

**Human induced pluripotent stem cell-based 3D  
neural in vitro models: development, quality  
control and disease modeling**

Dissertation to obtain the degree

Doctor rerum naturalium (Dr. rer. nat.)

at the Heinrich-Heine-University Düsseldorf

submitted by

**Julia Kapr**

from

Freiberg

Düsseldorf, 21.08.2023



**Neurale 3D in vitro Modelle basierend auf  
humanen induzierten pluripotenten  
Stammzellen: Entwicklung, Qualitätskontrolle  
und Krankheitsmodellierung**

Inaugural-Dissertation

zur Erlangung des Doktorgrades

der Mathematisch-Naturwissenschaftlichen Fakultät

der Heinrich-Heine-University Düsseldorf

vorgelegt von

**Julia Kapr**

aus

Freiberg

Düsseldorf, 21.08.2023



Angefertigt am IUF - Leibniz-Institut für umwelt-medizinische Forschung GmbH  
an der Heinrich-Heine-Universität Düsseldorf.

Gedruckt mit Genehmigung der  
Mathematisch-Naturwissenschaftlichen Fakultät der  
Heinrich-Heine-Universität Düsseldorf.

Referentin: Prof. Dr. Ellen Fritsche

Korreferentin: Prof. Dr. Vlada Urlacher

Tag der mündlichen Prüfung: 16.04.2024



Das Fragezeichen  
ist ein Symbol für das Unbekannte. Für unbeantwortete Fragen, ungelöste Rätsel.  
Unsere Aufgabe ist es, Fragen zu beantworten, Rätsel zu lösen  
und Geheimnisse jeglicher Art zu lüften.

*Justus Jonas, in Robert Arthurs': Die Drei ???*

# Table of Content

<b>ABSTRACT</b>	<b>1</b>
<b>ZUSAMMENFASSUNG</b>	<b>2</b>
<b>1 INTRODUCTION</b>	<b>3</b>
1.1 BRAIN DEVELOPMENT	3
1.1.1 <i>In health</i>	3
1.1.2 <i>In disease</i>	6
1.2 MODELING HUMAN BRAIN DEVELOPMENT AND ITS DISRUPTION	10
1.2.1 <i>In vitro models</i>	10
1.2.2 <i>Human iPSCs in brain disease modeling</i>	13
1.3 THE COCKAYNE SYNDROME B (CSB)	15
1.3.1 <i>Clinical phenotypes and the CSB protein</i>	16
1.3.2 <i>Modeling CSB brain development</i>	18
1.4 AIM OF THE THESIS	20
<b>2 MANUSCRIPTS</b>	<b>21</b>
2.1 STEM CELLS FOR NEXT LEVEL TOXICITY TESTING IN THE 21ST CENTURY	24
2.2 NEURAL IN VITRO MODELS FOR STUDYING SUBSTANCES ACTING ON THE CENTRAL NERVOUS SYSTEM	56
2.3 NEURONAL DIFFERENTIATION FROM INDUCED PLURIPOTENT STEM CELL-DERIVED NEUROSPHERES BY THE APPLICATION OF OXIDIZED ALGINATE-GELATIN-LAMININ HYDROGELS	88
2.4 HUMAN INDUCED PLURIPOTENT STEM CELL-DERIVED NEURAL PROGENITOR CELLS PRODUCE DISTINCT NEURAL 3D IN VITRO MODELS DEPENDING ON ALGINATE/GELLAN GUM/LAMININ HYDROGEL BLEND PROPERTIES	106
2.5 MEASUREMENT OF ELECTRICAL ACTIVITY OF DIFFERENTIATED HUMAN IPSC-DERIVED NEUROSPHERES RECORDED BY MICROELECTRODE ARRAYS (MEA)	122
2.6 ACADEMIC APPLICATION OF GOOD CELL CULTURE PRACTICE FOR INDUCED PLURIPOTENT STEM CELLS	140
2.7 HiPSC-DERIVED 3D NEURAL MODELS REVEAL NEURODEVELOPMENTAL PATHOMECHANISMS OF THE COCKAYNE SYNDROME B	162
<b>3 DISCUSSION</b>	<b>206</b>
3.1 HUMAN iPSCs AS BASIS FOR NEURAL IN VITRO MODELS	206
3.2 HUMAN IPSC-BASED NEURAL MODELS IN 2D AND 3D	208
3.2.1 <i>From 2D to 3D cultures</i>	208

3.2.2 <i>Scaffold-free and scaffold-based 3D models</i>	210
3.3 IN VITRO MODELING OF HUMAN BRAIN PATHOLOGY	217
3.4 THE COCKAYNE SYNDROME B (CSB)	220
3.4.1 <i>Fit-for-purpose models to study CSB in vitro</i>	221
3.4.2 <i>Mechanisms underlying the neuropathology of CSB</i>	222
3.5 IMPLICATIONS FOR THE FUTURE OF DISEASE MODELING	226
<b>ABBREVIATIONS</b>	<b>230</b>
<b>REFERENCES</b>	<b>234</b>
<b>DANKSAGUNG</b>	<b>267</b>
<b>EIDESSTÄTTLICHE ERKLÄRUNG/DECLARATION</b>	<b>269</b>

# Abstract

It is widely acknowledged that animal models do not often recapitulate human diseases with satisfactory results. Especially human brain development is difficult to model in animals due to a variety of structural and functional species-specificities. This causes significant discrepancies between predicted and apparent drug efficacies in clinical trials, and their subsequent failure. Emerging alternatives based on 3D in vitro approaches stride forward to close the current gaps, and ultimately reduce, replace and refine animal experiments. Therefore, this study aimed at the characterization and optimization of 3D culture conditions for the development of in vitro models mimicking neurodevelopmental disorders.

The first two manuscripts in this study review the existing and developing stem cell-based in vitro approaches, including their advantages and limitations (manuscript 2.1, manuscript 2.2). Specific focus on 2D and 3D human induced pluripotent stem cell (hiPSC)-based neural models and their comparison is set in manuscript 2.2. Since 2D models do not recapitulate the in vivo physiology, great efforts are made to augment these cultures into 3D. The establishment and characterization of oxidized alginate-gelatin-laminin and alginate-gellan gum-laminin hydrogel blends for 3D neural in vitro models is described in manuscript 2.3 and manuscript 2.4. These studies underline the necessity of adapted and fine-tuned hydrogel properties for neural network formation and electrical activity. A methods description on the measurement of electrical activity of hiPSC-based neural cultures using microelectrode arrays (MEAs) is given in manuscript 2.5. Owing to their properties, hiPSCs have proven to be a very promising tool to study human neurodevelopment. However, different cultivation protocols, storage conditions and contaminations can lead to reproducibility and reliability issues. This leads to a substantial need for quality controlled hiPSC cultures. Manuscript 2.6 provides a guideline for the implementation of quality control standards into academic settings.

The main manuscript 2.7 of this thesis describes the utilization of hiPSC-based neural models to gain valuable insights into neurological pathomechanisms of the Cockayne Syndrome B (CSB). CSB is a rare hereditary disease and is accompanied by severe neurologic defects, such as microcephaly, intellectual disability and demyelination. No treatment is currently available for affected children. Phenotypic analyses of two quality controlled hiPSC-based in vitro models of CSB link cellular mechanisms to the disease's cardinal neurological symptoms using a multi-omics approach. The thesis provides evidence, that HDAC-dependent and independent mechanisms lead to inhibited neural progenitor cell migration, altered electrical activity and disrupted oligodendrocyte maturation. These data add to the in-depth understanding of the CSB neuropathology.

The thesis shows that there are multiple ways of generating neural in vitro models from hiPSCs in 3D, which can be used in a fit-for-purpose manner. Applications of such models for studying human diseases, personalized and generic, opens new possibilities for the identification of human-relevant drug-targets in a physiologically relevant manner.

# Zusammenfassung

Es ist weithin anerkannt, dass Tiermodelle menschliche Krankheiten nur selten zufriedenstellend widerspiegeln. Insbesondere die Entwicklung des Gehirns ist aufgrund einer Vielzahl von artspezifischen strukturellen und funktionellen Besonderheiten schwer zu modellieren. Dies führt zu erheblichen Diskrepanzen zwischen vorhergesagter und tatsächlicher Wirksamkeit von Medikamenten. Alternativen, basierend auf 3D in vitro Methoden, erweisen sich als vielversprechend für die Beantwortung von offenen Fragen und zur Reduktion von Tierversuchen. Daher zielt diese Studie auf die Charakterisierung und Optimierung von 3D-Kulturbedingungen für die Untersuchung von Hirnkrankheiten ab.

Die ersten beiden Manuskripte in dieser Studie geben einen Überblick über stammzellbasierte in vitro Methoden (Manuskript 2.1, Manuskript 2.2). Ein spezieller Schwerpunkt liegt auf 2D- und 3D-Modellen des menschlichen Gehirns, welche auf induzierten pluripotenten Stammzellen (hiPSC) basieren (Manuskript 2.2). Da 2D-Modelle die in vivo Physiologie des Menschen nicht widerspiegeln, werden komplexere 3D-Kulturmodelle benötigt. Die Entwicklung und Charakterisierung von Hydrogelen aus oxidiertem Alginate-Gelatin-Laminin und Alginate-Gellan Gumm-Laminin für 3D neurale in vitro Modelle werden in Manuskript 2.3 und Manuskript 2.4 beschrieben. Diese Arbeiten unterstreichen die Notwendigkeit von speziell für Hirnmodelle angepasste Hydrogelen, um die Bildung elektrisch aktiver neuraler Netzwerke zu ermöglichen. Eine Methodenbeschreibung zur Messung der elektrischen Aktivität von hiPSC-basierten neuronalen Kulturen mittels Mikroelektrodenarrays (MEAs) erfolgt in Manuskript 2.5. Aufgrund ihrer Eigenschaften haben sich hiPSCs als vielversprechendes Werkzeug zur Untersuchung der Hirnentwicklung erwiesen. Unterschiedliche Kultivierungsprotokolle, Lagerbedingungen und Kontaminationen können jedoch zu Reproduzierbarkeits- und Zuverlässigkeitsproblemen führen. Manuskript 2.6 bietet eine Richtlinie für die Implementierung von Qualitätskontrollstandards in akademischen Einrichtungen, um solche Probleme zu minimieren. Das Hauptmanuskript 2.7 dieser Arbeit beschreibt die Verwendung von hiPSC-basierten neuronalen Modellen, um wertvolle Einblicke in die Pathomechanismen des Cockayne Syndroms B (CSB) zu gewinnen. CSB ist eine seltene erbliche Krankheit, die von schweren neurologischen Defekten begleitet wird, z.B. Mikrozephalie, geistige Behinderung und Demyelinisierung. Derzeit steht keine Behandlung für betroffene Kinder zur Verfügung. Unter Zuhilfenahme von Multiomics-Analysen werden die Endophänotypen von zwei hiPSC-basierten CSB in vitro Modellen den hirnspezifischen kardinalen Krankheitssymptomen zugeordnet. Das Manuskript liefert Hinweise darauf, dass HDAC-abhängige und -unabhängige Mechanismen zu gehemmter Migration von neuronalen Vorläuferzellen, veränderter elektrischer Aktivität und gestörter Reifung von Oligodendrozyten führen. Diese Daten tragen zu einem umfassenden Verständnis der CSB-Neuropathologie bei.

Die Studie zeigt, dass verschiedene hiPSC-basierte 3D in vitro Modelle zweckdienlich verwendet werden können. Ihre Anwendung für die Untersuchung menschlicher Krankheiten kann zur Identifizierung von pharmazeutisch relevanten Wirkstoffzielen beitragen.

# 1 Introduction

## 1.1 Brain development

The brain is one of the most complex organs of the human body and its development and function are an exceptional riddle, which is yet to be solved. A highly regulated spatiotemporal organization of different cell types and their interconnection is crucial for healthy brain development. Deviation from this delicate regulation leads to various adverse neurological effects. A brief introduction into brain development in health and disease is given below.

### *1.1.1 In health*

The human brain development is a highly orchestrated process that starts in the early prenatal phase and continues throughout life. Prenatal development is subdivided into two major periods: the embryonic period, from gestational week (GW) 4 to GW 8 when organ primordia are formed, and the subsequent fetal period, which is marked by organ maturation and stretches until birth (O’Rahilly and Müller 2005). Early postnatal development, until approx. 3 years after birth, also constitutes a crucial phase in children’s brain development (Figure 1.1). A human brain is fully matured at the age of approximately 25 years of age (Insel 2010; Paus, Keshavan, and Giedd 2008).

The embryonic period starts in GW 4 with the closure of the neural folds of the neural plate over the midline to form the neural tube (neural tube closure), during the process of neurulation. The neural tube subsequently forms the three vesicles, which give rise to the fore-, mid- and hindbrain (Jessell and Sanes 2000; Rash and Grove 2006; Rhinn, Picker, and Brand 2006; Stern 2001). A high rate of cell proliferation can be observed in the ventricular zone during GW 5-6, which marks a major key event (KE) in prenatal brain development (Jessell and Sanes 2000; Monk, Webb, and Nelson 2001; Pencea et al. 2001; Rash and Grove 2006). The ventricular zone hosts the majority of radial glia cells (RG), which give rise to glial progenitor cells, the source for astrocytes and oligodendrocytes, and early neurons. In parallel, neurogenesis initiates the start of laminar organization and patterning, where RG serve as guidance structure for neuronal migration. This

process continues until birth (Rakic 1982; Chao, Ma, and Shen 2009; Gressens 2000; Hatten 1999).

The embryonic period transitions into the fetal period during GW 8. Fetal development is generally characterized by immense growth, cell differentiation and accelerated synaptogenesis (O’Rahilly and Müller 2005). The brain’s weight increases 40-fold during that period, which is characterized not only by massive radial glia proliferation, but also neuronal migration, peaking during GW 12-20 (de Graaf-Peters and Hadders-Algra 2006; Tau and Peterson 2010). During this phase, radial glial activity shifts from neuron to astrocyte and oligodendrocyte generation, with internal and external factors, such as region-specific growth-factors, cellular microenvironment and transcription factors, determining the cell fate (Malatesta et al. 2003; Howard et al. 2008). In general, astrocytes are the major glia cell population in the human brain. As such, they have diverse functions, including neuroprotection and metabolic support. More precisely, astrocytes have antioxidative effects and facilitate synaptic cleft clearance, neurotransmitter recycling and nutrient supply in the brain. They also account for a significant part of the blood-brain-barriers (BBB) protective power (Peuchen et al. 1997; Santello, Toni, and Volterra 2019). The BBB develops between GW 8 and 35 and regulates the in- and efflux of molecules from the central nervous system (CNS; Saili et al. 2017). Its tight regulation protects the CNS from external factors like pathogens and neurotoxic blood components (Sweeney et al. 2019).

Oligodendrocytes account for a majority of the brains white matter. They generate the myelin sheath, which enwrap axons and thus enables rapid signal transmission. In this context, oligodendrocytes provide metabolites to maintain axonal health. They start to produce the first myelin, with myelinated gyri being detectable from GW 35. Although myelination peaks during early postnatal development (approx. 1-5% total brain myelination between GW 36 and 40), myelin production continues throughout life and increases to 50-60% in the white matter in adult brains (Kuhn et al. 2019; Snaidero and Simons 2014; Tau and Peterson 2010).

During GW 26-29, neurons reach their designated place and start to develop axons and dendrites to form synaptic connections (de Graaf-Peters and Hadders-Algra 2006; Huttenlocher et al. 1982; Petanjek et al. 2008; 2011). This process is accompanied by the formation of gyri and sulci during the third trimester (Garel et al. 2001). Specialized neuronal subtypes enable the transmission of information through spatiotemporal inhibitory and excitatory neurotransmitter signaling. Neurotransmitters are thereby released from the presynaptic neuron and taken up by the postsynaptic neuron from the synaptic cleft. Excitatory neurotransmitters, such as glutamate, acetylcholine and histamine, initiate the influx of positively charged ions through ion channels, which causes the depolarization of the cell, and subsequently generates the action potential. Postnatal inhibitory signaling through GABA prevents action potentials through the influx of negatively charged ions into the respective cell (Lovinger 2008). This fine-tuned communication between neuronal subtypes is crucial for healthy brain circuit formation. First electrophysiological measurements detect activity as early as GW 20. The electrical pattern changes throughout development, as transient connections are formed and remodeled. GW 34 marks the peak of synaptogenesis. However, this process reaches well into the early postnatal phase and follows a strict spatiotemporal regulation (Tau and Peterson 2010).

The postnatal phase features massive outgrowth, largely facilitated by further generation and expansion of glial cells and the progressing myelination. At 3 years of age, the child's brain reaches approx. 81-88% of its final weight (Dekaban and Sadowsky 1978; Barnea-Goraly et al. 2005). As neural circuits progress from transient to stable connections in the postnatal phase, the excitatory-to-inhibitory GABA switch marks a crucial neurodevelopmental KE (Peerboom and Wierenga 2021). The GABA switch is initiated by downregulation of the chloride importer Na-K-2Cl cotransporter isoform 1 (NKCC1) and upregulation of the exporter K-Cl cotransporter isoform 2 (KCC2). As active chloride transporters, they are responsible for the high pre-GABA switch and low post-GABA switch intracellular chlorine concentrations (Ben-Ari 2002), contributing to stable brain circuit formation. Subsequently, higher-order cognition and behavioral learning evolves.

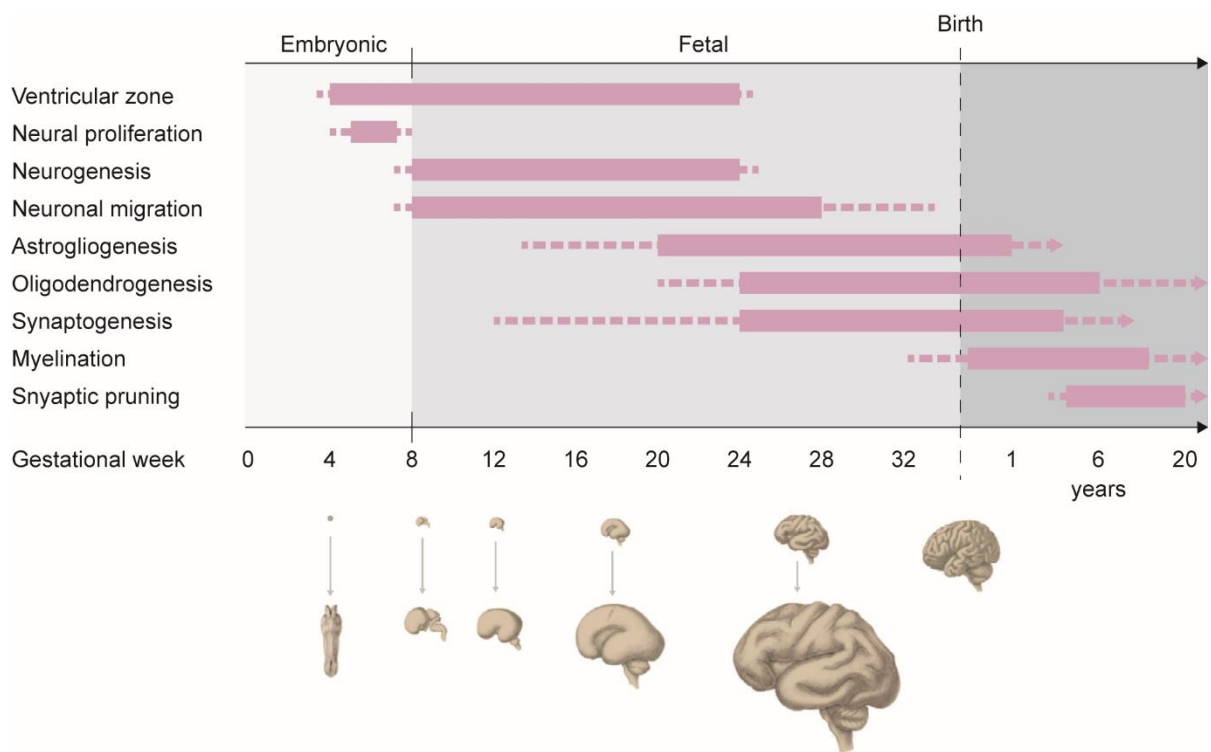


**Figure 1.1. Timeline of key processes in human brain development.** The figure summarizes selected crucial events in neurodevelopment and their rough chronology from conception to postnatal year 20. The bars represent the peak period of each process, with dotted lines indicating further timepoints during which the process occurs. Arrows indicate that the process is continued during later developmental stages. Schematics of brain images illustrate the rough features of development over time. This figure was adapted from Silbereis et al. 2016 and Tau and Peterson 2010. Figure made using biorender.com.

### 1.1.2 In disease

The human brain passes through many checkpoints during its development. Proliferation, migration, differentiation and neural network formation belong to these identified checkpoints, defined as neurodevelopmental KEs. The disruption of one or more KE by genetic or environmental factors can cause detrimental defects (Figure 1.2; Tau and Peterson 2010; Silbereis et al. 2016; Bal-Price et al. 2018). Notably, a high number of adverse neurodevelopmental effects arises already during embryonic development (Silbereis et al. 2016). Defects of the neural tube closure (NTC) are amongst the most common birth defects and can be caused by various genetic or environmental risk

factors, such as poor nutrition (e.g. low folate level) or certain maternal medications (e.g. agents to treat epilepsy or seizures). Exemplary resulting diseases include anencephaly (missing brain and skull vault, often stillbirth) and spina bifida (malformation of the spinal cord; Nikolopoulou et al. 2017). Proliferation is crucial for substantiating the brains' mass early on. The disruption of proliferation during brain development has been linked to distinct clinical phenotypes, such as microcephaly and megalencephaly. Decreased proliferation can lead to congenital microcephaly and the Seckel syndrome, while increased neuronal proliferation can cause the Megalencephaly-polymicrogyria-polydactyly-hydrocephalus (MPPH) syndrome (Pirozzi, Nelson, and Mirzaa 2018). The brains' spatial organization relies on precisely timed cellular migration. When neuronal migration is altered, malformations in cortical development occur, amongst others leading to intellectual disabilities (Buchsbaum and Cappello 2019; Poirier et al. 2013; Becerra-Solano, Mateos-Sánchez, and López-Muñoz 2021). Periventricular heterotopia is an X-linked disease caused by complete migratory failure of a subset of neurons, leading to aggregates in the ventricular zone. Clinically, the disease manifests in epilepsy (mild to severe) and brain anatomical abnormalities (Fox and Walsh 1999). Other migration-driven disorders belong to the lissencephaly spectrum. These diseases can be caused by viral infections during pregnancy or a lack of oxygenated blood in the fetus, subsequently leading to disrupted gyri and sulci formation and a "smooth brain" (Di Donato et al. 2017; Joseph, Pushpalatha, and Kuruvilla 2008; Tau and Peterson 2010). Depending on the severity of the adverse brain development, lissencephaly can lead to mild retardation but also early postnatal death (Tau and Peterson 2010). Disruption of cell migration during the fetal phase can also cause agenesis of the corpus callosum (ACC), a condition where the left and right hemispheres are not or insufficiently connected (Rotmensch and Monteagudo 2020). Moreover, the untimely or suppressed differentiation of neuronal and glia cells precedes a variety of severe disorders. For instance, the 1q21.1 microduplication syndrome causes a delay in neuronal differentiation, leading to adverse effects comprising developmental delay and cognitive impairment, in some cases including traits of autism spectrum disorder (Joy Yoon and Mao 2021). Similarly, premature neuronal differentiation can result in microcephaly and further developmental delays (Pirozzi, Nelson, and Mirzaa

2018). Oligodendrocyte differentiation is especially sensitive to oxidative stress, inflammation and toxicity, which can cause severe myelination pathologies when disrupted (Back et al. 2001; Ness et al. 2001; Tauheed, Ayo, and Kawu 2016; Stadelmann et al. 2019). Perivascular leukomalacia (PVL) can be caused by insufficient oxygenation in preterm infants, resulting in white matter damage, thereby negatively effecting oligodendrocyte maturation and myelination (Kinney and Back 1998; Motavaf and Piao 2021). Given that these lesions emerge during incomplete oligodendrogenesis, the consequences can encompass motor nerve damage and learning deficits. Furthermore, oligodendrocyte precursor (OPC) and oligodendrocyte abnormalities have been implicated with Parkinson's disease and Schizophrenia (Spaas et al. 2021). Another crucial aspect of neurodevelopment is the formation of neural networks. The intricacy of the brain's circuitry results in a diverse array of possible adverse effects. Disrupted brain function, such as altered synaptogenesis, is often intertwined with psychiatric conditions, such as Angelman syndrome, autism spectrum disorder and attention deficit hyperactivity disorder (ADHD; Lee et al. 2014; Stiles and Jernigan 2010; Tau and Peterson 2010; Margolis et al. 2015). As elucidated earlier, the postnatal GABA switch stands as a significant milestone in brain circuit formation, with a profound impact in postnatal brain development. A delay or failure of the GABA switch, triggered by factors like inflammatory stress during pregnancy, leads to increased excitatory GABA transmission in the brain. This increase in excitation is believed to be a contributing factor to the development of epilepsy (Treiman 2001). Imbalanced GABA signaling in early brain circuit formation was proposed to be involved in the development of a subset of autism spectrum disorder (Pizzarelli and Cherubini 2011), while altered migration and synaptogenesis in the GABAergic system was suggested to contribute to Schizophrenia (Schmidt and Mirnics 2015).

Only a diminutive subset of potential adverse effects on brain development has been listed above. The clinical heterogeneity, coupled with a lack of appropriate disease models, continues to limit our understanding of the underlying pathophysiology for a majority of disorders. Consequently, the understanding of underlying mechanisms and subsequent identification of drug targets remains a substantial challenge.

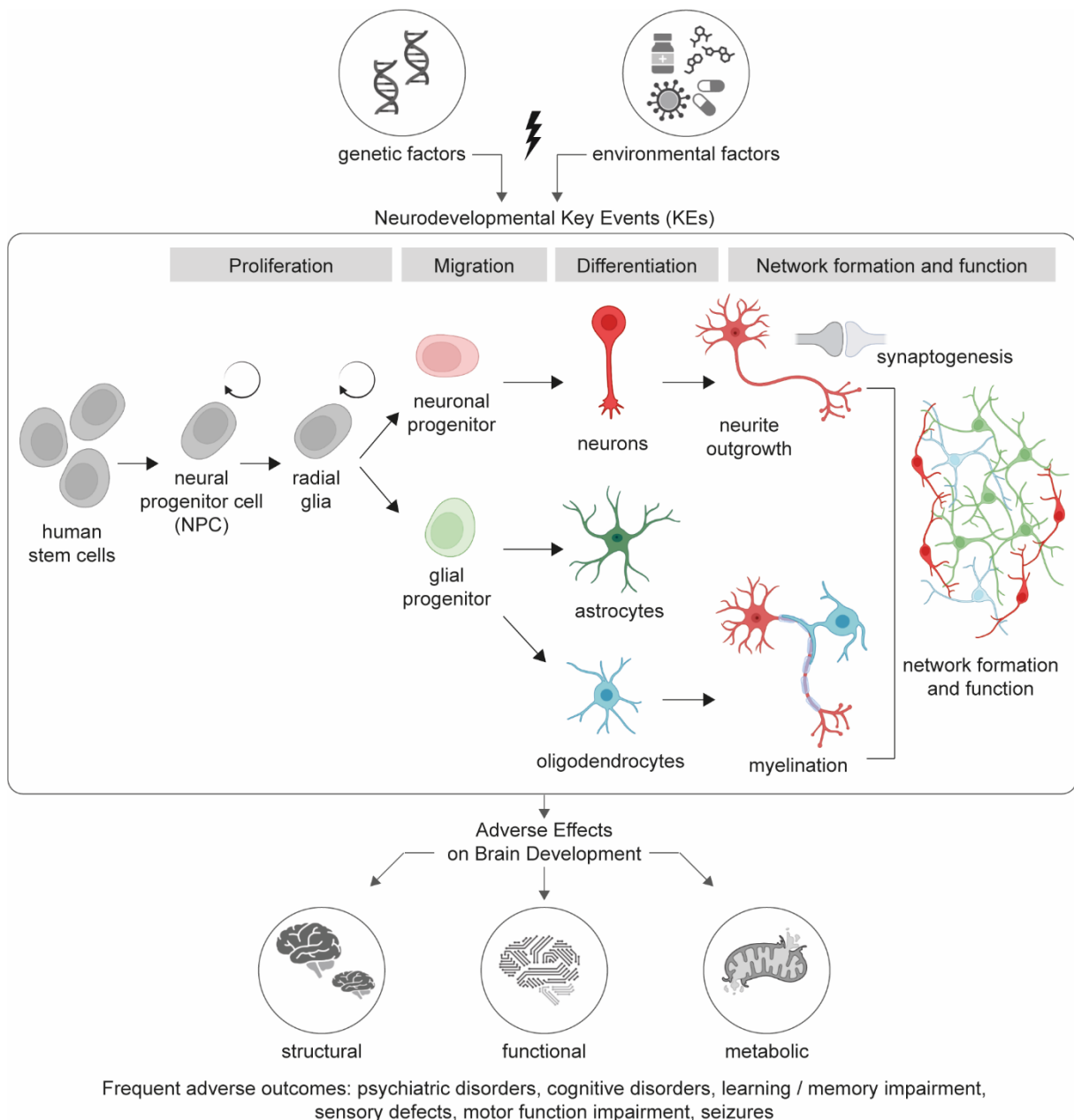


**Figure 1.2. Neurodevelopmental key events.** Genetic and environmental factors can negatively impact neurodevelopmental key events (KE). Depicted are the selected KEs proliferation, migration, differentiation and neural network formation, including respective cell types. Human stem cells form proliferating neural progenitor cells (NPC), which develop into radial glia (RG) and further into neuronal and glial progenitor cells. These cell types are able to migrate. The glial progenitor cells can further differentiate into astrocytes and oligodendrocytes. Neuronal progenitor cells differentiate into distinct neuronal subtypes. Together, neuronal outgrowth, synaptogenesis and myelination precede the subsequent formation of functional neural networks. Adverse effects in brain development can cause structural alterations, functional impairment and metabolic changes. Exemplary adverse outcomes are listed at the bottom. Figure made using biorender.com.

## 1.2 Modeling human brain development and its disruption

Throughout the past century, animal models have yielded valuable insights into mammalian brain development, basic function and disorders. Nevertheless, significant limitations arise from inter-species variations, ethical issues, as well as cost and time consumption. This dilemma is reflected in alarmingly high attrition rates of drugs aimed at treating neurological disorders (Arrowsmith and Miller 2013). As an example, drug development targeting Alzheimer's disease has encountered failure rates exceeding 99% (Cummings, Morstorf, and Zhong 2014). This situation undeniably calls for more physiologically relevant models with enhanced predictive power for humans. Current EU regulations already state that animals should only be used for scientific purposes, if no alternative is available (European Directive 2010/63/EU). Under the umbrella of the 3Rs initiative (Russell and Burch 1959), substantial efforts are made to reduce, replace and refine animal experiments by developing human-based alternative *in vitro* models.

### 1.2.1 *In vitro* models

The establishment of the cultivation of human primary neural cell cultures during the mid to late 20th century gave rise to new neural *in vitro* models and a closer insight into cellular and molecular processes on human brain development and associated disorders. Moreover, primary fetal human neural progenitor cells (hNPC) cultured as neurospheres are successfully employed in developmental neurotoxicity (DNT) testing for adverse outcome analyses (Koch et al. 2022), also as part of a DNT *in vitro* testing battery (Blum et al. 2023). In 2007, Takahashi et al. developed a method to genetically reprogram adult human fibroblasts into human induced pluripotent stem cells (hiPSC). Their origin is ethically uncritical and they are available in a nearly limitless abundance. This discovery has aided the development of a plethora of new opportunities throughout the fields of biology and medicine, also catalyzing the rise of hiPSC-based neurophysiological *in vitro* models. The widespread accessibility of hiPSCs enables their use in high-throughput applications, such as drug screenings and toxicological studies (manuscript 2.1, manuscript 2.2; Nimtz et al. 2020; Fritsche et al. 2018; Tukker et al. 2018; Pamies et al.

2021; Pei et al. 2016). Moreover, their physiological relevance, including patient-specific and customizable genetic attributes, positions hiPSC models as ideal tools for disease modelling and drug target identification (Lebedeva and Lagarkova 2018; Penney, Ralvenius, and Tsai 2020; A. Sharma et al. 2020).

Both primary hNPCs and hiPSCs can be utilized to generate a variety of two-dimensional (2D) and three-dimensional (3D) in vitro models (Figure 1.3). The CNS consists of a complex cellular network in which the microenvironment, meaning spatiotemporal exposure to signaling molecules and cell-cell and cell-matrix interactions, play a crucial role for its function (Farrukh, Zhao, and del Campo 2018). Given that such interactions are largely absent in 2D cell cultures, the frequent failure in translating 2D in vitro findings into in vivo applications is inevitable. Due to the increasing need for more physiologically relevant models, great efforts went into adding the third dimension to standard 2D cell cultures. Starting from the beginning of this century, several approaches for the generation of 3D neural models such as neurospheres, BrainSpheres, organoids and hydrogel scaffolds have been developed (Zhuang, Sun, et al. 2018). As such models have been improving over the decades, they initiated a paradigm shift in disease modeling, as well as in pharmacological and toxicological testing (Lancaster and Knoblich 2014; Lancaster et al. 2017; S. P. Pasca 2018).

Human iPSC-derived 3D neurospheres consist of proliferating human induced neural progenitor cells (hiNPCs). They are relatively quick and easy to generate during a time course of approximately three weeks and allow the investigation of neurodevelopmental KEs like proliferation, as well as migration and differentiation into neurons and astrocytes after plating in secondary 3D (Nimtz et al. 2020; Hofrichter et al. 2017; Alépée et al. 2014). BrainSpheres are based on hiNPCs, yet differentiate in 3D into neurons and glia cells after approx. 8 weeks of differentiation. They consist of relevant co-cultured cell types, such as neurons of different subtypes, astrocytes and – facultatively – oligodendrocytes. Subsequently, both differentiated neurospheres and BrainSpheres develop functional neural networks, measurable on multielectrode arrays (MEAs; manuscript 2.5; Nimtz et al. 2020; Hartmann et al. 2023). Human iPSC-based neurospheres were employed to analyze neurotoxicity during neural network formation

on MEAs (Hartmann et al. 2023; Bartmann et al. 2023). BrainSpheres have previously been employed to study myelin disruption and chemical-induced dopaminergic neuronal toxicity (Chesnut et al. 2021; Pamies et al. 2021). Both their extensive applicability, including the ability to model multiple neurodevelopmental KE, emphasizes the value of this model for the reproducible investigation of the neurodevelopment and pathophysiological changes (manuscript 2.7; Pamies et al. 2021; Hartmann et al. 2023). Organoids, in contrast to BrainSpheres, are larger cell aggregates that contain a certain degree of anatomical structure due to self-organization (Lancaster et al. 2017; Matsui et al. 2018; Qian et al. 2016; Paşca et al. 2022). Different protocols have been developed to obtain brain region-specific organoids and assembloids (Qian et al. 2016; Hu et al. 2016; López-Tobón et al. 2019; Bagley et al. 2017), with characteristics of maturation, such as spontaneous electrical activity, dendritic spines and myelinating oligodendrocytes (Quadrato et al. 2017; Matsui et al. 2018; Shaker et al. 2021). As an example, hiPSC-derived brain organoids have previously been implemented to study drug efficacy against ZIKA virus infections (Zhou et al. 2017). However, the time-consuming generation and high organoid-to-organoid variability limit their current application for high throughput and screening applications (Di Lullo and Kriegstein 2017). Engineering-based 3D models such as hydrogel scaffolds complement the existing 3D cell models, by providing an adaptable, controlled and consistent extracellular environment (Bahram, Mohseni, and Moghtader 2016; Haring, Sontheimer, and Johnson 2017). The interest in hydrogels as extracellular matrixes (ECM) in cell cultures increased largely since their discovery in 1960 (Wichterle and Lím). The gels can be classified through different attributes, such as natural (e.g. gellan gum, alginate, gelatin) vs. synthetic polymers (e.g. PEG, POE) or the mode of crosslinking (Bahram et al. 2016). Natural polymers, including gellan gum (GG) and alginate (ALG), are inherently suitable surrogates for ECM, due to their structural similarity, as well as their chemical versatility and biocompatibility (Sun and Tan 2013). Various “bioinks” have previously been employed to generate bioprinted and non-bioprinted 3D neural models (manuscript 2.3, manuscript 2.4; Fantini et al. 2019; Gu et al. 2018; Chai, Jiao, and Yu 2017; D’Antoni et al. 2023). Nevertheless, combining suitable gel properties for adequate cell culture

development and functionality, with printability and long-term integrity of the hydrogels remains challenging.

Although there are many options to choose from, the most beneficial model choice largely depends on the individual research aim and needs. Sometimes, a combined use of different fit-for-purpose models can be valuable.

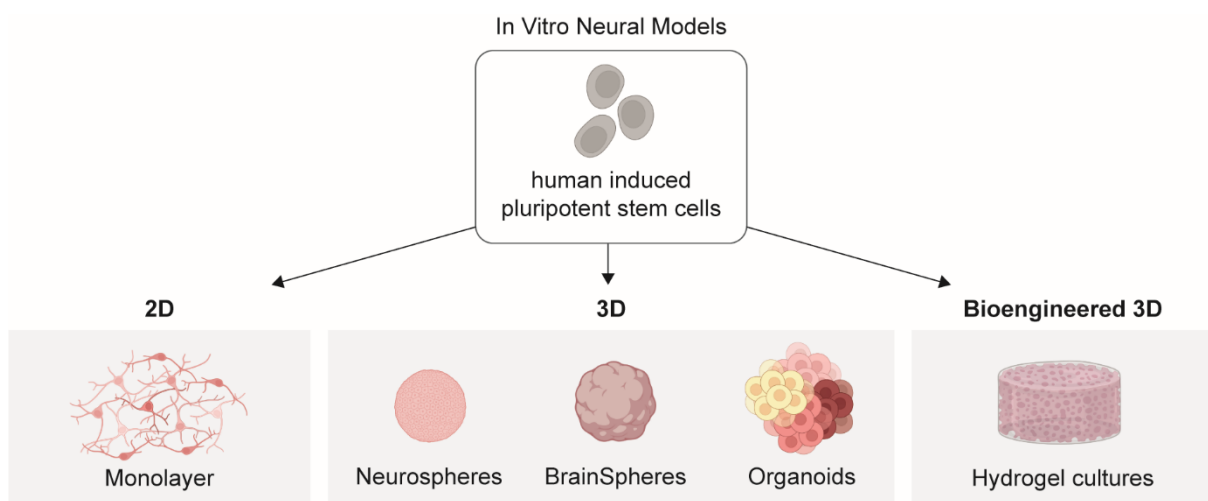


**Figure 1.3. In vitro neural models.** Human induced pluripotent stem cell (hiPSC)-based neural in vitro models can be generated in different dimensions. 2D monolayer cultures were originally used to model brain development in vitro. For more physiological relevance, in vitro models were augmented into 3D, including models like neurospheres, BrainSpheres and organoids. Bioengineered 3D hydrogel cultures additionally enable the tuning of specifically designed extracellular matrixes (ECMs). Figure made using biorender.com.

### 1.2.2 Human iPSCs in brain disease modeling

Human iPSCs are generated from somatic cells, primarily fibroblasts, of the respective donor in an ethically unproblematic manner. They have an unlimited capacity of self-renewal and possess the capacity to differentiate into all three germ layers: endoderm, ectoderm and mesoderm. The generation of hiPSCs can be achieved through different reprogramming techniques. In the original protocol, four transcription factors (Oct3/4, Sox2, Klf4, and c-Myc), collectively known as the “Yamanaka factors”, were integrated into the donor fibroblasts by retroviral transduction (Takahashi et al. 2007). These

original transcription factors identified for cell reprogramming remain widely utilized (I. H. Park, Lerou, et al. 2008; I. H. Park, Zhao, et al. 2008; Martins et al. 2021; Mittal et al. 2022). As time progressed, alternative reprogramming methods emerged, involving the exchange (J. Yu et al. 2007; Si-Tayeb et al. 2010), removal (Nakagawa et al. 2008) or addition (Zhao et al. 2008; Tsubooka et al. 2009) of different factors. Integration-free methods have also been developed (Zhou and Zeng 2013), such as employing episomal plasmids (Okita et al. 2011) or synthetic modified mRNA (Warren et al. 2010). The generated hiPSC can be neurally induced to obtain neural progenitor cells using a variety of 2D or 3D neural induction techniques (Galiakberova and Dashinimaev 2020). Amongst these methods, the dual-SMAD inhibition is the most widely used protocol, attributed to its simplicity and high efficiency. The protocol is based on the inhibition of both the bone morphogenic protein (BMP)- and transforming growth factor  $\beta$  (TGF $\beta$ )/Activin/Nodal-based pathways, which in turn suppress SMAD protein signaling (Chambers et al. 2009; Morizane et al. 2011). Modified approaches, such as using N2 and B27 supplemented media, have also proven efficient for the neural induction of hiPSCs (Hofrichter et al. 2017). The different protocols are adaptable to various adherent and spherical cultures, such as neural rosettes (Fedorova et al. 2019), embryoid bodies (EB; Kim et al. 2011; Rosati et al. 2018) and neurospheres (Hofrichter et al. 2017).

Neural models based on hiPSC provide an approximation of the embryonic phase, while concurrently developing functional neural networks. This combination positions them as optimal platforms for the investigation of neurodevelopmental diseases. Furthermore, the generation of patient-specific models enables the recapitulation of the disease-specific phenomic characteristics. These assets collectively offer us ideal tools to explore the fundamental cellular and molecular mechanisms at play, as well as to unravel the disease progression and subsequently identify potential drug targets (manuscript 2.2). Many hiPSC lines have by now been obtained from patients afflicted with various common and rare disorders, such as Parkinson's disease (Hartfield et al. 2014), Alzheimer's disease (Arber, Lovejoy, and Wray 2017; Barak et al. 2022), Down Syndrome (R. Xu et al. 2019), Cockayne Syndrome (Alexandre T. Vessoni et al. 2016) and Koolen-de-Vries-Syndrome (Linda et al. 2022). However, different reprogramming

techniques, cultivation protocols, storage conditions and contaminations can lead to reproducibility and reliability issues (Pamies et al. 2022). This leads to a substantial need for quality controlled hiPSC cultures. Manuscript 2.6 provides a guideline for the application of good cell culture practice for hiPSC cultures in academic settings. In a two tiered approach, an assay setup for the generation of quality-controlled master and working cell banks is described. Amongst others, morphological assessment, mycoplasma contamination checks, STR genotyping, karyotyping and pluripotency analyses are performed. In addition, the average cost per master cell bank is calculated. In another guidance, Pamies et al. (2022) list main principles that need to be considered in good cell and tissue culture practice, including culture characterization, documentation, safety, education and ethics. Following such guidelines will enable the generation of reliable data and support the transfer of knowledge from bench to bedside.

Taken together, hiPSCs emerge as promising tools for the patient-oriented investigation of neurodevelopmental pathomechanisms. Nevertheless, we do not yet harness their full potential in disease modeling. Especially, rare diseases and those lacking corresponding animal models stand to benefit from the ongoing development within the in vitro field.

### 1.3 The Cockayne Syndrome B (CSB)

The Cockayne Syndrome B (CSB) is a rare hereditary autosomal recessive disease characterized by severe dermatological and neurological symptoms. CSB manifests in different severities, with the most severe being fatal during early childhood (Laugel et al. 2010; Karikkineth et al. 2017). While considerable research has been conducted on the skin phenotype of CSB patients (Majora et al. 2018; Nakazawa et al. 2012; Rebel et al. 2005; Van der Horst et al. 1997), our understanding of the profound neurological defects remains very limited. This knowledge gap is largely attributed to the intricate nature of the disease and notable constraints in available model systems. Currently, there is no effective treatment strategy for children suffering from CSB.

### *1.3.1 Clinical phenotypes and the CSB protein*

E. A. Cockayne originally described the Cockayne Syndrome (CS) with the following symptoms: short stature, small head, retinal atrophy and deafness. Later it was discovered that patients are also sensitive to UV radiation (Schmickel and Chu 1977) and afflicted with severe neurological defects, such as microcephaly, demyelination and mental disabilities (Paddison, Moosy, and Derbres 1963; Moosy 1967; Sugarman, Landing, and Reed 1977). Hoar and Waghorne (1978) first suggested a defect of the excision repair pathway in CS patients, in connection to their UV-sensitivity. This suggestion was later confirmed in various studies (Lindenbaum et al. 2001; Rapin et al. 2000). Specifically, CSB was shown to be a main player in the transcription-coupled nucleotide excision repair (TC-NER) pathway. TC-NER is a mechanism to remove DNA lesions in actively transcribed regions, e.g. those induced by UV radiation or redox processes. The TC-NER pathway is triggered by damage-stalled RNA polymerase II in actively transcribed regions. This blockage stabilizes the binding of the CSB protein to the polymerase, which in turn induces the recruitment of CSA and other factors of the NER pathway. After the lesion is removed, the CSB is targeted for degradation and the transcription can be continued (Hanawalt and Spivak 2008; De Boer and Hoeijmakers 2000). Cell fusion experiments conducted by Tanaka et al. (1981) additionally revealed the involvement of two complementation groups in CS: CSA and CSB. Complementation groups generally refer to homozygous recessive mutations on different genes that cause the same phenotype and don't supplement each other. This thesis focuses on CSB, since approx. 80% of patients are affected by this type of CS (Mallery et al. 1998). However, it was not until 1992, that the CS was linked to the excision repair cross complementation (ERCC) gene family. Specifically, Troelstra et al. (1992) connected the CS complementation group B (CSB) to the ERCC6 gene on human chromosome 10q11-21. Various mutations in the ERCC6 gene, including short insertions and deletions, nonsense mutations, splice mutations, missense mutations, promoter mutations and polymorphisms have been described in relation to CSB (Figure 1.4 top; Laugel et al. 2010), together with variations in the patients' clinical severities. Nevertheless, no correlation of the type of mutation with the severity of the disease could be identified.

Over time, other rare diseases were identified to be caused by mutations in CSA or CSB and were thus associated to the CS spectrum. This led to the development of a clinical classifications system comprising three classes. CSI is the classical form of CSB, with first symptoms occurring during early childhood and a life expectancy of less than 16 years. CSII defines an early-onset phenotype with defects occurring in prenatal development. A very severe form of CSII is the Cerebro-oculofacio-skeletal syndrome (COFS), with a life expectancy of less than 5 years. The late-onset class CSIII comprises mild symptoms, such as in the UV-sensitivity syndrome (UVSS), where patients have a life expectancy of above 30 years (Vessoni et al. 2020). Laugel et al. (2008) provide a detailed description of the clinical manifestations of patients classified with COFS. As an example, patient 1 was, amongst others, afflicted with dysmorphic features, cataracts, severe seizures, cerebral and cerebellar atrophy, photosensitivity and microcephaly (Figure 1.4 bottom). This patient passed away at age 10 month from respiratory failure. The patient's fibroblasts were obtained for disease research by Prof. Egly (Strasbourg) and reprogrammed to hiPSCs using episomal plasmids (pCXLE-hUL, pCXLE-hSK, pCXLE-hOCT3/4-shp53-F; Okita et al 2011). The patient's hiPSCs were kindly provided for the usage in this dissertation.

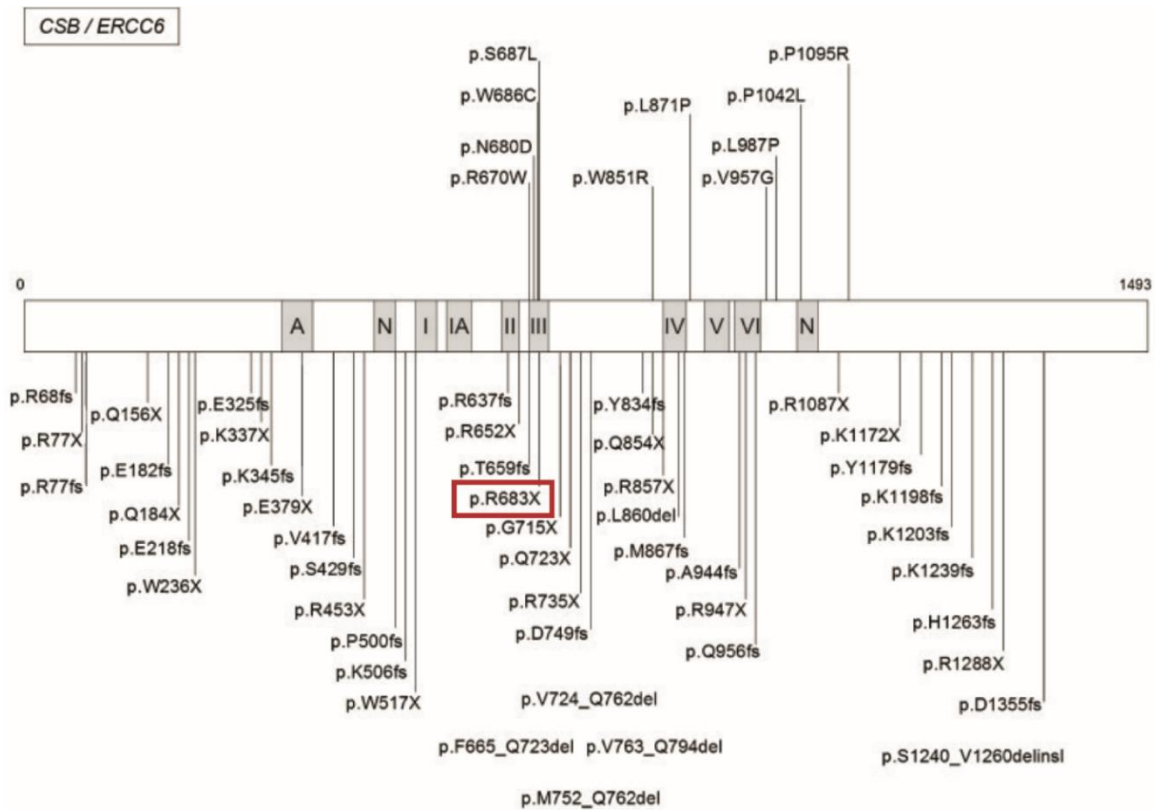
The CSB protein itself, encoded by the ERCC6 gene, is known to be involved in DNA repair, by tagging arrested RNA polymerase II in actively transcribed regions, subsequently recruiting the TC-NER machinery for DNA repair (Duan et al. 2021). DNA lesions caused by UV radiation account for a large number of transcription disruptions, which renders this mechanism especially important in the skin. However, the severe neuropathology of the patients cannot solely be explained with this mechanism. This becomes clear, when looking at phenotypes arising from mutations in genes encoding for Xeroderma pigmentosum (XP) proteins. XP proteins play a major role in the TC-NER, similar to CSB. Patients diagnosed with the Xeroderma pigmentosum share the characteristic increased photosensitivity with CSB patients, but not their severe neurological defects (Lehmann, McGibbon, and Stefanini 2011; Leung et al. 2022). Multiple studies have therefore suggested a role of CSB in the brain, which is independent of its involvement in the TC-NER pathway. Starting from the turn of the millennium, an increasing number of studies

suggested roles of CSB in different cellular mechanisms, such as p53 response (A. Yu et al. 2000; Sugita et al. 2001; Miyahara et al. 2015), chromatin remodeling (Citterio et al. 2000; Newman, Bailey, and Weiner 2006; I. Cho et al. 2013), mitochondrial maintenance (Tuo et al. 2002; Stevnsner et al. 2002; Scheibye-Knudsen et al. 2012) and autophagy (Majora et al. 2018). Yet, no underlying mechanisms for the clinical neurological phenotypes of CBS have been identified.

### *1.3.2 Modeling CSB brain development*

Due to the inherent complexity of human brain development, the deficit of data on the CSB neuropathology can be primarily attributed to the lack of suitable disease models. As human brain development is especially difficult to study, the data gap in CSB neuropathology largely results from a lack of adequate disease models. CSB rodent models show classic dermatological deficiencies, however, only very mild neurological defects (Scheibye-Knudsen et al. 2012; Murai et al. 2001; Revet et al. 2012; Y. Xu et al. 2019). *C. elegans* and zebrafish have also been employed to study CSB deficiency, mostly to investigate the effects of disrupted TC-NER and UV sensitivity (Boutin et al. 2022; Z. Wu et al. 2019). Prior efforts to uncover the underlying neuropathological mechanisms failed, as the phenotypes exhibited by the animals neither resembled the defects observed in human patients, nor their severity (Vessoni et al. 2020; Xu et al. 2019). Encouragingly, emerging in vitro alternatives stride forward to close the tremendous gap in human disease modeling and drug target identification (manuscript 2.1; Azar et al. 2021; David Pamies, Wiersma, et al. 2022). The use of hiPSCs in such models provides excellent tools to investigate diseases and their mechanisms (Martins et al. 2021; Pasca et al. 2015; Park et al. 2018). However, only few in vitro studies on CSB have employed patient-derived cells or even hiPSCs (Alexandre T. Vessoni et al. 2016; S. Wang et al. 2020; Liang et al. 2023).

Although previous in vivo and in vitro studies imply the impact of CSB on brain development, we still lack the necessary mechanistic understanding of why the diverse clinical phenotypes arise and how we can treat them.



Patient ID	CS789VI
Origin	UK
Mutation	Point mutation (2047C>T; p.Arg683x)
Donor Cell Type	Dermal fibroblasts, male
Clinical Classification	Cerebro-oculofacio-skeletal syndrome (COFS)
Growth failure	+
Low birth weight	+
Cachexia	-
Intellectual Disability	Severe
Microcephaly	Congenital
Seizures	+
Cataracts	Congenital
Microphthalmia	+
Retinal degradation	-
Deafness	+
Clinical photosensitivity	+
Dental anomalies	-
Arthrogyrosis	+
Age at Death	10 months

**Figure 1.4. Mutation spectrum of the Cockayne Syndrome B (CSB).** CSB can be caused by various mutations in the ERCC6 gene (top). The highlighted mutation (red box) was described for a patient classified with the Cerebro-oculofacio-skeletal syndrome (COFS), which is one of the most severe forms of CSB. The clinical phenotype of this patient is described in the bottom part of the figure. The upper photograph shows the newborn patient with dysmorphic features. The bottom image shows a magnetic resonance image of the patient brain after 1 month. The scan reveals global cerebral and cerebellar atrophy. The table on the right lists molecular and clinical characteristics of the COFS patient. Adapted from Laugel et al. (2008) and Laugel et al. (2010).

## 1.4 Aim of the thesis

The brain is one of the most complex tissues in the human body, making the task of modeling its development, and associated diseases, a difficult endeavor. Although animal models provided fundamental insights into brain function, species-differences between humans and rodents hinder the accurate recapitulation of human physiology. It is therefore not surprising, that drugs targeting CNS diseases exhibit alarmingly high attrition rates (Arrowsmith and Miller 2013). The pressing need for disease models that mirror human physiology has driven the quest for alternatives, and emerging human in vitro models based on hiPSCs offer promising tools to close the gaps in brain disease modeling and drug target identification (manuscript 2.1; David Pamies, Wiersma, et al. 2022; Shaker et al. 2021; A. M. Pasca et al. 2015; J. Park et al. 2018). However, we do not exploit their full potential yet. The Cockayne Syndrome B (CSB) is a rare hereditary disease with severe neuropathological defects (Newman, Bailey, and Weiner 2006; Laugel et al. 2008; Laugel et al. 2010; Kraemer et al. 2008; Melis, Van Steeg, and Luijten 2013). Although the skin phenotype of CSB has been well studied (Majora et al. 2018; Nakazawa et al. 2012; Rebel et al. 2005; Van der Horst et al. 1997), the origins of the neurological impairment remains enigmatic. Presently, a viable treatment strategy for children suffering from CSB remains elusive.

In order to utilize hiPSCs as tools to gain valuable insights into neurological pathomechanisms, the aims of this thesis are defined as follows:

1. Characterization and optimization of 3D culture conditions for the development of in vitro models phenocopying neurodevelopmental disorders.
2. Phenotypic analyses of two quality controlled hiPSC-based in vitro models of the Cockayne Syndrome B, focusing on the ubiquitous neurological clinical manifestations.
3. Identification of mechanisms underlying the CSB neuropathology based on a multi-omics approach.

## 2 Manuscripts

This thesis consists of 7 manuscripts.

In the first manuscript 2.1, 'Stem Cells for Next Level Toxicity Testing in the 21st Century' (Fritsche et al. 2020), a broad overview over existing and developing stem cell-based, including hiPSC-derived, in vitro models and assays for the main human organ systems is given, and innovative technologies are highlighted.

The second manuscript 2.2, 'Neural In Vitro Models for Studying Substances Acting on the Central Nervous System' (Fritsche et al. 2020) reviews the necessity, availability and limitations of 2D and 3D hiPSC-based neural models for safety and efficacy testing.

In the third manuscript 2.3, 'Neuronal Differentiation from Induced Pluripotent Stem Cell-Derived Neurospheres by the Application of Oxidized Alginate-Gelatin-Laminin Hydrogels' (Distler et al. 2021), the importance of laminin as ECM anchor for embedded hiNPCs is shown. Laminin supports cell survival and outgrowth within the hydrogels.

The fourth manuscript 2.4, 'Human Induced Pluripotent Stem Cell-Derived Neural Progenitor Cells Produce Distinct Neural 3D In Vitro Models Depending on Alginate/Gellan Gum/Laminin Hydrogel Blend Properties' (Kapr et al. 2021) presents the establishment and comparison of 3D hydrogel compositions, which allow for the differentiation and outgrowth of healthy and disease hiNPCs within the gel. Additionally, the bioprintability and subsequent survival of hydrogel-embedded single hiNPCs is shown.

In the fifth manuscript 2.5, 'Measurement of Electrical Activity of Differentiated Human iPSC-Derived Neurospheres Recorded by Microelectrode Arrays (MEA)' (Bartmann et al. 2021), the application of MEAs in toxicology assessment, including cell preparation, cultivation and measurement parameters, is described for the usage of hiPSC-based neurospheres.

The sixth manuscript 2.6, 'Academic Application of Good Cell Culture Practice for Induced Pluripotent Stem Cells' (Tigges et al. 2021) emphasizes the importance of quality-controlled hiPSC culture in academic settings, to ensure experiment reproducibility and high-value data.

In the last and main manuscript 2.7, 'HiPSC-derived 3D neural models reveal neurodevelopmental pathomechanisms of the Cockayne Syndrome B' (Kapr et al. submitted), we link cellular pathomechanisms caused by CSB-deficiency in hiPSC-based in vitro models, to the cardinal neuropathological symptoms of the CSB.



## 2.1 Stem Cells for Next Level Toxicity Testing in the 21st Century

*Ellen Fritsche, Thomas Haarmann-Stemmann, Julia Kapr, Saskia Galanjuk, Julia Hartmann, Peter R. Mertens, Angela A. M. Kämpfer, Roel P. F. Schins, Julia Tigges, Katharina Koch*

The call for a paradigm change in toxicology from the United States National Research Council in 2007 initiates awareness for the invention and use of human-relevant alternative methods for toxicological hazard assessment. Simple 2D in vitro systems may serve as first screening tools, however, recent developments infer the need for more complex, multicellular organotypic models, which are superior in mimicking the complexity of human organs. In this review article most critical organs for toxicity assessment, i.e., skin, brain, thyroid system, lung, heart, liver, kidney, and intestine are discussed with regards to their functions in health and disease. Embracing the manifold modes-of-action how xenobiotic compounds can interfere with physiological organ functions and cause toxicity, the need for translation of such multifaceted organ features into the dish seems obvious. Currently used in vitro methods for toxicological applications and ongoing developments not yet arrived in toxicity testing are discussed, especially highlighting the potential of models based on embryonic stem cells and induced pluripotent stem cells of human origin. Finally, the application of innovative technologies like organs-on-a-chip and genome editing point toward a toxicological paradigm change moves into action.

Journal:	Small
Impact factor:	15.15 (2021)
Contribution to the publication:	20%
	Section Text on Organ-on-a-Chip/Microphysiological Systems, Figure Layouts and Figure 7, Graphical Abstract
Type of authorship:	Co-author
Status of publication:	Published (23 December 2020)

# Stem Cells for Next Level Toxicity Testing in the 21st Century

Ellen Fritsche,\* Thomas Haarmann-Stemmann, Julia Kapr, Saskia Galanjuk, Julia Hartmann, Peter R. Mertens, Angela A. M. Kämpfer, Roel P. F. Schins, Julia Tigges, and Katharina Koch

The call for a paradigm change in toxicology from the United States National Research Council in 2007 initiates awareness for the invention and use of human-relevant alternative methods for toxicological hazard assessment. Simple 2D *in vitro* systems may serve as first screening tools, however, recent developments infer the need for more complex, multicellular organotypic models, which are superior in mimicking the complexity of human organs. In this review article most critical organs for toxicity assessment, i.e., skin, brain, thyroid system, lung, heart, liver, kidney, and intestine are discussed with regards to their functions in health and disease. Embracing the manifold modes-of-action how xenobiotic compounds can interfere with physiological organ functions and cause toxicity, the need for translation of such multifaceted organ features into the dish seems obvious. Currently used *in vitro* methods for toxicological applications and ongoing developments not yet arrived in toxicity testing are discussed, especially highlighting the potential of models based on embryonic stem cells and induced pluripotent stem cells of human origin. Finally, the application of innovative technologies like organs-on-a-chip and genome editing point toward a toxicological paradigm change moves into action.

For the last decades, human health risk assessment has been mainly based on results from animal experiments. These are stipulated, e.g., for chemicals in Organization for Economic Co-operation and Development (OECD) guidelines including acute toxicity (oral, inhalation, dermal), irritation (skin and eye), sensitization (skin and respiratory), repeated dose toxicity (28-day, 90-day, and chronic), mutagenicity and genotoxicity, reproductive and developmental toxicity, as well as carcinogenicity. Such animal experiments have been useful for hazard identification in the past and still guide the current risk assessment process. However, there are several drawbacks in this procedure that provoked a call for a paradigm change in toxicity testing by the United States National Research Council in the beginning of the century.<sup>[1,2]</sup> These drawbacks include the issues that animal experiments i) are extremely time- and cost-intensive, hence not suited for testing the

## 1. Introduction

Toxicology integrates biology, chemistry, pharmacology, and medicine to study adverse effects of exogenous noxae (e.g., chemicals, drugs, particles, radiation) on living organisms with the final goal of human and environmental health protection.

Prof. E. Fritsche, Dr. T. Haarmann-Stemmann, J. Kapr, S. Galanjuk, J. Hartmann, Dr. A. A. M. Kämpfer, Dr. R. P. F. Schins, Dr. J. Tigges, Dr. K. Koch

IUF – Leibniz Research Institute for Environmental Medicine  
Düsseldorf 40225, Germany  
E-mail: Ellen.Fritsche@iuf-duesseldorf.de

Prof. E. Fritsche  
Medical Faculty  
Heinrich-Heine University Düsseldorf  
Düsseldorf 40225, Germany

Prof. P. Mertens  
Department of Nephrology and Hypertension  
Diabetes and Endocrinology  
Otto-von-Guericke-University Magdeburg  
Magdeburg 39106, Germany

 The ORCID identification number(s) for the author(s) of this article can be found under <https://doi.org/10.1002/smll.202006252>.

© 2020 The Authors. Small published by Wiley-VCH GmbH. This is an open access article under the terms of the Creative Commons Attribution License, which permits use, distribution and reproduction in any medium, provided the original work is properly cited.

DOI: 10.1002/smll.202006252

wealth (in the ten-thousands) of chemicals that need hazard characterization,<sup>[3–5]</sup> ii) might produce results that are questionable in their translation to humans due to interspecies differences in pharmaco-/toxico-kinetics and -dynamics,<sup>[6–10]</sup> best studied for the drug development process,<sup>[11–14]</sup> iii) are not designed for generating mechanistic understanding,<sup>[15,16]</sup> iv) do not cover the complexity of human diseases like immunotoxicity, developmental neurotoxicity, chronic neurological disorders, neuropsychological diseases, or endocrine disorders,<sup>[15]</sup> v) do not consider coexposures,<sup>[15]</sup> and vi) are ethically not in concordance with the 3R (replacement, reduction, and refinement of animal studies) principle.<sup>[5,17]</sup> Therefore, the new approach envisions a transformation from apical endpoint assessments in animals to mechanistically relevant studies that primarily rely on *in vitro* assays and computational (in silico) methods based on human biology, thereby circumventing species differences and increasing hazard prediction.<sup>[2,18,19]</sup> In particular, this strategy aims at i) covering a broad range of chemicals, chemical mixtures, endpoints, and life stages, ii) reducing the cost and increasing the throughput of testing, iii) using fewer animals and causing minimal suffering of the animals used, and iv) developing a robust scientific basis for assessing health effects of environmental agents.<sup>[2]</sup>

A promising tool for bridging between species or from health to disease are *in vitro* cell cultures and accordingly the field of *in vitro* toxicology has been emerging over the last decades. Mainly primary animal cells, tissue specimens, and immortalized

as well as tumor cell lines have been used. However, similar to Garbage In, Garbage Out in informatics,<sup>[20]</sup> data produced with *in vitro* test systems that do not contain high extrapolative power for physiology, might lead to unsatisfactory toxicity predictions.<sup>[21]</sup> For example, this might be the study of physiologic, tissue-specific cell proliferation in a tumor cell line.<sup>[22,23]</sup> Therefore, the emergence of stem cell systems in the early 21st century—as exemplified for the field of neurotoxicity<sup>[24–26]</sup>—was a big gain for *in vitro* science. Especially the development of the human-induced pluripotent stem cell (hiPSC) technology<sup>[27]</sup> was a significant milestone for many research areas including toxicology. Due to their pluripotent nature these reprogrammed cells provide an ethically innocuous, standardized and reproducible<sup>[28]</sup> human cell source with high similarity to blastocyst-derived human embryonic stem cells (hESCs).<sup>[29–31]</sup> Furthermore, hiPSCs and their differentiated progeny closely resemble their human *in vivo* counterparts in health and disease which is a prerequisite for successful translational research, with brain and liver providing examples.<sup>[32–35]</sup> However, since the ground-breaking publication of brain organoids by Lancaster et al. in 2013,<sup>[36]</sup> a variety of hiPSC-derived *in vitro* models have been taken to the next, 3D level by assembling organ-specific cell clusters containing secondary anatomical structures.<sup>[37–39]</sup> These are promising for application in basic research, disease modeling, drug development, personalized treatment, and regenerative medicine. However, they are also understood as promising tools for species-specific *in vitro* toxicological studies.<sup>[40]</sup>

This review will provide a state-of-the-art summary on advanced *in vitro* methods using stem cells for drug and chemical evaluation. Here, primary target organs, i.e., skin, lung, and intestine that come in direct contact with potentially hazardous substances, as well as secondary exposure organs, i.e., cardiovascular system, liver, kidney, thyroid gland, and brain are highlighted. Structural and/or functional units of each organ that are necessary for its function and thus need modeling for comprehensive toxicity assessment are depicted in respective figures. Benefits of overarching technologies like genome editing and “organ-on-a-chip (OOAC)” methods for toxicological applications are discussed and achievements and challenges in the field are pointed out.

## 2. Human Organ Structure and Functions and Their Modeling *In Vitro*

### 2.1. Skin

With  $\approx 2 \text{ m}^2$  and around 15% of total body mass, the skin is one of the largest organs of the human body.<sup>[41]</sup> Its multilayered architecture consists of epidermis, dermis, and hypodermis (subcutaneous fat) and combines crucial functions such as thermoregulation, energy storage, water homeostasis, removal of waste metabolites through sweat, and production of pigments protecting against sunlight.<sup>[42,43]</sup> In addition, the skin is capable of xenobiotic metabolism (reviewed by Oesch et al.<sup>[44]</sup>) and is one of the major endocrine sites of peripheral vitamin D synthesis.<sup>[45]</sup> The skin is also a sensory organ equipped with specialized sensory nerve endings for perception of touch, pain, heat, cold, acid, and pressure.<sup>[42]</sup> From a toxicological point of view, it is a primary target organ for toxicant exposure<sup>[46]</sup> since it

constitutes an important barrier to the outside environment,<sup>[47]</sup> protecting the body from penetrating pathogens and chemical exposure. The skin barrier is a complex interaction of different barrier compartments: i) the physical barrier consisting of the stratum corneum (SC) corneocytes, the cornified envelope, and the tight junctions of keratinocytes within the stratum granulosum (SG), ii) the chemical barrier formed by antimicrobial peptides, which are produced by keratinocytes, and to a lesser extent by immune cells, and protect against bacterial infections together with reactive oxygen species (ROS)-scavenging molecules secreted by keratinocytes, iii) the immunological barrier consisting of T-cells and Langerhans cells in the lower epidermal layers as well as pattern recognition receptors expressed and immunomodulatory factors secreted by keratinocytes in the SG, and iv) the microbial barrier formed by the commensal skin microbiome preventing infections by pathogenic microbes (Figure 1).<sup>[48]</sup> All these factors contributing to the barrier function of human skin together with the multitude of cell types involved (keratinocytes, melanocytes, fibroblasts, adipocytes, immune, and endothelial cells, not to mention the different sensory cells and skin appendages) make the reconstruction of human skin *in vitro* challenging, yet important for future toxicological testing of cosmetics and topical drugs as well as for hazard assessment of chemicals.

The development of human-based *in vitro* skin models for toxicological hazard assessment is probably more advanced compared to the other organs described in this review,<sup>[49,50]</sup> due to the ban of animal tests for cosmetic products by the European Union (EU) in 2004, followed by an *in vivo* test ban for cosmetic ingredients in 2013.<sup>[51]</sup> An exception is the current *in vitro* test battery for mutagenicity/genotoxicity consisting of i) a bacterial reverse mutation assay (Ames; TG 471),<sup>[52]</sup> ii) an *in vitro* mammalian cell gene mutation test (TG 476),<sup>[53]</sup> and iii) an *in vitro* micronucleus or *in vitro* mammalian chromosome aberration test (TG 473).<sup>[54]</sup> Due to its low specificity<sup>[55,56,57–65]</sup> this battery needs validated *in vitro* follow up tests which are currently not available.<sup>[66]</sup> Therefore, efforts are made to improve the specificity of the existing *in vitro* test battery<sup>[55,67–72]</sup> and to develop new *in vitro* assays.<sup>[71,73–75]</sup>

Those *in vitro* models accepted by the OECD include *ex vivo* human skin (TG 428),<sup>[76]</sup> an immortalized keratinocyte reporter cell line (TG 442D),<sup>[77]</sup> and a human monocytic leukemia cell line (TG 442E),<sup>[78]</sup> as well as reconstructed human epidermis (RhE) models (TG 431, 439).<sup>[79,80]</sup> So far four RhE models are accepted by the regulatory authorities for studies on skin irritation<sup>[79]</sup> and skin corrosion.<sup>[80]</sup> EpiSkin, EpiDerm, SkinEthic, and epiCS.<sup>[81]</sup> They consist of human primary epidermal keratinocytes which are cultured in cell culture inserts and then lifted to the air-liquid-interphase (ALI) to induce differentiation, epithelial stratification, and cornification. These RhEs then closely resemble a normal human epidermis with a basement membrane, proliferating keratinocytes, and an SC with an intact physical barrier function and xenobiotic metabolizing capacity similar to human skin,<sup>[46,82]</sup> thereby overcoming the limitations of classical cell monolayers<sup>[83]</sup> and making them suitable for topical applications of test compounds.<sup>[81]</sup> As a drawback, these models consisting of a single cell type (epidermal keratinocytes) resemble only the physical skin barrier and disregard other barrier components and cell types. A variety of full thickness skin models (FTM) exist, which are composed of

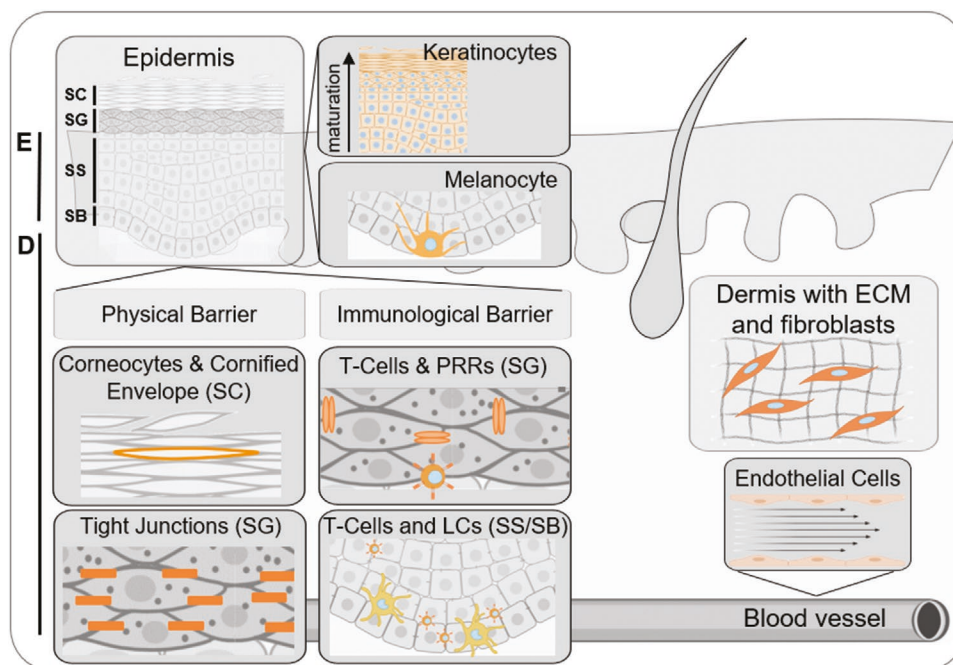


**Figure 1.** Schematic overview of important cell types and functional units of the skin. Abbreviations: E, epidermis; D, dermis; SC, stratum corneum; SG, stratum granulosum; SS, stratum spinosum; SB, stratum basale; PRR, pattern recognition receptors; LC, Langerhans cell; ECM, extracellular matrix. Figure created with BioRender.com.

an epidermal layer comparable to RhEs and a dermal layer of human dermal fibroblasts embedded in a collagen matrix.<sup>[50,84]</sup> Basic research studies investigated the inclusion of other cell types like melanocytes,<sup>[85]</sup> Langerhans cells,<sup>[86]</sup> or dendritic cells,<sup>[87]</sup> resulting in improved modeling of skin sensitization, while others included endothelial cells,<sup>[88–90]</sup> sweat glands,<sup>[91]</sup> or hair follicles.<sup>[92]</sup>

A key challenge in the development of more sophisticated skin *in vitro* models is to use a combination of cells that best mimic the *in vivo* responses.<sup>[46]</sup> Although human skin derived from plastic surgeries undisputedly is the best starting material for 3D skin models, the supply of material is limited and subjected to donor variation.<sup>[47,93]</sup> Human iPSCs provide a solution for overcoming the obstacle of restricted supply,<sup>[46]</sup> since hiPSC-derived RhE exhibits differentiation and barrier properties similar to *in vivo* epidermis.<sup>[94]</sup> Recently, the combination of hiPSC and 3D bioprinting technologies led to more physiological *in vitro* skin models, containing vasculature, appendages, pigment, innervation, and adipose tissue, which could be used for pharmaceutical screening (reviewed by Abaci et al.<sup>[95]</sup>). The group of Christiano<sup>[96–99]</sup> and others<sup>[100]</sup> reported on FTM build from hiPSC-derived fibroblasts, keratinocytes, and/or melanocytes containing a functional hiPSC-derived epidermal-melanin unit and hiPSC-derived keratinocytes participating in melanin uptake and transfer.<sup>[99]</sup> The same group incorporated functional hiPSC-derived endothelial cells into FTMs using a sacrificial layer of alginate microchannels in 3D-printed molds as basis for the dermal and epidermal compartment, which was dissolved by sodium citrate treatment followed by endothelial cell seeding. This system allows *in vitro* perfusion of skin vasculature and evaluation of endothelial barrier function, and therefore the study of systemic delivery

of therapeutics or toxicants, making it a promising model for future toxicological testing.<sup>[101]</sup> Interestingly, while hiPSC-derived dendritic cells are used for clinical applications and have the potential of large-scale production,<sup>[102,103]</sup> to date none of the developed hiPSC-based RhEs or FTMs have incorporated immune cells.<sup>[104,105]</sup> Recently, the generation of hESC-derived skin organoids was achieved by coinducing cranial epithelial cells and neural crest cells within a spherical cell aggregate. After long-time cultivation (4–5 month) this resulted in a cyst-like skin organoid composed of stratified epidermis, dermis, and pigmented hair follicles with sebaceous glands. Together with a network of sensory neurons and Schwann cells from nerve-like bundles that target Merkel cells in organoid hair follicles, the authors report that their model resembles facial skin of human fetuses in the second trimester of development, making it suitable to investigate cellular dynamics of developing human skin and its appendages,<sup>[106]</sup> but not relevant for toxicological testing in the near future due to its complexity and maturation status.

A known limitation of *in vitro* models for human skin is the altered barrier formation and resulting impaired functionality compared to native human skin (NHS).<sup>[48,107–109]</sup> One issue contributing to this is that these models, independent of their cell origin, are traditionally maintained at atmospheric oxygen levels of 160 mmHg (21%).<sup>[110]</sup> However, with  $\approx 26.6$  mmHg or 3.5% O<sub>2</sub><sup>[111]</sup> oxygen concentration *in vivo* (physioxia of the skin) is significantly lower, with oxygen levels increasing from apical to basal throughout different skin layers:  $\approx 8.5$  mmHg ( $\approx 1\%$ ) in the superficial region at 5–10  $\mu\text{m}$  depth,  $\approx 25$  mmHg ( $\approx 3\%$ ) in dermal papillae at 45–64  $\mu\text{m}$ , and  $\approx 37$  mmHg ( $\approx 5\%$ ) in the subpapillary plexus at 100–120  $\mu\text{m}$  skin depth.<sup>[112,113]</sup> Comparative studies of organotypic skin cultures under normoxia

(21% oxygen) and hypoxia/physioxia (1–3% oxygen) revealed that epidermal structure, SC barrier formation, and epidermal proliferation index better mimics NHS when models are cultured under hypoxic/physioxic conditions.<sup>[110,114]</sup>

With regard to skin models, the squamous oral epithelium and the superficial mucus layer of the oral mucosa play a special role. They are the first line of protection against toxicants derived from food, oral care products, and tobacco smoke.<sup>[115]</sup> Since mucositis and ulceration are frequent causes of toxicants,<sup>[116]</sup> chemicals are evaluated for acute (TG 420, 423, 425),<sup>[117–119]</sup> subacute (TG 407),<sup>[120]</sup> and subchronic (TG 408)<sup>[121]</sup> oral toxicity according to OECD guidelines in rodent animal studies.<sup>[122]</sup> Multiple *in vitro* 3D models of the human oral epithelium were designed as partial thickness oral mucosa or full-thickness oral mucosa (FTOM) models either from primary,<sup>[123–126]</sup> immortalized,<sup>[127]</sup> or malignant oral epithelial cells.<sup>[128]</sup> The majority of these models are grown in ALI-cultures to ensure partial stratification of the epithelial layer.<sup>[124,127]</sup> Incorporation of artificial lamina propria composed of collagen-embedded fibroblasts in the FTOM models promotes the differentiation of the epithelial layer, thus increasing the *in vivo* resemblance.<sup>[129]</sup> Although several models have been applied in toxicological studies evaluating oral consumers products,<sup>[123,124]</sup> dental composite resins,<sup>[128]</sup> or tobacco heating systems,<sup>[125]</sup> none of these approaches uses stem cell-derived cell sources, instead relying on primary cells and immortalized or malignant cell lines, the first representing a very restricted cell source and the latter two cells which do not resemble the physiology

of primary cells, respectively. Moreover, no medium- or high-throughput approaches were developed. Therefore, the *in vitro* oral mucosa models are far away from application in toxicological screening approaches.

While basic research is making huge progress in the development of hiPSC-based 3D skin models, it is yet a long way to a standardized toxicological application. Future efforts should focus on the development of standardized models with high tissue complexity and an adequate representation of the *in vivo* situation (e.g., by addition of immune cells). Moreover, testing throughput can be increased by the use of multiwell plates. Finally, such complex systems need validation for application in toxicology and disease modeling.<sup>[130]</sup>

## 2.2. Brain

The brain is the most complex organ of the human body, composed of billions of cells and subdivided in multiple regions each containing a specific cytoarchitecture necessary for its particular function. It is mainly composed of two superordinate cell types, neurons and glial cells. In the fully developed brain, neurons transmit information via electrical and chemical stimuli and, depending on the brain region, differ tremendously in size, morphology, neurotransmitters expression pattern, and overall function (Figure 2).<sup>[131]</sup> Although there is a certain amount of neurogenesis in adulthood due to residual neural progenitor cells (NPCs), e.g., in hippocampus,<sup>[132,133]</sup>

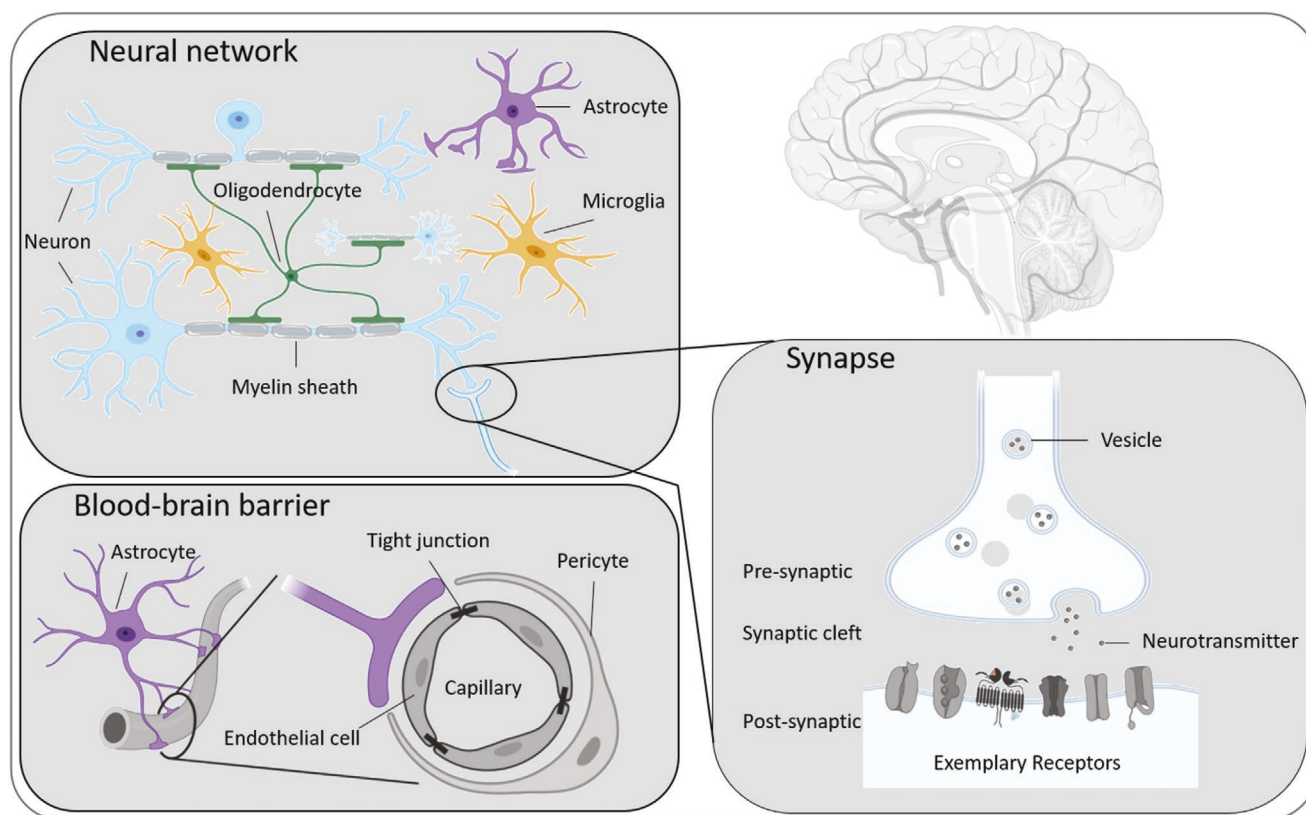


**Figure 2.** Schematic overview of important cell types and functional units of the brain. Figure created with BioRender.com.

neurons are terminally differentiated post-mitotic cells, which cannot divide to compensate for the neuronal loss after neurotoxic exposure.<sup>[134]</sup> Glia cells constitute about half of the cells within the developed central nervous system (CNS)<sup>[135]</sup> and can be divided into oligodendrocytes, astrocytes, microglia, and ependymal cells. Oligodendrocytes facilitate rapid saltatory conduction by insulating neuronal axons with myelin sheaths to guarantee adequate motor, sensory, and cognitive function.<sup>[136]</sup> Astrocytes exhibit a variety of morphological and physiological properties reflecting their diverse functions in the CNS: They i) regulate synaptogenesis and synaptic transmission, ii) provide neurons with nutrients and neurotransmitters, iii) maintain the blood-brain barrier (BBB), iv) build scar tissue in case of injury, and v) form structural scaffolds.<sup>[137]</sup> Microglia are the resident immune cells of the brain which orchestrate the inflammatory response and guide neuronal expansion and maturation.<sup>[138]</sup> The brain is protected from most environmental chemicals by the BBB and the blood-cerebrospinal fluid barrier. Although both provide highly selective permeability, several substances can penetrate or disrupt the barrier structures to eventually reach the brain (Figure 2).<sup>[139]</sup>

Due to the brain's complexity, neurotoxicity summarizes various modes-of-action (MoA) including i) neuronal injury or death (neuronopathies), ii) axon degeneration and secondary myelin degeneration (axonopathies), iii) separation of myelin sheets or selective myelin loss (myelinopathies), iv) altered astrocyte function (astrocyte neurotoxicity), v) disturbance of intercellular communication (neurotransmission-associated neurotoxicity) as well as vi) changes in cognitive function, level of consciousness and vigilance (toxic encephalopathy) including compromised adult neurogenesis.<sup>[140]</sup> According to the OECD guidelines, neurotoxicity testing is performed in rodent animal studies, however species differences between rodent and human brains including astrocyte morphology,<sup>[141]</sup> neuronal subtype ratios,<sup>[142]</sup> and receptor affinities<sup>[143–145]</sup> questions the predictivity of rodent models for human health. Therefore, the development of *in vitro* assays based on hiPSC or NPCs has led to promising alternative approaches.

Zhang et al. first described the differentiation of hESCs into a mixed culture of neurons, astrocytes, and oligodendrocytes.<sup>[146]</sup> Moreover, targeted differentiation of hESCs and hiPSCs into neuronal subtypes including dopaminergic neurons, spinal motoneurons, and electrically active glutamatergic and GABAergic neurons can be either performed directly<sup>[147–151]</sup> or following neural induction into NPCs.<sup>[152–154]</sup> Of note, direct comparison of the neural-differentiation capacity of hiPSCs and hESCs revealed that both cell types produce neuronal cell types over the same developmental time course, however, hiPSCs exhibited a reduced differentiation potency and increased variability.<sup>[155]</sup> Several 2D *in vitro* models based on neurally induced human pluripotent SCs<sup>[156–160]</sup> or primary hNPCs<sup>[144,161–163]</sup> have been used in neurotoxicity testing, predominantly in a developmental context focusing on i) neural progenitor proliferation, ii) neuronal differentiation, outgrowth, and network formation, iii) oligodendrocyte differentiation and maturation, iv) ROS accumulation, and v) epigenetic and transcriptional reprogramming. However, in a multiparametric high content approach, 36 chemicals were analyzed according to their potential to

induce acute neurotoxicity in hESC-derived neurons with cell viability, cytotoxicity, neurite length, and mitochondrial area as readouts.<sup>[164]</sup>

Since cerebral 2D cultures cannot depict the complex *in vivo* cytoarchitecture of the brain, self-assembling 3D multicellular brain organoids emerged as an alternative especially in developmental research.<sup>[36,165,166]</sup> Several approaches successfully generated brain-region-specific organoids recapitulating the specific cytoarchitecture, epigenome, and transcriptome of the fore-brain, midbrain or hypothalamus.<sup>[167–169]</sup> Fusions of different region-specific organoids demonstrated interneuron migration between fused parts, highlighting their applicability to model complex interactions between brain regions *in vitro*.<sup>[170]</sup> To study the inflammatory response and increase the physiological relevance, functional, cytokine-secreting microglia have been cultured as immortalized cell lines or differentiated from hPSCs and incorporated into cerebral organoids.<sup>[171–173]</sup> Since their early developmental stage limits the applicability of organoids for nondevelopmental testing, efforts have been made to increase the maturity, thereby generating stem cell-derived organoids including dendritic spines, active neuronal networks, mature oligodendrocytes, and myelinated axons.<sup>[174–177]</sup> Another limitation for toxicity testing using organoids is their high variability.<sup>[178]</sup> A compromise for staying in 3D yet with reduced variability are brain spheres, multicellular 3D brain aggregates that can be derived from ESCs or hiPSC, but lack higher anatomical structures.<sup>[171,176,179–181]</sup> Such brain spheres have already been used for toxicity evaluation and proved useful to identify neurotoxicants causing mitochondrial dysfunction, ROS accumulation, and metabolic disruption.<sup>[180–182]</sup> Moreover, Sandström et al. tested the effect of non-neurotoxic and neurotoxic compounds in hESC-derived brain spheres exhibiting myelinated axons and functional neuronal networks and confirmed their usefulness for *in vitro* neurotoxicity testing.<sup>[183]</sup> Schwartz et al. showed that self-assembled hESC-derived neural constructs composed of multiple neuronal and glial cell types, microglia, and interconnected vascular networks respond to toxic compounds as measured by RNA sequencing and confirmed in a cross-validation experiment that machine learning techniques can be used to correctly predict chemical effects. However, chemical effects on viability or cytotoxicity were not assessed.<sup>[184]</sup>

Since the BBB is crucial for neuroprotection, lack of blood vessels is one of the major shortcomings of most *in vitro* models. Implementing such an interorgan crosstalk was realized by incorporating vasculature to cerebral organoids. This was achieved by either adding ETV2 variant 2 (ETV2)-expressing hESCs during organoid formation or by re-embedding organoids in Matrigel droplets containing hiPSC-derived endothelial cells.<sup>[185,186]</sup> Of note, vasculature-like structures enhanced organoid maturity and induced BBB-like characteristics.<sup>[185]</sup> Moreover, several functional BBB models have been developed as spheroids<sup>[187,188]</sup> or in microfluidics devices.<sup>[189–191]</sup> Since they show comparable permeabilities to *in vivo* measurements, promising candidates for drug-permeability screenings and neurotoxicity testing have been identified. However, these BBB models not only consist of stem cell-derived cells, but also contain human and rodent primary cells as well as immortalized cell lines.

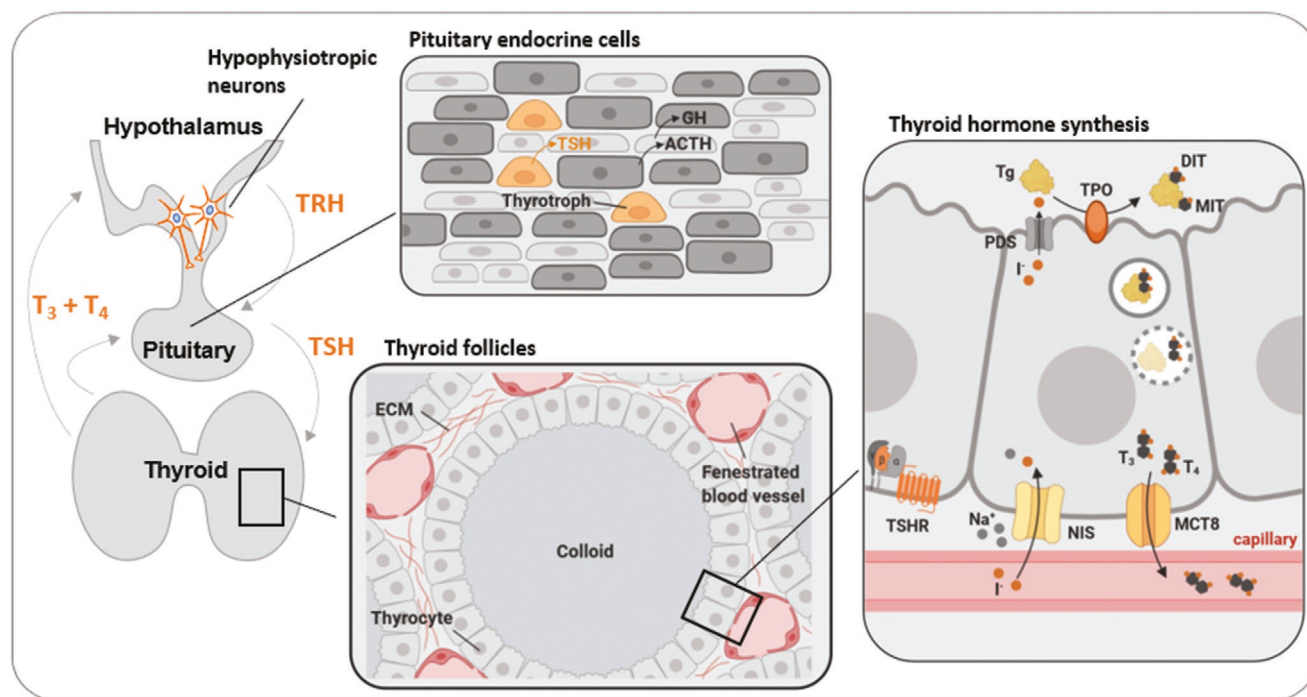


**Figure 3.** Cell types and functional units of the HPT axis necessary for TH production. Abbreviations: ACTH, adrenocorticotropic hormone; DIT, diiodotyrosine; ECM, extracellular matrix; GH, growth hormone; MCT8, monocarboxylate transporter 8; MIT, monoiodotyrosines; NIS, sodium-iodide symporter; PDS, pendrin; T<sub>3</sub>, triiodothyronine; T<sub>4</sub>, thyroxine; Tg, thyroglobulin; TPO, thyroperoxidase; TRH, thyrotropin-releasing hormone; TSH, thyroid-stimulating hormone/thyrotropin; TSHR, thyroid-stimulating hormone receptor. Figure created with BioRender.com.

Vascularization would not only increase the resemblance to the native *in vivo* situation, but further eliminate the gradient of nutrients and oxygen from the outer spherical shell to the spheroid core. This gradient results in zonation of the spheroid, the formation of a hypoxic core, and an uneven distribution of the test substance.<sup>[192,193]</sup>

Cultures of different hiPSC-derived neuronal subtypes, astrocytes and microglia (iCell, Cellular Dynamics; CNS.4U, Ncardia; SynFire, ReproCELL) as well as multicellular brain organoids (microBrain 3D, StemoniX) are commercially available and already applied in neurotoxicity testing in high-throughput, high-content approaches in 384 multiwell plates.<sup>[179,194]</sup> Moreover, comparative electrophysiological analysis and neurotoxic exposure of neuronal models revealed differences in sensitivity and the degree of chemical-induced effects, but the models performed reproducibly and even outperformed primary rat cortical neurons in terms of sensitivity to detect seizurogenicity.<sup>[195]</sup>

### 2.3. Thyroid System

The thyroid system is a neuroendocrine axis which regulates the production of the thyroid hormones (THs) thyroxine (T<sub>4</sub>), and triiodothyronine (T<sub>3</sub>). THs control a variety of physiological processes including energy metabolism,<sup>[196]</sup> nervous system development,<sup>[197]</sup> and thermoregulation,<sup>[198]</sup> and are particularly important during perinatal development. Thyroid function is regulated by a fine-tuned interplay between the hypothalamus, the pituitary gland, and the thyroid (HPT axis) and is initiated by the secretion of thyrotropin-releasing hormone (TRH)

from hypophysiotropic neurons within the hypothalamus (Figure 3). TRH enters the pituitary portal circulation and binds to receptors on the plasma membrane of thyrotropes within the anterior pituitary.<sup>[199]</sup> Binding causes the acute release of thyroid-stimulating hormone (TSH) from secretory granules, an essential regulator of thyroid function, differentiation, and growth.<sup>[200]</sup> The thyroid's task is the production of THs, which involves uptake of iodide and its utilization during TH synthesis. Iodide absorption from the plasma is mediated by the sodium-iodide symporter (NIS) located within the basal membrane of polarized follicular thyrocytes.<sup>[201]</sup> Thyrocyte follicles are vascularized spherical secretory units filled with a protein-rich substance called the colloid. Within the colloid, iodide is oxidized and bound to tyrosine residues of the colloid-protein thyroglobulin (Tg) in an organification reaction catalyzed by the enzyme thyroperoxidase (TPO) generating both monoiodotyrosines (MIT) and diiodotyrosines (DIT) within the Tg protein. Subsequent coupling of two neighboring DIT molecules generates T<sub>4</sub> whereas the coupling of one MIT and one DIT molecule yields T<sub>3</sub>.<sup>[202,203]</sup> Endocytosis of Tg and lysosomal proteolysis releases T<sub>4</sub> and T<sub>3</sub> from Tg and the transporter MCT8 within the basolateral membrane releases the THs into the circulation.<sup>[204]</sup> The amount of TSH secreted by the anterior pituitary substantially determines the TH production rate since TSH receptor (TSHR) activation positively regulates iodide uptake by NIS, Tg expression, and TH synthesis. Moreover, THs exert a negative feedback on the secretion of TSH and TRH by the pituitary and hypothalamus, respectively (Figure 3).<sup>[200]</sup>

Environmental chemicals deregulate the thyroid system by various routes of interference (e.g., TH synthesis, metabolism,

transport, elimination, or TH receptor activation).<sup>[205]</sup> However, the ability to influence circulating levels of TH or TSH in vivo is the only readout used to identify thyroid disruptors in toxicity testing. TH levels are mandatorily assessed in OECD in vivo toxicity guideline studies (i.e., TG 408, 414, 421, 422, and 443),<sup>[121,206–209]</sup> however, they do not provide information about the mechanism of TH disruption complicating the extrapolation of study results across species. Moreover, high costs, ethical concerns, and the low-throughput of animal-based assays in contrast to the numerous chemicals which need to be tested have driven efforts to develop and validate in vitro assays based on key molecular initiating events (MIEs) in thyroid disruption.<sup>[198,210–212]</sup> To facilitate their regulatory application, a thyroid-related adverse outcome pathway (AOP) network has been established linking the MIEs to toxicity-mediated thyroid dysgenesis and downstream adverse outcomes.<sup>[213]</sup> Several high-throughput screening (HTS) assays have been developed,<sup>[198]</sup> however, the uncertainty of these assays to predict functional effects on the tissue-level questions their physiological relevance and elucidates the need for organotypic cell culture models. The use of a tiered screening approach in which positive hits from HTS assays (Tier 1) are further verified in organotypic medium-throughput models (Tier 2) as a preselection for final Tier 3 in vivo testing significantly reduces costs, the testing throughput and guarantees the predictivity of the risk assessment.<sup>[198,214]</sup> Since the HPT axis comprises several organs, the establishment of a single organotypic Tier 2 model is insufficient. By contrast, models depicting interim steps within the thyroid system including TRH and TSH secretion, iodide uptake, and TH production are needed.

Already in the 1980s, thyroid tissue was reconstructed in collagen gels from primary human thyrocytes.<sup>[215,216]</sup> The cells formed follicles secreting Tg into the colloid in response to TSH stimulation. Moreover, they proved functional in vitro concentration-dependently responding to TSH exposure with iodide uptake and T<sub>3</sub> secretion. Exposure to the TPO inhibitor methimazole further confirmed response to chemical interference.<sup>[216]</sup> Studies on thyroid models derived from primary mouse thyrocytes further confirmed in vivo functionality and yielded follicles capable of TSH-dependent iodide uptake and TH secretion after transplantation into hypothyroid mice.<sup>[217,218]</sup> In order to increase the applicability for toxicological screenings, Deisenroth et al. developed a medium-throughput organotypic screening assay in a 96-well plate format.<sup>[219]</sup> Functional follicular structures expressing genes of mature thyrocytes (NIS, TPO, TSHR, Tg), capable of iodide uptake and TH production, were derived from human thyrocyte tissue. Of note, screening of reference compounds identified in established HTS assays for thyroid disruption (i.e., NIS and TPO enzyme activity) revealed both similar effects and potencies in the microtissue model, highly indicating its applicability for a tiered screening approach. However, the use of primary thyrocytes for toxicological testing is challenging. Their low turnover rate (five renewals per lifetime) and general impurities in primary cultures limit their application in a regulatory context.<sup>[220]</sup> Therefore, the development of 3D models based on ESCs or iPSCs is more promising. Two different approaches successfully generated functional thyroid follicles from ESCs and iPSCs in 3D Matrigel cultures: i) the enrichment of cells

expressing the transcription factors Pax6 and Nkx2.1 by genetic modification or FACS sorting and ii) the induction of anterior foregut endoderm (AFE) by treatment with Activin A, Noggin, SB431542 followed by cultivation in thyroid differentiation medium supplemented with insulin, IGF-1, FGF2, FGF10, and bone-morphogenic 4 (BMP4). Both protocols generated follicular thyroid tissue expressing NIS, TSHR, and TPO from human and mouse ESCs<sup>[221–224]</sup> and iPSCs.<sup>[223,225,226]</sup> The follicles increased iodide uptake upon TSH stimulation and secreted Tg into the colloid. Furthermore, TH production was observed both in vitro<sup>[223–225]</sup> and in vivo<sup>[222,223]</sup> after transplantation into hypothyroid mice. Direct comparison of 2D and 3D cultivation approaches revealed increased expression of TSHR, TPO, and Tg in 3D cultures. Moreover, NIS expression and TH secretion was completely limited to Matrigel-embedded follicular 3D cultures, highlighting the increased functionality of organoid compared to monolayer models.<sup>[219]</sup> The stem cell-based thyroid models seem promising in identifying chemical interference with iodide uptake, Tg production, and TH synthesis and thus represent interesting candidates for application in tiered approaches in toxicity testing. Bioprinting of primary thyroid and allantoic spheroids as sources of thyroid and endothelial cells, respectively, resulted in follicles containing microvascular networks which proved functional in vivo after grafting into mice. Since folliculogenesis is guided by angiogenesis and iodide is taken up from the bloodstream, vascularization could increase the functionality of the thyroid 3D model and the technique could be adapted to stem cell-derived thyroid and endothelial cells.<sup>[217]</sup> Additional optimization of the culture parameters could further promote the differentiation into thyroid tissues, since hypoxia (2% O<sub>2</sub>) was reported to increase the expression of thyroid transcription factors (Pax8 and Nkx2.1), the expression of NIS and TSHR, and the uptake of iodide.<sup>[227]</sup>

Fewer efforts have been directed at developing 3D models for the initiating steps of the HPT axis within the hypothalamus and the pituitary. However, coinduction of hypothalamic and oral ectoderm from ESCs<sup>[228,229]</sup> and hiPSCs<sup>[230]</sup> facilitated the formation of 3D organoids with different hormone-producing pituitary cells adjacent to functional hypothalamic tissue. The protocol is based on the formation of large cell aggregates in suspension culture and the concurrent activation of BMP4 and sonic hedgehog signaling pathways. Of note, interactions between the two juxtaposed tissues were critical for the development of hormone-producing pituitary cells, elucidating the importance of the hypothalamus for pituitary maturation.<sup>[228]</sup> Although the model gave rise to high amounts of adrenocorticotrophic hormone (ACTH)- and growth hormone (GH)-producing pituitary cells both in vitro and after transplantation into hypopituitary mice in vivo, only few TSH-producing thyrotropes were observed. Therefore, additional optimization of the protocol is needed to make it suitable for the screening of chemicals interfering with TSH synthesis and secretion.

#### 2.4. Lung

The respiratory tract is one of the principle barrier organs of the human body. Its main function is to facilitate the exchange of oxygen and carbon dioxide between the air and the blood. An

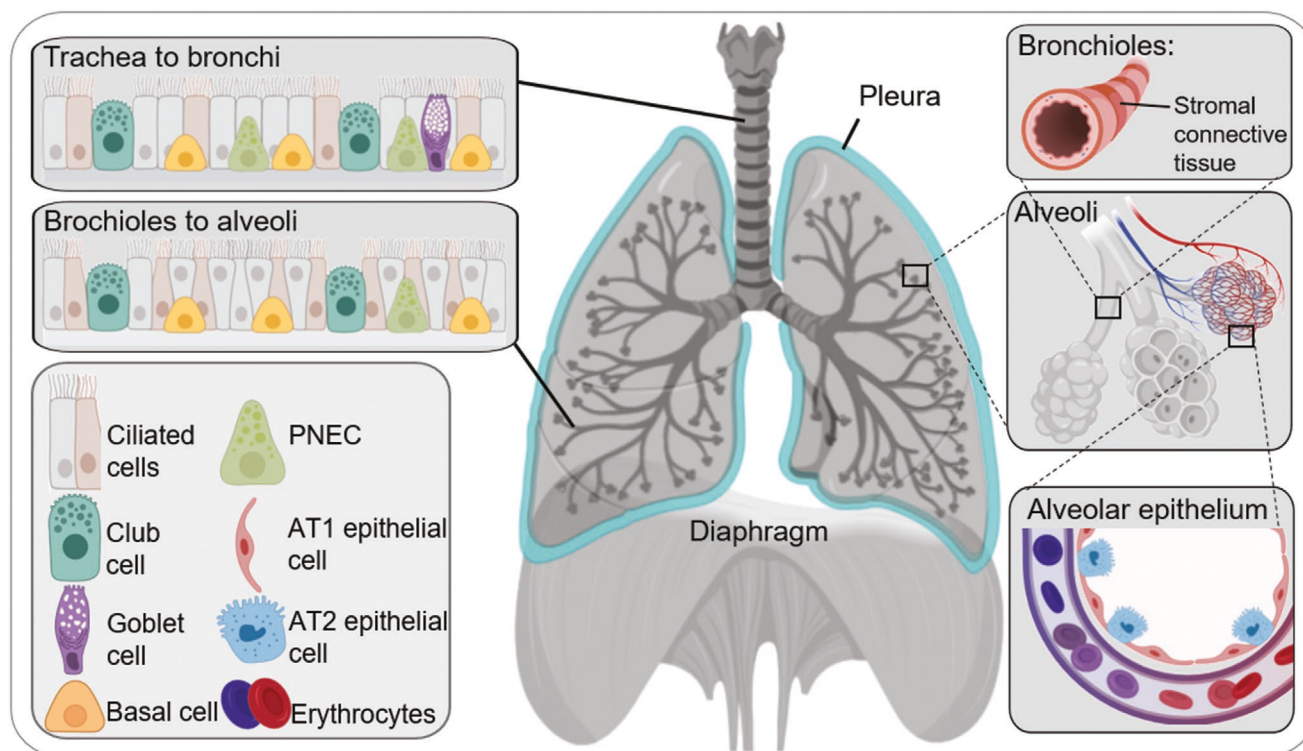


**Figure 4.** Schematic overview of important cell types and functional units of the respiratory tract. Abbreviations: PNEC, pulmonary neuroendocrine cell; AT, alveolar type. Figure created with BioRender.com.

adult human inhales  $\approx 15$  to  $20 \text{ m}^3$  of air per day and as such the lung epithelium, with an estimated surface area of  $30\text{--}130 \text{ m}^2$ ,<sup>[231,232]</sup> can be directly exposed to gaseous and particulate contaminants of chemical and biological origin. Apart from being a target for occupational and environmental airborne toxicants, the respiratory tract represents a dominant uptake route for noxious agents affecting other organs. In turn, the lung can be affected by toxicants that reach this organ via other uptake pathways. Considering the multitude of resident cell types (over 40),<sup>[233]</sup> architectural and physiological particularities in terms of airflow dynamics, and stretch as well as shear stress effects (Figure 4), the development of robust and realistic *in vitro* models to replace *in vivo* inhalation studies is a major challenge. Risk assessment of inhalable toxicants traditionally relies on the in-depth (histo-)pathological and clinical/biochemical investigation of experimental animals, predominantly rodents, following acute or long-term repeated inhalation exposures.<sup>[234]</sup> Such studies often include analysis of further endpoints, such as inflammation (by bronchoalveolar lavage), genotoxicity, or even lung function.<sup>[235]</sup> Inhalation studies are laborious, expensive, and complex, not only regarding the evaluation of effects, but also in view of the requirements for the controlled, reproducible, and safe generation and monitoring of the exposure cloud.<sup>[236]</sup>

*In vitro* methods have been used since long in inhalation toxicology research and major developments in the last decades yielded innovative approaches that aim for high throughput analysis and models that better mimic specific aspects of the complex anatomy and physiology of the human respiratory tract. Model developments have mostly focused on the selection

of epithelial cells as they represent the first target for inhaled toxicants.<sup>[237]</sup> Anatomically and functionally, the respiratory tract can be subdivided into two principle regions. i) The conducting airways are represented by mucus producing goblet cells, ciliated cells, club cells, and neuroendocrine cells as well as basal cells, the progenitor cells for the airway epithelium.<sup>[238–240]</sup> ii) The epithelium of the alveolar region, where the gas exchange takes place, is composed of alveolar type I epithelial (AT1) cells and type II (AT2) cells. The surfactant producing AT2 cells serve as progenitors to replace damaged alveolar epithelial cells.<sup>[238,241]</sup> When designing or selecting the type(s) of epithelial cells for an *in vitro* model the target site specificity of a toxicant must be taken into account. Its airborne concentration and its physicochemical properties (e.g., water-solubility and reactivity of gases, aerodynamic size and shape of particles) as well as host factors (e.g., breathing pattern, activity) determine the predominant region of interaction.<sup>[242–244]</sup>

For decades, *in vitro* studies addressing effects on epithelial cells have used primary cells, explant cultures or immortalized cell lines from (fetal) lungs of rodents or human origin.<sup>[245–248]</sup> The adenocarcinoma cell line A549 represents by far the most investigated human AT2-like epithelial cell model.<sup>[249]</sup> Effects on AT1 cells can be modeled by the immortalized human alveolar type-I-like epithelial cell line TT1.<sup>[250]</sup> Novel methods have been developed in recent years to improve the collection of human primary bronchial epithelial cells, e.g., to investigate disease susceptibility.<sup>[251,252]</sup>

Besides epithelial cells, various other cell types of the lung have been used, or included in coculture with epithelial cells, for *in vitro* inhalation toxicology research purposes. This

includes mesenchymal cells to study fibrosis hazards and mechanisms,<sup>[253,254]</sup> primary alveolar macrophages obtained from experimental animals or humans by lung lavage to study host defense and particle clearance,<sup>[255–258]</sup> monocytes/macrophages, neutrophils, dendritic cells, and mast cells to simulate lung inflammation processes,<sup>[259–261]</sup> and pleural cells to study mechanisms and hazards of pleural disease and malignant pleural mesothelioma.<sup>[262–265]</sup> Vascular and capillary endothelial cells have been introduced in coculture models together with lung epithelial cells to explore epithelial–endothelial crosstalk mechanisms, airway or alveolar barrier impairments and systemic uptake of inhaled chemicals and particles.<sup>[266–268]</sup>

Specific model developments for lung research have focused on the recreation of physiological aspects of this organ. Herein, major milestones have been achieved through the ongoing development of ALI systems, using monocultures,<sup>[269,270]</sup> multiple cell types,<sup>[260,271]</sup> or commercially available human lung tissue.<sup>[272]</sup> ALI approaches allow for the controlled testing of gases, particles or their mixtures in immediate contact with epithelial cells, unlike models in which cells are submerged in (testing) medium. Combined with advanced exposure systems ALI cultures enable *in vitro* testing scenarios that better mimic inhalation exposure. This is particularly the case for inhalable particles in terms of their complex kinetics of particle deposition and initial interaction with the epithelial lining fluid. Mechanical stretch models mimicking breathing movements have been introduced to study its role in lung development,<sup>[273]</sup> repair of damaged lung epithelium,<sup>[274]</sup> and possible modulation of toxicant effects.<sup>[275]</sup> Sophisticated human lung-on-a-chip models have been developed using microfluidic devices that mimic both architectural and physiological aspects of the alveolar-capillary region, by combining breathing–mimicking mechanical strain with respective air and blood-flow characteristics in epithelial and endothelial compartments.<sup>[276]</sup>

Stem-cell based technologies brought major innovations into lung research. The developments and methodological advancements of stem cell-based tissue engineering focused on elaboration of mechanisms of lung development, damage repair, regeneration, and the pathogenesis of lung diseases.<sup>[277,278]</sup> Principal approaches to generate mature adult lung cells from ESCs or iPSCs include coculture approaches with mesenchymal cells or successive treatment and selection protocols that mimic lung development. Early developments include the generation of AT2 and club cells from murine ESCs. When cultivated under ALI conditions, these ESCs can grow into a differentiated airway epithelium comprising basal, ciliated, intermediate, and club cells.<sup>[279]</sup> Lung progenitor cells can also be derived from the circulation<sup>[280]</sup> and used to generate AT2-like cells from CD34<sup>(+)</sup> cells.<sup>[281]</sup> Major progress in the field was achieved with the generation of human epithelial cells from AFE-derived from hESC and hiPSC, whereby caudal region of the AFE gives rise to the tracheal and lung.<sup>[282]</sup> Along these lines, bronchial and alveolar progenitors can be derived for the generation of both airway and alveolar epithelial cells from iPSCs.<sup>[283,284]</sup> Of note, hypoxia of 1% O<sub>2</sub> enhanced both the spontaneous and activin A-dependent formation of definitive endoderm from mouse ESCs and the subsequent differentiation into AT2 and club cells in a hypoxia-inducible factor 1 alpha (HIF1 $\alpha$ )-dependent manner. This indicates, that a careful timing of hypoxia may

increase the efficiency of *in vitro* differentiation processes into the lung lineage.<sup>[285]</sup> Scaffold-based methods have been used to generate alveolar-like structures, characterized by AT1 and AT2-like epithelial cells from murine lung stem/progenitor cells using 3D-gelatin microbubbles.<sup>[286]</sup> Also human alveolar organoids, composed of a pool of self-renewable AT2-like cells and AT1-like cells have been successfully created from hiPSCs.<sup>[287]</sup> These and various further protocols to develop lung organoids and AT2 cells from hiPSCs are nowadays at hand, offering great potential for *in vitro* inhalation toxicology testing.<sup>[288–290]</sup> However, also concern has been expressed especially regarding the generation of mature, differentiated AT2 cells.<sup>[291]</sup> Chen et al. described the construction of lung bud organoids from hPSCs containing pulmonary endoderm and mesoderm which, following xenotransplantation or in Matrigel 3D cultures, develop into branching airway and alveolar like structures.<sup>[292]</sup> They also showed the potential of their model to study molecular and morphological hallmarks of diseases, like fibrosis. In combination with gene editing approaches innovative lung organoid developments are envisaged to benefit research on susceptibility toward idiopathic or toxicant-induced lung diseases.<sup>[293,294]</sup>

In the future, stem cell-based technologies in combination with the latest developments in tools that reliably mimic the specific physiology of the respiratory tract are anticipated to bring major advancements to the field. However, the complexity of the respiratory tract needs to be critically considered here. Promising advancements can be achieved by combining stem-cell and lung-on-a-chip approaches (reviewed by Nawroth et al.<sup>[295]</sup>). However, the authors also promote the inclusion of lung physiology aspects in such models, especially concerning toxicological or drug safety testing. Moreover, while elegant systems are available for controlled exposure of epithelial cells or tissues at the ALI interface,<sup>[296]</sup> they do not yet allow for a straightforward incorporation of complex (scaffold-based) lung organoid models. Toxicological hazard assessment analysis calls for reliable, robust, and reproducible models to generate valid concentration-response data. And it is precisely this dosimetry aspect that fuels the complexity of inhalation toxicology research, on gases, vapors, and especially particles.

## 2.5. Cardiovascular System

Together with the circulatory system the heart orchestrates an unidirectional continuous blood flow to provide all organs with oxygen, nutrients, and hormones.<sup>[297]</sup> It is composed of four chambers that are divided into two blood receiving atria and two pumping ventricles. The ability to beat requires a thick wall robust enough to withstand the continuous movement and the associated shear forces. The inner wall of the heart is lined with the endocardium, followed by the thick myocardium containing cardiomyocytes (CMs) embedded in extracellular matrix and the electrical conduction system composed of specialized muscle fibers capable of signal conduction. The outer epicardium consists of elastic fibers, which protect the heart and reduce friction (**Figure 5**; reviewed by Bauer<sup>[298]</sup>). The complex structure of the heart with its multiple cell types, the permanent blood flow, the shear forces caused by the contraction, and the electrical stimulation are all factors complicating

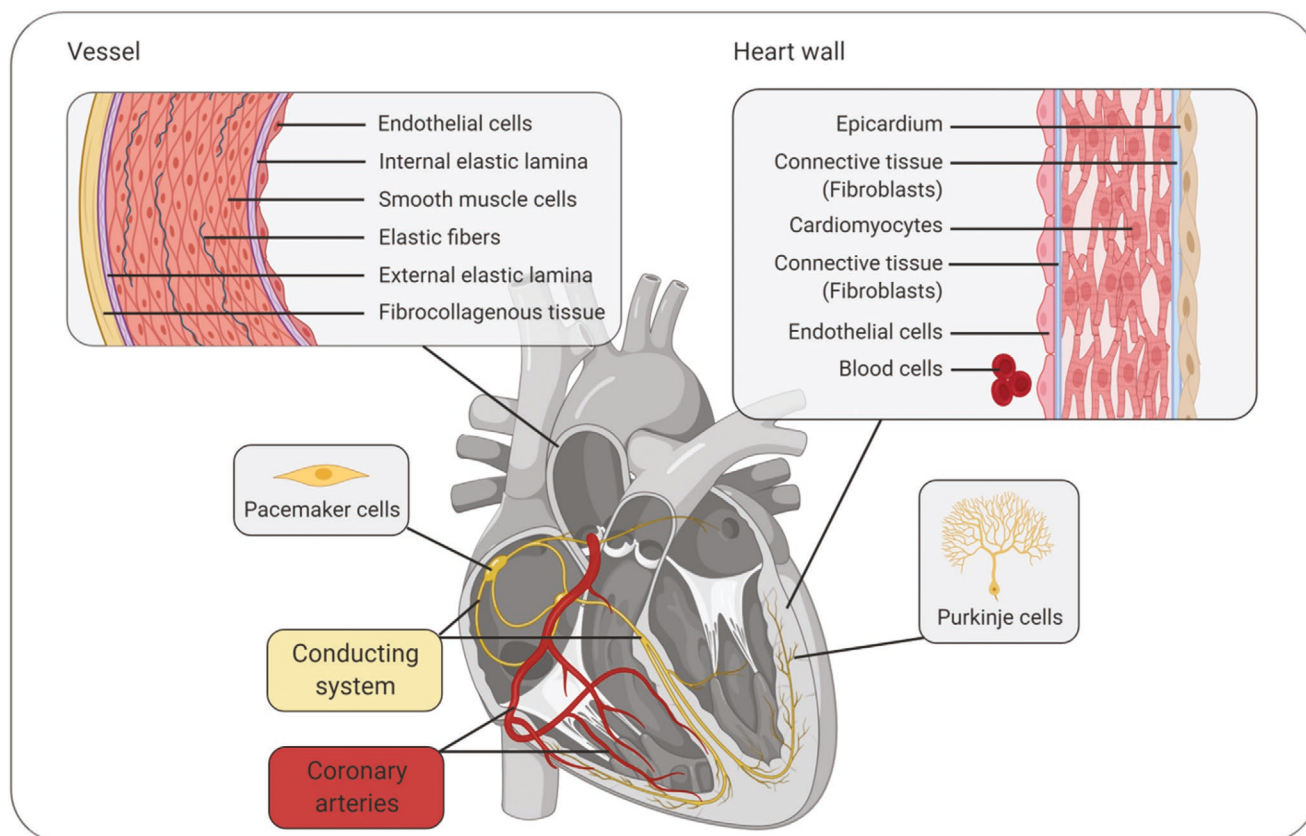


**Figure 5.** Schematic overview of important cell types, tissues and functional units of the heart. Figure created with BioRender.com.

the development of predictive *in vitro* systems for cardiotoxicity testing. Nevertheless, cardiotoxicity is the most crucial adverse event in drug development, making cardiovascular safety issues the number one reason why drug candidates fail in preclinical trials or have to be withdrawn from the market.<sup>[299]</sup> Therefore, arrhythmia, altered QT intervals, channelopathies in general, decreased cell viability, and structural cell damage are possible heart-related effects of substances which have to be ruled out prior to drug release.

Typically, first line drug testing includes the hERG *in vitro* assay detecting inhibitors of potassium channels essential for the repolarization phase of action potentials.<sup>[300]</sup> The human ether-a-go-go related gene (hERG) encodes for a channel subunit whose blockage results in QT interval prolongation potentially followed by Torsade de Pointe (TdP), a drug-induced lethal arrhythmia.<sup>[301]</sup> The QT interval represents the time from the Q wave (first depolarization of the ventricles) to the T wave (total repolarization) and abnormalities in interval lengths are associated with tremendous adverse effects making QT prolongation one of the most common reasons for drug withdrawal.<sup>[302,303]</sup> The classic hERG assay utilizes patch clamp recording in immortalized human embryonic kidney (HEK) 293 cells heterologously expressing hERG channels.<sup>[301]</sup> This setup in noncardiac cells exhibits limited predictive power and thus is inferior to novel approaches with hiPSC-derived CM cultures.<sup>[300]</sup> In addition to the hERG assay, the proarrhythmic potential of chemicals is further tested in nonclinical *in vivo* animal studies according to ICH S7B and E14 guidelines.<sup>[304,305]</sup> However, species

differences, especially in terms of ion channel expression and phenotypic causes of channel inhibition, question the predictivity of rodent experiments for human health.<sup>[297,306]</sup>

Stem cell research revolutionized the development of alternative *in vitro* methods for cardiotoxicity testing, generating spontaneously contracting CMs from pluripotent stem cells which express most of the ion channels and sarcomeric proteins found *in vivo*. For the induction of functional CMs from hESCs or hiPSCs, numerous 2D and 3D culture protocols exist which slightly differ in factors like cell source, culture media, days of preculture, and days of toxicant exposure.<sup>[307–309]</sup> The *in vitro* cardiotoxicity assessment can be divided according to the functional readout into models evaluating electrophysiology, cardiac cellular contractility, and cytotoxicity. Electrophysiological cardiotoxicity is either measured by i) microelectrode arrays (MEAs),<sup>[310,311]</sup> ii) by patch clamp techniques which are extremely sensitive but exhibit reduced throughput<sup>[312]</sup> or iii) by optical imaging of voltage sensitive dyes.<sup>[313]</sup> In order to implement a next-generation, mechanism-based standard for preclinical risk assessment of proarrhythmic chemicals, the comprehensive *in vitro* proarrhythmia assay initiative combines *in vitro* assays with *in silico* reconstructions of cardiac electrophysiological activity, thereby encouraging a paradigm change in cardiotoxicity testing beyond the hERG assay to better understand and predict TdP risk.<sup>[314,315]</sup> As part of that ongoing movement, drugs linked to low, intermediate, and high TdP risk are tested with respect to their proarrhythmic potential in hiPSC-CMs using MEAs or voltage-sensing optical approaches.

Besides proarrhythmic effects, the impact on cardiac cellular contractility is a key element of cardiotoxicity risk assessment, therefore, altered contractility of CMs is addressed in several *in vitro* assays. Since the direct measurement of the force component of contractility in cell culture is technically challenging, indirect readouts like sarcomere shortening, Ca<sup>2+</sup> flux or mitochondrial membrane potential changes are used.<sup>[316,317]</sup> Moreover, hiPSC-derived CMs are responsive to inotropic drugs like norepinephrine and their beating frequency can be modulated via electrical stimulation.<sup>[318]</sup> Sharma et al. recently established the cardiac safety index (CSI) as a measure to evaluate cardiotoxic chemicals in a HTS format in 384 multiwells.<sup>[319]</sup> The CSI is based on several *in vitro* readouts for measuring chemical effects on contractility and cytotoxicity in hiPSC-derived CMs.

Although CM-based models are functional and widely applied in cardiotoxicity testing, the impact of multiple cardiac cell types like fibroblasts, epithelial cells (epicardium), and endothelial cells (endocardium) on cardiotoxicity is neglected. Kurokawa et al. showed that the cardiotoxic effects of the ErbB2 (HER2) inhibitor Trastuzumab can only be recapitulated *in vitro* within a coculture model of hiPSC-CMs and endothelial cells, highlighting the relevance of organotypic, preferably 3D models containing multiple cardiac cell types.<sup>[320]</sup> Challenges in recapitulating the cellular complexity of the heart *in vitro* with its continuous movement and perfusion by the cardiovascular system impedes the development of functional cardiac organoids.<sup>[321]</sup> However, multicellular spheroids have been constructed from hiPSC-CMs, coronary artery endothelial cells, and cardiac fibroblasts using the hanging drop method.<sup>[322]</sup> Doxorubicin exposure evoked responses comparable to primary cardiac cultures, however, this system is not yet ready for high throughput cardiotoxicity testing. Within a high throughput approach, human 3D cardiac microtissues were assembled from the same cell types in 384 multiwell plates, exposed to known cardiotoxins and the mitochondrial membrane potential, endoplasmic reticulum integrity, and cell viability were used as readouts to evaluate the risk for cardiotoxicity.<sup>[323]</sup> Although the model could detect cardiotoxicity at clinically relevant concentrations, it is still lacking toxicological relevant cell types like smooth muscle fibers and the influence of shear stress caused by the continuous blood flow is neglected.

TdP can be modeled in human 3D cardiac tissue sheets (CTSs) which are constructed from hiPSC-CMs and non-myocytes.<sup>[324]</sup> The arrhythmias are detected by simultaneous measurement of the extracellular field potential on MEAs and evaluation of the contractile movement by a high-precision live cell imaging system capturing the beating motion. Of note, TdP could predominantly be detected in multilayered 3D CTSs composed of cell mixtures, highlighting the superiority of multicellular 3D models for *in vitro* cardiotoxicity testing compared to pure CM 2D cultures.

Although stem cell-based *in vitro* assays have been successfully applied in cardiotoxicity testing, the available systems do not live up to the cellular and structural complexity of the heart and do not model the blood flow. A limitation of the widely used hiPSC-CMs is their insufficient maturity rather representing fetal CMs.<sup>[321]</sup> The choice of *in vitro* culture parameters like media supplementation or oxygen content significantly affect

CM maturation. Glucose rich media promote anaerobic glycolysis in CM cultures, a metabolic phenotype observed in fetal hearts *in vivo* or under hypoxic condition. By contrast, glucose deprivation or HIF1 $\alpha$  inhibition increase oxidative phosphorylation in CM cultures which is an indicator of metabolic maturation observed in adult hearts *in vivo*.<sup>[325]</sup> Efforts have been made to accelerate hiPSC-CMs maturation but so far, no mature CMs have been established *in vitro*. However, the use of a testing battery of *in vitro* assays detecting specific cardiotoxic events like ion channel blockage, altered electrophysiology or contractility and cardio cytotoxicity could be a promising approach to circumvent the limitations of the individual assays.

## 2.6. Liver

Connecting the gastrointestinal tract with the systemic circulation, the liver is of tremendous importance for the metabolism and elimination of first pass doses of drugs, food contaminants, microbial metabolites, and other xenobiotics. The structural unit of the liver is the hepatic lobule, which consists of hexagonally arranged hepatocytes infused by a network of liver sinusoids. Nutrient- and oxygen-rich blood coming from the portal vein and the hepatic artery, respectively, enters the lobule via the interlobular portal triad (i.e., hepatic arteriole, portal venule, and bile duct), passes the sinusoid network and drains into the central vein of the lobule. The resulting oxygen gradient, ranging from normoxic to hypoxic conditions, and the associated activation of signal transduction pathways, i.e.,  $\beta$ -catenin and hedgehog signaling, contribute to the zonation of the liver, which critically determines spatial enzyme expression and corresponding metabolic activity.<sup>[326]</sup> In addition, hepatic blood flow through the liver sinusoids causes shear stress not only in the endothelial cells but also in the lining hepatocytes, which shapes various hepatic functions, including xenobiotic metabolism and hepatocyte maturation.<sup>[327]</sup> Liver zonation, shear stress, and other parameters, such as the crosstalk between hepatocytes and nonparenchymal cells, in particular sinusoidal endothelial cells, Kupffer cells, stellate cells, and lymphocytes, have a critical impact on hepatic functions and thus challenge the development and implementation of appropriate *in vitro* test systems for predictive hepatotoxicity testing (Figure 6).

In fact, hepatotoxicity is a major safety concern for the pharmaceutical industry. Adverse drug reactions are responsible for a remarkable high attrition rate of new chemical entities of up to 90%,<sup>[328]</sup> with hepatotoxic effects being causative second to cardiovascular safety issues.<sup>[329]</sup> Moreover, drug-induced liver injury, which in severe cases may cause life-threatening acute liver failure, is the most frequent cause of postmarketing warnings and withdrawals.<sup>[330,331]</sup> Thus, existing (preclinical) testing strategies, combining *in vivo* and *in vitro* studies as well as *in silico* predictions, are of obvious limited success.

Besides ethical considerations, animal studies face the challenge of considerable interspecies differences in the toxicopharmacokinetics and -dynamics of a chemical or drug and thus often fail to predict human hepatotoxicity.<sup>[332,333]</sup> The current gold standard for *in vitro* hepatotoxicity testing during drug development are human primary hepatocytes grown in monolayer culture. Obvious limitations of these cells are their

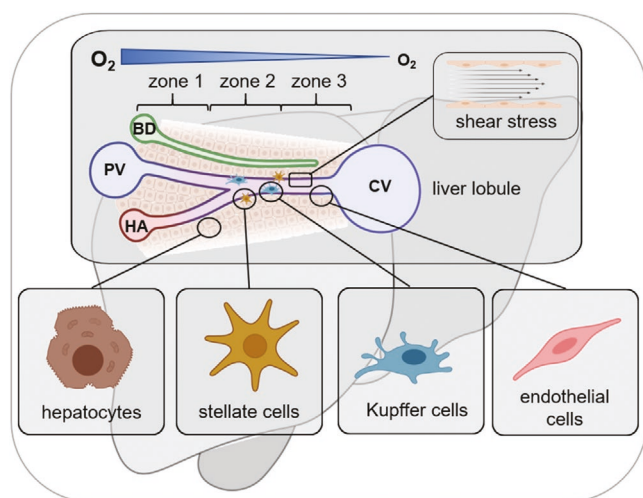


**Figure 6.** Structural and functional aspects and cell-types of the liver. Abbreviations: BD, bile duct; CV, central vein; HA, hepatic arteriole; PV, portal venule. Figure created with BioRender.com.

scarce availability, short life span, and tendency to rapidly dedifferentiate in culture, which is associated with a substantial downregulation of phase I and phase II enzymes.<sup>[334]</sup> Other cell models that are widely employed to assess potential hepatotoxicity are human hepatoma cell-lines, such as HepG2, Hep3B, and HepaRG. However, these cell-lines have a tumor background, rendering them less sensitive toward chemical threats, and lack the expression of major xenobiotic-metabolizing enzymes.<sup>[334]</sup>

The use of 3D *in vitro* models for hepatotoxicity testing is superior to monolayer cultures of hepatocytes or hepatoma cells, as these models, at least to some extent, resemble liver architecture and cellular diversity and thus are closer to liver physiology. In fact, 3D culture maintains the viability and hepatic functionality of incorporated primary human hepatocytes or hepatoma cells for up to several weeks.<sup>[335]</sup> As thoroughly summarized in various recent overview articles,<sup>[333,335,336]</sup> there is an ever-growing list of novel 3D liver models with each having its individual advantages and drawbacks. Today, several 3D liver models are on the market, an up-to-date list of commercially available models can be found here.<sup>[290]</sup> Liver spheroids, e.g., derived by the hanging drop technique, consisting of primary human hepatocytes or hepatoma cells are relatively easy to handle and are already more sensitive and specific in predicting hepatotoxicity and drug-induced liver injury than the corresponding plain monolayer cultures.<sup>[333,337,338]</sup> Spheroid and higher organized organoid models allow the incorporation of nonparenchymal cell-types, which is of particular importance for the screening of complex adverse effects, such as inflammation and fibrosis. The complex liver architecture and cellular complexity, including endothelial cells, can also be reconstituted by means of 3D bioprinting<sup>[339]</sup> and usage of organ-on-a-chip-platforms, such as microfluidic biochips or microfluidic multiorgan chips, enabling a more physiologically relevant supply with nutrients, oxygen, and test compounds.<sup>[333,337]</sup> For instance, different approaches, including the generation of 3D hepatic zonal channels and biochips, enabling the mounting of an oxygen gradient (from normoxia to hypoxia) across

hepatocytes, exists that mimic hepatic zonation and spatially distributed metabolic activities.<sup>[340–342]</sup>

However, most of these models depend on primary human hepatocytes with all their limitations. Hepatocyte-like cells have been successfully differentiated from pluripotent stem cells including iPSCs, and used for hepatotoxicity testing.<sup>[343,344]</sup> However, when cultured in 2D monolayers these cells lose morphology, proper cell–cell contact (tight junctions), and metabolic capacity.<sup>[345]</sup> Self-organizing 3D hepatic organoid systems derived from PSCs or iPSCs may overcome these limitations by closely mimicking the hepatic microenvironment and physiology.<sup>[336]</sup> Stem cell-derived 3D liver models can be cultured for month or years without losing their metabolic capacity or other hepatic functions. Several methodological approaches exist, including scaffold-free (decellularized liver matrices, spheroids, and organoids) and scaffold-based (nanofiber- and hydrogel-based, nanoscaffolds) setups.<sup>[333]</sup> Moreover, PSC/iPSC-derived 3D liver organoids can be generated by starting either with a coculture of cell-types, for instance, iPSC-derived endodermal, endothelial, and mesenchymal cells,<sup>[346]</sup> or with a homogeneous cell population that during the culture protocol differentiates into the different hepatic cell-lineages.<sup>[347,348]</sup> The use of PSCs/iPSCs allows to generate multicellular 3D models with all hepatic cell lineages incorporated being genetically identical.<sup>[336,347]</sup> Human iPSCs derived from fibroblasts, blood cells or any other cell-type of a donor, can be differentiated in all hepatic cell-types and thus present an unlimited pool of cellular material for diagnostic purposes or toxicity testing. The simultaneous generation of 3D liver organoids from hiPSCs of different donors in combination with high-throughput hepatotoxicity testing enables comparative compound testing, and thus tackles the issue of population diversity/interindividual susceptibility. In fact, a high-throughput approach with hiPSC-derived hepatocytes grown in 2D and 3D cultures assessing the impact of 48 substances on cell number, viability, nuclear integrity, mitochondrial membrane potential, apoptosis, and other parameters, demonstrated that hiPSC-derived 3D liver models are suitable for high-throughput testing.<sup>[349]</sup> Powerful gene engineering techniques, such as transcription activator-like effector nucleases (TALENs) and the CRISPR/Cas system, allow the introduction of point mutations, smaller deletions, etc. and thus the creation of hiPSC cultures, which in a 3D context may phenocopy functionally relevant single nucleotide polymorphisms (SNP) and rare mutations that frequently occur in genes coding for xenobiotic-metabolizing enzymes.<sup>[350]</sup> Stem cell-derived 3D liver organoids can also be used to model complex hepatic diseases. Ouchi et al., for instance, successfully simulated the sequential pathogenesis of steatohepatitis, consisting of steatosis, inflammation, and fibrosis, by treating PSC-derived 3D models made of hepatocyte-, macrophage-, cholangiocyte-, and stellate-like cells with free fatty acids.<sup>[347]</sup> By incorporating human fetal liver mesenchymal cells into human ESC-derived expandable hepatic organoids, Wang and co-workers generated another intriguing test model, which is suitable to investigate the pathophysiology of alcoholic liver injury. Specifically, under ethanol treatment, the model allows to assess the generation of oxidative stress, steatosis, the secretion of inflammatory mediators, and fibrosis.<sup>[351]</sup>

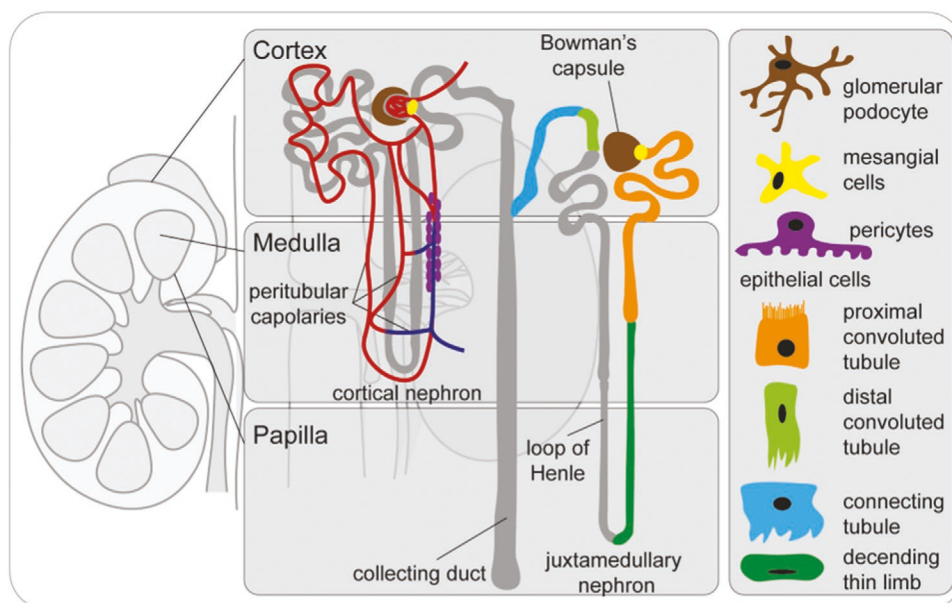


**Figure 7.** Schematic overview of important cell types and functional units of the kidney. Adapted under the terms of the Creative Commons Attribution license.<sup>[531]</sup> Copyright 2013, The Author(s). Published by Wiley (<https://staging.onlinelibrary.wiley.com/page/journal/20011326/open-access-license-and-copyright.html>). Figure created with BioRender.com.

Even though there is an urgent need for the development, characterization, and validation of new *in vitro* models suitable for a solid prediction of the hepatotoxic properties of chemicals and drugs, the use of stem cell-derived 3D models still remains a challenging task. Besides improving the model systems toward hepatic functionality, for instance, by optimizing hepatocyte polarization, oxygen and nutrient gradients and cell–cell interactions, it is also important to consider how simple or complex, for instance, in terms of the number of incorporated cell-types, a model should be to adequately predict a certain toxicological/pharmacological readout or address a specific scientific question. In order to get PSC-derived 3D liver models employed, *i.e.*, accepted by industry and regulatory authorities, in the current test battery for hepatotoxicity, a proper standardization of the protocols and a comparison of the different protocols and models assessing the same adverse outcome across laboratories is urgently needed.

## 2.7. Kidney

Kidney functions are closely linked with homeostasis of the inner body milieu, electrolyte and fluid balance, acid base handling, and retention of amino acids. Furthermore, kidneys are major players in the excretion of water-soluble waste products and xenobiotics, toxins, and “end-products” such as uric acid. At the same time kidneys achieve retainment of serum proteins and glucose within the body, a process that requires numerous active transport processes.<sup>[352]</sup> This plethora of functions is achieved through the interplay of different kidney cell types, *i.e.*, podocytes, parietal epithelial, mesangial, glomerular endothelial, juxtaglomerular, specialized epithelial cells (proximal and distal tubules, loops of Henle, collecting ducts),

interstitial, endothelial, stromal, dendritic and stem cells, that are organized in structural units, denoted nephrons (**Figure 7**). At the one end of the nephron a filtration barrier, the glomerulus, produces a primary urine volume of 180 l per day into the Bowman’s capsule. This urine is further concentrated and processed within the renal tubular structures. The anatomy and transporter/ion channel distribution allows to distinguish five different nephron sections with individual functions, *i.e.*, the proximal tubule, the thick part of Henle’s loop, the distal convolute, and the collecting ducts.<sup>[353]</sup> The tubules are lined by at least 20 different epithelial cell types that are highly differentiated, linked through tight junctions and have a high oxygen consumption rate due to their metabolic activities, which demands constant high nutrition, oxygen, and energy supply. Which kidney structures transport renal malfunctions can be specified by shedding light on acute or chronic kidney injury, which are due to multiple causes with hypocirculatory, immune, and direct toxic effects being most frequent.<sup>[354]</sup> Transient interruptions of adequate blood supply in the course of blood volume contractions or vasoconstriction are common reasons for acute kidney injury. These can originate from severe bleeding episodes or nonsteroidal anti-inflammatory drug applications, the latter inhibiting prostaglandin synthesis and abrogating the vasodilatory effects of endogenous prostaglandins thereby reducing glomerular blood flow.<sup>[355]</sup> Some drugs are notorious for increasing the vascular tone with similar effects on blood flow especially on the afferent capillaries that enter the glomerular structures, *e.g.* calcineurin inhibitors often prescribed as immunosuppressive drugs in organ transplanted patients.<sup>[356]</sup> These “hypocirculatory” events result in regional or complete kidney ischemia with cellular damage incited in those cells that are most dependent on energy and oxygen supply, the tubular cells, which respond with necrosis and apoptosis.

At the cellular level the kidneys have the potential to recover from such acute kidney injuries by tubular cell proliferation and endocycle-related tubular cell hypertrophy.<sup>[357]</sup> Direct toxic effects of pharmaceutical compounds and environmental toxins are common phenomena and drug-induced kidney toxicity accounts for about 25% of the reported severe adverse drug reactions.<sup>[358]</sup> Drug- or toxin-induced kidney damage might occur in different nephron sections. For example, the heavy metal mercury induces proximal tubule dysfunction due to its uptake by the organic anion transporters OAT1 and OAT3, which are preferably expressed in the proximal tubule.<sup>[359]</sup> Fluoride yet acts on the ascending limb of the loop of Henle by interfering with chloride transport.<sup>[360]</sup> On the contrary, kidney toxicity induced by amphotericin B mainly targets the distal tubule. This seems to be due to the impaired cellular repair mechanism at low urine pH values that counteracts toxicity in the proximal tubule due to a higher urine pH at this part of the nephron.<sup>[361]</sup> Another phenomena in the kidney following tubular cell injury is an immunological response, such as tubulointerstitial cell infiltration. The infiltrating immune cells release inflammatory cytokines that propagate fibrosis on the one side, and are thought to coordinate tissue reparative processes on the other side.<sup>[362]</sup>

Keeping the aforementioned mechanisms of acute kidney injury in mind with a large cellular repertoire at risk, toxicological studies have to address the aspects of cell-specific drug levels and adverse effects including phenotypic and functional alterations. The number of different cell types within the glomerulus, the tubular structures and tubulointerstitial compartment are even growing with the advent of single cell sequencing.<sup>[363–365]</sup> Homogenous cell cultures of the respective cells have been established earlier. One success story in the early 2000s was the establishment of immortalized podocyte cells that grow or differentiate in dependence of environmental temperature.<sup>[366]</sup> However, economics should balance testing efforts and therefore compound testing across the at least 26 individual renal cell types identified so far<sup>[367]</sup> does not seem feasible – or physiological, as they are devoid of cell–cell interactions and higher complex organization. Modeling different functional nephron sections with their complex architectures including cell–cell interactions, presence of capillaries, differences in oxygen tensions and shear fluid stress in vitro remains challenging. To cover especially these complex context-dependent changes in cellular compartments, fibrogenic niches, capillaries, pericapillary cells, mesangium or due to differing oxygen tensions, most studies dealing with kidney toxicity combine in vitro with in vivo approaches. In vivo studies concerning kidney using rodents bear the drawback of interspecies differences<sup>[368]</sup> when extrapolating to humans, and most former in vitro models do not picture the architectural complexity of the kidney. Here, stem cell technology has been offering a sky-rocketing development toward organotypic cultures including hiPSC-derived kidney organoids and adult stem cell-derived tubuloids bridging the gap between traditional 2D cultures and animal models.<sup>[369]</sup> Although organoids contain a large variety of renal cells, they are still largely devoid of mesangial cells, immune cells, glomerular endothelium, principal and intercalated cells and their functionality has hardly been studied.<sup>[369]</sup> One example of a valuable

development in the kidney organoid field is the establishment of reporter human pluripotent stem cell lines that encompass all kidney cell types of the glomerulus, proximal and distal tubule as well as an extensive endothelial network, and renal interstitium. These “whole kidney organoids” enable live assessment of kidney cell differentiation and organoid development in a toolbox format.<sup>[370]</sup> For phenotypic screening including toxicity testing, renal organoid production was also brought to the next level by setting up a robotic platform for miniaturizing and speeding up kidney organoid formation in microwell formats for high-throughput screening.<sup>[371]</sup> Some kidney organoids even produce renin,<sup>[372]</sup> an endopeptidase synthesized by juxtaglomerular cells, which is crucial for blood pressure regulation. Such functional aspects are valuable additions to the descriptive nature of organoid cellular composition and structure. Protocols for kidney organoids derived from human inducible progenitor stem cells have proven successful to mimic late capillary loop stage nephrons on day 14 of cultures. Later on, some cells are not sufficiently supplied by oxygen and nutrients resulting in cell damage with ensuing fibrosis.<sup>[373]</sup> Despite these achievements in cellular differentiation and organizational features at the nephron level, significant challenges remain. i) Kidney organoids represent a very immature, i.e., fetal kidney system.<sup>[363]</sup> ii) Current protocols do not embrace the whole array of renal cells, especially heterogeneous stromal cell populations and the minimal requirement for kidney toxicity assessment is uncertain. iii) Functional vasculature and a common urinary collecting system are currently not depicted even in complex in vitro systems.<sup>[374]</sup> iv) More “physiological” culture conditions, e.g., with varying fluid shear stress or oscillating pressure<sup>[375]</sup> will be of paramount relevance to mimic the milieu of the kidney. Given the low oxygen tension in most parts of kidney tissue cell culture protocols with organoids also need to address the issue of reduced oxygen supply. Drug nephrotoxicity testing by kidney-on-a-chip testing has been adopted by some groups with experimental setups that also include fluid shear stress. Such test systems will likely revolutionize toxicity testing when they succeed to be standardized.<sup>[376–379]</sup>

## 2.8. Intestine

The intestine is comprised of subsections with substantial anatomical and physiological heterogeneity in luminal pH, presence or abundance of cell types, and presence and composition of the microbiome. The intestine is an organ of superlatives: its epithelium is one of the fastest renewing tissues within the human body with a maximum cellular life span of 5 days.<sup>[380]</sup> It harbors the largest pool of microbial communities, which is contained by a semipermeable epithelial barrier forming one of the largest interfaces between the endogenous and exogenous environment. To safeguard the uptake of exogenous compounds and to govern the host–microbiome interactions, vast numbers of immune cells reside along the gut, resulting in a major compartment of the immune system.<sup>[381]</sup> Apart from its most commonly known tasks, the regulation of water balance, digestion of food and nutrient absorption, the intestine is recognized for its impact on overall physical and mental health with endocrine activity, immune regulatory functions, and

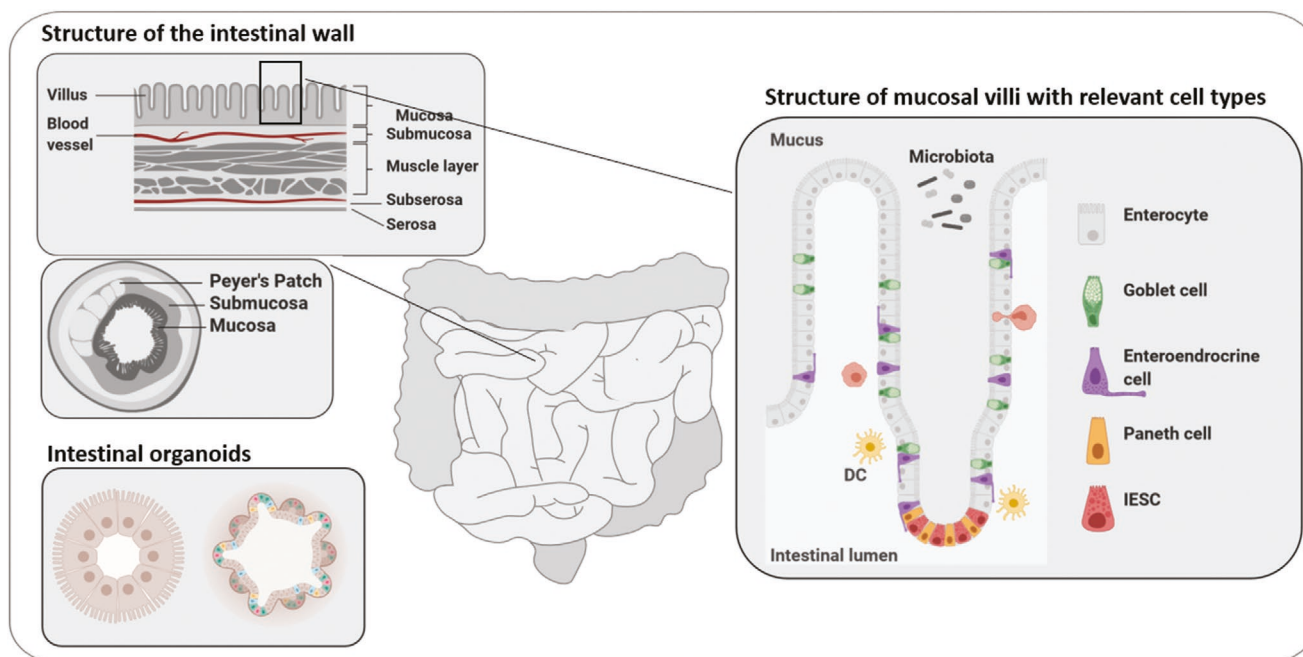


**Figure 8.** Structural and functional units of the intestine. Abbreviations: DC, dendritic cell; M $\phi$ , macrophage; IESC, intestinal epithelial stem cell. Figure created with BioRender.com.

extensive neuronal network (reviewed in refs. [382,383]). Its basic structure folds into villi and crypts and is lined with a single layer of intestinal epithelial cells (IECs) of which enterocytes and goblet cells make up the majority, while Paneth cells, endocrine cells and Microfold cells account for the rest (**Figure 8**). All IECs develop from intestinal stem cell (ISC)-derived progenitors and differentiate while traveling along the crypt-villus axis.

This complexity of the intestine is challenging to mimic experimentally, as summarized by Costa and Ahluwalia.<sup>[384]</sup> However, the availability of relevant intestinal models is indispensable. Intestinal disorders, e.g., intestinal cancer, inflammatory bowel disease and infections, affect millions of people worldwide and present a substantial economic and societal burden.<sup>[385,386]</sup> Furthermore, oral toxicity testing is a requirement for pharmaceutical and chemical development.<sup>[387,388]</sup> The oral route is preferred for the application of pharmaceuticals, but gastrointestinal adverse events (GI AE), e.g., diarrhea, abdominal pain, and nausea, are common side effects. Though hardly ever the reason for market removal or clinical attrition, AE can significantly affect treatment compliance.<sup>[389–391]</sup> To facilitate and standardize noxae investigations, the OECD has specified test guidelines for rodent (e.g., TG 408)<sup>[121]</sup> and non-rodent species (e.g., TG 409).<sup>[392]</sup> Models of larger vertebrate species (e.g., dog and pig) as well as invertebrate organisms (e.g., zebrafish and *C. elegans*) are available, but the majority of studies is conducted in rodents. The most suitable way of exposure is based on the intended application and physicochemical properties of the test substance. To address questions in non-regulatory context, e.g., on intestinal inflammation, digestion, and the microbiome, specialized *in vivo* models are available (reviewed in refs. [393–395]). However, the predictive quality of animal models for intestinal effects in humans is increasingly disputed as substantial anatomical, biochemical, and

microbiological differences prevail.<sup>[396–398]</sup> Especially the role of the microbiome has been neglected with regard to preclinical reproducibility and clinical translation efficacy, which might be a factor in the low congruence in drug toxicity testing between humans and other animals.<sup>[9,399–401]</sup>

In context of the 3Rs, a variety of intestinal *in vitro* models has been developed in the last three decades, of which cancer-derived cell lines are the most commonly applied system.<sup>[402–404]</sup> Although these cell lines are inherently diseased and do not fully match healthy tissue biochemically and genetically,<sup>[404,405]</sup> good correlations to human tissue were found.<sup>[406,407]</sup> Since then, highly sophisticated models have been developed by combining multiple cell types, mimicking the intestinal architecture, luminal flow or peristalsis, and even incorporating the microbiota.<sup>[408–410]</sup> In this context, hypoxia has emerged as potentially important factor for intestinal systems. Unlike other organs, the intestine is characterized by a substantial heterogeneity in oxygen levels to a nearly anaerobic environment in the lumen (reviewed by Zeitouni et al.<sup>[411]</sup>). Chen et al.<sup>[412]</sup> have developed a scaffold-based 3D coculture model, where the oxygen tension can be adapted to create micro- to anaerobic conditions within the lumen. As the group demonstrated, the consideration of oxygen levels in intestinal models may affect their applicability especially for studies on host–microbial interactions.<sup>[412–414]</sup> But also the toxicity of nanomaterials may change depending on the availability of oxygen.<sup>[415]</sup> However, many of these elaborate models stagnate at a proof of concept stage with little or no routine application in toxicity testing. Whereas strong agreement exists on the suitability of transwell cultures over undifferentiated monocultures, studies failed to demonstrate a clear advantage of more complex models.<sup>[416,417]</sup>

As GI AE still commonly occur at clinical stages and are frequent side effects of marketed drugs, the suitability and

adequacy of existing models needs to be considered. The use of stem cells is investigated to improve the predictive quality of *in vitro* models for toxicity testing. Different approaches are available: i) the use of ISCs of isolated intestinal crypts, and ii) ESCs or iPSCs, which result in the formation of self-organized 3D spheroids. The studies by Sato et al.<sup>[418,419]</sup> are regarded as game changer in the field, as they enabled the long-term culture of primary intestinal cells in absence of mesenchymal tissue—until then the bottleneck for primary intestinal cultures.<sup>[420]</sup> Methods for the targeted differentiation of human iPSC<sup>[421]</sup> or murine ESCs<sup>[422]</sup> into intestinal tissue further expanded the stem cell toolbox. It is noteworthy that the differentiation protocols for ESC and iPSC cultures are generally more complex and time intensive—requiring at least 28–34 days.<sup>[421,423]</sup> They span three differentiation stages: i) to definitive endoderm, ii) to hindgut-like tissue, and iii) toward organoids resembling intestine-like tissue.<sup>[421,423,424]</sup> In stem cell-derived organoids, all major IEC types are detectable, including enterocytes, goblet cells, Paneth cells, and endocrine cells. In iPSC-based models, ISC markers are only present after an extensive differentiation time.<sup>[421]</sup> The resulting organoids were found to resemble fetal rather than mature adult tissue,<sup>[425]</sup> which might be a critical limitation.<sup>[426]</sup> To improve maturation, different approaches were reported, e.g., using interleukin 2,<sup>[427]</sup> cell sorting,<sup>[423,428]</sup> or *in vivo* engraftment.<sup>[424,425]</sup>

Notwithstanding these limitations, stem cell-derived intestinal cultures have been applied for a range of research questions, including biological processes of intestinal tissue,<sup>[429]</sup> organ development,<sup>[430,431]</sup> intestinal pathologies,<sup>[423]</sup> and to lesser extent the toxicity of xenobiotics.<sup>[432,433]</sup> They appear to be a promising tool for the study of host–microbiome or host–pathogen interactions, using passive colonization<sup>[434]</sup> or active microinjection into the lumen.<sup>[435]</sup> Although these models were found to be suitable to investigate drug transport and metabolism, only few reports are available to date.<sup>[436–439]</sup> Their limited application in exposure studies may be due to the organoids' physiology and morphology—a polarized status with the apical side facing inward. This restricts their suitability as the absorption of nutrients and drugs as well as the interaction with noxae and the microbiota are initiated from the apical side. Studies aimed to push these boundaries by luminal injection of organoids,<sup>[435]</sup> establishment of flow through the lumen<sup>[440]</sup> or development of “apical-out” organoids.<sup>[441]</sup> Others have turned to approaches that break up the organoid structure to seed 2D barriers on transwells or microchips using the whole organoid<sup>[442–444]</sup> or selected cell types.<sup>[445,446]</sup>

Altogether, stem cells have the potential to greatly advance the field of intestinal research, including toxicity testing. Apart from the use of physiologically healthy tissue, patient-specific organoids may be developed to investigate intestinal disease development and treatment strategies.<sup>[447]</sup> However, questions remain on the regional identity as well the maturity status of the stem cell-derived organoids.<sup>[425,448]</sup> Undoubtedly, the intestine is important in itself, but its full impact only emerges in the interplay with other organs, e.g., the liver, the CNS, and the microbiome, which remains a shortcoming in these models.<sup>[447]</sup> Although the protocols are described as “highly efficient” and “robust,”<sup>[421,449]</sup> they greatly exceed the intricacy of most *in vitro*

systems. Their superiority over these established, less complex models for toxicity and safety evaluations remains to be demonstrated, and will likely determine their implementation rate and application range.

### 3. Genome Editing

Genome manipulation using zinc finger nucleases and TALENs<sup>[450,451]</sup> realized insertion of genetic elements into specific sites of the genome. The CRISPR revolution<sup>[452,453]</sup> substantially improved this procedure by making genome editing fairly easy to achieve. A comprehensive overview about the rapidly evolving field of applications and protocols of CRISPR/Cas and related genome editing tools is provided by the following review articles.<sup>[454–456]</sup> Toxicology benefits from such genome editing approaches in several ways. Reporter lines with fluorescent or luminescent reporters under endogenous promoter control can be used for following stem cell differentiation and target cell toxicity, e.g., for neurons,<sup>[457]</sup> kidney cells<sup>[370]</sup> or CMs.<sup>[458]</sup> Also, genetically encoded indicators, e.g., for calcium signaling, are useful tools for assessing calcium transients. These can be combined with other functional indicators as, e.g., for voltage. Such lines offer the possibility for functional studies in target cells without the use of dyes like Fura-2 and thus offer a great possibility for functional toxicity testing in high throughput formats using high content imaging.<sup>[459,460]</sup>

Besides value in generation of stem cell reporter lines, genome editing techniques can also be used for disease modeling, in toxicology particularly relevant for studying gene–environmental interactions. Human PSC knockout lines or the targeted integration of specific mutations for the establishment of isogenic disease models is definitely of great significance for such applications with the combined effort of CRISPR in hiPSC-derived organoids representing cutting-edge toolsets.<sup>[461–464]</sup>

Also, in mechanistic toxicology the CRISPR/Cas system has already proven its great value. CRISPR/Cas-based approaches identified genes critically involved in determining the toxicity of various chemicals, including arsenic trioxide, formaldehyde, and paraquat.<sup>[465–467]</sup> For example, a CRISPR-based positive-selection screen identified the genes coding for CYP oxidoreductase, copper transporter ATP7A, and sucrose transporter SLC45A4, as critical mediators of paraquat-induced cell-death.<sup>[466]</sup> Moreover, the study revealed CYP oxidoreductase as a major source for paraquat-induced oxidative stress. In another study, CRISPR/Cas technology was used to identify targets of anticancer small molecules by a mutagenesis scanning of essential genes.<sup>[468]</sup> Hence, CRISPR/Cas-based functional genomic screening approaches are suitable to provide unprecedented mechanistic insight in modern toxicology and pharmacology.<sup>[469]</sup>

Finally, combining genome editing with iPSC technology enables the integration of genetic variation, which may determine the interindividual susceptibility toward a given drug or xenobiotic, into modern toxicity testing. In fact, genome-wide association studies have contributed to the identification of a large number of SNPs and rare genetic variants in genes, amongst others encoding xenobiotic-metabolizing,

antioxidative, and DNA repair enzymes, which critically shape the adverse and/or beneficial outcome of a certain chemical or drug.<sup>[470,471]</sup> A well-known example is the human cytochrome P450 (CYP) 2D6 monooxygenase, which accounts for the metabolism of ~15% of clinically used drugs, including opioids, beta-blockers, antiarrhythmics, and antidepressants.<sup>[472]</sup> More than 110 SNPs, some of them displaying allele frequencies of up to 32%, have been identified in the CYP2D6 gene to either enhance, attenuate or completely abolish its catalytic activity.<sup>[472]</sup> By generating iPSC-derived hepatocyte-like cells from hepatocytes of CYP2D6 polymorphic donors and subsequent analyses of the metabolism of CYP2D6 substrates, i.e., desipramine and tamoxifen, Takayama et al. demonstrated that the application of iPSC-derived cells with different SNPs is suitable to predict the interindividual differences in the metabolism of drugs and associated biological effects.<sup>[473]</sup> In general, the use of donor cells with well-defined polymorphic genes for iPSC generation or the integration of mutations that resemble a certain SNP directly in the iPSC genome, would for sure improve the prediction of drug-induced cardiotoxicity, liver injury, neurotoxicity, and other frequent adverse drug reactions.<sup>[474,475]</sup> Besides CYP2D6, potential candidates for such a screening approach are genetic variants of glutathione S-transferases T1 and M1, N-acetyltransferase 2, and mitochondrial DNA polymerase- $\gamma$ . In fact, the mentioned gene variants are not only associated with a reduced catalytic activity of the respective enzyme, but also increase the individual's susceptibility to idiosyncratic drug-induced liver injury.<sup>[476–478]</sup> Along the same line, missense variants of genes encoding retinoic acid receptor- $\gamma$ , CYP2C19, and multidrug resistance protein-2 have been identified to enhance the risk for anthracycline-induced cardiotoxicity.<sup>[479–481]</sup> Recent studies reporting the generation of genome-edited hiPSC-derived hepatocyte-like cells resembling CYP2C19 poor metabolizers,<sup>[482]</sup> and CMs carrying the retinoic acid receptor- $\gamma$  missense variant S427L and exhibiting the associated enhanced sensitivity toward doxorubicin treatment,<sup>[481]</sup> illustrated the outstanding potential of genome-edited iPSC cells and organotypic models derived thereof for future compound testing in toxicology and pharmacology.

## 4. Biofabrication

### 4.1. Organ-on-a-Chip/Microphysiological Systems

Advances in material engineering and biofabrication enabled the development of highly adaptable microphysiological systems. Such systems integrate the biological complexity of 2D and 3D cell cultures with a defined spatial organization and a controlled microenvironment to closely mimic the *in vivo* situation, including naturalistic stimuli.<sup>[483]</sup> Microphysiological systems, such as OOAC systems, aim at reconstructing the complex mechanical and biochemical cellular environment of the human body. By complementing and enhancing standard cell culture models, these systems have the potential to improve toxicity testing, accelerate drug discovery, improve diseases modeling, and reduce the use of animal models. The high adaptability of OOACs allows their application in many different cell, tissue, and organ models.<sup>[483–487]</sup>

OOACs are extremely diverse and customizable, thriving toward the reproducible generation of single cell cultures, cocultures or even complex 3D scaffolds. The option for the compartmentalized cultivation of different cell types and their supplementation with distinct media, massively extends the possible applications for such systems including organ crosstalk. At the same time, OOACs require a very little amount of cell material, media, and test substances, thereby reducing cultivation costs.

OOACs have already been adapted to fit a diversity of applications, such as modeling the BBB,<sup>[191,488]</sup> assessing and driving cellular maturation,<sup>[489,490]</sup> (patient-specific) modeling of diseases,<sup>[491,492]</sup> mimicking the capillary formation,<sup>[493]</sup> and the capillary flow,<sup>[494]</sup> assessing the effect of stretch and strain on tissues<sup>[495,496]</sup> and showing the applicability of OOACs for drug and substance exposures and development.<sup>[378,490,495,497]</sup> OOACs have even been applied to study nanoparticles, which are currently of great public concern<sup>[498]</sup> thus allowing to study indirect adverse effects. No large-scale toxicity testing has been done with OOACs, yet. However, smaller scale applications that aim at the establishment of testing platforms have been developed, mainly with human, but nonstem cell-based cell systems.<sup>[376,498–500]</sup> Some toxicity biomarkers that have already been utilized with OOACs are summarized by Cong et al.<sup>[376]</sup>

Even though the development of the OOACs for the field of toxicology is still heavily under construction, strong beneficial aspects can already be anticipated. The system will add complexity to the conventional cell culture models by recapitulating the physiological forces, increasing the reproducibility due to the controllable environment and improving long-term viability by enhancing the nutrient and waste flux within the samples. By implementing human-based stem cell systems, the OOACs could help reduce animal experiments by providing relevant indication of substance MoA and their impact on toxicity in humans, prior to animal experiments or clinical testing. Mechanistic questions concerning MoAs can be investigated with OOACs by including molecular and cellular readout methods. Coexposures and cocultures are also easily implementable due to the modularity of most OOAC systems. This increases the predictivity for example in drug design and substance testing. Maoz et al. developed a multichip system to model the BBB, which could be used to test the efficiency of drug flux across the BBB.<sup>[488]</sup>

The evaluation of organ crosstalk *in vitro* was long thought to be beyond the bounds of possibility, but these fast-developing OOAC systems and the option to combine them to form integrated body-on-a-chip (BOC) systems have opened up the unique opportunity to make the impossible possible. In BOC systems, organ chips can be connected to transfer flow-through from one chip to another, thereby not only transferring nutrients, but also metabolites as well as waste- and by-products. BOCs could therefore give valuable insights into substance metabolism and toxicological effects across tissues.<sup>[377,501]</sup> Tsamandouras et al. developed a fluidic platform that allows for the study of pharmacokinetics in a multiorgan setting.<sup>[502]</sup> They successfully tested their platform using gut and liver interconnected chips. Another impressive study was performed by Oleaga et al.,<sup>[503]</sup> who generated a functional model to evaluate human multiorgan toxicity under continuous flow conditions.

The group tested their four integrated modules, namely cardiac, muscle, neuronal and liver modules, for their pharmacological relevance, by evaluating their response to five drugs with known side effects. Their culture model exhibited a multiorgan toxicity response and the results were in general agreement with published toxicity data.

Besides the relatively high manufacturing costs and the usually medium to low scalability, one of the greater challenges with OOAC systems is the design of biocompatible materials that support cell survival and growth, and at the same time allow for the appropriate readouts. Although ready-to-use chips can be purchased from commercial manufacturers such as TissueUse GmbH, Mimetas, and EmulateBio, the majority of the research community working in this field produce their own chips. Many OOACs so far rely on imaging methods to assess the culture, which requires a clear and thin imaging surface. Silicon-based and polydimethylsiloxane are currently used in the field,<sup>[504]</sup> however, the development is still striving forward. Additional points of consideration for substance testing in OOACs are the resistance of the material toward the uptake of the tested substances to avoid unintended postexposures, and the integration of endpoint-specific readouts needed for each specific model type. The material of the chip has to be biocompatible, meaning that it has to be resistant to leaching and must not interfere with the test compound thereby altering exposure concentrations. Moreover, most OOAC models are unsuitable for screening applications that require parallelization (96- and 384-well plates). However, high-throughput modules that hold up to 96 microfluidic structures have been established and are commercially available (OrganoPlate, Mimetas). These modules are compatible with automation and HTS instruments and have already been tested using SCs as cell source.<sup>[505,506]</sup> In summary, OOAC and BOC models still need to be validated against established toxicity assays using a library of compounds with known toxicological effects. The biological functionalities of the chips must be highly reproducible and reliable to gain acceptance in toxicity studies. Moreover, they have to be user-friendly, cost-effective, and should be compatible with the standard cell culture equipment and HTS devices. Keeping this in mind, there are promising developments in the field of OOAC and BOC, that will very likely lead to a leap forward in toxicological testing, disease modeling and fundamental research.

#### 4.2. Bioprinting

Bioprinting is a biofabrication technique to generate organotypic tissue or organ models. Goal of this strategy is to augment the complexity of the models to recapitulate the *in vivo* 3D physiology in more detail than manually generated 3D models. There are a variety of printing technologies available, the most popular of which are inkjet-based, extrusion-based, and laser-assisted.<sup>[507]</sup> Each technology has its own advantages and disadvantages, e.g., concerning the bioink property requirements, printing resolution, possible cell densities, and shear stress effecting cell viability.<sup>[507]</sup> The printing process itself is influenced by three main variables: i) the material (bioink), ii) the cell source, and iii) biomechanical factors, such as viscosity, elasticity, and stress relaxation.<sup>[508–510]</sup> The right choice of

bioink is crucial to adequately mimic the cellular microenvironment.<sup>[511]</sup> Widely used materials are natural hydrogels (gellan gum, alginate, chitosan) and synthetic hydrogels poly(ethylene oxide), poly(vinyl alcohol), poly(pro-pylene fumarate)). Their high water content and tunable properties render them ideal for 3D models.<sup>[512–515]</sup> The choice of material heavily depends on the cell type and the intended 3D differentiation or growth process. Studies looking at bioprinted models often focus on basic cellular processes within the printed gels (i.e., cell survival, cell growth, and differentiation), or aim at the highest possible accuracy in recapitulating the physiological *in vivo* situation.<sup>[516]</sup> Additionally, bioprinting rises great hopes to fabricate vascularized tissues, thereby diminishing the dead core effect. Bioprinting of ES- and hiPSC-based models has been intensively reviewed in Romanazzo et al.<sup>[517]</sup> and Ong et al.,<sup>[518]</sup> discussing advantages, limitations, and future perspectives. In brief, ESCs and iPSCs are ideal cell sources for bioprinting applications. They are available in virtually unlimited quantity and can proliferate and differentiate into various cell types within the bioink. Among others, SCs have been used for bioprinting of cardiac,<sup>[519]</sup> neural,<sup>[520]</sup> and hepatic<sup>[521]</sup> tissues. An advanced printing strategy using a triculture of hiPSC-derived hepatic progenitors, human umbilical vein endothelial cells, and adipose-derived stem cells, developed an organotypic 3D liver model which recapitulates the native *in vivo* structure and is able to secrete products of liver metabolism.<sup>[339]</sup> Challenges of SC bioprinting include the search for suitable bioinks supporting cell growth and differentiation, the need for printing parameters that the cells can withstand, and the optimization of long-term cultivation parameters allowing adequate in- and efflux of nutrients and oxygen. However, these challenges also apply for other cell sources like primary cells and immortalized cell lines. Regarding a toxicological application, bioprinted organotypic models are very rarely intended to work in a high-throughput context, which is mandatory for screening approaches. Moreover, the influx and efflux of the test substance within the hydrogel as well as interactions with hydrogel components are difficult to predict. Nevertheless, the automated printing process provides a higher degree of consistency and decreased batch-to-batch variations compared to manual 3D fabrication techniques, thereby increasing the reproducibility and reliability.

#### 5. Challenges and Opportunities

With toxicology moving from apical endpoint testing in *in vivo* to human cell-based *in vitro* assays, comprehensive cellular models are needed that cover the organ- and cell type-specific MoA for a large variety of toxicants. In this review article we discussed which structural and functional units of the skin, brain, thyroid system, lung, heart, liver, kidney, and intestine are targets of or mediate toxicity and disease and thus have to be modeled *in vitro* for human health prediction without using animals. Moreover, we summarized which preferably stem cell-based *in vitro* models have been developed for modeling the respective organs and evaluate their coverage of all necessary functional and structural criteria discussed above. Additionally, we highlighted organotypic models can be taken

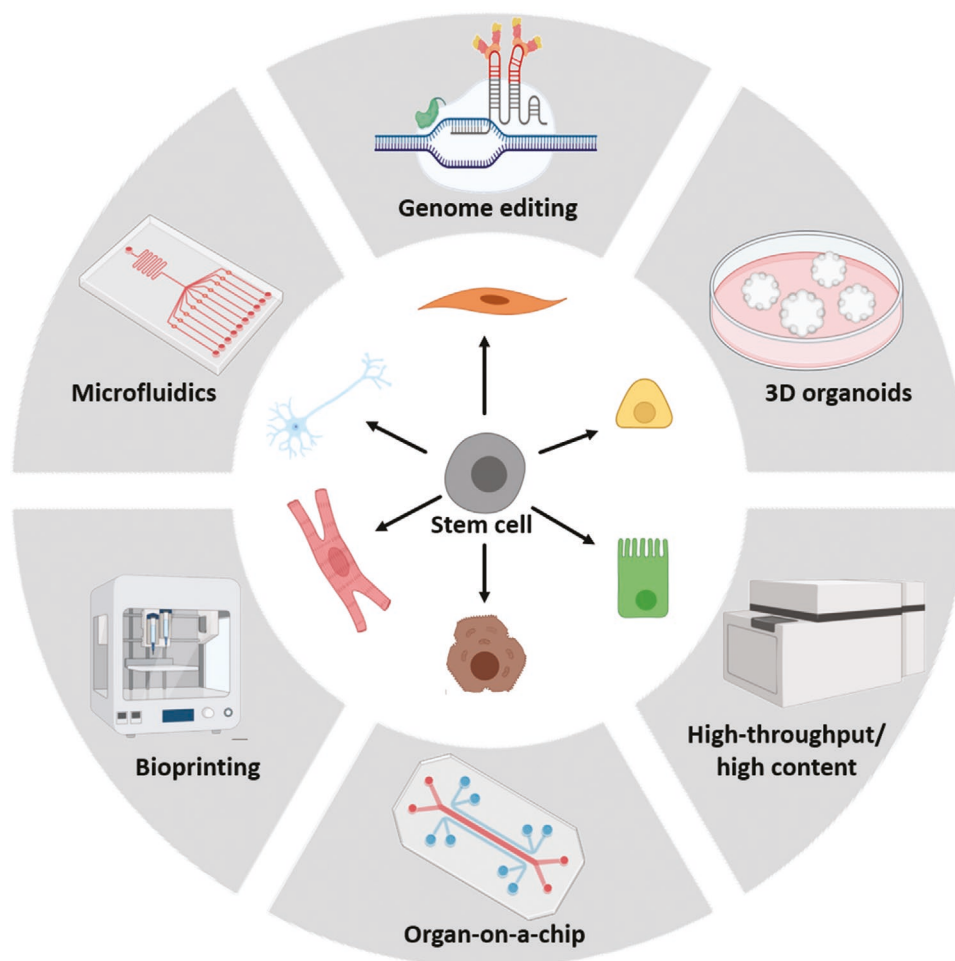


**Figure 9.** Opportunities of stem-cell based models for future toxicological testing. Figure created with BioRender.com.

to the next level using cutting edge technologies like genome editing and bioprinting in combination with sophisticated culturing methods (e.g., microfluidic systems and OOAC) with the final goal to facilitate high throughput/high content screening in the near future (Figure 9). Through targeted differentiation into multiple cell types, stem cell-based in vitro models can be accurate representations of human cell physiology and widely applied to study adversity on the cellular level in toxicity and disease without the necessity to rely on primary cells, tumor cell models or immortalized cell lines. They can even model functional properties of the organ like hormone production<sup>[223,224]</sup> or generate complex 3D structures including multiple tissues and several functional units in one model.<sup>[170,372]</sup> The use of human instead of rodent cell cultures substantially decreased the uncertainties arising from species differences concerning cellular functions, cytoarchitecture, hormonal regulation, and sensitivity to internal/external stimuli or toxicants.<sup>[8,10,142,297,368]</sup> Moreover, hiPSCs-based techniques in combination with targeted genome editing enable the development of patient-specific disease models and the generation of cell type-specific transgenes in a human genetic background.<sup>[226,453,457,458]</sup> However, human iPSC technology still struggles from issues such as variability among iPSC lines,<sup>[522]</sup> genomic instability,<sup>[523]</sup> low

reprogramming efficiency,<sup>[524]</sup> which might be improved by keeping the cells under hypoxic conditions for a limited time span after reprogramming,<sup>[525]</sup> preservation of an epigenetic memory of the parental cell,<sup>[526]</sup> and difficulties in achieving a mature phenotype of iPSC-derived cells.<sup>[46]</sup> Cultivation techniques have evolved quickly in the last decade with 2D monolayer models representing the classical approach which is well established and documented by broad literature. 2D cultivation is rather inexpensive, highly reproducible, and advantageous to study specific effects of factors on the individual cell. Coculturing of different cell types increases the complexity and predictivity of the model and enables the elucidation of cell-cell interactions. However, the still limited complexity, lack of cell-ECM interactions and the insufficient representation of the complex in vivo cytoarchitecture of the respective organ, suggests limitations of the predictivity of 2D models for toxicity testing. The development of 3D organoid techniques led to models exhibiting highly complex organotypic cytoarchitectures including cell-cell and cell-ECM interactions. Organoids enable the analysis of not only molecular but also functional readouts which strengthen the methods' clinical and toxicological relevance. However, increasing complexity comes with increased batch-to-batch variability, reduced reproducibility and

decreased testing throughput. Moreover, organoid culture is technically challenging and more expensive than 2D monolayer culture. Although organoids comprise a complex organotypic cytoarchitecture, they still represent immature developmental stages of the respective organ (reviewed by Logan et al.<sup>[527]</sup>). Lack of complexity common to all organs reviewed comprises missing immune cells and blood vessels. First steps for the incorporation of microvascular structures<sup>[101,185,186]</sup> and immune cells<sup>[171,172,188,268,408]</sup> have been made. However, the complex crosstalk between organs, the involvement of the nervous, endocrine, and immunological system, as well as the impact of the blood flow and serum components are barely covered. Recent approaches are moving to the multiorgan level by tissue-on-a-chip methods enabling the evaluation of organ crosstalk in vitro.<sup>[410,444,494,498,500]</sup>

## 6. Conclusion

From a toxicological point of view, making systemic predictions based on cellular effects is challenging. Therefore, the AOP concept was developed that helps placing cellular hazards into a systemic context.<sup>[528,529]</sup> Advanced pharmaco- and toxicokinetics including computational modeling are also needed to predict internal exposure as well as in vitro kinetics combining both by IVIVE (in vitro–in vivo extrapolation).<sup>[530]</sup> Another obstacle is the necessary willingness to consider innovative methods in the field. Although it is known that the predictivity of animal studies is limited, the year-long experience conveys a feeling of security in contrast to the use of alternative approaches, which are perceived as bearing higher uncertainties due to their novelty.

## Acknowledgements

J.T. and K.K. contributed equally to this work. The authors thank Thomas Nentwich and Jakob Fritsche for the biography pictures of Ellen Fritsche and Katharina Koch, respectively. This work was supported by the project CERST (Center for Alternatives to Animal Testing) of the Ministry for culture and science of the State of North-Rhine Westphalia, Germany (File No. 233-1.08.03.03-121972/131–1.08.03.03–121972), and the European Union's Horizon 2020 Research and Innovation Program, under the Grant Agreement No. 825759 of the ENDPoiNTs project. P.R.M. was supported by the German Research Foundation (funding code 97850925, SFB 854 project A1; GRK 2408 project 8, Grant Nos. ME-1365/7-2 and ME-1365/9-2).

Open access funding enabled and organized by Projekt DEAL.

## Conflict of Interest

The authors declare no conflict of interest.

## Keywords

3R, alternative methods, high throughput, human-induced pluripotent stem cells, organoids, risk assessment

Received: October 8, 2020  
Revised: November 13, 2020  
Published online:

- [1] F. S. Collins, G. M. Gray, J. R. Bucher, *Science* **2008**, 319, 906.
- [2] National Research Council (2007), *Toxicity Testing in the 21st Century: A Vision and a Strategy*, The National Academies Press, Washington, DC **2007**
- [3] D. Krewski, M. E. Andersen, M. G. Tyshenko, K. Krishnan, T. Hartung, K. Boekelheide, J. F. Wambaugh, D. Jones, M. Whelan, R. Thomas, C. Yauk, T. Barton-Maclaren, I. Cote, *Arch. Toxicol.* **2020**, 94, 1.
- [4] L. Meigs, L. Smirnova, C. Rovida, M. Leist, T. Hartung, *ALTEX* **2018**, 35, 275.
- [5] T. Höfer, I. Gerner, U. Gundert-Remy, M. Liebsch, A. Schulte, H. Spielmann, R. Vogel, K. Wettig, *Arch. Toxicol.* **2004**, 78, 549.
- [6] K. Gassmann, J. Abel, H. Bothe, T. Haarmann-Stemmann, H. F. Merk, K. N. Quasthoff, T. D. Rockel, T. Schreiber, E. Fritsche, *Environ. Health Perspect.* **2010**, 118, 1571.
- [7] A. R. Green, M. V. King, S. E. Shortall, K. C. F. Fone, *Br. J. Pharmacol.* **2012**, 166, 1523.
- [8] A. Strasser, H. J. Wittmann, A. Buschauer, E. H. Schneider, R. Seifert, *Trends Pharmacol. Sci.* **2013**, 34, 13.
- [9] M. Clark, T. Steger-Hartmann, *Regul. Toxicol. Pharmacol.* **2018**, 96, 94.
- [10] S. Herculano-Houzel, *Brain. Behav. Evol.* **2011**, 78, 22.
- [11] A. Knight, *ALTEX* **2007**, 24, 320.
- [12] M. J. Waring, J. Arrowsmith, A. R. Leach, P. D. Leeson, S. Mandrell, R. M. Owen, G. Pairaudeau, W. D. Pennie, S. D. Pickett, J. Wang, O. Wallace, A. Weir, *Nat. Rev. Drug Discovery* **2015**, 14, 475.
- [13] I. W. Y. Mak, N. Evaniew, M. Ghert, *Am. J. Transl. Res.* **2014**, 6, 114.
- [14] M. Leist, T. Hartung, *Arch. Toxicol.* **2013**, 87, 563.
- [15] S. H. Bennekou, *EFSA J.* **2019**, 17, e170711.
- [16] A. Lanzoni, A. F. Castoldi, G. E. Kass, A. Terron, G. De Seze, A. Bal-Price, F. Y. Bois, K. B. Deldos, D. R. Doerge, E. Fritsche, T. Halldorsson, M. Kolossa-Gehring, S. Hougaard Bennekou, F. Koning, A. Lampen, M. Leist, E. Mantus, C. Rousselle, M. Siegrist, P. Steinberg, A. Tritscher, B. Van de Water, P. Vineis, N. Walker, H. Wallace, M. Whelan, M. Younes, *EFSA J.* **2019**, 17, e170712.
- [17] T. Hartung, *J. Toxicol. Environ. Health, Part B* **2010**, 13, 277.
- [18] National Academies of Sciences Engineering and Medicine, *Using 21st Century Science to Improve Risk-Related Evaluations*, National Academies Press, Washington, DC **2017**.
- [19] E. Fritsche, H. T. Hogberg, *Front. Toxicol.* **2020**, 2, 3.
- [20] J. D. Clark, *Ignition! An Informal History of Liquid Rocket Propellants*, Rutgers University Press, New Brunswick, NJ **1972**.
- [21] R. S. Thomas, M. B. Black, L. Li, E. Healy, T. M. Chu, W. Bao, M. E. Andersen, R. D. Wolfinger, *Toxicol. Sci.* **2012**, 128, 398.
- [22] W. Oehlert, *Cell Proliferation* **1973**, 6, 325.
- [23] D. Hanahan, R. A. Weinberg, *Cell* **2011**, 144, 646.
- [24] E. Fritsche, H. Alm, J. Baumann, L. Geerts, H. Hakansson, S. Masjosthusmann, H. Witters, *EFSA Support. Publ.* **2015**, 12, 186.
- [25] S. Masjosthusmann, M. Barenys, M. El-Gamal, L. Geerts, L. Gerosa, A. Gorreja, B. Kühne, N. Marchetti, J. Tigges, B. Viviani, H. Witters, E. Fritsche, *EFSA Support. Publ.* **2018**, 15, 125.
- [26] M. Barenys, E. Fritsche, *Toxicol. Sci.* **2018**, 165, 10.
- [27] K. Takahashi, K. Tanabe, M. Ohnuki, M. Narita, T. Ichisaka, K. Tomoda, S. Yamanaka, *Cell* **2007**, 131, 861.
- [28] G. N. Stacey, *Stem Cell Rev. Rep.* **2009**, 5, 301.
- [29] J. Munoz, T. Y. Low, Y. J. Kok, A. Chin, C. K. Frese, V. Ding, A. Choo, A. J. R. Heck, *Mol. Syst. Biol.* **2011**, 7, 550.
- [30] D. H. Phanstiel, J. Brumbaugh, C. D. Wenger, S. Tian, M. D. Probasco, D. J. Bailey, D. L. Swaney, M. A. Tervo, J. M. Bolin, V. Ruotti, R. Stewart, J. A. Thomson, J. J. Coon, *Nat. Methods* **2011**, 8, 821.
- [31] R. S. Lindoso, T. H. Kasai-Brunswick, G. Monnerat Cahli, F. Collino, A. Bastos Carvalho, A. C. Campos de Carvalho, A. Vieyra, *Cells* **2019**, 8, 703.
- [32] Y. Du, J. Wang, J. Jia, N. Song, C. Xiang, J. Xu, Z. Hou, X. Su, B. Liu, T. Jiang, D. Zhao, Y. Sun, J. Shu, Q. Guo, M. Yin, D. Sun, S. Lu, Y. Shi, H. Deng, *Cell Stem Cell* **2014**, 14, 394.

- [33] B. Hanger, A. Couch, L. Rajendran, D. P. Srivastava, A. C. Vernon, *Front. Psychiatry* **2020**, *11*, 789.
- [34] T. A. Juopperi, W. R. Kim, C. H. Chiang, H. Yu, R. L. Margolis, C. A. Ross, G. L. Ming, H. Song, *Mol. Brain* **2012**, *5*, 17.
- [35] M. A. Cayo, J. Cai, A. Delaforest, F. K. Noto, M. Nagaoka, B. S. Clark, R. F. Coltery, K. Si-Tayeb, S. A. Duncan, *Hepatology* **2012**, *56*, 2163.
- [36] M. A. Lancaster, M. Renner, C. A. Martin, D. Wenzel, L. S. Bicknell, M. E. Hurler, T. Homfray, J. M. Penninger, A. P. Jackson, J. A. Knoblich, *Nature* **2013**, *501*, 373.
- [37] T. Takahashi, *Annu. Rev. Pharmacol. Toxicol.* **2019**, *59*, 447.
- [38] C. Olgasi, A. Cucci, A. Follenzi, *Int. J. Mol. Sci.* **2020**, *21*, 6215.
- [39] P. de Carvalho Ribeiro, L. F. Oliveira, M. A. Filho, H. C. Caldas, *Stem Cells Int.* **2020**, *2020*, 8894590.
- [40] J. Augustyniak, A. Bertero, T. Coccini, D. Baderna, L. Buzanska, F. Caloni, *J. Appl. Toxicol.* **2019**, *39*, 1610.
- [41] M. Rauma, A. Boman, G. Johanson, *Adv. Drug Delivery Rev.* **2013**, *65*, 306.
- [42] K. M. Albers, B. M. Davis, *Neuroscientist* **2007**, *13*, 371.
- [43] A. A. H. Deniz, E. A. Abdik, H. Abdik, S. Aydın, F. Şahin, P. N. Taşlı, *Adv. Exp. Med. Biol.* **2020**, *1247*, 157.
- [44] F. Oesch, E. Fabian, R. Landsiedel, *Arch. Toxicol.* **2018**, *92*, 2411.
- [45] M. Gaur, M. Dobke, V. V. Lunyak, *Int. J. Mol. Sci.* **2017**, *18*, 208.
- [46] N. Alépée, A. Bahinski, M. Daneshian, B. De Wever, E. Fritsche, A. Goldberg, J. Hansmann, T. Hartung, J. Haycock, H. T. Hogberg, L. Hoelting, J. M. Kelm, S. Kadereit, E. McVey, R. Landsiedel, M. Leist, M. Lübberstedt, F. Noor, C. Pellevoisin, D. Petersohn, U. Pfannenbecker, K. Reisinger, T. Ramirez, B. Rothen-Rutishauser, M. Schäfer-Korting, K. Zeilinger, M. G. Zurich, *ALTEX* **2018**, *31*, 441.
- [47] C. Riebeling, A. Luch, T. Tralau, *Exp. Dermatol.* **2018**, *27*, 526.
- [48] H. Niehues, J. A. Bouwstra, A. El Ghalbzouri, J. M. Brandner, P. L. J. M. Zeeuwen, E. H. van den Bogaard, *Exp. Dermatol.* **2018**, *27*, 501.
- [49] S. H. Mathes, H. Ruffner, U. Graf-Hausner, *Adv. Drug Delivery Rev.* **2014**, *69–70*, 81.
- [50] C. S. Pridgeon, C. Schlott, M. W. Wong, M. B. Heringa, T. Heckel, J. Leedale, L. Launay, V. Gryshkova, S. Przyborski, R. N. Bearon, E. L. Wilkinson, T. Ansari, J. Greenman, D. F. G. Hendriks, S. Gibbs, J. Sidaway, R. L. Sison-Young, P. Walker, M. J. Cross, B. K. Park, C. E. P. Goldring, *Arch. Toxicol.* **2018**, *92*, 557.
- [51] Council of the European Union and the European Parliament, Directive 2003/15/EC of the European Parliament and of the Council of 27 February 2003 Amending Council Directive 76/768/EEC on the Approximation of the Laws of the Member States Relating to Cosmetic Products, **2003**.
- [52] OECD (2020), Test No. 471: *Bacterial Reverse Mutation Test*, OECD Publishing, Paris **2020**.
- [53] OECD (1997), Test No. 476: *In Vitro Mammalian Cell Gene Mutation Test*, OECD Publishing, Paris **1997**.
- [54] OECD (2016), Test No. 473: *In Vitro Mammalian Chromosomal Aberration Test*, OECD Publishing, Paris **2016**.
- [55] G. Ates, T. Y. Doktorova, M. Pauwels, V. Rogiers, *Mutagenesis* **2014**, *29*, 115.
- [56] D. Kirkland, M. Aardema, L. Henderson, L. Müller, *Mutat. Res., Genet. Toxicol. Environ. Mutagen.* **2005**, *584*, 1.
- [57] D. Kirkland, M. Aardema, L. Müller, M. Hayashi, *Mutat. Res., Genet. Toxicol. Environ. Mutagen.* **2006**, *608*, 29.
- [58] E. J. Matthews, N. L. Kruhlak, M. C. Cimino, R. D. Benz, J. F. Contrera, *Regul. Toxicol. Pharmacol.* **2006**, *44*, 83.
- [59] E. J. Matthews, N. L. Kruhlak, M. C. Cimino, R. D. Benz, J. F. Contrera, *Regul. Toxicol. Pharmacol.* **2006**, *44*, 97.
- [60] V. Rogiers, M. Pauwels, *Curr. Probl. Dermatol.* **2008**, *36*, 129.
- [61] V. Rogiers, M. Pauwels, *Curr. Probl. Dermatol.* **2008**, *36*, XVII.
- [62] V. Rogiers, M. Pauwels, *Curr. Probl. Dermatol.* **2008**, *36*, 58.
- [63] V. Rogiers, M. Pauwels, *Curr. Probl. Dermatol.* **2008**, *36*, 1.
- [64] V. Rogiers, M. Pauwels, *Curr. Probl. Dermatol.* **2008**, *36*, 29.
- [65] G. Speit, *Mutat. Res., Genet. Toxicol. Environ. Mutagen.* **2009**, *678*, 108.
- [66] EU SCHER/SCENIHR/SCCP, Risk Assessment Methodologies and Approaches for Genotoxic and Carcinogenic Substances, **2009**.
- [67] P. Fowler, R. Smith, K. Smith, J. Young, L. Jeffrey, D. Kirkland, S. Pfuhrer, P. Carmichael, *Mutat. Res., Genet. Toxicol. Environ. Mutagen.* **2012**, *747*, 104.
- [68] P. Fowler, R. Smith, K. Smith, J. Young, L. Jeffrey, P. Carmichael, D. Kirkland, S. Pfuhrer, *Mutat. Res., Genet. Toxicol. Environ. Mutagen.* **2014**, *767*, 28.
- [69] D. Kirkland, S. Pfuhrer, D. Tweats, M. Aardema, R. Corvi, F. Darroudi, A. Elhajouji, H. Glatt, P. Hastwell, M. Hayashi, P. Kasper, S. Kirchner, A. Lynch, D. Marzin, D. Maurici, J. R. Meunier, L. Müller, G. Nohynek, J. Parry, E. Parry, V. Thybaud, R. Tice, J. van Benthem, P. Vanparys, P. White, *Mutat. Res., Genet. Toxicol. Environ. Mutagen.* **2007**, *628*, 31.
- [70] D. Kirkland, L. Reeve, D. Gatehouse, P. Vanparys, *Mutat. Res., Genet. Toxicol. Environ. Mutagen.* **2011**, *721*, 27.
- [71] S. Pfuhrer, A. Kirst, M. Aardema, N. Banduhn, C. Goebel, D. Araki, M. Costabel-Farkas, E. Dufour, R. Fautz, J. Harvey, N. J. Hewitt, J. Hibatallah, P. Carmichael, M. Macfarlane, K. Reisinger, J. Rowland, F. Schelllauf, A. Schepky, J. Scheel, *Regul. Toxicol. Pharmacol.* **2010**, *57*, 315.
- [72] S. Pfuhrer, M. Fellows, J. Van Benthem, R. Corvi, R. Curren, K. Dearfield, P. Fowler, R. Frötschl, A. Elhajouji, L. Le Hégarat, T. Kasamatsu, H. Kojima, G. Ouédraogo, A. Scott, G. Speit, *Mutat. Res., Genet. Toxicol. Environ. Mutagen.* **2011**, *723*, 101.
- [73] T. Y. Doktorova, M. Pauwels, M. Vinken, T. Vanhaecke, V. Rogiers, *Crit. Rev. Toxicol.* **2012**, *42*, 91.
- [74] T. Y. Doktorova, G. Ates, M. Vinken, T. Vanhaecke, V. Rogiers, *T. Vitro* **2014**, *28*, 54.
- [75] P. Vanparys, R. Corvi, M. J. Aardema, L. Gribaldo, M. Hayashi, S. Hoffmann, L. Schechtman, *Mutat. Res., Genet. Toxicol. Environ. Mutagen.* **2012**, *744*, 111.
- [76] OECD (2004), Test No. 428: *Skin Absorption: In Vitro Method*, OECD Publishing, Paris **2004**.
- [77] OECD (2018), Test No. 442D: *In Vitro Skin Sensitisation: ARE-Nrf2 Luciferase Test Method*, OECD Publishing, Paris **2018**.
- [78] OECD (2016), Test No. 442E: *In Vitro Skin Sensitisation*, OECD Publishing, Paris **2016**.
- [79] OECD (2013), Test No. 431: *In Vitro Skin Corrosion: Reconstructed Human Epidermis (RHE) Test Method*, OECD Publishing, Paris **2013**.
- [80] OECD (2019), Test No. 439: *In Vitro Skin Irritation: Reconstructed Human Epidermis Test Method*, OECD Guidelines for the Testing of Chemicals, Section 4, OECD Publishing, Paris **2019**.
- [81] A. Almeida, B. Sarmento, F. Rodrigues, *Int. J. Pharm.* **2017**, *519*, 178.
- [82] C. Götz, R. Pfeiffer, J. Tigges, P. Blatz, C. Jäckh, E. M. Freytag, E. Fabian, R. Landsiedel, H. F. Merk, J. Krutmann, R. J. Edwards, C. Pease, C. Goebel, N. Hewitt, E. Fritsche, *Exp. Dermatol.* **2012**, *21*, 358.
- [83] B. Sarmento, F. Andrade, S. B. Da Silva, F. Rodrigues, J. Das Neves, D. Ferreira, *Expert Opin. Drug Metab. Toxicol.* **2012**, *8*, 607.
- [84] S. Gordon, M. Daneshian, J. Bouwstra, F. Caloni, S. Constant, D. E. Davies, G. Dandekar, C. A. Guzman, E. Fabian, E. Haltner, T. Hartung, N. Hasiwa, P. Hayden, H. Kandarova, S. Khare, H. F. Krug, C. Kneuer, M. Leist, G. Lian, U. Marx, M. Metzger, K. Ott, P. Prieto, M. S. Roberts, E. L. Roggen, T. Tralau, C. Van Den Braak, H. Walles, C. M. Lehr, *ALTEX* **2015**, *32*, 327.
- [85] C. Duval, C. Chagnoleau, F. Pouradier, P. Sextius, E. Condom, F. Bernerd, *Tissue Eng., Part C* **2012**, *18*, 947.
- [86] I. J. Kosten, S. W. Spiekstra, T. D. de Gruijl, S. Gibbs, *Toxicol. Appl. Pharmacol.* **2015**, *287*, 35.
- [87] D. Y. S. Chau, C. Johnson, S. Macneil, J. W. Haycock, A. M. Ghaemmaghami, *Biofabrication* **2013**, *5*, 035011.

- [88] P. L. Tremblay, F. Berthod, L. Germain, F. A. Auger, *J. Pharmacol. Exp. Ther.* **2005**, 315, 510.
- [89] M. Matsusaki, K. Fujimoto, Y. Shirakata, S. Hirakawa, K. Hashimoto, M. Akashi, *J. Biomed. Mater. Res., Part A* **2015**, 103, 3386.
- [90] T. Akagi, M. Nagura, A. Hiura, H. Kojima, M. Akashi, *Tissue Eng., Part A* **2017**, 23, 481.
- [91] S. Huang, Y. Xu, C. Wu, D. Sha, X. Fu, *Biomaterials* **2010**, 31, 5520.
- [92] M. Michel, N. L'Heureux, R. Pouliot, W. Xu, F. A. Auger, L. Germain, *In Vitro Cell. Dev. Biol.: Anim.* **1999**, 35, 318.
- [93] S. Lönnqvist, K. Briheim, G. Kratz, *Toxicol. Mech. Methods* **2016**, 26, 82.
- [94] A. Petrova, A. Celli, L. Jacquet, D. Dafou, D. Crumrine, M. Hupe, M. Arno, C. Hobbs, A. Cvor, P. Karagiannis, L. Devito, R. Sun, L. C. Adame, R. Vaughan, J. A. McGrath, T. M. Mauro, D. Ilic, *Stem Cell Rep.* **2014**, 2, 675.
- [95] H. E. Abaci, Z. Guo, Y. Doucet, J. Jacków, A. Christiano, *Exp. Biol. Med.* **2017**, 242, 1657.
- [96] M. Itoh, M. Kiuru, M. S. Cairo, A. M. Christiano, *Proc. Natl. Acad. Sci. USA* **2011**, 108, 8797.
- [97] M. Itoh, N. Umegaki-Arao, Z. Guo, L. Liu, C. A. Higgins, A. M. Christiano, *PLoS One* **2013**, 8, 77673.
- [98] N. Umegaki-Arao, A. M. G. Pasmooij, M. Itoh, J. E. Cerise, Z. Guo, B. Levy, A. Gostyrski, L. R. Rothman, M. F. Jonkman, A. M. Christiano, *Sci. Transl. Med.* **2014**, 6, 264ra164.
- [99] K. Gledhill, Z. Guo, N. Umegaki-Arao, C. A. Higgins, M. Itoh, A. M. Christiano, *PLoS One* **2015**, 10, 0136713.
- [100] Y. Kim, N. Park, Y. A. Rim, Y. Nam, H. Jung, K. Lee, J. H. Ju, *Stem Cell Res. Ther.* **2018**, 9, 217.
- [101] H. E. Abaci, Z. Guo, A. Coffman, B. Gillette, W. Lee, S. K. Sia, A. M. Christiano, *Adv. Healthcare Mater.* **2016**, 5, 1800.
- [102] Y. Li, M. Liu, S.-T. Yang, *World J. Stem Cells* **2014**, 6, 1.
- [103] Y. Li, T. Ma, *J. Hematol. Malign.* **2011**, 1, 35.
- [104] A. Pupovac, B. Senturk, C. Griffoni, K. Maniura-Weber, M. Rottmar, S. L. McArthur, *Adv. Healthcare Mater.* **2018**, 7, 1701405.
- [105] A. Thélou, S. Catoire, S. Kerdine-Römer, *Toxicol. In Vitro* **2020**, 62, 104691.
- [106] J. Lee, C. C. Rabbani, H. Gao, M. R. Steinhart, B. M. Woodruff, Z. E. Pflum, A. Kim, S. Heller, Y. Liu, T. Z. Shipchandler, K. R. Koehler, *Nature* **2020**, 582, 399.
- [107] V. S. Thakoersing, G. S. Gooris, A. Mulder, M. Rietveld, A. E. I. Ghalbzouri, J. A. Bouwstra, *Tissue Eng., Part C* **2012**, 18, 1.
- [108] S. Schreiber, A. Mahmoud, A. Vuia, M. K. Rübhelke, E. Schmidt, M. Schaller, H. Kandırová, A. Haberland, U. F. Schäfer, U. Bock, H. C. Korting, M. Liebsch, M. Schäfer-Korting, *Toxicol. In Vitro* **2005**, 19, 813.
- [109] F. P. Schmook, J. G. Meingassner, A. Billich, *Int. J. Pharm.* **2001**, 215, 51.
- [110] R. Koh, I. Szeverényi, B. Lee, S. L. I. J. Denil, S. Y. J. Lim, P. A. Benny, N. Grasset, B. K. Tan, E. B. Lane, *J. Invest. Dermatol.* **2020**, 140, 235.
- [111] A. Carreau, B. E. I. Hafny-Rahbi, A. Matejuk, C. Grillon, C. Kieda, *J. Cell. Mol. Med.* **2011**, 15, 1239.
- [112] W. Wang, C. P. Winlove, C. C. Michel, *J. Physiol.* **2003**, 549, 855.
- [113] K. R. Rivera, M. A. Yokus, P. D. Erb, V. A. Pozdin, M. Daniele, *Analyst* **2019**, 144, 3190.
- [114] A. Mieremet, A. Vázquez García, W. Boiten, R. van Dijk, G. Gooris, J. A. Bouwstra, A. El Ghalbzouri, *Sci. Rep.* **2019**, 9, 7811.
- [115] E. Fröhlich, E. Roblegg, *Toxicology* **2012**, 291, 10.
- [116] G. R. Betton, *Cell Biol. Toxicol.* **2013**, 29, 321.
- [117] OECD (2002), *Test No. 420: Acute Oral Toxicity – Fixed Dose Procedure*, OECD Publishing, Paris **2002**.
- [118] OECD (2002), *Test No. 423: Acute Oral Toxicity – Acute Toxic Class Method*, OECD Publishing, Paris **2002**.
- [119] OECD (2008), *Test No. 425: Acute Oral Toxicity: Up-and-Down Procedure*, OECD Publishing, Paris **2008**.
- [120] OECD (2008), *Test No. 407: Repeated Dose 28-Day Oral Toxicity Study in Rodents*, OECD Publishing, Paris **2008**.
- [121] OECD (2018), *Test No. 408: Repeated Dose 90-Day Oral Toxicity Study in Rodents*, OECD Publishing, Paris **2018**.
- [122] A. Rodríguez-Lara, M. D. Mesa, J. Aragón-Vela, R. A. Casuso, C. C. Vázquez, J. M. Zúñiga, J. R. Huertas, *Nutrients* **2019**, 11, 2133.
- [123] J. N. Norton, L. A. Rylander, J. L. Richards, *Toxicol. In Vitro* **1995**, 9, 67.
- [124] M. Klausner, S. Ayejunie, B. A. Breyfogle, P. W. Wertz, L. Bacca, J. Kubilus, *Toxicol. In Vitro* **2007**, 21, 938.
- [125] F. Zanetti, A. Sewer, C. Mathis, A. R. Iskandar, R. Kostadinova, W. K. Schlage, P. Leroy, S. Majeed, E. Guedj, K. Trivedi, F. Martin, A. Elamin, C. Merg, N. V. Ivanov, S. Frenzel, M. C. Peitsch, J. Hoeng, *Chem. Res. Toxicol.* **2016**, 29, 1252.
- [126] L. Pindáková, V. Kašpárková, K. Kejlová, M. Dvořáková, D. Krsek, D. Jírová, L. Kašparová, *Int. J. Pharm.* **2017**, 527, 12.
- [127] A. Dongari-Bagtzoglou, H. Kashleva, *Nat. Protoc.* **2006**, 1, 2012.
- [128] K. Moharamzadeh, I. M. Brook, A. M. Scutt, M. H. Thornhill, R. Van Noort, *J. Dent.* **2008**, 36, 331.
- [129] M. B. Kautsky, P. Fleckman, B. A. Dale, *J. Invest. Dermatol.* **1995**, 104, 224.
- [130] D. G. Nguyen, S. L. Pentoney, *Drug Discovery Today Technol.* **2017**, 23, 37.
- [131] T. Kumamoto, C. Hanashima, *Neurosci. Res.* **2014**, 86, 37.
- [132] S. M. G. Braun, S. Jessberger, *Development* **2014**, 141, 1983.
- [133] P. S. Eriksson, E. Perfilieva, T. Björk-Eriksson, A. M. Alborn, C. Nordborg, D. A. Peterson, F. H. Gage, *Nat. Med.* **1998**, 4, 1313.
- [134] A. Aranda-Anzaldo, *Commun. Integr. Biol.* **2012**, 5, 134.
- [135] C. S. von Bartheld, J. Bahney, S. Herculano-Houzel, *J. Comp. Neurol.* **2016**, 524, 3865.
- [136] K. A. Nave, H. B. Werner, *Annu. Rev. Cell Dev. Biol.* **2014**, 30, 503.
- [137] L. Ben Haim, D. H. Rowitch, *Nat. Rev. Neurosci.* **2016**, 18, 31.
- [138] D. Nayak, T. L. Roth, D. B. McGavern, *Annu. Rev. Immunol.* **2014**, 32, 367.
- [139] W. Zheng, *J. Toxicol., Clin. Toxicol.* **2001**, 39, 711.
- [140] S. Weis, A. Büttner, in *Handbook of Clinical Neurology*, Elsevier B.V., Amsterdam **2018**, pp. 181–192.
- [141] N. A. Oberheim, T. Takano, X. Han, W. He, J. H. C. Lin, F. Wang, Q. Xu, J. D. Wyatt, W. Pilcher, J. G. Ojemann, B. R. Ransom, S. A. Goldman, M. Nedergaard, *J. Neurosci.* **2009**, 29, 3276.
- [142] J. DeFelipe, L. Alonso-Nanclares, J. I. Arellano, *J. Neurocytol.* **2002**, 31, 299.
- [143] M. Schmidt, B. Raghavan, V. Müller, T. Vogl, G. Fejer, S. Tchaptchet, S. Keck, C. Kalis, P. J. Nielsen, C. Galanos, J. Roth, A. Skerra, S. F. Martin, M. A. Freudenberg, M. Goebeler, *Nat. Immunol.* **2010**, 11, 814.
- [144] K. Dach, F. Bendt, U. Huebenthal, S. Giersiefer, P. J. Lein, H. Heuer, E. Fritsche, *Sci. Rep.* **2017**, 7, 44861.
- [145] J. Klose, J. Tigges, S. Masjosthusmann, K. Schmuck, F. Bendt, U. Huebenthal, P. Petzsch, K. Köhrer, K. Koch, E. Fritsche, *ALTEX* **2020**, DOI 10.14573/altex.2007201.
- [146] S. C. Zhang, M. Wernig, I. D. Duncan, O. Brüstle, J. A. Thomson, *Nat. Biotechnol.* **2001**, 19, 1129.
- [147] H. J. Rhee, A. H. Shaib, K. Rehbach, C. K. Lee, P. Seif, C. Thomas, E. Gideons, A. Guenther, T. Krutenko, M. Heibisch, M. Peitz, N. Brose, O. Brüstle, J. S. Rhee, *Cell Rep.* **2019**, 27, 2212.
- [148] Y. Shi, P. Kirwan, F. J. Livesey, *Nat. Protoc.* **2012**, 7, 1836.
- [149] R. Nehme, E. Zuccaro, S. D. Ghosh, C. Li, J. L. Sherwood, O. Pietilainen, L. E. Barrett, F. Limone, K. A. Worringer, S. Kommineni, Y. Zang, D. Cacchiarelli, A. Meissner, R. Adolfsson, S. Haggarty, J. Madison, M. Muller, P. Arolla, Z. Fu, G. Feng, K. Eggan, *Cell Rep.* **2018**, 23, 2509.
- [150] M. Frega, S. H. C. Van Gestel, K. Linda, J. Van Der Raadt, J. Keller, J. R. Van Rhijn, D. Schubert, C. A. Albers, N. N. Kasri, *J. Vis. Exp.* **2017**, 8, 54900.

- [151] N. Yang, S. Chanda, S. Marro, Y. H. Ng, J. A. Janas, D. Haag, C. E. Ang, Y. Tang, Q. Flores, M. Mall, O. Wapinski, M. Li, H. Ahlenius, J. L. Rubenstein, H. Y. Chang, A. A. Buylla, T. C. Südhof, M. Wernig, *Nat. Methods* **2017**, *14*, 621.
- [152] S. M. Chambers, C. A. Fasano, E. P. Papapetrou, M. Tomishima, M. Sadelain, L. Studer, *Nat. Biotechnol.* **2009**, *27*, 275.
- [153] L. Nimtz, J. Hartmann, J. Tigges, S. Masjosthusmann, M. Schmuck, E. Keßel, S. Theiss, K. Köhler, P. Petzsch, J. Adjaye, C. Wigmann, D. Wiczorek, B. Hildebrandt, F. Bendt, U. Hübenthal, G. Brockerhoff, E. Fritsche, *Stem Cell Res.* **2020**, *45*, 101761.
- [154] M. Hofrichter, L. Nimtz, J. Tigges, Y. Kabiri, F. Schröter, B. Royer-Pokora, B. Hildebrandt, M. Schmuck, A. Epanchintsev, S. Theiss, J. Adjaye, J. M. Egly, J. Krutmann, E. Fritsche, *Stem Cell Res.* **2017**, *25*, 72.
- [155] B. Y. Hu, J. P. Weick, J. Yu, L. X. Ma, X. Q. Zhang, J. A. Thomson, S. C. Zhang, *Proc. Natl. Acad. Sci. USA* **2010**, *107*, 4335.
- [156] J. A. Harrill, T. Freudenrich, K. Wallace, K. Ball, T. J. Shafer, W. R. Mundy, *Toxicol. Appl. Pharmacol.* **2018**, *354*, 24.
- [157] E. Rempel, L. Hoelting, T. Waldmann, N. V. Balmer, S. Schildknecht, M. Grinberg, J. A. Das Gaspar, V. Shinde, R. Stöber, R. Marchan, C. van Thriel, J. Liebing, J. Meisig, N. Blüthgen, A. Sachinidis, J. Rahnenführer, J. G. Hengstler, M. Leist, *Arch. Toxicol.* **2015**, *89*, 1599.
- [158] V. Shinde, S. Klima, P. S. Sureshkumar, K. Meganathan, S. Jagtap, E. Rempel, J. Rahnenführer, J. G. Hengstler, T. Waldmann, J. Hescheler, M. Leist, A. Sachinidis, *J. Vis. Exp.* **2015**, 52333.
- [159] N. V. Balmer, M. K. Weng, B. Zimmer, V. N. Ivanova, S. M. Chambers, E. Nikolaeva, S. Jagtap, A. Sachinidis, J. Hescheler, T. Waldmann, M. Leist, *Hum. Mol. Genet.* **2012**, *21*, 4104.
- [160] F. Pistollato, J. Louise, B. Scelfo, M. Mennecozzi, B. Accordi, G. Basso, J. A. Gaspar, D. Zagoura, M. Barilari, T. Palosaari, A. Sachinidis, S. Bremer-Hoffmann, *Toxicol. Appl. Pharmacol.* **2014**, *280*, 378.
- [161] S. Masjosthusmann, C. Siebert, U. Hübenthal, F. Bendt, J. Baumann, E. Fritsche, *Chemosphere* **2019**, *235*, 447.
- [162] M. Barenys, K. Gassmann, C. Baksmeier, S. Heinz, I. Reverte, M. Schmuck, T. Temme, F. Bendt, T. C. Zschauer, T. D. Rockel, K. Unfried, W. Wätjen, S. M. Sundaram, H. Heuer, M. T. Colomina, E. Fritsche, *Arch. Toxicol.* **2017**, *91*, 827.
- [163] K. Gassmann, T. Schreiber, M. M. L. Dingemans, G. Krause, C. Roderigo, S. Giersiefer, J. Schuwald, M. Moors, K. Unfried, Å. Bergman, R. H. S. Westerink, C. R. Rose, E. Fritsche, *Arch. Toxicol.* **2014**, *88*, 1537.
- [164] M. S. Wilson, J. R. Graham, A. J. Ball, *Neurotoxicology* **2014**, *42*, 33.
- [165] M. A. Lancaster, N. S. Corsini, S. Wolfinger, E. H. Gustafson, A. W. Phillips, T. R. Burkard, T. Otani, F. J. Livesey, J. A. Knoblich, *Nat. Biotechnol.* **2017**, *35*, 659.
- [166] A. M. Pasca, S. A. Sloan, L. E. Clarke, Y. Tian, C. D. Makinson, N. Huber, C. H. Kim, J. Y. Park, N. A. O'Rourke, K. D. Nguyen, S. J. Smith, J. R. Huguenard, D. H. Geschwind, B. A. Barres, S. P. Pasca, *Nat. Methods* **2015**, *12*, 671.
- [167] X. Qian, H. N. Nguyen, M. M. Song, C. Hadiono, S. C. Ogden, C. Hammack, B. Yao, G. R. Hamersky, F. Jacob, C. Zhong, K. J. Yoon, W. Jeang, L. Lin, Y. Li, J. Thakor, D. A. Berg, C. Zhang, E. Kang, M. Chickering, D. Nauen, C. Y. Ho, Z. Wen, K. M. Christian, P. Y. Shi, B. J. Maher, H. Wu, P. Jin, H. Tang, H. Song, G. L. Ming, *Cell* **2016**, *165*, 1238.
- [168] C. Luo, M. A. Lancaster, R. Castanon, J. R. Nery, J. A. Knoblich, J. R. Ecker, *Cell Rep.* **2016**, *17*, 3369.
- [169] A. López-Tobón, C. E. Villa, C. Cheroni, S. Trattaro, N. Caporale, P. Conforti, R. Iennaco, M. Lachgar, M. T. Rigoli, B. Marcó de la Cruz, P. Lo Riso, E. Tenderini, F. Troglia, M. De Simone, I. Liste-Noya, G. Macino, M. Pagani, E. Cattaneo, G. Testa, *Stem Cell Rep.* **2019**, *13*, 847.
- [170] J. A. Bagley, D. Reumann, S. Bian, J. Lévi-Strauss, J. A. Knoblich, *Nat. Methods* **2017**, *14*, 743.
- [171] C. M. Abreu, L. Gama, S. Krasemann, M. Chesnut, S. Odwin-Dacosta, H. T. Hogberg, T. Hartung, D. Pamies, *Front. Microbiol.* **2018**, *9*, 2766.
- [172] M. Brüll, A. S. Spreng, S. Gutbier, D. Loser, A. Krebs, M. Reich, U. Kraushaar, M. Britschgi, C. Patsch, M. Leist, *ALTEX* **2020**, *37*, 409.
- [173] J. Muffat, Y. Li, B. Yuan, M. Mitalipova, A. Omer, S. Corcoran, G. Bakiasi, L. H. Tsai, P. Aubourg, R. M. Ransohoff, R. Jaenisch, *Nat. Med.* **2016**, *22*, 1358.
- [174] G. Quadrato, T. Nguyen, E. Z. Macosko, J. L. Sherwood, S. M. Yang, D. R. Berger, N. Maria, J. Scholvin, M. Goldman, J. P. Kinney, E. S. Boyden, J. W. Lichtman, Z. M. Williams, S. A. McCarroll, P. Arlotta, *Nature* **2017**, *545*, 48.
- [175] T. K. Matsui, M. Matsubayashi, Y. M. Sakaguchi, R. K. Hayashi, C. Zheng, K. Sugie, M. Hasegawa, T. Nakagawa, E. Mori, *Neurosci. Lett.* **2018**, *670*, 75.
- [176] D. Pamies, P. Barreras, K. Block, G. Makri, A. Kumar, D. Wiersma, L. Smirnova, C. Zhang, J. Bressler, K. M. Christian, G. Harris, G. L. Ming, C. J. Berlinicke, K. Kyro, H. Song, C. A. Pardo, T. Hartung, H. T. Hogberg, *ALTEX* **2017**, *34*, 362.
- [177] R. M. Marton, Y. Miura, S. A. Sloan, Q. Li, O. Revah, R. J. Levy, J. R. Huguenard, S. P. Pasca, *Nat. Neurosci.* **2019**, *22*, 484.
- [178] G. Quadrato, P. Arlotta, *Curr. Opin. Cell Biol.* **2017**, *49*, 47.
- [179] O. Sirenko, F. Parham, S. Dea, N. Sodhi, S. Biesmans, S. Mora-Castilla, K. Ryan, M. Behl, G. Chandy, C. Crittenden, S. Vargas-Hurlston, O. Guicherit, R. Gordon, F. Zanella, C. Carromeu, *Toxicol. Sci.* **2019**, *167*, 249.
- [180] L. Hoelting, B. Scheinhardt, O. Bondarenko, S. Schildknecht, M. Kapitza, V. Tanavde, B. Tan, Q. Y. Lee, S. Mecking, M. Leist, S. Kadereit, *Arch. Toxicol.* **2013**, *87*, 721.
- [181] L. Smirnova, G. Harris, J. Delp, M. Valadares, D. Pamies, H. T. Hogberg, T. Waldmann, M. Leist, T. Hartung, *Arch. Toxicol.* **2016**, *90*, 2725.
- [182] D. Pamies, K. Block, P. Lau, L. Gribaldo, C. A. Pardo, P. Barreras, L. Smirnova, D. Wiersma, L. Zhao, G. Harris, T. Hartung, H. T. Hogberg, *Toxicol. Appl. Pharmacol.* **2018**, *354*, 101.
- [183] J. Sandström, E. Eggermann, I. Charvet, A. Roux, N. Toni, C. Greggio, A. Broyer, F. Monnet-Tschudi, L. Stoppini, *Toxicol. In Vitro* **2017**, *38*, 124.
- [184] M. P. Schwartz, Z. Hou, N. E. Propson, J. Zhang, C. J. Engstrom, V. S. Costa, P. Jiang, B. K. Nguyen, J. M. Bolin, W. Daly, Y. Wang, R. Stewart, C. D. Page, W. L. Murphy, J. A. Thomson, *Proc. Natl. Acad. Sci. USA* **2015**, *112*, 12516.
- [185] B. Cakir, Y. Xiang, Y. Tanaka, M. H. Kural, M. Parent, Y. J. Kang, K. Chapeton, B. Patterson, Y. Yuan, C. S. He, M. S. B. Raredon, J. Dengelegi, K. Y. Kim, P. Sun, M. Zhong, S. Lee, P. Patra, F. Hyder, L. E. Niklason, S. H. Lee, Y. S. Yoon, I. H. Park, *Nat. Methods* **2019**, *16*, 1169.
- [186] M. T. Pham, K. M. Pollock, M. D. Rose, W. A. Cary, H. R. Stewart, P. Zhou, J. A. Nolte, B. Waldau, *Neuroreport* **2018**, *29*, 588.
- [187] C. F. Cho, J. M. Wolfe, C. M. Fadzen, D. Calligaris, K. Hornburg, E. A. Chiocca, N. Y. R. Agar, B. L. Pentelute, S. E. Lawler, *Nat. Commun.* **2017**, *8*, 15623.
- [188] G. Nzou, R. T. Wicks, E. E. Wicks, S. A. Seale, C. H. Sane, A. Chen, S. V. Murphy, J. D. Jackson, A. J. Atala, *Sci. Rep.* **2018**, *8*, 7413.
- [189] G. Adriani, D. Ma, A. Pavesi, R. D. Kamm, E. L. K. Goh, *Lab Chip* **2017**, *17*, 448.
- [190] M. Campisi, Y. Shin, T. Osaki, C. Hajal, V. Chiono, R. D. Kamm, *Biomaterials* **2018**, *180*, 117.
- [191] Y. I. Wang, H. E. Abaci, M. L. Shuler, *Biotechnol. Bioeng.* **2017**, *114*, 184.
- [192] S. R. Horman, C. Hogan, K. D. Reyes, F. Lo, C. Antczak, *Future Med. Chem.* **2015**, *7*, 513.

- [193] R. I. Dmitriev, A. V. Zhdanov, Y. M. Nolan, D. B. Papkovsky, *Biomaterials* **2013**, *34*, 9307.
- [194] K. R. Ryan, O. Sirenko, F. Parham, J. H. Hsieh, E. F. Cromwell, R. R. Tice, M. Behl, *Neurotoxicology* **2016**, *53*, 271.
- [195] A. M. Tukker, R. G. D. M. van Kleef, F. M. J. Wijnolts, A. de Groot, R. H. S. Westerink, *ALTEX* **2020**, *37*, 121.
- [196] R. Mullur, Y. Y. Liu, G. A. Brent, *Physiol. Rev.* **2014**, *94*, 355.
- [197] S. Horn, H. Heuer, *Mol. Cell. Endocrinol.* **2010**, *315*, 19.
- [198] A. T. J. Murk, E. Rijntjes, B. J. Blaauboer, R. Clewell, K. M. Crofton, M. M. L. Dingemans, J. D. Furlow, R. Kavlock, J. Köhrle, R. Opitz, T. Traas, T. J. Visser, M. Xia, A. C. Gutleb, *Toxicol. In Vitro* **2013**, *27*, 1320.
- [199] H. J. Steinfeldt, P. Hauser, Y. Nakayama, S. Radovick, J. H. McClaskey, T. Taylor, B. D. Weintraub, F. E. Wondisford, *Proc. Natl. Acad. Sci. USA* **1991**, *88*, 3130.
- [200] T. M. Ortega-Carvalho, M. I. Chiamolera, C. C. Pazos-Moura, F. E. Wondisford, *Compr. Physiol.* **2016**, *6*, 1387.
- [201] G. Dai, O. Levy, N. Carrasco, *Nature* **1996**, *379*, 458.
- [202] D. P. Carvalho, C. Dupuy, *Mol. Cell. Endocrinol.* **2017**, *458*, 6.
- [203] C. E. Citterio, H. M. Targovnik, P. Arvan, *Nat. Rev. Endocrinol.* **2019**, *15*, 323.
- [204] C. Di Cosmo, X. H. Liao, A. M. Dumitrescu, N. J. Philp, R. E. Weiss, S. Refetoff, *J. Clin. Invest.* **2010**, *120*, 3377.
- [205] F. Brucker-Davis, *Thyroid* **1998**, *8*, 827.
- [206] OECD (2018), *Test No. 414: Prenatal Developmental Toxicity Study*, OECD Publishing, Paris **2018**.
- [207] OECD (1995), *Test No. 421: Reproduction/Developmental Toxicity Screening Test*, OECD Publishing, Paris **1995**.
- [208] OECD (2016), *Test No. 422: Combined Repeated Dose Toxicity Study with the Reproduction/Developmental Toxicity Screening Test*, OECD Publishing, Paris **2016**, p. 2016.
- [209] OECD (2018), *Test No. 443: Extended One-Generation Reproductive Toxicity Study*, OECD Publishing, Paris **2018**.
- [210] N. Andersson, M. Arena, D. Auteri, S. Barmaz, E. Grignard, A. Kienzler, P. Lepper, A. M. Lostia, S. Munn, J. M. Parra Morte, F. Pellizzato, J. Tarazona, A. Terron, S. Van der Linden, *EFSA J.* **2018**, *16*, e05311.
- [211] U.S. Environmental Protection Agency, *Endocrine Disruptor Screening Program (EDSP) Comprehensive Management Plans*, Washington, D.C. **2014**.
- [212] OECD (2017), *New Scoping Document on in Vitro and Ex Vivo Assays for the Identification of Modulators of Thyroid Hormone Signalling*, OECD Publishing, Paris **2017**.
- [213] P. D. Noyes, K. P. Friedman, P. Browne, J. T. Haselman, M. E. Gilbert, M. W. Hornung, S. Barone, K. M. Crofton, S. C. Laws, T. E. Stoker, S. O. Simmons, J. E. Tietge, S. J. Degitz, *Environ. Health Perspect.* **2019**, *127*, 95001.
- [214] R. S. Thomas, T. Bahadori, T. J. Buckley, J. Cowden, C. Deisenroth, K. L. Dionisio, J. B. Frithsen, C. M. Grulke, M. R. Gwinn, J. A. Harrill, M. Higuchi, K. A. Houck, M. F. Hughes, E. Sidney Hunter, K. K. Isaacs, R. S. Judson, T. B. Knudsen, J. C. Lambert, M. Linnenbrink, T. M. Martin, S. R. Newton, S. Padilla, G. Patlewicz, K. Paul-Friedman, K. A. Phillips, A. M. Richard, R. Sams, T. J. Shafer, R. W. Setzer, I. Shah, J. E. Simmons, S. O. Simmons, A. Singh, J. R. Sobus, M. Strynar, A. Swank, R. Tornero-Valez, E. M. Ulrich, D. L. Villeneuve, J. F. Wambaugh, B. A. Wetmore, A. J. Williams, *Toxicol. Sci.* **2019**, *169*, 317.
- [215] C. Thomas-Morvan, B. Caillou, M. Schlumberger, P. Fragu, *Biol. Cell* **1988**, *62*, 247.
- [216] C. Massart, B. Hody, D. Condé, G. Leclech, G. Edan, M. Nicol, *Mol. Cell. Endocrinol.* **1988**, *56*, 227.
- [217] E. A. Bulanova, E. V. Koudan, J. Degosserie, C. Heymans, F. D. A. S. Pereira, V. A. Parfenov, Y. Sun, Q. Wang, S. A. Akhmedova, I. K. Sviridova, N. S. Sergeeva, G. A. Frank, Y. D. Khesuani, C. E. Pierreux, V. A. Mironov, *Biofabrication* **2017**, *9*, 34105.
- [218] Y. Saito, N. Onishi, H. Takami, R. Seishima, H. Inoue, Y. Hirata, K. Kameyama, K. Tsuchihashi, E. Sugihara, S. Uchino, K. Ito, H. Kawakubo, H. Takeuchi, Y. Kitagawa, H. Saya, O. Nagano, *Biochem. Biophys. Res. Commun.* **2018**, *497*, 783.
- [219] C. Deisenroth, V. Y. Soldatow, J. Ford, W. Stewart, C. Brinkman, E. L. Lecluyse, D. K. MacMillan, R. S. Thomas, *Toxicol. Sci.* **2020**, *174*, 63.
- [220] J. Coclet, F. Foureau, P. Ketelbant, P. Galand, J. E. Dumont, *Clin. Endocrinol.* **1989**, *31*, 655.
- [221] R. Ma, R. Latif, T. F. Davies, *Thyroid* **2015**, *25*, 455.
- [222] F. Antonica, D. F. Kasprzyk, R. Opitz, M. Iacovino, X. H. Liao, A. M. Dumitrescu, S. Refetoff, K. Peremans, M. Manto, M. Kyba, S. Costagliola, *Nature* **2012**, *491*, 66.
- [223] A. A. Kurmann, M. Serra, F. Hawkins, S. A. Rankin, M. Mori, I. Astapova, S. Ullas, S. Lin, M. Bilodeau, J. Rossant, J. C. Jean, L. Ikonou, R. R. Deterding, J. M. Shannon, A. M. Zorn, A. N. Hollenberg, D. N. Kotton, *Cell Stem Cell* **2015**, *17*, 527.
- [224] K. Dame, S. Cincotta, A. H. Lang, R. M. Sanghrajka, L. Zhang, J. Choi, L. Kwok, T. Wilson, M. M. Kařduřa, S. Monti, A. N. Hollenberg, P. Mehta, D. N. Kotton, L. Ikonou, *Stem Cell Rep.* **2017**, *8*, 216.
- [225] A. Arauchi, K. Matsuura, T. Shimizu, T. Okano, *Front. Endocrinol.* **2017**, *8*, 22.
- [226] R. Ma, S. A. Morshed, R. Latif, T. F. Davies, *Front. Endocrinol.* **2015**, *6*, 56.
- [227] Y. Yang, Y. Lu, T. Chen, S. Zhang, B. Chu, Y. Gong, W. Zhao, J. Zhu, Y. Liu, *Int. J. Dev. Biol.* **2016**, *60*, 85.
- [228] H. Suga, T. Kadoshima, M. Minaguchi, M. Ohgushi, M. Soen, T. Nakano, N. Takata, T. Wataya, K. Muguruma, H. Miyoshi, S. Yonemura, Y. Oiso, Y. Sasai, *Nature* **2011**, *480*, 57.
- [229] C. Ozone, H. Suga, M. Eiraku, T. Kadoshima, S. Yonemura, N. Takata, Y. Oiso, T. Tsuji, Y. Sasai, *Nat. Commun.* **2016**, *7*, 10351.
- [230] T. Kasai, H. Suga, M. Sakakibara, C. Ozone, R. Matsumoto, M. Kano, K. Mitsumoto, K. Ogawa, Y. Kodani, H. Nagasaki, N. Inoshita, M. Sugiyama, T. Onoue, T. Tsunekawa, Y. Ito, H. Takagi, D. Hagiwara, S. Iwama, M. Goto, R. Banno, J. Takahashi, H. Arima, *Cell Rep.* **2020**, *30*, 18.
- [231] P. Gehr, M. Bachofen, E. R. Weibel, *Respir. Physiol.* **1978**, *32*, 121.
- [232] E. Fröhlich, A. Mercuri, S. Wu, S. Salar-Behzadi, *Front. Pharmacol.* **2016**, *7*, 181.
- [233] T. J. Franks, T. V. Colby, W. D. Travis, R. M. Tuder, H. Y. Reynolds, A. R. Brody, W. V. Cardoso, R. G. Crystal, C. J. Drake, J. Engelhardt, M. Frid, E. Herzog, R. Mason, S. H. Phan, S. H. Randell, M. C. Rose, T. Stevens, J. Serge, M. E. Sunday, J. A. Voynow, B. M. Weinstein, J. Whitsett, M. C. Williams, *Proc. Am. Thorac. Soc.* **2008**, *5*, 763.
- [234] OECD (2018), *Guidance Document on Inhalation Toxicity Studies*, OECD Publishing, Paris, **2018**.
- [235] H. G. Hoymann, *J. Pharmacol. Toxicol. Methods* **2007**, *55*, 16.
- [236] L. C. Chen, M. Lippmann, *Curr. Protoc. Toxicol.* **2015**, *63*, 24.4.1.
- [237] P. S. Hiemstra, G. Grootaers, A. M. van der Does, C. A. M. Krul, I. M. Kooter, *Toxicol. In Vitro* **2018**, *47*, 137.
- [238] J. D. Crapo, B. E. Barry, P. Gehr, M. Bachofen, E. R. Weibel, *Am. Rev. Respir. Dis.* **1982**, *126*, 332.
- [239] D. E. Johnson, M. K. Georgieff, *Am. Rev. Respir. Dis.* **1989**, *140*, 1807.
- [240] K. U. Hong, S. D. Reynolds, S. Watkins, E. Fuchs, B. R. Stripp, *Am. J. Pathol.* **2004**, *164*, 577.
- [241] B. D. Uhal, K. M. Flowers, D. E. Rannels, *Am. J. Physiol. Cell. Mol. Physiol.* **1991**, *261*, 110.
- [242] M. A. Medinsky, J. A. Bond, *Toxicology* **2001**, *160*, 165.
- [243] M. Lippmann, D. B. Yeates, R. E. Albert, *Br. J. Ind. Med.* **1980**, *37*, 337.
- [244] B. Asgharian, T. P. Owen, E. D. Kuempel, A. M. Jarabek, *Toxicol. Appl. Pharmacol.* **2018**, *361*, 27.

- [245] T. T. Crocker, T. V. O'Donnell, L. L. Nunes, *Cancer Res.* **1973**, *33*, 88.
- [246] J. E. Craighead, B. T. Mossman, B. J. Bradley, *Environ. Health Perspect.* **1980**, *34*, 37.
- [247] U. Mohr, M. Emura, *Food Chem. Toxicol.* **1985**, *23*, 233.
- [248] K. E. Driscoll, J. M. Carter, P. T. Iype, H. L. Kumari, L. L. Crosby, M. J. Aardema, R. J. Isfort, D. Cody, M. H. Chestnut, J. L. Burns, R. A. LeBoeuf, *In Vitro Cell. Dev. Biol.: Anim.* **1995**, *31*, 516.
- [249] M. Lieber, G. Todaro, B. Smith, A. Szakal, W. Nelson-Rees, *Int. J. Cancer* **1976**, *17*, 62.
- [250] I. W. H. Jarvis, Z. Enlo-Scott, E. Nagy, I. S. Mudway, T. D. Tetley, V. M. Arlt, D. H. Phillips, *Environ. Mol. Mutagen.* **2018**, *59*, 290.
- [251] N. Fujino, H. Kubo, C. Ota, T. Suzuki, S. Suzuki, M. Yamada, T. Takahashi, M. He, T. Suzuki, T. Kondo, M. Yamaya, *Am. J. Respir. Cell Mol. Biol.* **2012**, *46*, 422.
- [252] P. Khan, K. Fytianos, L. Tamò, M. Roth, M. Tamm, T. Geiser, A. Gazdhar, K. E. Hostettler, *Respir. Res.* **2018**, *19*, 204.
- [253] M. A. Shatos, J. M. Doherty, J. P. Marsh, B. T. Mossman, *Environ. Res.* **1987**, *44*, 103.
- [254] G. Vietti, S. Ibouaadaten, M. Palmi-Pallag, Y. Yakoub, C. Bailly, I. Fenoglio, E. Marbaix, D. Lison, S. van den Brule, *Part. Fibre Toxicol.* **2013**, *10*, 52.
- [255] A. C. Allison, J. S. Harington, M. Birbeck, *J. Exp. Med.* **1966**, *124*, 141.
- [256] M. C. Jaurand, J. Bignon, A. Gaudichet, L. Magne, A. Oblin, *Environ. Res.* **1978**, *17*, 216.
- [257] P. Gosset, P. Lassalle, D. Vanh e, B. Wallaert, C. Aerts, C. Voisin, A. B. Tonnel, *Am. J. Respir. Cell Mol. Biol.* **1991**, *5*, 431.
- [258] R. P. F. Schins, P. J. A. Borm, *Ann. Occup. Hyg.* **1999**, *43*, 7.
- [259] A. M. Knaapen, R. P. F. Schins, P. J. A. Borm, F. J. van Schooten, *Carcinogenesis* **2005**, *26*, 1642.
- [260] F. Herzog, M. J. D. Clift, F. Piccapietra, R. Behra, O. Schmid, A. Petri-Fink, B. Rothen-Rutishauser, *Part. Fibre Toxicol.* **2013**, *10*, 11.
- [261] S. G. Klein, T. Serchi, L. Hoffmann, B. Bl omeke, A. C. Gutleb, *Part. Fibre Toxicol.* **2013**, *10*, 31.
- [262] H. Batra, V. B. Antony, *J. Thorac. Dis.* **2015**, *7*, 964.
- [263] C. Blanquart, M. C. Jaurand, D. Jean, *Front. Oncol.* **2020**, *10*, 388.
- [264] A. Renier, M. Yegles, A. Buard, H. Dong, L. Kheuang, L. Saint-Etienne, P. Laurent, M. C. Jaurand, *Cell Biol. Toxicol.* **1992**, *8*, 133.
- [265] F. A. Murphy, A. Schinwald, C. A. Poland, K. Donaldson, *Part. Fibre Toxicol.* **2012**, *9*, 8.
- [266] M. I. Hermans, R. E. Unger, K. Kehe, K. Peters, C. J. Kirkpatrick, *Lab. Invest.* **2004**, *84*, 736.
- [267] K. Luyts, D. Napierska, D. Dinsdale, S. G. Klein, T. Serchi, P. H. M. Hoet, *Toxicol. In Vitro* **2015**, *29*, 234.
- [268] A. Costa, C. de Souza Carvalho-Wodarz, V. Seabra, B. Sarmento, C. M. Lehr, *Acta Biomater.* **2019**, *91*, 235.
- [269] K. B. Adler, P. W. Cheng, K. C. Kim, *Am. J. Respir. Cell Mol. Biol.* **1990**, *2*, 145.
- [270] F. Blank, B. M. Rothen-Rutishauser, S. Schurch, P. Gehr, *J. Aerosol Med.* **2006**, *19*, 392.
- [271] G. Lacroix, W. Koch, D. Ritter, A. C. Gutleb, S. T. Larsen, T. Loret, F. Zanetti, S. Constant, S. Chortarea, B. Rothen-Rutishauser, P. S. Hiemstra, E. Frejafon, P. Hubert, L. Gribaldo, P. Kearns, J. M. Aublant, S. Diabat , C. Weiss, A. De Groot, I. Kooter, *Appl. In Vitro Toxicol.* **2018**, *4*, 91.
- [272] S. Huang, B. Boda, J. Vernaz, E. Ferreira, L. Wiszniewski, S. Constant, *Eur. J. Pharm. Biopharm.* **2017**, *118*, 68.
- [273] M. Liu, S. J. M. Skinner, J. Xu, R. N. N. Han, A. K. Tanswell, M. Post, *Am. J. Physiol.: Lung Cell. Mol. Physiol.* **1992**, *263*, 376.
- [274] U. Savla, C. M. Waters, *Am. J. Physiol.: Lung Cell. Mol. Physiol.* **1998**, *274*, 883.
- [275] C. Schmitz, J. Welck, I. Tavernaro, M. Grinberg, J. Rahnenf hrer, A. K. Kiemer, C. van Thriel, J. G. Hengstler, A. Kraegeloh, *Nanotoxicology* **2019**, *13*, 1227.
- [276] D. Huh, D. C. Leslie, B. D. Matthews, J. P. Fraser, S. Jurek, G. A. Hamilton, K. S. Thorneloe, M. A. McAlexander, D. E. Ingber, *Sci. Transl. Med.* **2012**, *4*, 159ra147.
- [277] S. Gotoh, I. Ito, T. Nagasaki, Y. Yamamoto, S. Konishi, Y. Korogi, H. Matsumoto, S. Muro, T. Hirai, M. Funato, S. I. Mae, T. Toyoda, A. Sato-Otsubo, S. Ogawa, K. Osafune, M. Mishima, *Stem Cell Rep.* **2014**, *3*, 394.
- [278] M. C. Basil, J. Katzen, A. E. Engler, M. Guo, M. J. Herriges, J. J. Kathiriyai, R. Windmueller, A. B. Ysasi, W. J. Zacharias, H. A. Chapman, D. N. Kotton, J. R. Rock, H. W. Snoeck, G. Vunjak-Novakovic, J. A. Whitsett, E. E. Morrissey, *Cell Stem Cell* **2020**, *26*, 482.
- [279] C. Coraux, B. Nawrocki-Raby, J. Hinnrasky, C. Kileztky, D. Gaillard, C. Dani, E. Puchelle, *Am. J. Respir. Cell Mol. Biol.* **2005**, *32*, 87.
- [280] B. Mehrad, M. P. Keane, B. N. Gomperts, R. M. Strieter, *Expert Rev. Respir. Med.* **2007**, *1*, 157.
- [281] L. Srikanth, K. Venkatesh, M. M. Sunitha, P. S. Kumar, C. Chandrasekhar, B. Vengamma, P. V. G. K. Sarma, *Biotechnol. Lett.* **2016**, *38*, 237.
- [282] M. D. Green, A. Chen, M. C. Nostro, S. L. D'Souza, C. Schaniel, I. R. Lemischka, V. Gouon-Evans, G. Keller, H. W. Snoeck, *Nat. Biotechnol.* **2011**, *29*, 267.
- [283] F. Hawkins, D. N. Kotton, *Ann. Am. Thorac. Soc.* **2015**, *12*, S50.
- [284] M. Ghaedi, L. E. Niklason, in *Methods in Molecular Biology*, Humana Press Inc., Totowa **2019**, pp. 55–92.
- [285] P. Pimton, S. Lecht, C. T. Stabler, G. Johannes, E. S. Schulman, P. I. Lelkes, *Stem Cells Dev.* **2015**, *24*, 663.
- [286] T. Y. Ling, Y. L. Liu, Y. K. Huang, S. Y. Gu, H. K. Chen, C. C. Ho, P. N. Tsao, Y. C. Tung, H. W. Chen, C. H. Cheng, K. H. Lin, F. H. Lin, *Biomaterials* **2014**, *35*, 5660.
- [287] Y. Yamamoto, S. Gotoh, Y. Korogi, M. Seki, S. Konishi, S. Ikeo, N. Sone, T. Nagasaki, H. Matsumoto, S. Muro, I. Ito, T. Hirai, T. Kohno, Y. Suzuki, M. Mishima, *Nat. Methods* **2017**, *14*, 1097.
- [288] S. X. L. Huang, M. D. Green, A. T. De Carvalho, M. Mumau, Y. W. Chen, S. L. D'souza, H. W. Snoeck, *Nat. Protoc.* **2015**, *10*, 413.
- [289] A. J. Miller, B. R. Dye, D. Ferrer-Torres, D. R. Hill, A. W. Overeem, L. D. Shea, J. R. Spence, *Nat. Protoc.* **2019**, *14*, 518.
- [290] X. Zhang, T. Jiang, D. Chen, Q. Wang, L. W. Zhang, *Crit. Rev. Toxicol.* **2020**, *50*, 279.
- [291] M. F. Beers, Y. Moodley, *Am. J. Respir. Cell Mol. Biol.* **2017**, *57*, 18.
- [292] Y. W. Chen, S. X. Huang, A. L. R. T. De Carvalho, S. H. Ho, M. N. Islam, S. Volpi, L. D. Notarangelo, M. Ciancanelli, J. L. Casanova, J. Bhattacharya, A. F. Liang, L. M. Palermo, M. Porotto, A. Moscona, H. W. Snoeck, *Nat. Cell Biol.* **2017**, *19*, 542.
- [293] A. Jacob, M. Morley, F. Hawkins, K. B. McCauley, J. C. Jean, H. Heins, C. L. Na, T. E. Weaver, M. Vedaie, K. Hurley, A. Hinds, S. J. Russo, S. Kook, W. Zacharias, M. Ochs, K. Traber, L. J. Qinton, A. Crane, B. R. Davis, F. V. White, J. Wambach, J. A. Whitsett, F. S. Cole, E. E. Morrissey, S. H. Guttentag, M. F. Beers, D. N. Kotton, *Cell Stem Cell* **2017**, *21*, 472.
- [294] R. Wang, K. B. McCauley, D. N. Kotton, F. Hawkins, in *Methods Cell Biol.*, Academic Press Inc., Cambridge **2020**, pp. 95–114.
- [295] J. C. Nawroth, R. Barrile, D. Conegliano, S. van Riet, P. S. Hiemstra, R. Villenave, *Adv. Drug Delivery Rev.* **2019**, *140*, 12.
- [296] Y. Ding, P. Weindl, A. G. Lenz, P. Mayer, T. Krebs, O. Schmid, *Part. Fibre Toxicol.* **2020**, *17*, 44.
- [297] M. R. Tanner, C. Beeton, *Front. Biosci., Landmark* **2018**, *23*, 43.
- [298] M. Bauer, in *Basic Science In Anesthesia*, Springer International Publishing, Basel, **2017**, pp. 195–228.
- [299] N. Ferri, P. Siegl, A. Corsini, J. Herrmann, A. Lerman, R. Benghozi, *Pharmacol. Ther.* **2013**, *138*, 470.
- [300] M. Takeda, S. Miyagawa, S. Fukushima, A. Saito, E. Ito, A. Harada, R. Matsuura, H. Iseoka, N. Sougawa, N. Mochizuki-Oda, M. Matsusaki, M. Akashi, Y. Sawa, *Tissue Eng., Part C* **2018**, *24*, 56.

- [301] T. Jin, B. Hu, S. Chen, Q. Wang, X. Dong, Y. Zhang, Y. Zhu, Z. Zhang, *Front. Pharmacol.* **2018**, *9*, 577.
- [302] J. Cuadros, N. Dugarte, S. Wong, P. Vanegas, V. Morocho, R. Medina, *J. Healthcare Eng.* **2019**, *2019*, 6371871.
- [303] B. Darpo, *Br. J. Pharmacol.* **2010**, *159*, 49.
- [304] B. D. Guth, S. Germeyer, W. Kolb, M. Markert, *J. Pharmacol. Toxicol. Methods* **2004**, *49*, 159.
- [305] I. Cavero, W. Crumb, *Expert Opin. Drug Saf.* **2005**, *4*, 509.
- [306] C. L. Mummery, *Stem Cell Rep.* **2018**, *11*, 1306.
- [307] M. Zhang, J. S. Schulte, A. Heinick, I. Piccini, J. Rao, R. Quaranta, D. Zeuschner, D. Malan, K. P. Kim, A. Röpke, P. Sasse, M. Araúzo-Bravo, G. Seebohm, H. Schöler, L. Fabritz, P. Kirchhof, F. U. Müller, B. Greber, *Stem Cells* **2015**, *33*, 1456.
- [308] P. W. Burridge, E. Matsa, P. Shukla, Z. C. Lin, J. M. Churko, A. D. Ebert, F. Lan, S. Diecke, B. Huber, N. M. Mordwinkin, J. R. Plews, O. J. Abilez, B. Cui, J. D. Gold, J. C. Wu, *Nat. Methods* **2014**, *11*, 855.
- [309] X. Lian, J. Zhang, S. M. Azarin, K. Zhu, L. B. Hazeltine, X. Bao, C. Hsiao, T. J. Kamp, S. P. Palecek, *Nat. Protoc.* **2013**, *8*, 162.
- [310] H. Ando, T. Yoshinaga, W. Yamamoto, K. Asakura, T. Uda, T. Taniguchi, A. Ojima, T. Osada, S. Hayashi, C. Kasai, N. Miyamoto, H. Tashibu, D. Yamazaki, A. Sugiyama, Y. Kanda, K. Sawada, Y. Sekino, H. Ando, T. Yoshinaga, K. Asakura, T. Osada, S. Hayashi, C. Kasai, H. Tashibu, A. Sugiyama, K. Sawada, Y. Sekino, H. Ando, T. Uda, T. Yoshinaga, T. Taniguchi, A. Ojima, R. Shinkyo, K. Kikuchi, N. Miyamoto, K. Sawada, W. Yamamoto, K. Asakura, S. Hayashi, T. Osada, C. Kasai, H. Tashibu, D. Yamazaki, Y. Kanda, Y. Sekino, A. Sugiyama, *J. Pharmacol. Toxicol. Methods* **2017**, *84*, 111.
- [311] M. Shi, N. T. Tien, L. de Haan, J. Lousse, I. M. C. M. Rietjens, H. Bouwmeester, *Toxicol. In Vitro* **2020**, *67*, 104891.
- [312] S. Stoelzle, A. Haythornthwaite, R. Kettenhofen, E. Kolossov, H. Bohlen, M. George, A. Brüggemann, N. Fertig, *J. Biomol. Screen.* **2011**, *16*, 910.
- [313] K. Blinova, J. Stohman, J. Vicente, D. Chan, L. Johannesen, M. P. Hortigon-Vinagre, V. Zamora, G. Smith, W. J. Crumb, L. Pang, B. Lyn-Cook, J. Ross, M. Brock, S. Chvatal, D. Millard, L. Galeotti, N. Stockbridge, D. G. Strauss, *Toxicol. Sci.* **2017**, *155*, 234.
- [314] T. Colatsky, B. Fermini, G. Gintant, J. B. Pierson, P. Sager, Y. Sekino, D. G. Strauss, N. Stockbridge, *J. Pharmacol. Toxicol. Methods* **2016**, *81*, 15.
- [315] K. Blinova, Q. Dang, D. Millard, G. Smith, J. Pierson, L. Guo, M. Brock, H. R. Lu, U. Kraushaar, H. Zeng, H. Shi, X. Zhang, K. Sawada, T. Osada, Y. Kanda, Y. Sekino, L. Pang, T. K. Feaster, R. Kettenhofen, N. Stockbridge, D. G. Strauss, G. Gintant, *Cell Rep.* **2018**, *24*, 3582.
- [316] B. R. Berridge, A. E. Schultze, J. R. Heyen, G. H. Searfoss, R. D. Sarazan, *ILAR J.* **2016**, *57*, 120.
- [317] G. Gintant, P. T. Sager, N. Stockbridge, *Nat. Rev. Drug Discovery* **2016**, *15*, 457.
- [318] E. G. Navarrete, P. Liang, F. Lan, V. Sanchez-Freire, C. Simmons, T. Gong, A. Sharma, P. W. Burridge, B. Patlolla, A. S. Lee, H. Wu, R. E. Beygui, S. M. Wu, R. C. Robbins, D. M. Bers, J. C. Wu, *Circulation* **2013**, *128*.
- [319] A. Sharma, W. L. McKeithan, R. Serrano, T. Kitani, P. W. Burridge, J. C. del Álamo, M. Mercola, J. C. Wu, *Nat. Protoc.* **2018**, *13*, 3018.
- [320] Y. K. Kurokawa, M. R. Shang, R. T. Yin, S. C. George, *Toxicol. Lett.* **2018**, *285*, 74.
- [321] B. Nugraha, M. F. Buono, L. von Boehmer, S. P. Hoerstrup, M. Y. Emmert, *Clin. Pharmacol. Ther.* **2019**, *105*, 79.
- [322] L. Polonchuk, M. Chabria, L. Badi, J. C. Hoflack, G. Figtree, M. J. Davies, C. Gentile, *Sci. Rep.* **2017**, *7*, 7005.
- [323] C. R. Archer, R. Sargeant, J. Basak, J. Pilling, J. R. Barnes, A. Pointon, *Sci. Rep.* **2018**, *8*, 10160.
- [324] M. Kawatou, H. Masumoto, H. Fukushima, G. Morinaga, R. Sakata, T. Ashihara, J. K. Yamashita, *Nat. Commun.* **2017**, *8*, 1078.
- [325] D. Hu, A. Linders, A. Yamak, C. Correia, J. D. Kijlstra, A. Garakani, L. Xiao, D. J. Milan, P. Van Der Meer, M. Serra, P. M. Alves, I. J. Domian, *Circ. Res.* **2018**, *123*, 1066.
- [326] T. Kietzmann, *Redox Biol.* **2017**, *11*, 622.
- [327] H. Rashidi, S. Alhaque, D. Szkolnicka, O. Flint, D. C. Hay, *Arch. Toxicol.* **2016**, *90*, 1757.
- [328] M. Hay, D. W. Thomas, J. L. Craighead, C. Economides, J. Rosenthal, *Nat. Biotechnol.* **2014**, *32*, 40.
- [329] M. Z. Sakatis, M. J. Reese, A. W. Harrell, M. A. Taylor, I. A. Baines, L. Chen, J. C. Bloomer, E. Y. Yang, H. M. Ellens, J. L. Ambroso, C. A. Lovatt, A. D. Ayrton, S. E. Clarke, *Chem. Res. Toxicol.* **2012**, *25*, 2067.
- [330] J. L. Stevens, T. K. Baker, *Drug Discovery Today* **2009**, *14*, 162.
- [331] N. Kaplowitz, *Nat. Rev. Drug Discovery* **2005**, *4*, 489.
- [332] T. Hartung, *Nature* **2009**, *460*, 208.
- [333] A. Natale, K. Vanmol, A. Arslan, S. Van Vlierberghe, P. Dubruel, J. Van Erps, H. Thienpont, M. Buzgo, J. Boeckmans, J. De Kock, T. Vanhaecke, V. Rogiers, R. M. Rodrigues, *Arch. Toxicol.* **2019**, *93*, 1789.
- [334] P. Godoy, N. J. Hewitt, U. Albrecht, M. E. Andersen, N. Ansari, S. Bhattacharya, J. G. Bode, J. Bolley, C. Borner, J. Böttger, A. Braeuning, R. A. Budinsky, B. Burkhardt, N. R. Cameron, G. Camussi, C. S. Cho, Y. J. Choi, J. Craig Rowlands, U. Dahmen, G. Damm, O. Dirsch, M. T. Donato, J. Dong, S. Dooley, D. Drasdo, R. Eakins, K. S. Ferreira, V. Fonsato, J. Fraczek, R. Gebhardt, A. Gibson, M. Glanemann, C. E. P. Goldring, M. J. Gómez-Lechón, G. M. M. Groothuis, L. Gustavsson, C. Guyot, D. Hallifax, S. Hammad, A. Hayward, D. Häussinger, C. Hellerbrand, P. Hewitt, S. Hoehme, H. G. Holzhütter, J. B. Houston, J. Brach, K. Ito, H. Jaeschke, V. Keitel, J. M. Kelm, B. Kevin Park, C. Kordes, G. A. Kullak-Ublick, E. L. Lecluyse, P. Lu, J. Luebke-Wheeler, A. Lutz, D. J. Maltman, M. Matz-Soja, P. McMullen, I. Merfort, S. Messner, C. Meyer, J. Mwinyi, D. J. Naisbitt, A. K. Nussler, P. Olinga, F. Pampaloni, J. Pi, L. Pluta, S. S. A. Przyborski, A. Ramachandran, V. Rogiers, C. Rowe, C. Schelcher, K. Schmic, M. Schwarz, B. Singh, E. H. K. Stelzer, B. Stieger, R. Stöber, Y. Sugiyama, C. Tetta, W. E. Thasler, T. Vanhaecke, M. Vinken, T. S. Weiss, A. Widera, C. G. Woods, J. J. Xu, K. M. Yarborough, J. G. Hengstler, *Arch. Toxicol.* **2013**, *87*, 1315.
- [335] V. M. Lauschke, D. F. G. Hendriks, C. C. Bell, T. B. Andersson, M. Ingelman-Sundberg, *Chem. Res. Toxicol.* **2016**, *29*, 1936.
- [336] W. L. Thompson, T. Takebe, in *Methods in Cell Biology*, Academic Press Inc., Cambridge **2020**, pp. 47–68.
- [337] C. C. Bell, D. F. G. Hendriks, S. M. L. Moro, E. Ellis, J. Walsh, A. Renblom, L. Fredriksson Puigvert, A. C. A. Dankers, F. Jacobs, J. Snoeys, R. L. Sison-Young, R. E. Jenkins, Å. Nordling, S. Mkrtrchian, B. K. Park, N. R. Kitteringham, C. E. P. Goldring, V. M. Lauschke, M. Ingelman-Sundberg, *Sci. Rep.* **2016**, *6*, 25187.
- [338] W. R. Proctor, A. J. Foster, J. Vogt, C. Summers, B. Middleton, M. A. Pilling, D. Shienson, M. Kijanska, S. Ströbel, J. M. Kelm, P. Morgan, S. Messner, D. Williams, *Arch. Toxicol.* **2017**, *91*, 2849.
- [339] X. Ma, X. Qu, W. Zhu, Y. S. Li, S. Yuan, H. Zhang, J. Liu, P. Wang, C. S. E. Lai, F. Zanella, G. S. Feng, F. Sheikh, S. Chien, S. Chen, *Proc. Natl. Acad. Sci. USA* **2016**, *113*, 2206.
- [340] F. Tonon, G. G. Giobbe, A. Zambon, C. Luni, O. Gagliano, A. Floreani, G. Grassi, N. Elvassore, *Sci. Rep.* **2019**, *9*, 13557.
- [341] J. Ahn, J. H. Ahn, S. Yoon, Y. S. Nam, M. Y. Son, J. H. Oh, *J. Biol. Eng.* **2019**, *13*, 22.
- [342] Y. B. Kang, J. Eo, B. Bulutoglu, M. L. Yarmush, O. B. Usta, *Bio-technol. Bioeng.* **2020**, *117*, 763.
- [343] F. A. Grimm, Y. Iwata, O. Sirenko, M. Bittner, I. Rusyn, *Assay Drug Dev. Technol.* **2015**, *13*, 529.
- [344] O. Sirenko, J. Hesley, I. Rusyn, E. F. Cromwell, *Assay Drug Dev. Technol.* **2014**, *12*, 43.

- [345] P. Horvath, N. Aulner, M. Bickle, A. M. Davies, E. Del Nery, D. Ebner, M. C. Montoya, P. Östling, V. Pietiäinen, L. S. Price, S. L. Shorte, G. Turcatti, C. Von Schantz, N. O. Carragher, *Nat. Rev. Drug Discovery* **2016**, *15*, 751.
- [346] T. Takebe, K. Sekine, M. Kimura, E. Yoshizawa, S. Ayano, M. Koido, S. Funayama, N. Nakanishi, T. Hisai, T. Kobayashi, T. Kasai, R. Kitada, A. Mori, H. Ayabe, Y. Ejiri, N. Amimoto, Y. Yamazaki, S. Ogawa, M. Ishikawa, Y. Kiyota, Y. Sato, K. Nozawa, S. Okamoto, Y. Ueno, H. Taniguchi, *Cell Rep.* **2017**, *21*, 2661.
- [347] R. Ouchi, S. Togo, M. Kimura, T. Shinozawa, M. Koido, H. Koike, W. Thompson, R. A. Karns, C. N. Mayhew, P. S. McGrath, H. A. McCauley, R. R. Zhang, K. Lewis, S. Hakozaiki, A. Ferguson, N. Saiki, Y. Yoneyama, I. Takeuchi, Y. Mabuchi, C. Akazawa, H. Y. Yoshikawa, J. M. Wells, T. Takebe, *Cell Metab.* **2019**, *30*, 374.
- [348] F. Wu, D. Wu, Y. Ren, Y. Huang, B. Feng, N. Zhao, T. Zhang, X. Chen, S. Chen, A. Xu, *J. Hepatol.* **2019**, *70*, 1145.
- [349] O. Sirenko, M. K. Hancock, J. Hesley, D. Hong, A. Cohen, J. Gentry, C. B. Carlson, D. A. Mann, *Assay Drug Dev. Technol.* **2016**, *14*, 381.
- [350] A. K. Daly, *Nat. Rev. Genet.* **2010**, *11*, 241.
- [351] S. Wang, X. Wang, Z. Tan, Y. Su, J. Liu, M. Chang, F. Yan, J. Chen, T. Chen, C. Li, J. Hu, Y. Wang, *Cell Res.* **2019**, *29*, 1009.
- [352] J. L. Zhuo, X. C. Li, *Compr. Physiol.* **2013**, *3*, 1079.
- [353] N. O. Lindström, M. L. Lawrence, S. F. Burn, J. A. Johansson, E. R. M. Bakker, R. A. Ridgway, C. H. Chang, M. J. Karolak, L. Oxburgh, D. J. Headon, O. J. Sansom, R. Smits, J. A. Davies, P. Hohenstein, *eLife* **2014**, *3*, e04000.
- [354] M. A. Perazella, *Clin. J. Am. Soc. Nephrol.* **2018**, *13*, 1897.
- [355] M. Carlström, C. S. Wilcox, W. J. Arendshorst, *Physiol. Rev.* **2015**, *95*, 405.
- [356] E. J. Hoorn, S. B. Walsh, J. A. McCormick, A. Fürstenberg, C. L. Yang, T. Roeschel, A. Paliege, A. J. Howie, J. Conley, S. Bachmann, R. J. Unwin, D. H. Ellison, *Nat. Med.* **2011**, *17*, 1304.
- [357] E. Lazzeri, M. L. Angelotti, A. Peired, C. Conte, J. A. Marschner, L. Maggi, B. Mazzinghi, D. Lombardi, M. E. Melica, S. Nardi, E. Ronconi, A. Sisti, G. Antonelli, F. Becherucci, L. De Chiara, R. R. Guevara, A. Burger, B. Schaefer, F. Annunziato, H. J. Anders, L. Lasagni, P. Romagnani, *Nat. Commun.* **2018**, *9*, 1344.
- [358] M. A. Perazella, *Clin. J. Am. Soc. Nephrol.* **2009**, *4*, 1275.
- [359] M. H. Hazelhoff, R. P. Bulacio, A. M. Torres, *Int. J. Mol. Sci.* **2012**, *13*, 10523.
- [360] R. J. Roman, J. R. Carter, W. C. North, M. L. Kauker, *Anesthesiology* **1977**, *46*, 260.
- [361] I. Walev, S. Bhakdi, *Antimicrob. Agents Chemother.* **1996**, *40*, 1116.
- [362] A. Bernhardt, A. Fehr, S. Brandt, S. Jerchel, T. M. Ballhause, L. Philipsen, S. Stolze, R. Geffers, H. Weng, K. D. Fischer, B. Isermann, M. C. Brunner-Weinzierl, A. Batra, B. Siegmund, C. Zhu, J. A. Lindquist, P. R. Mertens, *Kidney Int.* **2017**, *92*, 1157.
- [363] H. Wu, B. D. Humphreys, *Clin. J. Am. Soc. Nephrol.* **2020**, *15*, 550.
- [364] Y. Kiritani, H. Wu, K. Uchimura, P. Wilson, B. Humphreys, *Proc. Natl. Acad. Sci. USA* **2020**, *117*, 15874.
- [365] H. Li, B. Humphreys, *Kidney Int.* **2020**, *S0085–2538*, 30817.
- [366] M. A. Saleem, M. J. O'Hare, J. Reiser, R. J. Coward, C. D. Inward, T. Farren, Y. X. Chang, L. Ni, P. W. Mathieson, P. Mundel, *J. Am. Soc. Nephrol.* **2002**, *13*, 630.
- [367] Q. Al-Awqati, J. A. Oliver, *Kidney Int.* **2002**, *61*, 387.
- [368] E. Bigaeva, E. Gore, E. Simon, M. Zwick, A. Oldenburger, K. P. de Jong, H. S. Hofker, M. Schlepütz, P. Nicklin, M. Boersema, J. F. Rippmann, P. Olinga, *Arch. Toxicol.* **2019**, *93*, 3549.
- [369] F. A. Yousef Yengej, J. Jansen, M. B. Rookmaaker, M. C. Verhaar, H. Clevers, *Cells* **2020**, *9*, 1326.
- [370] S. E. Howden, M. H. Little, in *Methods in Molecular Biology*, Humana Press Inc., Totowa **2020**, pp. 183–192.
- [371] S. M. Czerniecki, N. M. Cruz, J. L. Harder, R. Menon, J. Annis, E. A. Otto, R. E. Gulieva, L. V. Islas, Y. K. Kim, L. M. Tran, T. J. Martins, J. W. Pippin, H. Fu, M. Kretzler, S. J. Shankland, J. Himmelfarb, R. T. Moon, N. Paragas, B. S. Freedman, *Cell Stem Cell* **2018**, *22*, 929.
- [372] A. S. Shankar, Z. Du, H. T. Mora, T. P. P. van den Bosch, S. S. Korevaar, I. M. Van den Berg – Garrelds, E. Bindels, C. Lopez-Iglesias, M. C. Groningen, J. Gribnau, C. C. Baan, A. H. J. Danser, E. J. Hoorn, M. J. Hoogduijn, *Kidney Int.* **2020**, *S0085–2538*, 30968.
- [373] A. Przepiorski, V. Sander, T. Tran, J. A. Hollywood, B. Sorrenson, J. H. Shih, E. J. Wolvetang, A. P. McMahon, T. M. Holm, A. J. Davidson, *Stem Cell Rep.* **2018**, *11*, 470.
- [374] R. Nishinakamura, *Nat. Rev. Nephrol.* **2019**, *15*, 613.
- [375] P. R. Mertens, V. Espenkott, B. Venjakob, B. Heintz, S. Handt, H. G. Sieberth, *Hypertension* **1998**, *32*, 945.
- [376] Y. Cong, X. Han, Y. Wang, Z. Chen, Y. Lu, T. Liu, Z. Wu, Y. Jin, Y. Luo, X. Zhang, *Micromachines* **2020**, *11*, 381.
- [377] R. Novak, M. Ingram, S. Marquez, D. Das, A. Delahanty, A. Herland, B. M. Maoz, S. S. F. Jeanty, M. R. Somayaji, M. Burt, E. Calamari, A. Chalkiadaki, A. Cho, Y. Choe, D. B. Chou, M. Cronce, S. Dauth, T. Divic, J. Fernandez-Alcon, T. Ferrante, J. Ferrier, E. A. FitzGerald, R. Fleming, S. Jalili-Firoozinezhad, T. Grevesse, J. A. Goss, T. Hamkins-Indik, O. Henry, C. Hinojosa, T. Huffstater, K. J. Jang, V. Kujala, L. Leng, R. Mannix, Y. Milton, J. Nawroth, B. A. Nestor, C. F. Ng, B. O'Connor, T. E. Park, H. Sanchez, J. Sliz, A. Sontheimer-Phelps, B. Swenor, G. Thompson, G. J. Touloumes, Z. Tranchemontagne, N. Wen, M. Yadid, A. Bahinski, G. A. Hamilton, D. Levner, O. Levy, A. Przekwas, R. Prantil-Baun, K. K. Parker, D. E. Ingber, *Nat. Biomed. Eng.* **2020**, *4*, 407.
- [378] S. Musah, A. Mammoto, T. C. Ferrante, S. S. F. Jeanty, M. Hirano-Kobayashi, T. Mammoto, K. Roberts, S. Chung, R. Novak, M. Ingram, T. Fatanat-Didar, S. Koshy, J. C. Weaver, G. M. Church, D. E. Ingber, *Nat. Biomed. Eng.* **2017**, *1*, 0069.
- [379] F. Schutgens, M. B. Rookmaaker, T. Margaritis, A. Rios, C. Ammerlaan, J. Jansen, L. Gijzen, M. Vormann, A. Vonk, M. Viveen, F. Y. Yengej, S. Derakhshan, K. M. de Winter-de Groot, B. Artegiani, R. van Boxel, E. Cuppen, A. P. A. Hendrickx, M. M. van den Heuvel-Eibrink, E. Heitzer, H. Lanz, J. Beekman, J. L. Murk, R. Masereeuw, F. Holstege, J. Drost, M. C. Verhaar, H. Clevers, *Nat. Biotechnol.* **2019**, *37*, 303.
- [380] L. G. Van Der Flier, H. Clevers, *Annu. Rev. Physiol.* **2009**, *71*, 241.
- [381] W. W. Agace, K. D. McCoy, *Immunity* **2017**, *46*, 532.
- [382] J. König, J. Wells, P. D. Cani, C. L. Garcia-Ródenas, T. MacDonald, A. Mercenier, J. Whyte, F. Troost, R. J. Brummer, *Clin. Transl. Gastroenterol.* **2016**, *7*, e196.
- [383] T. C. Fung, C. A. Olson, E. Y. Hsiao, *Nat. Neurosci.* **2017**, *20*, 145.
- [384] J. Costa, A. Ahluwalia, *Front. Bioeng. Biotechnol.* **2019**, *7*, 144.
- [385] J. Tack, V. Stanghellini, F. Mearin, Y. Yiannakou, P. Layer, B. Coffin, M. Simren, J. Mackinnon, G. Wiseman, A. Marciniak, *BMC Gastroenterol.* **2019**, *19*, 69.
- [386] S. J. O'Brien, in *Encyclopedia of Food Safety*, Elsevier, Amsterdam **2014**, pp. 302–311.
- [387] European Medicines Agency, ICH Guideline M3(R2) on Non-Clinical Safety Studies for the Conduct of Human Clinical Trials and Marketing Authorisation for Pharmaceuticals, **2009**.
- [388] Regulation (EC) No 1907/2006, European Parliament, Regulation Concerning the Registration, Evaluation, Authorisation and Restriction of Chemicals (REACH), **2006**.
- [389] C. Federer, M. Yoo, A. C. Tan, *Assay Drug Dev. Technol.* **2016**, *14*, 557.
- [390] H. L. Philpott, S. Nandurkar, J. Lubel, P. R. Gibson, *Postgrad. Med. J.* **2014**, *90*, 411.
- [391] R. Düsing, K. Lottermoser, T. Mengden, *Nephrol. Dial. Transplant.* **2001**, *16*, 1317.
- [392] OECD (1998), *Test No. 409: Repeated Dose 90-Day Oral Toxicity Study in Non-Rodents*, OECD Publishing, Paris **1998**.

- [393] J. A. Jiminez, T. C. Uwiera, G. D. Inglis, R. R. E. Uwiera, *Gut Pathog.* **2015**, *7*, 29.
- [394] A. E. Tammariello, J. A. Milner, *J. Nutr. Biochem.* **2010**, *21*, 77.
- [395] J. C. Park, S. H. Im, *Exp. Mol. Med.* **2020**, *52*, 1383.
- [396] G. B. Hatton, V. Yadav, A. W. Basit, H. A. Merchant, *J. Pharm. Sci.* **2015**, *104*, 2747.
- [397] X. Cao, S. T. Gibbs, L. Fang, H. A. Miller, C. P. Landowski, H. C. Shin, H. Lennernas, Y. Zhong, G. L. Amidon, L. X. Yu, D. Sun, *Pharm. Res.* **2006**, *23*, 1675.
- [398] R. Nagpal, S. Wang, L. C. Solberg Woods, O. Seshie, S. T. Chung, C. A. Shively, T. C. Register, S. Craft, D. A. McClain, H. Yadav, *Front. Microbiol.* **2018**, *9*, 2897.
- [399] B. D. Wallace, H. Wang, K. T. Lane, J. E. Scott, J. Orans, J. S. Koo, M. Venkatesh, C. Jobin, L. A. Yeh, S. Mani, M. R. Redinbo, *Science* **2010**, *330*, 831.
- [400] J. Zhan, Y. Liang, D. Liu, X. Ma, P. Li, C. Liu, X. Liu, P. Wang, Z. Zhou, *Microbiome* **2018**, *6*, 224.
- [401] A. Vich Vila, V. Collij, S. Sanna, T. Sinha, F. Imhann, A. R. Bourgonje, Z. Mujagic, D. M. A. E. Jonkers, A. A. M. Masclee, J. Fu, A. Kurilshikov, C. Wijmenga, A. Zhernakova, R. K. Weersma, *Nat. Commun.* **2020**, *11*, 1.
- [402] A. R. Hilgers, R. A. Conradi, P. S. Burton, *Pharm Res.* **1990**, *7*, 902.
- [403] W. Rubas, N. Jezyk, G. M. Grass, *Pharm Res.* **1993**, *10*, 113.
- [404] T. Lesuffleur, A. Barbat, E. Dussaulx, A. Zweibaum, *Cancer Res.* **1990**, *50*, 6334.
- [405] S. Djelloul, M. E. Forgue-Lafitte, B. Hermelin, M. Mareel, E. Bruyneel, A. Baldi, A. Giordano, E. Chastre, C. Gespach, *FEBS Lett.* **1997**, *406*, 234.
- [406] A. M. Sääf, J. M. Halbleib, X. Chen, T. Y. Siu, Y. L. Suet, W. J. Nelson, P. O. Brown, *Mol. Biol. Cell* **2007**, *18*, 4245.
- [407] K. Lenaerts, F. K. Bouwman, W. H. Lamers, J. Renes, E. C. Mariman, *BMC Genomics* **2007**, *8*, 91.
- [408] R. Lehner, W. Wohlleben, D. Septiadi, R. Landsiedel, A. Petri-Fink, B. Rothen-Rutishauser, *Arch. Toxicol.* **2020**, *94*, 2463.
- [409] L. Cacopardo, J. Costa, N. Guazzelli, S. Giusti, S. Meucci, A. Corti, G. Mattei, A. Ahluwalia, *Biomed. Sci. Eng.* **2020**, *3*, 104.
- [410] H. J. Kim, D. Huh, G. Hamilton, D. E. Ingber, *Lab Chip* **2012**, *12*, 2165.
- [411] N. E. Zeitouni, S. Chotikatam, M. von Köckritz-Blickwede, H. Y. Naim, *Mol Cell Pediatr.* **2016**, *3*, 14.
- [412] Y. Chen, Y. Lin, K. M. Davis, Q. Wang, J. Rnjak-Kovacina, C. Li, R. R. Isberg, C. A. Kumamoto, J. Mecsas, D. L. Kaplan, *Sci. Rep.* **2015**, *5*, 13708.
- [413] N. E. Zeitouni, P. Dersch, H. Y. Naim, M. Von Köckritz-Blickwede, *PLoS One* **2016**, *11*, 0146103.
- [414] Y. Tazuke, R. A. Drongowski, D. H. Teitelbaum, A. G. Coran, *Pediatr. Surg. Int.* **2003**, *19*, 316.
- [415] H. Xu, F. Qu, H. Xu, W. Lai, Y. A. Wang, Z. P. Aguilar, H. Wei, *BioMetals* **2012**, *25*, 45.
- [416] J. Susewind, C. De Souza Carvalho-Wodarz, U. Repnik, E. M. Collnot, N. Schneider-Daum, G. W. Griffiths, C. M. Lehr, *Nanotoxicology* **2016**, *10*, 53.
- [417] A. A. M. Kämpfer, M. M. Busch, V. Büttner, G. Bredeck, B. Stahlmecke, B. Hellack, I. Masson, A. Sofranko, C. Albrecht, R. P. F. Schins, *Small* **2020**, *66*, 402.
- [418] T. Sato, R. G. Vries, H. J. Snippert, M. Van De Wetering, N. Barker, D. E. Stange, J. H. Van Es, A. Abo, P. Kujala, P. J. Peters, H. Clevers, *Nature* **2009**, *459*, 262.
- [419] T. Sato, D. E. Stange, M. Ferrante, R. G. J. Vries, J. H. Van Es, S. Van Den Brink, W. J. Van Houdt, A. Pronk, J. Van Gorp, P. D. Siersema, H. Clevers, *Gastroenterology* **2011**, *141*, 1762.
- [420] M. Kedinger, P. M. Simon-Assmann, B. Lacroix, A. Marxer, H. P. Hauri, K. Haffen, *Dev. Biol.* **1986**, *113*, 474.
- [421] J. R. Spence, C. N. Mayhew, S. A. Rankin, M. F. Kuhar, J. E. Vallance, K. Tolle, E. E. Hoskins, V. V. Kalinichenko, S. I. Wells, A. M. Zorn, N. F. Shroyer, J. M. Wells, *Nature* **2011**, *470*, 105.
- [422] L. Cao, J. D. Gibson, S. Miyamoto, V. Sail, R. Verma, D. W. Rosenberg, C. E. Nelson, C. Giardina, *Differentiation* **2011**, *81*, 1.
- [423] A. Mithal, A. Capilla, D. Heinze, A. Berical, C. Villacorta-Martin, M. Vedaie, A. Jacob, K. Abo, A. Szymaniak, M. Peasley, A. Stuffer, J. Mahoney, D. N. Kotton, F. Hawkins, G. Mostoslavsky, *Nat. Commun.* **2020**, *11*, 215.
- [424] C. L. Watson, M. M. Mahe, J. Múnera, J. C. Howell, N. Sundaram, H. M. Poling, J. I. Schweitzer, J. E. Vallance, C. N. Mayhew, Y. Sun, G. Grabowski, S. R. Finkbeiner, J. R. Spence, N. F. Shroyer, J. M. Wells, M. A. Helmrath, *Nat. Med.* **2014**, *20*, 1310.
- [425] S. R. Finkbeiner, D. R. Hill, C. H. Altheim, P. H. Dedhia, M. J. Taylor, Y. H. Tsai, A. M. Chin, M. M. Mahe, C. L. Watson, J. J. Freeman, R. Nattiv, M. Thomson, O. D. Klein, N. F. Shroyer, M. A. Helmrath, D. H. Teitelbaum, P. J. Dempsey, J. R. Spence, *Stem Cell Rep.* **2015**, *4*, 1140.
- [426] Y. S. Son, S. J. Ki, R. Thanavel, J. J. Kim, M. O. Lee, J. Kim, C. R. Jung, T. S. Han, H. S. Cho, C. M. Ryu, S. H. Kim, D. S. Park, M. Y. Son, *FASEB J.* **2020**, *34*, 9899.
- [427] K. B. Jung, H. Lee, Y. S. Son, M. O. Lee, Y. D. Kim, S. J. Oh, O. Kwon, S. Cho, H. S. Cho, D. S. Kim, J. H. Oh, M. Zilbauer, J. K. Min, C. R. Jung, J. Kim, M. Y. Son, *Nat. Commun.* **2018**, *9*, 3039.
- [428] N. Arora, J. I. Alsous, J. W. Guggenheim, M. Mak, J. Munera, J. M. Wells, R. D. Kamm, H. H. Asada, S. Y. Shvartsman, L. G. Griffith, *Development* **2017**, *144*, 1128.
- [429] T. Grabinger, L. Luks, F. Kostadinova, C. Zimmerlin, J. P. Medema, M. Leist, T. Brunner, *Cell Death Dis.* **2014**, *5*, 1228.
- [430] M. Navis, T. Martins Garcia, I. B. Renes, J. L. Vermeulen, S. Meisner, M. E. Wildenberg, G. R. van den Brink, R. M. van Elburg, V. Muncan, *EMBO Rep.* **2019**, *20*, 46221.
- [431] K. B. Jung, O. Kwon, M.-O. Lee, H. Lee, Y. S. Son, O. Habib, J.-H. Oh, H.-S. Cho, C.-R. Jung, J. Kim, M.-Y. Son, *J. Clin. Med.* **2019**, *8*, 976.
- [432] W. Lu, E. Rettenmeier, M. Paszek, M. F. Yueh, R. H. Tukey, J. Trottier, O. Barbier, S. Chen, *Drug Metab. Dispos.* **2017**, *45*, 748.
- [433] D. G. Belair, R. J. Visconti, M. Hong, M. Marella, M. F. Peters, C. W. Scott, K. L. Kolaja, *Toxicol. In Vitro* **2020**, *68*, 104928.
- [434] Y. G. Zhang, S. Wu, Y. Xia, J. Sun, *Physiol. Rep.* **2014**, *2*, 12147.
- [435] J. L. Leslie, S. Huang, J. S. Opp, M. S. Nagy, M. Kobayashi, V. B. Young, J. R. Spence, *Infect. Immun.* **2015**, *83*, 138.
- [436] T. Iwao, N. Kodama, Y. Kondo, T. Kabeya, K. Nakamura, T. Horikawa, T. Niwa, K. Kurose, T. Matsunaga, *Drug Metab. Dispos.* **2015**, *43*, 603.
- [437] T. Kabeya, S. Mima, Y. Imakura, T. Miyashita, I. Ogura, T. Yamada, T. Yasujima, H. Yuasa, T. Iwao, T. Matsunaga, *Drug Metab. Pharmacokin.* **2020**, *35*, 374.
- [438] T. Akazawa, S. Yoshida, S. Ohnishi, T. Kanazu, M. Kawai, K. Takahashi, *Drug Metab. Dispos.* **2018**, *46*, 1497.
- [439] K. Mayumi, T. Akazawa, T. Kanazu, S. Ohnishi, H. Hasegawa, *J. Pharm. Sci.* **2020**, *109*, 1605.
- [440] B. Sidar, B. R. Jenkins, S. Huang, J. R. Spence, S. T. Walk, J. N. Wilking, *Lab Chip* **2019**, *19*, 3552.
- [441] J. Y. Co, M. Margalef-Català, X. Li, A. T. Mah, C. J. Kuo, D. M. Monack, M. R. Amieva, *Cell Rep.* **2019**, *26*, 2509.
- [442] T. Roodsant, M. Navis, I. Aknouch, I. B. Renes, R. M. van Elburg, D. Pajkr, K. C. Wolthers, C. Schultsz, K. C. H. van der Ark, A. Sridhar, V. Muncan, *Front. Cell. Infect. Microbiol.* **2020**, *10*, 272.
- [443] L. R. Madden, T. V. Nguyen, S. Garcia-Mojica, V. Shah, A. V. Le, A. Peier, R. Visconti, E. M. Parker, S. C. Presnell, D. G. Nguyen, K. N. Retting, *iScience* **2018**, *2*, 156.
- [444] M. Kasendra, A. Tovaglieri, A. Sontheimer-Phelps, S. Jalili-Firoozinezhad, A. Bein, A. Chalkiadaki, W. Scholl, C. Zhang,

- H. Rickner, C. A. Richmond, H. Li, D. T. Breault, D. E. Ingber, *Sci. Rep.* **2018**, *8*, 2871.
- [445] S. Yoshida, H. Miwa, T. Kawachi, S. Kume, K. Takahashi, *Sci. Rep.* **2020**, *10*, 5989.
- [446] M. J. Workman, J. P. Gleeson, E. J. Troisi, H. Q. Estrada, S. J. Kerns, C. D. Hinojosa, G. A. Hamilton, S. R. Targan, C. N. Svendsen, R. J. Barrett, *Cell. Mol. Gastroenterol. Hepatol.* **2018**, *5*, 669.
- [447] K. L. Sinagoga, J. M. Wells, *EMBO J.* **2015**, *34*, 1149.
- [448] Y. H. Tsai, R. Nattiv, P. H. Dedhia, M. S. Nagy, A. M. Chin, M. Thomson, O. D. Klein, J. R. Spence, *Development* **2017**, *144*, 1045.
- [449] K. W. McCracken, J. C. Howell, J. M. Wells, J. R. Spence, *Nat. Protoc.* **2011**, *6*, 1920.
- [450] D. Carroll, *Genetics* **2011**, *188*, 773.
- [451] J. Boch, *Nat. Biotechnol.* **2011**, *29*, 135.
- [452] L. Cong, F. A. Ran, D. Cox, S. Lin, R. Barretto, N. Habib, P. D. Hsu, X. Wu, W. Jiang, L. A. Marraffini, F. Zhang, *Science* **2013**, *339*, 819.
- [453] P. Mali, L. Yang, K. M. Esvelt, J. Aach, M. Guell, J. E. DiCarlo, J. E. Norville, G. M. Church, *Science* **2013**, *339*, 823.
- [454] J. A. Doudna, *Nature* **2020**, *578*, 229.
- [455] F. Hille, H. Richter, S. P. Wong, M. Bratovič, S. Ressel, E. Charpentier, *Cell* **2018**, *172*, 1239.
- [456] J. Lee, D. Bayarsaikhan, G. Bayarsaikhan, J. S. Kim, E. Schwarzbach, B. Lee, *Pharmacol. Ther.* **2020**, *209*, 107501.
- [457] G. Vöfely, T. Berecz, E. Szabó, K. Szébényi, E. Hathy, T. I. Orbán, B. Sarkadi, L. Homolya, M. C. Marchetto, J. M. Réthelyi, Á. Apáti, *Mol. Cell. Neurosci.* **2018**, *88*, 222.
- [458] R. Shinnawi, I. Huber, L. Maizels, N. Shaheen, A. Gepstein, G. Arbel, A. J. Tijssen, L. Gepstein, *Stem Cell Rep.* **2015**, *5*, 582.
- [459] S. Li, M. Xia, *Arch. Toxicol.* **2019**, *93*, 3387.
- [460] Á. Apáti, N. Varga, T. Berecz, Z. Erdei, L. Homolya, B. Sarkadi, *Expert Opin. Drug Metab. Toxicol.* **2019**, *15*, 61.
- [461] C. Pires, B. Schmid, C. Petráeus, A. Poon, N. Nimsanor, T. T. Nielsen, G. Waldemar, L. E. Hjermind, J. E. Nielsen, P. Hyttel, K. K. Freude, *Stem Cell Res.* **2016**, *17*, 285.
- [462] S. Merkert, U. Martin, *Int. J. Mol. Sci.* **2016**, *17*, 1000.
- [463] C. Cheroni, N. Caporale, G. Testa, *Mol. Autism* **2020**, *11*, 69.
- [464] J. W. Lunden, M. Durens, J. Nestor, R. F. Niescier, K. Herold, C. Brandenburg, Y. C. Lin, G. J. Blatt, M. W. Nestor, *Advances in Neurobiology*, Springer, Berlin **2020**, pp. 259–297.
- [465] A. Sobh, A. Loguinov, G. N. Yazici, R. S. Zeidan, A. Tagmount, N. S. Hejazi, A. E. Hubbard, L. Zhang, C. D. Vulpe, *Toxicol. Sci.* **2019**, *169*, 108.
- [466] C. R. Reczek, K. Birsoy, H. Kong, I. Martínez-Reyes, T. Wang, P. Gao, D. M. Sabatini, N. S. Chandel, *Nat. Chem. Biol.* **2017**, *13*, 1274.
- [467] Y. Zhao, L. Wei, A. Tagmount, A. Loguinov, A. Sobh, A. Hubbard, C. M. McHale, C. J. Chang, C. D. Vulpe, L. Zhang, *Chemosphere* **2020**.
- [468] J. E. Negggers, B. Kwanten, T. Dierckx, H. Noguchi, A. Voet, L. Bral, K. Minner, B. Massant, N. Kint, M. Delforge, T. Vercruysse, E. Baloglu, W. Senapedis, M. Jacquemyn, D. Daelemans, *Nat. Commun.* **2018**, *9*, 502.
- [469] H. Shen, C. M. McHale, M. T. Smith, L. Zhang, *Mutat. Res.: Rev. Mutat. Res.* **2015**, *764*, 31.
- [470] S. Ahmed, Z. Zhou, J. Zhou, S. Q. Chen, *Genomics, Proteomics Bioinf.* **2016**, *14*, 298.
- [471] M. Bachtiar, B. N. S. Ooi, J. Wang, Y. Jin, T. W. Tan, S. S. Chong, C. G. L. Lee, *Pharmacogenomics J.* **2019**, *19*, 516.
- [472] S. C. Preissner, M. F. Hoffmann, R. Preissner, M. Dunkel, A. Gewiess, S. Preissner, *PLoS One* **2013**, *8*, 82562.
- [473] K. Takayama, Y. Morisaki, S. Kuno, Y. Nagamoto, K. Harada, N. Furukawa, M. Ohtaka, K. Nishimura, K. Imagawa, F. Sakurai, M. Tachibana, R. Sumazaki, E. Noguchi, M. Nakanishi, K. Hirata, K. Kawabata, H. Mizuguchi, *Proc. Natl. Acad. Sci. USA* **2014**, *111*, 16772.
- [474] D. P. Williams, *Philos. Trans. R. Soc., B* **2018**, *373*, 20170228.
- [475] V. Schwach, R. H. Slaats, R. Passier, *Front. Cardiovasc. Med.* **2020**, *7*, 50.
- [476] J. D. Stewart, R. Horvath, E. Baruffini, I. Ferrero, S. Bulst, P. B. Watkins, R. J. Fontana, C. P. Day, P. F. Chinnery, *Hepatology* **2010**, *52*, 1791.
- [477] M. I. Lucena, R. J. Andrade, C. Martínez, E. Ulzurrun, E. García-Martín, Y. Borraz, M. C. Fernández, M. Romero-Gomez, A. Castiella, R. Planas, J. Costa, S. Anzola, J. A. G. Agúndez, *Hepatology* **2008**, *48*, 588.
- [478] C. S. Ng, A. Hasnat, A. Al Maruf, M. U. Ahmed, M. Pirmohamed, C. P. Day, G. P. Aithal, A. K. Daly, *Eur. J. Clin. Pharmacol.* **2014**, *70*, 1079.
- [479] J. L. Mega, S. L. Close, S. D. Wiviott, L. Shen, R. D. Hockett, J. T. Brandt, J. R. Walker, E. M. Antman, W. Macias, E. Braunwald, M. S. Sabatine, *N. Engl. J. Med.* **2009**, *360*, 354.
- [480] L. Wojnowski, B. Kulle, M. Schirmer, G. Schlüter, A. Schmidt, A. Rosenberger, S. Vonhof, H. Bickeböller, M. R. Toliat, E. K. Suk, M. Tzvetkov, A. Kruger, S. Seifert, M. Kloess, H. Hahn, M. Loeffler, P. Nürnberg, M. Pfreundschuh, L. Trümper, J. Brockmüller, G. Hasenfuss, *Circulation* **2005**, *112*, 3754.
- [481] E. Christidi, H. Huang, S. Shafaattalab, A. Maillet, E. Lin, K. Huang, Z. Laksman, M. K. Davis, G. F. Tibbits, L. R. Brunham, *Sci. Rep.* **2020**, *10*, 10363.
- [482] S. Deguchi, T. Yamashita, K. Igai, K. Harada, Y. Toba, K. Hirata, K. Takayama, H. Mizuguchi, *Drug Metab. Dispos.* **2019**, *47*, 632.
- [483] J. Parrish, K. Lim, B. Zhang, M. Radisic, T. B. F. Woodfield, *Trends Biotechnol.* **2019**, *37*, 1327.
- [484] M. Karimi, S. Bahrami, H. Mirshekari, S. M. M. Basri, A. B. Nik, A. R. Aref, M. Akbari, M. R. Hamblin, *Lab Chip* **2016**, *16*, 2551.
- [485] S. Ahadian, R. Civitarese, D. Bannerman, M. H. Mohammadi, R. Lu, E. Wang, L. Davenport-Huyer, B. Lai, B. Zhang, Y. Zhao, S. Mandla, A. Korolj, M. Radisic, *Adv. Healthcare Mater.* **2018**, *7*, 1700506.
- [486] B. Zhang, M. Radisic, *Lab Chip* **2017**, *17*, 2395.
- [487] T. Osaki, Y. Shin, V. Sivathanu, M. Campisi, R. D. Kamm, *Adv. Healthcare Mater.* **2018**, *7*.
- [488] B. M. Maoz, A. Herland, E. A. Fitzgerald, T. Grevesse, C. Vidoudez, A. R. Pacheco, S. P. Sheehy, T. E. Park, S. Dauth, R. Mannix, N. Budnik, K. Shores, A. Cho, J. C. Nawroth, D. Segrè, B. Budnik, D. E. Ingber, K. K. Parker, *Nat. Biotechnol.* **2018**, *36*, 865.
- [489] S. Sances, R. Ho, G. Vatine, D. West, A. Laperle, A. Meyer, M. Godoy, P. S. Kay, B. Mandefro, S. Hatata, C. Hinojosa, N. Wen, D. Sareen, G. A. Hamilton, C. N. Svendsen, *Stem Cell Rep.* **2018**, *10*, 1222.
- [490] Y. Wang, H. Wang, P. Deng, W. Chen, Y. Guo, T. Tao, J. Qin, *Lab Chip* **2018**, *18*, 3606.
- [491] G. Wang, M. L. McCain, L. Yang, A. He, F. S. Pasqualini, A. Agarwal, H. Yuan, D. Jiang, D. Zhang, L. Zangi, J. Geva, A. E. Roberts, Q. Ma, J. Ding, J. Chen, D. Z. Wang, K. Li, J. Wang, R. J. A. Wanders, W. Kulik, F. M. Vaz, M. A. Laflamme, C. E. Murry, K. R. Chien, R. I. Kelley, G. M. Church, K. K. Parker, W. T. Pu, *Nat. Med.* **2014**, *20*, 616.
- [492] T. Tao, Y. Wang, W. Chen, Z. Li, W. Su, Y. Guo, P. Deng, J. Qin, *Lab Chip* **2019**, *19*, 948.
- [493] M. R. Zanolli, H. Ardalani, J. Zhang, Z. Hou, E. H. Nguyen, S. Swanson, B. K. Nguyen, J. Bolin, A. Elwell, L. L. Bischel, A. W. Xie, R. Stewart, D. J. Beebe, J. A. Thomson, M. P. Schwartz, W. L. Murphy, *Acta Biomater.* **2016**, *35*, 32.
- [494] B. W. Ellis, A. Acun, U. Isik Can, P. Zorlutuna, *Biomicrofluidics* **2017**, *11*, 024105.
- [495] J. Ribas, Y. S. Zhang, P. R. Pitrez, J. Leijten, M. Miscuglio, J. Rouwkema, M. R. Dokmeci, X. Nissan, L. Ferreira, A. Khademhosseini, *Small* **2017**, *13*, 1603737.
- [496] K. K. Lee, H. A. McCauley, T. R. Broda, M. J. Kofron, J. M. Wells, C. I. Hong, *Lab Chip* **2018**, *18*, 3079.

- [497] K. Achberger, C. Probst, J. C. Haderspeck, S. Bolz, J. Rogal, J. Chuchuy, M. Nikolova, V. Cora, L. Antkowiak, W. Haq, N. Shen, K. Schenke-Layland, M. Ueffing, S. Liebau, P. Loskill, *Elife* **2019**, *8*, e46188.
- [498] M. Zhang, C. Xu, L. Jiang, J. Qin, *Toxicol. Res.* **2018**, *7*, 1048.
- [499] E. M. Materne, A. P. Ramme, A. P. Terrasso, M. Serra, P. M. Alves, C. Brito, D. A. Sakharov, A. G. Tonevitsky, R. Lauster, U. Marx, *J. Biotechnol.* **2015**, *205*, 36.
- [500] D. Bovard, A. Sandoz, K. Luettich, S. Frentzel, A. Iskandar, D. Marescotti, K. Trivedi, E. Guedj, Q. Dutertre, M. C. Peitsch, J. Hoeng, *Lab Chip* **2018**, *18*, 3814.
- [501] M. B. Esch, T. L. King, M. L. Shuler, *Annu. Rev. Biomed. Eng.* **2011**, *13*, 55.
- [502] N. Tsamandouras, W. L. K. Chen, C. D. Edington, C. L. Stokes, L. G. Griffith, M. Cirit, *AAPS J.* **2017**, *19*, 1499.
- [503] C. Oleaga, C. Bernabini, A. S. T. Smith, B. Srinivasan, M. Jackson, W. McLamb, V. Platt, R. Bridges, Y. Cai, N. Santhanam, B. Berry, S. Najjar, N. Akanda, X. Guo, C. Martin, G. Ekman, M. B. Esch, J. Langer, G. Ouedraogo, J. Cotovio, L. Breton, M. L. Shuler, J. J. Hickman, *Sci. Rep.* **2016**, *6*, 20030.
- [504] A. Sharma, S. Sances, M. J. Workman, C. N. Svendsen, *Cell Stem Cell* **2020**, *26*, 309.
- [505] N. R. Wevers, R. Van Vught, K. J. Wilschut, A. Nicolas, C. Chiang, H. L. Lanz, S. J. Trietsch, J. Joore, P. Vulto, *Sci. Rep.* **2016**, *6*, 38856.
- [506] E. Naumovska, G. Aalderink, C. W. Valencia, K. Kosim, A. Nicolas, S. Brown, P. Vulto, K. S. Erdmann, D. Kurek, *Int. J. Mol. Sci.* **2020**, *21*, 4964.
- [507] F. Salaris, A. Rosa, *Brain Res.* **2019**, *1723*, 146393.
- [508] H. Cui, M. Nowicki, J. P. Fisher, L. G. Zhang, *Adv. Healthcare Mater.* **2017**, *6*.
- [509] P. Zhuang, J. An, L. P. Tan, C. K. Chua, in *Proc. Int. Conf. Progress in Additive Manufacturing*, ISSN National Centre For Singapore, Singapore **2018**, pp. 183–188.
- [510] Z. Gu, J. Fu, H. Lin, Y. He, *Asian J. Pharm. Sci.* **2020**, *15*, 529.
- [511] L. de la Vega, C. Lee, R. Sharma, M. Amereh, S. M. Willerth, *Brain Res. Bull.* **2019**, *150*, 240.
- [512] S. Ilkhanizadeh, A. I. Teixeira, O. Hermanson, *Biomaterials* **2007**, *28*, 3936.
- [513] J. Sun, H. Tan, *Materials* **2013**, *6*, 1285.
- [514] C. Licht, J. C. Rose, A. O. Anarkoli, D. Blondel, M. Roccio, T. Haraszti, D. B. Gehlen, J. A. Hubbell, M. P. Lutolf, L. De Laporte, *Biomacromolecules* **2019**, *20*, 4075.
- [515] M. Bahram, N. Mohseni, M. Moghtader, in *Emerging Concepts Anal. Appl. Hydrogels*, IntechOpen Limited, London **2016**.
- [516] N. Noor, A. Shapira, R. Edri, I. Gal, L. Wertheim, T. Dvir, *Adv. Sci.* **2019**, *6*, 1900344.
- [517] S. Romanazzo, S. Nemeč, I. Roohani, *Materials* **2019**, *12*, 2453.
- [518] C. S. Ong, P. Yesantharao, C. Y. Huang, G. Mattson, J. Boktor, T. Fukunishi, H. Zhang, N. Hibino, *Pediatr. Res.* **2018**, *83*, 223.
- [519] F. Maiullari, M. Costantini, M. Milan, V. Pace, M. Chirivi, S. Maiullari, A. Rainer, D. Baci, H. E. S. Marei, D. Seliktar, C. Gargioli, C. Bearzi, R. Rizzi, *Sci. Rep.* **2018**, *8*, 13532.
- [520] Q. Gu, E. Tomaskovic-Crook, G. G. Wallace, J. M. Crook, in *Methods in Molecular Biology*, Humana Press Inc., Totowa **2018**, pp. 129–138.
- [521] A. Faulkner-Jones, C. Fyfe, D. J. Cornelissen, J. Gardner, J. King, A. Courtney, W. Shu, *Biofabrication* **2015**, *7*, 044102.
- [522] R. Lister, M. Pelizzola, Y. S. Kida, R. D. Hawkins, J. R. Nery, G. Hon, J. Antosiewicz-Bourget, R. Ogmalley, R. Castanon, S. Klugman, M. Downes, R. Yu, R. Stewart, B. Ren, J. A. Thomson, R. M. Evans, J. R. Ecker, *Nature* **2011**, *471*, 68.
- [523] L. C. Laurent, I. Ulitsky, I. Slavin, H. Tran, A. Schork, R. Morey, C. Lynch, J. V. Harness, S. Lee, M. J. Barrero, S. Ku, M. Martynova, R. Semechkin, V. Galat, J. Gottesfeld, J. C. I. Belmonte, C. Murry, H. S. Keirstead, H. S. Park, U. Schmidt, A. L. Laslett, F. J. Muller, C. M. Nievergelt, R. Shamir, J. F. Loring, *Cell Stem Cell* **2011**, *8*, 106.
- [524] T. M. Schlaeger, L. Daheron, T. R. Brickler, S. Entwisle, K. Chan, A. Cianci, A. DeVine, A. Ettenger, K. Fitzgerald, M. Godfrey, D. Gupta, J. McPherson, P. Malwadkar, M. Gupta, B. Bell, A. Doi, N. Jung, X. Li, M. S. Lynes, E. Brookes, A. B. C. Cherry, D. Demirbas, A. M. Tsankov, L. I. Zon, L. L. Rubin, A. P. Feinberg, A. Meissner, C. A. Cowan, G. Q. Daley, *Nat. Biotechnol.* **2015**, *33*, 58.
- [525] Y. Yoshida, K. Takahashi, K. Okita, T. Ichisaka, S. Yamanaka, *Cell Stem Cell* **2009**, *5*, 237.
- [526] K. Kim, R. Zhao, A. Doi, K. Ng, J. Unternaehrer, P. Cahan, H. Hongguang, Y. H. Loh, M. J. Aryee, M. W. Lensch, H. Li, J. J. Collins, A. P. Feinberg, G. Q. Daley, *Nat. Biotechnol.* **2011**, *29*, 1117.
- [527] S. Logan, T. Arzua, S. G. Canfield, E. R. Seminary, S. L. Sison, A. D. Ebert, X. Bai, *Compr. Physiol.* **2019**, *9*, 565.
- [528] D. L. Villeneuve, D. Crump, N. Garcia-Reyero, M. Hecker, T. H. Hutchinson, C. A. LaLone, B. Landesmann, T. Lettieri, S. Munn, M. Nepelska, M. A. Ottinger, L. Vergauwen, M. Whelan, *Toxicol. Sci.* **2014**, *142*, 312.
- [529] D. L. Villeneuve, D. Crump, N. Garcia-Reyero, M. Hecker, T. H. Hutchinson, C. A. LaLone, B. Landesmann, T. Lettieri, S. Munn, M. Nepelska, M. A. Ottinger, L. Vergauwen, M. Whelan, *Toxicol. Sci.* **2014**, *142*, 321.
- [530] S. M. Bell, X. Chang, J. F. Wambaugh, D. G. Allen, M. Bartels, K. L. R. Brouwer, W. M. Casey, N. Choksi, S. S. Ferguson, G. Fraczkiwicz, A. M. Jarabek, A. Ke, A. Lumen, S. G. Lynn, A. Paini, P. S. Price, C. Ring, T. W. Simon, N. S. Sipes, C. S. Sprankle, J. Strickland, J. Troutman, B. A. Wetmore, N. C. Kleinstreuer, *Toxicol. In Vitro* **2018**, *47*, 213.
- [531] Y. Li, R. A. Wingert, *Clin. Transl. Med.* **2013**, *2*, 11.



## 2.2 Neural In Vitro Models for Studying Substances Acting on the Central Nervous System

*Ellen Fritsche, Julia Tigges, Julia Hartmann, Julia Kapr, Melania M. Serafini, Barbara Viviani*

Animal models have been greatly contributing to our understanding of physiology, mechanisms of diseases, and toxicity. Yet, their limitations due to, e.g., interspecies variation are reflected in the high number of drug attrition rates, especially in central nervous system (CNS) diseases. Therefore, human-based neural in vitro models for studying safety and efficacy of substances acting on the CNS are needed. Human iPSC-derived cells offer such a platform with the unique advantage of reproducing the “human context” in vitro by preserving the genetic and molecular phenotype of their donors. Guiding the differentiation of hiPSC into cells of the nervous system and combining them in a 2D or 3D format allows to obtain complex models suitable for investigating neurotoxicity or brain-related diseases with patient-derived cells. This chapter will give an overview over stem cell-based human 2D neuronal and mixed neuronal/astrocyte models, in vitro cultures of microglia, as well as CNS disease models and considers new developments in the field, more specifically the use of brain organoids and 3D bioprinted in vitro models for safety and efficacy evaluation.

Journal:	Springer Handbook of Experimental Pharmacology
Impact factor:	not calculated for book chapters
Contribution to the publication:	15%
	Section Text on 3D Bioprinted In Vitro Neural Models
Type of authorship:	Co-author
Status of publication:	Published (28 June 2020)



# Neural In Vitro Models for Studying Substances Acting on the Central Nervous System

Ellen Fritsche, Julia Tigges, Julia Hartmann, Julia Kapr, Melania Maria Serafini, and Barbara Viviani

## Contents

- 1 Introduction into In Vitro Neurotoxicity Evaluation
    - 1.1 Stem Cell-Based Human 2D Neuronal and Mixed Neuronal/Astrocyte Models
    - 1.2 In Vitro Cultures of Microglia
    - 1.3 Moving In Vitro Cultures into the Third Dimension with Brain Organoids
    - 1.4 3D Bioprinted In Vitro Neural Models
    - 1.5 CNS Disease Models
  - 2 Summary and Conclusion
- References

## Abstract

Animal models have been greatly contributing to our understanding of physiology, mechanisms of diseases, and toxicity. Yet, their limitations due to, e.g., interspecies variation are reflected in the high number of drug attrition rates, especially in central nervous system (CNS) diseases. Therefore, human-based neural in vitro models for studying safety and efficacy of substances acting on the CNS are needed. Human iPSC-derived cells offer such a platform with the unique advantage of reproducing the “human context” in vitro by preserving the genetic

Ellen Fritsche, Julia Tigges, Julia Hartmann, Julia Kapr, Melania Maria Serafini, and Barbara Viviani contributed equally to this work.

E. Fritsche (✉) · J. Tigges · J. Hartmann · J. Kapr  
IUF-Leibniz Research Institute for Environmental Medicine at the Heinrich-Heine-University  
Dusseldorf gGmbH, Dusseldorf, Germany  
e-mail: ellen.fritsche@iuf-duesseldorf.de; julia.tigges@iuf-duesseldorf.de;  
julia.hartmann@iuf-duesseldorf.de; julia.kapr@iuf-duesseldorf.de

M. M. Serafini · B. Viviani (✉)  
Department of Pharmacological and Biomolecular Sciences, University of Milan, Milan, Italy  
e-mail: melania.serafini@unimi.it; barbara.viviani@unimi.it

and molecular phenotype of their donors. Guiding the differentiation of hiPSC into cells of the nervous system and combining them in a 2D or 3D format allows to obtain complex models suitable for investigating neurotoxicity or brain-related diseases with patient-derived cells. This chapter will give an overview over stem cell-based human 2D neuronal and mixed neuronal/astrocyte models, in vitro cultures of microglia, as well as CNS disease models and considers new developments in the field, more specifically the use of brain organoids and 3D bioprinted in vitro models for safety and efficacy evaluation.

---

### Keywords

Bioprinted neuronal models · Brain organoids · CNS disease models · Developmental neurotoxicity (DNT) · Human induced pluripotent stem cells (hiPSCs) · Microglia culture · Neurotoxicity (NT)

---

## 1 Introduction into In Vitro Neurotoxicity Evaluation

Adult *neurotoxicity* occurs when exposure to natural or human-made toxic substances (*neurotoxicants*) alters the normal activity of the nervous system. It can eventually disrupt or even kill *neurons* or the surrounding *glial* cells, influencing the transmission and processing of signals in the brain and other parts of the *nervous system*. Neurotoxicity can result from exposure to substances used in radiation treatment, chemotherapy, other drug therapies, and organ transplants, as well as exposure to heavy metals such as lead and mercury; certain foods and food additives; pesticides; industrial and/or cleaning solvents; cosmetics, i.e., mercury for skin bleaching or new actives with unknown systemic effects; and some naturally occurring substances (Massaro 2002). Symptoms may appear immediately after exposure or be delayed. They may include limb weakness or numbness; loss of memory or vision; headache; intellect, cognitive, and behavioral problems; and visceral, including sexual dysfunction. Individuals with certain disorders may be especially vulnerable to neurotoxicants (National Institute of Health Neurotoxicity Information 2019).

The recognized test method for evaluating the neurotoxic potential of chemicals is the OECD Guideline 424 (Neurotoxicity studies in rodents). This method uses complex in vivo tests which are often labor-intensive and expensive (Crofton et al. 2012) and might also not well reflect the human situation because of interspecies variation (Leist and Hartung 2013). Such interspecies variation is also thought to be one of the reasons for the high attrition rates in drug development. Before a drug candidate can be taken into human clinical trials, it must be tested for safety and efficacy in animals that display relevant disease characteristics. This poses unique challenges in *central nervous system* (CNS) research, because of the difficulties to induce or quantify, e.g., depression, anxiety, or impairment of social interaction. In addition, pharmacokinetics and pharmacodynamics might differ between species

and thus cause poor prediction for beneficial or adverse effects in humans (Toutain et al. 2010). It stands to reason that diseases with the most complex and least understood etiologies are typically the ones that are the hardest to develop treatments for, which is reflected in the translation failure of CNS drug discovery (Danon et al. 2019; Gribkoff and Kaczmarek 2017).

Understanding compounds' modes of action (*MoA*) and pathophysiology of disease in the human context is of high importance for correct safety and efficacy predictions. This is exemplified by the activation of peroxisome proliferator-activated receptor alpha (PPAR $\alpha$ ) via PPAR $\alpha$  agonists inducing liver tumors in rodents, yet not in humans, probably due to lower PPAR $\alpha$  and/or co-activators/co-repressors expression in the latter (Klaunig et al. 2003). Here, animal models overestimate PPAR $\alpha$  agonists' hazard for human health. In the case of searching for drugs curing Alzheimer's disease, animal models, which are genetically predisposed to generate A $\beta$  plaques or neurofibrillary tangles of Tau protein, have been used. Yet no results have translated from these animal disease models into effective human medication, probably because they do not represent human AD pathophysiology sufficiently (Danon et al. 2019).

These two examples nicely pin down the issue of model predictivity in compound safety and efficacy evaluation and their translation to human health. One strategy to overcome such translational shortcomings lies in the use of test systems of human origin. Therefore, the biomedical achievement of producing human induced pluripotent stem cells (*hiPSC*) from somatic cells (Takahashi et al. 2007) opened up a whole new arena in the ethically sound production of an unlimited number of human cells, including neurons and glia. In addition, the recent surge in tissue modeling, by culturing such cells in three dimensions (*3D*), is producing a paradigm shift in disease modeling and in pharmacological as well as toxicological testing strategies (Lancaster and Knoblich 2014; Lancaster et al. 2017; Pasca 2018). In vitro cultures are currently also taken to the next level by their growth in bioreactors, which, when connected, can be assembled as organs-on-the-chip and designed to mimic in vivo environments (Park et al. 2019).

Such *new approach methods* (NAMs) cannot be used in an isolated manner, as a cell culture does not represent a whole organism, even if cells grow in 3D. Therefore, frameworks are needed that allow the interpretation of data generated with human 2D or 3D in vitro methods (Fig. 1). One general deficiency of in vitro methods is the lack of picturing pharmacokinetics that is crucial for toxicity and efficacy evaluation. Here, physiology-based pharmacokinetics modeling can be of great help (Paini et al. 2019; Zhuang and Lu 2016) as it provides wet-lab researchers with target tissue concentrations as rationales for their in vitro studies. Finding that human exposure-relevant concentrations is fundamental, yet how to choose and proceed with the readouts of in vitro studies? Here, the "Adverse Outcome Pathway" (AOP) concept is of tremendous help. The AOP is an organizational model that identifies a sequence of biochemical and cellular events (*molecular initiating event*, MIE; *key events*, KE) required to produce a toxic effect (*adverse outcome*, AO) when an organism is exposed to a substance (Fig. 1). Construction of an AOP can (1) organize information about biological interactions and toxicity mechanisms into models that describe

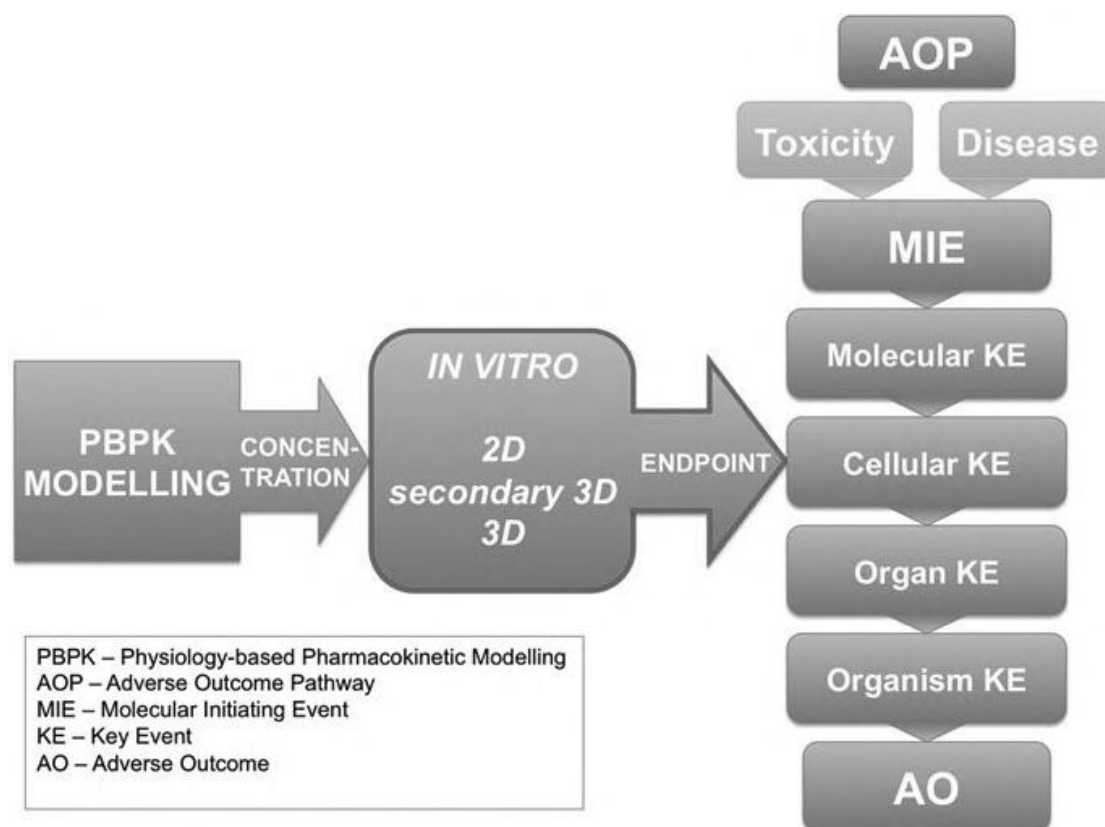


**Fig. 1** Framing of data from in vitro models with pharmacokinetics information from PBPK modeling and endpoint judgment according to the AOP concept

how exposure to a substance might cause illness or injury, (2) suggest cell- or biochemical-based tests for pathway elements that could be used to develop testing strategies for targeted toxicity, and (3) identify data gaps in a pathway of toxicity that need more information with the final goal of using fewer resources and experimental animals (Ankley et al. 2010). This concept was soon also applied to neurotoxicity (Bal-Price et al. 2015). Recently it was suggested that the AOP framework is also applicable to understanding disease pathways for prevention, diagnosis, and treatment and in biomedical and clinical research for drug discovery, efficacy, and safety testing (Carusi et al. 2018). Studying cellular effects with in vitro methods in a conceptual framework for toxicity or disease provides drug developers and basic or regulatory scientists with greater confidence in the meaningfulness and thus applicability of generated in vitro data (Fig. 1). In the end, higher human relevance of scientific outcomes will protect society and the individual and also reduce health-care costs.

Neurotoxicity can be triggered by a multitude of MoA (Masjosthusmann et al. 2018). In vitro, this MoA can either be measured as specific changes in endpoints, like effects on ion currents, specific receptor activation, or loss in myelin. In addition, MoA can cause neuronal cell death, an endpoint relevant for in vitro and in vivo neurotoxicology. For example, excitatory cell death can occur through stimulation of glutamatergic neurotransmission, or dopaminergic cell death can be

induced via mitochondrial dysfunction. Although neural cell death is indeed a relevant endpoint, it does not inform on the underlying MIE. Moreover, a compound not inducing neural cell death cannot be excluded as a neurotoxicant. When studying neurotoxicity in vitro, knowledge about molecular equipment of cells is crucial for defining the application domain of the respective model.

This chapter now intends to fill the red box in Fig. 1 by summarizing the current state of the art on hiPSC/ESC-based 2D or secondary 3D neuronal and mixed neuronal/glial as well as microglial models, neural organoids, bioprinted neural models, and 2D or 3D neurological disease models. Such find their application in pharma- and toxicological studies by investigating endpoints in vitro that lead to AOs or possibly represent relevant therapeutic targets. A summary of the main toxicological targets is given in Table 1. Although historically most brain-related in vitro data has been derived from rodents (Masjosthusmann et al. 2018), this chapter will focus on published human test systems due to the species specificities discussed above.

## **1.1 Stem Cell-Based Human 2D Neuronal and Mixed Neuronal/Astrocyte Models**

*Stem cells* (SC) are divided into adult stem cells and *embryonic stem cells* (ESC), depending on their origin and potency (Singh et al. 2015). ESCs are derived from the inner cell mass of the blastocyst and have the ability to self-renew and to generate all cell types of the body except extraembryonic cells (placenta) and are therefore termed pluripotent (Guenther 2011). In 1998 the first human ESC line was isolated from human embryos initially produced for in vitro fertilization (Thomson et al. 1998).

Yamanaka and co-workers created the basis for a new generation of neural in vitro models by developing the Nobel Prize-winning cell system of *human induced pluripotent stem cells* (hiPSC). These cells can be derived from human mature somatic cells by different reprogramming methods (Janabi et al. 1995; Lowry and Plath 2008; Warren et al. 2010; Zhang et al. 2013; Victor et al. 2014) and thus avoid the ethical issues of human ESC (Takahashi et al. 2007; Yu et al. 2007). Human iPSC can be differentiated into cells from all three germ layers (Takahashi et al. 2007; Shi et al. 2017).

Using hiPSC, it is possible to induce a variety of neural cell types. *Neural stem cells* (NSCs) and *neuronal progenitor cells* (NPCs) can be differentiated from hiPSC in large quantities with high reproducibility (Farkhondeh et al. 2019). Cheng and co-workers describe a method to generate NPC from hiPSC using a multistep protocol including embryoid body formation and formation of neural rosettes, followed by multidimensional fluorescence-activated cell sorting (FACS) to purify NPCs by using a set of cell surface markers (Cheng et al. 2017). The authors claim that these cells are suitable for probing human neuroplasticity and mechanisms underlying CNS disorders using high-content, single-cell level automated microscopy assays. Still, a proof-of-concept study remains to be published.

**Table 1** Mode of action (MoA) relevant for human neurotoxicity identified within a systematic review investigating 248 individual chemical compounds, 23 compound classes, and 212 natural neurotoxins (Masjosthusmann et al. 2018; modified from Appendix D)

#	Mode of action	MoA related to
1	Stimulation of cholinergic neurotransmission	Neurotransmission
2	Inhibition of cholinergic neurotransmission	
3	Stimulation of GABAergic neurotransmission	
5	Inhibition of glycinergic neurotransmission	
6	Stimulation of glutamatergic neurotransmission	
7	Inhibition of glutamatergic neurotransmission	
8	Stimulation of adrenergic neurotransmission	
9	Inhibition of adrenergic neurotransmission	
10	Stimulation of serotonergic neurotransmission	
11	Inhibition of serotonergic neurotransmission	
12	Inhibition of dopaminergic neurotransmission	
13	Neurotransmission in general	
14	Activation of sodium channels	
15	Inhibition of sodium channels	
16	Inhibition of potassium channels	
17	Inhibition of calcium channels	
18	Activation of chloride channels	
19	Inhibition of chloride channels	
20	Effects on other neuronal receptors	
21	Mitochondrial dysfunction/oxidative stress/apoptosis	Cell biology
22	Redox cycling	
23	Altered calcium signaling	
24	Cytoskeletal alterations	
25	Neuroinflammation	
26	Axonopathies	
27	Myelin toxicity	
28	Delayed neuropathy	
29	Enzyme inhibition	
30	Other	

Human iPSC-derived neurons can be generated directly from hiPSC or with NSCs/NPCs as an intermediate step (Yu et al. 2014; Ghaffari et al. 2018). The latter protocol takes about 2 weeks and can be used for the evaluation of drug efficacy, although purity and maturity of the cells are in question and need further characterization (Farkhondeh et al. 2019; Dai et al. 2016).

Numerous protocols have been published describing the generation of specific neuronal subtypes as well as glial cells from hiPSC such as *cortical neurons* (Shi et al. 2014; Eiraku et al. 2008; Boissart et al. 2013), *glutamatergic neurons* (Boissart et al. 2013; Cheng et al. 2017; Wang et al. 2017; D’Aiuto et al. 2014; Sanchez-Danes et al. 2012; Yu et al. 2009; Nehme et al. 2018), *GABAergic neurons* (Yang et al. 2017; Liu et al. 2013; Flames et al. 2007; Manabe et al. 2005), *serotonergic and*

*dopaminergic neurons* (Chambers et al. 2009; Cooper et al. 2012; Kriks et al. 2011; Sanchez-Danes et al. 2012; Li et al. 2017), *motor neurons* (Corti et al. 2012; Sareen et al. 2012, 2013; Kiskinis et al. 2014; Maury et al. 2015), *sensory neurons* (Boisvert et al. 2015; Stacey et al. 2018), *astrocytes* (Lundin et al. 2018; Suga et al. 2019), *oligodendrocytes* (Osaki et al. 2018; Ehrlich et al. 2017; García-León et al. 2018b), and *microglia* (McQuade et al. 2018), just to name a few. In this chapter, we will focus on published in vitro systems that have already been used for screening approaches or are at a state of assay development that will allow substance screening in the near future.

Malik and co-workers established a high-throughput screening platform using hiPSC-derived NSCs and rat cortical cells to screen a compound library of 2,000 chemicals including known drugs (50%), natural products (30%), and bioactive compounds (20%) for their cytotoxic potential (Malik et al. 2014; Efthymiou et al. 2014). In a follow-up study, a subset of 100 compounds was screened in hiPSC, NSC-derived neurons (Efthymiou et al. 2014), and fetal astrocytes. This approach enabled the authors to identify species- and cell type-specific differences in responses to compounds. Specifically, they found that human NSCs were more sensitive to the screened compounds than rodent cultures. In addition, they identified compounds with cell type-specific toxicities. A limitation of the study is the assessment of cytotoxicity as the sole endpoint, which might not be the most sensitive one. Another restriction of this approach is the lack of co-culture of neuronal and glial cells. Moreover, in the species comparison, cells from different maturation stages and single (human) versus co-cultures (rat) were related, making data interpretation difficult.

Another study used small molecule-based NPCs differentiated from three different hiPSC lines, which were then differentiated into neurons and astrocytes within 15 days, using a highly standardized protocol (Seidel et al. 2017). The authors used *multi-microelectrode arrays* (MMEA) for monitoring neuronal network activities via field potential measurements. Such recordings assess multiple endpoints stipulating that different neuronal receptors are expressed by the cells (Table 1). Here, they show reactivity towards dopamine, GABA, serotonin, acetylcholine, and glutamic acid, but not norepinephrine. To date, there are no general guidelines for the analysis and quantification of MMEA measurements. Seidel et al. use single electrodes as the statistical unit, but using different chips or experiments as an individual “n” number would be preferable to assess the reproducibility and standardization between experiments (Masjosthusmann et al. 2018).

In recent years, more and more companies have been offering commercially available hiPSC-based neuronal cells. One study compared different commercially available hiPSC-derived mature neurons (excitatory and inhibitory) from different suppliers, with and without astrocyte co-culture, again utilizing MMEA activity as a functional readout, this time in combination with measurements of calcium signaling (Tukker et al. 2016). Treatment with glutamate and GABA strongly reduced the mean spike rate of the analyzed cultures. Calcium transients of individual neurons were generated upon treatment with glutamate, GABA, and acetylcholine. Here, astrocytes seem to be crucial for *neuronal network* generation because pure neuronal

cultures in the absence of astrocytes lack bursting, a sign for neuronal network maturity. In this study, the statistical unit was chosen as one well of a 48-well plate, not allowing assessment of reproducibility and standardization between experiments (Masjosthusmann et al. 2018). A follow-up study in 2018 also used commercially available hiPSC-derived neurons and astrocytes, this time exploring the effect of the ratio of mixed neurons and astrocytes (Tukker et al. 2018). This study strongly supports the previous observation that the addition of astrocytes to the model in near-physiological proportions of 50% (glia/neuron ratio 1:1; von Bartheld et al. 2017) and a ratio of 1:5 for GABAergic inhibitory neurons and excitatory neurons (Hendry et al. 1987; Sahara et al. 2012) indeed promotes neuronal network formation and maturation best. This study primarily indicates that hiPSC-derived neuronal models must be carefully designed and characterized before their large-scale use in neurotoxicity screenings, as each model exerts different responses to compounds, depending on the composition of the networks. The importance of the presence of astrocytes was also assessed by another study using commercially available cortical neurons on MMEAs (Kayama et al. 2018).

For controlled plating of neuron/astrocyte ratios, cells must be differentiated separately. A recent protocol instructs how to differentiate hiPSC into astroglia (NES-Astro) within 28 days (Lundin et al. 2018). These cells were extensively characterized using transcriptomics, proteomics, glutamate uptake, inflammatory competence, calcium signaling response, and APOE secretion and were compared to primary astrocytes, commercially available hiPSC-derived astrocytes, and an astrocytoma cell line. The data show large diversity among the different analyzed astrocytic models and strongly suggest to take the cellular context into account when studying astrocyte biology. Taking this to the next level, it indicates the importance of choosing the right astrocytic model to combine with hiPSC-derived neurons for the testing of substances acting on the CNS.

One major challenge in the field is the availability of a sufficient number of cells for large-scale screening approaches. Stacey et al. (2018) describe the concept of cryopreserved “near-assay-ready” cells, which decouples complex cell production from assay development and screening. Using this approach, the authors developed a 384-well veratridine-evoked calcium flux assay which assesses neuronal excitability and screened 2,700 compounds to profile the range of target-based mechanisms able to inhibit veratridine-evoked excitability using hiPSC-derived sensory neurons. In order to be able to use this approach for the identification of active compounds with unknown MoA, further secondary assays (e.g., using MMEA-technology) need to be developed to characterize the hits on a mechanistic level (Stacey et al. 2018). In addition, experiments were performed using pure neuronal cultures without the addition of astrocytes, probably leading to different neuronal responses than with astrocytes present.

Along those lines another high-throughput screening using 11 different compound libraries with a total of 4,421 unique substances, all bioactive small molecules, which include approved drugs, well-characterized tool compounds, natural products, and human metabolites, has been described lately (Sherman and Bang 2018). The authors use high-content image analysis, focusing on neurite outgrowth

of commercially available hiPSC-derived neurons, consisting primarily of GABAergic and glutamatergic neurons, but no astrocytes. They identified 108 hit compounds containing 38 approved drugs (outgrowth: erlotinib, clomiphene, tamoxifen, 17 $\beta$ -estradiol, dehydroepiandrosterone-3-acetate (DHEA), alfacalcidol, lynestrenol, benztropine, dibucaine, fluphenazine, perphenazine, prochlorperazine, trifluoperazine, sertindole, quetiapine, ifenprodil, meclizine, alverine, econazole, oxiconazole, letrozole, SAHA (Vorinostat); inhibition: methyltestosterone, thioridazine, methotrimeprazine, colchicine, docetaxel, vincristine, mebendazole, emetine, daunorubicin, doxorubicin, mitoxantrone, topotecan, hexachlorophene, ouabain, digoxin, suramin) which fall into the following categories: kinase inhibitors, steroid hormone receptor modulators, and channel and neurotransmitter system modulators (Sherman and Bang 2018). Inhibition of neurite outgrowth is one key characteristic in developmental neurotoxicity (Fritsche et al. 2018a, b), yet its implication in adult neurotoxicity is not clear.

Using a similar readout, hiPSC-derived peripheral-like neurons were applied to study the effect of chemotherapeutic agents on neuronal cytotoxicity and neurite length, again using high-content image analysis (Rana et al. 2017). This approach identified compounds that cause interference in microtubule dynamics but failed to depict the adverse effects of platinum and anti-angiogenic chemotherapeutics, which are compounds that do not act directly on neuronal processes. Here the addition of astrocytes to the model might lead to a higher predictivity, as the administration of fluorocitrate, an astrocyte-specific metabolic inhibitor, increased the pain tolerance of the animals in a rat model of oxaliplatin-induced neuropathic pain (Di Cesare et al. 2014; Kanat et al. 2017), indicating the role of astrocytes in sustaining platinum-mediated neurotoxicity.

One important cell type for neurotoxicological assessment of substances is myelin-producing oligodendrocytes. Yet publications on hiPSC-derived oligodendrocyte are scarce, and the protocols that are available are very time-consuming and of limited efficiency (Wang et al. 2013; Douvaras et al. 2014; Djelloul et al. 2015). Therefore, they are not suitable for medium- to high-throughput screening approaches. In contrast, the three transcription factors SOX10, OLIG2, and NKX6.2 produced 80% O4<sup>+</sup> oligodendrocytes from hiPSC within 28 days and might thus be a promising approach for future neurotoxicological applications (Ehrlich et al. 2017). Another recent study even reports that the overexpression of the transcription factor SOX10 alone is sufficient to generate 60% O4<sup>+</sup> and 10% MBP<sup>+</sup> cells in only 22 days (García-León et al. 2018b).

Although this part of the chapter primarily covers the use of hiPSC for the generation of neural in vitro models for studying substances acting on the CNS, the method of direct reprogramming of neuronal cells from somatic cells should not be disregarded. Lee et al. (2015) directly reprogrammed human blood to NPC without the intermediate step of hiPSC generation. These induced neurons (iNs) can be generated by overexpression of a set of transcription factors (Ichida and Kiskinis 2015; Vierbuchen et al. 2010; Ambasadhan et al. 2011; Hu et al. 2015; Wapinski et al. 2017) or miRNAs (Victor et al. 2014; Yoo et al. 2011; Abernathy et al. 2017) that promote chromatin remodeling and drive direct neural lineage

differentiation (Silva and Haggarty 2019). Especially for research regarding age-associated neurodegenerative diseases, like Alzheimer's disease (AD) or Parkinson's disease (PD), this method is of high interest, as bypassing the hiPSC reprogramming process reduces the disruption of epigenetic markers associated with the age of the somatic cell, therefore allowing to create neuronal models at "pathogenic ages" (Mertens et al. 2018). This method preserves multiple age-associated markers, including DNA methylation patterns, transcriptomic and microRNA profiles, oxidative stress, DNA damage (loss of heterochromatin and nuclear organization), and telomere length (Mertens et al. 2018; Silva and Haggarty 2019), and is therefore a promising approach to study substances acting on the aged CNS or screening for pharmaceuticals as a treatment for these conditions.

When working with either of these models, it is of utmost importance to have a well-characterized cell system, which suits the research question in case of basic research or contains a defined application domain for neurotoxic MoA (Table 1) when used for screening applications. Lack of characterization or definition of the application domain might result in false-negative data due to a lack of cellular targets. In addition, as with other *in vitro* approaches, the multicellular context of cultures seems to be crucial, possibly resulting in false predictions of chemicals when pure neuronal cultures lacking glia are used.

## 1.2 In Vitro Cultures of Microglia

Microglia constitute 5–10% of total brain cells and represent the resident innate immune cells of the CNS (Arcuri et al. 2017). Microglia discovery dates back to the end of the nineteenth century, but the name was coined in the 1920s by del Rio Hortega who phenotypically characterized the only immune cells resident in the brain parenchyma (Pérez-Cerdá et al. 2015). The function of microglia was for a long time underestimated because of the misconception that the brain is an immune-privileged site; moreover it was initially wrongly thought that this cell type originates from the neuroectoderm. To date, it is known that microglia arise from embryonic yolk sac (YS) precursors (Ginhoux et al. 2010) which give rise to YS macrophages that colonize the embryo, including the brain, to generate all types of tissue-resident macrophages (Li and Barres 2018). In the CNS, microglia maintain their population by self-renewal (Ajami et al. 2007) and by recruiting monocytes from the bloodstream (Hashimoto et al. 2013). The presence of microglia in the brain parenchyma is fundamental because of the variety of functions they perform from early brain development throughout the entire life of the organism, both in brain homeostasis and disease (for an extensive review, see Li and Barres 2018).

Considering the pivotal contribution of microglia to brain functions, it is important to have *in vitro* models containing microglia when studying the influence of drugs and toxicants on the brain. The majority of published *in vitro* studies mainly used primary microglia cultures from embryonic/neonatal rodent brain (mouse or rat). Still, fetal microglia seem to be quite different from adult ones. Due to ethical reasons, it is challenging to obtain brain-derived microglia from humans. The few

human microglia cell lines generated, such as HMO6 (Nagai et al. 2005) and HMC3 (Janabi et al. 1995), are not considered as an optimal model because long-term culture and genetic manipulation altered their functions and morphology. Finally, the low number of cells collected from humans does not allow large-scale neurotoxicity in vitro studies.

Starting from these premises, Leone and colleagues set up a monocyte-derived microglia-like cell model by culturing human monocytes with astrocyte-conditioned medium (Leone et al. 2006). This protocol was successively standardized using human peripheral blood mononuclear cells (PBMCs) stimulated with four recombinant human cytokines. The microglia cells obtained display a ramified morphology after 2 weeks in culture and express surface markers typical for the known pattern of microglia (Etemad et al. 2012).

More recently, human microglia-like cells were obtained from hESC and hiPSC. As previously stated, microglia derive from non-monocytic primitive myeloid cells, unlike adult bone marrow-derived macrophages. Thus microglia-like cells derived from PBMCs do not mirror this ontogeny. Muffat and co-workers established a robust protocol that allows the derivation of microglia-like cells from hiPSC, obtained from reprogrammed fibroblasts, using a serum-free medium that mimics the environment of the CNS interstitial milieu and adding interleukin 34 (IL-34), an alternative ligand for colony-stimulating factor 1 receptor. The microglia-like cells obtained with this protocol are highly phagocytic, and their gene expression profile resembles human primary microglia. They progressively adopt a ramified morphology when cultured in isolation, while when co-cultured in the presence of hiPSC-derived neurons, microglia-like cells refine their molecular signature. In terms of activity and response to stressors, unstimulated microglia-like cells secrete detectable levels of various cytokines and chemokines, which were enhanced after stimulation with lipopolysaccharide (Muffat et al. 2016) (Fig. 2).

Similar protocols were published a few months later reprogramming fibroblasts or PBMCs. In the paper of Pandya et al. (2017), hiPSCs were sequentially differentiated into myeloid progenitor-like intermediate cells and then into cells with the phenotypic, transcriptional, and in vitro functional signatures of brain-derived microglia. Abud and co-workers demonstrated that microglia-like cells obtained from hiPSC secrete cytokines in response to inflammatory stimuli, migrate, undergo calcium transients, and phagocytose (Abud et al. 2017). All those protocols require from 30 to about 70 days of time to obtain mature glia (McComish and Caldwell 2018). Taken together, those data suggest that microglia obtained from reprogrammed hiPSC better mirror the developmental stages of microglia maturation and ontogeny, in comparison to microglia-like cells derived from PBMCs stimulated with a cocktail of factors.

The potential applications of hiPSC-derived microglia include drug discovery studies, neurotoxicity screening assays, and use in disease modeling. Microglia-mediated inflammation can negatively impact the brain, and much evidence shows that microglial activation plays a role in neurodegeneration, contributing to the etiology of neurodegenerative disorders (Ransohoff and El Khoury 2016). The availability of robust protocols to generate and maintain microglia from patients with different brain dysfunctions in culture would facilitate the study of the

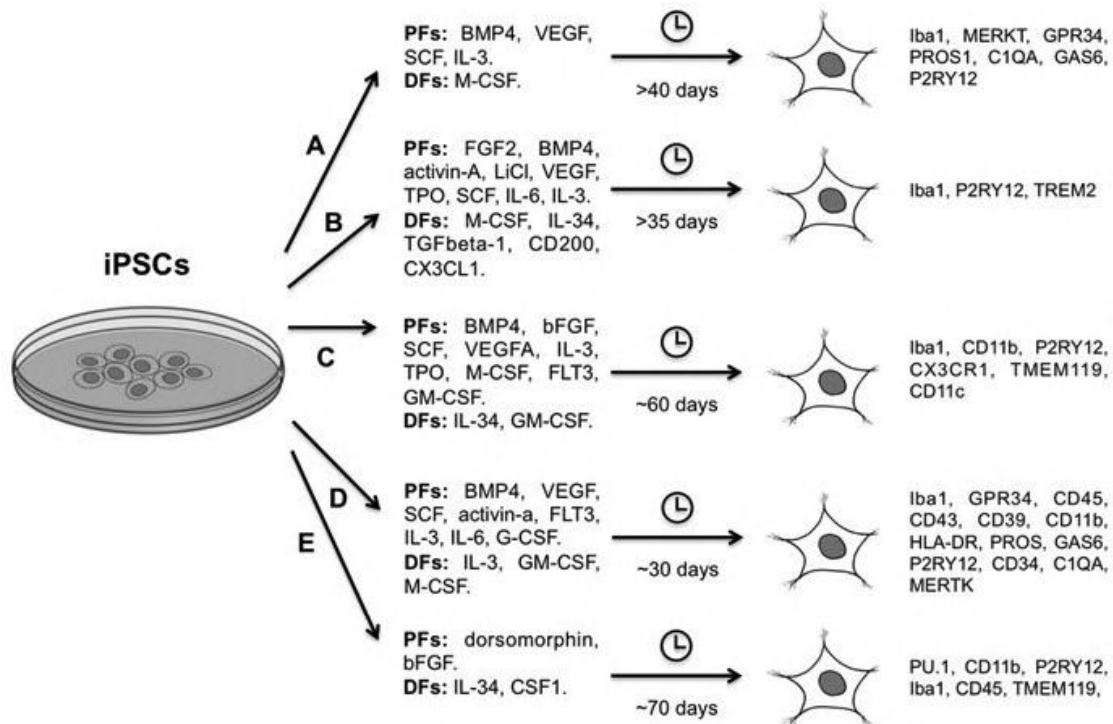


**Fig. 2** Human iPSC-derived microglia protocols. (a) Haenseler et al. (2017), (b) Abud et al. (2017), (c) Douvaras et al. (2017), (d) Pandya et al. (2017), (e) Muffat et al. (2016). *PFs* patterning factors, *DFs* differentiation factors, *BMP4* brain morphogenetic protein 4, *VEGF* vascular endothelial growth factor, *SCF* stem cell factor, *IL-3* interleukin 3, *M-CSF* macrophage colony-stimulating factor, *FGF2* or *bFGF* fibroblast growth factor 2, *TPO* thrombopoietin, *IL-6* interleukin 6, *IL-34* interleukin 34, *TGFbeta-1* transforming growth factor beta 1, *CD200* cluster of differentiation 200, *CX3CL1* fractalkine, *VEGF-A* vascular endothelial growth factor A, *FLT-3* fm-like tyrosine kinase 3, *GM-CSF* granulocyte-macrophage colony-stimulating factor, *G-CSF* granulocyte colony-stimulating factor, *CSF1* colony-stimulating factor 1, *Iba1* ionized calcium-binding adapter molecule 1, *MERTK* tyrosine kinase phagocytic receptor, *GPR34* G protein-coupled receptor 34, *PROS1* protein S1, *C1QA* complement C1q subcomponent subunit A, *GAS6* growth arrest-specific 6, *P2RY12* purinergic receptor P2Y, *TREM2* triggering receptor expressed on myeloid cells 2, *CD11b* cluster of differentiation 11b, *CX3CR1* CX3C chemokine receptor 1, *TMEM119* transmembrane protein 119, *CD11c* cluster of differentiation 11c, *CD45* cluster of differentiation 45, *CD43* cluster of differentiation 43, *CD39* cluster of differentiation 39, *HLA-DR* human leukocyte antigen – DR isotype, *CD34* cluster of differentiation 34

pathology and the discovery of new pharmacological approaches. The first evidence of in vitro culturing disease-related microglia cells from patients was in 2012, when Almeida and colleagues generated multiple induced hiPSC lines from subjects with frontotemporal dementia (Almeida et al. 2012). More recently, Ryan and co-workers performed, on human monocyte-derived microglia-like cells, a quantitative expression trait locus study to examine the effects of common genetic variation on the expression of genes found in susceptibility loci for Alzheimer's disease, Parkinson's disease, and multiple sclerosis (Ryan et al. 2017). Microglia-like cells obtained by reprogramming PBMCs were also combined with neural progenitor cells and synaptosomes from hiPSC-derived neurons to create patient-specific cellular models useful to model CNS diseases facilitating high-throughput drug screening and neurotoxicity assays based on microglia function in the future (Sellgren et al. 2017).

In conclusion, different protocols for the derivation of human microglia are available that enable experiments in authentic human in vitro systems. Unlike methods for the derivation of neurons and astrocytes, protocols for microglia lack regionality and do not reflect microglia subtypes found within the brain (Grabert et al. 2016), which is a true challenge for the future.

### **1.3 Moving In Vitro Cultures into the Third Dimension with Brain Organoids**

For investigating possible CNS disease mechanisms or screening drugs or toxins for safety and efficacy, it is thought to be advantageous to use complex 3D systems such as *brain organoids*. The benefits of organoids compared to “conventional” cultures lie in their composition of multiple cell types, which are functional in an in vivo-like manner and display morphological features of the organ to be modeled (Lancaster and Knoblich 2014). Yet, one has to be aware that there are major differences between in vivo embryogenesis or organogenesis and in vitro organoid formation, since even extremely well-controlled in vitro conditions strongly differ from real, regionally defined, physiological in vivo conditions (Bayir et al. 2019).

Different protocols for generating brain organoids have been established. Lancaster et al. (2017) used a floating scaffold out of poly(lactide-co-glycolide) copolymer (PLGA) fiber microfilaments to generate elongated embryoid bodies, called microfilament-engineered cerebral organoids (enCORs). Other groups used shaking platforms (Matsui et al. 2018), self-made spinning bioreactors (Qian et al. 2016), or soft matrices for embedding the cells (Lindborg et al. 2016; Bian et al. 2018) to let them form self-organized brain organoids. While neural organoids mostly mimic the early phases of embryonic development of the human brain, Matsui et al. (2018) cultivated their organoids up to 6 months and showed cell differentiation into functional neurons and myelin basic protein (MBP)-positive oligodendrocytes. The cerebral organoids fabricated by Quadrato et al. (2017) contained mature neurons including dendritic spine-like structures that generated spontaneously active neuronal networks as well as photosensitive cells after 8–9 months. These CNS models that display a later developmental status can now be used for safety and efficacy evaluations in medium to high throughput. One has to note that integration of microglia into organoids will be necessary in the future to better model toxicity and disease. This advanced technology is currently evolving (Ormel et al. 2018). In addition, although seemingly much more complex than 2D models, organoids also need definition of their applicability domains, with regard to the presence of cellular targets mediating neurotoxicity or drug efficacy (Table 1). Because reproducibility of organoid formation is still an issue with high variation making well-to-well comparison difficult, this neurotoxicity/efficacy target characterization has to be performed with great caution focusing on reproducibility of results.

As an example, hiPSC-derived brain organoids were recently employed for drug efficacy screening against ZIKA virus infection (Zhou et al. 2017) indicating that it is

possible to use such complex in vitro systems for medium- to high-throughput applications. The authors' high-content imaging approach identified a compound prohibiting organoid ZIKA virus infection and eliminating virus from infected organoids (Zhou et al. 2017). Other ZIKA virus-infected organoids were also published recently (Cugola et al. 2016; Garcez et al. 2016; Dang et al. 2016; Qian et al. 2016). Two groups (Watanabe et al. 2017; Xu et al. 2016) used these organoids similar to Zhou et al. (2017), for drug screening against ZIKA virus. Since the declaration of a public health emergency of international concern by the World Health Organization in 2016, a lot of drug candidates against ZIKA virus were tested in in vitro as well as in in vivo systems, but only few of them with anti-ZIKA virus activity in animal models made it to clinical trials (Bernatchez et al. 2019).

Due to the higher throughput of such models, they are logistically superior over the low-throughput mouse models and can thus screen a large number of compounds. Moreover, their translational success to the human in vivo situation might be higher due to the human nature of cells. However, as already pointed out in Fig. 1, kinetic modeling is crucial for correct predictions that has to go hand in hand with the in vitro work.

While brain organoids are good models to examine the effects of disease and genetic aberrances on brain development, they lack to model the blood-brain barrier (BBB) of the adult human cortex. Many drugs for neurologic diseases and disorders fail to pass the BBB; therefore, there is a need for a BBB model that enables the examination of the permeability of these drugs. BBB organoid models can be derived from three (Cho et al. 2017; Bergmann et al. 2018) or from six (Nzou et al. 2018) different cell types that include astrocytes, pericytes, and endothelial cells. Both models are able to reproduce the properties and functions of the BBB through the exhibition of tight/adherent junctions, efflux pumps, and transporters. Nzou et al. (2018) showed in their organoids also the impenetrability of the BBB for specific molecules: by adding MPTP, MPP+, and mercury chloride to the medium they proofed that their models indeed have a charge-selective barrier. Data from such models might also be useful for feeding PBPK models.

In conclusion, there are currently several different organoid models in development, both normal and disease models. However, these are still in the process of establishment and characterization and are not yet in use for substance screenings.

## 1.4 3D Bioprinted In Vitro Neural Models

The next generation of in vitro models already arising is fabricated by 3D *bioprinting*. The state of the art of 3D bioprinting of brain cells was recently comprehensively reviewed by Antill-O'Brien et al. (2019). 3D bioprinting of brain cells is faced with a variety of challenges needing sophisticated solutions. The first is the choice of biomaterial biomimicking brain tissue from extracellular matrix components as well as the mechanical, structural, biochemical, and diffusive properties of the brain with high cellular biocompatibility. Here, especially, the tremendous softness of brain tissue poses a great challenge for bioengineers.

Biomaterials currently used for neural cell culture are *hydrogels*. These hydrophilic polymers can be reversibly or irreversibly cross-linked via chemical or physical triggers to maintain their structure over a long period of time. Hydrogels are an attractive material for culturing cells in 3D due to their biocompatibility, high water content, and tuneable physical and chemical properties. For neuronal cultures, the pore structure of the hydrogel must be able to support neural cell bodies, which are 10–50  $\mu\text{m}$  in diameter, and allow neurite extension (Antill-O'Brien et al. 2019). Once a suitable biomaterial is identified, the biofabrication strategy has to be defined. Prior to printing, 3D neural tissue can be manufactured via layering. Cell embedding in gels and manual layering thereby allow studying cytocompatibility of hydrogels. Printing of soft materials is often challenging. A major hurdle to 3D biofabrication of such soft structures is their shaping into 3D structures with high spatial resolution to achieve an anisotropically accurate mimic of the brain microstructure. Sacrificial scaffolds, e.g., from gelatine, have previously been used to support soft gels like 0.5% alginate, which otherwise fall below the printable viscosity range. Usage of this sacrificial scaffold improved cell survival in the hydrogel (Naghieh et al. 2019). For scaffold-free 3D bioprinting, extrusion-based printing has mainly been employed due to its economy, ease of use, and capability to print with high cell density with a wide range of materials. Despite a small number of studies using rat or hiPSC-derived neurons for extrusion-based bioprinting, one study should be highlighted. Joung et al. (2018) developed a bioengineered spinal cord combining bioprinting with 3D printed scaffolds in the only example of functional neurons with extensive axon propagation from bioprinted neural precursor cells. Pre-differentiated spinal NPC and oligodendrocyte progenitor cells from hiPSC were bioprinted in precise alternating points in silicon channels. After 4 days,  $\beta$ -III tubulin-positive axons spread throughout the channel, and after 14 days the cells were found to have differentiated into mature glutamate-responsive neurons with synchronous responses to  $\text{K}^+$  and glutamate (Joung et al. 2018). This method of a spinal cord model could be applied to CNS neural tissue engineering.

This paragraph is not supposed to give a comprehensive overview of 3D bioprinting of neural structures, yet should touch on the challenges of this rising technique. 3D bioprinting of neural models is still in the early stages of development and offers great potential for exquisite spatial bioink patterning to recapitulate the microarchitecture of brain tissue. Although 3D bioprinted neural disease models have not yet been developed, the potential advantages over animal models include species- and patient-specific disease modeling. For more detailed information on cells, materials, techniques, and readouts, the reader is referred to Antill-O'Brien et al. (Antill-O'Brien et al. 2019).

## 1.5 CNS Disease Models

Improvement of the hiPSC technology allows to obtain and culture neurological patient-specific hiPSC lines, which recapitulate molecular and cellular phenotypic aspects of the respective disease. These offer a unique opportunity to generate

physiologically relevant in vitro models to understand disease etiology and progression, as well as to support preclinical drug discovery. Genomically unaltered human iPSC-derived neurons and astrocytes have been derived from Alzheimer's disease (AD), Parkinson's disease (PD), *Huntington's disease* (HD), *amyotrophic lateral sclerosis* (ALS), and *idiopathic autistic spectrum disorder* (ASD) patients (Table 2), to provide 2D and, most recently, 3D cultures reproducing features of these neurological diseases. In addition to patient-derived iPSCs, inserting genetic changes manually into iPSCs can also generate disease models. Manipulating gene expression of *LIS1*, the most common gene mutated in patients with *lissencephaly*, and using an on-chip organoid approach as an exciting example, allowed studying the emergence of folding during in vitro development and the physical mechanisms of folding reproducing pathogenesis of lissencephaly using organoids (Karzbrun et al. 2018).

In 2D cultures, patient-derived iPSCs are generally committed to differentiate into neuronal monoculture representative of the affected cell type: in PD research iPSCs are differentiated into dopaminergic neurons (TH-positive) functionally characterized by dopamine decarboxylase and the dopamine transporter (Hartfield et al. 2014), while cortical glutamatergic neuron or motor neurons are derived to best represent AD or ALS features, respectively.

More recently, greater attention has been dedicated to both microglia (Haenseler et al. 2017) and patient-derived astrocytes (Kondo et al. 2013; Qian et al. 2017; Hsiao et al. 2015), due to the recognition of the relevance of glial cells in contributing to disease initiation and progression. Similar to toxicity evaluation described above, the aim here is to develop co-cultures, which take the complexity of neuron-glia interactions into account, hence also considering inflammatory responses, which have a high impact on the course of pathology (Haenseler et al. 2017). In addition, the presence of multiple cell type allows to address neuron-glia cross-talk in drug discovery. The diversity of cell types in a single culture is also retained in organoid models, which add a further step of complexity by respecting brain cytoarchitecture.

A clarifying example on the potentiality of patient-derived stem cell models comes from AD patients (for extensive review, see Arber et al. 2017). Extracellular amyloid plaques composed of amyloid beta peptide ( $A\beta$ ) and Tau protein intracellular neurofibrillary tangles are considered hallmarks of AD.  $A\beta$  is the product of  $\beta$ - and  $\gamma$ -secretase processing of amyloid precursor protein (APP). Autosomal dominant mutations in APP and alternative subunits of  $\gamma$ -secretase presenilin 1 and 2 (PSEN1 and PSEN2) have been detected in AD patients, implicating an altered APP processing and  $A\beta$  imbalance in AD pathogenesis. Reprogramming cells derived from patients with genetic predisposition to AD into cortical glutamatergic neurons, cortical interneurons, and cholinergic neurons (Table 2) allowed to reproduce AD features like increased  $A\beta_{42:40}$  ratio and enhanced Tau phosphorylation (Table 2). These models were then used to gain insight into biochemical pathomechanisms of AD (Kondo et al. 2013), contribution of neurons and astrocytes to pathophysiology (Kondo et al. 2013; Oksanen et al. 2017) and identify drug targets potentially relevant in the progression of the disease. In these studies, also

**Table 2** Patients' iPSC-derived neurons as disease models for investigating neurological disorders

	Mutations investigated	Cell type	Pathological hallmarks	Reference
<i>Alzheimer's disease</i>				
fAD	PSEN1 A246E PSEN1 N141I	Neurons	Increased A $\beta$ Increased A $\beta$ 42:40 ratio	Yagi et al. (2011)
fAD sAD	APP duplication	Neurons Glutamatergic GABAergic Cholinergic	Increased A $\beta$ 40 Increased pTau Activated GSK3b	Israel et al. (2012)
fAD sAD	APP E693 $\Delta$ APP V717L	Cortical neurons <sup>1</sup> or astrocytes <sup>2</sup>	Increased A $\beta$ 42:40 ratio <sup>1</sup> Extracellular A $\beta$ oligomers <sup>1,2</sup>	Kondo et al. (2013)
fAD	PSEN1 $\Delta$ E9	Neurons	Increased A $\beta$ 42:40 ratio	Woodruff et al. (2013)
sAD	ApoE3/E4 (AD-E3/E4)	Cholinergic neurons	Increased A $\beta$ 42:40 ratio	Duan et al. (2014)
fAD	APPV717I	Neurons	Increased A $\beta$ 42:40 ratio Increased A $\beta$ 38:40 ratio Increased total and phosphorylated Tau	Muratore et al. (2014)
fAD	PSEN1 $\Delta$ E9	Astrocytes	Accumulation of full-length PS-1 Increased A $\beta$ 42:40 ratio Disturbance in ER calcium signaling Development of a pro-inflammatory profile	Oksanen et al. (2017)
fAD sAD	PSEN 1 M146L <i>ApoE4</i> <sup>+/+</sup>	Astrocytes		Jones et al. (2017)
fAD	APP duplication PSEN 1 M146I PSEN 1 A264E	3D organoids	Amyloid aggregation Hyperphosphorylated tau protein Endosome abnormalities	Raja et al. (2016)
Down syndrome		Cortical glutamatergic neurons	Increased A $\beta$ 40 Increased A $\beta$ 42 A $\beta$ aggregates	Shi et al. (2012)
Down syndrome		Neurons with forebrain characteristics	A $\beta$ aggregates Tau protein hyperphosphorylation Tau intracellular redistribution	Chang et al. (2015)

(continued)

**Table 2** (continued)

	Mutations investigated	Cell type	Pathological hallmarks	Reference
<i>Parkinson's disease</i>				
	PARK2/Parkin V324A PINK1 Q456X	Midbrain DA neurons	Increased $\alpha$ -synuclein expression	Chung et al. (2016)
	SNCA gene triplication	DA neurons	Increased $\alpha$ -synuclein expression	Oliveira et al. (2015)
	a-synuclein A53T	Cortical neurons and glia	$\alpha$ -Synuclein expression	Chung et al. (2013)
<i>Amyotrophic lateral sclerosis</i>				
sALS	Patients presented symptoms relating to motor-neurons degeneration of the spinal cord (not in brainstem or cortex) in the absence of C9ORF72 gene mutations	Astrocytes	Increased GFAP immunofluorescence	Qian et al. (2017)
	GGGGCC repeat expansions in C9ORF72	Motor neurons	Aging increased DNA damage	Lopez-Gonzalez et al. (2016)
	VCP mutations R191Q or R155C	Enriched cultures of motor neurons and astrocytes	Increased percentage of cytosolic TDP-43	Hall et al. (2017)
	SOD1 E100G	Spinal motor neurons	Significant decline in survival compared with the healthy control MNs	Bhingre et al. (2017)
fALS	TDP-43	Motor neurons	Cytosolic aggregates Shorter neurites	Egawa et al. (2012)
<i>Huntington's disease</i>				
HD	43 CAG repeats	Astrocytes	Increased vascular endothelial growth factor A	Hsiao et al. (2015)
HD Juvenile HD	109 CAG repeats		Contain both normal and mutant huntingtin	Szlachcic et al. (2015)
Juvenile HD	60 and 109 CAG repeats	Mixed culture: Neurons, glia, and progenitor cells	Alterations in genes and gene pathways that are associated with a pathological CAG repeat length	Consortium TH iPSC (2017)
HD	180 CAG repeats	Striatal-like cultures	Significantly lower ATP levels than control	Rindt et al. (2017)

fAD familial AD, sAD sporadic AD, sALS sporadic ALS, DA dopaminergic

novel mechanisms like endoplasmic reticulum and oxidative stress were identified (Kondo et al. 2013; Muratore et al. 2014). In addition, iPSCs derived from patients carrying multiple genetic variants allow investigations of AD risk factors, i.e., linking mutations to increased risk of late onset AD (Duan et al. 2014; Young et al. 2015; Huang et al. 2017; Schröter et al. 2016). The organization of genomically unaltered iPSC-derived neurons in a 3D structure, thereby reproducing brain cytoarchitecture, favors the retention of proteins secreted by cells that are lost in a 2D culture, like A $\beta$  peptides. In 3D their local concentration is increased and pathology better recapitulated (Raja et al. 2016). 2D and 3D models obtained from iPSCs derived from AD patients have been used to investigate drug efficacy and toxicity, so far targeting  $\beta$ - and  $\gamma$ -secretase with specific inhibitors (Yagi et al. 2011; Shi et al. 2012; Kondo et al. 2013; Duan et al. 2014; Raja et al. 2016; Woodruff et al. 2013) and inflammation with nonsteroidal anti-inflammatory drugs (Yahata et al. 2011).

Although the models obtained from patients' hiPSCs exhibit clear advantages, their use to model aging and neurodegenerative diseases poses a relevant challenge due to the fact that differentiation protocols mimic neurodevelopmental processes. Indeed, derived cells retain molecular characteristics closer to the fetal than the adult stage (Patani et al. 2012; Camp et al. 2015), which might limit the full development of an AD model. For example, Tau isoform expression is tightly regulated during development (Bunker et al. 2004), and the lack of formation of aggregated Tau in non-manipulated patients' hiPSCs might reflect the absence of the adult isoforms. In general, this implicates that any disease phenotype has to be discriminated from phenotypes of earlier developmental stages. So far this issue that represents a possible limit in drug discovery has been solved by generating footprint-free triple MAPT-mutant human iPSCs (García-León et al. 2018a), overexpressing mutant PSEN1 (DE9) and APP (K670N/M671L plus V7171; Choi et al. 2014), or could be overcome by direct reprogramming, thus skipping the intermediate step of hiPSC (for details on this, see second to last paragraph of Sect. 1.1 of this chapter).

In the context of CNS pathologies recapitulated by an hiPSC approach, neurodevelopmental and psychiatric diseases are worth a note. CNS cells derived from patients by reprogramming allow to capture a complex genetic architecture of diseases that are highly polygenic in nature, overcoming the difficulty to generate genetically accurate animal models of psychiatric disorders. Patient hiPSC-derived neural cells allow to dissect the gene network associated with features of altered neurodevelopment that controls the phenotypic trait and the signaling pathways involved (Mariani et al. 2015; Haggarty et al. 2016).

As listed in Table 2, patients' hiPSCs replicate disease phenotypes to an extent to represent clinically relevant features of the illness, thus providing human cellular assays that may improve drug preclinical evaluation and translation of the results to clinical trial in the process of drug discovery (Silva and Haggarty 2019). Clinically relevant targets and phenotypes displayed in hiPSC-derived disease models may drive the testing of candidate drugs selected on a hypothesis-driven screening or the screening of large compound libraries for identification of novel molecules for their ability to rescue disease phenotypes. In addition, the generation of large numbers of

patients' cell models representative of the heterogeneity of each disorder may represent a strategy to identify patient subpopulations with specific responsiveness to therapeutic agents. Finally, by interlinking a patient's genetic background with specific disease characteristics, hiPSCs apply to the concept of personalized medicine, possibly allowing the development of personalized drug evaluation in the future (Engle and Puppala 2013).

---

## 2 Summary and Conclusion

Animal models have been greatly contributing to our understanding of physiology, mechanisms of diseases, and toxicity. Yet, they have limitations due to interspecies variation, which determines the lack of information of the “human context,” and deficiency in pathophysiologically relevant disease models. This deficiency has a tremendous negative impact on the understanding of basic physiology, human disease, mechanisms of toxicity, and the process of successful drug discovery.

Human iPSC-derived cells offer a platform with the unique advantage of reproducing the “human context” missing in animal models, by preserving the genetic and the molecular phenotype of donors. Forcing the differentiation of hiPSC into cells of the nervous system and combining them in a 2D or 3D format allows obtaining complex models suitable to investigate neurodevelopmental processes and to reproduce neurodegenerative diseases with patient-derived cells. This has the potentiality to drive the identification of molecular targets that may be predictive for the evolution of specific human diseases as well as for beneficial and/or adverse drug responses. Thus, with such cell platforms, screening assays can be set up that are based on human-relevant targets and thus are useful for drug testing and discovery with the hope of overcoming the low success rate of CNS drug development due to poor clinical efficacy or elevated toxicity. Cell culture standardization is mandatory in this process. Well-characterized and overall reproducible cell systems that contain neural and immune cells of the CNS, are based on standardized protocols and procedures to generate differentiated and mature cells representative of different brain areas, and are able to address the fundamental unanswered questions of drug discovery and toxicity are urgently needed.

---

## References

- Abernathy DG, Kim WK, McCoy MJ, Lake AM, Ouwenga R, Lee SW, Xing X, Li D, Lee HJ, Heuckeroth RO, Dougherty JD, Wang T, Yoo AS (2017) MicroRNAs induce a permissive chromatin environment that enables neuronal subtype-specific reprogramming of adult human fibroblasts. *Cell Stem Cell* 21:332–348.e9. <https://doi.org/10.1016/j.stem.2017.08.002>
- Abud EM, Ramirez RN, Martinez ES, Healy LM, Nguyen CHH, Newman SA, Yeromin AV, Scarfone VM, Marsh SE, Fimbres C, Caraway CA, Fote GM, Madany AM, Agrawal A, Kaye R, Gyls KH, Cahalan MD, Cummings BJ, Antel JP, Mortazavi A et al (2017) iPSC-derived human microglia-like cells to study neurological diseases. *Neuron* 94:278–293.e9. <https://doi.org/10.1016/j.neuron.2017.03.042>

- Ajami B, Bennett JL, Krieger C, Tetzlaff W, Rossi FMV (2007) Local self-renewal can sustain CNS microglia maintenance and function throughout adult life. *Nat Neurosci* 10:1538–1543
- Almeida S, Zhang Z, Coppola G, Mao W, Futai K, Karydas A, Geschwind MD, Tartaglia MC, Gao F, Gianni D, Sena-Esteves M, Geschwind DH, Miller BL, Farese RV, Gao FB (2012) Induced pluripotent stem cell models of progranulin-deficient frontotemporal dementia uncover specific reversible neuronal defects. *Cell Rep* 2:789–798
- Ambasudhan R, Talantova M, Coleman R, Yuan X, Zhu S, Lipton SA (2011) Brief report direct reprogramming of adult human fibroblasts to functional neurons under defined conditions. *Stem Cell* 9:113–118. <https://doi.org/10.1016/j.stem.2011.07.002>
- Ankley GT, Bennett RS, Erickson RJ, Hoff DJ, Hornung MW, Johnson RD, Mount DR, Nichols JW, Russom CL, Schmieder PK, Serrano JA, Tietge JE, Villeneuve DL (2010) Adverse outcome pathways: a conceptual framework to support ecotoxicology research and risk assessment. *Environ Toxicol Chem* 29:730–741
- Antill-O'Brien N, Bourke J, O'Connell CD (2019) Layer-by-layer: the case for 3D bioprinting neurons to create patient-specific epilepsy models. *Materials (Basel)* 12:3218
- Arber C, Lovejoy C, Wray S (2017) Stem cell models of Alzheimer's disease: progress and challenges. *Alzheimers Res Ther* 9:1–17
- Arcuri C, Mecca C, Bianchi R, Giambanco I, Donato R (2017) The pathophysiological role of microglia in dynamic surveillance, phagocytosis and structural remodeling of the developing CNS. *Front Mol Neurosci* 10:1–22
- Bal-Price A, Crofton KM, Sachana M, Shafer TJ, Behl M, Forsby A, Hargreaves A, Landesmann B, Lein PJ, Louise J, Monnet-Tschudi F, Painsi A, Rolaki A, Schrattenholz A, Suñol C, van Thriel C, Whelan M, Fritsche E (2015) Putative adverse outcome pathways relevant to neurotoxicity. *Crit Rev Toxicol* 45:83–91
- Bayir E, Sendemir A, Missirlis YF (2019) Mechanobiology of cells and cell systems, such as organoids. *Biophys Rev* 11:721–728
- Bergmann S, Lawler SE, Qu Y, Fadzen CM, Wolfe JM, Regan MS, Pentelute BL, Agar NYR, Cho CF (2018) Blood–brain-barrier organoids for investigating the permeability of CNS therapeutics. *Nat Protoc* 13:2827–2843
- Bernatchez JA, Tran LT, Li J, Luan Y, Siqueira-Neto JL, Li R (2019) Drugs for the treatment of Zika virus infection. *J Med Chem*
- Bhinge A, Namboori SC, Zhang X, VanDongen AMJ, Stanton LW (2017) Genetic correction of SOD1 mutant iPSCs reveals ERK and JNK activated AP1 as a driver of neurodegeneration in amyotrophic lateral sclerosis. *Stem Cell Rep* 8:856–869. <https://doi.org/10.1016/j.stemcr.2017.02.019>
- Bian S, Repic M, Guo Z, Kavirayani A, Burkard T, Bagley JA, Krauditsch C, Knoblich JA (2018) Genetically engineered cerebral organoids model brain tumor formation. *Nat Methods* 15:748–748. <http://www.nature.com/articles/s41592-018-0118-8>
- Boissart C, Poulet A, Georges P, Darville H, Julita E, Delorme R, Bourgeron T, Peschanski M, Benchoua A (2013) Differentiation from human pluripotent stem cells of cortical neurons of the superficial layers amenable to psychiatric disease modeling and high-throughput drug screening. *Transl Psychiatry* 3:e294–e211. <https://doi.org/10.1038/tp.2013.71>
- Boisvert EM, Engle SJ, Hallowell SE, Liu P, Wang Z (2015) The specification and maturation of nociceptive neurons from human embryonic stem cells. *Nat Publ Gr*:1–12. <https://doi.org/10.1038/srep16821>
- Bunker JM, Leslie W, Jordan MA, Feinstein SC (2004) Modulation of microtubule dynamics by tau in living cells: implications for development and neurodegeneration. *Mol Biol Cell* 15:2720–2728
- Camp JG, Badsha F, Florio M, Kanton S, Gerber T, Wilsch-Bräuninger M, Lewitus E, Sykes A, Hevers W, Lancaster M, Knoblich JA, Lachmann R, Pääbo S, Huttner WB, Treutlein B (2015) Human cerebral organoids recapitulate gene expression programs of fetal neocortex development. *Proc Natl Acad Sci U S A* 112:15672–15677

- Carusi A, Davies MR, de Grandis G, Escher BI, Hodges G, KMY L, Whelan M, Willett C, Ankley GT (2018) Science of the total environment harvesting the promise of AOPs: an assessment and recommendations. *Sci Total Environ* 628–629:1542–1556. <https://doi.org/10.1016/j.scitotenv.2018.02.015>
- Chambers SM, Fasano CA, Papapetrou EP, Tomishima M, Sadelain M, Studer L (2009) Highly efficient neural conversion of human ES and iPS cells by dual inhibition of SMAD signaling. *Nat Biotechnol* 27:275–280. <http://www.nature.com/nbt/journal/v27/n3/abs/nbt.1529.html>
- Chang CY, Chen SM, Lu HE, Lai SM, Lai PS, Shen PW, Chen PY, Shen CI, Harn HJ, Lin SZ, Hwang SM, Su HL (2015) N-butylidenephthalide attenuates Alzheimer’s disease-like cytopathy in down syndrome induced pluripotent stem cell-derived neurons. *Sci Rep* 5:1–7
- Cheng C, Fass DM, Folz-Donahue K, MacDonald ME, Haggarty SJ (2017) Highly expandable human iPS cell-derived neural progenitor cells (NPC) and neurons for central nervous system disease modeling and high-throughput screening. *Curr Protoc Hum Genet* 93:21.8.1–21.8.21
- Cho CF, Wolfe JM, Fadzen CM, Calligaris D, Hornburg K, Chiocca EA, Agar NYR, Pentelute BL, Lawler SE (2017) Blood-brain-barrier spheroids as an in vitro screening platform for brain-penetrating agents. *Nat Commun* 8:1–14. <https://doi.org/10.1038/ncomms15623>
- Choi SH, Kim YH, Hebesch M, Sliwinski C, Lee S, D’Avanzo C, Chen H, Hooli B, Asselin C, Muffat J, Klee JB, Zhang C, Wainger BJ, Peitz M, Kovacs DM, Woolf CJ, Wagner SL, Tanzi RE, Kim DY (2014) A three-dimensional human neural cell culture model of Alzheimer’s disease. *Nature* 515:274. <https://doi.org/10.1038/nature13800>
- Chung CY, Khurana V, Auluck PK, Tardiff DF, Mazzulli JR, Soldner F, Baru V, Lou Y, Freyzo Y, Cho S, Mungenast AE, Muffat J, Mitalipova M, Pluth MD, Jui NT, Schulze B, Lippard SJ, Tsai LH, Krainc D, Buchwald SL et al (2013) Identification and rescue of  $\alpha$ -synuclein toxicity in Parkinson patient-derived neurons. *Science* 342:983–987
- Chung SY, Kishinevsky S, Mazzulli JR, Graziotto J, Mrejeru A, Mosharov EV, Puspita L, Valiulahi P, Sulzer D, Milner TA, Taldone T, Krainc D, Studer L, won Shim J (2016) Parkin and PINK1 patient iPSC-derived midbrain dopamine neurons exhibit mitochondrial dysfunction and  $\alpha$ -synuclein accumulation. *Stem Cell Reports* 7:664–677. <https://doi.org/10.1016/j.stemcr.2016.08.012>
- Consortium TH iPSC (2017) Developmental alterations in Huntington’s disease neural cells and pharmacological rescue in cells and mice. *Nat Neurosci* 20:648–660
- Cooper O, Seo H, Andrabi S, Guardia-Laguarta C, Graziotto J, Sundberg M, McLean JR, Carrillo-Reid L, Xie Z, Osborn T, Hargus G, Deleidi M, Lawson T, Bogetofte H, Perez-Torres E, Clark L, Moskowitz C, Mazzulli J, Chen L, Volpicelli-Daley L et al (2012) Pharmacological rescue of mitochondrial deficits in iPSC-derived neural cells from patients with familial Parkinson’s disease. *Sci Transl Med* 4:141ra90
- Corti S, Nizzardo M, Simone C, Falcone M, Nardini M, Ronchi D, Donadoni C, Salani S, Riboldi G, Magri F, Menozzi G, Bonaglia C, Rizzo F, Bresolin N, Comi GP (2012) Genetic correction of human induced pluripotent stem cells from patients with spinal muscular atrophy. *Sci Transl Med* 4:1–32
- Crofton KM, Mundy WR, Shafer TJ (2012) Developmental neurotoxicity testing: a path forward. *Congenit Anom* 52:140–146
- Cugola FR, Fernandes IR, Russo FB, Freitas BC, Dias JLM, Guimarães KP, Benazzato C, Almeida N, Pignatari GC, Romero S, Polonio CM, Cunha I, Freitas CL, Brandaõ WN, Rossato C, Andrade DG, Faria DDP, Garcez AT, Buchpiguel CA, Braconi CT et al (2016) The Brazilian Zika virus strain causes birth defects in experimental models. *Nature* 534:267–271
- D’Aiuto L, Zhi Y, Kumar Das D, Wilcox MR, Johnson JW, Mc Clain L, Macdonald ML, Di Maio R, Schurdak ME, Piazza P, Viggiano L, Sweet R, Kinchington PR, Bhattacharjee AG, Yolken R, Nimgaonka VL (2014) Large-scale generation of human ipsc-derived neural stem cells/early neural progenitor cells and their neuronal differentiation. *Organogenesis* 10:365–377
- Dai S, Li R, Long Y, Titus S, Zhao J, Huang R, Xia M, Zheng W (2016) One-step seeding of neural stem cells with vitronectin- supplemented medium for high throughput screening assays. *J Biomol Screen* 21:1112–1124

- Dang J, Tiwari SK, Lichinchi G, Qin Y, Patil VS, Eroshkin AM, Rana TM (2016) Zika virus depletes neural progenitors in human cerebral organoids through activation of the innate immune receptor TLR3. *Cell Stem Cell* 19:258–265
- Danon JJ, Reekie TA, Kassiou M (2019) Challenges and opportunities in central nervous system drug discovery. *Trends Chem* 1:612–624. <https://doi.org/10.1016/j.trechm.2019.04.009>
- Di Cesare ML, Pacini A, Micheli L, Tani A, Zanardelli M, Ghelardini C (2014) Glial role in oxaliplatin-induced neuropathic pain. *Exp Neurol* 261. <https://doi.org/10.1016/j.expneurol.2014.06.016>
- Djelloul M, Holmqvist S, Boza-Serrano A, Azevedo C, Yeung MS, Goldwurm S, Frisén J, Deierborg T, Roybon L (2015) Alpha-synuclein expression in the oligodendrocyte lineage: an in vitro and in vivo study using rodent and human models. *Stem Cell Rep* 5:174–184
- Douvaras P, Wang J, Zimmer M, Hanchuk S, O'Bara MA, Sadiq S, Sim FJ, Goldman J, Fossati V (2014) Efficient generation of myelinating oligodendrocytes from primary progressive multiple sclerosis patients by induced pluripotent stem cells. *Stem Cell Rep* 3:250–259. <https://doi.org/10.1016/j.stemcr.2014.06.012>
- Douvaras P, Sun B, Wang M, Kruglikov I, Lалlos G, Zimmer M, Terrenoire C, Zhang B, Gandy S, Schadt E, Freytes DO, Noggle S, Fossati V (2017) Directed differentiation of human pluripotent stem cells to microglia. *Stem Cell Rep* 8:1516–1524. <https://doi.org/10.1016/j.stemcr.2017.04.023>
- Duan L, Bhattacharyya BJ, Belmadani A, Pan L, Miller RJ, Kessler JA (2014) Stem cell derived basal forebrain cholinergic neurons from Alzheimer's disease patients are more susceptible to cell death. *Mol Neurodegener* 9:1–14
- Efthymiou A, Shaltouki A, Steiner JP, Jha B, Heman-Ackah SM, Swistowski A, Zeng X, Rao MS, Malik N (2014) Functional screening assays with neurons generated from pluripotent stem cell-derived neural stem cells. *J Biomol Screen* 19:32–43
- Egawa N, Kitaoka S, Tsukita K, Naitoh M, Takahashi K, Yamamoto T, Adachi F, Kondo T, Okita K, Asaka I, Aoi T, Watanabe A, Yamada Y, Morizane A, Takahashi J, Ayaki T, Ito H, Yoshikawa K, Yamawaki S, Suzuki S et al (2012) Drug screening for ALS using patient-specific induced pluripotent stem cells. *Sci Transl Med* 4:145ra104
- Ehrlich M, Mozafari S, Glatza M, Starost L, Velychko S, Hallmann AL, Cui QL, Schambach A, Kim KP, Bachelin C, Marteyn A, Hargus G, Johnson RM, Antel J, Sternecker J, Zaehres H, Schöler HR, Baron-Van Evercooren A, Kuhlmann T (2017) Rapid and efficient generation of oligodendrocytes from human induced pluripotent stem cells using transcription factors. *Proc Natl Acad Sci U S A* 114:E2243–E2252
- Eiraku M, Watanabe K, Matsuo-takasaki M, Kawada M, Yonemura S, Matsumura M, Wataya T, Nishiyama A, Muguruma K, Sasai Y (2008) Article self-organized formation of polarized cortical tissues from ESCs and its active manipulation by extrinsic signals. *Stem Cell* 3:519–532. <https://doi.org/10.1016/j.stem.2008.09.002>
- Engle SJ, Puppala D (2013) Integrating human pluripotent stem cells into drug development. *Cell Stem Cell* 12:669–677. <https://doi.org/10.1016/j.stem.2013.05.011>
- Etemad S, Zamin RM, Ruitenber MJ, Filgueira L (2012) A novel in vitro human microglia model: characterization of human monocyte-derived microglia. *J Neurosci Methods* 209:79–89
- Farkhondeh A, Li R, Gorshkov K, Chen KG, Might M, Rodems S, Lo DC, Zheng W (2019) Induced pluripotent stem cells for neural drug discovery. *Drug Discov Today* 24:992–999. <https://doi.org/10.1016/j.drudis.2019.01.007>
- Flames N, Gelman DM, Rubenstein JLR, Puelles L, Mari O, Herna UM, Joan S (2007) Delineation of multiple subpallial progenitor domains by the combinatorial expression of transcriptional codes. *J Neurosci* 27:9682–9695
- Fritsche E, Barenys M, Klose J, Masjosthusmann S, Nimtz L, Schmuck M, Wuttke S, Tigges J (2018a) Current availability of stem cell-based in vitro methods for developmental neurotoxicity (DNT) testing. *Toxicol Sci* 165:21–30

- Fritsche E, Barenys M, Klose J, Masjosthusmann S, Nimtz L, Schmuck M, Wuttke S, Tigges J (2018b) Development of the concept for stem cell-based developmental neurotoxicity evaluation. *Toxicol Sci* 165:14–20. <https://academic.oup.com/toxsci/article/165/1/14/5046970>
- Garcez P, Loiola E, Madeiro da Costa R, Higa L, Trindade P, Delvecchio R, Nascimento J, Brindeiro R, Tanuri A, Rehen S (2016) Zika virus impairs growth in human neurospheres and brain organoids. *Science* 351:816–818
- García-León JA, Cabrera-Socorro A, Eggermont K, Swijssen A, Terryn J, Fazal R, Nami FA, Ordoñas L, Quiles A, Lluís F, Serneels L, Wierda K, Sierksma A, Kreir M, Pestana F, Van Damme P, De Strooper B, Thorrez L, Ebner A, Verfaillie CM (2018a) Generation of a human induced pluripotent stem cell-based model for tauopathies combining three microtubule-associated protein TAU mutations which displays several phenotypes linked to neurodegeneration. *Alzheimers Dement* 14:1261–1280
- García-León JA, Kumar M, Boon R, Chau D, One J, Wolfs E, Eggermont K, Berckmans P, Gunhanlar N, de Vrij F, Lendemeijer B, Pavie B, Corthout N, Kushner SA, Dávila JC, Lambrechts I, Hu WS, Verfaillie CM (2018b) SOX10 single transcription factor-based fast and efficient generation of oligodendrocytes from human pluripotent stem cells. *Stem Cell Rep* 10:655–672
- Ghaffari LT, Starr A, Nelson AT, Sattler R (2018) Representing diversity in the dish: using patient-derived in vitro models to recreate the heterogeneity of neurological disease. *Front Neurosci* 12:1–18
- Ginhoux F, Greter M, Leboeuf M, Nandi S, See P, Gokhan S, Mehler MF, Conway SJ, Ng LG, Stanley ER, Samokhvalov IM, Merad M (2010) Fate mapping analysis reveals that adult microglia derive from primitive macrophages. *Science* 330:841–845
- Grabert K, Michoel T, Karavolos MH, Clohisey S, Kenneth Baillie J, Stevens MP, Freeman TC, Summers KM, McColl BW (2016) Microglial brain region-dependent diversity and selective regional sensitivities to aging. *Nat Neurosci* 19:504–516
- Gribkoff VK, Kaczmarek LK (2017) The need for new approaches in CNS drug discovery: why drugs have failed, and what can be done to improve outcomes. *Neuropharmacology* 120:11–19. <https://doi.org/10.1016/j.neuropharm.2016.03.021>
- Guenther MG (2011) Transcriptional control of embryonic and induced pluripotent stem cells. *Epigenomics* 3:323–343
- Haenseler W, Sansom SN, Buchrieser J, Newey SE, Moore CS, Nicholls FJ, Chintawar S, Schnell C, Antel JP, Allen ND, Cader MZ, Wade-Martins R, James WS, Cowley SA (2017) A highly efficient human pluripotent stem cell microglia model displays a neuronal-co-culture-specific expression profile and inflammatory response. *Stem Cell Rep* 8:1727–1742. <https://doi.org/10.1016/j.stemcr.2017.05.017>
- Haggarty SJ, Silva MC, Cross A, Brandon NJ, Perlis RH (2016) Advancing drug discovery for neuropsychiatric disorders using patient-specific stem cell models. *Mol Cell Neurosci* 73:104–115. <https://doi.org/10.1016/j.mcn.2016.01.011>
- Hall CE, Yao Z, Choi M, Tyzack GE, Serio A, Luisier R, Harley J, Preza E, Arber C, Crisp SJ, Watson PMD, Kullmann DM, Abramov AY, Wray S, Burley R, Loh SHY, Martins LM, Stevens MM, Luscombe NM, Sibley CR et al (2017) Progressive motor neuron pathology and the role of astrocytes in a human stem cell model of VCP-related ALS. *Cell Rep* 19:1739–1749. <https://doi.org/10.1016/j.celrep.2017.05.024>
- Hartfield EM, Yamasaki-Mann M, Ribeiro Fernandes HJ, Vowles J, James WS, Cowley SA, Wade-Martins R (2014) Physiological characterisation of human iPS-derived dopaminergic neurons. *PLoS One* 9:e87388
- Hashimoto D, Chow A, Noizat C, Teo P, Beasley MB, Leboeuf M, Becker CD, See P, Price J, Lucas D, Greter M, Mortha A, Boyer SW, Forsberg EC, Tanaka M, van Rooijen N, García-Sastre A, Stanley ER, Ginhoux F, Frenette PS et al (2013) Tissue-resident macrophages self-maintain locally throughout adult life with minimal contribution from circulating monocytes. *Immunity* 38:792–804

- Hendry SH, Schwark HD, Jones EG, Yan J (1987) Numbers and proportions of GABA-immunoreactive neurons in different areas of monkey cerebral cortex. *J Neurosci* 7:1503–1519
- Hsiao HY, Chen YC, Huang CH, Chen CC, Hsu YH, Chen HM, Chiu FL, Kuo HC, Chang C, Chern Y (2015) Aberrant astrocytes impair vascular reactivity in Huntington disease. *Ann Neurol* 78:178–192
- Hu W, Qiu B, Guan W, Wang Q, Wang M, Li W, Gao L, Shen L (2015) Short article direct conversion of normal and Alzheimer's disease human fibroblasts into neuronal cells by small molecules short article direct conversion of normal and Alzheimer's disease human fibroblasts into neuronal cells by small molecules. *Stem Cell* 17:204–212. <https://doi.org/10.1016/j.stem.2015.07.006>
- Huang YWA, Zhou B, Wernig M, Südhof TC (2017) ApoE2, ApoE3, and ApoE4 differentially stimulate APP transcription and A $\beta$  secretion. *Cell* 168:427–441.e21
- Ichida JK, Kiskinis E (2015) Probing disorders of the nervous system using reprogramming approaches. *EMBO J* 34:1456–1477
- Israel MA, Yuan SH, Bardy C, Reyna SM, Mu Y, Herrera C, Hefferan MP, Van Gorp S, Nazor KL, Boscolo FS, Carson CT, Laurent LC, Marsala M, Gage FH, Remes AM, Koo EH, Goldstein LSB (2012) Probing sporadic and familial Alzheimer's disease using induced pluripotent stem cells. *Nature* 482:216–220. <https://doi.org/10.1038/nature10821>
- Janabi N, Peudenier S, Héron B, Ng KH, Tardieu M (1995) Establishment of human microglial cell lines after transfection of primary cultures of embryonic microglial cells with the SV40 large T antigen. *Neurosci Lett* 195:105–108
- Jones VC, Atkinson-Dell R, Verkhatsky A, Mohamet L (2017) Aberrant iPSC-derived human astrocytes in Alzheimer's disease. *Cell Death Dis* 8:1–11. <https://doi.org/10.1038/cddis.2017.89>
- Joung D, Truong V, Neitzke CC, Guo SZ, Walsh PJ, Monat JR, Meng F, Park SH, Dutton JR, Parr AM, McAlpine MC (2018) 3D printed stem-cell derived neural progenitors generate spinal cord scaffolds. *Adv Funct Mater* 28:1–10
- Kanat O, Ertas H, Caner B (2017) Platinum-induced neurotoxicity: a review of possible mechanisms. *World J Clin Oncol* 8:329–336
- Karzbrun E, Kshirsagar A, Cohen SR, Hanna JH, Reiner O (2018) Human brain organoids on a chip reveal the physics of folding. *Nat Phys* 14:515–522
- Kayama T, Suzuki I, Odawara A, Sasaki T, Ikegaya Y (2018) Temporally coordinated spiking activity of human induced pluripotent stem cell-derived neurons co-cultured with astrocytes. *Biochem Biophys Res Commun* 495:1028–1033. <https://doi.org/10.1016/j.bbrc.2017.11.115>
- Kiskinis E, Sandoe J, Williams LA, Boulting GL, Moccia R, Wainger BJ, Han S, Peng T, Thams S, Mikkilineni S, Mellin C, Merkle FT, Davis-dusenbery BN, Ziller M, Oakley D, Ichida J, Dicostanza S, Atwater N, Maeder ML, Goodwin MJ et al (2014) Article pathways disrupted in human ALS motor neurons identified through genetic correction of mutant SOD1. *Stem Cell* 43:1–15. <https://doi.org/10.1016/j.stem.2014.03.004>
- Klaunig JE, Babich MA, Baetcke KP, Cook JC, Corton JC, David RM, DeLuca JG, Lai DY, McKee RH, Peters JM, Roberts RA, Fenner-Crisp PA (2003) PPAR $\alpha$  agonist-induced rodent tumors: modes of action and human relevance. *Crit Rev Toxicol* 33:655–780
- Kondo T, Asai M, Tsukita K, Kutoku Y, Ohsawa Y, Sunada Y, Imamura K, Egawa N, Yahata N, Okita K, Takahashi K, Asaka I, Aoi T, Watanabe A, Watanabe K, Kadoya C, Nakano R, Watanabe D, Maruyama K, Hori O et al (2013) Modeling Alzheimer's disease with iPSCs reveals stress phenotypes associated with intracellular A $\beta$  and differential drug responsiveness. *Cell Stem Cell* 12:487–496. <https://doi.org/10.1016/j.stem.2013.01.009>
- Kriks S, Shim J, Piao J, Ganat YM, Wakeman DR, Xie Z, Carrillo-reid L (2011) Dopamine neurons derived from human ES cells efficiently engraft in animal models of Parkinson's disease. *Nature* 480:547–551. <https://doi.org/10.1038/nature10648>
- Lancaster MA, Knoblich JA (2014) Organogenesis in a dish: modeling development and disease using organoid technologies. *Science* 345:1247125

- Lancaster MA, Corsini NS, Wolfinger S, Gustafson EH, Phillips AW, Burkard TR, Otani T, Livesey FJ, Knoblich JA (2017) Guided self-organization and cortical plate formation in human brain organoids. *Nat Biotechnol* 35:659–666
- Lee JH, Mitchell RR, McNicol JD, Shapovalova Z, Laronde S, Tanasijevic B, Milsom C, Casado F, Fiebig-Comyn A, Collins TJ, Singh KK, Bhatia M (2015) Single transcription factor conversion of human blood fate to NPCs with CNS and PNS developmental capacity. *Cell Rep* 11:1367–1376. <https://doi.org/10.1016/j.celrep.2015.04.056>
- Leist M, Hartung T (2013) Reprint: inflammatory findings on species extrapolations: humans are definitely no 70-kg mice. *ALTEX* 30:227–230
- Leone C, Le Pavec G, Mème W, Porcheray F, Samah B, Dormont D, Gras G (2006) Characterization of human monocyte-derived microglia-like cells. *Glia* 54:183–192
- Li Q, Barres BA (2018) Microglia and macrophages in brain homeostasis and disease. *Nat Rev Immunol* 18:225–242. <https://doi.org/10.1038/nri.2017.125>
- Li Y, Muffat J, Omer A, Bosch I, Lancaster MA, Sur M, Gehrke L, Knoblich JA, Jaenisch R (2017) Induction of expansion and folding in human cerebral organoids. *Cell Stem Cell* 20:385–396.e3. <https://doi.org/10.1016/j.stem.2016.11.017>
- Lindborg BA, Brekke JH, Vegoe AL, Ulrich CB, Haider KT, Subramaniam S, Venhuizen SL, Eide CR, Orchard PJ, Chen W, Wang Q, Pelaez F, Scott CM, Kokkoli E, Keirstead SA, Dutton JR, Tolar J, O'Brien TD (2016) Rapid induction of cerebral organoids from human induced pluripotent stem cells using a chemically defined hydrogel and defined cell culture medium. *Stem Cells Transl Med* 5:970–979. <https://doi.org/10.5966/sctm.2015-0305>
- Liu Y, Liu H, Sauvey C, Yao L, Zarnowska ED, Zhang S (2013) Directed differentiation of forebrain GABA interneurons from human pluripotent stem cells. *Nat Protoc* 8:1670–1679. <https://doi.org/10.1038/nprot.2013.106>
- Lopez-Gonzalez R, Lu Y, Gendron TF, Karydas A, Tran H, Yang D, Petrucelli L, Miller BL, Almeida S, Gao FB (2016) Poly(GR) in C9ORF72-related ALS/FTD compromises mitochondrial function and increases oxidative stress and DNA damage in iPSC-derived motor neurons. *Neuron* 92:383–391. <https://doi.org/10.1016/j.neuron.2016.09.015>
- Lowry WE, Plath K (2008) The many ways to make an iPSC cell. *Nat Biotechnol* 26:1246–1248
- Lundin A, Delsing L, Clausen M, Ricchiuto P, Sanchez J, Sabirsh A, Ding M, Synnergren J, Zetterberg H, Brolén G, Hicks R, Herland A, Falk A (2018) Human iPSC-derived astroglia from a stable neural precursor state show improved functionality compared with conventional astrocytic models. *Stem Cell Rep* 10:1030–1045. <https://linkinghub.elsevier.com/retrieve/pii/S221367111830047X>
- Malik N, Efthymiou AG, Mather K, Chester N, Wang X, Nath A, Rao MS, Steiner JP (2014) Compounds with species and cell type specific toxicity identified in a 2000 compound drug screen of neural stem cells and rat mixed cortical neurons. *Neurotoxicology* 45:192–200
- Manabe T, Tatsumi K, Inoue M, Matsuyoshi H, Makinodan M, Yokoyama S, Wanaka A (2005) L3/Lhx8 is involved in the determination of cholinergic or GABAergic cell fate. *J Neurochem* 94:723–730
- Mariani J, Coppola G, Zhang P, Abyzov A, Provini L, Tomasini L, Amenduni M, Szekely A, Palejev D, Wilson M, Gerstein M, Grigorenko EL, Chawarska K, Pelphrey KA, Howe JR, Vaccarino FM (2015) FOXP1-dependent dysregulation of GABA/glutamate neuron differentiation in autism spectrum disorders. *Cell* 162:375–390
- Masjosthusmann S, Barenys M, El-Gamal M, Geerts L, Gerosa L, Gorreja A, Kühne B, Marchetti N, Tigges J, Viviani B, Witters H, Fritsche E (2018) Literature review and appraisal on alternative neurotoxicity testing methods. *EFSA Support Publ* 15:1–108
- Massaro EJ (2002) *Handbook of neurotoxicology*. Springer Science + Business Media, New York
- Matsui TK, Matsubayashi M, Sakaguchi YM, Hayashi RK, Zheng C, Sugie K, Hasegawa M, Nakagawa T, Mori E (2018) Six-month cultured cerebral organoids from human ES cells contain matured neural cells. *Neurosci Lett* 670:75–82. <https://doi.org/10.1016/j.neulet.2018.01.040>

- Maury Y, Côme J, Piskorowski RA, Salah-Mohellibi N, Chevaleyre V, Peschanski M, Martinat C, Nedelec S (2015) Combinatorial analysis of developmental cues efficiently converts human pluripotent stem cells into multiple neuronal subtypes. *Nat Biotechnol* 33:89–96
- McComish SF, Caldwell MA (2018) Generation of defined neural populations from pluripotent stem cells. *Philos Trans R Soc B Biol Sci* 373:20170214
- McQuade A, Coburn M, Tu CH, Hasselmann J, Davtyan H, Blurton-Jones M (2018) Development and validation of a simplified method to generate human microglia from pluripotent stem cells. *Mol Neurodegener* 13:1–13
- Mertens J, Reid D, Lau S, Kim Y, Gage FH (2018) Aging in a dish: iPSC-derived and directly induced neurons for studying brain aging and age-related neurodegenerative diseases. *Annu Rev Genet* 52:271–293
- Muffat J, Li Y, Yuan B, Mitalipova M, Omer A, Corcoran S, Bakiasi G, Tsai LH, Aubourg P, Ransohoff RM, Jaenisch R (2016) Efficient derivation of microglia-like cells from human pluripotent stem cells. *Nat Med* 22:1358–1367
- Muratore CR, Rice HC, Srikanth P, Callahan DG, Shin T, Benjamin LNP, Walsh DM, Selkoe DJ, Young-Pearse TL (2014) The familial alzheimer's disease APPV717I mutation alters APP processing and Tau expression in iPSC-derived neurons. *Hum Mol Genet* 23:3523–3536
- Nagai A, Mishima S, Ishida Y, Ishikura H, Harada T, Kobayashi S, Kim SU (2005) Immortalized human microglial cell line: phenotypic expression. *J Neurosci Res* 81:342–348
- Naghieh S, Sarker MD, Abelseth E, Chen X (2019) Indirect 3D bioprinting and characterization of alginate scaffolds for potential nerve tissue engineering applications. *J Mech Behav Biomed Mater* 93:183–193
- National Institute of Health Neurotoxicity Information (2019). <https://www.ninds.nih.gov/disorders/all-disorders/neurotoxicity-information-page#disorders-r1>
- Nehme R, Zuccaro E, Ghosh SD, Fu Z, Ghosh SD, Li C, Sherwood JL, Pietilainen O (2018) Combining NGN2 programming with developmental patterning generates human excitatory neurons with NMDAR-mediated synaptic transmission resource combining NGN2 programming with developmental patterning generates human excitatory neurons with NMDAR-mediated. *Cell Rep* 23:2509–2523. <https://doi.org/10.1016/j.celrep.2018.04.066>
- Nzou G, Wicks RT, Wicks EE, Seale SA, Sane CH, Chen A, Murphy SV, Jackson JD, Atala AJ (2018) Human cortex spheroid with a functional blood brain barrier for high-throughput neurotoxicity screening and disease modeling. *Sci Rep* 8:1–10. <https://doi.org/10.1038/s41598-018-25603-5>
- Oksanen M, Petersen AJ, Naumenko N, Puttonen K, Lehtonen Š, Gubert Olivé M, Shakirzyanova A, Leskelä S, Sarajärvi T, Viitanen M, Rinne JO, Hiltunen M, Haapasalo A, Giniatullin R, Tavi P, Zhang SC, Kanninen KM, Hämäläinen RH, Koistinaho J (2017) PSEN1 mutant iPSC-derived model reveals severe astrocyte pathology in Alzheimer's disease. *Stem Cell Rep* 9:1885–1897
- Oliveira LMA, Falomir-Lockhart LJ, Botelho MG, Lin KH, Wales P, Koch JC, Gerhardt E, Taschenberger H, Outeiro TF, Lingor P, Schüle B, Arndt-Jovin DJ, Jovin TM (2015) Elevated  $\alpha$ -synuclein caused by SNCA gene triplication impairs neuronal differentiation and maturation in Parkinson's patient-derived induced pluripotent stem cells. *Cell Death Dis* 6:1–13
- Ormel PR, Vieira de Sá R, van Bodegraven EJ, Karst H, Harschnitz O, Sneeboer MAM, Johansen LE, van Dijk RE, Scheefhals N, Berdenis van Berlekom A, Ribes Martínez E, Kling S, MacGillavry HD, van den Berg LH, Kahn RS, Hol EM, de Witte LD, Pasterkamp RJ (2018) Microglia innately develop within cerebral organoids. *Nat Commun* 9:4167. <https://doi.org/10.1038/s41467-018-06684-2>
- Osaki T, Shin Y, Sivathanu V, Campisi M, Kamm RD (2018) In vitro microfluidic models for neurodegenerative disorders. *Adv Healthc Mater* 7
- Paini A, Leonard JA, Joossens E, Bessems JGM, Desalegn A, Dorne JL, Gosling JP, Heringa MB, Klaric M, Kliment T, Kramer NI, Loizou G, Louise J, Lumen A, Madden JC, Patterson EA, Proenca S, Punt A, Setzer RW, Suciú N et al (2019) Next generation physiologically based

- kinetic (NG-PBK) models in support of regulatory decision making. *Comput Toxicol (Amsterdam, Netherlands)* 9:61–72
- Pandya H, Shen MJ, Ichikawa DM, Sedlock AB, Choi Y, Johnson KR, Kim G, Brown MA, Elkahoun AG, Maric D, Sweeney CL, Gossa S, Malech HL, McGavern DB, Park JK (2017) Differentiation of human and murine induced pluripotent stem cells to microglia-like cells. *Nat Neurosci* 20:753–759
- Park DY, Lee J, Chung JJ, Jung Y, Kim SH (2019) Integrating organs-on-chips: multiplexing, scaling, vascularization, and innervation. *Trends Biotechnol* 38:99–112. <https://doi.org/10.1016/j.tibtech.2019.06.006>
- Pasca SP (2018) The rise of three-dimensional human brain cultures. *Nature* 553:437–445. <https://doi.org/10.1038/nature25032>
- Patani R, Lewis PA, Trabzuni D, Puddifoot CA, Wyllie DJA, Walker R, Smith C, Hardingham GE, Weale M, Hardy J, Chandran S, Ryten M (2012) Investigating the utility of human embryonic stem cell-derived neurons to model ageing and neurodegenerative disease using whole-genome gene expression and splicing analysis. *J Neurochem* 122:738–751
- Pérez-Cerdá F, Sánchez-Gómez MV, Matute C (2015) Pío del Río hortega and the discovery of the oligodendrocytes. *Front Neuroanat* 9:7–12
- Qian X, Nguyen HN, Song MM, Hadiono C, Ogden SC, Hammack C, Yao B, Hamersky GR, Jacob F, Zhong C, Yoon KJ, Jeang W, Lin L, Li Y, Thakor J, Berg DA, Zhang C, Kang E, Chickering M, Nauen D et al (2016) Brain-region-specific organoids using mini-bioreactors for modeling ZIKV exposure. *Cell* 165:1238–1254. <https://doi.org/10.1016/j.cell.2016.04.032>
- Qian X, Nguyen HN, Jacob F, Song H, Ming GL (2017) Using brain organoids to understand Zika virus-induced microcephaly. *Dev* 144:952–957
- Quadrato G, Nguyen T, Macosko EZ, Sherwood JL, Min Yang S, Berger DR, Maria N, Scholvin J, Goldman M, Kinney JP, Boyden ES, Lichtman JW, Williams ZM, McCarroll SA, Arlotta P (2017) Cell diversity and network dynamics in photosensitive human brain organoids. *Nature* 545:48–53. <http://www.nature.com/articles/nature22047>
- Raja WK, Mungenast AE, Lin YT, Ko T, Abdurrob F, Seo J, Tsai LH (2016) Self-organizing 3D human neural tissue derived from induced pluripotent stem cells recapitulate Alzheimer's disease phenotypes. *PLoS One* 11:1–18
- Rana P, Luerman G, Hess D, Rubitski E, Adkins K, Soms C (2017) Toxicology in vitro utilization of iPSC-derived human neurons for high-throughput drug- induced peripheral neuropathy screening. *Toxicol Vitro* 45:111–118. <https://doi.org/10.1016/j.tiv.2017.08.014>
- Ransohoff RM, El Khoury J (2016) Microglia in health and disease. *Cold Spring Harb Perspect Biol* 8:a020560. <http://cshperspectives.cshlp.org/lookup/doi/10.1101/cshperspect.a020560>
- Rindt H, Tom CM, Lorson CL, Mattis VB (2017) Optimization of trans-splicing for Huntington's disease RNA therapy. *Front Neurosci* 11:1–13
- Ryan KJ, White CC, Patel K, Xu J, Olah M, Replogle JM, Frangieh M, Cimpean M, Winn P, McHenry A, Kaskow BJ, Chan G, Cuerdon N, Bennett DA, Boyd JD, Imitola J, Elyaman W, De Jager PL, Bradshaw EM (2017) A human microglia-like cellular model for assessing the effects of neurodegenerative disease gene variants. *Sci Transl Med* 9:1–13
- Sahara S, Yanagawa Y, O'Leary DDM, Stevens CF (2012) The fraction of cortical GABAergic neurons is constant from near the start of cortical neurogenesis to adulthood. *J Neurosci* 32:4755–4761
- Sanchez-Danes A, Richaud-patin Y, Carballo-carbajal I, Sa A, Caig C, Mora S, Di Guglielmo C, Ezquerro M, Vila M, Cuervo AM, Tolosa E, Consiglio A, Raya A (2012) Disease-specific phenotypes in dopamine neurons from human iPS-based models of genetic and sporadic Parkinson's disease. *EMBO Mol Med* 4:380–395
- Sareen D, Ebert AD, Heins BM, McGivern JV, Ornelas L, Svendsen CN (2012) Inhibition of apoptosis blocks human motor neuron cell death in a stem cell model of spinal muscular atrophy. *PLoS One* 7:e39113
- Sareen D, O'Rourke JG, Meera P, Muhammad AKMG, Grant S, Simpkinson M, Bell S, Carmona S, Ornelas L, Sahabian A, Gendron T, Petrucelli L, Baughn M, Ravits J, Harms

- MB, Rigo F, Bennett CF, Otis TS, Svendsen CN, Baloh RH (2013) Targeting RNA foci in iPSC-derived motor neurons from ALS patients with C9ORF72 repeat expansion. *Sci Transl Med* 5:1–57
- Schröter F, Slegers K, Van Cauwenberghe C, Bohndorf M, Wruck W, Van Broeckhoven C, Adjaye J (2016) Lymphoblast-derived integration-free iPSC lines from a female and male Alzheimer's disease patient expressing different copy numbers of a coding CNV in the Alzheimer risk gene CR1. *Stem Cell Res* 17:560–563. <https://doi.org/10.1016/j.scr.2016.10.003>
- Seidel D, Jahnke H, Englich B, Girard M, Robitzki AA (2017) In vitro field potential monitoring on a multi-microelectrode array for the electrophysiological long-term screening of neural stem cell maturation. *Analyst* 142:1929–1937. <http://xlink.rsc.org/?DOI=C6AN02713J>
- Sellgren CM, Sheridan SD, Gracias J, Xuan D, Fu T, Perlis RH (2017) Patient-specific models of microglia-mediated engulfment of synapses and neural progenitors. *Mol Psychiatry* 22:170–177
- Sherman SP, Bang AG (2018) High-throughput screen for compounds that modulate neurite growth of human induced pluripotent stem cell-derived neurons. *DMM Dis Model Mech* 11: dmm031906
- Shi Y, Kirwan P, Smith J, MacLean G, Orkin SH, Livesey FJ (2012) A human stem cell model of early Alzheimer's disease pathology in down syndrome. *Sci Transl Med* 4:124ra29. <https://doi.org/10.1016/j.jalz.2012.05.1946>
- Shi Y, Kirwan P, Smith J, Robinson HPC, Livesey FJ (2014) Human cerebral cortex development from pluripotent stem cells to functional excitatory synapses. *Nat Neurosci* 15:1–25. <http://www.pubmedcentral.nih.gov/articlerender.fcgi?artid=3882590&tool=pmcentrez&rendertype=abstract>
- Shi Y, Inoue H, Wu JC, Yamanaka S (2017) Induced pluripotent stem cell technology: a decade of progress. *Nat Rev Drug Discov* 16:115–130
- Silva MC, Haggarty SJ (2019) Human pluripotent stem cell-derived models and drug screening in CNS precision medicine. *Ann N Y Acad Sci*
- Singh VK, Kalsan M, Kumar N, Saini A, Chandra R (2015) Induced pluripotent stem cells: applications in regenerative medicine, disease modeling, and drug discovery. *Front Cell Dev Biol* 3:1–18
- Stacey P, Wassermann AM, Kammonen L, Impey E, Wilbrey A, Cawkill D (2018) Plate-based phenotypic screening for pain using human iPSC-derived sensory neurons. *SLAS Disc* 23:585–596
- Suga M, Kondo T, Inoue H (2019) Modeling neurological disorders with human pluripotent stem cell-derived astrocytes. *Int J Mol Sci* 20:9–14
- Szlachcic WJ, Switonski PM, Krzyzosiak WJ, Figlerowicz M, Figiel M (2015) Huntington disease iPSCs show early molecular changes in intracellular signaling, the expression of oxidative stress proteins and the p53 pathway. *Dis Model Mech* 8:1047–1057
- Takahashi K, Tanabe K, Ohnuki M, Narita M, Ichisaka T, Tomoda K, Yamanaka S (2007) Induction of pluripotent stem cells from adult human fibroblasts by defined factors. *Cell* 131:861–872. <http://www.ncbi.nlm.nih.gov/pubmed/18035408>
- Thomson JA, Itskovitz-eldor J, Shapiro SS, Waknitz MA, Swiergiel JJ, Marshall VS, Jones JM (1998) Embryonic stem cell lines derived from human blastocysts. *Science* 282:1145–1148
- Toutain P-L, Ferran A, Bousquet-Melou A (2010) Species differences in pharmacokinetics and pharmacodynamics. *Handb Exp Pharmacol*:19–48
- Tukker AM, De Groot MWGDM, Wijnolts FMJ, Kasteel EEJ, Hondebrink L, Westerink RHS (2016) Research article is the time right for in vitro neurotoxicity testing using human iPSC-derived neurons? *ALTEX* 33:261–271
- Tukker AM, Wijnolts FMJ, de Groot A, Westerink RHS (2018) Neurotoxicology human iPSC-derived neuronal models for in vitro neurotoxicity assessment. *Neurotoxicology* 67:215–225. <https://doi.org/10.1016/j.neuro.2018.06.007>
- Victor MB, Richner M, Hermansteyne TO, Ransdell JL, Sobieski C, Deng P, Klyachko VA, Nerbonne JM, Yoo AS (2014) NeuroResource generation of human striatal neurons by

- MicroRNA-dependent direct conversion of fibroblasts. *Neuron* 84:311–323. <https://doi.org/10.1016/j.neuron.2014.10.016>
- Vierbuchen T, Ostermeier A, Pang ZP, Kokubu Y, Südhof TC, Wernig M (2010) Direct conversion of fibroblasts to functional neurons by defined factors. *Nature* 463:1035–1041
- von Bartheld CS, Bahney J, Herculano-houzel S (2017) The search for true numbers of neurons and glial cells in the human brain: a review of 150 years of cell counting. *J Comp Neurol* 524:3865–3895
- Wang S, Bates J, Li X, Schanz S, Chandler-militello D, Levine C, Maherali N, Studer L, Hochedlinger K, Windrem M, Goldman SA (2013) Clinical progress progenitor cells can myelinate and rescue a mouse model of congenital hypomyelination. *Stem Cell* 12:252–264. <https://doi.org/10.1016/j.stem.2012.12.002>
- Wang C, Ward ME, Chen R, Liu K, Tracy TE, Chen X, Xie M, Sohn PD, Ludwig C, Meyer-Franke A, Karch CM, Ding S, Gan L (2017) Scalable production of iPSC-derived human neurons to identify Tau-Lowering compounds by high-content screening. *Stem Cell Rep* 9:1221–1233. <https://doi.org/10.1016/j.stemcr.2017.08.019>
- Wapinski OL, Lee QY, Chen AC, Li R, Corces MR, Ang CE, Treutlein B, Xiang C, Baubet V, Suchy FP, Sankar V, Sim S, Quake SR, Dahmane N, Wernig M, Chang HY (2017) Rapid chromatin switch in the direct reprogramming of fibroblasts to neurons. *Cell Rep* 20:3236–3247
- Warren L, Manos PD, Ahfeldt T, Loh YH, Li H, Lau F, Ebina W, Mandal PK, Smith ZD, Meissner A, Daley GQ, Brack AS, Collins JJ, Cowan C, Schlaeger TM, Rossi DJ (2010) Highly efficient reprogramming to pluripotency and directed differentiation of human cells with synthetic modified mRNA. *Cell Stem Cell* 7:618–630
- Watanabe M, Buth JE, Vishlaghi N, de la Torre-Ubieta L, Taxidis J, Khakh BS, Coppola G, Pearson CA, Yamauchi K, Gong D, Dai X, Damoiseaux R, Aliyari R, Liebscher S, Schenke-Layland K, Caneda C, Huang EJ, Zhang Y, Cheng G, Geschwind DH et al (2017) Self-organized cerebral organoids with human-specific features predict effective drugs to combat Zika virus infection. *Cell Rep* 21:517–532. <https://doi.org/10.1016/j.celrep.2017.09.047>
- Woodruff G, Young JE, Martinez FJ, Buen F, Gore A, Kinaga J, Li Z, Yuan SH, Zhang K, Goldstein LSB (2013) The Presenilin-1  $\delta E9$  mutation results in reduced  $\gamma$ -secretase activity, but not total loss of PS1 function, in isogenic human stem cells. *Cell Rep* 5:974–985. <https://doi.org/10.1016/j.celrep.2013.10.018>
- Xu M, Lee EM, Wen Z, Cheng Y, Huang WK, Qian X, Tcw J, Kouznetsova J, Ogden SC, Hammack C, Jacob F, Nguyen HN, Itkin M, Hanna C, Shinn P, Allen C, Michael SG, Simeonov A, Huang W, Christian KM et al (2016) Identification of small-molecule inhibitors of Zika virus infection and induced neural cell death via a drug repurposing screen. *Nat Med* 22:1101–1107
- Yagi T, Ito D, Okada Y, Akamatsu W, Nihei Y, Yoshizaki T, Yamanaka S, Okano H, Suzuki N (2011) Modeling familial Alzheimer's disease with induced pluripotent stem cells. *Hum Mol Genet* 20:4530–4539
- Yahata N, Asai M, Kitaoka S, Takahashi K, Asaka I, Hioki H, Kaneko T, Maruyama K, Saido TC, Nakahata T, Asada T, Yamanaka S, Iwata N, Inoue H (2011) Anti-A $\beta$  drug screening platform using human iPS cell-derived neurons for the treatment of Alzheimer's disease. *PLoS One* 6: e25788
- Yang N, Chanda S, Marro S, Ng YH, Janas JA, Haag D, Ang CE, Tang Y, Flores Q, Mall M, Wapinski O, Li M, Ahlenius H, Rubenstein JL, Chang HY, Buylly AA, Südhof TC, Wernig M (2017) Generation of pure GABAergic neurons by transcription factor programming. *Nat Methods* 14:621–628. <https://doi.org/10.1038/nmeth.4291>
- Yoo AS, Sun AX, Li L, Shcheglovitov A, Portmann T, Li Y, Lee-Messer C, Dometsch RE, Tsien RW, Crabtree GR (2011) MicroRNA-mediated conversion of human fibroblasts to neurons. *Nature* 476:228–231. <https://www.ncbi.nlm.nih.gov/pmc/articles/PMC3624763/pdf/nihms412728.pdf>
- Young JE, Boulanger-Weill J, Williams DA, Woodruff G, Buen F, Revilla AC, Herrera C, Israel MA, Yuan SH, Edland SD, Goldstein LSB (2015) Elucidating molecular phenotypes caused by

- the SORL1 Alzheimer's disease genetic risk factor using human induced pluripotent stem cells. *Cell Stem Cell* 16:373–385. <https://doi.org/10.1016/j.stem.2015.02.004>
- Yu J, Vodyanik MA, Smuga-Otto K, Antosiewicz-Bourget J, Frane JL, Tian S, Nie J, Jonsdottir GA, Ruotti V, Stewart R, Slukvin II, Thomson JA (2007) Induced pluripotent stem cell lines derived from human somatic cells. *Science* 318:1917–1920
- Yu J, Hu K, Smuga-otto K, Tian S, Stewart R, Igor I, Thomson JA (2009) Human induced pluripotent stem cells free of vector and transgene sequences. *Science* 324:797–801
- Yu D, Swaroop M, Wang M, Baxa U, Yang R, Yan Y, Coksaygan T, DeTolla L, Marugan JJ, Austin CP, Mckew JC, Gong D-W, Zheng W (2014) Niemann-Pick disease type C: induced pluripotent stem cell- derived neuronal cells for modeling neural disease and evaluating drug efficacy. *J Biomol Screen* 19:1164–1173
- Zhang Y, Pak CH, Han Y, Ahlenius H, Zhang Z, Chanda S, Marro S, Patzke C, Acuna C, Covy J, Xu W, Yang N, Danko T, Chen L, Wernig M, Südhof TC (2013) Rapid single-step induction of functional neurons from human pluripotent stem cells. *Neuron* 78:785–798
- Zhou T, Tan L, Cederquist GY, Fan Y, Hartley BJ, Mukherjee S, Tomishima M, Brennand KJ, Zhang Q, Schwartz RE, Evans T, Studer L, Chen S (2017) High-content screening in hPSC-neural progenitors identifies drug candidates that inhibit Zika virus infection in fetal-like organoids and adult brain. *Cell Stem Cell* 21:274–283.e5. <https://doi.org/10.1016/j.stem.2017.06.017>
- Zhuang X, Lu C (2016) PBPK modeling and simulation in drug research and development. *Acta Pharm Sin B* 6:430–440

## 2.3 Neuronal Differentiation from Induced Pluripotent Stem Cell-Derived Neurospheres by the Application of Oxidized Alginate-Gelatin-Laminin Hydrogels

*Thomas Distler, Ines Lauria, Rainer Detsch, Clemens M. Sauter, Farina Bendt, Julia Kapr, Stephan Rütten, Aldo R. Boccaccini, Ellen Fritsche*

Biodegradable hydrogels that promote stem cell differentiation into neurons in three dimensions (3D) are highly desired in biomedical research to study drug neurotoxicity or to yield cell-containing biomaterials for neuronal tissue repair. Here, we demonstrate that oxidized alginate-gelatin-laminin (ADA-GEL-LAM) hydrogels facilitate neuronal differentiation and growth of embedded human induced pluripotent stem cell (hiPSC) derived neurospheres. ADA-GEL and ADA-GELLAM hydrogels exhibiting a stiffness close to ~5 kPa at initial cell culture conditions of 37° C were prepared. Laminin supplemented ADA-GEL promoted an increase in neuronal differentiation in comparison to pristine ADA-GEL, with enhanced neuron migration from the neurospheres to the bulk 3D hydrogel matrix. The presence of laminin in ADA-GEL led to a more than two-fold increase in the number of neurospheres with migrated neurons. Our findings suggest that laminin addition to oxidized alginate–gelatin hydrogel matrices plays a crucial role to tailor oxidized alginate-gelatin hydrogels suitable for 3D neuronal cell culture applications.

Journal:	Biomedicines
Impact factor:	4.757 (2023)
Contribution to the publication:	10%
	Figure Assembly, Method Description, Figure 5
Type of authorship:	Co-author
Status of publication:	Published (05 March 2021)



## Article

# Neuronal Differentiation from Induced Pluripotent Stem Cell-Derived Neurospheres by the Application of Oxidized Alginate-Gelatin-Laminin Hydrogels

Thomas Distler <sup>1,\*</sup>,<sup>†</sup>, Ines Lauria <sup>2,†</sup>, Rainer Detsch <sup>1,†</sup>, Clemens M. Sauter <sup>2</sup>, Farina Bendt <sup>2</sup>, Julia Kapr <sup>2</sup>, Stephan Rütten <sup>3</sup>, Aldo R. Boccaccini <sup>1,\*</sup> and Ellen Fritsche <sup>2,4,\*</sup>

<sup>1</sup> Department of Materials Science and Engineering, Institute Biomaterials, University of Erlangen-Nuremberg, Cauerstr. 6, 91058 Erlangen, Germany; rainer.detsch@fau.de

<sup>2</sup> IUF-Leibniz Research Institute for Environmental Medicine, Auf'm Hennekamp 50, 40225 Duesseldorf, Germany; ines.lauria@rwth-aachen.de (I.L.); clemens.sauter@uni-tuebingen.de (C.M.S.); farina.bendt@iuf-duesseldorf.de (F.B.); julia.kapr@iuf-duesseldorf.de (J.K.)

<sup>3</sup> Electron Microscopy Facility, Institute of Pathology, RWTH Aachen University Hospital, Pauwelsstrasse 30, 52074 Aachen, Germany; sruetten@ukaachen.de

<sup>4</sup> Medical Faculty, Heinrich-Heine-University, 40225 Düsseldorf, Germany

\* Correspondence: thomas.distler@fau.de (T.D.); aldo.boccaccini@fau.de (A.R.B.); ellen.fritsche@iuf-duesseldorf.de (E.F.)

† These authors contributed equally to this work.



**Citation:** Distler, T.; Lauria, I.; Detsch, R.; Sauter, C.M.; Bendt, F.; Kapr, J.; Rütten, S.; Boccaccini, A.R.; Fritsche, E. Neuronal Differentiation from Induced Pluripotent Stem Cell-Derived Neurospheres by the Application of Oxidized Alginate-Gelatin-Laminin Hydrogels. *Biomedicines* **2021**, *9*, 261. <https://doi.org/10.3390/biomedicines9030261>

Academic Editors: Elvira De Giglio and Maria A. Bonifacio

Received: 9 February 2021

Accepted: 2 March 2021

Published: 5 March 2021

**Publisher's Note:** MDPI stays neutral with regard to jurisdictional claims in published maps and institutional affiliations.



**Copyright:** © 2021 by the authors. Licensee MDPI, Basel, Switzerland. This article is an open access article distributed under the terms and conditions of the Creative Commons Attribution (CC BY) license (<https://creativecommons.org/licenses/by/4.0/>).

**Abstract:** Biodegradable hydrogels that promote stem cell differentiation into neurons in three dimensions (3D) are highly desired in biomedical research to study drug neurotoxicity or to yield cell-containing biomaterials for neuronal tissue repair. Here, we demonstrate that oxidized alginate-gelatin-laminin (ADA-GEL-LAM) hydrogels facilitate neuronal differentiation and growth of embedded human induced pluripotent stem cell (hiPSC) derived neurospheres. ADA-GEL and ADA-GEL-LAM hydrogels exhibiting a stiffness close to ~5 kPa at initial cell culture conditions of 37 °C were prepared. Laminin supplemented ADA-GEL promoted an increase in neuronal differentiation in comparison to pristine ADA-GEL, with enhanced neuron migration from the neurospheres to the bulk 3D hydrogel matrix. The presence of laminin in ADA-GEL led to a more than two-fold increase in the number of neurospheres with migrated neurons. Our findings suggest that laminin addition to oxidized alginate—gelatin hydrogel matrices plays a crucial role to tailor oxidized alginate-gelatin hydrogels suitable for 3D neuronal cell culture applications.

**Keywords:** oxidized alginate; laminin; hydrogels; human induced pluripotent stem cells (hiPSC); neurospheres; tissue engineering; bioprinting

## 1. Introduction

The fate and organization of stem cells within the human body is dependent on a spatiotemporal exposure to growth factors, cell-cell contacts and physiological cues from the surrounding extracellular matrix (ECM) [1]. Together, these factors constitute the microenvironment or niche of a cell. Traditional in vitro cell cultures are grown in two dimensions and adherent to a flat surface, reflecting the in vivo microenvironment in a simplified manner. Unnatural cell morphology and a general lack of cell–cell interactions, as well as cell-ECM adhesions, represent the limitations of such two-dimensional (2D) models [2]. Depending on the scientific question, 2D cell models can be sufficient to provide a convenient and quick solution for high-throughput applications. However, given the low success rate of drugs targeting brain-related diseases, a need for more complex and physiological neural culture models exists [3–5]. Different strategies have emerged to create 3D neural cell models that display higher degrees of structural complexity. Conventional

cell biology-based models include spheroids, neurospheres, and organoids, each having their own merits and limitations [6–9].

While conventional 3D *in vitro* models might capture the structural and cytoarchitectural aspects of the human brain, they are also prone to variability [10,11]. A key issue regarding the development of consistent cell models is the precise control over their cell and matrix composition as well as spatial organization [12]. Taken together, reproducibility and controllability are critical factors for the implementation of 3D cell models in high-throughput test systems for compound assessment. The mechanical properties of the cells' environment play a significant role in regulating their behavior [13,14]. The brain is one of the softest tissues in the human body with a Young's modulus ( $E$ ) ranging from 0.5 to 50 kPa [15]. *In vitro* studies have demonstrated that rodent neural stem cells embedded in methacrylated hyaluronic acid (HA) based hydrogels show neuronal differentiation and survival is favored in soft hydrogels (approximately <1 kPa), while astrocytes prefer slightly stiffer gels (<10 kPa) [16,17], which was shown also on 2D peptide-functionalized polyacrylamide (pAAm) hydrogel substrates [16]. In the same context, primary neuronal cells grown on soft ( $G' < 300$  Pa) substrates exhibited increased neurite branching compared to those grown on stiffer ( $G' > 400$  Pa) gels [18]. Oxidized alginate, or alginate di-aldehyde (ADA) based ADA-gelatin (ADA-GEL) hydrogel is a promising biomaterial for tissue engineering (TE) as it offers a wide range of tunable properties such as controlled degradation and hydrogel stiffness [19,20]. It is further possible to tune the stiffness and mechanical properties of alginate-gelatin based hydrogels to mimic the stiffness and characteristics of neuronal tissues like brain (~1 kPa) [21,22]. The key advantage of ADA over pristine alginate is its capability to be functionalized with ligands, preferably proteins, to enhance cytocompatibility and cell attachment [23]. Free aldehyde groups of ADA can form Schiff's bases with available amino groups of proteins. As a result, gelatin can be retained in the hydrogel matrix, which is otherwise prone to fast release and degradation [20]. In addition, a more homogeneous cell growth has been observed in ADA-GEL hydrogels in comparison to alginate-GEL hydrogels, emphasizing the potential of this matrix as a 3D cell culture microenvironment [24]. The protein binding properties of ADA can be utilized to modify the hydrogel with matrix proteins such as laminin [25]. However, such a modification has only been used in combination with oxidized hyaluronic acid and pre-adipocyte/adipocyte delivery application [25,26], not investigating its potential as a 3D matrix for neural applications. While ADA-GEL has shown promising properties for e.g., vascular and bone tissue TE [27–29], the application of ADA-GEL modified with laminin might ideally facilitate the development of neuronal networks due to its softness, degradability and incorporation of native cell adhesion motifs via crosslinking of gelatin and laminin.

The aim of this study was to investigate laminin modified oxidized alginate-gelatin hydrogels (ADA-GEL-LAM) (Figure 1) as a 3D culture system to assess the influence of laminin addition on the differentiation and neuronal outgrowth of embedded hiPSC-derived neurospheres consisting of neural progenitor cells (hiNPC). The mechanical stiffness and microstructure of ADA-GEL-LAM hydrogels are characterized via nanoindentation and scanning electron microscopy techniques, respectively. Immunocytochemistry is used to analyze hiNPC differentiation into neurons in ADA-GEL and ADA-GEL-LAM hydrogels.

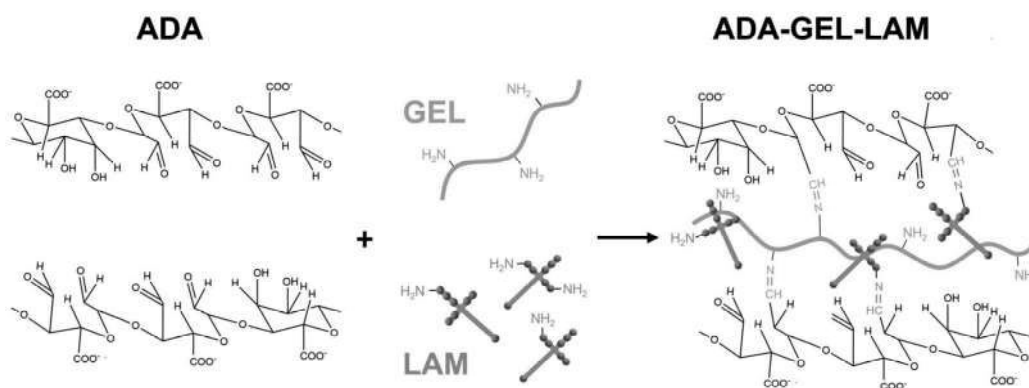


**Figure 1.** Schematic of ADA-GEL-LAM hydrogel. By oxidation of alginate, alginate di-aldehyde (ADA) is formed. The presence of aldehyde groups allows crosslinking with amine groups of proteins (gelatin, laminin) via nucleophilic attack of the amine on the aldehyde.

## 2. Materials and Methods

Sodium alginate (VIVAPHARM PH176 alginate, Ph. Eur.) was purchased from JRS PHARMA GmbH & Co. KG (Rosenberg, Germany). Ethylene glycol ( $\geq 99\%$  purity) was bought from VWR Chemicals International (Radnor, PA, USA). PBS (#L1825/L1835) for cell culture was purchased from Biochrom (Berlin, Germany). Murine sarcoma basement membrane laminin (LAM) was purchased from Sigma (#L2020). All other chemicals were purchased from Sigma Aldrich if not otherwise noted.

### 2.1. Materials Synthesis

Oxidized alginate was synthesized by controlled oxidation of sodium using sodium metaperiodate ( $\text{NaIO}_4$ , ACS reagent,  $\geq 99.8\%$ ) as described earlier [20]. In brief, sodium alginate (10 g) was transferred to equal amounts (100 mL in total) of  $\text{H}_2\text{O}$ :Ethanol (EtOH, absolute, EMSURE<sup>®</sup> ACS reagent,  $\geq 99.9\%$ ) containing 9.375 mmol  $\text{NaIO}_4$ . Oxidation of alginate was carried out for 6 h in the absence of light at room temperature (RT, 22 °C). The reaction was quenched using 10 mL ethylene glycol and stirred for additional 30 min. The dispersion was allowed to sediment for 5 min, the ethanol was decanted, and the ADA was transferred into dialysis tubes (MWCO: 6–8 kDa) and dialyzed for 7 days against ultrapure water (Type II, Merck MilliPore, Darmstadt, Germany). The final product was frozen for a minimum of 24 h and lyophilized using a freeze dryer (Alpha 1-2LD plus, Martin Christ, Osterode am Harz, Germany). The level of oxidation of the final ADA product amounted to  $\sim 19\%$ .

### 2.2. Preparation of Hydrogels

For the preparation of the ADA stock solution, ADA was weighed inside a beaker with a stirring bar. PBS (w/o  $\text{Ca}^{2+}$ / $\text{Mg}^{2+}$ ) was added to create a 5% or 10% (w/v) ADA stock solution. The solutions were stirred at 200 rpm (SU1200 magnetic stirring plate, Sunlab<sup>®</sup> Instruments, Mannheim, Germany) using a magnetic stirring bar at RT (5%) or 40 °C (10%) for  $\sim 3$ –4 h and the pH of the solutions (pH  $\sim 6.51$ ) was adjusted to pH 7.4 using 0.1 M NaOH. The ADA solutions were subsequently filtered with pre-warmed 0.45  $\mu\text{m}$  PVDF filters (37 °C) to allow in vitro cell culture. The ADA was stored at 4 °C until further use.

Gelatin was weighed inside a beaker with a stirring bar already inserted and supplemented with an appropriate volume of PBS (w/o  $\text{Ca}^{2+}$ / $\text{Mg}^{2+}$ ) to create a 5% or 20% (w/v) gelatin stock solution. The gelatin was dissolved by stirring at 200 rpm (SU1200 magnetic stirring plate, Sunlab<sup>®</sup> Instruments, Mannheim, Germany) using a magnetic stirring bar at 40 °C for  $\sim 3$ –4 h and the pH of the solutions (pH  $\sim 6.51$ ) was adjusted to pH 7.4 using 0.1 M NaOH. The gelatin solutions were heated to 50 °C prior to the filtration with pre-warmed

0.45  $\mu\text{m}$  PVDF filters (37 °C) to allow for suitability for in vitro cell culture. The gelatin was stored at 4 °C until further use.

ADA-GEL was prepared by mixing ADA and GEL solutions for 10 min at 37 °C in a volume ratio of ADA:GEL 50:50 to gain ADA-GEL hydrogel precursor solution with a final concentration of 2.5% (*w/v*)/2.5% (*w/v*) ADA-GEL.

ADA-GEL-LAM was prepared by adding 100  $\mu\text{L}$  LAM stock ( $c_{\text{stock}} = 0.1\%$ ) to 250  $\mu\text{L}$  GEL (10% *w/v*) and 150  $\mu\text{L}$  PBS, followed by mixing with 500  $\mu\text{L}$  ADA (5% (*w/v*)) for 10 min at 37 °C. The final hydrogel concentrations were 2.5% (*w/v*)/2.5% (*w/v*)/0.01% ADA-GEL-LAM.

ADA-LAM was prepared similarly by adding 100  $\mu\text{L}$  LAM stock to 400  $\mu\text{L}$  PBS and 500  $\mu\text{L}$  ADA (5% *w/v*), with final concentrations of 2.5% (*w/v*) ADA/0.01% LAM.

Hydrogel specimens were fabricated by casting hydrogel precursor solutions (200  $\mu\text{L}$ ) into custom-made cylindrical PDMS molds (diameter  $d = 10$  mm), allowing the solutions to set at RT for 10 min. Following this, the hydrogels were crosslinked using 0.1 M  $\text{CaCl}_2$  solution for 10 min. Hydrogels were removed from the molds and crosslinked for another 15 min in 0.1 M  $\text{CaCl}_2$  to ensure homogenous crosslinking throughout the hydrogels prior to the material's characterization.

### 2.3. Hydrogel Characterization

To investigate the influence of laminin on hydrogel stiffness, nanoindentation of ADA-GEL and ADA-GEL-LAM hydrogels was performed. The gels ( $n \geq 3$ ) were immersed in Hanks buffered salt solution (HBSS) to avoid dehydration during the measurement and indented directly after immersion as technical triplicates (three indentations each sample) with a cantilever (tip radius: 24.5  $\mu\text{m}$ ; 4.6 N/m; Optics II, HV Amsterdam

Amsterdam, NL using a nanoindentation setup (PIUMA Nanoindenter, Optics II, HV Amsterdam, The Netherlands). Indentation loading curves were recorded and the effective Young's Modulus was calculated using the Oliver & Pharr method [30] implemented in the PIUMA software. The effective Young's Modulus is reported as it accounts for the elastic displacements which occur in the specimen (Young's modulus  $E$ , Poisson's ratio  $\nu$ ) and the indenter tip ( $E_{\text{indenter}}$ ,  $\nu_{\text{indenter}}$ ) [31], while the Poisson's ratio of the hydrogel is unknown. All hydrogel samples were assessed at 22 °C (RT) and 37 °C.

The chemical composition of ADA, ADA-GEL, ADA-GEL-LAM, and ADA-LAM was assessed using attenuated total reflectance-Fourier transformed infrared spectroscopy (ATR-FTIR). Hydrogel samples were frozen and freeze-dried using a lyophilizer (LD12 plus, Martin Christ, Osterode am Harz, Germany). Dry samples were then assessed and attenuated total reflectance spectra were recorded using an infrared spectrometer (Nicolet 6700, Thermo Scientific, Waltham, MA, USA).

The hydrogel's microstructure was assessed using scanning electron microscopy (SEM). Samples were washed with PBS and fixed using 3% glutaraldehyde (#G5882) in PBS, 1 h at RT, and later stored at 4 °C until drying. Dehydration was employed by an ascending ethanol series followed by critical point drying in liquid  $\text{CO}_2$ . Prior to SEM imaging using the FEI-Philips XL30 ESEM FEG, a 12.5 nm palladium/gold (Science Services, Munich, Germany) film was deposited on the insulating surfaces using a Leica EM SCD500 high vacuum sputter coater to avoid sample charging.

### 2.4. Cell Culture and Maintenance

Human induced pluripotent stem cell (hiPSC) culture and neural induction were adapted from a previously published study [32]. In brief, hiPSCs were purchased (iPS(IMR90)-4; WiCell, Madison, WI, USA) and cultivated on Matrigel coated dishes (hESC-qualified matrix, LDEV-free, #354277, Corning, Corning, NY, USA) in mTeSR1 medium (#05850, StemCell Technologies, Cologne, Germany). After pre-incubation with 1  $\mu\text{M}$  ROCK-inhibitor (Y-27632, #1254, Tocris Biosciences, Bristol, UK) in mTeSR1 for 1 h, fragmented colonies were transferred onto a poly(2-hydroxyethyl methacrylate) (#P3932, Merck, Darmstadt, Germany)-coated dish and to neural induction medium (see Supple-

mentary Table S1) supplemented with 1  $\mu\text{M}$  ROCK-inhibitor. The medium was changed three times per week. Upon first medium change, ROCK inhibitor was excluded from the medium. Seven days after the start of the induction, 10 ng/mL recombinant human FGF (#233-FB, R&D Systems, Minneapolis, MN, USA) was added to the culture medium. Upon day 21, formed neurospheres (hiNPC, hiPSC-derived neural progenitor cells) were cultivated in proliferation medium (Supplementary Table S1). HiNPCs were controlled by FACS as already described [32,33]. Spheres were chopped approximately every week to 0.2  $\mu\text{m}$  using a McIlwain Tissue Chopper (Ted Pella, Redding, CA, USA). Cell viability was measured by the ability of cells to reduce resazurin to fluorescent resorufin using the CellTiter-Blue (#G8080, Promega, Madison, WI, USA). The cytotoxicity was verified by measuring the extracellular lactate dehydrogenase (LDH), which is based on the LDH release from dead and apoptotic cells and is indicative for cytotoxicity, using the CytoTox-ONE Homogeneous Membrane Integrity assay (#G7890, both Promega, Madison, WI, USA). All assays were performed in accordance with the manufacturer's instructions. The amount of cells in 2D, indicated in the instructions, was seeded onto laminin-coated surfaces, as well as permeabilized 2D samples, which were prepared using Triton-X to serve as positive and negative controls. A LIVE/DEAD Viability/Cytotoxicity Kit for mammalian cells was used to visualize living and dead cells (#L3224, Invitrogen, ThermoFisher Scientific, Waltham, MA, USA) simultaneously using 0.6  $\mu\text{M}$  Calcein-AM and 0.1  $\mu\text{M}$  EthD-1. Samples were incubated in the dark for approximately 45 min at 37 °C and 5% CO<sub>2</sub> and subsequently analyzed using the Cellomics Array Scan (ThermoFisher, Waltham, MA, USA).

### 2.5. Preparation of Sphere-Laden Hydrogels Subsection

Pre-filtered ADA and GEL solutions were heated to 37 °C prior to hydrogel preparation. GEL (20% (*v/w*)) and laminin (0.1% (*w/v*)) stock solutions were mixed in equal parts to create a GEL-LAM precursor gel (10% gelatin, 0.04% laminin). The pre-warmed ADA (10% (*w/v*)) was added in a 1:1 (*v/v*) ratio to create an ADA-GEL-LAM precursor gel solution (5% ADA, 5% gelatin and 0.02% laminin). The hydrogel solution was stirred for 10 min at 200 rpm (SU1200 magnetic stirring plate, Sunlab<sup>®</sup> Instruments, Mannheim, Germany) and 37 °C using a magnetic stirring bar. The previously prepared cell suspension of  $2 \times 10^4$  spheres/mL (one 0.1 mm sphere equaled approximately  $1 \times 10^3$  cells) was carefully mixed in equal parts with the ADA-GEL-LAM precursor gel, creating a cell-laden hydrogel solution with final concentrations of 2.5% ADA, 2.5% GEL, 0.01% laminin, and  $1 \times 10^7$  cells/mL. The ADA-GEL and ADA-LAM hydrogels were prepared in a similar manner by generating ADA-GEL (5% ADA, 5% GEL) and ADA-LAM (5% ADA, 0.02% laminin) precursor gels from the 5% (*w/v*) ADA and 5% (*w/v*) GEL stock solutions. The hydrogels were allowed to mix for 10 min at 37 °C (200 rpm, SU1200 magnetic stirring plate, Sunlab<sup>®</sup> Instruments, Mannheim, Germany) prior to mixing equal volumes of cell suspension ( $2 \times 10^7$  cells/mL) and hydrogel (1:1 *v/v*) with the hydrogels. The final hydrogels consisted of ADA-GEL (2.5% ADA, 2.5% GEL) and ADA-LAM (2.5% ADA, 0.01% laminin) with a cell density of  $1 \times 10^7$  cells/mL, respectively. Cell-laden hydrogels were crosslinked for 10 min at 37 °C in CaCl<sub>2</sub> solution (90 mM).

### 2.6. Cytocompatibility Study

To investigate the cytocompatibility of ADA-GEL, ADA-GEL-LAM, and ADA-LAM hydrogels for the culture of hiNSC derived neurospheres, the embedded cells were cultured for 7 days inside the hydrogels in differentiation medium (Supplementary Table S1). Cell viability was assessed using a resazurin conversion CellTiter-Blue (#G8080) assay. Cytotoxicity was investigated by LDH release using a CytoTox-ONE Homogeneous Membrane Integrity assay (#G7890, both Promega, Madison, WI, USA) according to the manufacturer's instructions. LIVE/DEAD Viability stainings were performed using 0.6  $\mu\text{M}$  Calcein-AM and 0.1  $\mu\text{M}$  EthD-1 (#L3224, Invitrogen). Samples were incubated for 45 min at 37 °C and 5% CO<sub>2</sub> and analyzed using the Cellomics Array Scan (ThermoFisher). Cells cultured in

2D on LAM-coated substrates as well as ADA-GEL served as positive 2D and 3D controls to LAM-supplemented ADA-GELs.

### 2.7. Immunocytochemistry

Samples were washed with pre-warmed DPBS and fixed with 4% paraformaldehyde (#P6148, Sigma-Aldrich, St. Louis, MO, USA) in DPBS (#14040, ThermoFisher Scientific, Waltham, MA, USA) for 1 h at RT. After fixation, samples were washed three times with DPBS for 10 min. Hydrogel samples were incubated in 10% (*v/v*) goat serum (#G9023)/0.1% (*v/v*) Triton X-100 (#T8787)/PBS, and TUBB3 antibody (1:200, rabbit polyclonal, #T2200, all Sigma-Aldrich, St. Louis, MO, USA), at 4 °C overnight. Specimens were washed three times for 2 h each with DPBS and subsequently incubated with anti-rabbit-Alexa546 (1:500, #A11010, Invitrogen), Phalloidin-Alexa488 (1:70, #A12379, ThermoFisher), and Hoechst (1%, bis-benzimide H33258, #B1155, Sigma) in 2% goat serum/PBS over night at 4 °C. Subsequently, samples were washed three times for 2 h each in PBS at RT and directly imaged by a confocal laser scanning microscope (CLSM, TCS SP8, Leica Microsystems, Wetzlar, Germany) using the objectives HC PL FLUOTAR 5x/0.15 DRY, HC PL APO CS2 10x/0.40 DRY, and HC PL APO CS2 20x/0.75 DRY. Maximum intensity projections of recorded z-stacks were constructed using Fiji Image J 1.52p [34]. ADA-GEL hydrogel served as control to LAM-supplemented ADA-GEL hydrogels.

### 2.8. Statistical Analysis

Data were analyzed using Graphpad Prism<sup>TM</sup> (GraphPad Software Inc., San Diego, CA, USA) and Origin<sup>®</sup>Lab (OriginLab Corporation, Northampton, MA, USA) software. Means  $\pm$  standard deviations (SD) of individual experiments are displayed ( $n \geq 3$  (nanoindentation),  $n = 3$  (cell culture studies)). Statistical analysis was performed by one-way ANOVA (Origin 2019, OriginLab Software, v9.6.0.172), using a post-hoc Bonferroni's pairwise mean comparison between multiple groups. Image analysis was performed using ImageJ (ImageJ Software, <https://imagej.nih.gov/ij/>, accessed on 20 October 2019).

## 3. Results

### 3.1. Material Characterization

By the addition of gelatin and laminin to ADA, FTIR analysis showed the presence of amine I ( $1620\text{ cm}^{-1}$ ) and amine II ( $1546\text{ cm}^{-1}$ ) peaks in ADA-GEL, ADA-GEL-LAM, and ADA-LAM spectra, characteristic for the presence of primary and secondary amine groups of gelatin and laminin protein [20,35] inside the hydrogels (Figure 2A). The peak shift of primary amines I and II (GEL spectrum) from  $1629\text{ cm}^{-1}$  and  $1525\text{ cm}^{-1}$  towards lower ( $1620\text{ cm}^{-1}$ ) and higher ( $1546\text{ cm}^{-1}$ ) wave numbers in ADA-GEL and ADA-GEL-LAM indicate Schiff's base formation of gelatin and laminin with ADA [20]. Peaks at  $\sim 1546\text{ cm}^{-1}$  in ADA-LAM are indicative of the presence of laminin in comparison to the pristine ADA spectrum [35]. Both, ADA-GEL and ADA-GEL-LAM formed hydrogels featuring a microporous microstructure, which was confirmed via SEM analysis (Figure 2B). ADA-GEL and ADA-GEL-LAM present a similar microstructure and porosity (Figure 2B).

Indentation analysis showed that by the addition of laminin to ADA-GEL, the hydrogel stiffness decreased from approximately  $17 \pm 2\text{ kPa}$  to  $12 \pm 2\text{ kPa}$  (Figure 2C). Heating of the samples to 37 °C to mimic cell culture conditions revealed a stiffness reduction of both ADA-GEL and ADA-GEL-LAM hydrogels, by almost 60% (ADA-GEL) and 35% (ADA-GEL-LAM) (Figure 2C), resulting in stiffnesses in the range of  $\sim 5\text{--}7\text{ kPa}$ . The qualitative nanoindentation force-penetration behavior was similar for all hydrogels and independent of laminin addition (Figure 2D), with ADA-GEL-LAM at 37 °C leading to slightly less stiff hydrogels in comparison to ADA-GEL. Statistical analysis indicated no significant differences in mean stiffness of ADA-GEL and ADA-GEL-LAM.

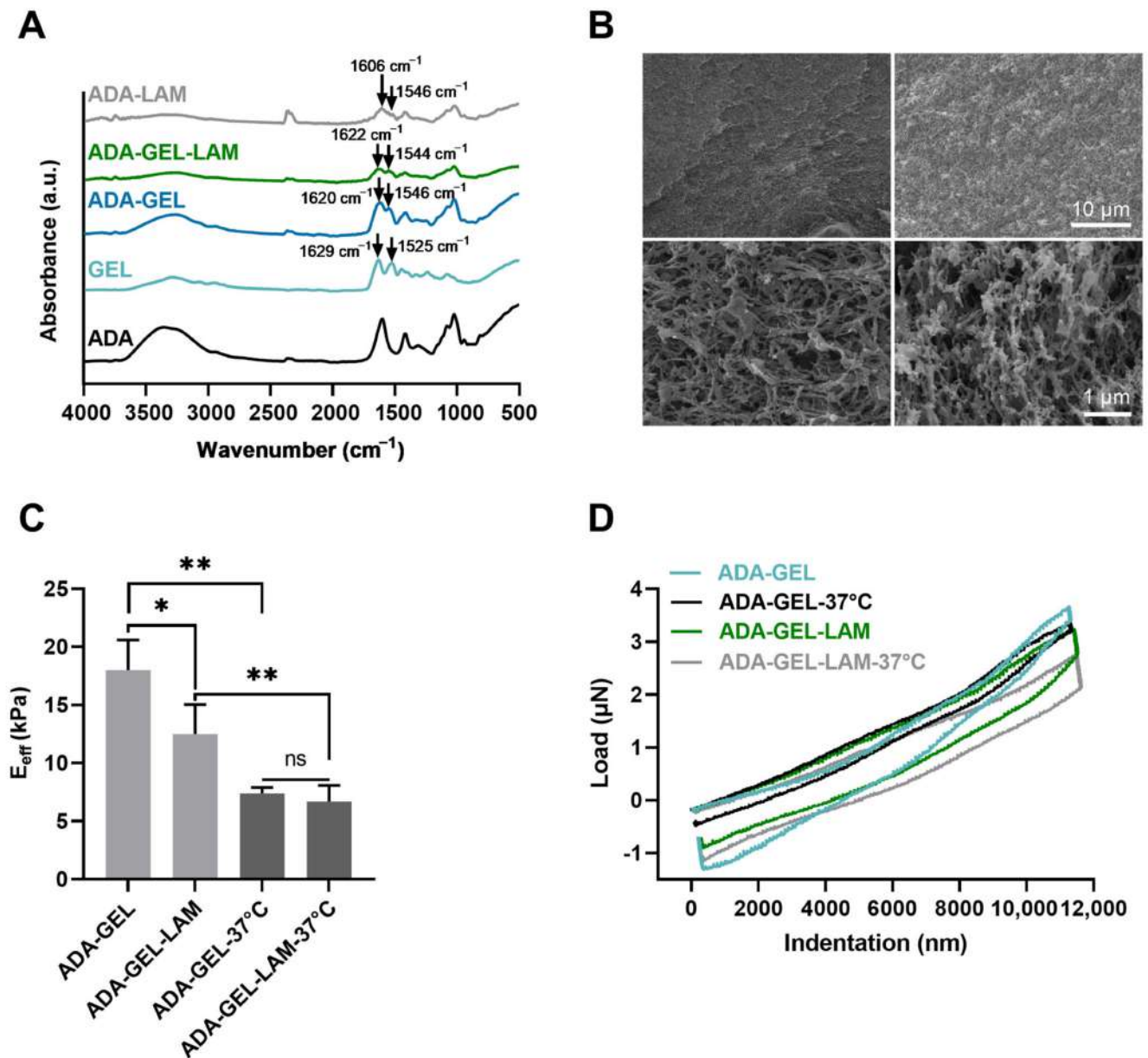


**Figure 2.** Material characterization. (A) Fourier transformed infrared spectroscopy (FTIR) analysis, absorbance spectra of ADA, GEL, ADA-GEL, ADA-GEL-LAM, and ADA-LAM hydrogels. (B) Scanning electron microscopy images of ADA-GEL and ADA-GEL-LAM hydrogels. Both hydrogels feature micro porosity (bottom row). (C) Nanoindentation of ADA-GEL and ADA-GEL-LAM showing the effective Young's modulus ( $E_{\text{eff}}$ ) of the hydrogels at 22 °C and 37 °C. Data are displayed as mean  $\pm$  SD. (D) Qualitative load-indentation behavior of the hydrogels. Statistically significant differences of means analyzed using one-way ANOVA with \*  $p < 0.05$ , \*\*  $p < 0.01$ , not significant (ns,  $p \geq 0.05$ ). Scale bar 1–10  $\mu\text{m}$ .

### 3.2. Cytocompatibility of ADA-GEL-LAM Hydrogels

Neurospheres were generated from hiPSC by neural induction as described earlier [32] and subsequently embedded into ADA-GEL, ADA-GEL-LAM, and ADA-LAM hydrogels after chopping neurospheres to 0.1 mm and mixing with the hydrogel precursor (Figure 3A). Cross-linked cell-laden hydrogels were further incubated in cell-differentiation medium to start neuronal differentiation. In order to assess the compatibility of the hydrogels with the neurospheres, cell viability was measured by resazurin reduction to fluorescent resorufin on days 1, 3, and 7 (Figure 3B).

Fluorescence intensities in all tested ADA-hydrogels was approximately 30% of the 2D control at day one. From the day 1 samples, LDH release as a readout for cytotoxicity was measured (Figure 3C). Cytotoxicity was above 40% of 2D lysis controls in 2D samples, indicating that the cell preparation induces high cell death. In hydrogel samples LDH release was approximately 30% of the 2D lysis controls. Cell viability slightly decreased over the time period of seven days for all tested hydrogels. However, the detected fluorescence was lower for ADA-LAM compared to the other materials (Figure 3B) despite the similar LDH release measured for all conditions (Figure 3C). To visualize the neurospheres in the hydrogels and to investigate the cell viability in situ, LIVE/DEAD fluorescence microscopy analysis was used (Figure 4). One day after hydrogel preparation, few dead (red stained) cells were visible outside of the embedded neurospheres, irrespective of the hydrogel composition. In ADA-GEL-LAM, protrusions from spheres appeared, which were visible in brightfield phase contrast images. At day seven, the observed protrusions or outgrowths of cells had increased. In addition, LIVE staining indicated viable cells in the observed protrusions, indicating cells actively migrating out of the spheres after seven days.

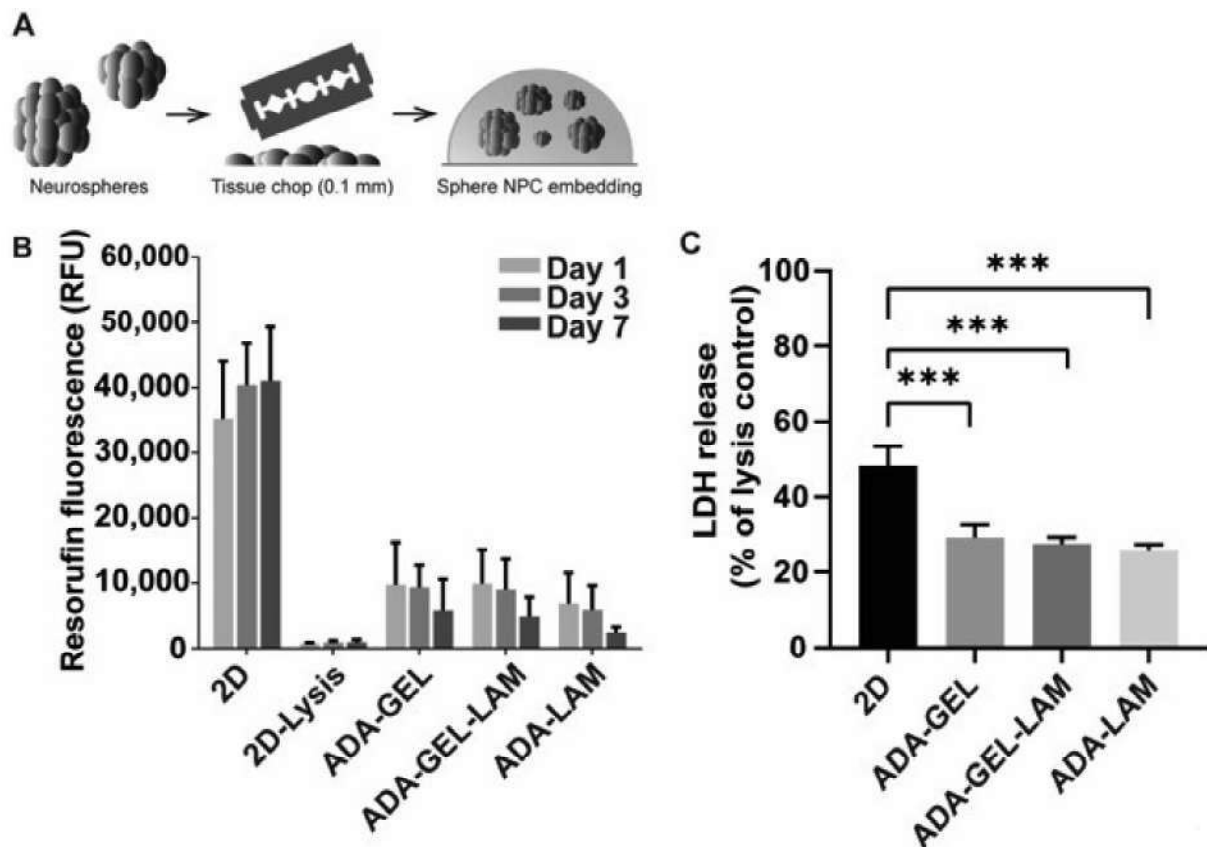


**Figure 3.** Cell viability and toxicity of iPSC-derived NPCs. (A) Cell embedding scheme. Neurospheres were freshly chopped to 0.1 mm, mixed with ADA-GEL-X precursor at a density of 10,000 spheres/mL (corresponds to  $1 \times 10^7$  cells/mL), crosslinked, and maintained in differentiation medium. (B) Viability of neurospheres in the hydrogels measured via resazurin reduction to resorufin. Data shown as relative fluorescence units (RFU). 2D as positive and negative (2D lysis, TritonX-100 treated) controls. (C) Cytotoxicity assessment via LDH release after one day of incubation in differentiation medium, normalized to 2D TritonX-100 treated lysis control ( $n = 3$  with 4 technical replicates; \*\*\*  $p < 0.001$  compared to 2D control).

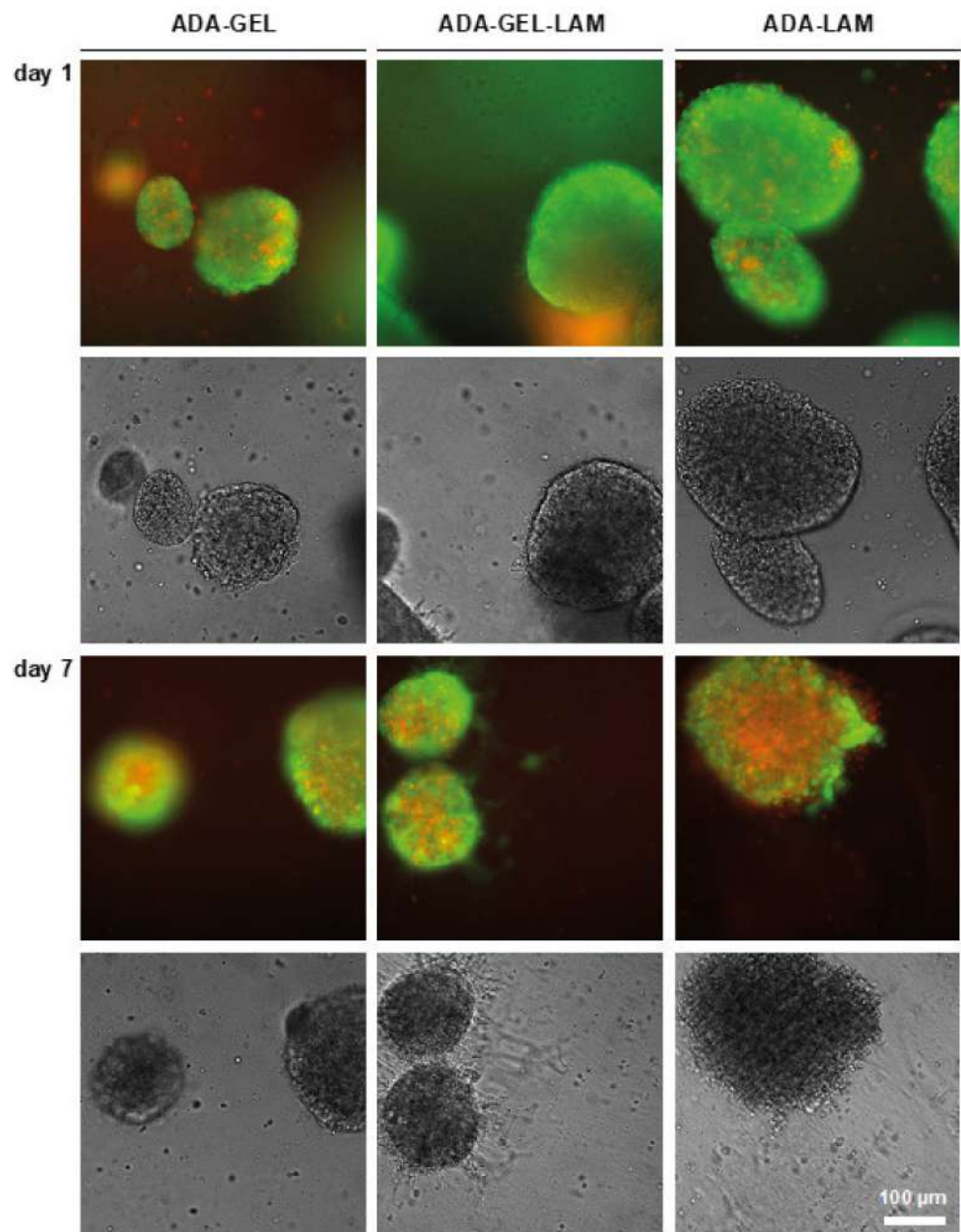


**Figure 4.** LIVE/DEAD staining of neurospheres in ADA-X hydrogels. Neurospheres were embedded in the indicated hydrogels and cultivated in differentiation medium. Samples were stained with Calcein-AM (LIVE, green) and Ethidium-homodimer (DEAD, red) and analyzed by light-microscopy in fluorescence and brightfield mode. Cell outgrowth was indicated in ADA-GEL-LAM (white arrows). Scale bar 100  $\mu\text{m}$ .

In contrast, for ADA-LAM without the presence of gelatin, the core of the neurospheres exhibited a high degree of necrosis, with spheres seeming to disintegrate as indicated by the red EthD-1-stained cells. In phase contrast images, the defined interface between the neurospheres and the bulk hydrogel vanished compared to ADA-GEL or ADA-GEL-LAM hydrogels.

### 3.3. Neurospheres Differentiate into Neurons

Cell differentiation was further monitored after a time period of 14 days using confocal laser scanning fluorescence microscopy. Filamentous (F-)actin as well as the neuronal

marker tubulin- $\beta$ -III (TUBB3) were labeled by phalloidin and specific antibodies, respectively (Figure 5). ADA-LAM showed dispersed spheres with cells appearing necrotic as indicated by cell viability LIVE/DEAD stainings, similar to earlier time points (data not shown). However, neurospheres in ADA-GEL were interconnected via neuronal paths, indicated by TUBB3-positive neurites (Figure 5A, red). Moreover, in laminin-crosslinked ADA-GEL-LAM, the cellular outgrowth of spheres was stronger and omnidirectional (Supplementary Videos S1 and S2), suggesting laminin-supported cell migration (Figure 5A). This observation was quantified by determination of the number of spheres with migrated cells and measurement of the migration distance.

Although migration distance showed no significant difference, laminin presence stimulated cell migration out of the spheres by 2.7-fold (Figure 5B). The results thus suggest that laminin supports cell differentiation and migration.

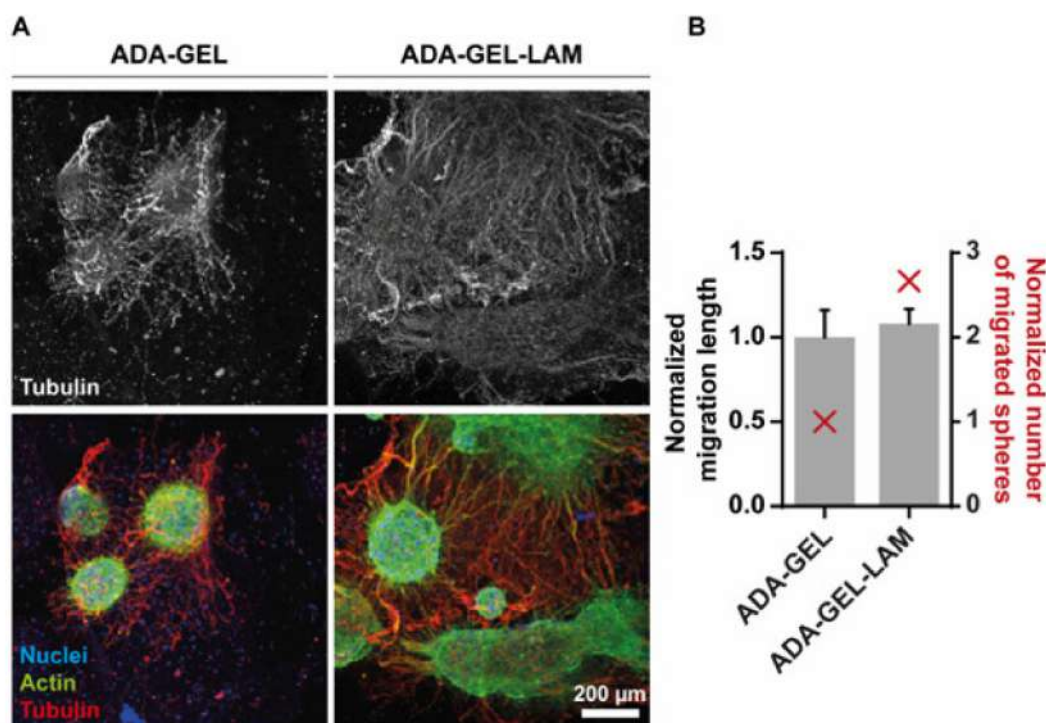


**Figure 5.** Laminin supports neuronal migration out of neurospheres. (A) Confocal fluorescence microscopy of immunostainings for tubulin- $\beta$ -III (red, Alexa546), filamentous actin (green, Phalloidin-Alexa488) and nuclei (blue, Hoechst) after 14 days of gel differentiation. The upper panel displays the tubulin- $\beta$ -III positive neuronal outgrowth only. Representative maximum intensity projections are shown in the lower panel. (B) Quantification of the migration distance (black), measured from the edge of the sphere core to the distal end, normalized to the length of ADA-GEL. Number of spheres showing migration, normalized to ADA-GEL (red). Scale bar 200  $\mu$ m.

#### 4. Discussion

Our work demonstrates for the first time that ADA-GEL hydrogel is cytocompatible with hiPSC-derived neurospheres, opening the possibility of the application of this gel base for 3D tissue modeling. Both neuronal outgrowth and migration in 3D are supported by ADA-GEL hydrogels and are further enhanced in the presence of laminin, resulting in dense neuronal differentiation in 3D. Although different alginate-based hydrogels were previously used for neural applications—including rodent spinal cord, neurite outgrowth activity and cell-matrix-adhesion [36–39]—the application of oxidized alginate-gelatin-laminin hydrogels for central nervous system neuronal differentiation from hiPSC-derived NPC represents a novel approach in the field.

We suggest the following functions of each material inside ADA-GEL-LAM: ADA provides the main 3D hydrogel environment by ionic crosslinking using  $\text{Ca}^{2+}$  ions. GEL

may offer initial cell adhesion motifs for neurosphere attachment, as shown for other cell types in ADA-GEL [20,32,40,41]. The availability of amine groups by GEL facilitates Schiff's base formation with aldehyde groups of ADA, saturating the aldehyde groups in ADA, which is indicated by the higher cell viability inside ADA-GEL-LAM in comparison to ADA-LAM (Figures 3 and 4). ADA and GEL degrade over time [20], providing space for neuron outgrowth. LAM provides integrin binding motifs for hiNPC similar to human neural stem cell (hNSC)-derived neurons [42,43] and PC-12 cell neuron outgrowth [38], thus providing adhesion and guidance for neuron outgrowth in comparison to pristine ADA-GEL (Figure 5). In addition, amine groups of LAM crosslink to aldehyde groups of ADA via Schiff's base formation [25]. The network formation of LAM at 37 °C contributes to the ADA-GEL-LAM hydrogel network supplying an environment for cell adhesion and migration. LAM seems to be the key contributor to the enhanced 3D differentiation of hiNPC's inside the ADA-GEL-LAM hydrogels.

The ECM is capable of influencing cellular differentiation by activating different downstream signaling pathways through interaction with cellular adhesion receptors [44]. Laminin influences cellular attachment and differentiation in multiple native tissue environments [45,46]. It is expressed during the development of the ventricular zone in rodents, which represents the neural stem/precursor cell niche in the developing cortex [43,47,48]. In the early human developing brain, laminin is expressed in the cortex after approximately 17 weeks of gestation [43,49] and was found to be involved in the neuronal differentiation of cultured neural tube neurons [50]. As a result, laminin may represent a key ECM component influencing neural differentiation among other cytokines and stimuli. Laminin also impacts the differentiation of hNSC in vitro [42,51,52] involving the interplay of laminin with different growth factors [52]. An increased number of neurons differentiated from hNSC on laminin-coated substrates, which has been associated to laminin-binding integrins  $\alpha 3$ ,  $\alpha 6$ ,  $\alpha 7$ ,  $\beta 1$ ,  $\beta 4$  found on the surface of hNSCs [43]. Our results on laminin addition to ADA-GEL hydrogels, which increased 3D neuron outgrowth of hiNPC-derived neurospheres, are in accordance with those findings. Laminin peptides, and here especially the IKVAV sequence, also impact neural cell differentiation in vitro [44,51,53], providing a more cost-efficient solution than using the whole laminin protein. IKVAV-functionalized nanofibers were shown to amplify the presence of bioactive IKVAV epitopes in comparison to 2D control substrates [51], while IKVAV increased migration, attachment, and differentiation of hNSC into neurons in polyethyleneglycol (PEG) hydrogels [44] and enhanced neural migration of primary hiNPC in functionalized hydrogels in 3D [53]. In sum, evidence from the literature highlights the interplay of neuronal stem cells by laminin interaction, capable of influencing neuronal differentiation efficiency, neuronal cell adhesion, and migration. We add to this knowledge base by demonstrating the positive impact of laminin for neuronal differentiation and outgrowth in 3D ADA-GEL-LAM hydrogels.

Peak shifts of amine I and amine II peaks in FTIR analysis from  $1525\text{ cm}^{-1}$  to  $\sim 1546\text{ cm}^{-1}$  and  $1629\text{ cm}^{-1}$  to  $1620\text{ cm}^{-1}$  indicate the formation of a Schiff's base (imine bond) [20] in ADA-GEL-LAM and ADA-LAM hydrogels, inducing the crosslinking of laminin and GEL protein components to the ADA polysaccharide. Mechanical assessments showed that the stiffness of ADA-GEL decreased with laminin addition, with a relatively higher decrease in stiffness of ADA-GEL in comparison to ADA-GEL-LAM once incubated at 37 °C (Figure 2). This behavior might be associated to laminin crosslinking at 37 °C, which counteracts the stiffness loss due from the release of excess gelatin and ADA-GEL degradation after incubation [20,27,54]. Previous studies have shown a decrease in hydrogel stiffness with increasing laminin concentration for laminin-conjugated PEG hydrogels [55]. The addition of laminin may lower the initial stiffness of ADA-GEL by sterically hindering the formation of a dense ADA-GEL network. However, the reduction of stiffness can be in favor for neuron growth, due to its higher similarity to brain tissue stiffness ( $<5\text{ kPa}$ ) [21]. An increased neuronal stem cell proliferation and enhancement of neuronal  $\beta$ III-tubulin markers has been shown in soft hydrogels ( $\sim 100\text{ Pa}$ – $1\text{ kPa}$ ) compared to stiffer hydrogels ( $10$ – $20\text{ kPa}$ ) [56]. Due to ADA-GEL degradation [20], a further decrease

in hydrogel stiffness after day 14 can be expected for the ADA-GEL-LAM hydrogels investigated here, which may result in a lower stiffness than measured initially at 37 °C (Figure 2). A decrease in stiffness during incubation may explain the observed differentiation despite initial ADA-GEL-LAM hydrogel stiffness values of >1 kPa. ADA-GEL hydrogels degrade over time by a controlled release of GEL [20]. Therefore, we assume that this process also takes place in ADA-GEL-LAM hydrogels reducing their stiffness during incubation. In addition, hydrogel degradation was shown to be a crucial factor for the maintenance of neuronal progenitor stemness in 3D [57]. As a result, the ADA-GEL-LAM hydrogel stiffness is likely to adapt closer to brain tissue stiffness over incubation time, possibly enabling the observed neuronal migration by hydrogel degradation. The stiffness of 2.5% ADA—2.5% GEL hydrogels at 37 °C were reported to be in the range of 5 kPa [54], which is in accordance with the 2.5% ADA—2.5% GEL—0.01% LAM hydrogels here. Enzymatically crosslinked GEL-LAM hydrogels with a bulk stiffness of ~8.4 kPa (surface elastic modulus:  $24.1 \pm 12.9$  kPa, via AFM) facilitated the growth of hiPSC derived spinal spheroids [58]. While the cells detached on enzymatically crosslinked GEL substrates after two days [58], the combination of GEL and LAM lead to sustained cell attachment and growth [58]. We confirm the increased growth of hiNPC-derived neurospheres in GEL-LAM supplemented ADA in comparison to pure ADA-LAM, which is in accordance with that study. In sum, the ADA-GEL-LAM hydrogels presented here are in an initial stiffness range shown suitable for neuronal cell culture earlier. As the uncertainty of the mechanical properties and degradation of the ADA-GEL-LAM hydrogels over incubation time are one limitation of this study, we will assess the degradation of ADA-GEL-LAM and corresponding effects on the mechanical properties and hiNPC response to the hydrogels in future investigations.

ADA-LAM showed higher cytotoxicity in LIVE/DEAD staining analysis as well as disintegration of neurospheres in phase contrast images compared to ADA-GEL-LAM (Figures 3 and 4). The low laminin concentration (0.01%) might not have yielded complete saturation of aldehyde groups of ADA by Schiff's base crosslinking. Consequently, un-crosslinked aldehyde groups could act as a cytotoxic fixative similar to e.g., formaldehyde [59]. In addition, LAM-peptide AG73 interacts with cell syndecan transmembrane-proteins by ionic interaction of the LAM-peptide with the syndecan's heparansulfate domain [38,60]. The anionic properties of ADA in the ADA-LAM system may counteract the LAM-heparansulfate interaction [38]. In contrast, the cationic properties of Typ A GEL at pH 7.4 (isoelectric point pH ~8–9) in ADA-GEL-LAM may lead to an enhanced LAM-heparansulfate interaction. This may further explain the increased cell survival in ADA-GEL-LAM besides the integrin binding sites offered by GEL [40]. Hence, the ADA-LAM system would require additional engineering to yield hydrogels of LAM concentration and oxidation degree tuned to ensure complete crosslinking of aldehyde groups with LAM. However, the overall lower resorufin adsorption measured in gels compared to 2D cultures without gels is likely not due to lower cell viability, but the result of assay compounds not diffusing into the gels easily. This notion is also supported by the lack of differences between ADA-GEL-LAM and ADA-LAM in this assay (Figure 3). Hence, the CellTiter-Blue assay is not well suited for the viability assessment of neurospheres embedded in hydrogels. Here, LIVE/DEAD stainings are preferred.

The use of hydrogels for neural cell applications, i.e., neuronal tissue regeneration, has been reviewed previously [61], identifying various LAM-modified hydrogels [55,62–64] among other modifications to be promising matrices for the promotion of neurite outgrowth, a process which is necessary for neuronal network formation. Exemplary, hyaluronic acid-laminin hydrogels facilitate *in vivo* migration of neural progenitor/stem cells (NPSC) [65]. Collagen-based hydrogels were modified using LAM or LAM-derived polypeptides, demonstrating that LAM promotes superior neural cell growth and neural differentiation in 3D *in vitro* [66–68]. Laminin- and poly-L-ornithine (PLO)-modified alginate improved axonal growth, neurite outgrowth, and cell adhesion of rat dorsal root ganglia cells (DRG), and increased regenerative capacity and cell-ingrowth in PLO/LAM hydrogel microchannels was observed [36]. Similarly, improved nerve outgrowth of DRG by the use

of laminin-alginate hydrogel capillaries has been reported [37]. Alginate functionalized with three different laminin peptides (A99, AG73, EF1zz) supported neurite outgrowth of rat pheochromocytoma (PC12) cells dependent on alginate and laminin peptide concentrations [38], while not triggering cell adhesion of fibroblasts [39]. Due to the different cells, gels, applications, and types of laminin, it is challenging to derive an overall conclusion from these studies. Yet, the data indicate that laminin in general supports neural cell performance in 3D cultures. In contrast to the present study, previous studies utilized oxidized alginate conjugated specific mouse LAM-based cys-peptides, like A99a, EF1XmRk, and A99T [69], or chitosan [70], instead of GEL and LAM which were used here. The advantages of the ADA-GEL-LAM system presented here are based on its cost-efficiency and ease of production, as it is based on mainly ADA and GEL (2.5%/2.5%) with only a small amount of supplemented LAM (0.01%), which already supported hiPSC-derived dense neuronal differentiation and migration in 3D. This ADA-GEL composition was previously used for 3D bioprinting [19], yet without the addition of laminin. The applicability of ADA-GEL-LAM for the 3D culture of hiPSC-derived neurospheres and the suitability of a 3D printable ADA-GEL based hydrogel composition [19] for the culture of neurospheres provides an exciting ground for future neurosphere-based 3D TE. The results confirm that ADA-GEL-LAM represents a cost-efficient and promising in vitro hydrogel model system to study neuronal cells in 3D, with the potential to create 3D printed in vitro models in future research.

LAM-modified hydrogels seem to be promising for a variety of different biomedical applications besides neural cultures. Exemplary, functionalized alginate wound dressings using laminin-derived peptides promote wound healing [71], oxidized alginate-laminin hydrogels have a potential as autologous fat grafting models [25,26], and ADA-LAM has shown to be a suitable carrier matrix for pre-adipocytes [72]. A selection of laminin peptides was identified to enhance pancreatic islet function in alginate-based microcapsules [73] and LM-111-containing fibrin hydrogels enhanced VEGF production and reduction of IL-6 of C2C12 myoblasts relevant for skeletal muscle engineering [74]. In contrast to these studies [25,26,75] and other ADA-based ADA-LAM systems [36,38,69], we here use a distinct cell type, i.e., hiNPC-derived neurospheres, different laminin, and GEL as an additional hydrogel component. Hence, the ADA-GEL-LAM hydrogels developed in this study might provide a benefit for the development and optimization of various TE applications.

## 5. Conclusions

We demonstrate that adding laminin as an important matrix component to oxidized alginate-gelatin hydrogels can be an effective tool to enhance cell adhesion, migration, and differentiation of embedded iPSC derived neurospheres. ADA-GEL-LAM showed lower cytotoxicity than ADA-LAM, associated to the complete crosslinking of aldehyde groups of ADA with excess amine groups of GEL and to the higher concentration of RGD-sequence containing GEL proteins in the matrix. All hydrogels showed initial stiffness values of approximately 5 kPa close to the relevant range of native brain tissue. Initial neuron out-growth was observed after 7 days in vitro, with higher spatial distribution and neuron migration observed after 14 days for ADA-GEL-LAM in comparison to ADA-GEL. Our study suggests that ADA-GEL-LAM can be a promising and cost-effective 3D hydrogel system for neural cell culture, with the future option for 3D-bioprinting. Finding matrices for building neural cell models in 3D in vitro is crucial in light of TE. Such 3D-models with tissue-like properties are increasingly gaining attention in regenerative medicine, basic research, drug development, and toxicity testing [76]. They should be of human relevance, allow physiological processes, permit application-oriented processing like 3D bioprinting, and be cost-effective. The successful application of ADA-GEL-LAM hydrogels for 3D hiPSC-derived neural culture contributes to this fast developing field of TE by meeting the mentioned criteria to some extent. In future, the application of ADA-GEL-LAM hydrogels

may thus aid in replacing and reducing animal experiments in accordance with the 3R principle [75].

**Supplementary Materials:** The following are available online at <https://www.mdpi.com/2227-9059/9/3/261/s1>, Table S1: Cell culture media compositions utilized for neural induction and differentiation. Video S1: ADA-GEL-LAM (0.01% lam)—day 14. Video S2: 3D\_System\_Neurospheres\_in\_ADA-GEL-LAM.

**Author Contributions:** Conceptualization, T.D., I.L., R.D., A.R.B., E.F.; methodology, T.D., I.L., R.D.; J.K., S.R., A.R.B., E.F.; formal analysis, T.D., I.L., C.M.S., F.B., J.K.; investigation, T.D., C.M.S., J.K., S.R.; resources, A.R.B., E.F.; writing—original draft preparation, T.D., I.L.; writing—review and editing, T.D., I.L., R.D., C.M.S., F.B., J.K., S.R., A.R.B., E.F.; visualization, T.D., I.L., J.K., S.R.; supervision, A.R.B., E.F.; funding acquisition, A.R.B., E.F.; All authors have read and agreed to the published version of the manuscript.

**Funding:** This research received no external funding.

**Institutional Review Board Statement:** Not applicable.

**Informed Consent Statement:** Not applicable.

**Data Availability Statement:** The data presented in this study are available on request from the corresponding authors.

**Acknowledgments:** The CLSM was performed at the Imaging Facility of the Cologne Excellence Cluster of Aging Research (CECAD) with the excellent support of Christian Jüngst. The study was supported by a grant from the Bayer AG.

**Conflicts of Interest:** Authors declare no conflict of interest.

## References

1. Discher, D.E.; Mooney, D.J.; Zandstra, P.W. Growth factors, matrices, and forces combine and control stem cells. *Science* **2009**, *324*, 1673–1677. [CrossRef] [PubMed]
2. Hopkins, A.M.; DeSimone, E.; Chwalek, K.; Kaplan, D.L. 3D in vitro modeling of the central nervous system. *Prog. Neurobiol.* **2015**, *125*, 1–25. [CrossRef] [PubMed]
3. Allison, M. Reinventing clinical trials. *Nat. Biotechnol.* **2012**, *30*, 41–49. [CrossRef]
4. Gribkoff, V.K.; Kaczmarek, L.K. The need for new approaches in CNS drug discovery: Why drugs have failed, and what can be done to improve outcomes. *Neuropharmacology* **2017**, *120*, 11–19. [CrossRef] [PubMed]
5. Langhans, S.A. Three-Dimensional in Vitro Cell Culture Models in Drug Discovery and Drug Repositioning. *Front. Pharmacol.* **2018**, *9*, 6. [CrossRef] [PubMed]
6. D’Aiuto, L.; Naciri, J.; Radio, N.; Tekur, S.; Clayton, D.; Apodaca, G.; Di Maio, R.; Zhi, Y.; Dimitrion, P.; Piazza, P.; et al. Generation of three-dimensional human neuronal cultures: Application to modeling CNS viral infections. *Stem Cell Res. Ther.* **2018**, *9*, 1–9. [CrossRef] [PubMed]
7. Centeno, E.G.Z.; Cimarosti, H.; Bithell, A. 2D versus 3D human induced pluripotent stem cell-derived cultures for neurodegenerative disease modelling. *Mol. Neurodegener.* **2018**, *13*, 1–15. [CrossRef] [PubMed]
8. Elliott, N.T.; Yuan, F. A review of three-dimensional in vitro tissue models for drug discovery and transport studies. *J. Pharm. Sci.* **2011**, *100*, 59–74. [CrossRef]
9. Ko, K.R.; Frampton, J.P. Developments in 3D neural cell culture models: The future of neurotherapeutics testing? *Expert Rev. Neurother.* **2016**, *16*, 739–741. [CrossRef]
10. Quadrato, G.; Brown, J.; Arlotta, P. The promises and challenges of human brain organoids as models of neuropsychiatric disease. *Nat. Med.* **2016**, *22*, 1220–1228. [CrossRef]
11. Huch, M.; Knoblich, J.A.; Lutolf, M.P.; Martinez-Arias, A. The hope and the hype of organoid research. *Development* **2017**, *144*, 938–941. [CrossRef]
12. Ozbolat, I.T.; Hospodiuk, M. Current advances and future perspectives in extrusion-based bioprinting. *Biomaterials* **2016**, *76*, 321–343. [CrossRef]
13. Engler, A.J.; Sen, S.; Sweeney, H.L.; Discher, D.E. Matrix Elasticity Directs Stem Cell Lineage Specification. *Cell* **2006**, *126*, 677–689. [CrossRef] [PubMed]
14. DuFort, C.C.; Paszek, M.J.; Weaver, V.M. Balancing forces: Architectural control of mechanotransduction. *Nat. Rev. Mol. Cell Biol.* **2011**, *12*, 308–319. [CrossRef] [PubMed]
15. Leipzig, N.D.; Shoichet, M.S. The effect of substrate stiffness on adult neural stem cell behavior. *Biomaterials* **2009**, *30*, 6867–6878. [CrossRef] [PubMed]

16. Saha, K.; Keung, A.J.; Irwin, E.F.; Li, Y.; Little, L.; Schaffer, D.V.; Healy, K.E. Substrate Modulus Directs Neural Stem Cell Behavior. *Biophys. J.* **2008**, *95*, 4426–4438. [CrossRef]
17. Seidlits, S.K.; Khaing, Z.Z.; Petersen, R.R.; Nickels, J.D.; Vanscoy, J.E.; Shear, J.B.; Schmidt, C.E. The effects of hyaluronic acid hydrogels with tunable mechanical properties on neural progenitor cell differentiation. *Biomaterials* **2010**, *31*, 3930–3940. [CrossRef]
18. Flanagan, L.A.; Ju, Y.-E.; Marg, B.; Osterfield, M.; Janmey, P.A. Neurite branching on deformable substrates. *Neuroreport* **2002**, *13*, 2411–2415. [CrossRef] [PubMed]
19. Zehnder, T.; Sarker, B.; Boccaccini, A.R.; Detsch, R. Evaluation of an alginate-gelatine crosslinked hydrogel for bioplotting. *Biofabrication* **2015**, *7*, 025001. [CrossRef]
20. Sarker, B.; Papageorgiou, D.G.; Silva, R.; Zehnder, T.; Gul-E-Noor, F.; Bertmer, M.; Kaschta, J.; Chrissafis, K.; Detsch, R.; Boccaccini, A.R. Fabrication of alginate-gelatin crosslinked hydrogel microcapsules and evaluation of the microstructure and physico-chemical properties. *J. Mater. Chem. B* **2014**, *2*, 1470–1482. [CrossRef] [PubMed]
21. Budday, S.; Sommer, G.; Birkl, C.; Langkammer, C.; Haybaeck, J.; Kohnert, J.; Bauer, M.; Paulsen, F.; Steinmann, P.; Kuhl, E.; et al. Mechanical characterization of human brain tissue. *Acta Biomater.* **2017**, *48*, 319–340. [CrossRef] [PubMed]
22. Distler, T.; Schaller, E.; Steinmann, P.; Boccaccini, A.R.; Budday, S. Alginate-based hydrogels show the same complex mechanical behavior as brain tissue. *J. Mech. Behav. Biomed. Mater.* **2020**, *111*, 103979. [CrossRef]
23. Sarker, B.; Singh, R.; Silva, R.; Roether, J.A.; Kaschta, J.; Detsch, R.; Schubert, D.W.; Cicha, I.; Boccaccini, A.R. Evaluation of fibroblasts adhesion and proliferation on alginate-gelatin crosslinked hydrogel. *PLoS ONE* **2014**, *9*, e107952. [CrossRef] [PubMed]
24. Sarker, B.; Rompf, J.; Silva, R.; Lang, N.; Detsch, R.; Kaschta, J.; Fabry, B.; Boccaccini, A.R. Alginate-based hydrogels with improved adhesive properties for cell encapsulation. *Int. J. Biol. Macromol.* **2015**, *78*, 72–78. [CrossRef] [PubMed]
25. Chen, Y.; Chen, Y.; Hsueh, Y.; Tai, H.; Lin, F. Modifying alginate with early embryonic extracellular matrix, laminin, and hyaluronic acid for adipose tissue engineering. *J. Biomed. Mater. Res. Part A* **2015**, 669–677. [CrossRef]
26. Chen, Y.; Chen, Y.H.Y.; Tai, C.L.H.; Lin, F. Evaluation of a laminin-alginate biomaterial, adipocytes, and adipocyte-derived stem cells interaction in animal autologous fat grafting model using 7-Tesla magnetic resonance imaging. *J. Mater. Sci. Mater. Med.* **2017**. [CrossRef]
27. Distler, T.; Ruther, F.; Boccaccini, A.R.; Detsch, R. Development of 3D Biofabricated Cell Laden Hydrogel Vessels and a Low-Cost Desktop Printed Perfusion Chamber for In Vitro Vessel Maturation. *Macromol. Biosci.* **2019**, *19*, 1–13. [CrossRef] [PubMed]
28. Rottensteiner, U.; Sarker, B.; Heusinger, D.; Dafinova, D.; Rath, S.N.; Beier, J.P.; Kneser, U.; Horch, R.E.; Detsch, R.; Boccaccini, A.R.; et al. In vitro and in vivo biocompatibility of alginate dialdehyde/gelatin hydrogels with and without nanoscaled bioactive glass for bone tissue engineering applications. *Materials* **2014**, *7*, 1957–1974. [CrossRef]
29. Reakasame, S.; Boccaccini, A.R. Oxidized Alginate-Based Hydrogels for Tissue Engineering Applications: A Review. *Biomacromolecules* **2018**, *19*, 3–21. [CrossRef] [PubMed]
30. Oliver, W.C.; Pharr, G.M. An improved technique for determining hardness and elastic modulus using load and displacement sensing indentation experiments. *J. Mater. Res.* **1992**, *7*, 1564–1583. [CrossRef]
31. Oliver, W.C.; Pharr, G.M. Measurement of hardness and elastic modulus by instrumented indentation: Advances in understanding and refinements to methodology. *J. Mater. Res.* **2004**, *19*, 3–20. [CrossRef]
32. Hofrichter, M.; Nimtz, L.; Tigges, J.; Kabiri, Y.; Schröter, F.; Royer-Pokora, B.; Hildebrandt, B.; Schmuck, M.; Epanchintsev, A.; Theiss, S.; et al. Comparative performance analysis of human iPSC-derived and primary neural progenitor cells (NPC) grown as neurospheres in vitro. *Stem Cell Res.* **2017**, *25*, 72–82. [CrossRef]
33. Nimtz, L.; Hartmann, J.; Tigges, J.; Masjosthusmann, S.; Schmuck, M.; Keßel, E.; Theiss, S.; Köhrer, K.; Petzsch, P.; Adjaye, J.; et al. Characterization and application of electrically active neuronal networks established from human induced pluripotent stem cell-derived neural progenitor cells for neurotoxicity evaluation. *Stem Cell Res.* **2020**. [CrossRef] [PubMed]
34. Schindelin, J.; Arganda-Carreras, I.; Frise, E.; Kaynig, V.; Longair, M.; Pietzsch, T.; Preibisch, S.; Rueden, C.; Saalfeld, S.; Schmid, B.; et al. Fiji: An open-source platform for biological-image analysis. *Nat. Methods* **2012**, *9*, 676–682. [CrossRef] [PubMed]
35. Neal, R.A.; Tholpady, S.S.; Foley, P.L.; Swami, N.; Ogle, R.C.; Botchwey, E.A. Alignment and composition of laminin-polycaprolactone nanofiber blends enhance peripheral nerve regeneration. *J. Biomed. Mater. Res. Part A* **2012**, *100*, 406–423. [CrossRef] [PubMed]
36. Schackel, T.; Kumar, P.; Günther, M.; Liu, S.; Brunner, M.; Sandner, B.; Puttagunta, R.; Müller, R.; Weidner, N.; Blesch, A. Peptides and Astroglia Improve the Regenerative Capacity of Alginate Gels in the Injured Spinal Cord. *Tissue Eng. Part A* **2019**, *25*, 522–537. [CrossRef]
37. Anderson, A.W.A.; Willenberg, A.R.; Bosak, A.J.; Willenberg, B.J.; Lambert, S. Use of a Capillary Alginate Gel (Capgel™) to Study the Three-Dimensional Development of Sensory Nerves Reveals the Formation of a Rudimentary Perineurium. *J. Neurosci. Methods* **2018**. [CrossRef]
38. Yamada, Y.; Hozumi, K.; Katagiri, F.; Kikkawa, Y.; Nomizu, M. Biological activity of laminin peptide-conjugated alginate and chitosan matrices. *Biopolymers* **2010**, *94*, 711–720. [CrossRef]
39. Hozumi, K.; Nomizu, M. Cell Adhesion Activity of Peptides Conjugated to Polysaccharides. *Curr. Protoc. Cell Biol.* **2018**, *80*. [CrossRef]
40. Grigore, A.; Sarker, B.; Fabry, B.; Boccaccini, A.R.; Detsch, R. Behavior of Encapsulated MG-63 Cells in RGD and Gelatine-Modified Alginate Hydrogels. *Tissue Eng. Part A* **2014**, *20*, 2140–2150. [CrossRef] [PubMed]

41. Distler, T.; Solistio, A.A.; Schneidereit, D.; Friedrich, O.; Detsch, R.; Boccaccini, A.R. 3D printed oxidized alginate-gelatin bioink provides guidance for C2C12 muscle precursor cell orientation and differentiation via shear stress during bioprinting. *Biofabrication* **2020**. [CrossRef]
42. Wu, P.; Tarasenko, Y.I.; Gu, Y.; Huang, L.Y.M.; Coggeshall, R.E.; Yu, Y. Region-specific generation of cholinergic neurons from fetal human neural stem cells grafted in adult rat. *Nat. Neurosci.* **2002**, *5*, 1271–1278. [CrossRef] [PubMed]
43. Flanagan, L.A.; Rebaza, L.M.; Derzic, S.; Schwartz, P.H.; Monuki, E.S. Regulation of human neural precursor cells by laminin and integrins. *J. Neurosci. Res.* **2006**, *83*, 845–856. [CrossRef] [PubMed]
44. Li, X.; Liu, X.; Josey, B.; James Chou, C.; Tan, Y.; Zhang, N.; Wen, X. Short Laminin Peptide for Improved Neural Stem Cell Growth. *Stem Cells Transl. Med.* **2014**, *3*, 662–670. [CrossRef]
45. Tzu, J.; Marinkovich, M.P. Bridging structure with function: Structural, regulatory, and developmental role of laminins. *Int. J. Biochem. Cell Biol.* **2008**, *40*, 199–214. [CrossRef] [PubMed]
46. Paulsson, M. The role of laminin in attachment, growth, and differentiation of cultured cells: A brief review. *Cytotechnology* **1992**, *9*, 99–106. [CrossRef] [PubMed]
47. Georges-Labouesse, E.; Mark, M.; Messaddeq, N.; Gansmüller, A. Essential role of  $\alpha 6$  integrins in cortical and retinal lamination. *Curr. Biol.* **1998**, *8*, 983–986. [CrossRef]
48. Campos, L.S.; Leone, D.P.; Relvas, J.B.; Brakebusch, C.; Fässler, R.; Suter, U.; Ffrench-Constant, C.  $\beta 1$  integrins activate a MAPK signalling pathway in neural stem cells that contributes to their maintenance. *Development* **2004**, *131*, 3433–3444. [CrossRef] [PubMed]
49. Anlar, B.; Atilla, P.; Cakar, A.N.; Kose, M.F.; Beksac, M.S.; Dagdeviren, A.; Akcoren, Z. Expression of Adhesion and Extracellular Matrix Molecules in the Developing Human Brain. *J. Child. Neurol.* **2002**, *17*, 707–713. [CrossRef] [PubMed]
50. Heaton, M.B.; Swanson, D.J. The influence of laminin on the initial differentiation of cultured neural tube neurons. *J. Neurosci. Res.* **1988**, *19*, 212–218. [CrossRef] [PubMed]
51. Silva, G.A.; Czeisler, C.; Niece, K.L.; Beniash, E.; Harrington, D.A.; Kessler, J.A.; Stupp, S.I. Selective Differentiation of Neural Progenitor Cells by High-Epitope Density Nanofibers. *Science* **2004**, *303*, 1352–1355. [CrossRef]
52. Caldwell, M.A.; He, X.; Wilkie, N.; Pollack, S.; Marshall, G.; Wafford, K.A.; Svendsen, C.N. Growth factors regulate the survival and fate of cells derived from human neurospheres. *Nat. Biotechnol.* **2001**, *19*, 475–479. [CrossRef] [PubMed]
53. Hellwig, C.; Barenys, M.; Baumann, J.; Gassmann, K.; Casanellas, L.; Kauer, G.; Fritsche, E. Culture of human neurospheres in 3D scaffolds for developmental neurotoxicity testing. *Toxicol. In Vitro* **2018**, *52*, 106–115. [CrossRef]
54. Zehnder, T.; Boccaccini, A.; Detsch, R. Biofabrication of a co-culture system in an osteoid-like hydrogel matrix. *Biofabrication* **2017**, *9*, 25016. [CrossRef] [PubMed]
55. Marquardt, L.; Willits, R.K. Neurite growth in PEG gels: Effect of mechanical stiffness and laminin concentration. *J. Biomed. Mater. Res. Part. A* **2011**, *98A*, 1–6. [CrossRef]
56. Banerjee, A.; Arha, M.; Choudhary, S.S.; Ashton, R.R.; Bhatia, S.V.; Schaffer, D.S.; Kane, R. The Influence of Hydrogel Modulus on the Proliferation and Differentiation of Encapsulated Neural Stem Cells. *Biomaterials* **2009**, *30*, 4695–4699. [CrossRef] [PubMed]
57. Madl, C.M.; Lesavage, B.L.; Dewi, R.E.; Dinh, C.B.; Stowers, R.S.; Khariton, M.; Lampe, K.J.; Nguyen, D.; Chaudhuri, O.; Enejder, A.; et al. Maintenance of neural progenitor cell stemness in 3D hydrogels requires matrix remodelling. *Nat. Mater.* **2017**, *16*, 1233–1242. [CrossRef]
58. Besser, R.R.; Bowles, A.C.; Alassaf, A.; Carbonero, D.; Claire, I.; Jones, E.; Reda, J.; Wubker, L.; Batchelor, W.; Ziebarth, N.; et al. Enzymatically crosslinked gelatin–laminin hydrogels for applications in neuromuscular tissue engineering. *Biomater. Sci.* **2020**, *8*. [CrossRef] [PubMed]
59. Lopachin, R.M.; Gavin, T. Molecular Mechanisms of Aldehyde Toxicity: A Chemical Perspective. *Chem. Res. Toxicol.* **2014**, *27*, 1081–1091. [CrossRef] [PubMed]
60. Hozumi, K.; Ishikawa, M.; Hayashi, T.; Yamada, Y.; Katagiri, F.; Kikkawa, Y.; Nomizu, M. Identification of cell adhesive sequences in the N-terminal region of the laminin  $\alpha 2$  chain. *J. Biol. Chem.* **2012**, *287*, 25111–25122. [CrossRef]
61. Kornev, V.A.; Grebenik, E.A.; Solovieva, A.B.; Dmitriev, R.I.; Timashev, P.S. Hydrogel-assisted neuroregeneration approaches towards brain injury therapy: A state-of-the-art review. *Comput. Struct. Biotechnol. J.* **2018**, *16*, 488–502. [CrossRef]
62. Deister, C.; Aljabari, S.; Schmidt, C.E. Journal of Biomaterials Science, Effects of collagen 1, fibronectin, laminin and hyaluronic acid concentration in multi-component gels on neurite extension. *J. Biomater. Sci. Polym. Ed.* **2012**, *37*–41. [CrossRef]
63. Barros, D.; Conde-sousa, E.; Gonçalves, A.M.; Han, W.M.; García, A.J.; Amaral, I.F.; Pêgo, A.P. Biomaterials Science as 3D neural stem cell culture systems. *Biomater. Sci.* **2019**, *7*, 5338–5349. [CrossRef] [PubMed]
64. Francisco, A.T.; Mancino, R.J.; Bowles, R.D.; Brunger, J.M.; Tainter, D.M.; Chen, Y.; Richardson, W.J.; Guilak, F.; Setton, L.A. Biomaterials Injectable laminin-functionalized hydrogel for nucleus pulposus regeneration. *Biomaterials* **2013**, *34*, 7381–7388. [CrossRef] [PubMed]
65. Addington, C.; Dharmaway, S.; Heffernan, J.; Sirianni, R.; Stabenfeldt, S. Hyaluronic acid-laminin hydrogels increase neural stem cell transplant retention and migratory response to SDF-1 $\alpha$ . *Matrix Biol.* **2018**, 206–216. [CrossRef] [PubMed]
66. Nakaji-hirabayashi, T.; Kato, K.; Iwata, H. In Vivo Study on the Survival of Neural Stem Cells Transplanted into the Rat Brain with a Collagen Hydrogel That Incorporates Laminin-Derived Polypeptides. *Bioconjug. Chem.* **2013**, *24*, 1798–1804. [CrossRef] [PubMed]

67. Hoffman-kim, D.; Swindle-reilly, K.E.; Papke, J.B.; Kutosky, H.P.; Willits, R.K. The impact of laminin on 3D neurite extension in collagen gels. *J. Neural Eng.* **2012**, *9*, 046007. [CrossRef]
68. Yao, L.; Damodaran, G.; Nikolskaya, N.; Gorman, A.M.; Windebank, A.; Pandit, A. The effect of laminin peptide gradient in enzymatically cross-linked collagen scaffolds on neurite growth. *J. Biomed. Mater. Res. Part A* **2009**, *92*, 484–492. [CrossRef]
69. Fujimori, C.; Kumai, J.; Nakamura, K.; Gu, Y. Biological activity of peptide-conjugated polyion complex matrices consisting of alginate and chitosan. *Pept. Sci.* **2017**, 1–10. [CrossRef] [PubMed]
70. Wei, Z.; Zhao, J.; Chen, Y.M.; Zhang, P.; Zhang, Q. Self-healing polysaccharide-based hydrogels as injectable carriers for neural stem cells. *Sci. Rep.* **2016**, *6*, 1–12. [CrossRef]
71. Hashimoto, T.; Suzuki, Y.; Tanihara, M.; Kakimaru, Y. Development of alginate wound dressings linked with hybrid peptides derived from laminin and elastin. *Biomaterials* **2004**, *25*, 1407–1414. [CrossRef] [PubMed]
72. Hsueh, Y.S.; Chen, Y.S.; Tai, H.C.; Mestak, O.; Chao, S.C.; Chen, Y.Y.; Shih, Y.; Lin, J.F.; Shieh, M.J.; Lin, F.H. Laminin-Alginate Beads as Preadipocyte Carriers to Enhance Adipogenesis in Vitro and in Vivo. *Tissue Eng. Part A* **2017**, *23*, 185–194. [CrossRef] [PubMed]
73. Llacua, A.; De Haan, B.J.; Smink, A.M.; Vos, P. De Extracellular matrix components supporting human islet function in alginate-based immunoprotective microcapsules for treatment of diabetes. *J. Biomed. Mater. Res. Part A* **2016**, 1788–1796. [CrossRef]
74. Marcinczyk, M.; Elmashady, H.; Talovic, M.; Dunn, A. Laminin-111 enriched fibrin hydrogels for skeletal muscle regeneration. *Biomaterials* **2017**, *141*, 233–242. [CrossRef] [PubMed]
75. Russell, W.M.S.; Burch, R.L. *The Principles of Humane Experimental Technique*; Methuen: London, UK, 1959; ISBN 0900767782.
76. Fritsche, E.; Haarmann-Stemann, T.; Kapr, J.; Galanjuk, S.; Hartmann, J.; Mertens, P.R.; Kämpfer, A.A.M.; Schins, R.P.F.; Tigges, J.; Koch, K. Stem Cells for Next Level Toxicity Testing in the 21st Century. *Small* **2020**, 2006252. [CrossRef] [PubMed]

## 2.4 Human Induced Pluripotent Stem Cell-Derived Neural Progenitor Cells Produce Distinct Neural 3D In Vitro Models Depending on Alginate/Gellan Gum/Laminin Hydrogel Blend Properties

*Julia Kapr, Laura Petersilie, Thomas Distler, Ines Lauria, Farina Bendt, Clemens M. Sauter, Aldo R. Boccaccini, Christine R. Rose, Ellen Fritsche*

Stable and predictive neural cell culture models are a necessary premise for many research fields. However, conventional 2D models lack 3D cell-material/-cell interactions and hence do not reflect the complexity of the in vivo situation properly. Here two alginate/gellan gum/laminin (ALG/GG/LAM) hydrogel blends are presented for the fabrication of human induced pluripotent stem cell (hiPSC)-based 3D neural models. For hydrogel embedding, hiPSC-derived neural progenitor cells (hiNPCs) are used either directly or after 3D neural pre-differentiation. It is shown that stiffness and stress relaxation of the gel blends, as well as the cell differentiation strategy influence 3D model development. The embedded hiNPCs differentiate into neurons and astrocytes within the gel blends and display spontaneous intracellular calcium signals. Two fit-for-purpose models valuable for i) applications requiring a high degree of complexity, but less throughput, such as disease modeling and long-term exposure studies and ii) higher throughput applications, such as acute exposures or substance screenings are proposed. Due to their wide range of applications, adjustability, and printing capabilities, the ALG/GG/LAM based 3D neural models are of great potential for 3D neural modeling in the future.

Journal:	Advanced Healthcare Materials
Impact factor:	11.092 (2023)
Contribution to the publication:	75%
	Experiments for Figures 1-5, Lead Writing and Editing
Type of authorship:	First Author
Status of publication:	Published (01 July 2021)

# Human Induced Pluripotent Stem Cell-Derived Neural Progenitor Cells Produce Distinct Neural 3D In Vitro Models Depending on Alginate/Gellan Gum/Laminin Hydrogel Blend Properties

Julia Kapr, Laura Petersilie, Thomas Distler, Ines Lauria, Farina Bendt, Clemens M. Sauter, Aldo R. Boccaccini, Christine R. Rose, and Ellen Fritsche\*

Stable and predictive neural cell culture models are a necessary premise for many research fields. However, conventional 2D models lack 3D cell-material/-cell interactions and hence do not reflect the complexity of the in vivo situation properly. Here two alginate/gellan gum/laminin (ALG/GG/LAM) hydrogel blends are presented for the fabrication of human induced pluripotent stem cell (hiPSC)-based 3D neural models. For hydrogel embedding, hiPSC-derived neural progenitor cells (hiNPCs) are used either directly or after 3D neural pre-differentiation. It is shown that stiffness and stress relaxation of the gel blends, as well as the cell differentiation strategy influence 3D model development. The embedded hiNPCs differentiate into neurons and astrocytes within the gel blends and display spontaneous intracellular calcium signals. Two fit-for-purpose models valuable for i) applications requiring a high degree of complexity, but less throughput, such as disease modeling and long-term exposure studies and ii) higher throughput applications, such as acute exposures or substance screenings are proposed. Due to their wide range of applications, adjustability, and printing capabilities, the ALG/GG/LAM based 3D neural models are of great potential for 3D neural modeling in the future.

cell-matrix interactions, plays a crucial role for its proper development and function.<sup>[1]</sup> Given that such interactions are largely absent in 2D cell cultures, the frequent failure in translating in vitro findings into in vivo applications is inevitable.<sup>[2-5]</sup> The generation of stable and predictive neural cell culture models is central for many fields dealing with, for example, toxicological evaluation, disease modeling, drug development, and regenerative medicine. Therefore, there is a need for more sophisticated models that better mimic the physiology of the human brain.

Substantial efforts have been made to add the third dimension to standard 2D cell cultures. Starting from the beginning of this century, several approaches for the generation of 3D neural models such as neurospheres and hydrogel scaffolds were developed.<sup>[6]</sup> Essentially, 3D structure can be achieved by harnessing the self-organization properties of cells, for example, to drive the formation of

## 1. Introduction

The human central nervous system (CNS) consists of a complex cellular network in which the microenvironment, like spatiotemporal exposure to signaling molecules and cell-cell and

neurospheres, or by providing support and structure for cells with hydrogel scaffolds in an engineering-based manner. Neurospheres are cell aggregates that consist of neural progenitor cells (NPCs) and are cultivated in the presence of growth factors. In the absence of growth factors and when seeded

J. Kapr, Dr. I. Lauria, F. Bendt, C. M. Sauter, Prof. E. Fritsche  
IUF – Leibniz Research Institute for Environmental Medicine  
Düsseldorf 40225, Germany  
E-mail: Ellen.Fritsche@iuf-duesseldorf.de

L. Petersilie, Prof. C. R. Rose  
Institute of Neurobiology  
Heinrich Heine University  
Düsseldorf 40225, Germany  
T. Distler, Prof. A. R. Boccaccini  
Institute of Biomaterials  
Department of Materials Science and Engineering  
Friedrich-Alexander-University Erlangen-Nuremberg  
Erlangen 91054, Germany  
Prof. E. Fritsche  
Medical Faculty  
Heinrich Heine University  
Düsseldorf 40225, Germany

 The ORCID identification number(s) for the author(s) of this article can be found under <https://doi.org/10.1002/adhm.202100131>

© 2021 The Authors. Advanced Healthcare Materials published by Wiley-VCH GmbH. This is an open access article under the terms of the Creative Commons Attribution-NonCommercial-NoDerivs License, which permits use and distribution in any medium, provided the original work is properly cited, the use is non-commercial and no modifications or adaptations are made.

DOI: 10.1002/adhm.202100131

on 2D poly-D-lysine/laminin (PDL/LAM)-coated surfaces, NPC neurospheres migrate and differentiate into neurons, astrocytes, and oligodendrocytes, thereby generating complex networks.<sup>[7–13]</sup> The dimension of such neurospheres when plated for migration and differentiation is called “secondary 3D.”<sup>[14]</sup> NPCs generated from induced pluripotent stem cells (iPSCs), iNPCs, have been previously employed in neurotoxicity testing and modeling of Alzheimer’s and Parkinson’s disease.<sup>[13,15–20]</sup> These secondary 3D models were developed to improve the classical 2D-monolayer neuronal cultures.<sup>[21,22]</sup> However, plated neurospheres do not form a 3D network on 2D substrates. Engineered 3D biomaterial models such as hydrogel scaffolds complement the existing cell models by providing an adaptable, controlled, and consistent extracellular environment.<sup>[23]</sup> 3D models augment the complexity of conventional cell cultures, thus rendering them more predictive and physiologically relevant.<sup>[6,14]</sup> However, variability and reproducibility in these systems are still challenging, often due to the nature of the materials. Batch-to-batch variations in, for example, matrigel or limited cell-material interaction in synthetic gels play important roles.<sup>[24,25]</sup>

The interest in hydrogels has increased largely since their discovery in 1960.<sup>[26]</sup> These 3D matrices consist of hydrophilic polymers that hold large quantities of water. Due to this high water content (>90%), these gels can exhibit tissue-like properties.<sup>[27]</sup> Hydrogels maintain their structure by chemical, physical, or biochemical crosslinking of the polymer chains.<sup>[28]</sup> Ideally, extracellular matrix (ECM)-mimicking hydrogels should support cell survival, growth, differentiation, cell-cell, and cell-matrix adhesion, as well as facilitate proper nutrient flux.<sup>[29,30]</sup> In order to allow cellular outgrowth, a certain degree of hydrogel-degradation is desirable. The material stiffness also plays an important role for the generation of neural models. With a Young’s elastic modulus of 0.5 to 50 kPa, the brain is one of the softest tissues in the human body.<sup>[31,32]</sup> As an example, natural polymers such as alginate (ALG) and gellan gum (GG) are inherently suitable surrogates for ECM, due to their high water content and tunable stiffness, as well as their chemical versatility and biocompatibility.<sup>[33–37]</sup>

ALG is a seaweed-derived marine polysaccharide and one of the most commonly used biomaterials for hydrogel formation. It can be easily gelatinized with divalent cations and is highly biocompatible.<sup>[38]</sup> It is composed of D mannuronic acid (M) and L guluronic acid (G) monosaccharide units and forms hydrogels through crosslinking of the G residues with divalent cations.<sup>[34,39]</sup> GG is a natural extracellular polysaccharide produced by the bacterium *Sphingomonas paucimobilis*, which forms a gel after crosslinking of its double helices with divalent cations such as  $\text{Ca}^{2+}$  or  $\text{Mg}^{2+}$ .<sup>[33]</sup> Although many modifications and blends have been produced from ALG and GG,<sup>[34,40]</sup> no ALG/GG blend has yet been used for the development of 3D neural models. Since ALG and GG gels are biologically inert,<sup>[34,41]</sup> they are often functionalized with native ECM molecules, such as LAM, collagen, or fibronectin.<sup>[1,42–44]</sup> LAM has previously been used to support cell survival, network formation, and functional development of neural cultures *in vitro*.<sup>[1,45]</sup> Moreover, it was reported that ALG-based hydrogels can mimic the complex mechanical properties of brain tissue.<sup>[46]</sup>

The engineering of physiologically relevant structures and the recapitulation of spatiotemporal availability of signaling molecules in neural models is highly challenging. 3D bio-

printing offers a promising tool for the generation of such model systems.<sup>[36]</sup> Cell-supplemented biocompatible materials are printed with micrometric precision and may even combine several cell types, thus generating complex cellular networks. The printing process depends on three main variables: 1) the material (biomaterial ink), 2) the cells and 3) biomechanical factors.<sup>[25,47–49]</sup> Due to their highly tunable rheological properties, hydrogels are suitable for bioprinting applications.<sup>[35,50]</sup> However, neural cells require soft materials and are sensitive to shear stress, which only permits hydrogels with very specific properties.<sup>[51]</sup>

Bioinks based on ALG or GG, yet not in combination, have previously been employed to generate bioprinted and non-bioprinted 3D neural models.<sup>[37,52–55]</sup> Combining suitable gel properties for adequate cell-culture development and functionality, with printability and long-term integrity of the hydrogels remains a challenge. Although both ALG and GG are promising candidates for the generation of 3D neural cultures, they each lack desirable properties. While GG is not surface adherent, ALG deforms severely upon crosslinking. However, ALG appears surface adherent and is stable over long periods of time, which is important for long-term cultivation. The GG is printable in low concentrations and its softness appears favorable for neural cultures. To date, there is no gold standard for the generation of hydrogel-based 3D neural cultures and the full potential of such systems has yet to be exploited.

In this study, we chose ALG and GG for their complementary favorable properties and present two ALG/GG/LAM blends for the generation of functional 3D neural models. We chose the gel blends according to their gel integrity, surface adherence, cell survival, and neural outgrowth. We characterized the hydrogels via Fourier transformed infrared spectroscopy (FTIR), scanning electron microscopy (SEM), mechanical testing, and degradation studies. We additionally show the printability of the gel blends using an extrusion-based 3D bioprinter. Pre-differentiated and non-pre-differentiated hiNPC neurospheres were embedded into both 1.5% ALG/0.5% GG/0.01% LAM and 0.3% ALG/0.8% GG/0.01% LAM hydrogels. The growth and differentiation of these multicellular models into neurons and astrocytes within the gels were assessed via immunocytochemistry (ICC) and the network functionality was verified by intracellular calcium imaging.

## 2. Results

### 2.1. Material Characterization

Reproducibility and close characterization of the cellular microenvironment are important factors in cell culture maintenance and application. Physico-chemical tests are generally used to characterize material properties and to anticipate their behavior and performance under cell culture conditions. Therefore, we characterized the developed hydrogels and used pure ALG and GG as comparative materials. ALG and GG both formed clear and stable hydrogels and blends upon crosslinking with  $\text{CaCl}_2$ . Pure ALG deformed upon crosslinking (Supporting Information), whereas GG and the 0.3% ALG/0.8% GG blend retained their structural integrity. The 1.5% ALG/0.5% GG blend appeared slightly deformed after crosslinking (data not shown). All gels maintained their structure over at least 4 weeks, when

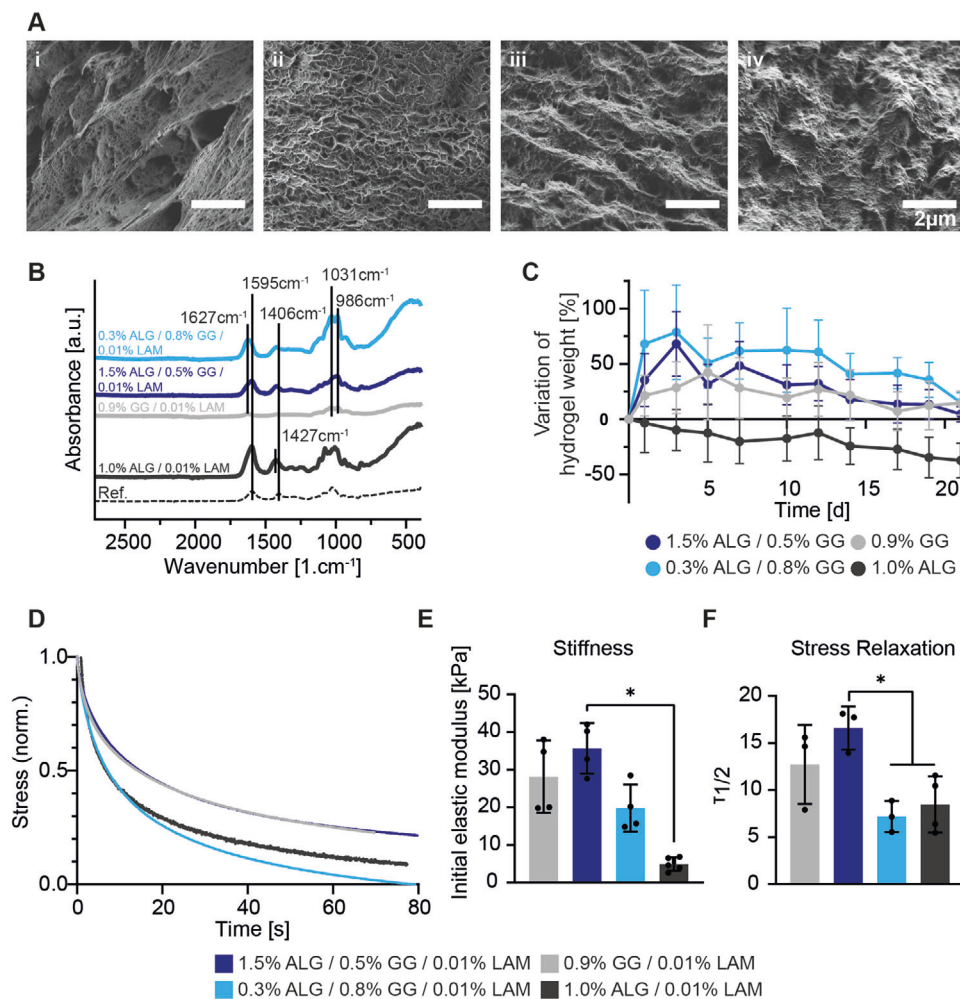


**Figure 1.** Physico-chemico characterization of ALG and GG based hydrogels. A) SEM images of i) 0.9% GG/0.01% LAM, ii) 1.5% ALG/0.5% GG/0.01% LAM, iii) 0.3% ALG/0.8% GG/0.01% LAM, and iv) 1.0% ALG/0.01% LAM hydrogels. B) FTIR analysis of ALG/GG/LAM composite hydrogels. 1.0% ALG serves as reference. C) Hydrogel swelling and degradation of i) 0.9% GG, ii) 1.5% ALG/0.5% GG, iii) 0.3% ALG/0.8% GG, and iv) 1.0% ALG hydrogels assessed for 21 days of incubation in PBS (37 °C;  $N = 7$ ). D) Qualitative stress relaxation behavior of the different hydrogels. E) Initial elastic modulus and F) stress relaxation time as the time after which 50% of the initial stress (at 15% strain) has been dissipated ( $N > 3$ ) of the hydrogels. The legend for (B), (D), (E), and (F) is shown on the bottom. Data are shown as mean  $\pm$  SD. Statistically significant differences among means between the different groups are indicated as  $*p < 0.05$ , analyzed using one-way ANOVA and Bonferroni post-hoc tests. Abbreviations: GG, gellan gum; FTIR, Fourier transformed infrared spectroscopy; SEM, Scanning electron microscopy; Ref., reference.

immersed in CINDA medium. ALG and both hydrogel blends reliably adhered to PDL/LAM-coated plastic and polymer surfaces, as well as to non-coated plastic surfaces, whereas GG is not surface adherent (Supporting Information).

All hydrogels formed microporous microstructures after crosslinking, as shown by SEM (Figure 1A). Peak shifts from 1406 to 1427  $\text{cm}^{-1}$  and 1595 to 1627  $\text{cm}^{-1}$  were indicative for the presence of LAM in all LAM containing samples, corresponding to amine and amide bonds (amide I  $\approx 1621 \text{ cm}^{-1}$ ; Figure 1B).<sup>[56,57]</sup> Peaks of GG at 1031 and 1627  $\text{cm}^{-1}$  corresponding to C—O stretching and COO<sup>-</sup> asymmetric stretching<sup>[58]</sup> confirmed the presence of GG in all GG-containing hydrogel blends, while the peak at 1627  $\text{cm}^{-1}$  cannot be well discerned from the amide I peak expected from LAM. In sum, the FTIR results indicated the successful presence of ALG, GG, and LAM in all respective hydrogel blends.

All GG-containing hydrogels show an initial swelling phase of 3–5 days, followed by water release and degradation (Figure 1C). 1.0% ALG/0.01% LAM lacks the initial swelling phase, but also degrades over time. All hydrogels are stable for at least 21 days under cell culture conditions (Figure 1C). Figure 1D,F displays the qualitative stress relaxation experiments, as well as the quantification of the stress relaxation time ( $t_{1/2}$ ), as the time point after which 50% of the initial stress (at 15% strain) has been dissipated from the hydrogels. All gels showed a fast stress relaxation ( $t_{1/2} < 20 \text{ s}$ ) with 0.3% ALG/0.8% GG/0.01% LAM having the shortest ( $\approx 7 \text{ s}$ ) and 1.5% ALG/0.5% GG/0.01% LAM having the longest ( $\approx 16 \text{ s}$ ) stress relaxation time (Figure 1D,F). The addition of 0.3% ALG to 0.8% GG and 0.01% LAM accelerated stress relaxation in comparison to pure 0.9% GG hydrogels, while the reduction of ALG content from 1.5% to 0.3% significantly ( $*p < 0.05$ ) reduced stress relaxation time of the hydrogels (Figure 1D,F).

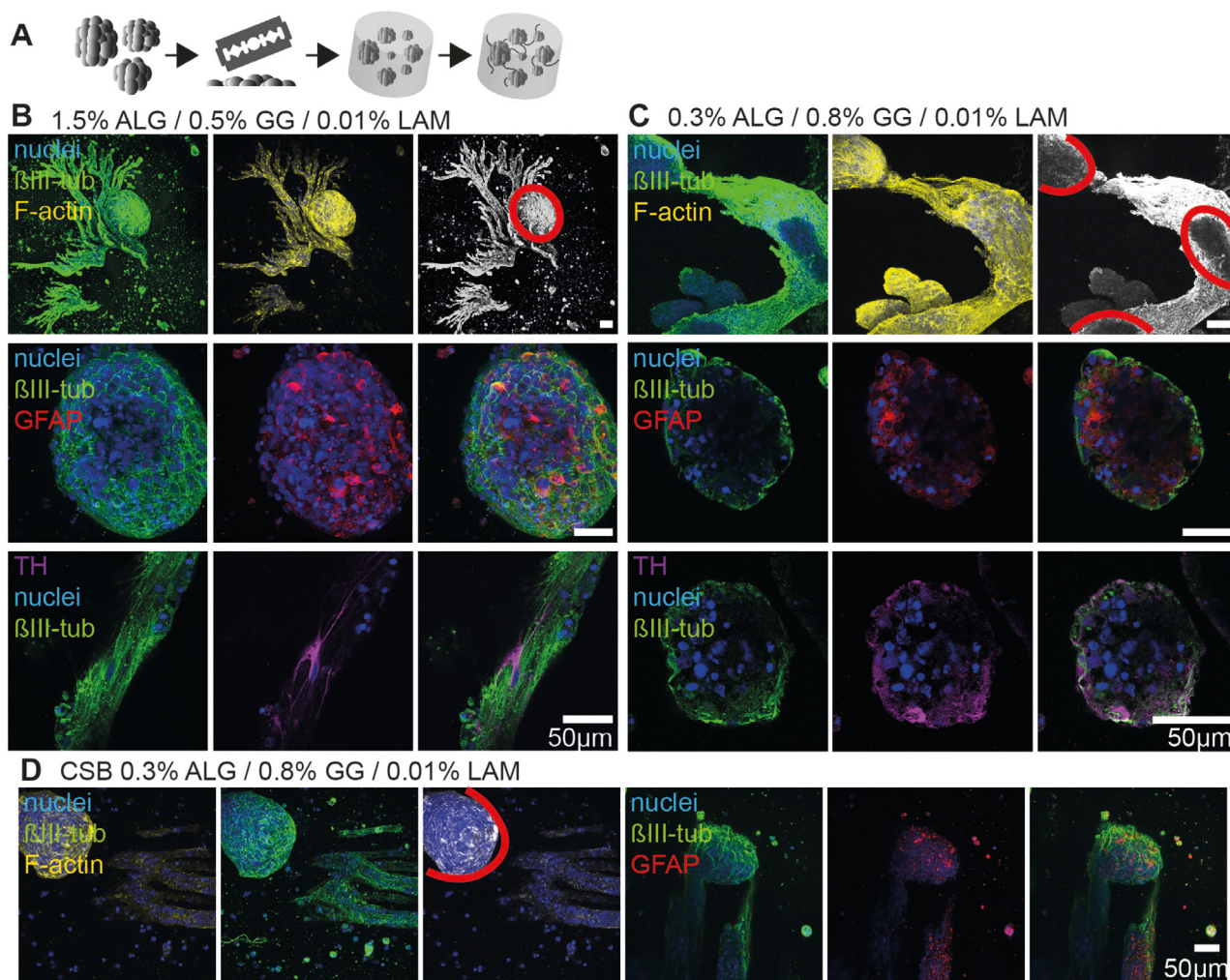


**Figure 2.** hiNPC differentiation in 1.5% ALG/0.5% GG/0.01% LAM and 0.3% ALG/0.8% GG/0.01% LAM gels. A) Proliferating hiNPC spheres were chopped (0.1 mm) and embedded into the respective gel ( $4.9 \times 10^3$  spheres  $\text{mL}^{-1}$  gel). The gels were then cultivated in differentiation medium for 21 days and subsequently stained. Confocal images of differentiated spheres in B) 1.5% ALG/0.5% GG/0.01% LAM or C) 0.3% ALG/0.8% GG/0.01% LAM gels are shown. The samples were stained for nuclei (Hoechst, blue),  $\beta$ III tubulin (Alexa 546, green), F-actin (phalloidin, Alexa 488, yellow or grey), dopaminergic neurons (TH, Alexa 546, magenta) and astrocytes (GFAP, Alexa 647, red). Images of the neural network formation are depicted in the upper row far right of (B) and (C). Differentiation into multiple cell types within the gels is shown in the lower two rows of (B) and (C). D) Proliferating 0.3 mm iNPC spheres generated from a disease cell line derived from a patient with Cockayne syndrome B (CSB), were embedded and differentiated as described above. The gels were subsequently stained for nuclei (Hoechst, blue),  $\beta$ III tubulin (Alexa 546), F-actin (phalloidin, Alexa 488, yellow or grey), and astrocytes (GFAP, Alexa 647, red). Left to right: F-actin,  $\beta$ III tubulin, F-actin incl. network formation,  $\beta$ III tubulin, GFAP,  $\beta$ III-GFAP merge. The red circles show the approximate size and location of the originally embedded spheres. Images represent sections through spheres in varying depths or maximum intensity projections of Z-stacks. Abbreviations: GG, gellan gum; hiNPCs, human induced pluripotent stem cell-derived neural progenitor cells.

Figure 1E indicates the gel stiffness between the different conditions, derived from uniaxial compression test.<sup>[59]</sup> The initial elastic modulus of the hydrogels revealed 1.5% ALG/0.5% GG/0.01% LAM as the stiffest ( $\approx 35$  kPa) and 1.0% ALG/0.01% LAM as the softest ( $\approx 5$  kPa) hydrogel, while 0.3% ALG/0.8% GG/0.01% LAM hydrogels showed a lower stiffness in comparison to the 1.5% ALG/0.5% GG/0.01% LAM composition ( $\approx 20$  kPa; Figure 1E).

We showed that the developed hydrogel blends are structurally stable and surface adherent, which is beneficial for long-term cultivations. Furthermore, all three components are contained within the crosslinked hydrogels, thereby excluding initial washout of ALG, GG, or LAM. The gel blends degrade

slowly over time, which is generally thought of as beneficial for cellular outgrowth and migration. The fast stress relaxation times may additionally support this effect. The elastic moduli of the hydrogel blends lay within the range of brain stiffness.

## 2.2. Long-Term Neural Differentiation

We tested the hydrogel blends for their applicability in long-term cultivation and differentiation of hiNPCs. HiNPC spheres were chopped to 0.1 mm and embedded into 1.5% ALG/0.5% GG/0.01% LAM and 0.3% ALG/0.8% GG/0.01% LAM blends (Figure 2A). Both ALG/GG blends exhibited satisfying cell

compatibility, as indicated by medium to high cell viability in calcein-AM (live) and ethidium-homodimer-1 (dead) double-stainings (LIVE/DEAD; Supporting Information). Spontaneous neural differentiation and the migration pattern of differentiating cells within the gel blends after 21 days were assessed using ICC staining. Migration of differentiating cells out of the sphere core into the surrounding gel matrix was observed in both gel blends (Figure 2B,C). Outgrowth within the gels occurred in thick bundles over the course of 3 weeks and was subsequently assessed by staining for the neuronal epitope  $\beta$ (III)-tubulin and the cytoskeletal marker F-actin. A more detailed characterization of the differentiation pattern revealed differentiation into neurons ( $\beta$ III-tubulin<sup>+</sup>), dopaminergic neurons (TH<sup>+</sup>), and astrocytes (GFAP<sup>+</sup>) in both hydrogel blends, as shown in Figure 2B,C.

Additionally, a disease cell line of a Cockayne Syndrome B (CSB) patient was cultivated and stained in the same manner as the IMR90 cells, in order to show the suitability of the 0.3% ALG/0.8% GG/0.01% LAM gel blend for disease modeling. We show outgrowth and differentiation of the disease cell line within the respective hydrogel blend.

In a second approach, 0.3 mm hiNPC spheres were allowed to pre-differentiate as floating spheres for 1 week in differentiation medium, before subsequent embedding into 1.5% ALG/0.5% GG/0.01% LAM and 0.3% Alg/0.8% GG/0.01% LAM hydrogels, where they were allowed to differentiate for another 7 days (Figure 3A). ICC stainings reveal a dense F-actin and  $\beta$ III-tubulin network, as well as TH-positive dopaminergic neurons and GFAP-positive astrocytes within the spheres (Figure 3B,C). However, no significant outgrowth or migration of pre-differentiated hiNPC spheres into the surrounding gel matrix was observed.

As a comparison to the second approach, we differentiated 0.3 mm NPC spheres as free-floating culture for 14 days and subsequently stained the spheres (Figure 3D). ICC images show an actin and tubulin network.

With the first approach, non-pre-differentiated NPCs developed into complex multicellular 3D microtissues within the course of 3 weeks. In contrast, pre-differentiated spheres did not extend into the hydrogel, but instead formed multicellular interspherical networks in 3D within 1 week. Here, two fit-for-purpose applications seem to emerge. Long-term cultivations of complex cellular models could be valuable for applications that require a higher degree of physiology, such as disease modeling, while the quick generation of complex models in an easy to handle 3D model could be beneficial for, for example, substance screening.

### 2.3. Calcium Signaling

In order to test the functionality of the neural networks developed in 3D, cellular activity was monitored using calcium imaging. The hiNPCs were embedded in either hydrogel blend and the resulting crosslinked sphere-laden hydrogels were differentiated for 21 days, before they were employed for calcium imaging (Figure 4A). The 1.5% ALG/0.5% GG/0.01% LAM and 0.3% ALG/0.8% GG/0.01% LAM gels exhibited an average frequency of  $\approx 1.5$  signals per 10 min (mean  $\pm$  SEM:  $1.6 \pm 0.2$ ,  $N = 3$ ,  $n = 51$ ,  $n_s = 21$ ; mean  $\pm$  SEM:  $1.5 \pm 0.1$ ,  $N = 4$ ,  $n = 89$ ,  $n_s = 28$ ; Figure 4E), the peak amplitude was 0.9 to 1.5% (mean  $\pm$  SEM:  $0.9 \pm 0.1$ ,  $N = 3$ ,  $n = 51$ ,  $n_a = 34$ ; mean  $\pm$  SEM:  $1.5 \pm 0.3$ ,  $N = 4$ ,  $n =$

89,  $n_a = 41$ ; Figure 4F) and the average length of the signals was  $\approx 100$  s (mean  $\pm$  SEM:  $102.3 \pm 14.6$ ,  $N = 3$ ,  $n = 51$ ,  $n_f = 32$ ; mean  $\pm$  SEM:  $92.1 \pm 10.3$ ,  $N = 4$ ,  $n = 89$ ,  $n_f = 35$ ; Figure 4G).

The 1-week pre-differentiated spheres were also embedded in both hydrogel blends and further differentiated for 7 days. Pre-differentiated spheres in 0.3% ALG/0.8% GG/0.01% LAM gels could not be sliced due to the softness of the gels, precluding calcium imaging. The pre-differentiated spheres in 1.5% ALG/0.5% GG/0.01% LAM gels were sliced and analyzed as described above. Spontaneous calcium signals were measured, with 74% of the cells being active (Figure 4D). The average frequency was  $\approx 3.2$  signals per 10 min (mean  $\pm$  SEM:  $3.2 \pm 0.3$ ,  $N = 3$ ,  $n = 76$ ,  $n_s = 56$ ; Figure 4E), the peak amplitude was  $\approx 4.5\%$  (mean  $\pm$  SEM:  $4.6 \pm 0.4$ ,  $N = 3$ ,  $n = 76$ ,  $n_a = 179$ ; Figure 4F) and the average length of the signal was  $\approx 40$  s (mean  $\pm$  SEM:  $40.1 \pm 3.0$ ,  $N = 3$ ,  $n = 76$ ,  $n_f = 177$ ; Figure 4G). In summary, these results show that in all conditions tested (3/4 models), cells generate spontaneous calcium signals, indicative of physiological activity.

### 2.4. Bioprinting

To evaluate whether the 3D bioprinting technology can be used to print the developed gel blends, we utilized an extrusion-based bioprinter. We intended to directly deposit the hydrogels onto the electrodes of a 24-well multielectrode array (MEA), which could later be used for the electrophysiological measurements of neural 3D networks. A general challenge of the MEA technology is the direct positioning of the cells onto the electrodes, so that electrical activity can be measured. This is especially challenging in 3D, where the cells are potentially far away from the electrodes. Our print pattern was therefore designed as 4 lines, surrounded by a stabilizing square, which lays directly on top of the electrodes. In a preliminary test trial using silicon, this grid was printed with the necessary precision onto 24-well MEAs. However, the mwMEA plates are manufactured with small deviations in the electrode position from plate to plate, resulting in variable position outcomes of the printed structures in relation to the electrodes (Figure 5A). Therefore, printability of the hydrogels was further examined in standard tissue culture 24-well plates. Suitable printing parameters were identified for 0.9% GG and both ALG/GG blends and the grid was successfully printed (Figure 5B, supplementary material). Both printed gel blend structures, but not pure GG structures were surface adherent. Pure ALG was not printable. As a proof of principle, we then embedded iPSC-derived single cell NPCs into the 1.5% ALG/0.5% GG/0.01% LAM gel blend, bioprinted them in the same manner as the cell-free gels and crosslinked the gels after printing. The cell-laden gels were then cultivated under differentiation conditions for 3 days and subsequently stained for live and dead cells (Figure 5C). The stainings show  $\approx 62\%$  live cells within the gels. We conclude, that the developed hydrogel blends are suitable for bioprinting applications, even for small scale structures.

## 3. Discussion and Conclusion

The establishment of complex and robust neural in vitro models and reliable cultivation systems that reflect human physiology becomes increasingly important. Gaining a deeper understanding of cell and tissue function in health and disease will

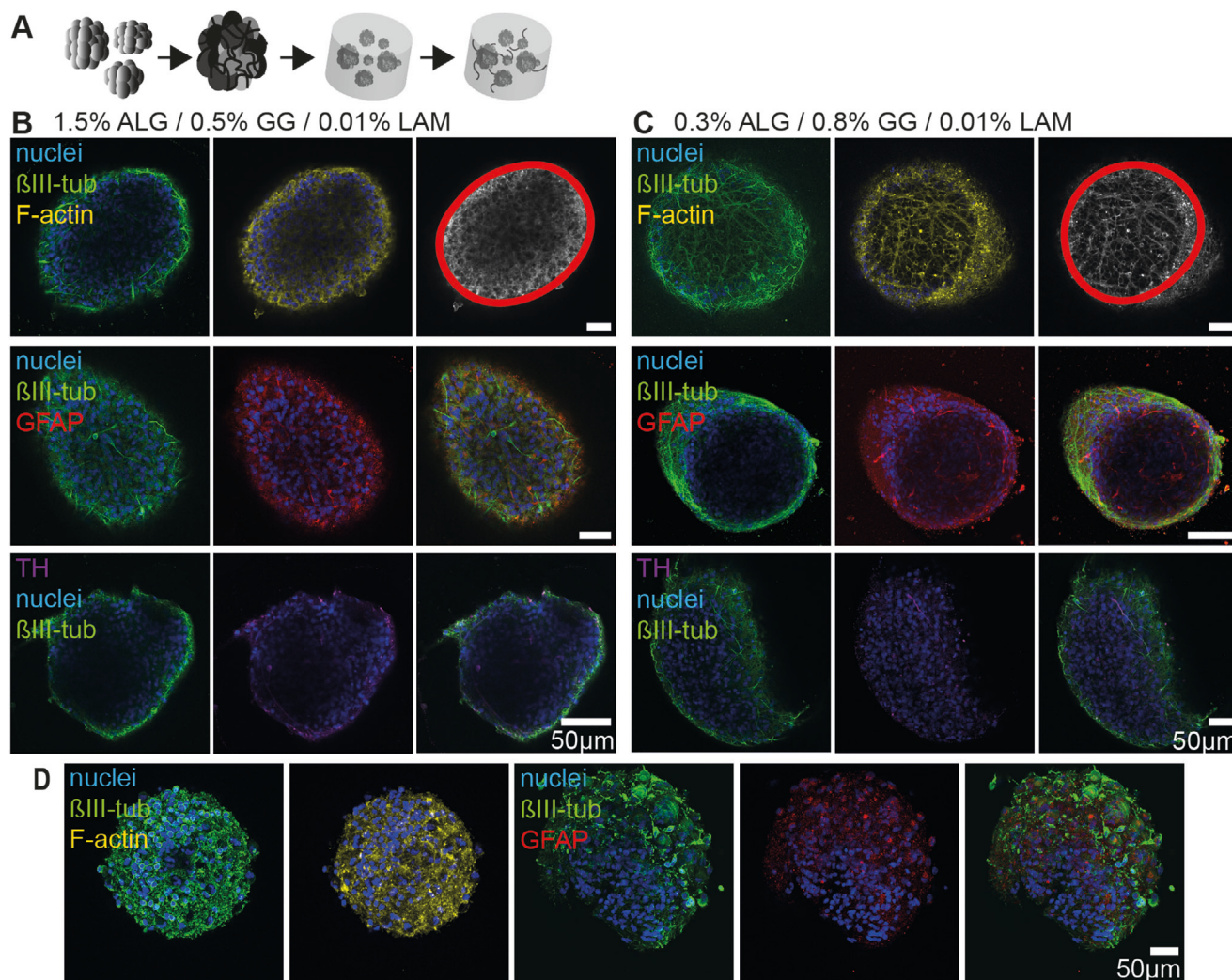


**Figure 3.** Pre-differentiated hiNPCs differentiated in 1.5% ALG/0.5% GG/0.01% LAM and 0.3% ALG/0.8% GG/0.01% LAM. A) Proliferating 0.3 mm hiNPC spheres were pre differentiated for 1 week and subsequently embedded into the respective gel. The gels were then cultivated in differentiation medium for 7 days and subsequently stained. Confocal images of differentiated spheres in B) 1.5% ALG/0.5% GG/0.01% LAM or C) 0.3% ALG/0.8% GG/0.01% LAM hydrogels. The samples were stained for nuclei (Hoechst, blue),  $\beta$ III tubulin (Alexa 546, green), F-actin (phalloidin, Alexa 488, yellow or grey), dopaminergic neurons (TH, Alexa 546, in magenta) and astrocytes (GFAP, Alexa 647, red). Images of the neural network formation are depicted in the upper row of (B) and (C). The red circles show the approximate size and location of the originally embedded spheres. Differentiation into multiple cell types within the gels is shown in the lower two rows of (B) and (C). D) As a comparison for the gel differentiation, proliferating 0.3 mm NPC spheres were differentiated as free-floating spheres without gel-embedding for 2 weeks and subsequently stained for nuclei (Hoechst, blue),  $\beta$ III tubulin (Alexa 546, green), F-actin (phalloidin, Alexa 488, yellow or grey) and astrocytes (GFAP, Alexa 647, red). Left to right:  $\beta$ III tubulin, F-actin,  $\beta$ III tubulin, GFAP,  $\beta$ III-GFAP merge. Images represent sections through spheres in varying depths or maximum intensity projections of Z-stacks. Abbreviations: GG, gellan gum; hiNPCs, human induced pluripotent stem cell-derived neural progenitor cells.

help us to understand pathomechanisms. Moreover, utilization of such in vitro models for assessing the neural responses to toxicants and drugs will improve hazard assessment. 3D models augment the complexity of conventional cell cultures, thus rendering them more predictive and physiologically relevant.<sup>[28,54,55,60,61]</sup> However, there is currently no gold standard for hydrogel-based 3D neural cultures, as limitations such as the high variability and the general low throughput of 3D models still need to be overcome. Here we suggest two cytocompatible ALG/GG/LAM hydrogel blends for the generation of human iPSC-based 3D neural models with spontaneous intracellular calcium signals.

Animal models and rodent primary cell cultures have given us great insights into the brain's development, basic function, disorders, and its reaction to substance exposure. However, interspecies differences suggest a limited predictive power of such models for humans,<sup>[12,13,22,62–66]</sup> especially when it comes to disease models.<sup>[67,68]</sup> This leads, amongst others, to high attrition rates for drugs.<sup>[2–4]</sup> Therefore, we developed our 3D models with widely available and ethically justifiable hiNPCs, that reflect the correct species. These pluripotent cells can be differentiated into multicellular networks containing cells of the neuronal and astroglia lineage. It is, however, not yet possible to obtain fully ma-

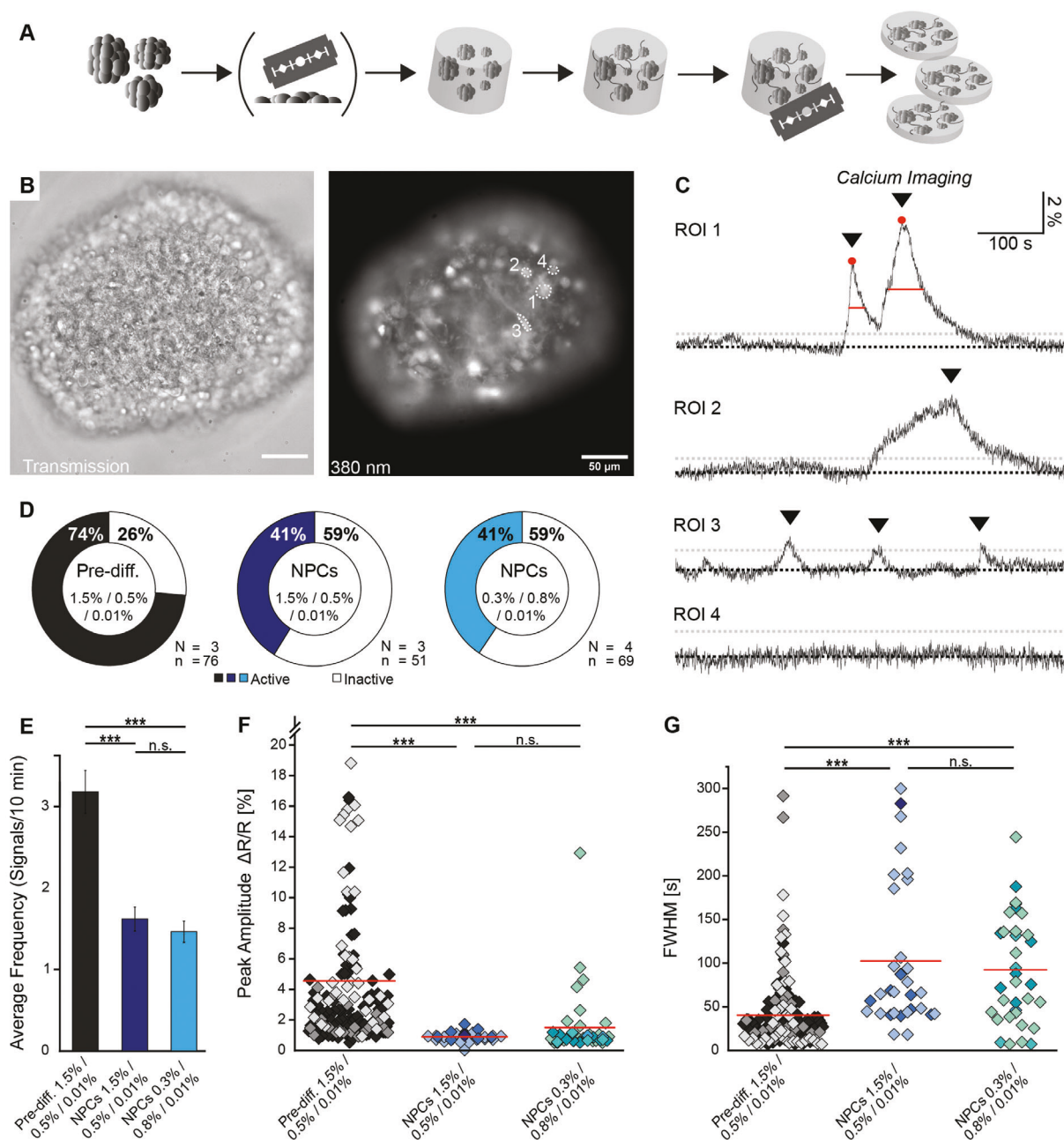


**Figure 4.** Calcium signaling in pre-differentiated and non-pre-differentiated hiNPC-derived neural networks in 1.5% ALG/0.5% GG/0.01% LAM and 0.3% ALG/0.8% GG/0.01% LAM gels. A) The hiNPCs were chopped to 0.1 mm size and subsequently embedded into the respective hydrogel blend. The hiNPCs were differentiated within the gel for 21 days before slicing and calcium imaging. 0.3 mm pre-differentiated spheres were not chopped, but sorted and pre-differentiated for 1 week in the absence of growth factors. Thereafter, the pre-differentiated spheres were embedded into the respective hydrogel blend and cultivated under differentiating conditions for 1 week. The sphere-laden gels were then sliced into 250  $\mu\text{m}$  thick slices before calcium imaging. B) Transmission and widefield images showing Fura-2 fluorescence (after excitation at 380 nm) of a pre-differentiated neural network in 1.5% ALG/0.5% GG hydrogel. Dashed lines illustrate regions of interest (ROIs) 1-4, representing cell bodies, as analyzed in (C). C) Corresponding ROIs showing spontaneous calcium signals during a 10 min recording period. Black dotted lines indicate the baseline and grey dotted lines indicate  $5 \times$  SD of the baseline. Black lines represent the smoothed traces (Savitzky Golay Filter: 15). Black triangles mark calcium signals; red dots mark the peak amplitudes  $\Delta R/R$ , red lines mark the Full Width at Half Maximum (FWHM) of two signals in one example trace. D) The pie charts display the percentages of active vs. inactive ROIs in all imaged samples of pre-differentiated spheres differentiated in 1.5% ALG/0.5% GG/0.01% LAM (black, left), non-differentiated hiNPCs differentiated in 1.5% ALG/0.5% GG/0.01% LAM (dark blue, middle) and non-differentiated hiNPCs differentiated in 0.3% ALG/0.8% GG/0.01% LAM (light blue, right). The graphs show E) the average frequency (mean  $\pm$  SEM) of calcium signals per 10 min, F) the peak amplitude  $\Delta R/R$  (in %) and G) the FWHM (in s) of each individual calcium signal, respectively. Each color in (F) and (G) represents individual Ns. For illustration purposes, seven data points of pre-differentiated hiNPCs in 1.5% ALG/0.5% GG, exhibiting amplitudes exceeding 20%, are not shown. Abbreviations: N, number of gels; n, number of cells. ALG, alginate; GG, gellan gum; LAM, laminin; ROI, region of interest; iPSCs, induced pluripotent stem cells; hiNPCs, human iPSC-derived neural progenitor cells; FWHM, full width at half maximum; pre-diff, pre-differentiated.

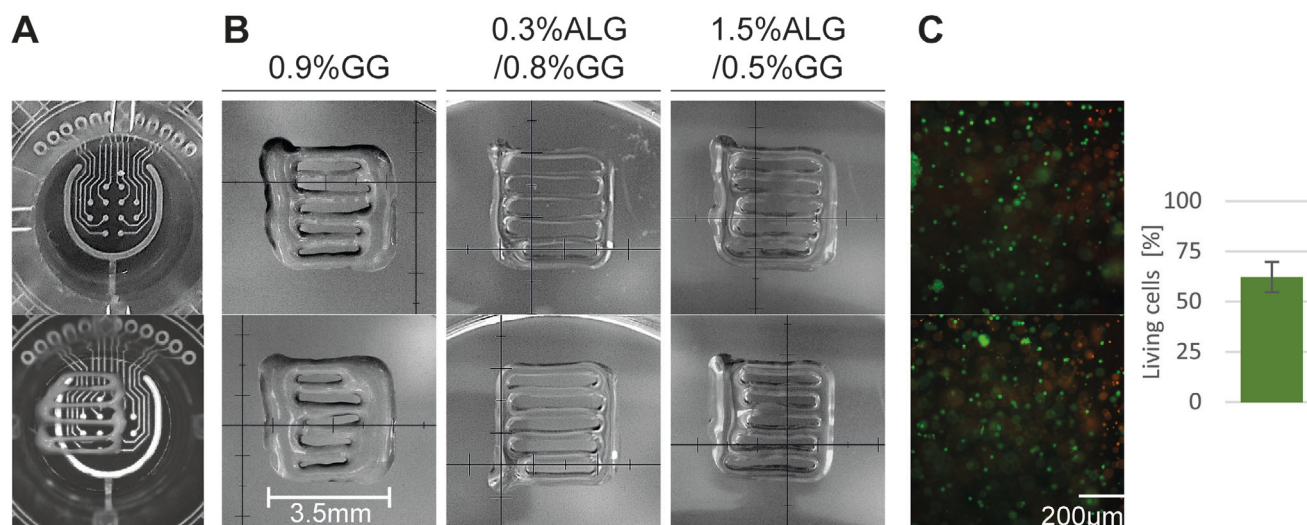


**Figure 5.** Bioprinting strategy. A) Detailed view of a well from a 24-well MEA plate (top). The silicon was printed in a square with four horizontal lines onto the electrodes with the currently highest possible accuracy (bottom). B) Representative microscopy images of 0.9% GG, 1.5% ALG/0.5% GG and 0.3% ALG/0.8% GG gels printed into a 24 well plate. Depicted are two representative images of the printing layer of the intended structure. All images were taken immediately after printing. C) Exemplary images of bioprinted single cells in 1.5% ALG/0.5% GG/0.01% LAM. Cells were differentiated for 3 days after printing and crosslinking, and subsequently stained with calcein-AM for live cells (green) and ethidium homodimer-1 for dead cells (red). The graph shows the living cells within the gels after 3 days ( $n = 4$  gels). Abbreviations: MEA, microelectrode array; GG, gellan gum; ALG, alginate; LAM, laminin.

ture networks in vitro, which needs to be considered, when utilizing hiPSC-based models.

### 3.1. 3D Outgrowth and Migration of hiPSC-Derived Neural Cells in Hydrogels

The brain is one of the softest tissues in the human body, with a Young's elastic modulus of 0.5–50 kPa.<sup>[31,32]</sup> Thus, mimicking the brains ECM in vitro is highly challenging.<sup>[69]</sup> Hydrogels feature advantageous properties for the 3D cultivation of neural models, such as the high water content (>90%), potential for functionalization, as well as chemical and physical tunability.<sup>[28]</sup> Studies demonstrated that soft hydrogels (<1.5 kPa) support neurite outgrowth<sup>[39]</sup> whereas stiffer hydrogels promote astrocyte differentiation.<sup>[70,71]</sup> Koivisto et al. embedded hiPSC-derived neurons into bioamine-crosslinked GG gels with compressive moduli ranging from 3.9 to 23 kPa and compared them to the rabbit brain (7–10 kPa).<sup>[29]</sup> They showed good cytocompatibility and migration of embedded hiPSC-derived neurons, as well as maturation of neuronal cultures underneath a gel cover. Electrical activity of the neurons was not assessed in their study. Matyash et al. plated primary rat and human neurons on 1% ALG gels with elastic moduli ranging from 20.8 to 0.64 kPa depending on the crosslinker concentration.<sup>[72]</sup> This group showed supported neurite outgrowth and increased resistance to oxidative stress of neurons cultured on soft ALGs. Moxon et al. generated even lower percentage GG gels with elastic moduli of  $\approx$ 10 kPa and applied sonication at various amplitudes to alter the gels properties.<sup>[73]</sup> However, very soft hydrogels are difficult to handle and tend to be incompatible with advanced biofabrication techniques, such as bioprinting or fluidic devices. Therefore, we approached the issue by generating hydrogel blends that are within an appropri-

ate range of stiffness and exhibit quick stress relaxation times. 0.3% ALG/0.8% GG/0.01% LAM gels are less stiff than 1.5% ALG/0.5% GG 0.01% LAM gels and exhibit significantly quicker stress relaxation times, which was attributed to the reduced ALG content in those hydrogels. Outgrowth of non-pre-differentiated spheres in 0.3% ALG/0.8% GG/0.01% LAM gels seems to occur slightly quicker and in thinner bundles. A significant difference between the gels was observed during calcium imaging of pre-differentiated spheres. Here, the higher stiffness of 1.5% ALG/0.5% GG/0.01% LAM gels allowed easy slicing, while 0.3% ALG/0.8% GG/0.01% LAM gels were more difficult to handle. The results suggest that, in ALG/GG blends, ALG and GG may sterically hinder each other in ionic crosslinking, suggesting that ALG or GG may act similarly to spacer molecules. Spacer molecules have already been introduced to PET and ALG-based hydrogels and were shown to control and accelerate stress relaxation of these materials.<sup>[59]</sup> Since natural ECM, specifically the brain ECM, are viscoelastic, with time-dependent mechanical responses to stress, the property of quick stress relaxation times seems not only beneficial, but crucial (reviewed by Madl et al. and Axpe et al.).<sup>[69,74]</sup> We suggest that the quick stress relaxation of our gel blends supports growth and migration of neural cultures, even in stiffer gels.

However, a deeper knowledge on the mechanics of the here identified optimal ALG/GG/LAM hydrogel composition (1.5% ALG/0.5% GG/0.01% LAM and 0.3% ALG/0.8% GG/0.01% LAM) should be scope of future research, as others indicated that multimodal mechanical testing is required to gain full knowledge on the complex mechanics of, for example, brain tissue and brain-mimicking materials.<sup>[31,46]</sup> As a result, further mechanical testing to complement the compressive modulus and stress relaxation data in the present study should be performed in future research, like rheological assessments on storage and loss

moduli ( $G'/G''$ ) of the gels, to gain knowledge on frequency dependent hydrogel viscoelasticity, as demonstrated earlier for GG hydrogels.<sup>[29]</sup> This would allow to better understand potential mechanical cues of the here presented hydrogels for future neural tissue engineering applications.

We present stiffness and stress relaxation measurements derived from uniaxial compression testing. We also confirm slow degradation of the hydrogel blends over time, which additionally benefits cellular outgrowth.<sup>[75]</sup> In future studies, we will assess calcium affinity to both ALG and GG, which may elucidate which component preferentially crosslinks through the available calcium ions, and if mutual weakening of the crosslinking is caused by using the here developed blends.

In general, there is no one-model-fits-all approach, when it comes to neural cultures and their various applications. Substance screenings usually require a medium to high throughput approach and very high reproducibility, while disease modeling is content with lower-throughput systems, but often relies on a higher degree of specificity and complexity. In vitro acute substance exposures commonly range from minutes to a few days, while chronic substance exposures are modeled over several days, however there is no common rule concerning the exposure length yet.<sup>[76]</sup> As a result, we developed two different materials and cultivation systems, which can be applied for different purposes.

### 3.2. Two Protocols for the Differentiation of hiNPC into Neurons and Astrocytes

The first system consists of hiNPCs embedded in the 0.3% ALG/0.8% GG/0.01% LAM gel. This softer hydrogel model combines cellular outgrowth and migration with differentiation into astrocytes and neurons thereby generating complex microtissues with spontaneous calcium signals, as confirmed by ICC and calcium imaging after 3 weeks in vitro. We suggest this model to be valuable for applications requiring a high degree of complexity, but less throughput, such as disease modeling and long-term exposure studies. We were able to show that also NPCs derived from a disease hiPSC line, that is, from a patient with Cockayne Syndrome B (CSB), can be differentiated in 0.3% ALG/0.8% GG/0.01% LAM gels to form 3D neural networks. Spheres showed outgrowth out of the sphere and clear differentiation into neurons. The astrocyte staining did not offer conclusive results, which might be due to the disease. This, however, needs to be further evaluated in future experiments yet offers a valuable starting point of cellular analyses of the pathomechanisms of this neurodevelopmental disease. We hereby show, that the gel blend is also suitable for studying patient-derived cells and that the here developed gel blend is a valuable tool for 3D disease modeling. In the future, more hiPSC lines from healthy and diseased donors need to be tested for their 3D migration and differentiation behavior using 0.3% ALG/0.8% GG/0.01% LAM gel blends.

The second system consists of pre-differentiated hiNPC spheres embedded in the 1.5% ALG/0.5% GG/0.01% LAM gel. These samples were easy to handle for calcium imaging due to their slightly higher stiffness and quickly produced dense intraspherical networks, consisting of neurons and astrocytes. This

model displays spontaneous calcium signals after only 1 week of differentiation within the hydrogel. However, it does not form microtissues due to the short cultivation time. In comparison to the spheres differentiated in suspension only, the neuronal network of 3D cultivated spheres appears more prominent and morphologically advanced. We believe that the 3D cultivated spheres are easier to handle, especially for staining and calcium imaging, since they do not need additional embedding. Combined with the fast and easy production of these 3D cultures, we suggest this model to be suitable for higher throughput applications, such as acute exposures to chemicals or substance screenings. The cultivation length for both models including the pre-differentiation phase could be optimized in future experiments, depending on the required complexity and maturity of the networks. With the TH stainings we confirm the presence of dopaminergic neurons not only in secondary 3D,<sup>[13]</sup> but also in the gel-based 3D models. This information is useful for applications concerning dopaminergic neurons, for example, for studying attention deficit hyperactivity disorder of Parkinson's disease.<sup>[77,78]</sup>

### 3.3. Calcium Signals in Differentiated 3D Models

Spontaneous calcium signaling plays an important role in the regulation of many cellular processes such as gene expression,<sup>[79,80]</sup> neuronal outgrowth,<sup>[81,82]</sup> neuronal differentiation, and other developmental progresses.<sup>[83]</sup> Calcium imaging is widely used for investigating calcium signaling in tissue slices. However, in the past calcium imaging has also been used to monitor calcium transients in human differentiated neural aggregates or brain organoids,<sup>[84–86]</sup> as well as in primary human neurospheres differentiated in secondary 3D.<sup>[87]</sup> We are, to the best of our knowledge, the first to establish calcium imaging in slices of in vitro 3D-cultivated neural samples. We detected calcium signals in both differentiation systems. The pre-differentiated hiNPC spheres in 1.5% ALG/0.5% GG/0.01% LAM gels displayed calcium signals with the highest average signal frequencies and peak amplitudes, plus shorter FWHM. Both hydrogels with non-pre-differentiated spheres showed lower frequencies and peak amplitudes plus longer FWHM. We therefore want to enhance the differentiation time in the non-pre-differentiated hydrogels to get a higher number of active cells and increased frequency rates. Within one sample we observed calcium signals with varying frequency, amplitude and length. This is in accordance with findings from Gualda et al., who imaged differentiated human midbrain-derived NPCs.<sup>[85]</sup> The observed heterogeneity in our samples may arise partly from the fact that the hiPSC-derived networks contain several neuronal subtypes and also astrocytes.<sup>[13]</sup> The calcium signals will be further analyzed during the future development of the 3D models. Here, application of saline containing high K<sup>+</sup> concentration could, for example, be employed to differentiate neurons from astrocytes. Alternatively, sodium signals could be analyzed to probe for glutamate transporters, which are highly expressed by astrocytes. After further development of the method, for example by embedding organoids, one might envision the development of human correlate to rodent brain slices. Additionally, basic exposures during calcium imaging, such as glutamate or bicuculline (GABAAR antagonist) treatment need to be used to further characterize the

developing networks. In addition, the proposed application scenario for both models has to be tested in the future.

### 3.4. Hydrogel Functionalization

ALG and GG are inexpensive materials and their processing for the generation of the ALG/GG gel blends is easy and fast. Although both gels are cytocompatible, no specific cell binding sites are present.<sup>[34,41]</sup> Since cell-matrix interactions are crucial for cell growth, proliferation, and differentiation of neural cultures, a lot of effort is going into functionalizing biologically inert hydrogels with native ECM molecules, such as LAM, collagen, or fibronectin. LAM is one of the major integrin interactor groups in the brain ECM and promotes cell survival, network formation, and functional development of hiPSC-derived neural cultures in vitro.<sup>[1,45]</sup> Improved progenitor cell and primary cortical neuron interaction with hydrogels were also achieved by integration of the RGD motif, which is part of the LAM structure.<sup>[52,88]</sup> In our study, we implemented LAM to support the cell-matrix interaction. This approach is sufficient for short-term cultures and high-throughput systems, such as in the 1.5% ALG/0.5% GG 0.01% LAM with embedded pre-differentiated spheres. As the brain ECM is very complex, additional steps toward improved functionalization are of grave importance, especially when it comes to long-term cultivations of complex neural models. Therefore, we aim at further enhancing specifically the 0.3% ALG/0.8% GG/0.01% LAM gel blend with additional native ECM molecules such as collagen and fibronectin in future studies. Both additives are widely studied for their effect on cell survival, growth, and adhesion, as well as their ability to provide growth factor binding sites in hydrogels.<sup>[89–91]</sup> However, these ECM molecules have not yet been fully evaluated for their potential in 3D neural modeling. Alternative fibrinogen,<sup>[92]</sup> hyaluronic acid,<sup>[71]</sup> and chitosan-based<sup>[91]</sup> hydrogels have also been proposed, featuring their individual advantages and disadvantages.

### 3.5. 3D Bioprinting of Hydrogels

Advanced biofabrication and cultivation methods, such as 3D bioprinting, are up and rising in many in vitro fields like tissue engineering and substance testing, as extensively reviewed by Parrish et al.<sup>[93]</sup> They are able to increase the reproducibility and complexity of 3D structures.<sup>[37,94]</sup> As a functional readout besides calcium imaging, the electrophysiological analysis of in vitro neural network is often performed on MEAs.<sup>[30,95]</sup> However, the measurement of 3D models on MEAs is highly challenging, due to the planar structure of the electrodes and difficulties in positioning the cell-containing material onto the electrodes. Here, 3D bioprinting of hiPSC-derived neural cells onto MEA electrodes might offer a valuable solution, especially for higher throughput applications. Although in this work we did not succeed in producing a ready-to-use 3D bioprinted neural model, we contribute to its generation by showing the printability and cytocompatibility of the developed ALG/GG/LAM gel blends. Notably, 1% ALG by itself cannot be 3D bioprinted, due to its softness in the uncrosslinked state, and the GG by itself is not adherent to PDL/LAM-coated surfaces. Hence, the established printability of the gel blends is

a big step forward in future brain tissue engineering. In addition, our preliminary and unpublished work demonstrates that hiNPC spheres embedded and differentiated in ALG gels exert electrical activity measured with 24-well MEA systems (Figure S5, Supporting Information). Hence, our data prepares the ground for future work in CNS tissue engineering using 3D bioprinting that needs to address two issues: 1) missing bioprinting precision arising from variable plate manufacturing needs to be overcome, for example by applying a camera-based printing approach and 2) more work needs to be performed on systematically optimizing and characterizing the MEA readouts after 3D bioprinting. In the future, these data will help to create physiologically-relevant and reproducible 3D in vitro systems for disease modeling or compound screening.

### 3.6. Summary and Conclusion

In summary, in our study we present data on ALG/GG/LAM blends, which, amongst others, revealed the proposed favorable property of quick stress relaxation. Although many studies in the field of 3D modeling rely on primary or rodent cell cultures, iPSC plays an important role in the development of 3D models, not only due to species difference, but also due to known, and potentially unknown, varying requirements in culture conditions.<sup>[12,13,22,62–65]</sup> Therefore we used iPSC-based cell culture models, which gain more and more importance in the context of alternative testing methods and the aims of 3R (replacement, reduction, and refinement of animal testing).<sup>[96]</sup> We characterized our differentiating cultures via ICC and verified calcium transients within the 3D models. The implementation of the CSB disease hiPSC line supports the applicability of our model. We also showed the suitability of our gel blends for biofabrication purposes, specifically for extrusion-based 3D bioprinting. With our proof-of-principle study we open the opportunity for the further development of our models in many directions, such as disease modeling, substance screening, as well as basic research concerning the adaptation of standard methods such as calcium imaging, ICC, and MEA measurement.

## 4. Experimental Section

**Hydrogel Preparation:** For the preparation of the 3% (w/v) ALG stock solution, sterile dH<sub>2</sub>O (100 mL) was pre-warmed to 37 °C, ALG (3 g; #71238, Sigma) was added and the solution was steered overnight at 60 °C and 750 rpm to fully dilute the ALG. Finally, the ALG solution was autoclaved and stored at 4 °C until further use. 1% (w/v) ALG was prepared by diluting the 3% (w/v) ALG stock solution with sterile dH<sub>2</sub>O or with sterile dH<sub>2</sub>O containing a 0.1% (w/v) LAM stock solution in tris-buffered saline (TBS; #L2020, Sigma), which resulted in a 1% ALG/0.01% LAM solution. For the preparation of the GG stock solution, 10% (w/v) sucrose (#84097, Sigma) was dissolved in dH<sub>2</sub>O and sterile filtered (0.2 µm filter, Stericap Plus). A total of 5 mL sterile sucrose solution was heated to 80 °C (MKR23, Hettich Lab Technology). The GG (#G1910, Sigma) was then added to the sucrose solution and fully dissolved at 80 °C for 45 min at 600 rpm, to create 1% or 1.5% (w/v) stock solutions. The GG was subsequently

sterile filtered through a pre-heated filter. 0.9% (w/v) GG was prepared by diluting the 1% (w/v) stock solution with sterile dH<sub>2</sub>O or 0.1% (w/v) LAM stock solution in TBS. The latter resulted in a 0.9% GG/0.01% LAM solution. GG was prepared in a 10% sucrose solution to reduce the osmotic pressure on the cells, as suggested by Koivisto et al. 2017.<sup>[29]</sup> For both ALG/GG blends, the ALG stock solution was pre-warmed to 37 °C before addition. The 1.5% ALG/0.5% GG blend was prepared by mixing 3% (w/v) ALG stock solution to 1.5% (w/v) GG stock solution (pre-heated to 45 °C) and topping up the respective volume with sterile dH<sub>2</sub>O to yield the final concentrations. By additionally supplementing the sterile dH<sub>2</sub>O with 0.1% (w/v) LAM stock solution in TBS, a final blend of 1.5% ALG/0.5% GG/0.01% LAM was obtained. Similarly, 0.3% ALG/0.8% GG blends were prepared by mixing the 3% (w/v) ALG stock solution to the 1% (w/v) GG stock solution and topping up the volume with sterile dH<sub>2</sub>O. The addition of 0.1% (w/v) LAM stock solution in TBS resulted in a 0.3% ALG/0.8% GG/0.01% LAM blend. Both blends were cooled down to 37 °C before the addition of LAM or sphere-laden LAM. The hydrogels were crosslinked with CaCl<sub>2</sub> (0.09 M; #1023780500, Merck) for 5 min.

**FTIR:** To assess the chemical composition of the hydrogel blends, 1.5% ALG/0.5% GG/0.01% LAM and 0.3% ALG/0.8% GG/0.01% LAM hydrogels were analyzed using FTIR. The 0.9% GG and 1% ALG gels served as controls. The gels were frozen (−80 °C) and freeze-dried using a lyophilizer (LD-12 plus, Martin Christ). Attenuated total reflectance (ATR-FTIR) spectra were recorded with an infrared spectrometer (Nicolet 6700, Thermo Scientific, USA).

**SEM:** The hydrogels were washed using phosphate buffered saline (PBS +/+; 14040133, Gibco) and fixed using 3% (v/v) glutaraldehyde and 3% (v/v) paraformaldehyde solution (in 0.2 M sodium cacodylate buffer, pH 7.4, all Sigma Aldrich) for 1 h at 22 °C (room temperature), respectively. Next, the samples were dehydrated by an ascending ethanol series (30, 50, 70, 75, 80, 85, 90, 95, and 99.8%) for 30 min each and subsequently critical point dried by liquid CO<sub>2</sub> exchange using a critical point dryer (EM CPD300, Leica). SEM images were recorded at 1 kV using secondary electron (SE) detection with an Auriga CrossBeam unit (Carl Zeiss Microscopy GmbH).

**Mechanical Testing:** To assess the mechanical properties of the hydrogels, cylindrical hydrogel specimens were fabricated using custom made cylindrical silicone molds (diameter = 10 mm, height = 5 mm). Unconfined compression tests were performed using an Instron 5967 mechanical testing setup (Instron GmbH) using a 100 N load-cell and a compression deformation rate of 1 mm × min<sup>−1</sup>. The samples were compressed until reaching 15% compressional strain. Initial bulk gel stiffness was derived as the slope in the linear elastic deformation regime of stress–strain diagrams derived from stress relaxation experiments and was evaluated as the slope of the linear elastic region between 5% and 10% strain. Next, the samples were held at 15% strain and the stress was recorded over time. Stress relaxation of the hydrogel cylinders was monitored, and the stress relaxation time  $t_{1/2}$  was quantified as the time after which 50% of the initial stress at 15% strain was dissipated in the hydrogels ( $n > 3$ ), as described earlier.<sup>[59]</sup>

**Degradation Study:** The degradation of 0.9% GG, 1% ALG, 1.5% ALG/0.5% GG, and 0.3% ALG/0.8% GG gels was assessed

by measuring the hydrogel mass over time. Therefore, six 50 µL gels per condition were separately deposited in 60 mm petri dishes (BD-Falcon) and cross-linked with CaCl<sub>2</sub> (0.09 M) for 5 min. Hydrogels were stored in PBS (+/+) at 37 °C and 5% CO<sub>2</sub> between measurements. The weight of the hydrogels was measured with an analytical scale (A200S, Olympus) every other day, by carefully removing the surrounding liquid completely, without drying out the gel itself.

**Cell Culture and Maintenance:** The cultivation and neural induction of hiPSCs was adapted from Hofrichter and Nimtz et al.<sup>[13,19]</sup> Briefly, hiPSC-IMR90 lines were obtained from WiCell and maintained under feeder-free conditions on Matrigel-coated 6-well plates (LDEV-free, #354277, Corning) in mTeSR1 medium (#05850, StemCell Technologies), at 37 °C in a humidified atmosphere of 5% CO<sub>2</sub>. The medium was changed on 6 days per week by completely removing and replacing the medium with fresh mTeSR1 (2 mL) culture medium. On the sixth day of feeding, mTeSR1 (4 mL) was added, to substitute for the feeding-free seventh day.

The neural induction of hiPSC cultures was performed by incubating the cells with ROCK inhibitor (1 µM; Y-27632, #1254, Tocris Biosciences) in mTeSR1 medium for 1 h at 37 °C and 5% CO<sub>2</sub>. Subsequently, the cells were washed with PBS including Penicillin/Streptomycin (PAN-Biotech) and neural induction medium (NIM; 1 mL) was added. Colonies were then fragmented with a StemPro EZPassage Disposable Stem Cell Passaging Tool (Thermo Fisher Scientific) and transferred into Poly-HEMA-coated 6 cm dishes (#P3932, Merck) with NIM (5 mL). ROCK inhibitor (10 µM) was added for at least 24 h. The medium was changed every second day. On day 7, spheres were collected and transferred into new Poly-HEMA-coated 6 cm dishes with NIM and hFGF (10 ng mL<sup>−1</sup>; #233-FB, R&D Systems) and the spheres were cultured for another 14 days. On day 21 the generated hiNPCs were transferred into new Poly-HEMA-coated 10 cm dishes with NPC proliferation medium and hFGF (20 ng mL<sup>−1</sup>). Cells were fed every second day with NPC proliferation medium and chopped to 0.2 mm when exceeding a size of ≈0.5 mm, or when clumping occurs (McIlwain Tissue Chopper, Ted Pella). All media compositions are listed in Supporting Information.

**Preparation of Sphere-Laden Hydrogels:** Proliferating hiNPC spheres were pooled and chopped to a diameter of 0.1 mm. The spheres were then resuspended in CINDA differentiation medium and counted in a Nageotte chamber (Marienfeld). The desired number of spheres ( $4.9 \times 10^3$  spheres mL<sup>−1</sup> gel) was centrifuged at 2500 rpm for 5 min and resuspended in 0.1% (w/v) LAM in TBS (final concentration 0.01% (w/v)). The cell-LAM suspension was then added to the respective gel blend and distributed by careful pipetting. For the generation of pre-differentiated spheres, 0.3 mm proliferating spheres were sorted into a small dish with CINDA medium.<sup>[13]</sup> Subsequently, one sphere per well was added to a Poly-HEMA coated 96-well U-bottom plate (Sarstedt). The spheres were pre-differentiated in CINDA medium for 1 week at 37 °C in a humidified atmosphere at 5% CO<sub>2</sub> and subsequently embedded as described above.

**ICC:** Samples were fixed with 4% paraformaldehyde (#P6148, Sigma Aldrich) for 30 min at 37 °C, followed by three PBS (+/+) washing steps, 5 min each. Gels were then pre-blocked for 2 h with 10% (v/v) goat serum (#G9023, Sigma Aldrich) in 0.1% (v/v) Triton X 100 (#T8787) in PBS (PBS-T).

The desired primary antibodies were diluted in 10% goat serum in PBS-T. Subsequently, the antibody solution was added to the samples and incubated at 4 °C overnight. Samples were washed three times for 1 h with PBS (+/+). Then, the relevant secondary antibodies and Phalloidin-Alexa488 (1:70, A12379, Life Technologies) were added to 1% Hoechst (33258, Sigma Aldrich) and 2% goat serum in PBS (+/+). The samples were again incubated at 4 °C overnight. Finally, the samples were washed three times for 1 h with PBS (+/+) and stored in PBS (+/+) until they were imaged with the confocal laser scanning microscope TCS SP8 (Inverse DMI8CS, Leica Microsystems). Maximum intensity projections of recorded Z-stacks were constructed using Fiji Image J 1.52p.<sup>[97]</sup> All antibodies are listed in Supporting Information.

**Calcium Imaging:** Non-pre-differentiated hiNPCs were embedded in 50  $\mu$ L gels and cultured in 96-well plates in differentiation medium for 21 days. 1-week pre-differentiated spheres were embedded in 100  $\mu$ L gels and cultured in a 96-well plates in differentiation medium for 1 week. Gels were subsequently transferred into small Petri dishes containing standard artificial cerebrospinal fluid (ACSF, containing in mM: 130 NaCl, 2.5 KCl, 2 CaCl<sub>2</sub>, 1 MgCl<sub>2</sub>, 1.25 NaH<sub>2</sub>PO<sub>4</sub>, 26 NaHCO<sub>3</sub>, and 10 glucose, bubbled with 95% O<sub>2</sub> and 5% CO<sub>2</sub>; pH: 7.4 & osmolarity: 305–310 mOsm/l). Subsequently, gels were placed in a bath filled with ACSF and cut into 250  $\mu$ m thick slices using a vibratome (HM650 V, Thermo Fisher Scientific). For ratiometric calcium imaging, slices were transferred into standard ACSF which contained 15  $\mu$ M Fura-2 AM (Molecular Probes, Invitrogen) and loaded for 30 min at 36 °C in a humidified incubator at 5% CO<sub>2</sub>/95% O<sub>2</sub>, followed by a washing step in ACSF for 30 min. Fura-2 loaded slices were then placed in a recording chamber, fixed with a grid, and continuously perfused with ACSF. Experiments were performed at room temperature (20–24 °C).

Calcium signals were recorded using a widefield epifluorescence imaging system based on an Eclipse FN-PT upright microscope (Nikon), equipped with an Orca FLASH 4.0 camera (Hamamatsu Photonics) and a 40 $\times$ /0.80 LUMPlanFI water immersion objective (Olympus). Imaging was controlled by the software NIS-Elements AR 4.5 (Nikon). Fura-2 was alternately excited at 357 nm (insensitive) and 380 nm (sensitive wavelength) at an imaging frequency of 10 Hz. After background correction, the ratio of the fluorescence emission (R) obtained from individual regions of interest representing cell bodies (ROIs) was calculated using the software NIS-Elements AR 5.0 (Nikon). Measurements were analyzed using OriginPro 2020 (OriginLab Corporation) and Microsoft Excel 2016 (Microsoft Corporation). Background-corrected traces of the Fura-2 ratio of the individual ROIs were normalized to their initial baseline (as determined during the first signal-free 30 s of measurement), baseline corrected and a smoothing filter (Savitzky-Golay: 15 Points) was applied. Cells were considered “active,” if they exhibited calcium signals with peaks  $\geq$  the fivefold standard deviation relative to their individual baseline fluorescence. For each ROI and calcium signal, the average frequency (number of signals during a 10 min recording), the peak amplitude  $\Delta R/R$  (in %), and the Full Width at Half Maximum (FWHM, in s) were analyzed.

**3D Bioprinting:** A computer-aided design model for the bioprinting of hydrogels onto the electrodes of a 24-well multiwell

microelectrode array (MEA) plate was designed in Autodesk Inventor Professional 2020. The printing was carried out with an EnvisioTEC 3D-Bioplotter (Manufacturers Series), using a nozzle with 200  $\mu$ m inner diameter (7018417, Nordson EFD). The printing parameters were optimized and ideal parameters were identified. The respective parameters for printing of 0.9% GG and the gel blend 1.5% ALG/0.5% GG and 0.3% ALG/0.8% GG are listed in Supporting Information.

**Statistical Analyses:** The material characterization data were statistically analyzed in GraphPad Prism 9.0, using one-way ANOVA and Bonferroni post-hoc tests. Significant differences among means between the different materials were indicated as \* $p < 0.05$ . Data derived from calcium imaging measurements were tested using a Mann–Whitney–U-test. “N” represents the number of hydrogels, “n” the number of single cells.  $P$  values were represented as follows: \*  $p < 0.05$ , \*\*  $p < 0.01$ , \*\*\*  $p < 0.001$ .

## Supporting Information

Supporting Information is available from the Wiley Online Library or from the author.

## Acknowledgements

The authors thank the Center for Advanced Imaging (CAi) at the Heinrich Heine University Düsseldorf for their support with the imaging. Furthermore, the authors thank Dr. Katharina Koch (IUF – Leibniz Research Institute for Environmental Medicine, Düsseldorf, Germany) for useful discussions and comments. This work was supported by Bayer AG. CRR received support from the DFG (FOR2795 “Synapses under Stress,” Ro2327/13-1).

Open access funding enabled and organized by Projekt DEAL.

## Conflict of Interest

The authors declare no conflict of interest.

## Author Contributions

The author and co-author contributions are allocated in accordance with CRediT. E.F.: conceptualization, funding, supervision, writing—review & editing; A.R.B.: supervision, writing—review & editing; C.R.R.: supervision, writing—review & editing; C.M.S.: writing—review & editing; F.B.: investigation; I.L.: conceptualization, supervision, writing—review & editing; T.D.: investigation, visualization, resources, writing—review & editing; L.P.: investigation, methodology, resources, visualization, writing—review & editing; J.K.: conceptualization, investigation, methodology, project administration, resources, visualization, writing—original draft.

## Data Availability Statement

Research data are not shared.

## Keywords

alternative methods, bioprinting, brain spheres, extracellular matrix, human induced pluripotent stem cells, neurospheres, spheroids

Received: January 21, 2021

Revised: June 1, 2021

Published online:

- [1] A. Farrukh, S. Zhao, A. del Campo, *Front. Mater.* **2018**, *5*, 62.
- [2] K. Smietana, M. Siatkowski, M. Möller, *Nat. Rev. Drug Discovery* **2016**, *15*, 379.
- [3] R. K. Harrison, *Nat. Rev. Drug Discovery* **2016**, *15*, 817.
- [4] R. C. Mohs, N. H. Greig, *Alzheimer's Dementia* **2017**, *3*, 651.
- [5] P. Pound, M. Ritskes-Hoitinga, *J. Transl. Med.* **2018**, *16*, 304.
- [6] P. Zhuang, A. X. Sun, J. An, C. K. Chua, S. Y. Chew, *Biomaterials* **2018**, *154*, 113.
- [7] B. A. Reynolds, S. Weiss, *Science* **1992**, *255*, 1707.
- [8] B. A. Reynolds, W. Tetzlaff, S. Weiss, *J. Neurosci.* **1992**, *12*, 4565.
- [9] M. A. Caldwell, X. He, N. Wilkie, S. Pollack, G. Marshall, K. A. Wafford, C. Svendsen, *Nat. Biotechnol.* **2001**, *19*, 475.
- [10] Y. H. Chiang, V. Silani, F. C. Zhou, *Cell Transplant.* **1996**, *5*, 179.
- [11] M. Moors, T. D. Rockel, J. Abel, J. E. Cline, K. Gassmann, T. Schreiber, J. Schuwald, N. Weinmann, E. Fritsche, *Environ. Health Perspect.* **2009**, *117*, 1131.
- [12] J. Baumann, K. Gassmann, S. Masjosthusmann, D. DeBoer, F. Bendt, S. Giersiefer, E. Fritsche, *Arch. Toxicol.* **2016**, *90*, 1415.
- [13] L. Nimtz, J. Hartmann, J. Tigges, S. Masjosthusmann, M. Schmuck, E. Keßel, S. Theiss, K. Köhrer, P. Petzsch, J. Adjaye, C. Wigmann, D. Wieczorek, B. Hildebrandt, F. Bendt, U. Hübenthal, G. Brockerhoff, E. Fritsche, *Stem Cell Res.* **2020**, *45*, 101761.
- [14] N. Alépée, A. Bahinski, M. Daneshian, B. De Wever, E. Fritsche, A. Goldberg, J. Hansmann, T. Hartung, J. Haycock, H. Hogberg, L. Hoelting, J. Kelm, S. Kadereit, E. McVey, R. Landsiedel, M. Leist, M. Lübberstedt, F. Noor, C. Pellevoisin, D. Petersohn, U. Pfannenbecker, K. Reisinger, T. Ramirez, B. Rothen-Rutishauser, M. Schäfer-Korting, K. Zeilinger, M. Zurich, *ALTEX* **2014**, *31*, 441.
- [15] S. Kamata, R. Hashiyama, H. Hana-ika, I. Ohkubo, R. Saito, A. Honda, Y. Anan, N. Akahoshi, K. Noguchi, Y. Kanda, I. Ishii, *Toxicol. In Vitro* **2020**, *69*, 104999.
- [16] Y. J. Choi, S. Chae, J. H. Kim, K. F. Barald, J. Y. Park, S. H. Lee, *Sci. Rep.* **2013**, *3*, 1921.
- [17] Y. Pei, J. Peng, M. Behl, N. S. Sipes, K. R. Shockley, M. S. Rao, R. Tice, X. Zeng, *Brain Res.* **2016**, *1638*, 57.
- [18] D. Simão, C. Pinto, S. Piersanti, A. Weston, C. J. Peddie, A. E. P. Bastos, V. Licursi, S. Schwarz, L. Collinson, S. Salinas, M. Serra, A. Teixeira, I. Saggio, P. Lima, E. Kremer, G. Schiavo, C. Brito, P. Alves, *Tissue Eng., Part A* **2015**, *21*, 654.
- [19] M. Hofrichter, L. Nimtz, J. Tigges, Y. Kabiri, F. Schröter, B. Royer-Pokora, B. Hildebrandt, M. Schmuck, A. Epanchintsev, S. Theiss, J. Adjaye, J. Egly, J. Krutmann, E. Fritsche, *Stem Cell Res.* **2017**, *25*, 72.
- [20] D. Pamies, K. Block, P. Lau, L. Gribaldo, C. A. Pardo, P. Barreras, L. Smirnova, D. Wiersma, L. Zhao, G. Harris, T. Hartung, H. Hogberg, *Toxicol. Appl. Pharmacol.* **2018**, *354*, 101.
- [21] T. Shirakawa, I. Suzuki, *Curr. Pharm. Biotechnol.* **2020**, *21*, 780.
- [22] A. M. Tukker, R. Van Kleef, F. M. J. Wijnolts, A. De Groot, R. H. S. Westerink, *ALTEX* **2020**, *37*, 121.
- [23] A. P. Haring, H. Sontheimer, B. N. Johnson, *Stem Cell Rev. Rep.* **2017**, *13*, 381.
- [24] E. R. Aurand, K. J. Lampe, K. B. Bjugstad, *Neurosci. Res.* **2012**, *72*, 199.
- [25] P. Zhuang, J. An, L. P. Tan, C. K. Chua, *Proc. of the 3rd Int. Conf. on Progress in Additive Manufacturing*, Nanyang Technological University, Singapore **2018**, pp. 183–188.
- [26] O. Wichterle, D. Lim, *Nature* **1960**, *185*, 117.
- [27] O. Z. Fisher, A. Khademhosseini, R. Langer, N. A. Peppas, *Acc. Chem. Res.* **2010**, *43*, 419.
- [28] M. Bahram, N. Mohseni, M. Moghtader, *Emerging Concepts in Analysis and Applications of Hydrogels*, IntechOpen, Rijeka **2016**.
- [29] J. T. Koivisto, T. Joki, J. E. Parraga, R. Paakkönen, L. Ylä-Outinen, L. Salonen, I. Jönkkari, M. Peltola, T. Ihalainen, S. Narkilahti, M. Kellomaki, *Biomed. Mater.* **2017**, *12*, 025014.
- [30] L. Ylä-Outinen, J. M. A. Tanskanen, F. E. Kapucu, A. Hyysalo, J. A. K. Hyttinen, S. Narkilahti, *Adv. Neurobiol.* **2019**, *22*, 299.
- [31] N. D. Leipzig, M. S. Shoichet, *Biomaterials* **2009**, *30*, 6867.
- [32] S. Budday, G. Sommer, J. Haybaeck, P. Steinmann, G. A. Holzapfel, E. Kuhl, *Acta Biomater.* **2017**, *60*, 315.
- [33] A. M. Smith, R. M. Shelton, Y. Perrie, J. J. Harris, *J. Biomater. Appl.* **2007**, *22*, 241.
- [34] J. Sun, H. Tan, *Materials* **2013**, *6*, 1285.
- [35] A. Blaeser, D. F. Duarte Campos, H. Fischer, *Curr. Opin. Biomed. Eng.* **2017**, *2*, 58.
- [36] L. Moroni, J. A. Burdick, C. Highley, S. J. Lee, Y. Morimoto, S. Takeuchi, J. J. Yoo, *Nat. Rev. Mater.* **2018**, *3*, 21.
- [37] V. Fantini, M. Bordoni, F. Scocozza, M. Conti, E. Scarian, S. Carelli, A. M. Di Giulio, S. Marconi, O. Pansarasa, F. Auricchio, *Cells* **2019**, *8*, 830.
- [38] K. Y. Lee, D. J. Mooney, *Prog. Polym. Sci.* **2012**, *37*, 106.
- [39] M. Matyash, F. Despang, C. Ikonomidou, M. Gelinsky, *Tissue Eng., Part C* **2014**, *20*, 401.
- [40] K. M. Zia, S. Tabasum, M. F. Khan, N. Akram, N. Akhter, A. Noreen, M. Zuber, *Int. J. Biol. Macromol.* **2018**, *109*, 1068.
- [41] C. J. Ferris, K. J. Gilmore, G. G. Wallace, M. i. h. Panhuis, *Soft Matter* **2013**, *9*, 3705.
- [42] S. Plantman, M. Patarroyo, K. Fried, A. Domogatskaya, K. Tryggvason, H. Hammarberg, S. Cullheim, *Mol. Cell. Neurosci.* **2008**, *39*, 50.
- [43] K. E. Swindle-Reilly, J. B. Papke, H. P. Kutosky, A. Throm, J. A. Hammer, A. B. Harkins, R. Willits, *J. Neural Eng.* **2012**, *9*, 046007.
- [44] Y. Yamada, K. Hozumi, A. Aso, A. Hotta, K. Toma, F. Katagiri, M. Nomizu, *Biomaterials* **2012**, *33*, 4118.
- [45] H. Wen, W. Xiao, S. Biswas, Z. Q. Cong, X. M. Liu, K. S. Lam, Y. H. Liao, W. Deng, *ACS Appl. Mater. Interfaces* **2019**, *11*, 5821.
- [46] T. Distler, E. Schaller, P. Steinmann, A. R. Boccaccini, S. Budday, *J. Mech. Behav. Biomed. Mater.* **2020**, *111*, 103979.
- [47] H. Cui, M. Nowicki, J. P. Fisher, L. G. Zhang, *Adv. Healthcare Mater.* **2017**, *6*, 1601118.
- [48] Z. Gu, J. Fu, H. Lin, Y. He, *Asian J Pharm. Sci.* **2020**, *15*, 529.
- [49] F. Salaris, A. Rosa, *Brain Res.* **2019**, *1723*, 146393.
- [50] D. Bociaga, M. Bartniak, J. Grabarczyk, K. Przybyszewska, *Materials* **2019**, *12*, 2669.
- [51] L. de la Vega, C. Lee, R. Sharma, M. Amereh, S. M. Willerth, *Brain Res. Bull.* **2019**, *150*, 240.
- [52] R. Lozano, L. Stevens, B. C. Thompson, K. J. Gilmore, R. Gorkin, E. M. Stewart, M. in het Panhuis, M. Romero-Ortega, G. G. Wallace, *Biomaterials* **2015**, *67*, 264.
- [53] Q. Gu, E. Tomaskovic-Crook, R. Lozano, Y. Chen, R. M. Kapsa, Q. Zhou, G. G. Wallace, J. M. Crook, *Adv. Healthcare Mater.* **2016**, *5*, 1429.
- [54] Q. Chai, Y. Jiao, X. Yu, *Gels* **2017**, *3*, 6.
- [55] Q. Gu, E. Tomaskovic-Crook, G. G. Wallace, J. M. Crook, *Biomaterials for Tissue Engineering: Methods and Protocols*, Vol. 1758 (Ed: K. Chawla), Springer, New York **2018**, pp. 129–138.
- [56] N. Zhu, M. G. Li, Y. J. Guan, D. J. Schreyer, X. B. Chen, *Biofabrication* **2010**, *2*, 045002.
- [57] R. A. Neal, S. S. Tholpady, P. L. Foley, N. Swami, R. C. Ogle, E. A. Botchwey, *J. Biomed. Mater. Res., Part A* **2012**, *100A*, 406.
- [58] J. Silva-Correia, J. M. Oliveira, S. G. Caridade, J. T. Oliveira, R. A. Sousa, J. F. Mano, R. L. Reis, *J. Tissue Eng. Regen. Med.* **2011**, *5*, e97.
- [59] H. P. Lee, L. Gu, D. J. Mooney, M. E. Levenston, O. Chaudhuri, *Nat. Mater.* **2017**, *16*, 1243.
- [60] M. Karimi, S. Bahrami, H. Mirshekari, S. M. M. Basri, A. B. Nik, A. R. Aref, M. Akbari, M. R. Hamblin, *Lab Chip* **2016**, *16*, 2551.
- [61] D. Pacitti, R. Privolizzi, B. E. Bax, *Front. Cell. Neurosci.* **2019**, *13*, 129.
- [62] E. Fritsche, K. Gassmann, T. Schreiber, *In Vitro Neurotoxicology: Methods and Protocols*, Vol. 758 (Eds: L. Costa, G. Giordano, M. Guizzetti), Humana Press, Totowa, NJ **2011**, pp. 99–114.

- [63] M. Leist, T. Hartung, *Arch. Toxicol.* **2013**, *87*, 563.
- [64] K. Dach, F. Bendt, U. Huebenthal, S. Giersiefer, P. J. Lein, H. Heuer, E. Fritsche, *Sci. Rep.* **2017**, *7*, 44861.
- [65] L. J. Martin, Q. Chang, *J. Neuropathol. Exp. Neurol.* **2018**, *77*, 636.
- [66] M. Dragunow, *Trends Pharmacol. Sci.* **2020**, *41*, 777.
- [67] I. Kola, J. Landis, *Nat. Rev. Drug Discovery* **2004**, *3*, 711.
- [68] A. M. Palmer, F. A. Stephenson, *Drug News Perspect.* **2005**, *18*, 51.
- [69] E. Axpe, G. Orive, K. Franze, E. A. Appel, *Nat. Commun.* **2020**, *11*, 10.
- [70] P. C. Georges, W. J. Miller, D. F. Meaney, E. S. Sawyer, P. A. Janmey, *Biophys. J.* **2006**, *90*, 3012.
- [71] S. K. Seidlits, Z. Z. Khaing, R. R. Petersen, J. D. Nickels, J. E. Vanscoy, J. B. Shear, C. E. Schmidt, *Biomaterials* **2010**, *31*, 3930.
- [72] M. Matyash, F. Despang, R. Mandal, D. Fiore, M. Gelinsky, C. Ikonomidou, *Tissue Eng., Part A* **2012**, *18*, 55.
- [73] S. R. Moxon, A. M. Smith, *Int. J. Biol. Macromol.* **2016**, *84*, 79.
- [74] C. M. Madl, S. C. Heilshorn, *Annu. Rev. Biomed. Eng.* **2018**, *20*, 21.
- [75] L. Yildirim, A. M. Seifalian, *Biotechnol. Adv.* **2014**, *32*, 984.
- [76] A. Bal-Price, H. T. Hogberg, K. M. Crofton, M. Daneshian, R. E. FitzGerald, E. Fritsche, T. Heinonen, S. H. Bennekou, S. Klima, A. H. Piersma, M. Sachana, T. J. Shafer, A. Terron, F. Monnet-Tschudi, B. Viviani, T. Waldmann, R. H. S. Westerink, M. F. Wilks, H. Witters, M. G. Zurich, M. Leist, *ALTEX* **2018**, *35*, 306.
- [77] W. Dauer, P. S. Parkinson's, *Neuron* **2003**, *39*, 889.
- [78] B. K. Madras, G. M. Miller, A. J. Fischman, *Biol. Psychiatry* **2005**, *57*, 1397.
- [79] R. E. Dolmetsch, K. Xu, R. S. Lewis, *Nature* **1998**, *392*, 933.
- [80] A. E. West, W. G. Chen, M. B. Dalva, R. E. Dolmetsch, J. M. Kornhauser, A. J. Shaywitz, M. A. Takasu, X. Tao, M. E. Greenberg, *Proc. Natl. Acad. Sci. U. S. A.* **2001**, *98*, 11024.
- [81] K. L. Lankford, P. C. Letourneau, *J. Cell Biol.* **1989**, *109*, 1229.
- [82] D. J. Sutherland, Z. Pujic, G. J. Goodhill, *Trends Neurosci.* **2014**, *37*, 424.
- [83] S. S. Rosenberg, N. C. Spitzer, *Cold Spring Harbor Perspect. Biol.* **2011**, *3*, a004259.
- [84] M. A. Lancaster, M. Renner, C. A. Martin, D. Wenzel, L. S. Bicknell, M. E. Hurler, T. Homfray, J. M. Penninger, A. P. Jackson, J. A. Knoblich, *Nature* **2013**, *501*, 373.
- [85] E. J. Gualda, D. Simão, C. Pinto, P. M. Alves, C. Brito, *Front. Cell. Neurosci.* **2014**, *8*, 221.
- [86] H. Sakaguchi, Y. Ozaki, T. Ashida, T. Matsubara, N. Oishi, S. Kihara, J. Takahashi, *Stem Cell Rep.* **2019**, *13*, 458.
- [87] K. Gassmann, J. Baumann, S. Giersiefer, J. Schuwald, T. Schreiber, H. F. Merk, E. Fritsche, *Toxicol. In Vitro* **2012**, *26*, 993.
- [88] N. A. Silva, M. J. Cooke, R. Y. Tam, N. Sousa, A. J. Salgado, R. L. Reis, M. S. Shoichet, *Biomaterials* **2012**, *33*, 6345.
- [89] M. Antman-Passig, S. Levy, C. Gartenberg, H. Schori, O. Shefi, *Tissue Eng., Part A* **2017**, *23*, 403.
- [90] C. Licht, J. C. Rose, A. O. Anarkoli, D. Blondel, M. Rocco, T. Haraszti, D. B. Gehlen, J. A. Hubbell, M. P. Lutolf, L. De Laporte, *Biomacromolecules* **2019**, *20*, 4075.
- [91] S. Mousavi, A. B. Khoshfetrat, N. Khatami, M. Ahmadian, R. Rahbarghazi, *Biochem. Biophys. Res. Commun.* **2019**, *518*, 625.
- [92] R. Sharma, I. P. M. Smits, L. De, L. Vega, C. Lee, S. M. Willerth, *Front. Bioeng. Biotechnol.* **2020**, *8*, 57.
- [93] J. Parrish, K. Lim, B. Zhang, M. Radisic, T. B. F. Woodfield, *Trends Biotechnol.* **2019**, *37*, 1327.
- [94] N. Antill-O'Brien, J. Bourke, C. D. O'Connell, *Materials* **2019**, *12*, 3218.
- [95] T. J. Shafer, *In Vitro Neuronal Networks: From Culturing Methods to Neuro-Technological Applications*, Vol. 22 (Eds: M. Chiappalone, V. Pasquale, M. Frega), Springer, Cham **2019**, pp. 275–297.
- [96] E. Fritsche, T. Haarmann-Stemmann, J. Kapr, S. Galanjuk, J. Hartmann, P. R. Mertens, A. A. M. Kämpfer, R. P. F. Schins, J. Tigges, K. Koch, *Small* **2021**, *17*, 2006252.
- [97] J. Schindelin, I. Arganda-Carrera, E. Frise, K. Verena, L. Mark, P. Tobias, S. Preibisch, C. Rueden, S. Saalfeld, B. Schmid, J. Y. Tinevez, D. J. White, V. Hartenstein, K. Eliceiri, P. Tomancak, A. Cardona, *Nat. Methods* **2009**, *9*, 676.



## 2.5 Measurement of Electrical Activity of Differentiated Human iPSC-Derived Neurospheres Recorded by Microelectrode Arrays (MEA)

*Kristina Bartmann, Julia Hartmann, Julia Kapr, Ellen Fritsche*

Neurotoxicity is caused by a large variety of compound classes and affects all life stages from the developing child to the elderly. Studying for neurotoxicity often involves animal models, which are very resource-intensive and bear the problem of species-differences. Thus, alternative human-based models are needed to overcome these issues. Over the last years, far-reaching advancements in the field of neurotoxicity were made possible by the ability to reprogram human somatic cells into induced pluripotent stem cells (hiPSC). These hiPSCs can be differentiated into neurons and astrocytes, which spontaneously form functional neuronal networks (NN) in vitro. Microelectrode arrays (MEA) are a valuable tool to assess the electrophysiology of such networks. This chapter explains the neural induction of hiPSCs to human neural progenitor cells (hiNPC) in the form of free-floating spheres and their subsequent differentiation into functional neurons on MEAs. The measurement of the electrical network activity, as well as the evaluation of the received data is described.

Journal:	Springer Protocols
Impact factor:	not calculated for book chapters
Contribution to the publication:	10%
	Writing and Editing
Type of authorship:	Co-author
Status of publication:	Published (30 July 2021)



## Measurement of Electrical Activity of Differentiated Human iPSC-Derived Neurospheres Recorded by Microelectrode Arrays (MEA)

Kristina Bartmann, Julia Hartmann, Julia Kapr, and Ellen Fritsche

### Abstract

Neurotoxicity is caused by a large variety of compound classes and affects all life stages from the developing child to the elderly. Studying for neurotoxicity often involves animal models, which are very resource-intensive and bear the problem of species-differences. Thus, alternative human-based models are needed to overcome these issues. Over the last years, far-reaching advancements in the field of neurotoxicity were made possible by the ability to reprogram human somatic cells into induced pluripotent stem cells (hiPSC). These hiPSCs can be differentiated into neurons and astrocytes, which spontaneously form functional neuronal networks (NN) in vitro. Microelectrode arrays (MEA) are a valuable tool to assess the electrophysiology of such networks. This chapter explains the neural induction of hiPSCs to human neural progenitor cells (hiNPC) in the form of free-floating spheres and their subsequent differentiation into functional neurons on MEAs. The measurement of the electrical network activity, as well as the evaluation of the received data is described.

**Key words** Neurotoxicology, Neurotoxicity, Human induced pluripotent stem cells (hiPSC), Human induced neural progenitor cells (hiNPC), Microelectrode array (MEA), Neuronal network, Electrical activity

---

## 1 Introduction

Adverse effects on the peripheral or central nervous system caused by chemical, biological, or physical agents are referred to as neurotoxicity [1]. Substances such as metals (e.g., lead), industrial chemicals (e.g., acrylamide), pharmaceutical drugs (e.g., doxorubicin), pesticides (e.g., deltamethrin), and natural toxins (e.g., domoic acid) have been shown to cause neurotoxicity [1, 2]. They are often included in industrial, agricultural, and consumer products, which must then be registered and approved by the European Chemical Agency (ECHA) and the European Food Safety

---

Kristina Bartmann and Julia Hartmann are contributed equally to this chapter.

Authority (EFSA), prior to entering the European market. Depending on the production volume, different toxicity tests have to be conducted. Current neurotoxicity guideline studies [3, 4] that precede the approval of such products are performed *in vivo* and are thus highly resource-intensive with regard to time, money, and animals [5]. Additionally, animal and human interspecies variations greatly challenge the translation of the generated data, especially for the nervous system [6–8]. Therefore, we are in urgent need of animal-free alternatives that better mimic human nervous system physiology [9]. The ability to reprogram human somatic cells into induced pluripotent stem cells (hiPSC) [10] has extensively advanced the field of neurotoxicity evaluation [11–14].

The use of human cellular models gave rise to a very important component of hazard identification—the neurophysiological assessment. Cultured *in vitro*, hiPSCs are able to grow, migrate, and differentiate into functional neuronal networks (NN) [15–19]. Important tools to study the electrophysiology of such NN are microelectrode arrays (MEA). These integrated arrays of electrodes, photoetched into a glass slide or “chip”, allow the simultaneous extracellular recording of electrical activity from a large number of individual sites in one tissue [20]. So far, neurotoxicological testing with MEAs has mainly been performed with rodent NN [21–30]. However, the use of human *in vitro* cultures is preferred, because responses to test compounds might be affected by species differences in toxicodynamics [31–35]. For this reason, human cells are increasingly used to measure neurotoxicity on MEAs [36–40]. In this chapter, we describe the neural induction of hiPSCs to free-floating neural progenitor cells (hiNPC), their differentiation on poly-d-lysine (PDL)/laminin-coated MEAs and the subsequent formation and measurement of functional NN (Fig. 1) [15, 16].

---

## 2 Materials

All cell culture procedures need to be performed in a Class II Biological Safety Cabinet under sterile conditions. The cells are cultivated in an incubator at 37 °C and 5% CO<sub>2</sub>.

### 2.1 Generation of Human Induced Neural Progenitor Cells (hiNPC)

#### 2.1.1 Preparation of Neural Induction Medium (NIM)

Mix **DMEM** (high glucose, GlutaMAX™ Supplement, pyruvate, Thermofisher Scientific #31966-021) and **Ham’s F12 Nutrient Mix** (GlutaMAX™ Supplement, Thermofisher Scientific #31765-027) 3:1 and add **1% Penicillin-Streptomycin** (10.000 U/mL, Thermofisher Scientific #15140-122), **2% B27™ supplement** (serum-free (50×), Thermofisher Scientific #17504-044), **0.2% Human recombinant epidermal growth factor** (EGF, Thermofisher Scientific #PHG0313), **1% N2 Supplement** (100×, Thermofisher Scientific #17502-048), **20% KnockOut™ Serum**

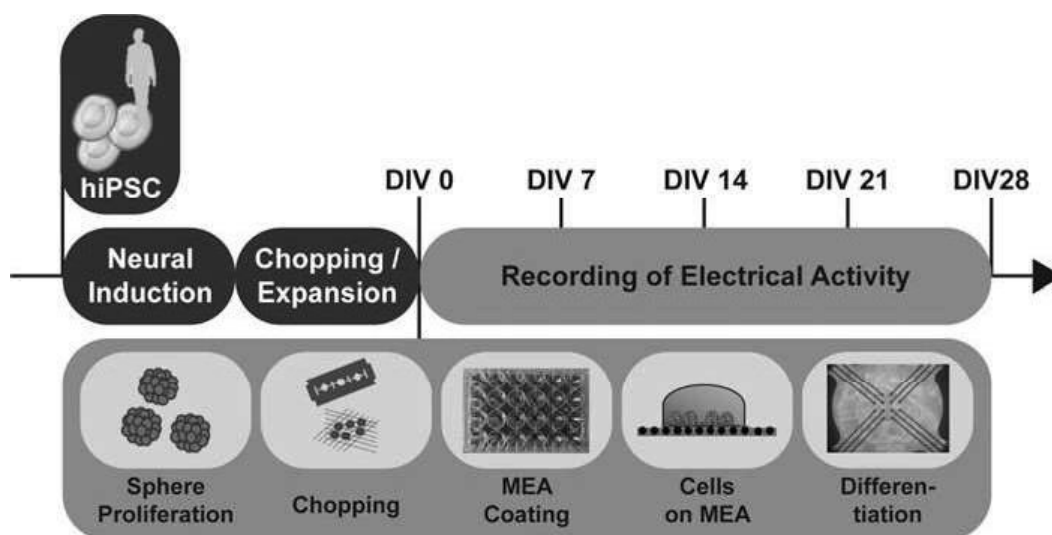


**Fig. 1** Experimental setup (adapted from Nimitz et al. [15]). Human iPSCs were neurally induced to hiNPC and cultivated as free-floating 3D neurospheres. Neurospheres proliferate in neural proliferation medium (NPM) supplemented with basic fibroblast growth factor (FGF2) and epidermal growth factor (EGF). By mechanical passaging with a razorblade (chopping), neurospheres are cut into small pieces (100 $\mu$ m) and directly plated onto a PDL-Laminin-coated mwMEA plate. In CINDA the NN differentiate and can be cultured for multiple weeks. The electrical activity can be measured from day 7. *DIV*: days in vitro

**Replacement** (KSR, Thermofisher Scientific #10828-028), **10 $\mu$ M SB-431542 hydrate** (Sigma #S4317, dissolved at 10 mM in DMSO), and **0.5 $\mu$ M LDN-193189 hydrochloride** (Sigma #SML0559, dissolved at 500 $\mu$ M in ultrapure water).

The medium can be stored at 2–8 °C for at least 3 weeks. Warm it to 37 °C prior to use.

### 2.1.2 Preparation of Neural Proliferation Medium (NPM)

Mix **DMEM** (high glucose, GlutaMAX™ Supplement, pyruvate, Thermofisher Scientific #31966-021) and **Ham's F12 Nutrient Mix** (GlutaMAX™ Supplement, Thermofisher Scientific #31765-027) 3:1 and add **1% Penicillin-Streptomycin** (10,000 U/mL, Thermofisher Scientific #15140-122), **2% B27™ supplement** (serum-free (50 $\times$ ), Thermofisher Scientific #17504-044), and **0.2% human recombinant epidermal growth factor** (EGF, Thermofisher Scientific #PHG0313). Previously, EGF is dissolved at 10 $\mu$ g/mL in sterile PBS, containing 0.1% bovine serum albumin (BSA, Serva #11920) and 1 mM DL-Dithiothreitol solution (DTT, Sigma #646563-10 $\times$ ). EGF is stored at –20 °C.

The NPM, containing supplements, antibiotics, and growth factors, can be stored up to 2 weeks at 2–8 °C. Prior to use, warm it to 37 °C and add **basic human recombinant fibroblast growth factor** (FGF2, R&D Systems #233-FB) to a final concentration of **20 ng/mL**. FGF2 is dissolved at 10 $\mu$ g/mL in sterile PBS, containing 0.1% bovine serum albumin (BSA, Serva #11920) and 1 mM DL-Dithiothreitol solution (DTT, Sigma #646563-10 $\times$ ). The reconstituted FGF2 can be stored for a maximum of 3 months at –20 °C.

### 2.1.3 Preparation of Poly-HEMA Solution

Dissolve 1.2 g of Poly(2-hydroxyethyl methacrylate) (Poly-HEMA, Sigma-Aldrich #P3932) in 40 mL ethanol (94.8%) using a magnetic stirrer for 5–16 h (*see Note 1*).

### 2.1.4 Neural Induction

- iPSC (IMR90) clone (#4), WiCell (*see Note 2*).
- mTeSR1, Stemcell Technologies #05850.
- Corning® Matrigel® Growth Factor Reduced (GFR) Basement Membrane Matrix, Phenol Red-free, LDEV-free, Corning #356231.
- Y-27632 (Rock Inhibitor), Tocris #1254, diluted to 10 mM in ultrapure water.
- StemPro™ EZPassage™ Disposable Stem Cell Passaging Tool, Thermofisher Scientific #23181010.
- Corning® cell lifter, Merck #CLS3008.
- McIlwain tissue chopper, Mickle Laboratory Engineering Co. Ltd.
- NIM (*see Subheading 2.1.1*).
- NPM (*see Subheading 2.1.2*).
- Dulbecco's phosphate-buffered saline with CaCl<sub>2</sub> and MgCl<sub>2</sub> (DPBS, 1×, Gibco).
- Culture dish (Ø10 cm and Ø6 cm).

## 2.2 Multiwell Microelectrode Arrays (mwMEAs)

### 2.2.1 Preparation of Differentiation Medium—CINDA

Mix **DMEM** (high glucose, GlutaMAX™ Supplement, pyruvate, Thermofisher Scientific #31966-021) and **Ham's F12 Nutrient Mix** (GlutaMAX™ Supplement, Thermofisher Scientific #31765-027) 3:1 and add **1% Penicillin-Streptomycin** (10.000 U/mL, Thermofisher Scientific #15140-122), **2% B27™ supplement** (serum-free (50×), Thermofisher Scientific #17504-044), **1% N2 Supplement** (100×, Thermofisher Scientific #17502-048), **5 mM creatine monohydrate** (Sigma #C3630), **100 U/mL human recombinant interferon-γ** (IFN-γ, Peprtech #300-02), **20 ng/mL human recombinant neurotrophin-3** (Peprtech #450-03) and **20 μM L-Ascorbic acid** (Sigma #A5960).

Store the medium at 2–8 °C for up to 2 weeks. Warm the differentiation medium to 37 °C and add **300 μM N<sup>6</sup>,2'-O-Dibutyryl adenosine 3',5'-cyclic monophosphate sodium salt** (Dibutyryl cAMP, Sigma #D0260) prior to use (*see Note 3*).

### 2.2.2 Differentiation on Poly-D-Lysin/ Laminin-Coated 24-Multiwell MEAs

- 24-Well plate with PEDOT electrodes on glass (mw-MEA), Multichannelsystems #24W300/30G-288.
- Poly-D-lysine hydrobromide (PDL), Sigma #P0899.
- Laminin from Engelbreth-Holm-Swarm sarcoma basement membrane (Laminin, working solution:  $c = 1$  mg/mL), Sigma #L2020 (*see Note 4*).

- Autoclaved ultrapure water.
- McIlwain tissue chopper, Mickle Laboratory Engineering Co. LTD.
- Dulbecco's phosphate-buffered saline with  $\text{CaCl}_2$  and  $\text{MgCl}_2$  (DPBS, 1 $\times$ , Gibco).
- Counting Chamber Nageotte, Marienfeld #KHY3.1.

### 2.2.3 Devices and Software for mwMEA Recordings and Analysis

- Multiwell-MEA headstage, Multi Channel Systems MCS GmbH.
- Multiwell-Screen, Version 1.11.6.0, Multi Channel Systems MCS GmbH.
- Multiwell-Analyzer, Version 1.8.6.0, Multi Channel Systems MCS GmbH.

### 2.3 Lactate- Dehydrogenase Assay

- CytoTox-ONE Homogenous Membrane Integrity Assay Kit (#G7891, Promega;  $-20\text{ }^\circ\text{C}$ ).
  - Substrate mix.
  - Assay buffer.
- Triton X-100 (10% in  $\text{H}_2\text{O}$ ), Sigma-Aldrich #T8787.
- CINDA (*see* Subheading 2.2.1).
- 96-Well plate compatible with fluorometer.
- Fluorescence plate reader with excitation 530–570 nm and emission 580–620 nm filter pair.

---

## 3 Methods

All experiments need to be performed under sterile conditions.

### 3.1 Neural Induction of hiPSCs into Human Induced Neural Progenitor Cells (hiNPC)

During embryogenesis the human central nervous system develops from the ectoderm, one of the three germ layers that compose the entire body. These complex procedures can now be taken into a dish due to the unique technique of stem cell differentiation. In vitro, pluripotent stem cells, such as hiPSCs, can be directed to the ectodermal lineage by using neural induction media (NIM). The NIM used in this protocol is based on dual SMAD inhibition, and contains the small molecules LDN-193189 and SB431542 [15]. These factors inhibit TGF- $\beta$  and SMAD signaling pathways and thereby prevent differentiation into non-neural ectodermal directions [41]. The neural induction is performed in Poly-HEMA-coated culture dishes to prevent cell adhesion to the dishes' surface and to ensure neurosphere formation. From day 7, 10 ng/mL FGF2 are added to the NIM. On day 21, the NPCs are

transferred to the NPM for further maintenance. With time, the neurospheres grow and need to be reduced in size by cutting into smaller pieces in order to avoid a necrotic sphere core (chopping; [42]). By using this method, neurospheres can be expanded and cultivated over several months. The number of possible passages depends on the cell line.

1. Add 1.5 mL Poly-HEMA solution to a 6 cm, or 3 mL to a 10 cm, culture dish and distribute the solution evenly across the surface. Let the solution evaporate overnight under sterile conditions or at least for 2 h (*see Note 5*).
2. The iPSC colonies are cultivated on Matrigel in a 6-well plate, with mTeSR1 medium. Assess the cell morphology under a microscope. If there are differentiated cells, mark the culture dish at the respective point and scratch off the cells with a pipette (*see Note 6*).
3. Add 10 $\mu$ M Y-27632 into the culture medium and swivel the plate in order to distribute it evenly.
4. Incubate the cells for 1 h at 37 °C and 5% CO<sub>2</sub>.
5. After the incubation, discard the medium and wash each well with 1 mL pre-warmed DPBS.
6. Add 1 mL NIM with 10 $\mu$ M Y-27632 to the culture and cut the iPSC colonies into pieces by rolling them with StemPro™ EZPassage™ Disposable Stem Cell Passaging Tool once from top to bottom and once from left to right (*see Note 7*).
7. Scrape the resulting cell-clusters off the plate using a cell lifter. Use a microscope to make sure that uncut colonies are not lifted from the edge of the well.
8. Transfer the scratched colonies of each two wells to one 6 cm Poly-HEMA-coated culture dish and add 5 mL NIM including 10 $\mu$ M Y-27632 to each dish to reach a final volume of 7 mL.
9. After 2 days, move the culture dish in small circles to collect the formed neurospheres in the middle of the dish and replace 3.5 mL culture medium with the same volume NIM, without Y-27632.
10. Place the dishes into the incubator and carefully move the dish six times horizontally left and right as well as back and forth to distribute the spheres evenly and to avoid clumping.
11. Replace half of the medium every other day by following instructions 9 and 10.
12. Starting from day 7, add 10 ng/mL FGF2 to the NIM.
13. On day 21, collect all neurospheres by gathering them in the middle of the dish and transfer them into a 10 cm Poly-HEMA-coated culture dish. Further cultivate them in 20 mL NPM with 20 ng/mL FGF2.

14. Replace half of the media with fresh NPM every other day, by following instructions 9 and 10.
15. Neurospheres with a diameter of 0.7 mm or above are mechanically passaged with a razor blade (chopped). This is necessary approximately every 7 days.
16. For chopping, use the McIlwan tissue chopper and attach a sterilized razor blade onto the chopping arm. Make sure the razor blade is positioned correctly and screwed on tightly (*see Note 8*).
17. Adjust the chop distance to 0.25 mm.
18. Transfer neurospheres from the culture dish to the lid of a sterile 6 cm culture dish, with less medium as possible. Remove the supernatant medium, to prevent moving of neurospheres during the process.
19. Place the lid in the holder of the tissue chopper, move it to the start position, and start the device, by pressing “reset”.
20. Stop the tissue chopper when the razor blade reached the end of the dish lid, rotate the lid 90°, and repeat **step 19**.
21. Resuspend the chopped neurospheres in 1 mL NPM by carefully pipetting up and down. Equally distribute the cell suspension into two to three new Poly-HEMA-coated culture dishes (Ø 10 cm), each with 20 mL NPM.
22. Cultivate the cells in an incubator at 37 °C and 5% CO<sub>2</sub>.

### **3.2 Recording Electrical Activity of Neural Networks with mwMEAs**

By plating the neurospheres as a monolayer onto an extracellular matrix, here PDL and laminin, and cultivating them in neural differentiation medium, they differentiate into an electrically active NN. Laminin is one of the major integrin interaction factors and, besides facilitating cell adherence, it supports growth, survival, and functional development in iPSC-based neural cultures in vitro [43]. The differentiation medium CINDA contains additional maturation supporting factors (**C**reatine, **I**nterferon- $\gamma$ , **N**eurotrophin-3, **D**ibutyl cAMP and **A**scorbic acid) that support neuronal maturation, synapse formation, and spontaneous NN activity [15]. This NN activity can be measured on MEAs, which simultaneously derive the membrane potential of numerous neurons via an electrode recording field. The here used 24-multiwell MEAs have an electrode field of 12 PEDOT-coated gold-electrodes plus four reference electrodes per well. Each electrode has a diameter of 30 $\mu$ m and an interelectrode distance of 300 $\mu$ m. The measured neuronal activity is detected and displayed as spikes and bursts, whereas each spike is derived from one action potential and several consecutive spikes are defined as one burst. Another measurable parameter is network bursts, which occur when the network matures over time and develops a synchronous bursting pattern.

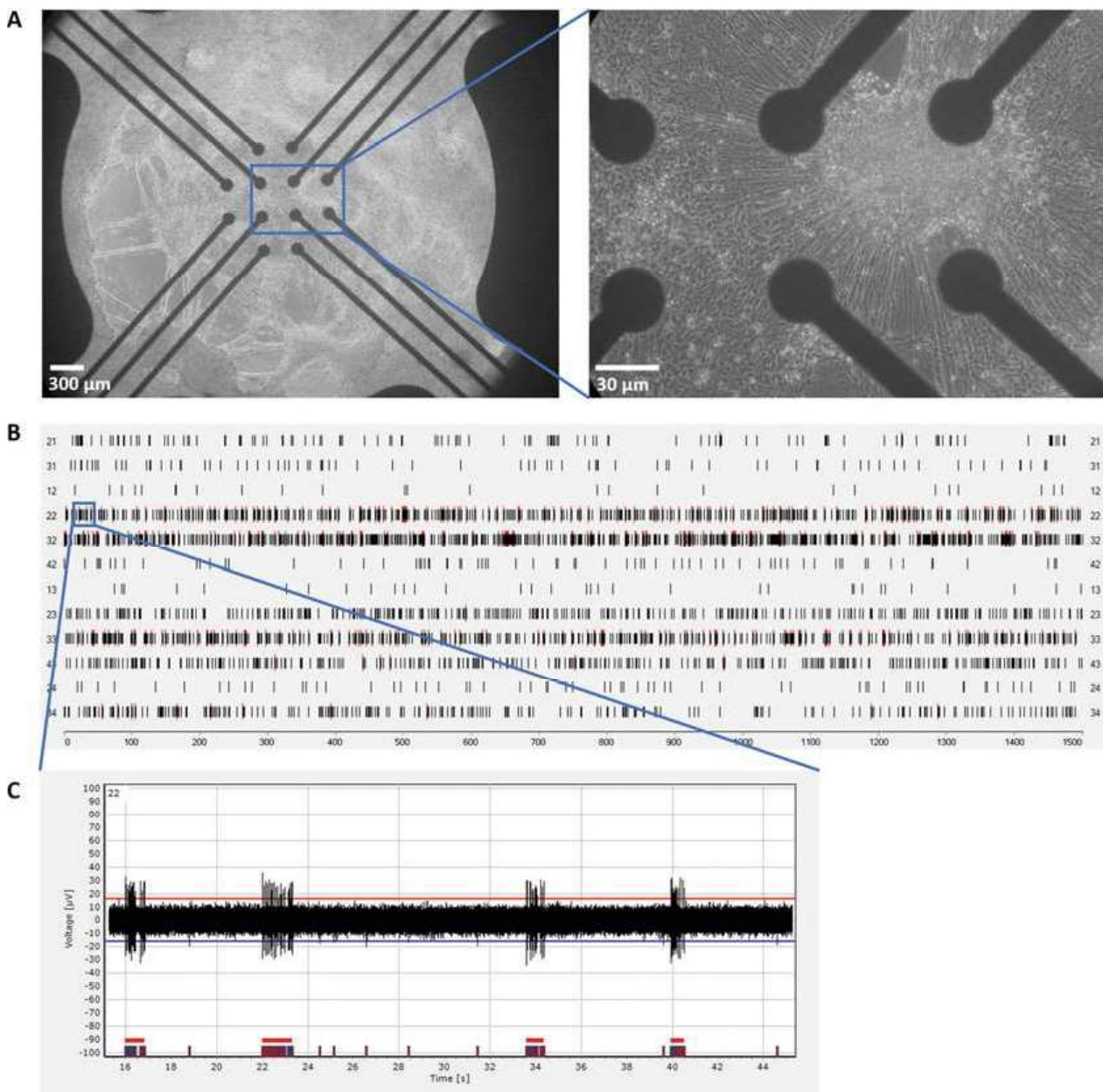


**Fig. 2** Measurement of electrical NN activity on mwMEA. (a) Representative phase-contrast images of a human NN, differentiated on mwMEA electrodes for 12 days. (b) SRP of one well of a 24-mwMEA, after 10 days of differentiation. Each vertical black line represents a spike and each horizontal red bar represents a burst. (c) Spike train of the blue marked position in the SRP

During the measurement, the signals are shown as spike raster plots (SRP) and spike trains (Figs. 2 and 3). By setting certain values and thresholds, which have to be adapted for each network, the sensitivity of the measurement can be adjusted and the background noise can be filtered. The measurement data give information about spike count, spike rate [Hz], burst count, mean burst duration [ $\mu$ s], mean burst spike count, percentage of spikes in a burst, mean interburst interval [ $\mu$ s], and number of active electrodes, as well as the same information about network bursts. The combined data set allows a good characterization of the network activity and

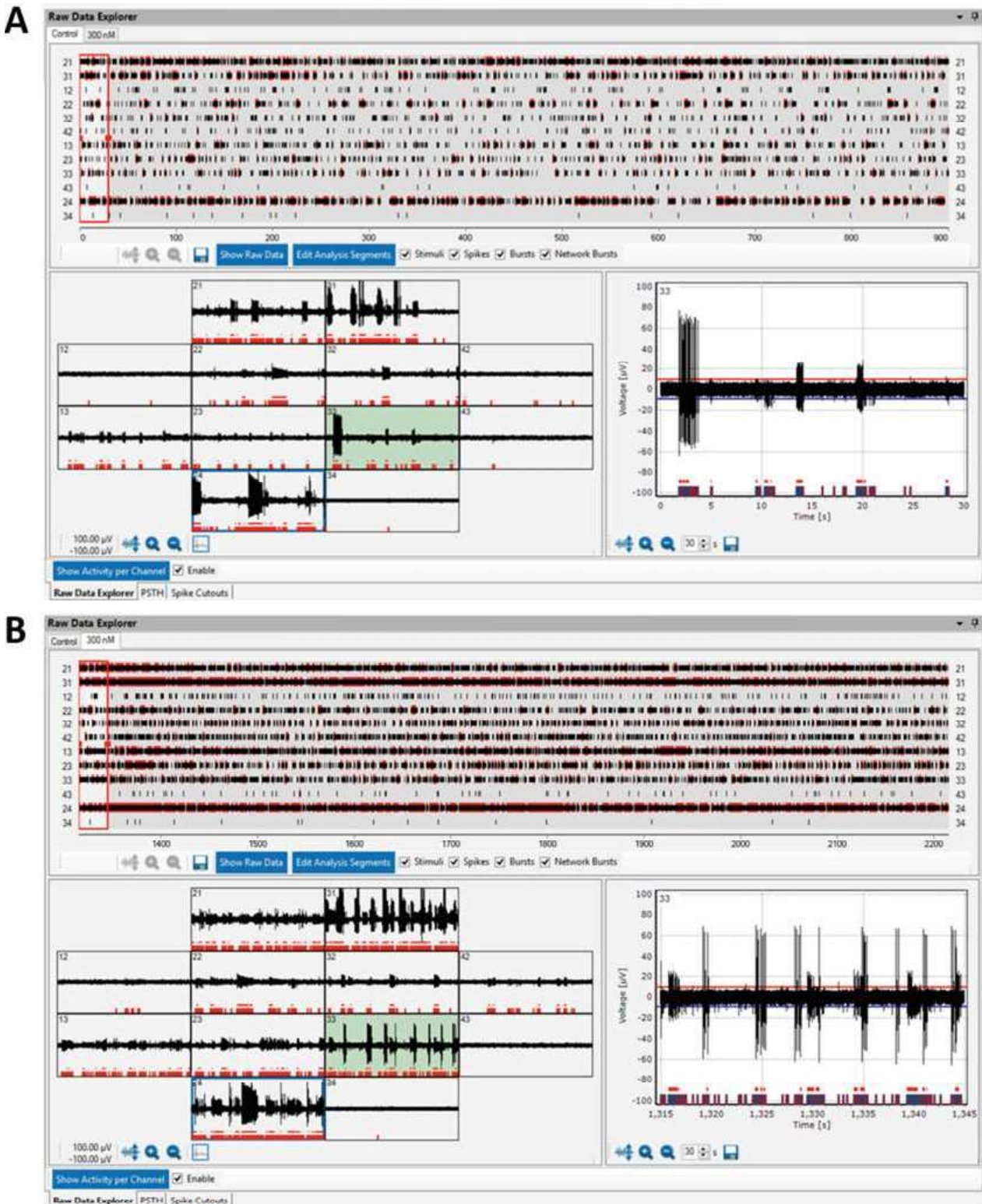


**Fig. 3** Neuronal network activity before and during treatment with domoic acid. Domoic acid binds to glutamate receptors with a higher affinity than glutamate itself. This results in an overreaction that can lead to excitotoxicity and finally to cell death. The images show representative software screen shots after 10 DIV of the **a**) baseline activity and **b**) the activity during the treatment with 300 nM domoic acid (after wash-in-phase of 5 min). Each vertical black line represents a spike and each horizontal red line represents a burst. Software: Multiwell-Analyzer, Version 1.8.6.0, Multi Channel Systems MCS GmbH

its response to neurotoxic substance exposure. In order to define a valid experiment, the two parameters minimum spike rate/electrode and number of active electrodes/well need to be monitored. The limit values for these parameters can vary depending on the cell line used.

### 3.2.1 Differentiation on PDL/Laminin-Coated 24-Multiwell MEAs

1. Dilute PDL in sterile ultrapure water to reach a final concentration of 100µg/mL and store working stocks at  $-20^{\circ}\text{C}$  until use. Prior to coating, thaw the PDL solution at  $37^{\circ}\text{C}$ .
2. Add 100µL PDL solution (100µg/mL) to each well of a 24-mwMEA plate and incubate at least for 1 h at  $37^{\circ}\text{C}$  or for 48 h at  $4^{\circ}\text{C}$ .
3. Thaw laminin in the fridge ( $4-8^{\circ}\text{C}$ ) to avoid gel formation and dilute the laminin with sterile ultrapure water 1:80 to obtain a final concentration of 12.5 ng/mL.
4. Aspirate the PDL solution and wash wells once with sterile ultrapure water.
5. Add 100µL laminin (12.5µg/mL) solution to each well and incubate at least for 1 h at  $37^{\circ}\text{C}$  (*see Note 9*).
6. Aspirate the laminin solution, wash the wells once with sterile ultrapure water, and directly use the coated plate.
7. Chop the neurospheres to a size of 0.1 mm (for details *see* Subheading 3.1, **step 16–21**).
8. Resuspend the cut spheres in 1 mL prewarmed CINDA.
9. Transfer 80µL of the cut spheres suspension into a Nageotte counting chamber and count the sphere parts. Dilute the cut spheres solution if necessary to reach a maximum of 4000 sphere parts/mL.
10. Collect 200 sphere parts in up to 100µL CINDA and carefully pipet them directly onto the electrodes of a mwMEA well. The solution should form a droplet on top of the electrodes. Allow the spheres to settle and adhere to the well surface, by incubating the droplet for 2 h at  $37^{\circ}\text{C}$  and 5%  $\text{CO}_2$ .
11. Add 1 mL CINDA to each well and incubate the plate at  $37^{\circ}\text{C}$  and 5%  $\text{CO}_2$ .
12. Feed the cells once a week, by replacing half of the medium in each well.
13. From day 7, measure the electrical activity twice a week as long as the neurons are electrically active (*see Note 10*). Preheat the mwMEA headstage to  $37^{\circ}\text{C}$  and gas the device with carbogen, before adding the mwMEA. For parameter settings *see* Table 1.
14. Let the mwMEA acclimatize for 15 min, before starting the 15 min baseline recording.

**Table 1**  
**Parameter settings for mwMEA measurement**

Parameter	Setting
Sampling rate	20,000 Hz
Low-pass filter type	Butterworth
Low-pass-filter order	4
Low-pass filter cutoff frequency	3,500 Hz
High-pass filter type	Butterworth
High-pass-filter order	2
High-pass filter cutoff frequency	300 Hz

15. For acute toxicity measurements, stick to the following time schedule:
  - Baseline measurement: 15 min recording.
  - Wash-in-phase: add the substance and equilibrate for 5 min.
  - Treatment: 15 min recording.
  - Cytotoxicity analysis: remove the medium and transfer it into a new 24-well plate for cytotoxicity analysis (*see* Sub-heading 3.3 for further details).
  - Wash-out-phase: wash each well twice with CINDA to wash out the substance.
16. Further cultivate the cells in fresh CINDA medium at 37 °C and 5% CO<sub>2</sub>.

### 3.2.2 Analysis of mwMEA Recordings

1. Load the .mwr file, which is automatically generated during recording, into the Multiwell-Analyzer Software.
2. Set the “Spike Detector Configuration” to an automatic threshold estimation of 500 ms baseline duration and rising/falling edge of 5× standard deviation (*see* **Note 11**).
3. For the “Burst Detector Configuration” choose the following settings (*see* **Note 12**):
  - Max. Interval to start burst: 100 ms.
  - Max. Interval to end burst: 100 ms.
  - Min. Interval between bursts: 20 ms.
  - Min. Duration of burst: 10 ms.
  - Min. Spike count in burst: 3.
4. To select active wells only, set the “Channel Selection Configuration” to a minimum of 5 spikes/minute (=0.083 Hz) for

each channel and a minimum of 3 active channels for each well [21].

5. Run the analysis.
6. Check each channel for artifacts and defective electrodes (*see Note 13*).
7. Export the analysis of all intact electrodes without artifacts as a .csv file.
8. Open the .csv file and copy the data into a software for statistical analysis and data plotting.

### **3.3 Assessment of Cytotoxicity via the Lactate-Dehydrogenase Assay**

To ensure that the adverse effects are due to neurotoxicity and not cytotoxicity, we perform the Lactate-Dehydrogenase (LDH) Assay. The substrate mix contains lactate, NAD<sup>+</sup>, and resazurin. If the cell membrane is damaged, the cytosolic lactate dehydrogenase enzyme is released into the cell culture medium and can be quantified by subsequent enzymatic reactions. LDH first catalyzes the conversion of lactate to pyruvate, with a simultaneous reduction of NAD<sup>+</sup> to NADH. By oxidation of NADH to NAD<sup>+</sup>, the enzyme diaphorase reduces resazurin to resorufin, which can be measured with a fluorometer (excitation: 540 nm; emission: 590 nm). The amount of produced resorufin is thus proportional to the amount of released LDH. Cells with an intact membrane do not release LDH and therefore no fluorescence is measurable in the culture medium. Two controls are required to perform this assay: a 100% cell lysis control (LC) and a background control (BG; culture medium without cells). By lysing the cells of the LC with Triton X-100, the maximum amount of LDH present is determined.

1. Prepare the CytoTox-ONE Reagent as indicated in the supplier's manual and protect it from light (*see Note 14*).
2. For the LC, add 10% (v/v) Triton X-100 solution 1:5 to the desired number of wells (final concentration 2%).
3. Preincubate the LC for 30 min at 37 °C and 5% CO<sub>2</sub>.
4. Transfer the complete medium of each well into a new 24-well plate.
5. Transfer 50µL medium of each well of interest of the 24-well plate into a 96-well plate, including the LC and the BG.
6. Add 50µL CytoTox-ONE Reagent to each of the wells.
7. Incubate at room temperature for 2 h, protected from light.
8. Measure the fluorescence of the samples at an excitation wavelength of 540 nm and an emission wavelength of 590 nm in a plate reader (*see Note 15*).
9. Calculate the mean of all technical replicate measurements and normalize data by subtracting the mean of the BG from the mean of the different conditions.

10. Calculate the values of each condition as percent of the mean of the LC.
11. The results of at least three independent experiments are pooled, and mean, standard deviation (SD), and standard error of the mean (SEM) are calculated. Data analyses, statistical analyses, and data plotting are performed in GraphPad Prism, using OneWay ANOVA and Bonferroni's post hoc test.

---

## 4 Notes

1. The Poly-HEMA solution is stable for up to 2 months at 4 °C.
2. When using a different hiPSC line, the protocol may have to be adapted.
3. Dibutyl cAMP is sensitive to light and moisture. The CINDA medium should therefore not be exposed to light for more than 1 h.
4. The product concentration depends on the batch number and has to be adjusted to 1 mg/mL with autoclaved ultrapure water.
5. Poly-HEMA-coated dishes can be used for up to 3 months if stored sealed at room temperature and in the dark.
6. iPSCs are small and round in shape and have a high nucleus-to-cytoplasm ratio, with prominent nucleoli. Differentiating cells have a lower nucleus-to-cytoplasm ratio and the morphology differs visibly from the original round shape.
7. We banked our hiPSCs so that we can start each neural induction with a similar passage number. We use the cells starting from passage 3 post-thawing at the earliest and up to passage 10 post-thawing at the latest. This must be adapted for other cell lines.
8. Each side of a razor blade can be used three times.
9. PDL/Laminin-coated plates can be stored in the refrigerator (4–8 °C) for a maximum of 2 weeks prior to use.
10. During cell differentiation, the burst behavior changes and begins to synchronize as the network matures. For this reason, exposure to the same substance in different experiments should always be carried out in the same time frame.
11. This eliminates the detected background signals.
12. These settings need to be adapted to the specific cell signals and vary depending on the cell line.
13. An artifact can be caused by external influences and is visible as an exactly simultaneous signals on all electrodes. Furthermore,

artifacts and defective electrodes can be excluded by observing the spike signal that should resemble a waveform.

14. Aliquot unused CytoTox-ONE reagent and protect the reagent from light. Aliquots should be labeled with preparation date and reagent number and can be stored tightly capped at  $-20\text{ }^{\circ}\text{C}$  for 6–8 weeks.
15. If the plate reader measures from above, remove the lid of the plate before measurement.

## References

1. Costa LG, Giordano G, Guizzetti M, Vitalone A (2008) Neurotoxicity of pesticides: a brief review. *Front Biosci* 13:1240–1249. <https://doi.org/10.2741/2758>
2. Massaro EJ (2002) *Handbook of neurotoxicology*. Humana Press, Totowa, NJ
3. OECD guideline for the testing of Chemicals (1997) Test no. 424: neurotoxicity study in rodents. In: *OECD guideline for the testing of chemicals*. OECD, Paris, pp 1–15
4. Forum RA (1998) *Guidelines for neurotoxicity risk assessment*
5. Bal-Price AK, Suñol C, Weiss DG et al (2008) Application of in vitro neurotoxicity testing for regulatory purposes: symposium III summary and research needs. *Neurotoxicology* 29:520–531. <https://doi.org/10.1016/j.neuro.2008.02.008>
6. Leist M, Hartung T (2013) Inflammatory findings on species extrapolations: humans are definitely no 70-kg mice. *Arch Toxicol* 87:563–567
7. Borrell V, Götz M (2014) Role of radial glial cells in cerebral cortex folding. *Curr Opin Neurobiol* 27:39–46
8. Toutain P-L, Ferran A, Bousquet-Melou A (2010) Species differences in pharmacokinetics and pharmacodynamics. In: *Comparative and Veterinary Pharmacology, Handbook of Experimental Pharmacology*, Springer, pp 19–48. [https://doi.org/10.1007/978-3-642-10324-7\\_2](https://doi.org/10.1007/978-3-642-10324-7_2)
9. Masjosthusmann S, Barenys M, El-Gamal M et al (2018) Literature review and appraisal on alternative neurotoxicity testing methods. *EFSA Support Publ* 15:1–108. <https://doi.org/10.2903/sp.efsa.2018.en-1410>
10. Takahashi K, Tanabe K, Ohnuki M et al (2007) Induction of pluripotent stem cells from adult human fibroblasts by defined factors. *Cell* 131:861–872. <https://doi.org/10.1016/j.cell.2007.11.019>
11. Pei Y, Peng J, Behl M et al (2016) Comparative neurotoxicity screening in human iPSC-derived neural stem cells, neurons and astrocytes. *Brain Res* 1638:57–73. <https://doi.org/10.1016/j.brainres.2015.07.048>
12. Barenys M, Fritsche E (2018) A historical perspective on the use of stem/progenitor cell-based in vitro methods for neurodevelopmental toxicity testing. *Toxicol Sci* 165:10–13. <https://doi.org/10.1093/toxsci/kfy170>
13. de Groot MWGDM, Westerink RHS, Dingemans MML (2013) Don't judge a neuron only by its cover: neuronal function in in vitro developmental neurotoxicity testing. *Toxicol Sci* 132:1–7. <https://doi.org/10.1093/toxsci/kfs269>
14. Tukker AM, De Groot MWGDM, Wijnolts FMJ et al (2016) Research article is the time right for in vitro neurotoxicity testing using human iPSC-derived neurons? *ALTEX* 33:261–271. <https://doi.org/10.14573/altex.1510091>
15. Nimtz L, Hartmann J, Tigges J et al (2020) Characterization and application of electrically active neuronal networks established from human induced pluripotent stem cell-derived neural progenitor cells for neurotoxicity evaluation. *Stem Cell Res* 45:101761. <https://doi.org/10.1016/j.scr.2020.101761>
16. Hofrichter M, Nimtz L, Tigges J et al (2017) Comparative performance analysis of human iPSC-derived and primary neural progenitor cells (NPC) grown as neurospheres in vitro. *Stem Cell Res* 25:72–82. <https://doi.org/10.1016/j.scr.2017.10.013>
17. Izsak J, Seth H, Andersson M et al (2019) Robust generation of person-specific, synchronously active neuronal networks using purely isogenic human iPSC-3D neural aggregate cultures. *Front Neurosci* 13. <https://doi.org/10.3389/fnins.2019.00351>

18. Hyvärinen T, Hyysalo A, Kapucu FE et al (2019) Functional characterization of human pluripotent stem cell-derived cortical networks differentiated on laminin-521 substrate: comparison to rat cortical cultures. *Sci Rep* 9:17125. <https://doi.org/10.1038/s41598-019-53647-8>
19. Pamies D, Barreras P, Block K et al (2017) A human brain microphysiological system derived from induced pluripotent stem cells to study neurological diseases and toxicity. *ALTEX* 34:362–376. <https://doi.org/10.14573/altext.1609122>
20. Johnstone AFM, Gross GW, Weiss DG et al (2010) Microelectrode arrays: a physiologically based neurotoxicity testing platform for the 21st century. *Neurotoxicology* 31:331–350
21. McConnell ER, McClain MA, Ross J et al (2012) Evaluation of multi-well microelectrode arrays for neurotoxicity screening using a chemical training set. *Neurotoxicology* 33:1048–1057. <https://doi.org/10.1016/j.neuro.2012.05.001>
22. Hogberg HT, Sobanski T, Novellino A et al (2011) Application of micro-electrode arrays (MEAs) as an emerging technology for developmental neurotoxicity: evaluation of domoic acid-induced effects in primary cultures of rat cortical neurons. *Neurotoxicology* 32:158–168. <https://doi.org/10.1016/j.neuro.2010.10.007>
23. Mack CM, Lin BJ, Turner JD et al (2014) Burst and principal components analyses of MEA data for 16 chemicals describe at least three effects classes. *Neurotoxicology* 40:75–85
24. Shafer TJ, Brown JP, Lynch B et al (2019) Evaluation of chemical effects on network formation in cortical neurons grown on microelectrode arrays. *Toxicol Sci* 169:436–455. <https://doi.org/10.1093/toxsci/kfz052>
25. Alloisio S, Nobile M, Novellino A (2015) Multiparametric characterisation of neuronal network activity for in vitro agrochemical neurotoxicity assessment. *Neurotoxicology* 48:152–165. <https://doi.org/10.1016/j.neuro.2015.03.013>
26. Shafer TJ, Rijal SO, Gross GW (2008) Complete inhibition of spontaneous activity in neuronal networks in vitro by deltamethrin and permethrin. *Neurotoxicology* 29:203–212. <https://doi.org/10.1016/j.neuro.2008.01.002>
27. Defranchi E, Novellino A, Whelan M et al (2011) Feasibility assessment of microelectrode chip assay as a method of detecting neurotoxicity in vitro. *Front Neuroeng* 4:1–12. <https://doi.org/10.3389/fneng.2011.00006>
28. Valdivia P, Martin M, LeFew WR et al (2014) Multi-well microelectrode array recordings detect neuroactivity of ToxCast compounds. *Neurotoxicology* 44:204–217. <https://doi.org/10.1016/j.neuro.2014.06.012>
29. Wallace K, Strickland JD, Valdivia P et al (2015) A multiplexed assay for determination of neurotoxicant effects on spontaneous network activity and viability from microelectrode arrays. *Neurotoxicology* 49:79–85. <https://doi.org/10.1016/j.neuro.2015.05.007>
30. Novellino A, Scelfo B, Palosaari T et al (2011) Development of micro-electrode array based tests for neurotoxicity: assessment of Interlaboratory reproducibility with neuroactive chemicals. *Front Neuroeng* 4:1–14. <https://doi.org/10.3389/fneng.2011.00004>
31. Gassmann K, Abel J, Bothe H et al (2010) Species-specific differential ahr expression protects human neural progenitor cells against developmental neurotoxicity of PAHs. *Environ Health Perspect* 118:1571–1577. <https://doi.org/10.1289/ehp.0901545>
32. Dach K, Bendt F, Huebenthal U et al (2017) BDE-99 impairs differentiation of human and mouse NPCs into the oligodendroglial lineage by species-specific modes of action. *Sci Rep* 7:1–11. <https://doi.org/10.1038/srep44861>
33. Masjosthusmann S, Becker D, Petzuch B et al (2018) A transcriptome comparison of time-matched developing human, mouse and rat neural progenitor cells reveals human uniqueness. *Toxicol Appl Pharmacol* 354:40–55. <https://doi.org/10.1016/j.taap.2018.05.009>
34. Oberheim NA, Takano T, Han X et al (2009) Uniquely hominid features of adult human astrocytes. *J Neurosci* 29:3276–3287. <https://doi.org/10.1523/JNEUROSCI.4707-08.2009>
35. Perreault M, Feng G, Will S et al (2013) Activation of TrkB with TAM-163 results in opposite effects on body weight in rodents and non-human primates. *PLoS One* 8:e62616. <https://doi.org/10.1371/journal.pone.0062616>
36. Tukker AM, Wijnolts FMJ, de Groot A, Westerink RHS (2018) Human iPSC-derived neuronal models for in vitro neurotoxicity assessment. *Neurotoxicology* 67:215–225. <https://doi.org/10.1016/j.neuro.2018.06.007>
37. Tukker AM, Wijnolts FMJ, de Groot A, Westerink RHS (2020) Applicability of hiPSC-derived neuronal co-cultures and rodent primary cortical cultures for in vitro seizure liability assessment. *Toxicol Sci*. <https://doi.org/10.1093/toxsci/kfaa136>

38. Tukker AM, Bouwman LMS, van Kleef RGDM et al (2020) Perfluorooctane sulfonate (PFOS) and perfluorooctanoate (PFOA) acutely affect human  $\alpha 1\beta 2\gamma 2L$  GABAA receptor and spontaneous neuronal network function in vitro. *Sci Rep* 10. <https://doi.org/10.1038/s41598-020-62152-2>
39. Ylä-Outinen L, Heikkilä J, Skottman H et al (2010) Human cell-based micro electrode array platform for studying neurotoxicity. *Front Neuroeng* 3. <https://doi.org/10.3389/fneng.2010.00111>
40. Odawara A, Matsuda N, Ishibashi Y et al (2018) Toxicological evaluation of convulsant and anticonvulsant drugs in human induced pluripotent stem cell-derived cortical neuronal networks using an MEA system. *Sci Rep* 8:10416. <https://doi.org/10.1038/s41598-018-28835-7>
41. Qi Y, Zhang XJ, Renier N et al (2017) Combined small-molecule inhibition accelerates the derivation of functional cortical neurons from human pluripotent stem cells. *Nat Biotechnol* 35:154–163. <https://doi.org/10.1038/nbt.3777>
42. Svendsen CN, Ter Borg MG, Armstrong RJE et al (1998) A new method for the rapid and long term growth of human neural precursor cells. *J Neurosci Methods* 85:141–152. [https://doi.org/10.1016/S0165-0270\(98\)00126-5](https://doi.org/10.1016/S0165-0270(98)00126-5)
43. Farrukh A, Zhao S, del Campo A (2018) Microenvironments designed to support growth and function of neuronal cells. *Front Mater* 5:1–22. <https://doi.org/10.3389/fmats.2018.00062>



## 2.6 Academic Application of Good Cell Culture Practice for Induced Pluripotent Stem Cells

*Julia Tigges, Kevin Bielec, Gabriele Brockerhoff, Barbara Hildebrandt, Ulrike Hübenthal, Julia Kapr, Katharina Koch, Nadine Teichweyde, Dagmar Wieczorek, Andrea Rossi, Ellen Fritsche*

Human induced pluripotent stem cells (hiPSC) are a promising tool for replacing animal-based experiments. To warrant data reproducibility, quality-controlled research material is recommended. While the need for global harmonization of quality standards for stem cell banking centers, commercial providers, pre-clinical and clinical use of cells is well documented, there are no recommendations available for quality control of hiPSC in an academic research environment to date. To fill this gap, we here give an example of a quality-controlled, two-tiered banking process producing a fully characterized master cell bank (MCB) and partially characterized respective working cell banks (WCB). Characterization includes the study of morphology, mycoplasma contamination, cell line identity, karyotype stability, cell antigen expression and viability, gene expression, pluripotency, and post-thaw recovery. Costs of these procedures are calculated. We present the results of the proposed testing panel of two hiPSC MCBs and show that both fulfil the defined specifications regarding the above-mentioned characterization assays during and upon banking. In conclusion, we propose a panel of eight assays, which are practical and useful for an academic research laboratory working with hiPSCs. Meeting these proposed specifications ensures the quality of pluripotent stem cells throughout diverse experiments at moderate costs.

Journal:	Altex
Impact factor:	6.043 (2020)
Contribution to the publication:	5%
	Imaging and Image Assembly for Figure 6
Type of authorship:	Co-author
Status of publication:	Published (06 May 2021)



## Research Article

# Academic Application of Good Cell Culture Practice for Induced Pluripotent Stem Cells

Julia Tigges<sup>1</sup>, Kevin Bielec<sup>1</sup>, Gabriele Brockerhoff<sup>1</sup>, Barbara Hildebrandt<sup>2</sup>, Ulrike Hübenthal<sup>1</sup>, Julia Kapr<sup>1</sup>, Katharina Koch<sup>1</sup>, Nadine Teichweyde<sup>1</sup>, Dagmar Wiczorek<sup>2</sup>, Andrea Rossi<sup>1</sup> and Ellen Fritsche<sup>1,3</sup>

<sup>1</sup>IUF-Leibniz Research Institute for Environmental Medicine, Duesseldorf, Germany; <sup>2</sup>Institute of Human Genetics, Medical Faculty, Heinrich-Heine-University, Duesseldorf, Germany; <sup>3</sup>Medical Faculty, Heinrich-Heine-University, Duesseldorf, Germany

### Abstract

Human induced pluripotent stem cells (hiPSC) are a promising tool for replacing animal-based experiments. To warrant data reproducibility, quality-controlled research material is recommended. While the need for global harmonization of quality standards for stem cell banking centers, commercial providers, pre-clinical and clinical use of cells is well documented, there are no recommendations available for quality control of hiPSC in an academic research environment to date. To fill this gap, we here give an example of a quality-controlled, two-tiered banking process producing a fully characterized master cell bank (MCB) and partially characterized respective working cell banks (WCB). Characterization includes the study of morphology, mycoplasma contamination, cell line identity, karyotype stability, cell antigen expression and viability, gene expression, pluripotency, and post-thaw recovery. Costs of these procedures are calculated. We present the results of the proposed testing panel of two hiPSC MCBs and show that both fulfil the defined specifications regarding the above-mentioned characterization assays during and upon banking. In conclusion, we propose a panel of eight assays, which are practical and useful for an academic research laboratory working with hiPSCs. Meeting these proposed specifications ensures the quality of pluripotent stem cells throughout diverse experiments at moderate costs.

## 1 Introduction

The development of human induced pluripotent stem cells (hiPSCs; Takahashi et al., 2007) bears immense opportunities for basic research, toxicological screening efforts, and next generation human safety assessment (Pistollato et al., 2012; Fritsche et al., 2020). Human iPSCs have distinct advantages compared to human embryonic stem cells (hESC), including similar self-renewal and pluripotency capacity, while raising fewer ethical concerns regarding their derivation process (Fritsche et al., 2020). Especially during the last decade, the use of hiPSCs has become increasingly popular in basic research (Liu et al., 2020), which results in a need for standardized technologies for hiPSC applications to enable the comparison between various experiments and researchers from different laboratories (Maddah et al., 2014).

According to a *Nature* survey of over 1,500 researchers in 2016, between 70% and 50% failed to reproduce another sci-

entist's or even their own experiments, respectively (Baker and Penny, 2016; Miyakawa, 2020). Among the factors contributing to this reproducibility crisis are selective reporting, low statistical power, or poor analysis and experimental design (Baker and Penny, 2016). In addition, poor starting material – especially for hiPSC research – can be a severe source of irreproducibility (Stacey et al., 2013; Pamies et al., 2017). Therefore, already in 2013 “an urgent need” to establish routine screening methods for the characterization of quality-controlled stem cells was (Stacey et al., 2013; Crook et al., 2017).

While there is guidance available for Good *In Vitro* Methods Practices in general (OECD, 2018) or stem cell-based Good Cell Culture Practice (Pamies et al., 2017, 2018, 2020), giving detailed insights into the broad subject of quality assurance (QA) and quality control (QC) of *in vitro* (stem cell-based) methods, these leave the average academic researcher with a plethora of QC assays, discussing pros and cons that might or

Received January 22, 2021; Accepted April 29, 2021;  
Epub April 29, 2021; © The Authors, 2021.

ALTEX 38(4), 595-614. doi:10.14573/altex.2101221

Correspondence: Ellen Fritsche, PhD  
IUF – Leibniz Research Institute for Environmental Medicine  
Auf'm Hennekamp 50  
40225 Duesseldorf, Germany  
(Ellen.Fritsche@IUF-duesseldorf.de)

This is an Open Access article distributed under the terms of the Creative Commons Attribution 4.0 International license (<http://creativecommons.org/licenses/by/4.0/>), which permits unrestricted use, distribution and reproduction in any medium, provided the original work is appropriately cited.



might not be of relevance to their needs. More specific guidelines exist that address the need for global harmonization of quality standards for stem cell banking centers and commercial providers (ISCBI, 2009; Ntai et al., 2017; Pamies et al., 2017) or for future pre-clinical and clinical use of cells (McNutt, 2014; Baghbaderani et al., 2015; Kim et al., 2017, 2019; Abbot et al., 2018; Sullivan et al., 2018). But to date no “hands on” guidelines are available for cell culture, banking and characterization of hiPSC that have been accessed from external sources such as commercial vendors or iPSC biobanks for use in an academic basic research environment (Li et al., 2015; Baker, 2016). It is certainly not feasible for hypothesis-driven academic research to perform the QC requirements of legal authorities, but undoubtedly also academic research from applying some of the QC concepts developed for regulatory purposes (Dekant, 2016).

Uncertainties in the choice of QC procedures and their standardization as well as *prima facie* fears of high costs and demanding labor contribute to the fact that, despite their high importance for hiPSC research, QC assays are rarely standardized in academic laboratories (Lenz et al., 2015; Suter-Dick et al., 2015; Scudellari, 2016). However, two arguments clearly support the implementation of QC procedures into academic research: (i) costs for QC are negligible compared to the and reputational burden that might be incurred when years of research are in vain due to non-reproducibility of data (Suter-Dick et al., 2015) and (ii) the societal responsibility based on the public’s investment into research (Munafò et al., 2017) – not to mention the individual researcher’s satisfaction gained from reproducible experiments.

The United States National Institutes of Health (NIH) already recognized the issue of reproducibility in (academic) cell culture studies in 2015 (NIH, 2015). Aspects as crucial for quality assurance were (hiPSC) cell line identity, genomic stability, pluripotency, and residual reprogramming factors. Implementing routine tests for such QC parameters into the stem cell community is facing a lack of consensus about standards, policies and practices, yet is necessary to ensure the highest quality and uniformity of stem cell lines (Yaffe et al., 2016).

We tackled this challenge by proposing a two-tiered hiPSC banking approach as recommended by the International Stem Cell Banking Initiative (ISCBI, 2009) and others (Coecke et al., 2005; Pistollato et al., 2012). This approach combines easy to apply characterization assays and QC release criteria for an hiPSC master cell bank (MCB) and a shortened testing scheme for second-tiered working cell banks (WCB). This two-tiered scheme of culturing, banking, and testing will ensure consistent quality and performance of hiPSCs employed for basic research (Fig. 1). We show that a selection of assays for hiPSC character-

ization (Adler et al., 2007; Pistollato et al., 2012) is feasible, and affordable to achieve reproducible cellular models in an academic setting that can subsequently serve as the basis for further test development.

## 2 Materials and methods

Cell culture and characterization assays were performed according to detailed standard operation procedures (SOPs) developed and implemented within our laboratory.

### 2.1 Cell culture

#### 2.1.1 Cell lines

One vial of the hiPSC line IMR90-C4 was purchased (#iPS(IMR)90-4-DL-01, WiCell, Madison, Wisconsin, USA), and the knock-in IMR90-C4 *ACTB-2A-LifeAct-eGFP* line (DU22; short *Life-Act-eGFP*) was generated using CRISPR/Cas9 (Rossi et al., unpublished). IMR90-C4 were cultivated on laminin (LN) 521-coated 6-well plates (see 2.1.1.1) in iPS-Brew medium (see 2.1.1.2) except for assay 5 (cell antigen expression), for which the cells were transitioned to Matrigel (MG) and mTeSR (see 2.1.2.4). *Life-Act-eGFP* were cultivated on MG-coated 6-well plates (see 2.1.1.1) in mTeSR1 medium (see 2.1.1.2).

##### 2.1.1.1 Coating of plates

LN521: One vial of 5 mL LN521 (#LN521-05; BioLamina AB, Sweden) was slowly thawed at 4°C for approx. 45 min (solution should be transparent and clear without ice inside), aliquoted, and stored at -20°C until further use. Coating: LN521 stock solution was thawed at 4°C as described above and diluted 1:20 in PBS<sup>(+/+)</sup> by pipetting LN521/PBS solution up and down 5 times. 1 mL of this working solution (resulting in 0.5 µg/cm<sup>2</sup>) was added per 6-well plate well, and it was ensured that the entire well surface was covered. Cell culture plates were sealed using <sup>®</sup> to prevent evaporation and contamination and incubated at 4°C overnight. Coated plates can be used for up to 4 weeks. When plates were needed to seed cells, they were equilibrated at RT for at least 15 min. The remaining LN521/PBS solution was aspirated and directly replaced with 2 mL of fresh hiPSC medium before cells were plated (see 2.1.2.3).

MG: One vial of MG (#356231; Corning, USA; alternatively, #354277 can be used) was thawed overnight on ice at 4°C, and 1000 µL pipette tips were precooled at 4°C overnight. Once MG was thawed, it was swirled to ensure that the material was evenly dispersed. MG was kept on ice during the whole procedure described and diluted 1:1

#### Abbreviations

AB, antibody; aCGH, array comparative genomic hybridization; AFP, α-feto protein; D, day; d.o.p., depending on provider; EB, embryoid body; FISH, fluorescent *in situ* hybridization; FMO, fluorescence minus one; Fvs, fixable viability stain; hESC, human embryonic stem cells; hiPSC, human induced pluripotent stem cells; hPSC, human pluripotent stem cells; ISCBI, International Stem Cell Banking Initiative; kbs, kilobase pairs; LN, laminin; MCB, master cell bank; MG, Matrigel; N<sub>2</sub>, liquid nitrogen; n.a.c., no additional costs; NIH, National Institutes of Health; NS, novelty score; P, passage; PBS, phosphate-buffered saline; Pen/Strep, penicillin/streptomycin; PS, pluripotency score; p.t., post thawing; QA, quality assurance; QC, quality control; RT, room temperature; SMA, smooth muscle actin; SNP, single-nucleotide polymorphism; SOP, standard operation procedure; STR, short tandem repeat; TUBB3, β(III) tubulin; WCB, working cell bank

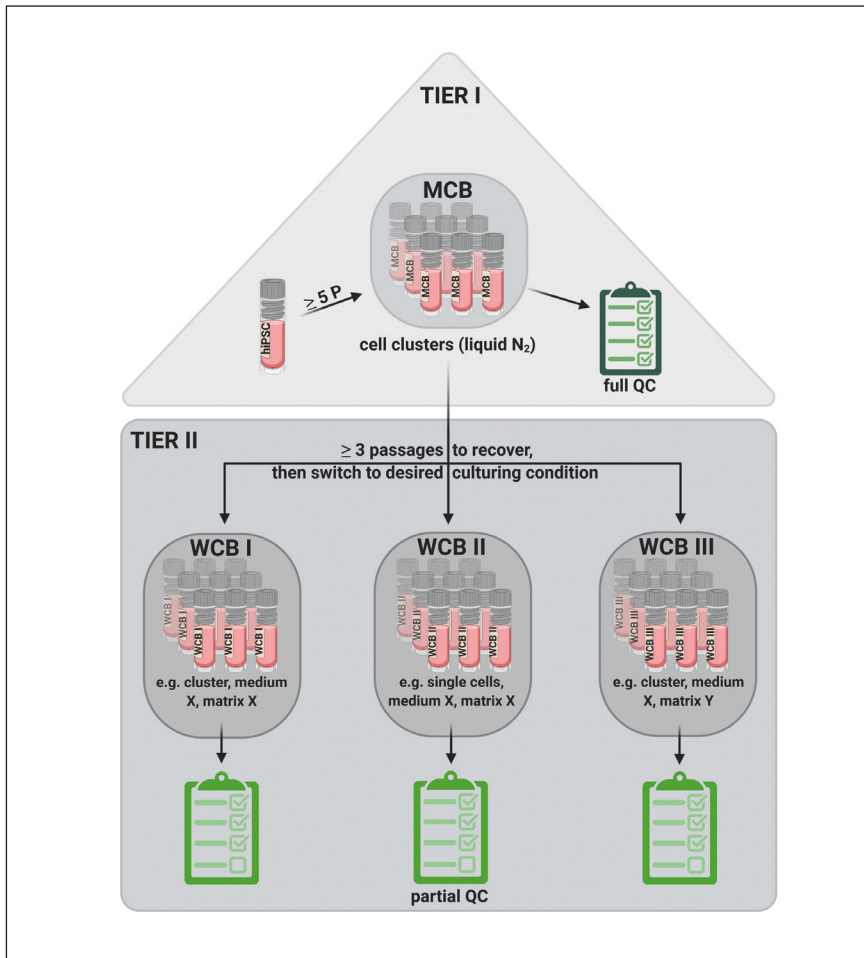


**Fig. 1: Schematic illustration of the proposed two-tiered banking process**

In tier I, a vial of hiPSC is thawed, cultivated, and expanded for at least 5 passages (P), and a Master Cell Bank (MCB) is prepared and stored in the vapor phase of liquid nitrogen (N<sub>2</sub>). Full quality control (QC) of cells including all 8 proposed assays (see Tab. 4) must be performed at the point of freezing to ensure the quality of the cells at the time of freezing. In tier II, a vial of the MCB is thawed and cultivated for at least 3 passages under the respective conditions. Then cells are switched to desired culturing conditions, expanded, and Working Cell Banks (WCBs) are frozen in vapor phase of N<sub>2</sub>. One WCB is generated for each culturing condition needed for the respective project for which the cells are designated (e.g., single cells vs. clusters, different media, different matrices). Here only partial QC is performed.

with cold KnockOut™ DMEM (#10829018; Thermo Fisher USA). A precooled pipette tip was used to gently pipette the MG and ensure homogeneity. 0.5 mL aliquots of diluted MG were prepared using precooled pipette tips (tips need to be changed every time MG starts to clog at the end of the tip). MG aliquots were stored at -20°C until further use. Coating: For coating of 6-well plates, one MG aliquot was placed into a class II biological safety cabinet, and 1 mL cold KnockOut™ DMEM medium was added on top of the still frozen MG and mixed by shaking and inverting of the tube. 13.5 mL KnockOut™ DMEM were added using a 10 mL serological pipette, and the solution was mixed by pipetting up and down (trying to avoid air bubbles and ensuring that no pellets were left inside the tube). Then 1 mL of this working solution was added per 6-well plate well, and it was ensured that the entire well surface was covered (one aliquot should yield 14 wells). Cell culture plates were sealed using <sup>®</sup> to prevent evaporation and contamination and were incubated at RT for 1 h. After this, the coated plates were stored at 4°C and could be used for up to 2 weeks. When plates were needed to seed cells, they were equilibrated at RT for at least 15 min.

Then the MG solution was removed, and 1 mL KnockOut™ DMEM was added to each coated well for washing. KnockOut™ DMEM was aspirated and directly replaced by 2 mL of fresh medium before cells were plated.

#### 2.1.1.2 Cell culture media

StemMACS™ iPS-Brew XF medium (iPSC-Brew; #130-104-368; Miltenyi Biotech, Bergisch Gladbach, Germany): For iPS-Brew medium preparation, the 10 mL vial of iPS-Brew 50x supplement and 5 mL of penicillin/streptomycin (Pen/Strep; #P06-07100; PAN Biotech, Aidenbach, Germany) were thawed at 4°C for approx. 2 h before combining them with one 500 mL bottle of iPS-Brew basal medium. Medium was mixed by shaking, aliquoted into labelled (name of medium, volume, expiration date and date of aliquoting) sterile 50 mL tubes and stored at -20°C until further use. Aliquots were thawed at 4°C overnight when needed.

mTeSR™1 (mTeSR; 85850; STEMCELL Technologies Inc., Canada): For mTeSR medium preparation, 5x supplement was thawed either overnight at 4°C or at RT and mixed thoroughly before adding it to mTeSR basal medium. 5 mL Pen/Strep was also added, and full medium was mixed well by shaking, aliquoted

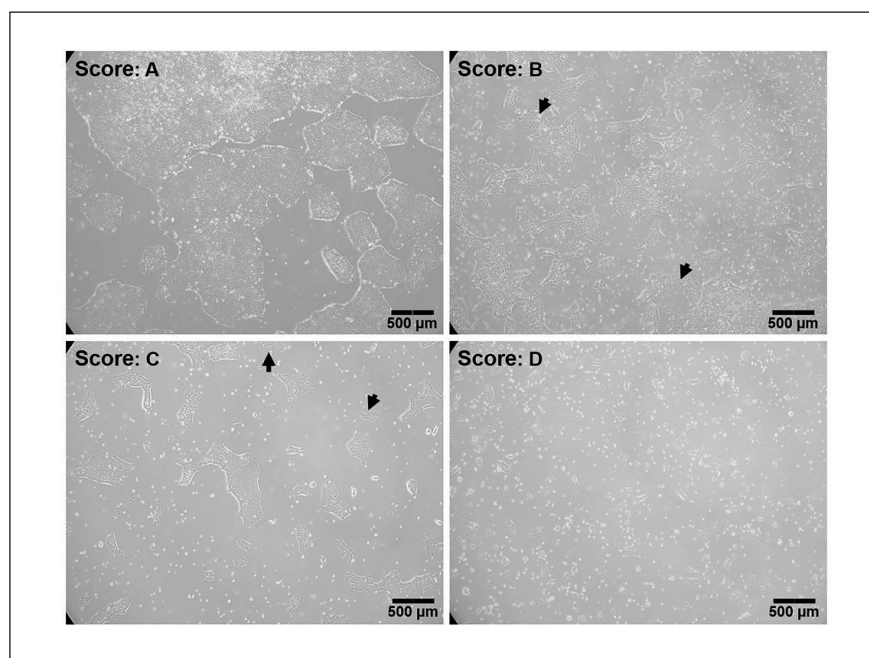


**Fig. 2: Representative images of IMR90-C4 scored for daily assessment**

Score A: Perfect culture (large, dense colonies; low to no differentiation visible) and > 70% confluent; Score B: Good culture (medium to large colonies; low to medium differentiation visible) and > 50% confluent; Score C: Fair culture (small to medium colonies; medium to low differentiation visible) and/or > 25% confluent; Score D: Poor culture (poor adherence, high amount of differentiation, and almost no iPSC visible). Arrowheads indicate areas of differentiation.

into labelled (name of medium, volume, expiration date and date of aliquoting) sterile 50 mL tubes, and stored at  $-20^{\circ}\text{C}$  until use. Aliquots were thawed at  $4^{\circ}\text{C}$  overnight when needed.

#### 2.1.1.3 Culture and splitting

Human iPSCs were supplied with 2 mL/well fresh medium 6 out of 7 days a week. On the 6<sup>th</sup> day, the cells received double the volume of medium (“double feed”) to survive the prolonged period without medium replacement. For routine feeding, the spent medium was aspirated and replaced immediately with fresh fully-supplemented medium equilibrated to RT. Human iPSCs were incubated at  $37^{\circ}\text{C}$  and 5%  $\text{CO}_2$ . Colonies were split when one of the following criteria was reached: (i) colonies reached approx. > 70% confluency, (ii) colonies were too dense, (iii) cultures showed increasing signs of differentiation, and/or (iv) individual colonies in the well were too large. Stock solution of 0.5 M EDTA (#15575020; Thermo Fisher Scientific, Waltham, MA, USA) was diluted 1:1000 in PBS<sup>(-/-)</sup> and then sterile aliquoted, and stored at RT (This 0.5 mM EDTA working solution is stable for 6 months at RT.). For the work presented here, only cluster-based passaging was used, and the standard splitting ratio was 1:8-1:12. Spent medium was aspirated, and cultures were washed twice with 1 mL/well 0.5 mM EDTA by swirling the wells gently and aspirating the EDTA immediately. Then another 1 mL of EDTA was added and wells were incubated for 4 (cultures on LN521) to 5 (cultures on MG) min at  $37^{\circ}\text{C}$  and 5%  $\text{CO}_2$ . Afterwards, EDTA was aspirated again, and 1 mL of respective hiPSC medium was added to the well with force, using a 1000  $\mu\text{L}$  pipette tip. The medium was triturated exactly twice (again with force: top of the well, then bottom of the well) to loosen colonies from well surface. The exact volume of the calculated split ratio of the cell suspension

was transferred to an already prepared (see 2.1.1.1) new plate and cultured at  $37^{\circ}\text{C}$  and 5%  $\text{CO}_2$ . As a back-up, 1 mL fresh medium was added to the freshly split well. This back-up well was discarded the next day when split cells passed microscopic assessment. Once a month, the spent medium was transferred to a new well and incubated for an additional week (without cells) in order to detect possible contaminations with bacteria and/or fungi.

#### 2.1.1.4 Transition of matrix and medium

For assay 5 (cell antigen expression + cell count and viability), IMR90-C4 cells were transferred from LN521 and iPS-Brew to MG and mTeSR. When cells scored A (for further expansion) at daily assessment, they were split 1:8 onto MG, but the medium remained 100% iPS-Brew. The medium was then changed gradually: 75% iPS-Brew + 25% mTeSR on day 1 after splitting, 50% iPS-Brew + 50% mTeSR on day 2, 25% iPS-Brew + 75% mTeSR on day 3 until cells were fully transferred to 100% mTeSR medium on day 4 after splitting.

#### 2.1.1.5 Daily assessment and scoring

hiPSC colonies were microscopically assessed and scored 6 times a week before feeding of the cultures according to the following scoring system (Fig. 2): (A) perfect culture with large, dense colonies, low to no visible differentiation and > 70% confluency, (B) good culture with medium to large colonies, low to medium visible differentiation and > 50% confluency, (C) fair culture with small to medium colonies, medium to low visible differentiation and/or > 25% confluency, (D) poor culture with poor adherence, high differentiation and no visible hiPSC. Only cells that scored A were used for further analysis. Bright images were taken using an inverted light microscope (CKX41,



Olympus) equipped with a Color Mosaik 18.2 camera (Visitron Systems) and the SPOT Advanced software (version 4.6.3.8). Every time, overview (40x Olympus UPlanFLN, 4x/0.3 PhP) and close-up pictures (200x Olympus LCAchN, 20x/0.40 PhP) were taken and archived.

### 2.1.2 Banking of hiPSCs

When a cell line is to be used over many experimental cycles or in various projects, a two-tiered cell banking system consisting of a MCB and a WCB (Fig. 1) is state-of-the-art. The MCB is characterized extensively on the day of freezing (assays 1-8). Cells from the MCB are expanded to form the WCBs, which are characterized again (assays 1, 2, 3, 4, 5, and 8) on the day of freezing. *Life-Act-eGFP* hiPSC lines were cultured for 5 passages after thawing of the cells. Then hiPSCs were expanded to at least 6-8 full 6-well plates (36-48 individual wells), of which a part was used for quality control assays 1-8 (except for 4, see 2.5 for details) and the other wells were cryopreserved as described in 2.1.1.1. For different projects and culturing conditions (e.g., single cell culture instead of clusters), different WCBs must be established. One vial of the respective MCB is thawed, cells are cultured for at least 3 passages, and culturing conditions (e.g., matrix/medium) are adjusted as needed (see also 2.1.1.4) before cells are again expanded like for generation of a MCB, and wells are used either for required quality control assays or liquid nitrogen stocks.

#### 2.1.2.1 Cryopreservation of hiPSCs

Cryovials with internal thread (#710522; Biozym GmbH, Hessisch Oldendorf, Germany) were labelled with essential cell line information (MCB/WCB ID, vial number, name of cell line, passage number, date of freezing, initials of researcher) and introduced into a Class II biological safety cabinet. Plates with hiPSCs that were to be cryopreserved were introduced into the same biological safety cabinet, and spent medium was aspirated. It is important to not process more than three wells at a time to avoid prolonged processing time and therefore ensure consistent quality of frozen vials. Culture plates were tilted at a slight angle, and medium was removed by aspirating from the bottom edge of the well, ensuring minimal contact to the surface. Cells were then washed twice by adding 1 mL 0.5 mM EDTA (#15575020; Thermo Fisher USA) and gently swirled once before EDTA was aspirated immediately. Then another 1 mL of 0.5 mM EDTA was added to the respective well, and cells were incubated at 37°C and 5% CO<sub>2</sub> for 4 and 5 min (LN521 and MG, respectively; this incubation time should be adapted to the hiPSC line and matrix used). EDTA solution was aspirated and replaced immediately with 2 mL CryoStem™ freezing medium (#05-710-1E; Biological Industries, USA) and triturated exactly twice to loosen colonies from well surface – the upper part of the well (1), then the lower part of the well (2). 1 mL of cell suspension was aliquoted into each labelled cryovial, and cryovials were then placed in an isopropanol freezing container at -80°C overnight. Next day, cells were transferred to a liquid nitrogen tank for long-term storage. Of note, the cryopreservation process

described here does not, strictly speaking, yield a homogeneous batch of hiPSCs as not all hiPSCs of all wells were pooled and then equally redistributed before freezing (e.g., as described in Wagner and Welch, 2010; Liu and Chen, 2014; Shibamiya et al., 2020). However, in our opinion such a procedure is not feasible for all research laboratories, as often the infrastructure for such a large-scale freezing process is not available.

#### 2.1.2.2 Thawing of hiPSC clusters

Before starting the thawing procedure, appropriate amounts of matrix-coated wells (2 6-wells per line) were prepared (see 2.1.1.1). Plates were allowed to equilibrate at RT for at least 30 min prior to starting of the thawing process.

A 15 mL conical tube was introduced into a Class II biological safety cabinet and labelled according to the hiPSC line to be thawed. 4 mL of ice-cold and 4 mL of hiPSC medium equilibrated to RT were also placed into the Class II biological safety cabinet. Cells to be thawed were removed from the liquid nitrogen tank and devolatilized in the Class II biological safety cabinet before they were thawed quickly at 37°C using a water bath until only a small clump of ice (pea size) was still visible. Using a 1000 µL pipette tip, the cell solution was carefully transferred to the prepared 15 mL conical tube. 1 mL of fresh, cold hiPSC medium was added dropwise to the cell suspension, followed by 2 mL cold medium. The vial was shaken gently to allow gradual equilibration of the cells to the changing microenvironment after every few drops and each respective additional mL. Another 1 mL of cold hiPSC medium was added to the cryopreservation vial for washing and then also transferred dropwise to the 15 mL tube. Cells were centrifuged at 200 x g at RT for 5 min. The supernatant was carefully aspirated, 4 mL of hiPSC medium at RT were added, and the cell pellet was carefully dislodged using a 5 mL serological pipette by pipetting up and down not more than twice. The supernatant was removed from prepared matrix-coated wells, and they were washed if appropriate (see 2.1.1.1). 2 mL per well cell suspension was added to each prepared matrix-coated well, and the 6-well plate was moved in a shape of 8 three times to evenly distribute cells over the whole surface of the well. Human iPSCs were incubated at 37°C and 5% CO<sub>2</sub>, and medium was changed the next day.

## 2.2 Assay #1: Microscopic assessment of colony/cell morphology

Microscopic assessment of the cells was performed as described in 2.1.2.5. Colonies should represent score A (see also 2.1.1.5) and appear compact, have smooth edges, and not show signs of premature differentiation (e.g., cracks between the cells that appear almost white). Cells should be round, small, and have a high nucleus-to-cytoplasm ratio and prominent nucleoli (Wakui, 2017).

## 2.3 Assay #2: Mycoplasma PCR

Mycoplasma PCR was performed using the PCR Mycoplasma Test Kit I/C (PK-CA91-1024, PromoCell, Heidelberg, Germany) according to the manufacturer's instructions. The kit includes a



positive (DNA-fragment of the *M. orale* genome) and a negative control and detects: *A. laidlawii*, *M. agalactiae*, *M. arginini*, *M. arthritidis*, *M. bovis*, *M. cloacale*, *M. falconis*, *M. faucium*, *M. fermentans*, *M. hominis*, *M. hyorhinae*, *M. hyosynoviae*, *M. opalescens*, *M. orale*, *M. primateum*, *M. pulmonis*, *M. salivarium*, *M. spermatophilum*, and *M. timone*. It is not suitable for detection of *M. pneumoniae*, *Ureaplasma urealyticum*, or other clinically associated species that are not typically found as cell culture contaminants.

#### 2.4 Assay #3: Short tandem repeat (STR) genotyping

At the time of banking, genomic DNA of one 6-well of hiPSC was extracted using the peqGOLD Tissue DNA Mini Kit (VWR International GmbH, Darmstadt) following the manufacturer's instructions.

For STR-analysis (carried out at the Institute of Forensic Medicine, University Clinic Duesseldorf), a single-source template DNA (0.5 ng) was using the PowerPlex® 21 System (Promega, USA). products were mixed with WEN Internal Lane Standard 500 and analyzed with an ABI 3130 Genetic Analyzer (Applied Biosystems®, USA). Results were analyzed using GeneMapper® ID software, version 3.2. The following genetic loci were analyzed: Amelogenin, D3S1358, D1S1656, D6S1043, D13S317, Penta E, D16S539, D18S51, D2S1338, CSF1PO, Penta D, TH01, vWA, D21S11, D7S820, D5S818, TPOX, D8S1179, D12S391, D19S433, and FGA.

As it is theoretically possible to identify donors on the basis of published STR (Pamies et al., 2017), we decided against showing the results of all 21 analyzed STR loci (although all analyzed loci matched between IMR90-C4 and *Life-Act-eGFP* hiPSC lines). Instead, we focus on the 14 already published loci: D3S1358, D13S317, D16S539, D18S51, CSF1PO, TH01, vWA, D21S11, D5S818, D7S820, TPOX, D8S1179, FGA, AMEL (Cellosaurus CVCL\_0347<sup>1</sup>).

#### 2.5 Assay #4: Cytogenetic analysis by classical G-banding

Cytogenetic analyses were performed using GTG-banding of chromosomes adapted from Howe et al. (2014). In detail, when cells were expanded for banking, one matrix-coated T25 with respective hiPSCs was prepared in parallel to ensure that the cytogenetic analysis took place in the same passage the cells were banked in. Cells were transferred to the Institute of Human Genetics (University Clinic Duesseldorf) and analyzed after a resting period of 24 h (Note that cells must be in proliferative phase, therefore cultures should not exceed a of 50% at time of transport). Culture medium was replaced the next day (cells should have reached ~80% To arrest cells in metaphase, 10 µL/mL colcemid (a spindle poison) was added to the cultures and incubated for 2-5 h. An inverted microscope was used to check for rounded cells. Cell supernatant was transferred to a 15 mL conical tube, which was set aside for later use. Cells were gently washed with 2 mL Hanks' solution. 1 mL prewarmed (37°C) trypsin was added to the cells and incubated

for 2-5 min. The cells were tapped vigorously to dislodge cells and again checked under an inverted microscope. This cell suspension was then transferred back to the 15 mL conical tube with medium and centrifuged at 1000 x g for 10 min. Supernatant was discarded, and the cell pellet was resuspended using 10 mL 0.075 M prewarmed KCl (37°C) on a vortexer set to medium speed (the hypotonic KCl solution causes cell swelling). Cells were incubated in KCl for 20 min at RT, followed by centrifugation at 1000 x g for 10 min. The supernatant was removed, and the cell pellet was resuspended in 8 mL of fresh Carnoy's

(methanol/glacial acetic acid at a ratio of 3:1) on a vortexer (see above). Cells were centrifuged at 1000 x g for 10 min and supernatant was removed. The cell pellet was resuspended in Carnoy's

(can be stored at 4°C for up to one year). For preparation of slides, cells were centrifuged at 1000 x g for 10 min, and most of the supernatant was discarded, leaving only ~0.5 mL to gently resuspend the cells. Three drops of the cell suspension were dropped on a tilted slide (~45°) from a distance of 5-10 cm, and the suspension was left to run over the slide to ensure that chromosomes were properly separated. One large drop of fresh Carnoy's was added to the slide before it was left to dry for at least 10 min (slide should be completely dry). In the meantime, the following solutions were prepared in separate Coplin jars:

(i) 80 mL buffer solution (di-sodium hydrogen phosphate/potassium dihydrogen phosphate) + 1 mL 10x trypsin (0.5%), and (ii) 100 mL NaCl (0.9%). Each slide was dipped in jar (i) for 3 min and then rinsed shortly in jar (ii). Afterwards slides were allowed to dry. Fresh Giemsa staining solution (Gurr Buffer and Giemsa Stain in a ratio of 3:1) was prepared and used to cover the entire slide for 5 min. Then slides were washed with distilled water and dried at RT. Slides were covered using Entellan® (#107961, Merck, Darmstadt, Germany; avoiding air bubbles under the cover slip). This treatment allows to discriminate between the relatively gene-poor heterochromatic regions (AT-rich), which stain darkly, and more transcriptionally active euchromatic regions (GC-rich). Subsequently, 2-16 slides were scanned using the slide scanning system Metafer from MetaSystems (MetaSystems Hard & Software GmbH, Altlussheim, Germany). The cytogenetic analysis was done with the karyotyping system Ikaros from MetaSystems. Up to 24 metaphases were analyzed and karyotyped. The karyotype was described according to (ISCN, 2016), where a clonal aberration is as at least two cells with the same aberration if the aberration is a chromosome gain or structural rearrangement, or at least three cells if the abnormality is a loss of a chromosome. The quality of the karyotypes ranged from 200-350 band levels.

#### 2.6 Assay #5: Cell antigen expression (#5.1) and cell count and viability (#5.2)

Human iPSC cultures were analyzed at the time of banking (3 to 5 days after the last split at no more than 80% We used the BD™ Human Pluripotent Stem Cell Transcription Factor Analysis FACS Kit (RUO #560589; Becton, Dickinson and Company (BD), USA) including PE mouse anti-human Nanog,

<sup>1</sup>Cellosaurus CVCL\_0347 Web page Cellosaurus cell line IMR-90 (CVCL\_0347). [https://web.expasy.org/cellosaurus/CVCL\\_0347](https://web.expasy.org/cellosaurus/CVCL_0347) (accessed 18.01.2021)

**Tab. 1: Flow cytometry setup**

Fluorochrome	FITC	PE	PerCP	Alexa657	Fvs 510
Laser lines	488 nm	488 nm	488 nm	633 nm	405 nm
Emission filter	530/30	585/42	670 LP	660/20	510/50

PerCP-Cy<sup>TM</sup> 5.5 mouse anti-OCT3/4, Alexa Fluor<sup>®</sup> 647 mouse anti-Sox2, as well as the respective isotype controls PE mouse IgG1,  $\kappa$  isotype control, PerCP-Cy5.5 mouse IgG1,  $\kappa$  isotype control, and Alexa Fluor<sup>®</sup> 647 mouse IgG2a,  $\kappa$  isotype control. According to the manufacturer's manual, we combined this kit with an additional antibody against the membrane-bound glycolipid SSEA4 (#560126; BD, USA) and the respective isotype control (#555578; BD, USA). To be able to assess cell viability at the same time, we also included a live staining of the cells using viability stain (Fvs) 510 (#564406; BD, USA).

cells were microscopically assessed as described under 2.2 and used when scored A. Then 8-12 wells were singularized using TrypLE<sup>TM</sup> Select Enzyme (#12563-011; Thermo Fisher USA). Approx.  $1 \times 10^6$  cells per staining condition (unstained, Fvs 510 only, isotypes + Fvs 510, all stained (Nanog-PE, OCT3/4-PerCP, Sox2-Alexa657, SSEA4-FITC + Fvs 510), the minus one (FMO) control for SSEA-4 (Nanog-PE, OCT3/4-PerCP, Sox2-Alexa647 + Fvs 510)) and single stained controls for each were collected in respective Eppendorf tubes. Cells were stained with Fvs 510 for 15 min at RT. Then cells were washed using staining buffer (PBS<sup>(-/-)</sup> + 2% heat-inactivated KnockOut<sup>TM</sup> Serum Replacement (#10828010; Thermo Fisher USA)). After washing, cells were stained for SSEA4-FITC and respective isotype control for 25 min at RT. Then cells were again washed and in BD Cyto-buffer (provided) for 20 min at RT. Afterwards they were washed again and stored in PBS<sup>(-/-)</sup> at 4°C overnight. The next day, cells were permeabilized using BD Perm/Wash buffer (provided) for 20 min at RT before staining for Nanog-PE, OCT3/4-PerCP, Sox2-Alexa647 and respective isotype controls for 30 min at RT. Cells were washed in PermWash Buffer, re-suspended in staining buffer, and analyzed using a BD FACS-Canto<sup>TM</sup> II system (see Tab. 1 for setup) using BD FACS Diva Software Version 6.1.3. At least 20,000 events per condition were recorded from the scatter gate, the applied gating strategy is included in the respective Figures 3 and S1<sup>2</sup>. Further analysis was performed using Flow Jo V10.7.1.

### 2.7 Assay #6: Cell gene expression (PluriTest<sup>TM</sup>)

One 6-well of hiPSC at the time of banking was washed twice with 1 mL 0.5 mM EDTA. Cells were incubated with 1 mL EDTA for 5 min (37°C, 5% CO<sub>2</sub>). EDTA was then aspirated and discarded. Cells were resuspended in 1 mL medium and collected in a 1.5 mL Eppendorf tube. Samples were centrifuged for 3 min at 500 x g. Supernatant was aspirated, and cell pellets were stored at -80°C until they were shipped to Thermo Fisher

(USA) on dry ice where the PluriTest<sup>TM</sup> assay (#A38154) was performed.

The PluriTest<sup>TM</sup> assay compares the transcriptional of a sample to a reference set of > 450 cells and tissue types (incl. 223 hESCs, 41 iPSCs, somatic cells, and tissues). The pluripotency score (PS) indicates how strongly a model-based pluripotency signature is expressed in the analyzed samples. A PS over 20 indicates that the sample is more like the pluripotent samples of the reference set than the other samples. The novelty score (NS) indicates the general model for a given sample. A NS below 1.67 indicates that the tested samples can be well reconstructed based on existing data from other well-characterized iPSC and ESC lines (Müller et al., 2011; Müller, 2014).

### 2.8 Assay #7: Embryoid body (EB) formation

The EB formation protocol was adapted from Kurosawa (2007). In detail, for each hiPSC line, two wells of a 6-well plate were used for EB-formation at time of banking (Day 0). This yields enough material for both plating onto gelatine for subsequent immunocytochemical analysis (see 2.8.1) and pellet generation for Scorecard<sup>TM</sup> analysis (see 2.8.2). EB medium (50 mL: 39 mL DMEM, high glucose, GlutaMAX<sup>TM</sup> (#31966-021; gibco by life technologies<sup>TM</sup>, USA), 10 mL KnockOut<sup>TM</sup> Serum Replacement (#10828010; Thermo Fisher USA), 0.5 mL non-essential amino acids (#11140-050; gibco by life technologies<sup>TM</sup>, USA), 0.5 mL penicillin/streptomycin (#P06-07100; PAN Biotech, Aidenbach, Germany), 91  $\mu$ L 2-mercaptoethanol (#31350-010; gibco by life technologies<sup>TM</sup>, USA)) was equilibrated in a T75 with CO<sub>2</sub> permeable lid at 37°C and 5% CO<sub>2</sub> for 30 min. 10 cm ultralow adherence plates (Nunc<sup>TM</sup> HydroCell; #174911; Thermo Fisher USA; 2 per line – note that these plates are no longer available. Thermo Fisher suggests Nunclon<sup>TM</sup> Sphera<sup>TM</sup> dishes #174945 as an alternative) were with 19 mL EB medium plus 10  $\mu$ M Rock inhibitor (#HB2297; hellobio, UK). Medium of respective hiPSCs was aspirated and discarded. Cells were washed once with PBS<sup>(+/+)</sup>, and 1 mL EB medium + Rock inhibitor per well was added. StemPro<sup>®</sup> EZPassage<sup>TM</sup> passaging tool (#23181-010; Invitrogen by Thermo Fisher USA) was used once vertically, once horizontally on each well to assure hiPSC pieces of equal size. A cell scraper (#83.1832; Sarstedt AG & Co. KG, Nümbrecht, Germany) was used to harvest the hiPSC pieces, and the clusters of one well of the 6-well plate were transferred to one ultralow adherence plate containing 19 mL EB medium. Cell clusters were incubated at 37°C and 5% CO<sub>2</sub>. On days 2, 4 and 6, spent medium was replaced by fresh EB induction medium

<sup>2</sup> doi:10.14573/alltex.2101221s



(20 mL) by transferring the entire volume of each plate into a separate 50 mL conical falcon tube. EBs were allowed to settle at the bottom of the tube for 10 min at RT. Then the supernatant was cautiously removed using a 25 mL serological pipette, and 20 mL fresh EB medium was added to each tube. Cells were transferred back into the old culturing plates by pouring to avoid unnecessary shear stress. Proliferating EBs grew in size over the culture time of 7 days.

### 2.8.1 Assay #7.1: Immunocytochemistry of markers of all three germ layers

#### 2.8.1.1 Spontaneous differentiation of EBs

On day 7, three 24-well plates (black plates with imaging bottom would be preferable, here normal cell culture plates were used) were coated with 250  $\mu$ L 0.2% gelatin (diluted from 2% gelatin (#G1393-20ML; Sigma Aldrich, USA) using PBS<sup>(+/+)</sup>; gelatin should be prewarmed to 37°C in a heating cabinet before use) for 20 min at RT (open lid). Then gelatin solution was aspirated completely, and 750  $\mu$ L EB medium per well were added. One EB of approx. 300  $\mu$ m in size per well was gently plated using a 1000  $\mu$ L pipette and allowed to settle for 5 min. EBs were incubated at 37°C and 5% CO<sub>2</sub>, and half of the spent medium was replaced every other day while carefully avoiding EB wash-off.

On days 11, 14 and 21, differentiated EBs were by adding 12% PFA (#P6148-1KG; Merck KGaA, Darmstadt, Germany), resulting in a PFA concentration of 4%, and incubated for 15 min at RT. Then, EBs were washed twice using 1 mL PBS<sup>(-/-)</sup> per well, sealed with and stored at 4°C until staining (Note that even if EBs are washed off at some point during the differentiation phase, it is worthwhile to check for differentiated cells under a microscope before discarding the sample).

#### 2.8.1.2 Immunocytochemical staining of differentiated EBs

Before staining, all wells were analyzed under a light microscope to judge from the morphological structures of the differentiated cells which antibody staining (which germ layer marker) would be most promising as each well is stained with one marker. Afterwards 24-well plates were equilibrated at RT for 15 min. Then PBS was carefully removed, and 200  $\mu$ L/well permeabilization buffer (0.05% PBS-Tween20) was added and incubated at RT for 5 min. Wells were washed twice with 0.5 mL PBS<sup>(+/+)</sup> for 5 min, followed by addition of 200  $\mu$ L/well blocking solution (1% BSA in PBS<sup>(+/+)</sup>) and incubation at RT for 30 min. Primary antibody (AB) solutions were prepared in primary AB dilution buffer (10 mL: 1 mL 10% BSA, 7.5  $\mu$ L Tween20, up to 10 mL with PBS<sup>(+/+)</sup>): (i) 1:100 monoclonal anti- $\beta$ -tubulin III (TUBB3) antibody produced in mouse, clone SDL.3D10 (#T8660; Sigma Aldrich, USA), (ii) 1:200 monoclonal anti-actin, smooth muscle actin (SMA) produced in mouse, clone 1A4 (#M0851; Agilent Dako, USA), and (iii) 1:200 monoclonal anti- $\alpha$ -feto protein (AFP) antibody produced in mouse, clone 1G7 (#WH0000174M1; Sigma Aldrich, USA). Blocking solution was discarded and 200  $\mu$ L per well of the respective primary AB solution was added. Plates were incubated over night at 4°C on a rocking plate. Next day,

primary AB solution was discarded, and cells were washed twice with 0.5 mL PBS<sup>(+/+)</sup> for 5 min. Secondary ABs (For IMR90-C4 SMA and for all *Life-Act-eGFP* stainings 1:100 polyclonal goat anti-mouse IgG (H+L) highly cross-adsorbed secondary antibody, Alexa Fluor 546 was used (#A11030; Thermo Fisher Sci-

USA), for *Life-Act-eGFP* TUBB3 and AFP 1:200 polyclonal goat anti-mouse IgG (H+L) cross-adsorbed secondary antibody, Alex Fluor 488 was used (#A11001; Thermo Fisher USA).) were prepared in secondary AB dilution buffer (0.05% PBS-Tween20). 200  $\mu$ L/well of secondary AB solution were added, and wells were incubated at 37°C in the dark for 30 min. Wells were washed twice with 0.5 mL per well PBS<sup>(+/+)</sup> at RT for 5 min and covered with 200  $\mu$ L PBS<sup>(+/+)</sup> for visualization using a microscope. Pictures of differentiated EBs from IMR90-C4 were taken with an Olympus BX60 - cent microscope combined with an Olympus ColorView XS digital camera and Soft Imaging Systems analysis software. Images of *Life-Act-eGFP* EBs were taken at RT using a laser scanning microscope (LSM710, Zeiss) with an EC 10x/0.30 M27 objective lens and a photo-multiplier-tube point detector. Acquisition software was ZEN Black (Zeiss).

### 2.8.2 Assay #7.2: Scorecard™ assay

At least 7-day-old proliferating EBs that were 300  $\mu$ m in size were collected in a 50 mL tube and centrifuged at 500 x g for 3 min. The supernatant was discarded, and the pellet was resuspended in 1 mL PBS<sup>(+/+)</sup> and transferred to a 1.5 mL tube. EBs were again centrifuged at 500 x g for 3 min, and the supernatant was discarded. Dry pellets were stored at -80°C. As a control, a cell pellet of the respective undifferentiated hiPSC-line was generated as described under 2.7. The pellets were then shipped to Thermo Fisher (USA) on dry ice where the Scorecard™ assay (#A16179) was performed.

The Scorecard™ assay (Bock et al., 2011) uses a proprietary algorithm to predict trilineage differentiation potential based on a panel of 94 genes relative to a reference set of nine undifferentiated pluripotent stem cell lines.

### 2.9 Assay #8: Trypan blue exclusion, microscopic assessment

Human iPSCs were thawed as described under 2.1.1.2. Cell density and colony/cell morphology were assessed microscopically on day 1 after thawing and when the cells reached a - cy of approx. 80% and needed splitting (day 3 for IMR90-C4 and day 2 for *Life-Act-eGFP*). For the trypan blue exclusion assay, medium of one well per line was aspirated, and cells were washed twice with 1 mL PBS<sup>(-/-)</sup>. 1 mL/well TrypLE™ Select Enzyme (#12563-011; Thermo Fisher USA) was added, and cells were incubated at 37°C and 5% CO<sub>2</sub> for 5 min. The enzymatic reaction was stopped using 3 mL/well KnockOut™ DMEM medium with 10% KnockOut™ Serum Replacement (#10828010; Thermo Fisher USA). Cells were pipetted up and down 5 times to ensure a single cell solution. 50  $\mu$ L of this cell suspension was placed in a 1.5 mL tube, and 50  $\mu$ L 0.4% trypan blue solution (#T8154; Sigma Aldrich, USA) was added and mixed by pipetting up and down until an even distribution

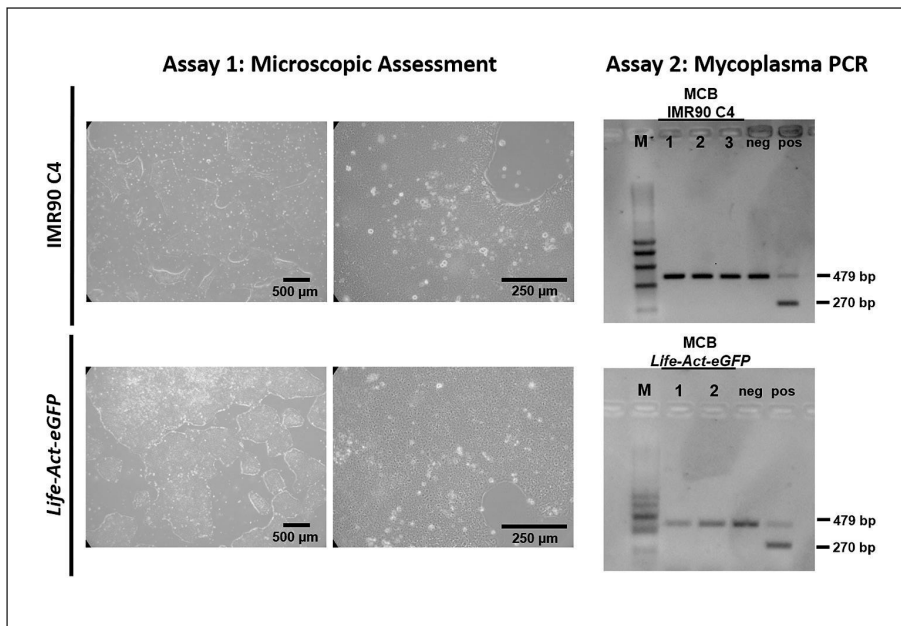


**Fig. 3: Results of microscopic assessment of colony/cell morphology (assay 1; left) and mycoplasma PCR (assay 2; right) for MCBs IMR90-C4 (upper panel) and *Life-Act-eGFP* (lower panel)**  
 Left: Representative microscopic images. Right: Results of mycoplasma PCR. M, marker; neg, negative (internal DNA) control (479 bp); pos, positive control (270 bp); bp, base pairs

of the color was reached. Cells were incubated for 2-3 min at RT, and 10 μL of the stained cells was transferred to a C-Chip disposable hemocytometer (#DHC-N01; NanoEnTek, Korea). Pictures were taken within the 5 min after the dye was added, as the dye itself will lead to cytotoxicity when incubated for too long. The percentage of viable cells was calculated using the following equation:

$$\% \text{ viable cells} = [1.00 - (\text{number of blue cells}/\text{number of total cells})] \times 100$$

Eq. 1

### 3 Results and discussion

#### 3.1 Assessment of colony/cell morphology (assay 1) and exclusion of mycoplasma contamination (assay 2)

It is well known that hiPSC cultures are prone to spontaneous differentiation, especially during longer culturing periods (Pamies et al., 2017). Therefore, we established a daily assessment of colony and cell morphology using a scoring system from (A) perfect culture with large, dense colonies, low to no visible differentiation, and > 70% to (D) poor culture with poor adherence, high amount of differentiation, and no visible hiPSC (for details see 2.1.2.5). We assessed the colony and cell morphology according to criteria previously (Pamies et al., 2017; Wakui, 2017). In recent years, there have been efforts to automate the quality ranking of hiPSC cultures by using time-lapse microscopy and automated image analysis assessing (i) hiPSC doubling time, (ii) compactness of colonies, (iii) smoothness of colony borders, (iv) sensitivity of colonies to change of medium, (v) degree of dead cells, and (vi) prevalence of spontaneously differentiated cells (Maddah et al., 2014). This non-invasive system to assess hiPSC colony and cell morphology might be useful for

high-throughput hiPSC laboratories, but for a normal academic lab we conclude that manually conducted daily microscopic assessment as described here is probably more feasible and, combined with the other assays described in this paper, to ensure quality of the cultures. Our two MCB cultures revealed a stem cell-like phenotype with compact, colonies consisting of small, round cells with a high nucleus-to-cytoplasm ratio, prominent nucleoli, and a general lack of spontaneously differentiated cells (Fig. 3, left panel).

It is estimated that up to 35% of cell cultures currently in use are contaminated by mycoplasma (Hay et al., 1989; Chi, 2013; Pamies et al., 2017), which can result in major changes of the cellular phenotype, e.g., increased sensitivity to apoptosis (Hay et al., 1989), changes in cellular morphology, growth and viability (Rottem and Barile, 1993; Langdon, 2004), occurrence of chromosomal aberrations (Drexler and Uphoff, 2002), altered cellular metabolism (Armstrong et al., 2010), changes in cell membrane antigenicity (Timenetsky et al., 2006), reduced transfection (Chi, 2013), and alterations of cytokine expression (Chi, 2013). Therefore, it is consensus that cultures should be screened for mycoplasma contamination at time of cell arrival and additionally every three months (Pamies et al., 2017). Our approach is in line with these standards, using a quarantine incubator in another laboratory and performing mycoplasma PCR analysis before the cells are transferred to the actual stem cell laboratory. Furthermore, we perform additional mycoplasma PCRs once a month, and cultures are discarded immediately upon a positive test result. Although no standardized PCR-based method exists to date (Pamies et al., 2017), we chose a commercial PCR-based kit for the detection of possible mycoplasma contamination in our cell cultures, as this is faster and more convenient than other assays including broth/agar culture, assays for mycoplasma-characteristic enzyme activities, and DNA staining (Pamies et al., 2017), which take from several



days to weeks and are therefore not practical in an academic research setting. The kit we chose is able to detect 19 (for details see 2.3) different mycoplasma types, including the ones that account for the vast majority of contaminations in cell culture, i.e., *M. hyorhinis*, *M. arginine*, *M. fermentans*, *A. laidlawii*, *M. hominis*, *M. orale*, *M. bovis* and *M. pulmonis* (Bruchmüller et al., 2006; ISCBI, 2009; Nikfarjam and Farzaneh, 2012). This test that the analyzed MCB samples of IMR90-C4 and *Life-Act-eGFP* were mycoplasma free (Fig. 3, right panel).

### 3.2 Identity assessment by short tandem repeat (STR) genotyping (assay 3)

One of the most important principles of Good Cell Culture Practice is cell line authentication (Coecke et al., 2005; Yaffe et al., 2016). Up to 40% of all analyzed cell lines have been falsely (Nelson-Rees et al., 1981; MacLeod et al., 1999; Stacey et al., 2000; Buehring et al., 2004; Hughes et al., 2007; Rojas et al., 2008; Dirks et al., 2010; Yu et al., 2015). Therefore, leading cell banks (ATCC, CellBank Australia, DSMZ, ECACC, JCRB, and RIKEN) introduced the technique of STR to address this issue (Pamies et al., 2017). According to the International Cell Line Authentication Committee (ICLAC), the analysis of at least eight STR loci is required for cell line authentication (et al., 2018), while ISCBI recommends the use of the core 13 loci commonly used in forensic medicine (Xu et al., 2013). Commercially available kits on the market typically use a common subset of 16 different STR loci, which ensures comparison between different providers (Andrews et al., 2015). Another approach is the analysis of single-nucleotide polymorphisms (SNPs), however they are discussed to be too detailed and expensive to be used for cell line authentication on a regular basis (Ntai et al., 2017). Comparing these two methods, individual STRs are more polymorphic (Freedman et al., 2015; et al., 2018) and are widely applied in forensic analysis (Almeida et al., 2016), but spontaneous mutations or epigenetic changes due to long term culture (Lorsch et al., 2014) and the possible cross-contamination with cell lines from other species (e.g., mice) will not be detected (Freedman et al., 2015). 52-plex SNP assays seem to have the same rate of discrimination as 16-plex STR assays, but a centralized, online reference database for SNP assays is lacking (Freedman et al., 2015; Pamies et al., 2017).

Therefore, we decided to use STR analysis for cell line authentication in cooperation with the Institute for Forensic Medicine at the University Clinic Duesseldorf. STR-analysis of gDNA isolated from both MCBs at the time of banking that IMR90-C4 are homozygous for two of the analyzed STR loci shown here (D18S51 and AMEL) and heterozygous for the other 12 (Tab. 2; middle column), which exactly matches the results for *Life-Act-eGFP* (Tab. 2; right column). This was expected, as IMR90-C4 is the parental line of *Life-Act-eGFP*. Both STR also match alleles of the initial IMR90-C4 parent line IMR90 lung (Tab. 2; left column) in the 14 STR loci that are publicly available on Cellosaurus (Bairoch, 2018). Performing STR-analysis not only for MCBs but also for WCB

### Tab. 2: Results of short tandem repeat (STR) genotyping (assay 3)

A single-source template DNA (0.5 ng) was amplified using the PowerPlex® 21 system (Promega). Amplification products were mixed with WEN Internal Lane Standard 500 and analyzed with an ABI 3130 Genetic Analyzer (Applied Biosystems®). Results were analyzed using GeneMapper® ID software, version 3.2. Only the previously published 14 loci of IMR90 lung fibroblasts are listed, see Section 2.4 for details.

STR locus	IMR90 lung fibroblasts	MCB IMR90-C4	MCB <i>Life-Act-eGFP</i>
D3S1358	14, 15	<b>14, 15</b>	<b>14, 15</b>
D13S317	11, 13	<b>11, 13</b>	<b>11, 13</b>
D16S539	10, 13	<b>10, 13</b>	<b>10, 13</b>
D18S51	17	<b>17</b>	<b>17</b>
CSF1PO	11, 13	<b>11, 13</b>	<b>11, 13</b>
TH01	8, 9.3	<b>8, 9.3</b>	<b>8, 9.3</b>
vWA	16, 19	<b>16, 19</b>	<b>16, 19</b>
D21S11	30.2, 31	<b>30.2, 31</b>	<b>30.2, 31</b>
D5S818	12, 13	<b>12, 13</b>	<b>12, 13</b>
D7S820	9, 12	<b>9, 12</b>	<b>9, 12</b>
TPOX	8, 9	<b>8, 9</b>	<b>8, 9</b>
D8S1179	13, 14	<b>13, 14</b>	<b>13, 14</b>
FGA	25, 26	<b>25, 26</b>	<b>25, 26</b>
AMEL	X	<b>X</b>	<b>X</b>

Bold: in accordance with the published STR profiles of ATCC IMR-90 (ATCC® CCL-186™) original lung fibroblasts, which IMR90 iPSCs were generated from (Cellosaurus CVCL\_0347, n.d.)x

should be considered. In our case, we decided against this as *Life-Act-eGFP* cells were made from an IMR90 C4 WCB, so their STR analysis result therefore also proved the correct identity of the IMR90-C4 WCB.

### 3.3 Cytogenetic analysis by classical G-banding (assay 4)

Certain types of aneuploidy have been recurrently in hiPSC cultures, including partial or complete gain of chromosome 8, 12, 17, or 20, trisomy X, and chromosome 1 - cation (Mayshar et al., 2010; Amps et al., 2011; Taapken et al., 2011; Kilpinen et al., 2017; Assou et al., 2018). Therefore, it is important to analyze the genetic stability of a given hiPSC line. Ideally, the technique of choice for this should be inexpensive, yield fast results, and have high resolution and sensitivity, but, unfortunately, this all-in-one solution does not exist (Assou et al., 2018). Nevertheless, different techniques are available: - orescent *in situ* hybridization (FISH), array comparative genomic hybridization (aCGH), SNP arrays, next-generation sequencing, quantitative PCR, and G-banding karyotype analysis

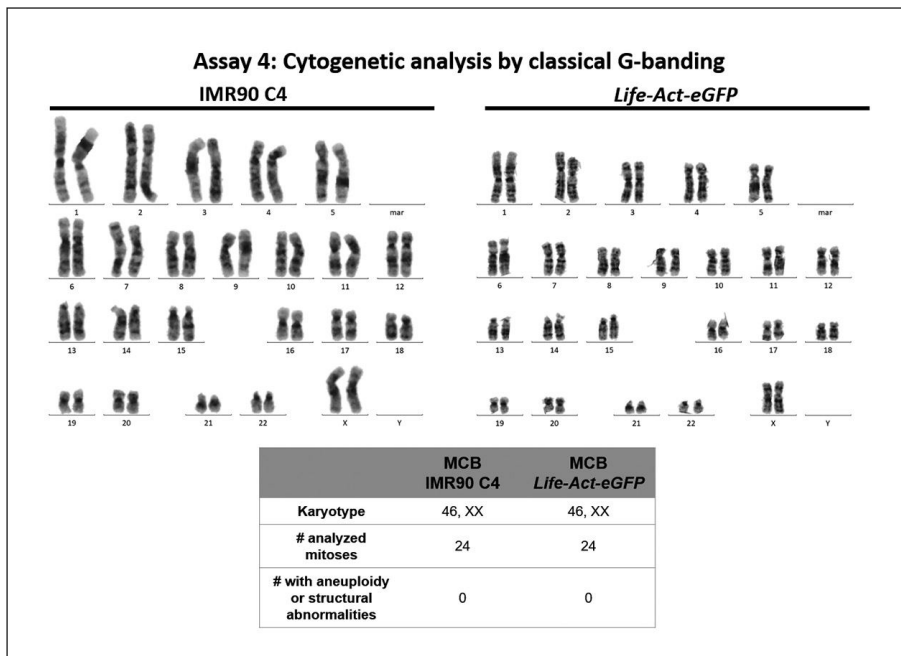


**Fig. 4: Results of cytogenetic analysis by classical G-banding (assay 4)**

24 mitoses for each MCB (IMR90-C4 and *Life-Act-eGFP*) were prepared and analyzed for aneuploidy or structural abnormalities using classical G-banding. Representative images of chromosomes are shown for each line, and results are summarized in the table.

(Assou et al., 2018). While FISH analysis reliably additional attributable chromosomal material (e.g., marker chromosomes), it has a resolution limit of > 1-2 Mb (MacArthur et al., 2014), only detecting larger abnormalities. CGH, SNP arrays, and whole genome sequencing on the other hand are extremely sensitive methods, capable of detecting chromosomal regions as small as 25 kbs as well as mosaicism (Conrad et al., 2010; Yaffe et al., 2016), but until recently were not able to detect inversions or balanced rearrangements (O’Shea et al., 2020). This has changed with technological progress, resulting in long reads (up to 60 kbs), which allow the detection of both inversions and rearrangements (Bartalucci et al., 2019; Zhang et al., 2019; Lei et al., 2020). Nevertheless, another drawback of these high-resolution methods is that while they provide a lot of data, they lack a of what differences may impact the reproducibility of research (Kleensang et al., 2016). Commercially available qPCR analysis kits, which detect the majority of karyotypic abnormalities reported in human ES and iPS cells, have the great disadvantage of bias: You only detect, what you look for. We believe that this method is to be preferred over not analyzing the cells at all, but it might create a false security compared to the other discussed unbiased approaches. ISCBi suggests using standard G-banding analysis, which can identify trisomy and gross chromosomal duplications/deletions and translocations. It is also the only major method that can detect structural abnormalities such as balanced translocations or inversions (Ntai et al., 2017; Rohani et al., 2018). According to ISCBi, a count of 20 metaphases and the analysis of the banding pattern of at least 8 metaphases (Bickmore, 2001; Loring et al., 2007; ISCBi, 2009) should be performed. 95% of the analyzed metaphases should hereby possess a normal karyotype (Pamies et al., 2017). chromo-

somal abnormalities of clonal origin should be in an independent analysis. Abnormalities in single cells could be due to a technical artefact but could also point towards a beginning clonal abnormality or low-level mosaicism (Hook, 1977; Sikke-ma-Raddatz et al., 1997). Here, again, a repeated analysis is suggested to allow interpretation of the results. In cooperation with the Institute of Human Genetics at the University Clinic Dues-seldorf, we analyzed the chromosomes of 24 metaphase spreads, none of them displaying any abnormalities (Fig. 4).

It is important to note that the analysis of genomic stability, regardless of the chosen method, is only a current snapshot, and it has been reported that a genetically abnormal clone can completely overtake a culture (Baker et al., 2007) in less than passages (Bai et al., 2013). Therefore, others have proposed to test for genomic integrity on a regular basis, at least every 12 weeks (WHO, 2013; Assou et al., 2018) or every 15 passages (WHO, 2013; Pamies et al., 2017). To bypass this laborious and time-intensive G-banding analysis every 12 weeks, we analyze hiPSC at the time of banking and culture them after thawing for only 8 passages in total (ca. 6 weeks), i.e., three passages to ensure full recovery after cryoconservation plus 5 passages for use in different assays. Hence, our cells never reach 15 passages or 12 weeks in culture.

### 3.4 Expression of stem cell markers on protein (assay 5) and mRNA (assay 6) level

Commonly used characterization methods to assess the self-renewal capacity of hiPSCs include immunocytochemical staining for alkaline phosphatase and intracellular markers (Nanog, POUF1, GDF3, DNMT3B), of cell surface stem cell markers (SSEA3, SSEA4, TRA-1-60, TRA-1-81) via

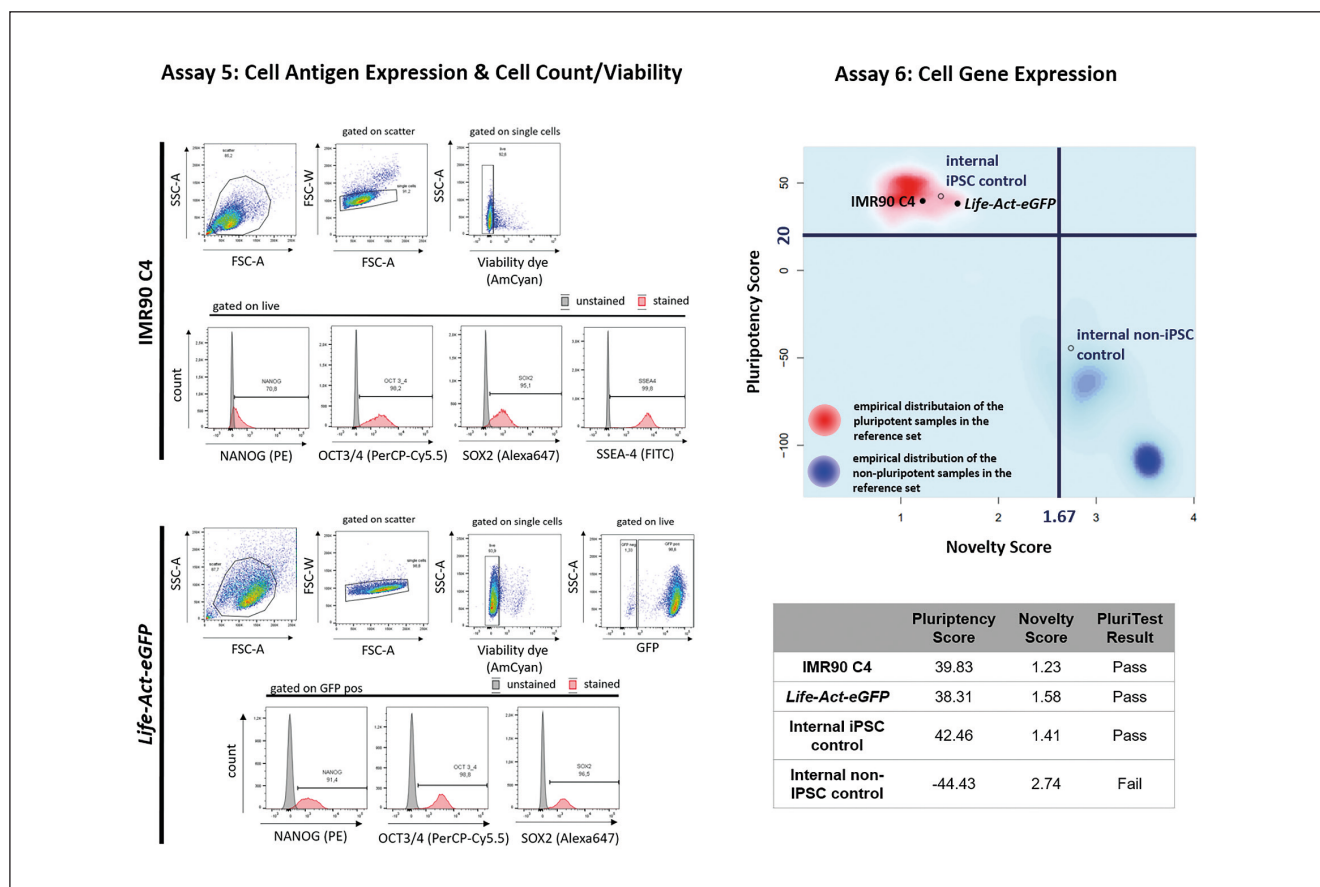


**Fig. 5: Results of cell antigen expression and cell count/viability (assay 5) and cell gene expression (assay 6)**

Assay 5: Cell antigen expression assessed by multipanel flow cytometric analysis for the stem cell markers Nanog-PE, OCT3/4-PerCP-Cy5.5, Sox2-Alexa Fluor 647, and SSEA-4-FITC (assay #5.1) plus Fvs 510 (AmCyan; assay #5.2) as live/dead discriminator. Acquisition and analysis were performed on a BD FACSCanto™ II system using BD FACS Diva Software Version 6.1.3. Analysis was performed using Flow Jo V10.7.1. Assay 6: Cell gene expression assessed by the PluriTest™ assay (assay #6) as pluripotency plot. Transcriptomes of MCBs IMR90-C4 (upper panel) and *Life-Act-eGFP* (lower panel) were analyzed and processed in the PluriTest™ algorithm to generate pluripotency and novelty score. Depicted are pluripotency score (y-axis) and novelty score (x-axis). The red and blue background visualize the empirical distribution of the pluripotent (red) and non-pluripotent (blue) samples in the reference dataset. A non-iPSC sample was included in this experiment to serve as a control for non-pluripotency.

cytometry, and assessment of OCT4 and Sox2 expression in a lineage commitment assay (Pamies et al., 2017). While all of these methods and markers are widely accepted and commonly used, a standardized set of markers has yet to be established (Pamies et al., 2017). We choose to use a commercially available FACS antibody kit for stem cell transcription factors to analyze the expression of stem cell markers on the protein level at the time of banking. This ensures a quantitative outcome, a relatively easy establishment in the laboratory, and includes three markers of the standard human pluripotent stem cell (hPSC) panel, OCT3/4, Sox2, and Nanog, of which an analysis of at least two has been stated as mandatory (Sullivan et al., 2018). It also yields the possibility to expand the assay for an additional canonical cell surface marker, in our case SSEA-4, which has also been proposed (Pamies et al., 2017; Sullivan et al., 2018). Performing the analysis for our MCBs revealed that although OCT3/4,

Sox2, and SSEA-4 were all expressed in well above 95% of the IMR90-C4 MCB cells cultivated on LN521 (98.2, 96.3, and 99.9%), Nanog expression fell short of the quality criterion of > 70% marker expression (Pamies et al., 2017; Sullivan et al., 2018; Fig. S1<sup>2</sup>). When the cultivation conditions were changed to MG and mTeSR medium (according to 2.1.2.4), expression of OCT3/4, Sox2, and SSEA-4 remained at the high level observed on LN521 (98.2, 95.1, and 99.8%, respectively), but Nanog was now expressed in 70.8% of the cells (Fig. 5; left, upper panel), indicating the of the chosen culturing conditions on hiPSC performance. This observation is supported by others, who already stated that there is no culture method that provides optimal conditions for all hiPSC lines (Christensen et al., 2018). With these results in mind, *Life-Act-eGFP* cells were directly cultured and banked on MG and expressed Nanog (91.4%), OCT3/4 (98.8%) and Sox2 (96.5%) (Fig. 5; left,

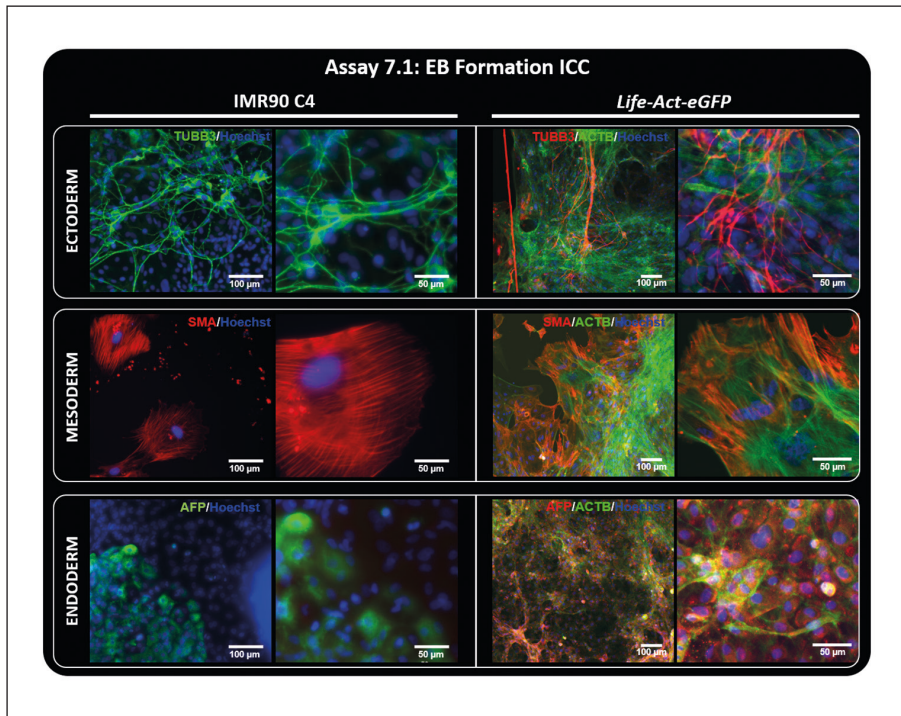


**Fig. 6: Results of EB formation assessed by immunocytochemistry (assay 7.1)**

Representative immunofluorescent images of plated EBs of the MCBs of IMR90-C4 (left) and *Life-Act-eGFP* (right). EBs were generated, differentiated under proliferating conditions for 7 days, and then plated on gelatin-coated 24-well plates and fixed after 7 and 14 days of differentiation. Cells were stained for markers of the three germ layers:  $\beta$ (III) tubulin (TUBB3) for ectoderm, smooth muscle actin (SMA) for mesoderm and  $\alpha$ -feto protein (AFP) for endoderm. All images were taken from cells fixed on day 14 after plating, except for IMR90-C4 TUBB3, which represents day 7.

lower panel). We wish to point out that using animal-free matrices is highly desirable, yet such matrices need to be shown to yield comparable results to Matrigel. Note that SSEA-4 expression was not analyzed, as 98.6% of the *Life-Act-eGFP* cells express GFP, which is detected in the same channel as the SSEA4-FITC antibody. Using a different marker for this marker might be an option for future analyses. Cell viability assessed using Fvs 510 was at 92.6 and 93.9% for IMR90-C4 and *Life-Act-eGFP*, respectively (Fig. 5; left).

To assess the expression of stem cell markers on mRNA level, we chose the commercially available PluriTest™ assay (Müller et al., 2011), which is a high-density microarray comparing the transcriptome of a test cell line to that of a large number of known pluripotent cell lines (ISCI, 2018). It is not able to account for heterogeneous cell populations (D'Antonio et al., 2017) and is therefore restricted to the assessment of self-renewal patterns (Pamies et al., 2017). Nevertheless, this assay provides valid insights into the stem cell character of cells based on a large number of analyzed genes (D'Antonio et al., 2017). Cell gene expression analyses of our banked hiPSC lines assessed by the PluriTest™ assay revealed that both cluster with the pluripotent samples in the reference set and yield a pluripotency score (PS) of 39.83 and 38.31 and a novelty score (NS) of 1.23 and 1.58 for IMR90-C4 and *Life-Act-eGFP*, respectively (Fig. 5; right). This is well within the range of the threshold values of  $> 20$  for PS, indicating that the samples are more similar to the pluripotent samples of the reference set than to the other samples, and  $< 1.67$  for NS, demonstrating that the tested samples can be well reconstructed based on existing data from other well-characterized iPSC and ESC lines established for this assay (Müller et al., 2011; Müller, 2014).

### 3.5 Assessment of pluripotency (assay 7)

While the *in vivo* teratoma assay identifying cell types of ectodermal, mesodermal and endodermal origin using H/E stained histological sections is still considered to be the gold standard for pluripotency assessment of a given hPSC line, it holds the ethical burden of animal testing (Gertow et al., 2007; Gropp et al., 2012; Pamies et al., 2017), is cost- and time-intensive, is associated with reproducibility problems, and requires special expertise (ISCBI, 2009). Therefore, alternative, low-burden, high-throughput molecular methods are on the rise (Buta et al., 2013; Pamies et al., 2017). While also other methods, e.g., directed differentiation (Borowiak et al., 2009; Chambers et al., 2009; Kattman et al., 2011; Burrige et al., 2012) exist, positive detection of trilineage markers (e.g., SMA for mesoderm, TUBB3 for ectoderm, and AFP for endoderm) in spontaneously differentiating EBs is an accepted method to verify the pluripotency of PSCs (Sathananthan and Trounson, 2005; de Miguel et al., 2010; Pistollato et al., 2012). As suggested by ISCI (2018), we chose to combine *in vitro* spontaneous EB differentiation with bioinformatic Scorecard™ analyses. This commercially available assay is a medium/low density focused array that compares lineage expression levels to a reference standard (Pamies et al., 2017), thereby (i) the self-renewal capacity and (ii) the trilineage differentiation potential of an hiPSC line (Bock et al., 2011). Alternatively, it is an option to perform an in-house qPCR assay on the EBs, as suggested by O'Shea and co-workers (2020), analyzing three to markers for each germ layer. However, we believe that the additional information provided by the Scorecard™ assay the additional costs and effort.

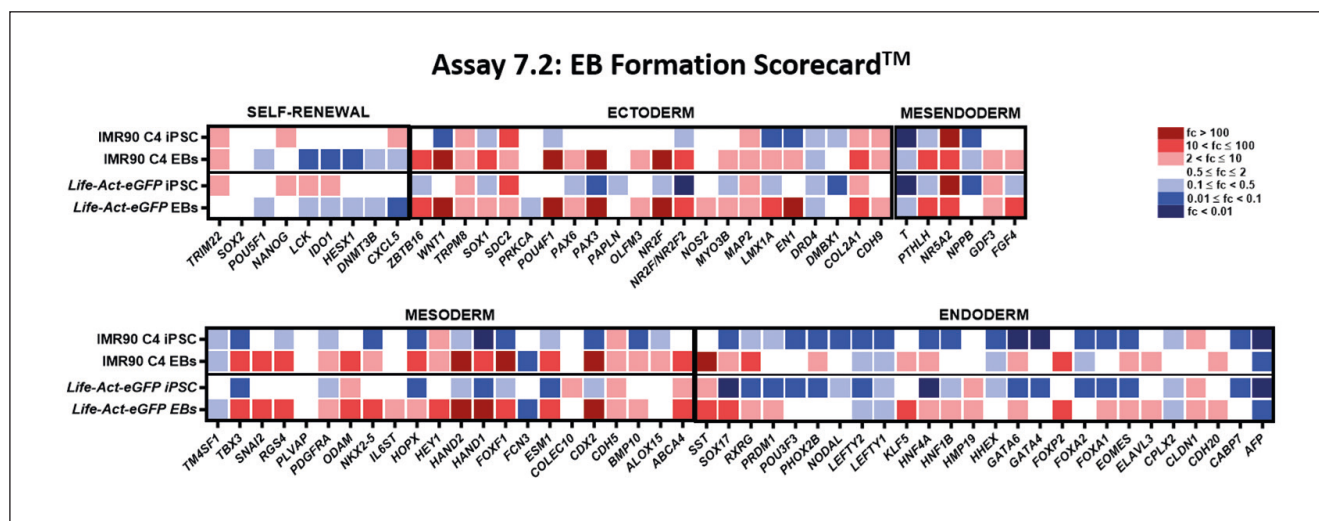


**Fig. 7: Results of EB formation assessed by the Scorecard™ assay (assay 7.2) for MCBs of IMR90-C4 (upper panel) and *Life-Act-eGFP* (lower panel)**

EBs were generated and cultured under proliferating conditions for 7 days before cell pellets were collected for analysis. The respective undifferentiated hiPSCs serve as undifferentiated controls. Colors correlate with the fold-change in expression of the indicated gene relative to the undifferentiated reference set.

Following this approach, ICC analyses of differentiated EBs of both analyzed hiPSC lines revealed that cells of both MCBs were able to spontaneously differentiate into cells expressing marker proteins for the three germ layers: TUBB3 for ectoderm, SMA for mesoderm, and AFP for endoderm (Fig. 6). Additional Scorecard™ gene expression analyses these Whereas marker genes for self-renewal such as *TRIM22* and *Nanog* were upregulated in undifferentiated hiPSCs of both MCBs, they were downregulated in the respective EBs, and at the same time marker genes for ectoderm, mesendoderm, mesoderm and endoderm were upregulated compared to the undifferentiated reference set (Fig. 7). Comparing the level of gene induction between the different germ layers, it is noticeable that while still upregulated compared to the undifferentiated hiPSCs, expression levels of endodermal markers seem to be lower (with the exception of *SST* for the IMR90 C4 cells, they are in the range of 10 to 100-fold induction) than expression of markers for ectoderm and mesoderm. Here, overall, more markers are upregulated, some also to over 100-fold. This might indicate that both analyzed hiPSC lines are less prone to differentiate into cells of the endodermal lineage.

### 3.6 Post-thaw recovery assessment (assay 8)

It has been reported that a post-thaw recovery assessment directly at the time of thawing might be misleading regarding the integrity of the cells (Pamies et al., 2017), therefore we chose to analyze the banked cells when they were split the time after thawing and assessed the of the colonies, cell morphology, and percentage of living cells.

We are aware that hiPSCs are affected by cryopreservation and thawing, which can lead to changes in cell morphology and altered proliferation behavior in the passage after cryopreservation (Archibald et al., 2016). Nevertheless, we believe it is im-

portant to assess the morphology of the thawed cells to get an idea of the quality of the banked cells. Later, cells are monitored on a daily basis and used for experiments only after a recovery period of three passages and with a morphology score of A.

To assess post-thaw recovery of the MCB vials, one vial each for IMR90-C4 and *Life-Act-eGFP* was thawed and cultivated until the cells reached approx. 70% and needed passaging for the time post thawing (p.t.). For IMR90-C4 this was on day 3 p.t. and for *Life-Act-eGFP* on day 2 p.t. The cultures were assessed microscopically (Fig. 8, right) and displayed characteristic stem cell morphology. Furthermore, the percentage of living cells was assessed using the trypan blue exclusion assay (Fig. 8, left), revealing 92% living cells for IMR90-C4 and 77.5% for *Life-Act-eGFP*.

### 3.7 Assay costs

All too often, QC assays are not regularly applied in academic labs, as the costs are believed to be high and, frankly speaking, it is commonly to get such work by third party funding. Nevertheless, we argue that the of performing QC assays resulting in high quality cell material, which is a prerequisite for reproducible data, by far outweighs the burden. To promote the integration of QC work into academic research projects, we have calculated the costs for the generation of quality controlled MCBs and WCBs.

A standard MCB of 50 vials with all eight QC assays described here totals approximately 2340€ (Tab. 3). Every additional WCB of 50 vials with 5 QC-assays will cost about another 1000€. Let's make a simple theoretical calculation: One MCB of 50 vials (2340€ in total, 46.80€/vial) yields 50 WCBs with 50 individual vials each (~21.20€/vial, considering the MCB vial that is needed to generate these WCBs), resulting in 2500 vials

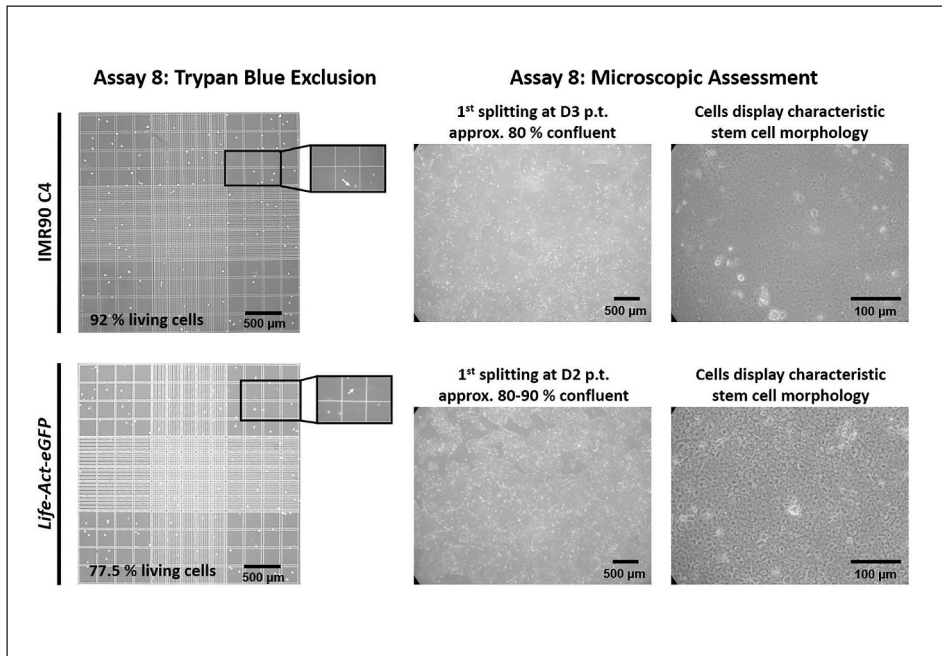


**Fig. 8: Results of trypan blue exclusion assay and microscopic assessment for post-thaw recovery testing (assay 8) of MCBs from IMR90-C4 (upper panel) and *Life-Act-eGFP* (lower panel) at the 1<sup>st</sup> split after re-thawing (D3 for IMR90-C4, D2 for *Life-Act-eGFP*)**

Left: Results of trypan blue exclusion assay. Right: Representative images of the respective cultures showing the density of the cultures (40x magnification) as well as the stem cell morphology of the cells (200x magnification). p.t., post thaw; D, day

**Tab. 3: Estimated costs for a MCB of 50 vials including all suggested assays for quality control**

A short summary of included techniques and analyses is included in brackets. Average costs are listed, with lowest and highest costs in brackets. Please note that this list is probably not complete and should only give a gross estimate of the costs. Not included are personnel costs, standard plastic ware, EtOH, pipette tips, etc. Procedures/assays that need to be performed for both MCB and WCB are indicated in blue italic font.

Assay #	Assay	Average costs/MCB (50 vials) (€) (lowest and highest costs)
	<i>Culturing costs from thawing to MCB (Matrigel, medium, EDTA)</i>	<i>509.45</i>
	<i>Cryopreservation (cryovials, EDTA, cryopreservation medium)</i>	<i>220.41</i>
1	<i>Colony morphology</i>	<i>n.a.c.</i>
2	<i>Mycoplasma PCR</i>	<i>34.83</i>
3	<i>STR genotyping (gDNA isolation, STR analysis)</i>	<i>72.94 (25.87-120) d.o.p.</i>
4	<i>Karyotype analysis</i>	<i>150.00 (0-300) d.o.p.</i>
5.1	<i>FACS analysis of stem cell markers (FACS kit, additional SSEA-4 antibody, and isotype control)</i>	<i>143.30</i>
5.2	<i>Cell count and viability (fixable viability stain for FACS analysis)</i>	<i>2.91</i>
6	<b>PluriTest™</b>	<b>283.90</b>
7	<b>EB formation</b> (culture dishes, gelatine solution, medium, PBS with and w/o Ca <sup>2+</sup> and Mg <sup>2+</sup> , EDTA)	<b>188.04</b>
7.1	<b>ICC of EBs</b> (PBS with Ca <sup>2+</sup> and Mg <sup>2+</sup> , BSA, Tween 20, Hoechst 33258, first antibodies against AFP, SMA and TUBB3, secondary antibody)	<b>132.52</b>
7.2	<b>Scorecard™</b>	<b>601.70</b>
8	<i>Post-thaw recovery assessment</i>	<i>n.a.c.</i>
	<b>Total costs</b>	<b>2340</b> (2142.93-2537.06)

n.a.c., no additional costs; d.o.p., depending on provider

**Tab. 4: Overview of proposed QC assays and respective specifications for hiPSC**

Assays (assay #) are numbered consecutively. Procedures/assays that need to be performed for both MCB and WCB are indicated in blue italic font. Release criteria represent acceptance criteria for further use of hiPSCs.

Information about	QC assay #	Proposed characterization assay	Release criteria
<i>Colony/cell morphology</i>	1	<i>Microscopic assessment at time of banking (+ daily assessment)</i>	<i>Characteristic stem cell morphology (see 2.2); lack of spontaneously differentiated cells</i>
<i>Mycoplasma</i>	2	<i>Mycoplasma PCR</i>	<i>No contamination detected</i>
<i>Identity</i>	3	<i>STR genotyping (gDNA isolation, STR analysis)</i>	<i>Shares all alleles of parent line</i>
<i>Karyotype</i>	4	<i>Classical G-banding</i>	<i>Normal diploid karyotype (without clonal aberrations; single aberrations in 5% of the analyzed metaphase spreads are acceptable)</i>
<i>Expression of stem-cell markers</i>	5.1	<i>Cell antigen expression: flow cytometric analysis of stem cell markers SSEA-4, OCT3/4, NANOG, SOX2</i>	<i>&gt; 70% expression of all analyzed markers</i>
	5.2	<i>Cell count and viability (fixable viability stain, flow cytometric analysis)</i>	<i>&gt; 80% viable cells at time of banking</i>
	6	<i>Cell gene expression: PluriTest™</i>	<i>Analyzed cells cluster with hPSC reference</i>
<i>Pluripotency</i>	7.1	<i>EB formation: ICC</i>	<i>At least one marker of each germ layer is detectable</i>
	7.2	<i>EB formation: Scorecard™</i>	
<i>Post-thaw recovery</i>	8	<i>Trypan blue exclusion assay, microscopic assessment</i>	<i>Assessed at 1<sup>st</sup> splitting after thawing (max. 7 days)</i>
			<i>&gt; 70% living cells</i>
			<i>&gt; 70% confluency</i>
			<i>Characteristic stem cell morphology</i>

costing 22.15€ each (21.20€ + (46.80€/50)). To ensure working with hiPSCs for experiments in passage 4-8, we thaw one vial every 4 weeks (12 per year), leading to pure cell costs of approx. 266€ per year (22.15€ x 12). This is by far less than the cost of your average commercially available hiPSC line. In this scenario, these 2.500 WCB vials would be to provide the laboratory with quality-controlled cell material for a little over 208 years (2.500/12).

We strongly believe that these numbers speak for themselves: Although the initial investment seems high, in the long run using quality-controlled cell material as a starting point for any research question pays off!

#### 4 Summary and conclusion

Human iPSCs are a promising tool to replace animal experiments for toxicity testing and other research questions. However, there is international consensus that only quality controlled cell material ensures reproducibility of data. Due to a lack of “hands-on” guidance on hiPSC QC in an academic research environment, we have assembled a set of assays that warrants hiPSC identity, genomic stability, and pluripotency by assessment of cell/colony morphology (assay 1), mycoplasma contamination (assay 2), cell line identity (assay 3), karyotype stability (assay 4), cell antigen

expression and viability (assays 5.1 + 5.2), cell gene expression (assay 6), pluripotency (assays 7.1 + 7.2), and post-thaw recovery (assay 8; Tab. 4) for the two hiPSC lines IMR90-C4 and *Life-Act-eGFP* (Fig. 9). Of note, these assays are intended for hiPSC lines accessed from external sources such as commercial vendors or iPSC biobanks. Additional QC, e.g., viral clearance assays, are necessary if researchers generate their own iPSC lines from primary human material. Furthermore, additional QC assays might be appropriate for genetically hiPSC lines, e.g., the assessment of viral clearance in case of the use of viral vectors. Using these or similar QC assays in the context of a two-tiered-banking approach consisting of one MCB per hiPSC line and respective WCBs provides researchers with reliable cell material for hiPSC-based applications, thereby safeguarding high hiPSC quality at all times. Our calculations demonstrate the feasibility of such an approach in an academic research set-up.

We conclude that an international consensus on QC for stem cell-based academic research, e.g., the strategy followed in this article, is highly warranted. Awareness of funding agencies and journals of QC as a requirement when sponsoring or publishing stem cell research is desirable for improving the current reproducibility crisis in cell-based research. This will not only produce more reliable and reproducible results in basic research but will also strongly support the application and decrease the uncertainty of stem cell-based methods in applied sciences like regulatory toxicology.

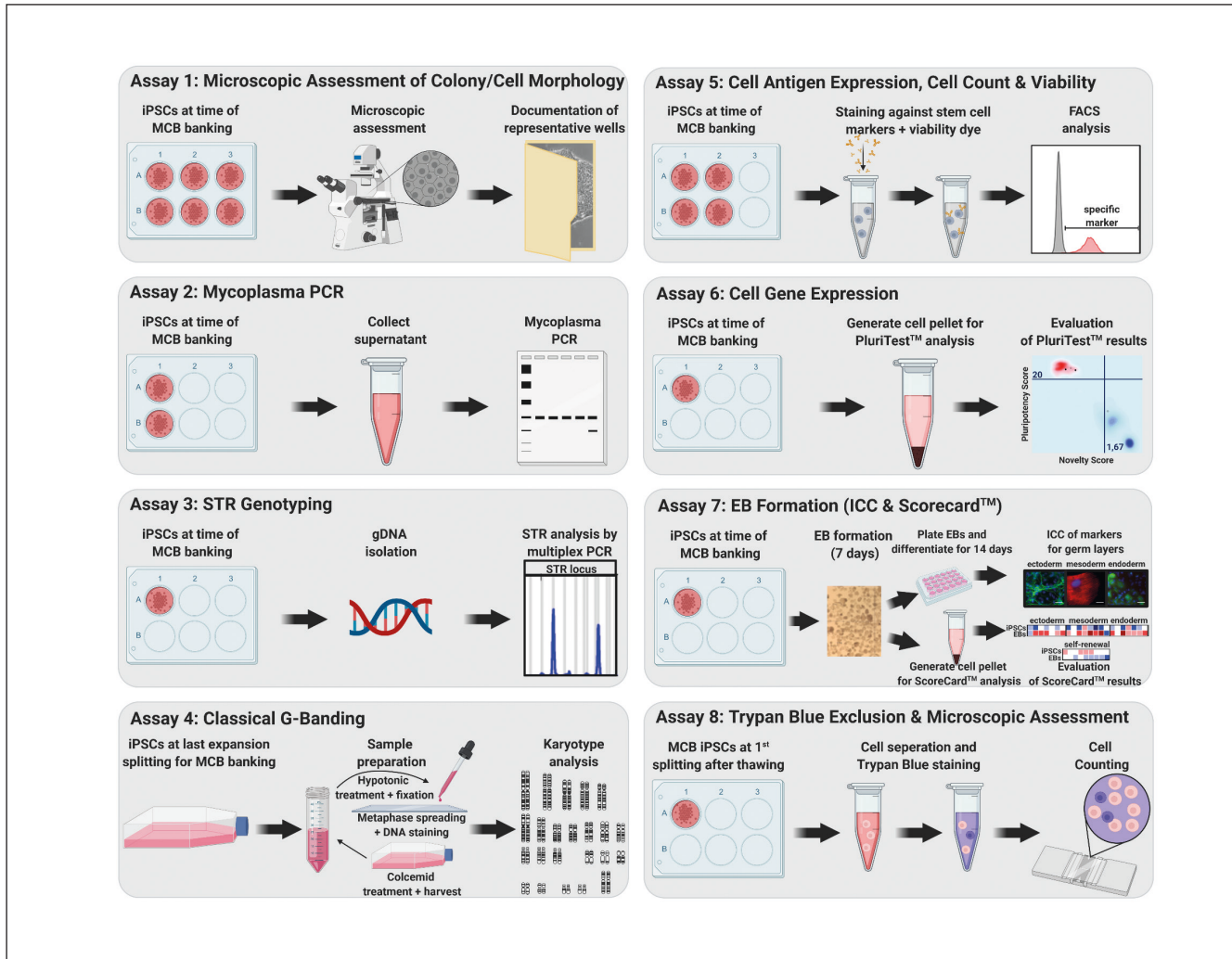


**Fig. 9: Summary of proposed quality control assays for iPSC in an academic research laboratory**

## References

- Abbot, S., Agbanyo, F., Ahlfors, J. E. et al. (2018). Report of the international conference on manufacturing and testing of pluripotent stem cells. *Biologicals* 56, 67-83. doi:10.1016/j.biologicals.2018.08.004
- Adler, S., Allsopp, T., Bremer, S. et al. (2007). hESC Technology for Toxicology and Drug Development: Summary of Current Status and Recommendations for Best Practice and Standardization The Report and Recommendations of an ECVAM Workshop.
- Almeida, J. L., Cole, K. D. and Plant, A. L. (2016). Standards for cell line authentication and beyond. *PLoS Biol* 14, e1002476. doi:10.1371/journal.pbio.1002476
- Amps, K., Andrews, P. W., Anyfantis, G. et al. (2011). Screening ethnically diverse human embryonic stem cells a chromosome 20 minimal amplicon conferring growth advantage. *Nat Biotechnol* 29, 1132-1144. doi:10.1038/nbt.2051
- Andrews, P. W., Baker, D., Benvenisty, N. et al. (2015). Points to consider in the development of seed stocks of pluripotent stem

cells for clinical applications: International stem cell banking initiative (ISCBI). *Regen Med* 10, Suppl 2, 1-44. doi:10.2217/rme.14.93

- Archibald, P. R. T., Chandra, A., Thomas, D. et al. (2016). Comparability of automated human induced pluripotent stem cell culture: A pilot study. *Bioprocess Biosyst Eng* 39, 1847-1858. doi:10.1007/s00449-016-1659-9
- Armstrong, S. E., Mariano, J. A. and Lundin, D. J. (2010). The scope of mycoplasma contamination within the biopharmaceutical industry. *Biologicals* 38, 211-213. doi:10.1016/j.biologicals.2010.03.002
- Assou, S., Bouckenheimer, J. and De Vos, J. (2018). Concise review: Assessing the genome integrity of human induced pluripotent stem cells: What quality control metrics? *Stem Cells* 36, 814-821. doi:10.1002/stem.2797
- Baghbaderani, B. A., Tian, X., Neo, B. H. et al. (2015). CGMP-manufactured human induced pluripotent stem cells are available for pre-clinical and clinical applications. *Stem Cell Reports* 5, 647-659. doi:10.1016/j.stemcr.2015.08.015



- Bai, Q., Desprat, R., Klein, B. et al. (2013). Embryonic stem cells or induced pluripotent stem cells? A DNA integrity perspective. *Curr Gene Ther* 13, 93-98. doi:10.2174/1566523211313020003
- Bairoch, A. (2018). The cellosaurus, a cell-line knowledge resource. *J Biomol Tech* 29, 25-38. doi:10.7171/jbt.18-2902-002
- Baker, D. E. C., Harrison, N. J., Maltby, E. et al. (2007). Adaptation to culture of human embryonic stem cells and oncogenesis in vivo. *Nat Biotechnol* 25, 207-215. doi:10.1038/nbt1285
- Baker, M. (2016). How quality control could save your science. *Nature* 529, 456-458. doi:10.1038/529456a
- Baker, M. and Penny, D. (2016). Is there a reproducibility crisis? *Nature* 533, 452-454. doi:10.1038/533452A
- Bartalucci, N., Romagnoli, S., Contini, E. et al. (2019). Long reads, short time: Feasibility of prenatal sample karyotyping by nanopore genome sequencing. *Clin Chem* 65, 1605-1608. doi:10.1373/clinchem.2019.310805
- Bickmore, W. A. (2001). Karyotype analysis and chromosome banding. In *Encyclopedia of Life Sciences*. Chichester, UK: John Wiley & Sons, Ltd. doi:10.1038/npg.els.0001160
- Bock, C., Kiskinis, E., Verstappen, G. et al. (2011). Reference maps of human ES and iPSC cell variation enable high-throughput characterization of pluripotent cell lines. *Cell* 144, 439-452. doi:10.1016/j.cell.2010.12.032
- Borowiak, M., Maehr, R., Chen, S. et al. (2009). Small molecules direct endodermal differentiation of mouse and human embryonic stem cells. *Cell Stem Cell* 4, 348-358. doi:10.1016/j.stem.2009.01.014
- Bruchmüller, I., Pirkil, E., Herrmann, R. et al. (2006). Introduction of a validation concept for a PCR-based Mycoplasma detection assay. *Cytotherapy* 8, 62-69. doi:10.1080/146532405000518413
- Buehring, G. C., Eby, E. A. and Eby, M. J. (2004). Cell line cross-contamination: How aware are mammalian cell culturists of the problem and how to monitor it? *In Vitro Cell Dev Biol Anim* 40, 211-215. doi:10.1290/1543-706x(2004)40<211:clcha>2.0.co;2
- Burridge, P. W., Keller, G., Gold, J. D. et al. (2012). Production of de novo cardiomyocytes: Human pluripotent stem cell differentiation and direct reprogramming. *Cell Stem Cell* 10, 16-28. doi:10.1016/j.stem.2011.12.013
- Buta, C., David, R., Dressel, R. et al. (2013). Reconsidering pluripotency tests: Do we still need teratoma assays? *Stem Cell Res* 11, 552-562. doi:10.1016/j.scr.2013.03.001
- Chambers, S. M., Fasano, C. A., Papapetrou, E. P. et al. (2009). Highly neural conversion of human ES and iPSC cells by dual inhibition of SMAD signaling. *Nat Biotechnol* 27, 275-280. doi:10.1038/nbt.1529
- Chi, K. R. (2013). Out, damned mycoplasma! Pointers for keeping your cell culture free of mycoplasma contamination. *The Scientist*. <https://www.the-scientist.com/?articles.view/articleNo/38381/> (accessed 13.01.2021)
- Christensen, K., Roudnicky, F., Patsch, C. et al. (2018). Requirements for using iPSC-based cell models for assay development in drug discovery. In *Advances in Biochemical Engineering/Biotechnology* (207-220). Springer Science and Business Media Deutschland GmbH. doi:10.1007/10\_2017\_23
- Coecke, S., Balls, M., Bowe, G. et al. (2005). Guidance on good cell culture practice: A report of the second ECVAM task force on good cell culture practice. *Altern to Lab Anim* 33, 261-287. doi:10.1177/026119290503300313
- Conrad, D. F., Pinto, D., Redon, R. et al. (2010). Origins and functional impact of copy number variation in the human genome. *Nature* 464, 704-712. doi:10.1038/nature08516
- Crook, J. M., Tomaskovic-Crook, E. and Ludwig, T. E. (2017). Cryobanking pluripotent stem cells. *Methods Mol Biol* 1590, 151-164. doi:10.1007/978-1-4939-6921-0\_11
- D'Antonio, M., Woodruff, G., Nathanson, J. L. et al. (2017). High-throughput and cost-effective characterization of induced pluripotent stem cells. *Stem Cell Reports* 8, 1101-1111. doi:10.1016/j.stemcr.2017.03.011
- de Miguel, M. P., Fuentes-Julián, S. and Alcaína, Y. (2010). Pluripotent stem cells: Origin, maintenance and induction. *Stem Cell Rev Reports* 6, 633-649. doi:10.1007/s12015-010-9170-1
- Dekant, W. (2016). Toxicology and the reproducibility crisis: Sci-publishing, hazard assessment and risk characterization. *Toxicol Lett* 263, 76-77. doi:10.1016/j.toxlet.2016.09.001
- Dirks, W. G., MacLeod, R. A. F., Nakamura, Y. et al. (2010). Cell line cross-contamination initiative: An interactive reference database of STR covering common cancer cell lines. *Int J Cancer* 126, 303-304. doi:10.1002/ijc.24999
- Drexler, H. G. and Uphoff, C. C. (2002). Mycoplasma contamination of cell cultures: Incidence, sources, effects, detection, elimination, prevention. *Cytotechnology* 90, 75-90. doi:10.1023/A:1022913015916
- Freedman, L. P., Gibson, M. C., Ethier, S. P. et al. (2015). Reproducibility: Changing the policies and culture of cell line authentication. *Nat Methods* 12, 493-497. doi:10.1038/nmeth.3403
- Fritsche, E., Haarmann-Stemmann, T., Kapr, J. et al. (2020). Stem cells for next level toxicity testing in the 21<sup>st</sup> century. *Small* 17, e2006252. doi:10.1002/smll.202006252
- Gertow, K., Przyborski, S., Loring, J. F. et al. (2007). Isolation of human embryonic stem cell-derived teratomas for the assessment of pluripotency. *Curr Protoc Stem Cell Biol*, Chapter 1, Unit1B.4. doi:10.1002/9780470151808.sc01b04s3
- Gropp, M., Shilo, V., Vainer, G. et al. (2012). Standardization of the teratoma assay for analysis of pluripotency of human ES cells and biosafety of their differentiated progeny. *PLoS One* 7, e45532. doi:10.1371/journal.pone.0045532
- Hay, R. J., Macy, M. L. and Chen, T. R. (1989). Mycoplasma infection of cultured cells. *Nature* 339, 487-488. doi:10.1038/339487a0
- Hook, E. B. (1977). Exclusion of chromosomal mosaicism: Tables of 90%, 95%, and 99% limits and comments on use. *Am J Hum Genet* 29, 94-97.
- Howe, B., Umrigar, A. and Tsien, F. (2014). Chromosome preparation from cultured cells. *J Vis Exp*, 50203. doi:10.3791/50203
- Hughes, P., Marshall, D., Reid, Y. et al. (2007). The costs of using unauthenticated, over-passaged cell lines: How much more data do we need? *Biotechniques* 43, 575-586. doi:10.2144/000112598
- ISCBI (2009). Consensus guidance for banking and supply of human embryonic stem cell lines for research purposes. *Stem Cell Rev Reports* 5, 301-314. doi:10.1007/s12015-009-9085-x
- ISCI (2018). Assessment of established techniques to determine de-

- velopmental and malignant potential of human pluripotent stem cells. *Nat Commun* 9, 1925. doi:10.1038/s41467-018-04011-3
- ISCN (2016). *An International System for Human Cytogenomic Nomenclature*. J. McGowan-Jordan, A. Simons and M. Schmid (eds.). S. Karger AG. doi:10.1159/isbn.978-3-318-06861-0
- Kattman, S. J., Witty, A. D., Gagliardi, M. et al. (2011). Stimulation and optimization of activin/nodal and BMP signaling promotes cardiac differentiation of mouse and human pluripotent stem cell lines. *Cell Stem Cell* 8, 228-240. doi:10.1016/j.stem.2010.12.008
- Kilpinen, H., Goncalves, A., Leha, A. et al. (2017). Common genetic variation drives molecular heterogeneity in human iPSCs. *Nature* 546, 370-375. doi:10.1038/nature22403
- Kim, J. H., Kurtz, A., Yuan, B. Z. et al. (2017). Report of the international stem cell banking initiative workshop activity: Current hurdles and progress in seed-stock banking of human pluripotent stem cells. *Stem Cells Transl Med* 6, 1956-1962. doi:10.1002/sctm.17-0144
- Kim, J. H., Alderton, A., Crook, J. M. et al. (2019). A report from a workshop of the international stem cell banking initiative, held in collaboration of global alliance for iPSC therapies and the harvard stem cell institute, Boston, 2017. *Stem Cells* 37, 1130-1135. doi:10.1002/stem.3003
- Kleensang, A., Vantangoli, M. M., Odwin-Dacosta, S. et al. (2016). Genetic variability in a frozen batch of MCF-7 cells invisible in routine authentication affecting cell function. *Sci Rep* 6, 28994. doi:10.1038/srep28994
- Kurosawa, H. (2007). Methods for inducing embryoid body formation: In vitro differentiation system of embryonic stem cells. *J Biosci Bioeng* 103, 389-398. doi:10.1263/jbb.103.389
- Langdon, S. P. (2004). Cell culture contamination: An overview. *Methods Mol Med* 88, 309-317. doi:10.1385/1-59259-406-9:309
- Lei, M., Liang, D., Yang, Y. et al. (2020). Long-read DNA sequencing fully characterized chromothripsis in a patient with Langer-Giedion syndrome and Cornelia de Lange syndrome-4. *J Hum Genet* 65, 667-674. doi:10.1038/s10038-020-0754-6
- Lenz, M., Goetzke, R., Schenk, A. et al. (2015). Epigenetic biomarker to support differentiation of human induced pluripotent cells. *Sci Rep* 5, 8973. doi:10.1038/srep08973
- Li, F., Hu, J., Xie, K. et al. (2015). Authentication of experimental materials: A remedy for the reproducibility crisis? *Genes Dis* 2, 283. doi:10.1016/j.gendis.2015.07.001
- Liu, G., David, B. T., Trawczynski, M. et al. (2020). Advances in pluripotent stem cells: History, mechanisms, technologies, and applications. *Stem Cell Rev Reports* 16, 3-32. doi:10.1007/s12015-019-09935-x
- Liu, W. and Chen, G. (2014). Cryopreservation of human pluripotent stem cells in chemically defined medium. *Curr Protoc Stem Cell Biol* 2014, 1c.17.1-1c.17.13. doi:10.1002/9780470151808.sc01c17s31
- Loring, J., Schwartz, P. and Wesselschmidt, R. (2007). *Human Stem Cell Manual*. 2<sup>nd</sup> edition. San Diego, CA, USA: Academic Press.
- Lorsch, J. R., Collins, F. S. and Lippincott-Schwartz, J. (2014). Fixing problems with cell lines. *Science* 346, 1452-1453. doi:10.1126/science.1259110
- MacArthur, D. G., Manolio, T. A., Dimmock, D. P. et al. (2014). Guidelines for investigating causality of sequence variants in human disease. *Nature* 508, 469-476. doi:10.1038/nature13127
- MacLeod, R. A. F., Dirks, W. G., Matsuo, Y. et al. (1999). Widespread intraspecies cross-contamination of human tumor cell lines arising at source. *Int J Cancer* 83, 555-563. doi:10.1002/(SICI)1097-0215(19991112)83:4<555::AID-IJC19>3.0.CO;2-2
- Maddah, M., Shoukat-Mumtaz, U., Nassirpour, S. et al. (2014). A system for automated, noninvasive, morphology-based evaluation of induced pluripotent stem cell cultures. *J Lab Autom* 19, 454-460. doi:10.1177/2211068214537258
- Mayshar, Y., Ben-David, U., Lavon, N. et al. (2010). Identification and characterization of chromosomal aberrations in human induced pluripotent stem cells. *Cell Stem Cell* 7, 521-531. doi:10.1016/j.stem.2010.07.017
- McNutt, M. (2014). Journals unite for reproducibility. *Science* 346, 679. doi:10.1126/science.aaa1724
- Miyakawa, T. (2020). No raw data, no science: Another possible source of the reproducibility crisis. *Mol Brain* 13, 24. doi:10.1186/s13041-020-0552-2
- Müller, F. J., Schuldt, B. M., Williams, R. et al. (2011). A bioinformatic assay for pluripotency in human cells. *Nat Methods* 8, 315-317. doi:10.1038/nmeth.1580
- Müller, F.-J. (2014). Assessment of human pluripotent stem cells with PluriTest. *StemBook*. doi:10.3824/stembook.1.84.1
- Munafò, M. R., Nosek, B. A., Bishop, D. V. M. et al. (2017). A manifesto for reproducible science. *Nat Hum Behav* 1, 0021. doi:10.1038/s41562-016-0021
- Nelson-Rees, W. A., Daniels, D. W. and Flandermeyer, R. R. (1981). Cross-contamination of cells in culture. *Science* 212, 446-451. doi:10.1126/science.6451928
- NIH (2015). NIH Workshop on Reproducibility in cell culture studies. [https://videocast.nih.gov/watch\\_16876](https://videocast.nih.gov/watch_16876)
- Nikfarjam, L. and Farzaneh, P. (2012). Prevention and detection of mycoplasma contamination in cell culture. *Cell J* 13, 203-212.
- Ntai, A., Baronchelli, S., La Spada, A. et al. (2017). A review of research-grade human induced pluripotent stem cell generation and biobanking processes. *Biopreserv Biobank* 15, 384-392. doi:10.1089/bio.2016.0097
- O'Shea, O., Steeg, R., Chapman, C. et al. (2020). Development and implementation of large-scale quality control for the European bank for induced pluripotent stem cells. *Stem Cell Res* 45, 101773. doi:10.1016/j.scr.2020.101773
- OECD (2018). Guidance Document on Good In Vitro Method Practices (GIVIMP). *OECD Series on Testing and Assessment, No. 286*. OECD Publishing, Paris. doi:10.1787/9789264304796-en
- Pamies, D., Bal-Price, A., Simeonov, A. et al. (2017). Good cell culture practice for stem cells and stem-cell-derived models. *ALTEX* 34, 95-132. doi:10.14573/altex.1607121
- Pamies, D., Bal-Price, A., Chesné, C. et al. (2018). Advanced good cell culture practice for human primary, stem cell-derived and organoid models as well as microphysiological systems. *ALTEX* 35, 353-378. doi:10.14573/altex.1710081
- Pamies, D., Leist, M., Coecke, S. et al. (2020). Good cell and



- tissue culture practice 2.0 (GCCP 2.0) – Draft for stakeholder discussion and call for action. *ALTEX* 37, 490-492. doi:10.14573/altext.2007091
- Pistollato, F., Bremer-Hoffmann, S., Healy, L. et al. (2012). Standardization of pluripotent stem cell cultures for toxicity testing. *Expert Opin Drug Metab Toxicol* 8, 239-257. doi:10.1517/17425255.2012.639763
- Rohani, L., Johnson, A. A., Naghsh, P. et al. (2018). Concise review: Molecular cytogenetics and quality control: Clinical guardians for pluripotent stem cells. *Stem Cells Transl Med* 7, 867-875. doi:10.1002/sctm.18-0087
- Rojas, A., Gonzalez, I. and Figueroa, H. (2008). Cell line cross-contamination in biomedical research: A call to prevent unawareness. *Acta Pharmacol Sin* 29, 877-880. doi:10.1111/j.1745-7254.2008.00809.x
- Rottem, S. and Barile, M. F. (1993). Beware of mycoplasmas. *Trends Biotechnol* 11, 143-151. doi:10.1016/0167-7799(93)90089-R
- R., Morato-Marques, M., Borsoi, J. et al. (2018). Monitoring cell line identity in collections of human induced pluripotent stem cells. *Stem Cell Res* 28, 66-70. doi:10.1016/j.scr.2018.01.030
- Sathananthan, A. H. and Trounson, A. (2005). Human embryonic stem cells and their spontaneous differentiation. *Ital J Anat Embryol* 110, Suppl, 151-157.
- Scudellari, M. (2016). A decade of: iPS Cells. *Nature* 534, 310-312. doi:10.1038/534310a
- Shibamiya, A., Schulze, E., Krauß, D. et al. (2020). Cell banking of hiPSCs: A practical guide to cryopreservation and quality control in basic research. *Curr Protoc Stem Cell Biol* 55, e127. doi:10.1002/cpsc.127
- Sikkema-Raddatz, B., Castedo, S. and Te Meerman, G. J. (1997). Probability tables for exclusion of mosaicism in prenatal diagnosis. *Prenat Diagn* 17, 115-118. doi:10.1002/(SICI)1097-0223(199702)17:2<115::AID-PD37>3.0.CO;2-A
- Stacey, G. N., Crook, J. M., Hei, D. et al. (2013). Banking human induced pluripotent stem cells: Lessons learned from embryonic stem cells? *Cell Stem Cell* 13, 385-388. doi:10.1016/j.stem.2013.09.007
- Stacey, G. N., Masters, J. R. W., Hay, R. J. et al. (2000). Cell contamination leads to inaccurate data: We must take action now. *Nature* 403, 356. doi:10.1038/35000394
- Sullivan, S., Stacey, G. N., Akazawa, C. et al. (2018). Quality control guidelines for clinical-grade human induced pluripotent stem cell lines. *Regen Med* 13, 859-866. doi:10.2217/rme-2018-0095
- Suter-Dick, L., Alves, P. M., Blaauboer, B. J. et al. (2015). Stem cell-derived systems in toxicology assessment. *Stem Cells Dev* 24, 1284-1296. doi:10.1089/scd.2014.0540
- Taapken, S. M., Nisler, B. S., Newton, M. A. et al. (2011). Karyotypic abnormalities in human induced pluripotent stem cells and embryonic stem cells. *Nat Biotechnol* 29, 313-314. doi:10.1038/nbt.1835
- Takahashi, K., Tanabe, K., Ohnuki, M. et al. (2007). Induction of pluripotent stem cells from adult human fibroblasts by defined factors. *Cell* 131, 861-872. doi:10.1016/j.cell.2007.11.019
- Timenetsky, J., Santos, L. M., Buzinhani, M. et al. (2006). Detection of multiple mycoplasma infection in cell cultures by PCR. *Brazilian J Med Biol Res* 39, 907-914. doi:10.1590/S0100-879X2006000700009
- Wagner, K. and Welch, D. (2010). Cryopreserving and recovering of human iPS cells using complete knockout serum replacement feeder-free medium. *J Vis Exp*, e2237. doi:10.3791/2237
- Wakui, T. (2017). Method for evaluation of human induced pluripotent stem cell quality using image analysis based on the biological morphology of cells. *J Med Imaging* 4, 1. doi:10.1117/1.jmi.4.4.044003
- WHO (2013). Annex 3. Recommendations for the evaluation of animal cell cultures as substrates for the manufacture of biological medicinal products and for the characterization of cell banks. Replacement of Annex 1 of WHO Technical Report Series, No. 878. [http://www.who.int/biologicals/vaccines/TRS\\_978\\_Annex\\_3.pdf](http://www.who.int/biologicals/vaccines/TRS_978_Annex_3.pdf) (accessed 13.01.2021)
- Xu, H., Baroukh, C., Dannenfelser, R. et al. (2013). ESCAPE: Database for integrating high-content published data collected from human and mouse embryonic stem cells. *Database* 2013, bat045. doi:10.1093/database/bat045
- Yaffe, M. P., Noggle, S. A. and Solomon, S. L. (2016). Raising the standards of stem cell line quality. *Nat Cell Biol* 18, 236-237. doi:10.1038/ncb3313
- Yu, M., Selvaraj, S. K., Liang-Chu, M. M. Y. et al. (2015). A resource for cell line authentication, annotation and quality control. *Nature* 520, 307-311. doi:10.1038/nature14397
- Zhang, S., Liang, F., Lei, C. et al. (2019). Long-read sequencing and haplotype linkage analysis enabled preimplantation genetic testing for patients carrying pathogenic inversions. *J Med Genet* 56, 741-749. doi:10.1136/jmedgenet-2018-105976

### Conflict of interest

The authors have no conflict of interest.

### Acknowledgements

The authors thank Dr Petra Boehme (Institute for Forensic Medicine, UKD), Dr Sebastian Hänsch (CAi, HHU Düsseldorf), and Kirstin K. Melton (Thermo Fischer) for excellent technical support. The graphical abstract and Figure 1 were created using BioRender.com. This work was supported by the project CERST (Center for Alternatives to Animal Testing) of the Ministry for Culture and Science of the State of North-Rhine Westphalia, Germany (number 233-1.08.03.03-121972/131 – 1.08.03.03 – 121972), the European Union's Horizon 2020 Research and Innovation Program, ENDpoiNTs project [grant agreement number: 825759], the DisCoVer VIP+ project of the Federal Ministry of Education and Research [BMBF; funding code: 03VP03792], and a project of the Leibniz Cooperative Excellence program [application number K246/2019].



## 2.7 HiPSC-derived 3D neural models reveal neurodevelopmental pathomechanisms of the Cockayne Syndrome B

*Julia Kapr, Ilka Scharkin, Haribaskar Ramachandran, Philipp Westhoff, Marius Pollet, Selina Dangeleit, Gabriele Brockerhoff, Andrea Rossi, Katharina Koch, Jean Krutmann, Ellen Fritsche*

Cockayne Syndrome B (CSB) is a hereditary multiorgan syndrome which - through largely unknown mechanisms - can affect the brain where it clinically presents with microcephaly, intellectual disability and demyelination. Using human induced pluripotent stem cell (hiPSC)-derived neural 3D models generated from CSB patient-derived and isogenic control lines, we here provide explanations for these three major neuropathological phenotypes. In our models, CSB deficiency is associated with (i) impaired cellular migration due to defective autophagy as an explanation for clinical microcephaly; (ii) altered neuronal network functionality and neurotransmitter GABA levels, which is suggestive of a disturbed GABA switch that likely impairs brain circuit formation and ultimately causes intellectual disability; and (iii) impaired oligodendrocyte maturation as a possible cause of the demyelination observed in children with CSB. Of note, some, but not all of these phenotypes could be rescued by pharmacological HDAC inhibition.

Journal:	Cell Stem Cell
Impact factor:	23.9 (2022)
Contribution to the publication:	75%
Type of authorship:	Experiments for all Figures, Lead Writing and Editing
Status of publication:	First Author
	Submitted to Cell Stem Cell (16 August 2023)

# Cell Stem Cell

## HiPSC-derived 3D neural models reveal neurodevelopmental pathomechanisms of the Cockayne Syndrome B --Manuscript Draft--

<b>Manuscript Number:</b>	
<b>Full Title:</b>	HiPSC-derived 3D neural models reveal neurodevelopmental pathomechanisms of the Cockayne Syndrome B
<b>Article Type:</b>	Research Article
<b>Keywords:</b>	disease modeling; in vitro; personalized; autophagy; brain development; HDAC; MEA; oligodendrocytes; GABA; migration
<b>Corresponding Author:</b>	Ellen Fritsche IUF – Leibniz Research Institute for Environmental Medicine Duesseldorf, GERMANY
<b>First Author:</b>	Julia Kapr
<b>Order of Authors:</b>	Julia Kapr Ilka Scharkin Haribaskar Ramachandran Philipp Westhoff Marius Pollet Selina Dangeleit Gabriele Brockerhoff Andrea Rossi Katharina Koch Jean Krutmann Ellen Fritsche
<b>Abstract:</b>	<p>Summary</p> <p>Cockayne Syndrome B (CSB) is a hereditary multiorgan syndrome which - through largely unknown mechanisms - can affect the brain where it clinically presents with microcephaly, intellectual disability and demyelination. Using human induced pluripotent stem cell (hiPSC)-derived neural 3D models generated from CSB patient-derived and isogenic control lines, we here provide explanations for these three major neuropathological phenotypes. In our models, CSB deficiency is associated with (i) impaired cellular migration due to defective autophagy as an explanation for clinical microcephaly; (ii) altered neuronal network functionality and neurotransmitter GABA levels, which is suggestive of a disturbed GABA switch that likely impairs brain circuit formation and ultimately causes intellectual disability; and (iii) impaired oligodendrocyte maturation as a possible cause of the demyelination observed in children with CSB. Of note, some, but not all of these phenotypes could be rescued by pharmacological HDAC inhibition.</p>
<b>Suggested Reviewers:</b>	
<b>Opposed Reviewers:</b>	
<b>Additional Information:</b>	
<b>Question</b>	<b>Response</b>
<b>Original Code</b>	No
Does this manuscript report original code?	

# HiPSC-derived 3D neural models reveal neurodevelopmental pathomechanisms of the Cockayne Syndrome B

Julia Kapr<sup>1</sup>, Ilka Scharkin<sup>1</sup>, Haribaskar Ramachandran<sup>1</sup>, Philipp Westhoff<sup>2</sup>, Marius Pollet<sup>1</sup>, Selina Dangeleit<sup>1</sup>, Gabriele Brockerhoff<sup>1</sup>, Andrea Rossi<sup>1</sup>, Katharina Koch<sup>1,4</sup>, Jean Krutmann<sup>1,3</sup>, Ellen Fritsche<sup>1,3,4\*</sup>

<sup>1</sup>IUF-Leibniz Research Institute for Environmental Medicine, 40225 Düsseldorf, Germany

<sup>2</sup>CEPLAS Metabolism and Metabolomics Laboratory, Cluster of Excellence on Plant Science (CEPLAS), Heinrich Heine University Düsseldorf, 40225 Düsseldorf, Germany

<sup>3</sup>Medical Faculty, University of Düsseldorf, 40225 Düsseldorf, Germany

<sup>4</sup>DNTOX GmbH, 40223 Düsseldorf

\*Corresponding author: [ellen.fritsche@iuf-duesseldorf.de](mailto:ellen.fritsche@iuf-duesseldorf.de)

## **Summary**

Cockayne Syndrome B (CSB) is a hereditary multiorgan syndrome which - through largely unknown mechanisms - can affect the brain where it clinically presents with microcephaly, intellectual disability and demyelination. Using human induced pluripotent stem cell (hiPSC)-derived neural 3D models generated from CSB patient-derived and isogenic control lines, we here provide explanations for these three major neuropathological phenotypes. In our models, CSB deficiency is associated with (i) impaired cellular migration due to defective autophagy as an explanation for clinical microcephaly; (ii) altered neuronal network functionality and neurotransmitter GABA levels, which is suggestive of a disturbed GABA switch that likely impairs brain circuit formation and ultimately causes intellectual disability; and (iii) impaired oligodendrocyte maturation as a possible cause of the demyelination observed in children with CSB. Of note, some, but not all of these phenotypes could be rescued by pharmacological HDAC inhibition.

## **Keywords**

disease modeling, in vitro, personalized, autophagy, brain development, HDAC, MEA, oligodendrocytes, GABA, migration

## Introduction

The Cockayne Syndrome B (CSB) is a rare hereditary disease with heterogeneous multi-organ defects including growth failure, retinal atrophy, deafness and a progeric skin phenotype. In addition, children with CSB develop severe neuropathological defects, with the cardinal phenotypes being microcephaly, intellectual disability and demyelination<sup>1-5</sup>. The disease is caused by several mutations in the excision repair 6 chromatin remodeling factor (ERCC) 6 gene and manifests with varying neurological severity, the most severe being fatal during early childhood<sup>6,7</sup>. CSB rodent models have proven very valuable for gaining insights into the clinical CSB phenotypes and the effects of CSB on the organism level<sup>8-12</sup>, which lead to a good understanding of the mechanistic underpinning of the skin phenotype of CSB<sup>13-15</sup>. However, the origin of the children's neurological defects is still enigmatic, because neurological defects cannot fully be modeled in rodents. Emerging in vitro approaches based on stem cells, e.g. human induced pluripotent stem cells (hiPSCs), can add to the current knowledge in human disease modeling and drug target identification, by providing excellent tools to investigate diseases and their underlying pathomechanisms<sup>16-22</sup>.

CSB was originally found to be involved in the transcription-coupled nucleotide excision repair pathway (TC-NER)<sup>23-26</sup>. However, the neuropathology of the patients cannot be well explained with this mechanism. Previous in vitro studies have therefore suggested a role of CSB in the brain, which is independent of its involvement in the TC-NER<sup>27-30</sup>. Main findings include hindered neuronal differentiation and neuritogenesis, linked to reduced MAP2, as well as SYT9 and BDNF levels in 2D small hairpin (shRNA)-based CSB models of immortalized human neural progenitor cells (hNPC) and SH-SY5Y neuroblastoma cells<sup>27,28</sup>. Vessoni et al.<sup>29</sup> found alterations in synapse density and reduced electrical activity in relation to a dysregulated Growth Hormone/Insulin-like Growth Factor-1 (GH/IGF-1) pathway in 2D iPSC-derived neuron/astrocyte mixed cultures and Liang et al.<sup>30</sup> identified Necdin as a CSB target, which promotes neuronal differentiation in 2D models of CS1AN human CSB fibroblasts and SH-SY5Y cells. Although these studies adumbrate the impact of CSB on brain development, we still lack the necessary understanding of why the clinical phenotypes arise and how we can treat them. Main limitations in current CSB models include non-physiological spatiotemporal microenvironments and low model complexity in 2D systems, missing cell types, such as oligodendrocytes, and a lack of appropriate control cell lines. These limitations outline the need for physiologically more relevant disease models, that better resemble the complexity of the developing human brain, and include isogenic controls.

Study designs using multiple isogenic control pairs from different hiPSC donors have been shown to have an absolute power advantage of up to 60% compared to study designs without isogenic control pairs<sup>31</sup>. Here, we use such a favorable two isogenic pair design to study different neurodevelopmental processes disrupted in CSB. We closed the current knowledge gap on CSB neuropathology, by utilizing two hiPSC-derived fit-for-purpose 3D cell culture models, including human induced neural progenitor cell (hiNPC) neurospheres and 3D-differentiated BrainSpheres<sup>32-35</sup>. The different fit-for-purpose models were applied to answer different research questions concerning the underlying mechanisms of CSB. While hiNPC neurospheres enable the investigation of early developmental key events (KE) such as NPC proliferation, migration and initial terminal differentiation into neurons and astrocytes, modeling later KEs such as neural network formation and oligodendrogenesis benefit from more complex models such as 3D differentiated BrainSpheres<sup>35</sup>. BrainSpheres have a complex 3D cytoarchitecture and consist of the relevant brain cell types, i.e. neurons of different subtypes, astrocytes and – facultatively – oligodendrocytes. Together, both in vitro models serve as ideal tools for investigating earlier and later neurodevelopmental processes and the underlying mechanisms of their disruption<sup>32-35</sup>.

## Results

### Two hiPSC models for neurodevelopmental key event analyses in the Cockayne Syndrome B

For investigating the CSB neuropathology, we established two distinct hiPSC disease models, each including a CSB-deficient and a CSB-expressing cell line. The first model consists of the commercially available hiPSC line IMR90<sup>WT</sup>, which expresses the CSB wildtype in a healthy donor genetic background and an IMR90<sup>KO</sup> line generated via CRISPR Cas technology, by introducing a 13bp deletion into exon 5 of the ERCC6 gene (Figure 1.A, left; supplemental information (SI) Figure S1). The second model consists of the patient-derived hiPSC line CS789 and the isogenic control line CS789<sup>Res</sup>. The patient cell line holds a point mutation (2047C>T) in exon 10 of the ERCC6 gene, which leads to a premature stop codon. The genetic rescue of the control line (CS789<sup>Res</sup>) was generated via CRISPR Cas technology, through a 9 bp in-frame deletion, which removes the stop codon (Figure 1.A, right; SI Figure S1). The donor of the patient hiPSCs was classified with Cerebro-oculofacio-skeletal syndrome (COFS), one of the most severe forms of CSB (supplemental information (SI) Table S1). The patient was, amongst others, afflicted with congenital microcephaly, severe intellectual disability and seizures. He passed away at 10 months of age. All hiPSC lines were quality controlled and banked as described in Tigges et al.<sup>36</sup>, to assure high cell quality throughout the experiments. The hiPSC lines were neurally induced into neurospheres containing hiNPCs, and subsequently either differentiated on an artificial extracellular matrix or floating as 3D BrainSpheres into neurons, astrocytes and facultatively oligodendrocytes (Figure 1.B), thereby generating different fit-for-purpose models.

First, we confirmed by western blot, that the CSB protein is expressed in hiNPC neurospheres of both healthy cell lines (IMR90<sup>WT</sup> and CS789<sup>Res</sup>), but not in either of the disease cell lines IMR90<sup>KO</sup> and CS789 (Figure 1.C left). Despite varying levels of expression (Figure 1.C right), the CSB protein was detected in both IMR90 and CS789<sup>Res</sup> lysates. Due to the non-isogenic nature of the two lines, such differences in expression levels of the CSB protein can be expected. We next confirmed that hiNPC neurospheres of all four cell lines are able to differentiate into cells of the neural lineage, containing both neurons and astrocytes (Figure 1.D).

To obtain an understanding of the consequences of CSB-deficiency for the hiNPCs' bulk transcriptome, we performed mRNA Sequencing (RNAseq) analyses. Here we decided for the control IMR90<sup>WT</sup> and the IMR90<sup>KO</sup> lines, in order to understand the effects of the clean CSB mutation and to exclude impacts of the patient specific genetic background. Transcriptome analyses were performed by plating hiNPC neurospheres onto a coated surface, and differentiating these for 3, 14 and 21 days in vitro (DIV). In total, 893 genes were differentially expressed in IMR90<sup>KO</sup> compared to IMR90<sup>WT</sup> cells across all time points (Figure 2.E). Only significantly regulated genes with a  $|\log_2|$  of  $\geq 1$  were analyzed. These differentially expressed genes (DEG) were mapped to kegg pathways and the top regulated pathways are depicted in Figure 2.F. Most DEGs map to autophagy (ID4140) and mitophagy (ID4137), as well as associated pathways such as MAPK (ID4010), RAP1 (ID4015), PI3K (ID4151) and Ras (ID4014) signaling. Another high number of DEGs map to Cell adhesion molecules (CAMs, ID4514), the regulation of the actin cytoskeleton (ID4810) and focal adhesions (ID4510), as well as calcium signaling (ID4020) and glutamatergic synapses (ID4724).

### CSB-deficiency is associated with inhibited neural progenitor cell migration and alterations in focal adhesion and autophagy

Microcephaly is a major neuropathological finding in CSB patients<sup>6,37</sup>. Two underlying cellular deficiencies that might cause microcephaly are inhibited NPC proliferation or<sup>38,39</sup>. Therefore, we investigated these neurodevelopmental KEs in the CSB proficient and deficient in vitro models. Proliferation was assessed in hiNPC neurospheres, by measuring the sphere diameter over time, and by quantifying the incorporation of Bromodeoxyuridine (BrdU) into newly synthesized DNA. No

significant differences between healthy and disease neurospheres were observed in either proliferation assay (SI Figure S2). Next, we assessed the migration capacity of plated hiNPC neurospheres by measuring total migration distance from the rim of the sphere core to the furthest cell that migrated out of the sphere core, and by counting the total number of migrated nuclei after 3 DIV within the migration area. We observed a significant reduction of the migration distance (25-35%), and a significantly decreased number of migrated nuclei (25-60%) within the migration area using hiNPCs from disease cell lines, compared to their respective controls (Figure 2.A). In support of the inhibited migration, transcriptome analyses present significant upregulation of the focal adhesion-specific gene expression markers *Integrin  $\beta$ 1* (*ITGB1*), *Integrin  $\beta$ 4* (*ITGB4*), *Talin-1* (*TLN1*) and *Vinculin* (*VCL*) in the IMR90<sup>KO</sup>, compared to the healthy IMR90<sup>WT</sup> hiNPC neurospheres after 3, 14 and 21 DIV (Figure 2.B). An important intracellular part of focal adhesions during migration are actin stress fibers. In line with the altered expression of genes involved in regulating the actin cytoskeleton (Figure 1.G), we observed thickened and elongated actin stress fibers in the migration area of plated disease hiNPC neurospheres after 3DIV (Figure 2.C). Inhibited focal adhesion turnover and subsequent migration inhibition thus seems to be one in vitro feature of CSB-deficiency.

In addition to the actin- and focal adhesion-related genes, 141 autophagy-associated mRNAs are significantly regulated in the disease IMR90<sup>KO</sup>, compared to IMR90<sup>WT</sup> differentiated neurospheres (Figure 2.D, right). Gene expression of the autophagosome markers *microtubule-associated proteins 1A/1B light chain 3A* (*LC3A*) and *3C* (*LC3C*) are highly upregulated in the disease differentiated neurospheres. Additionally, the lysosome marker *lysosomal-associated membrane protein-2* (*LAMP2*) and *p62*, a gene coding for a protein that tags intracellular material for targeted autophagy, are also upregulated in the disease differentiated neurospheres (Figure 2.D, left). On the protein level, we identified LAMP2 accumulation in immunocytochemical stainings (ICC, Figure 2.E) and confirmed significant LC3A and LAMP2 accumulation in both CSB-deficient IMR90<sup>KO</sup> and CS789 lines by Western Blot (WB) analyses of plated hiNPC neurospheres after 3 DIV (Figure 2.F). The accumulation of these proteins is a general marker for defective autophagy. Furthermore, a decreased level of mammalian target of rapamycin (mTOR), an autophagy-inhibitor, in IMR90<sup>KO</sup> hints towards an increased demand for autophagy in the disease cells (Figure 2.F).

### **The HDAC6-inhibitor Tubastatin A partially rescues the migration phenotype of disease hiNPC neurospheres**

A previous study on CSB-deficient fibroblasts suggested CSB to interact with  $\alpha$ -tubulin acetyltransferase MEC-17 and histone deacetylase 6 (HDAC6). MEC-17 acetylates  $\alpha$ -tubulin, thereby supporting cargo transport and autophagosome with lysosome fusion, while HDAC6 supports the opposite<sup>15</sup>. We observed significantly decreased acetyl- $\alpha$ -tubulin levels and increased HDAC6 levels in differentiated and plated disease hiNPC neurospheres after 3DIV, compared to their respective healthy controls (Figure 3.A). Low levels of  $\alpha$ -tubulin acetylation generally suggest inhibited autophagy in the cell.

Since targeted autophagy is an important facilitator of focal adhesion turnover, which in turn enables cell migration, we performed HDAC-inhibition experiments to link HDAC activity to altered migration of the CSB disease models. Therefore, we treated the migrating hiNPC spheres at the time of plating with the pan-HDAC inhibitor suberoylanilide hydroxamic acid (SAHA) or the HDAC-6-specific inhibitor Tubastatin A (TubA) for 3 DIV. SAHA did not significantly rescue the migration of the CSB-deficient cell lines, yet reduced the cell viability significantly even at low concentrations (SI Figure S3). Treatment with TubA, however, successfully rescued the reduced migration in both IMR90<sup>KO</sup> and CS789 disease lines, at non-cytotoxic concentrations (Figure 3.B left, see also SI Figure S3). To further strengthen the causal link between autophagy and migration, we inhibited the autophagy in migrating cells with chloroquine (CQ), a suppressor of autophagosome and lysosome fusion. Our results show a significant migration inhibition at non-cytotoxic CQ concentrations in both healthy cell lines (Figure

3.B right, SI Figure S3). Since autophagy is already compromised in the disease cell lines, CQ does not further reduce migration of IMR90<sup>KO</sup> or CS789 at non-cytotoxic concentrations.

### **Microelectrode Array measurements reveal altered neural network activity in CSB-deficient networks**

Next, we investigated the ability of the CSB-deficient cell lines to form functional neural networks as a possible pathomechanism for the intellectual disability seen in CSB patients<sup>1,6,37,40</sup>. These studies were inspired by the transcriptome analyses, which revealed strong alterations in the expression of genes involved in synapse formation, neurotransmitter synthesis and signaling (Figure 4.A). A number of genes involved in the biosynthesis (*CHAT*, *DDC*, *GAD1*, *GAD2*) and vesicular transport (*SLC32A1*, *SLC18A2*, *SLC18A3*) of neurotransmitters are significantly downregulated in IMR90<sup>KO</sup>, compared to IMR90<sup>WT</sup>. Genes for postsynaptic glutamate receptors (*GRIA2*, *GRIA3*, *GRIA4*, *GRIK4*, *GRIN1*, *GRIN2A*, *GRM8*), GABA receptors (*GABRB3*), acetylcholine receptors (*CHRNA2*) and serotonin receptors (*HTR6*) are significantly downregulated in the CSB-deficient cells, while few genes for glutamate and GABA receptors are significantly upregulated (*GRIA1*, *GRIK3*, *GABRG3*). Further differentially expressed genes are involved in postsynaptic density (*SHANK1*, *SHANK2*, *DLGAP1*), voltage-gated (*KCND2*, *KCNQ3*, *PLA2G4A*, *CACNA1D*, *KCNQ4*) and G-protein coupled (*ADCY2*, *ADCY7*, *GNG12*) signaling and neurotransmitter cycling (*MAOA*, *SLC1A2*, *SLC1A6*). Gene markers *MAP2* for neurons, *SYN* for pre-synapses and *PSD95* for post-synapses are not significantly differentially expressed (SI Figure S4).

To get a functional readout of the neural network formation, we recorded the electrical activity of neural networks derived from all cell models on microelectrode arrays (MEA). HiNPC neurospheres were plated onto 96-well MEAs and differentiated for neural network formation over a period of 7 weeks. This allows us to follow the formation of neural networks over time. Using MEAs, we can analyze multiple parameters, that are spike- burst- and network-related and represent single neuronal activity, single neuronal and network maturation, respectively (Figure 4.C)<sup>41</sup>. The number of active electrodes increased in all neural networks and plateaued at approx. 4-5 active electrodes per well (Figure 4.B). Representative spike raster plots (SRP) are shown in Figure 4.D. The SPR of each cell line depicts the spikes (black) and bursts (blue) of the first 30s of the 15 min measurement after 6 weeks in vitro (WIV). We observed differences in some of the measured MEA parameters, between CSB-deficient and -proficient networks, i.e. number of spikes, number of network bursts, area under normalized cross correlation (network synchrony) and number of spikes per network burst (Figure 4.E). The IMR90<sup>KO</sup> networks show no significant difference in the number of spikes compared to the IMR90<sup>WT</sup> networks. However, a significant reduction of network bursts and a significant increase in area under normalized cross correlation and number of spikes per network bursts can be seen, starting from 5 WIV. Similarly, CS789 shows significantly increased area under normalized cross correlation and number of spikes per network bursts. However, the parameters ‘number of network bursts’ and ‘number of spikes’ are both significantly increased in CS789 compared to its control CS789<sup>Res</sup>. Although the two different models cannot be directly compared, alterations on neural networks are similar. The significant changes in electrical activity of both model systems hint towards an altered neural network formation in the disease system and hence are in line with the transcriptome results. Noteworthy are especially the alterations of IMR90<sup>KO</sup> and CS789 in the network activity, compared to their respective controls. Rescue trials with above mentioned HDAC-inhibitors TubA and SAHA did not change the neural network activities of either network (data not shown).

## Altered GABA levels and KCC2 expression hint towards a delayed GABA switch in disease cell lines

In order to evaluate, whether the increase of spiking in CSB-deficient neural models is caused by excitatory neurotransmitter accumulation, we performed Mass Spectrometry (MS) analyses. For that hiNPC neurospheres were plated and differentiated for 14 DIV. Excitatory glutamate levels and GABA levels, show no significant difference between disease and control neurospheres (data not shown). However, their respective GABA/glutamate ratios, calculated from the relative metabolite concentrations, show an accumulation of GABA in both CSB-deficient systems, with significant accumulation in CS789 compared to CS789<sup>Res</sup> (Figure 5.A). The neurotransmitter GABA has excitatory consequences before the postnatal GABA-switch, and holds inhibitory functions thereafter. The transition of this GABA switch is initiated by crucial changes in gene expression of the chloride importer *Na-K-2Cl cotransporter isoform 1 (NKCC1)* and the exporter *K-Cl cotransporter isoform 2 (KCC2)*. During the GABA-switch, *NKCC1* expression decreases, while *KCC2* expression increases. As active chloride transporters, they are responsible for the high and low concentrations of intracellular chlorine before and after GABA switch, respectively<sup>42</sup>. The control IMR90<sup>WT</sup>-derived neural networks mimic this development over 21 DIV with increasing *NKCC1* and decreasing *KCC2* expression. In contrast, *KCC2* is not upregulated in the CSB-deficient networks derived from IMR90<sup>KO</sup>, indicating a disturbed GABA switch (analyzed via RNA Sequencing, Figure 5.B left). A similar picture is observed in the CS789<sup>Res</sup> and CS789 model, yet the GABA switch seems rather delayed, as *KCC2* expression is only significantly lower during the first 14 DIV (analyzed via qPCR, Figure 5.B right). *NKCC1* expression does not change over 21 DIV for this system.

## CSB-deficiency leads to hindered oligodendrocyte maturation

Demyelination is a common neuropathological phenotype of CSB patients<sup>1,6,11,37,40</sup>. Generating hiPSC-based BrainSpheres containing oligodendrocytes in addition to neurons and astrocytes in 3D requires a long-term protocol, that cultures the floating spheres in a shaking incubator (Figure 1.B). Here, BrainSpheres provide a more mature model compared to hiNPC neurospheres, due to their longer maturation period in 3D. After 8 weeks, BrainSpheres were analyzed by immunocytochemical staining for neurons ( $\beta$ III-tubulin) and oligodendrocytes (O4; Figure 6.A). No obvious morphological or numerical differences were observed in O4-stained oligodendrocytes differentiated from disease and respective control hiPSCs. In addition, hiNPC neurospheres were plated for subsequent adherent oligodendrocyte differentiation. After 4 weeks, cells were stained for the pan-oligodendrocyte marker O4 and scanned with a high-content imaging platform. Scanned images were then analyzed for the number of O4 positive cells, using a colocalization tool (Figure 6.B). No significant differences in O4 staining was detected. Myelin formation is dependent on oligodendrocyte differentiation and their maturation. Therefore, we explored if CSB-deficiency impacts oligodendrocyte maturation, by analyzing the gene expressions of pan- and maturation stage-specific oligodendrocyte markers (Figure 6.C). No significant difference in the expression of the pan-oligodendrocyte marker *SOX10* between CSB-proficient and -deficient BrainSpheres was observed. A second pan-oligodendrocyte marker, *Olig2*, was expressed significantly less in BrainSpheres from IMR90<sup>KO</sup>, compared to IMR90<sup>WT</sup>, yet this was not seen in CS789 compared to CS789<sup>Res</sup>. The oligodendrocyte progenitor cell (OPC) marker *FABP7* was overexpressed in both, IMR90<sup>KO</sup> (significantly) and CS789-derived BrainSpheres. The OPC and pre-oligodendrocyte (pre-OL) markers *NG2* and *PDGFRA* were both underexpressed in IMR90<sup>KO</sup>, while CS789 underexpressed *PDGFRA*, but not *NG2*. Correspondingly, expression of the immature and myelinating OL markers *CNPase* and *MBP* were underrepresented in both CSB-deficient BrainSpheres, compared to their respective controls. *PLP* was not differentially expressed in either cell system. These results point to a delayed maturation of developing oligodendrocytes in the CSB-deficient models, with an overexpression of the OPC-specific gene *FABP7* and an underexpression of genes specific for more mature oligodendrocyte stages.

In the next step we assessed, whether this impaired oligodendrocyte maturation is mediated by HDACs, similar to the CSB consequences on migration. Between 6 to 8 WIV, a time where oligodendrocyte maturation takes place in BrainSpheres, IMR90<sup>KO</sup> and CS789 BrainSpheres were treated with 740 nM TubA or 50 nM SAHA (Figure 6.D). Both HDAC inhibitors significantly antagonized the CSB deficiency-dependent underexpression of the pre-OL marker *PDGFR $\alpha$*  in IMR90<sup>KO</sup> and CS789. SAHA additionally induces a significant increase in the expression of the myelinating OL marker *MBP* in both CSB-deficient BrainSpheres (Figure 6.E).

## Discussion

CSB is a heterogeneous hereditary disease with a spectrum of clinical phenotypes highly depending on the associated mutant genotype. However, common pathophysiological brain features of CSB patients include microcephaly, intellectual disability and demyelination<sup>1,6,11,37</sup>. In this work, we provide for the first time mechanistic explanations for the cardinal brain phenotypes observed in CSB patients. We here use two 3D hiPSC-derived neural CSB models and their isogenic controls, a CSB patient-derived line and a genome-edited healthy donor hiPSC line carrying a truncating CSB mutation, both of which result in CSB protein deficiency. Specifically, our results suggest that CSB deficiency inhibits migration through defective autophagy, which is consistent with the clinical microcephaly observed in CSB patients. Further observations of altered electrophysiology and changes in GABA neurotransmitter levels in CSB-deficient neural networks indicate that a disturbed GABA switch is involved in altered brain circuit formation, ultimately leading to intellectual disability in patients. In addition, the impaired oligodendrocyte maturation we observed in CSB-deficient BrainSpheres provides an explanation for the demyelination observed in children with CSB. Therefore, using human-based 3D in vitro models, we identified multiple cellular pathomechanisms of CSB deficiency and were able to link them to the three cardinal brain phenotypes of CSB patients.

Microcephaly can be caused by dysfunctional NPC proliferation, migration, neuronal differentiation or apoptosis<sup>38,39</sup>. We are the first to show that deficiency of the CSB protein causes NPC migration defects. Others previously reported on disrupted neuronal differentiation and neurite outgrowth as a consequence of CSB-deficiency in 2D immortalized NPC and hiPSC-derived neurons, respectively<sup>27,28</sup>, which might also contribute to the microcephalic CSB phenotype. We did not observe an impairment of neuronal differentiation in the differentiating CSB-deficient neurospheres (SI Figure S4), which could be explained by the large heterogeneity of CSB phenotypes between patients. Yet, these differences might also arise due to the different cell systems (immortalized NPCs vs. hiNPCs) or dimensionality (2D vs. 3D). Next, we substantiated the findings of impaired migration by mechanistic understanding. The disrupted migration of CSB-deficient hiNPC neurospheres is accompanied by altered markers of autophagy, i.e. dysregulated auto- and mitophagy-related gene and protein expressions and a reduced amount of acetylated  $\alpha$ -tubulin. Disrupted autophagy based on malfunctioning HDACs was recently established as a major mechanism in the skin pathology of CSB patients<sup>15</sup>. Here we extend this mechanism from the skin to the developing brain, by showing that the HDAC6-specific inhibitor Tubastatin A rescues the inhibited migration in the CSB-deficient neurospheres. This leads us to hypothesize that HDAC-dependent defective autophagy is the cause for the impaired migration. This hypothesis is supported by the well-established knowledge that targeted autophagy plays a major role in focal adhesion turnover, which in turn facilitates cell migration (Figure 3C)<sup>43-45</sup>. HDAC-inhibitors can have highly context-dependent off-target effects, such as decreased proliferation, increased cell death or histone modifications, which need to be evaluated individually, ideally in an organism-specific manner. However, selective HDAC-inhibitors are expected to have a high molecular specificity<sup>46</sup>.

Besides migration, we also studied the functionalities of developing CSB-proficient and -deficient neural networks over 7 WIV on MEAs, as they provide a promising tool to investigate disease-associated alterations in neural circuit formation in vitro<sup>47,48</sup>. Brain circuit formation is precisely orchestrated during brain development and a disruption leads to numerous pathological defects, many of which culminate in intellectual disabilities<sup>49-51</sup>. Mutations in the CSB spectrum are also frequently accompanied by limited cognitive function and delayed neurodevelopment<sup>1,6,37</sup>, leading us to speculate that disrupted circuit formation might be one of the underlying causes. CSB-deficient in vitro neural networks show increased and/or accelerated electrophysiological parameters compared to the controls over time. In addition, neurotransmitter analyses coupled with transcriptional profiling identified elevated GABA levels, and a simultaneous delay in *KCC2* expression, as the possible underlying reason for the increased electrophysiological activities on MEAs. GABA is a fundamentally important neurotransmitter with prenatal excitatory functions and a postnatal shift towards inhibition. This shift is realized by

transcriptional up-regulation of the  $K^+/Cl^-$  co-transporter *KCC2*, which actively lowers intracellular chlorine levels and thereby reverses the passive  $Cl^-$  transport by the GABA receptor<sup>52</sup>. A disruption of this pivotal shift has so far not been described for CSB patients, however, it causes developmental delays and disorders in other neurodevelopmental diseases, such as autism spectrum disorder or attention deficit hyperactivity disorder (ADHD)<sup>52,53</sup>. Opposite electrophysiological findings in hiPSC-derived neuron/glia mixed cultures were published by Vessoni et al.<sup>29</sup>. Differences in activity might be explained by dissimilarity of patient and control cells' genetic backgrounds, endpoint measures only at one time point, general low network activity or other aspects of the MEA protocol. Treatment with Tubastatin A during the 7 WIV did not antagonize the elevated electrical activity suggesting a different, yet unknown, pathophysiological mode-of-action.

A third neuropathological phenotype found in CSB patients is hypomyelination<sup>6,11,37,40,54</sup>. Postnatal lack of myelin in offspring can be evoked by multiple causes ranging from disturbed oligodendrocyte precursor (OPC) cell proliferation, e.g. through Notch pathway inhibition<sup>55</sup>, OPC death e.g. by increased oxidative stress or excitotoxicity<sup>56</sup> to inhibited oligodendrocyte maturation, e.g. by deficiency of thyroid hormone<sup>57</sup>. Studying hypomyelination in human in vitro models has just recently become possible with appropriate protocols becoming available<sup>58-61</sup>. We employed hiPSC-based 3D BrainSpheres, which consist of neurons, astrocytes and oligodendrocytes<sup>59</sup> to investigate the hypomyelination phenotype of CSB-deficient BrainSpheres in vitro. While the quantitative ICC analyses showed no difference in the number of  $O4^+$  oligodendrocytes in both CSB-proficient and -deficient BrainSpheres, gene expression analyses revealed that CSB-deficient oligodendrocytes do not mature at the same pace as their respective isogenic controls. Similar to NPC migration, also the inhibited oligodendrocyte maturation can be partially rescued through HDAC-inhibition via the HDAC6-specific Tubastatin A and the pan-inhibitor SAHA. A number of studies have suggested a role of HDACs in the regulation of rodent oligodendrocyte differentiation and maturation, which renders them promising targets in different neurological pathologies<sup>62-64</sup>. Here we show for the first time that altered human oligodendrocyte maturation in an organotypic CSB disease model can be rescued by pharmacological intervention using HDAC inhibitors.

To date, clinically approved HDAC-inhibitors, such as SAHA (aka Vorinostat), are mainly employed as anti-cancer agents<sup>65,66</sup>. Newer developments however, have brought attention to HDAC-inhibitors in other applications, for instance to treat HIV infections, muscular dystrophies, inflammatory diseases, as well as neurodegenerative diseases, such as Alzheimer's Disease, frontotemporal dementia and Friedreich's ataxia<sup>67</sup>. HDACs might therefore also be promising targets for developing treatment strategies for CSB. However, our data suggests that a combination of drugs might be necessary to target the different cellular adversities observed in the CSB-deficient neural models.

### **Limitations of the study**

In our study we used fit-for-purpose hiPSC-derived 3D in vitro models to discover and investigate multiple neurodevelopmental endophenotypes caused by CSB-deficiency. Thereby, we broadly covered multiple cellular pathomechanisms on the expense of deeply uncovering single molecular mechanisms in full detail. Nevertheless, we were able to provide a first line of evidence that HDAC-dependent and -independent mechanisms converge on the pathophysiology of CSB patients. Especially the delayed GABA switch in CSB-deficient hiPSC-based neural in vitro models should be investigated in more detail, as was previously published for Rett Syndrome<sup>68</sup> and schizophrenia<sup>69</sup>. Another limitation of our study is the lack of microglia in the neural 3D models. Although not originating from neural stem cells, microglia colonize the developing brain between gestational weeks 4 and 24<sup>70</sup>. They influence brain development by refining CNS formation and function, e.g. synapse formation, circuit sculpting, myelination, plasticity, and cognition. Microglia functional alterations have been associated with neurodevelopmental diseases<sup>71,72</sup>. Therefore, especially for testing possible therapeutics in 3D neural models like BrainSpheres, microglia presence will further enhance the predictive value of the models.

With the different neural 3D in vitro models, we provide human-relevant multicellular systems that are already advantageous over tumor cell lines or pure neuronal cultures. However, these structures lack vascularization and, as elaborated above, immune cells. Therefore, these models have limitations when it comes to disease modelling involving inter-organ-crosstalk. Nevertheless, our study shows, that 3D in vitro brain models can provide what animal models often cannot: revealing fundamental disease mechanisms and therapeutic targets. With our work, we aim to spark further investigation into the pathophysiological mechanisms of CSB specifically, and increased usage of hiPSC-based 3D cultures for disease modelling and personalized medicine in general.

## **Authors Contributions**

The author and co-author contributions are allocated in accordance with CRediT. E.F.: conceptualization, funding acquisition, supervision, writing – review & editing. Je.Kr.: conceptualization, funding acquisition, writing – review & editing. K.K.: supervision, writing – review & editing. A.R.: resources, (writing – review & editing). G.B.: Investigation. S.D.: methodology, resources, investigation. M.P.: methodology, resources. P.W.: formal analysis, methodology, resources, investigation. H.R.: methodology, resources. I.S.: investigation, formal analysis. Ju.Ka.: conceptualization, formal analysis, investigation, methodology, project administration, visualization, supervision, writing – original draft.

## **Acknowledgements**

The authors thank the Center for Advanced Imaging (CAi) at the Heinrich Heine University Düsseldorf for their support with the imaging. Furthermore, the authors thank Julia Tigges, Marc Majora (IUF-Leibniz Research Institute for Environmental Medicine, 40225 Düsseldorf, Germany) and David Pamies (Biomedical Sciences, Université de Lausanne, CH-1005 Lausanne, France) for useful discussions and comments. This work is a Leibniz Competition (SAW) Cooperative Excellence project (K246/2019). The IUF is funded by the federal and state governments - the Ministry of Culture and Science of North Rhine-Westphalia (MKW) and the Federal Ministry of Education and Research (BMBF). The CEPLAS metabolism & metabolomics laboratory is funded by the Deutsche Forschungsgemeinschaft (DFG) under Germany's Excellence Strategy – EXC 2048/1 – project 390686111.

## **Declaration of interests**

K.K. and E.F. are founders and shareholders of and partly employed at the company DNTOX GmbH which provides DNT-IVB assay services. The funders had no role in the design of the study; in the collection, analyses, or interpretation of data; in the writing of the manuscript; or in the decision to publish the results.

## Main figure titles and legends

**Figure 1. Human iPSC-derived cell models to study adversities in neurodevelopmental key events linked to Cockayne Syndrome B (CSB).** (A) The two hiPSC-based CSB disease models used in this study include the commercially available IMR90<sup>WT</sup> cell line and its CSB-deficient control line IMR90<sup>KO</sup>, as well as the patient-derived cell line CS789 and its isogenic control CS789<sup>Res</sup>, with partially restored CSB expression. Both IMR90<sup>KO</sup> and CS789<sup>Res</sup> were produced via CRISPR Cas (see also Supplemental Information Figure S1). All hiPSC lines were quality controlled and cell banks were prepared according to Tigges et al.<sup>36</sup>. (B) Illustration depicting different fit-for-purpose models. Human iPSCs were neurally induced to hiNPC neurospheres, which were used to assess NPC proliferation after. HiNPCs were plated onto coated surfaces for subsequent differentiation, to assess NPC migration and differentiated into neurons and astrocytes after 3 DIV (middle). In order to obtain electrically active neural networks, hiNPC neurospheres were plated onto coated MEA plates for subsequent differentiation and electrical activity measurement over 7 WIV (left). The differentiation of oligodendrocytes requires a long-term differentiation protocol. HiNPC neurospheres were differentiated in a shaking incubator for 8 WIV to obtain BrainSpheres, which consist of neurons, astrocytes and oligodendrocytes (right). (C) Immunoblotting of CSB levels in neurospheres of the four hiNPC lines, normalized to the housekeeping protein HSP90 and to the respective control (left) or IMR90<sup>WT</sup> (right). Representative images are depicted and graphs visualize differences in protein content due to mutations in the CSB gene or between CSB expressing lines, respectively. Graphs depict N=3 biological replicates, mean  $\pm$  SEM. Statistical analyses were performed using unpaired two-tailed t-tests. A p-value below 0.05 was termed significant. (D) HiNPC spheres were plated, differentiated for 3DIV and subsequently stained for nuclei (Hoechst, blue), neurons (MAP2, yellow) and astrocytes (AQP4, magenta). (E) Transcriptome analyses were performed by plating hiNPC neurospheres onto a coated surface, and differentiating these for 3, 14 and 21 DIV. VENN Diagram of the significantly DEGs between IMR90<sup>WT</sup> and IMR90<sup>KO</sup> after 3, 14 and 21 DIV, as identified via RNAseq. DEG criteria:  $|\log_2| \geq 1$  and Qvalue of  $\leq 0.05$ . (F) 892 DEGs constantly regulated across the differentiation timepoints were mapped to KEGG pathways and the 30 pathways with the highest percentage of regulated genes are depicted. Abbreviations: hiPSC, human induced pluripotent stem cells; hiNPCs, human induced neural progenitor cells; MEA; microelectrode array (MEA); WIV, weeks in vitro; DIV, days in vitro; DEG, differentially expressed gene; RNAseq, RNA Sequencing.

**Figure 2. CSB-deficiency is associated with inhibited neural progenitor cell migration and alterations in focal adhesion and autophagy.** (A) 0.3 mm hiNPC neurospheres were plated and differentiated for 3 DIV. Cell migration was assessed by measuring both migration distance of furthest migrated cells (bars) and the total number of migrated nuclei (dots). Exemplary brightfield images are shown on the right. The graph depicts N=3 biological replicates with n=5-10 spheres each, mean  $\pm$  SEM. (B) The heat map shows selected significantly regulated DEGs of focal adhesion-related pathways, identified using RNA Sequencing. DEG criteria:  $|\log_2| \geq 1$  and Qvalue of  $\leq 0.05$ . (C) Representative stainings of the migration area of plated hiNPC neurospheres after 3 DIV, showing nuclei (blue) and the cytoskeletal marker F-actin (white). (D) Heatmap of the 140 differentially regulated autophagy-associated genes of IMR90<sup>KO</sup> compared to IMR90<sup>WT</sup> across 3, 14 and 21 DIV as identified using RNA Sequencing (right), and separately highlighted DEGs of interest (left). DEG criteria:  $|\log_2| \geq 1$  and Qvalue of  $\leq 0.05$ . (E) Representative ICC images of differentiating hiNPC neurospheres after 3DIV, showing nuclei (blue) and lysosomes (LAMP2, magenta). (F) Western Blot of plated and 3DIV differentiated hiNPC spheres, quantifying the fold change in LC3A, LAMP2 and mTOR protein levels, normalized to the housekeeper HSP90 and the respective CSB expressing control cell line. Graphs depict N=3 biological replicates, mean  $\pm$  SEM. For (A) and (F) a p-value below 0.05 was termed significant. Statistical analyses were performed using unpaired two-tailed t-tests. Abbreviations: NPCs, neural progenitor cells; DEG, differentially expressed gene; DIV, days in vitro; ICC, Immunocytochemistry.

**Figure 3. HDAC6-inhibitor Tubastatin A partially rescues the adverse migration phenotype of CSB-deficient cells.** (A) Exemplary images and quantifications of Western Blot analyses depicting the fold change in acetyl-alpha-tubulin and HDAC6 protein levels, normalized to the housekeeper HSP90 and the respective control cell line. Graphs depict N=3 biological replicates, mean  $\pm$  SEM. (B) 0.3 mm hiNPC neurospheres were plated and differentiated under exposure to TubA (left) or CQ (right), before the migration distance was measured on DIV 3. The migration distance of both healthy and disease cell lines was normalized to the solvent control (SC) of the respective healthy cell line within each graph. Viability and cytotoxicity were assessed in parallel (Supplemental Information Figure S3). Graphs depict N=3 biological replicates with n=5-10 spheres each. (C) Illustration of the presumed CSB mechanism: CSB-deficiency leads to defective autophagy, which in turn inhibits migration through inefficient focal adhesion turnover and altered regulation of the actin cytoskeleton. For (A) and (B), a p-value below 0.05 was termed significant. Statistical analyses in (A) were performed using unpaired two-tailed t-tests and in (B) using one-way ANOVA with post-hoc Dunnett tests. Abbreviations: NPCs, neural progenitor cells; TubA, Tubastatin A; CQ, Chloroquine. Figure created with biorender.com.

**Figure 4. Microelectrode Array measurements reveal altered neural network activity in CSB-deficient networks.** (A) Heatmap of the 36 differentially regulated synapse-associated genes of IMR90<sup>KO</sup> compared to IMR90<sup>WT</sup> across 3, 14 and 21 DIV. DEG criteria:  $|\log_2| \geq 1$  and Qvalue of  $\leq 0.05$ . (B) HiNPC neurospheres were plated onto MEA plates (96-well, 8 electrodes per well) and differentiated for neural network formation. The neural network development was assessed by measuring the electrical signals over 7 weeks. The graphs depict the number of active electrodes normalized to the number of wells over time (N=8-12 wells with n=64-96 electrodes each; mean  $\pm$  SEM). (C) Illustration of the MEA-derived parameters single spikes, bursts, network bursts and network synchrony. (D) Representative spike raster plots (SRP) of one well of each cell line after 6 DIV. Displayed are the spikes (black) and bursts (blue) of the first 30s of the 15 min total measurement. (E) The electrical activity of neural networks over time is depicted and compared to the respective control. The graphs show the mean  $\pm$  SEM of three biological replicates for the selected parameters number of spikes, number of network bursts, area under normalized cross correlation (network synchrony) and number of spikes per network burst (per replicate 8-12 wells with 64-96 electrodes were evaluated). Each time point comprises a 15 min measurement. A p-value below 0.05 was termed significant. Statistical analyses of MEA results were performed using Mixed-effects analysis with the Sidak test for multiple comparisons. Abbreviations: NPCs, neural progenitor cells; MEA, microelectrode array. Figure created with biorender.com.

**Figure 5. Elevated GABA/Glutamate ratios and delayed KCC2 induction hint towards a delayed GABA switch in CSB-deficient cells.** (A) HiNPC neurospheres were plated and differentiated for 14 DIV, before GC-MS was performed. Graphs depict the ratios of the relative metabolite concentrations of neurotransmitters glutamate and GABA (N=3 biological replicates, mean  $\pm$  SEM). (B) Left: Differential expression of *NKCC1* and *KCC2* in IMR90<sup>WT</sup> and IMR90<sup>KO</sup> was evaluated from RNA sequencing data. Graphs depict the FPKM raw values over 21 DIV. Right: *NKCC1* and *KCC2* mRNA expression in CS789<sup>Res</sup> and CS789 was analyzed via qPCR. Graphs depict the FGE over 21 DIV, normalized to  $\beta$ -actin and to d0 of CS789<sup>Res</sup> (not shown; N=3 biological replicates, mean  $\pm$  SEM). (C) Illustration of the presumed effects of CSB-deficiency on the brain circuit formation, possibly through GABA-switch delay. A p value below 0.05 was termed significant. Statistical analyses were performed using unpaired two-tailed t-tests. Abbreviations: DIV, days in vitro; FPKM, fragments per kilobase million; FGE, fold gene expression GC-MS, gas chromatography–mass spectrometry. Figure adapted from Tau et al.<sup>73</sup> created with biorender.com.

**Figure 6. CSB-deficiency leads to hindered oligodendrocyte maturation.** HiNPC neurospheres were pre-differentiated in designated oligodendrocyte differentiation medium for 8 weeks in an orbital shaking incubator to generate oligodendrocyte-containing BrainSpheres. (A) Representative 3D BrainSphere ICC stainings after 8 WIV, showing nuclei (Hoechst, blue), neurons ( $\beta$ -III tubulin, magenta) and oligodendrocytes (O4, cyan). (B) Quantification of O4 positive cells after 4 weeks of adherent oligodendrocyte differentiation, normalized to the respective healthy control cell line. (C) Analyses of oligodendrocyte marker mRNA expression via qPCR after 8 WIV. Left: Expression in IMR90<sup>KO</sup> compared to IMR90<sup>WT</sup>. Right: Expression in CS789 compared to CS789<sup>Res</sup>. Graphs depict N=3 biological replicates, mean  $\pm$  SEM. (D) After 6 WIV IMR90<sup>KO</sup> and CS789 BrainSpheres were treated with 250 nM TubA or 50 nM SAHA for two weeks, while remaining in the orbital shaking incubator. The graphs show marker gene expression at 8 WIV as assessed by qPCR. All graphs depict N=3 and mean  $\pm$  SEM. Marker gene expression is normalized to  $\beta$ -actin and respective expression in IMR90<sup>WT</sup>. (E) Illustration of the presumed effect of CSB-deficiency on HDAC-dependent oligodendrocyte maturation. A p-value below 0.05 was termed significant. Statistical analyses were performed using unpaired two-tailed t-tests. Abbreviations: NPCs, neural progenitor cells; WIV, weeks in vitro; ICC, Immunocytochemistry; TubA, Tubastatin A. Figure created with biorender.com.

## **STAR Methods**

### **Resource Availability**

#### *Lead Contact*

Requests for further information should be directed to and will be fulfilled by the lead contact, Prof. Dr. Ellen Fritsche (Ellen.Fritsche@IUF-Duesseldorf.de).

#### *Materials availability*

Requests for resources and reagents should be directed to and will be fulfilled by the lead contact.

#### *Data and code availability*

All data reported in this paper will be shared by the lead contact upon request. RNA Sequencing data have been deposited at GEO and are publicly available as of the date of publication. Accession numbers are listed in the key resources table.

This paper does not report original code.

Any additional information required to reanalyze the data reported in this paper is available from the lead contact upon request.

### **Experimental models and subject details**

#### *Cell Lines*

The commercial wild-type hiPSC-IMR90 line was obtained from WiCell (clone 4, Madison, USA). The patient-derived hiPSC-CS789 line was kindly provided by Prof. Egly from the IGBMC Strasbourg. ERCC6 CRISPR/Cas9 mutants CS789<sup>Res</sup> and IMR90<sup>KO</sup> were generated in house, as previously described<sup>74</sup>. In brief, gRNAs (supplemental information (SI) Figure S1) were designed using the CRISPR design tool CHOPCHOP (<https://chopchop.cbu.uib.no/>) and cloned into a modified version of the PX458 plasmid (Addgene #48138, Watertown, USA). The resulting bicistronic vector encoded the respective gRNA, Cas9 nuclease and GFP selection marker. gRNAs activity and efficiency were assessed via high resolution melt analysis (HRMA). HiPSCs cells were transfected with nuclease plasmids in antibiotic-free medium in a 6-well plate using Lipofectamine Stem (Thermo Fisher Scientific, Waltham, USA) or NEON electroporation system (Thermo Fisher Scientific, Waltham, USA). After 48 h, cells were sorted (FACS or MACS) and plated as single cells in a 96-well plate and duplicated after a week. Clones were lysed in proteinase K and genotyped by deep sequencing using a MiSeq Illumina (San Diego, CA)<sup>74</sup>. Briefly, libraries were quantified using qBit4 (Thermo Fisher Scientific, Waltham, USA) and deep sequencing was performed according to the manufacturer's protocol (Illumina, San Diego, CA) at around 2000 reads per clone using custom made barcodes. Data were obtained in FASTQ format and analyzed using CRISPRnano.de<sup>75</sup>.

To assure high and reliable cell culture quality, all hiPSC lines used in this study were quality controlled and banked, based on the recommendations of Tigges et al.<sup>36</sup>. Briefly, cells were characterized via karyotyping, STR analysis, FACS analysis for pluripotency markers and viability, mycoplasma test and colony morphology.

## Method Details

### Cell Culture

The neural induction of all hiPSC lines and subsequent cultivation of hiNPCs in 3D was performed according to the Hofrichter et al. NIM protocol<sup>32</sup>. HiPSCs were maintained under feeder-free conditions on Matrigel-coated 6-well plates (LDEV-free, #354277, Corning, New York, USA) in mTeSR1 medium, containing mTeSR1 (#05850, StemCell Technologies, Vancouver, Canada), 20% (v/v) mTeSR1 supplement (5850, StemCell Technologies, Vancouver, Canada) and 1% (v/v) Penicillin/Streptomycin (P06-07100, PAN-Biotech, Aidenbach, Germany) for CS789, CS789<sup>Res</sup> and IMR90<sup>KO</sup>, or on laminin-coated 6-well plates (#LN521-05, 50 µg/ml, Biolamina, Sundbyberg, Sweden) in iPSBrew iPSC medium, containing iPS-brew XF (human, 130-104-368, StemMACS, Miltenyi Biotec, Bergisch Gladbach, Germany), 2% (v/v) iPS Brew XF supplement (130-104-368, StemMACS, Miltenyi Biotec, Bergisch Gladbach, Germany) and 1% (v/v) Penicillin/Streptomycin for IMR90<sup>WT</sup>, at 37 °C in a humidified atmosphere of 5% CO<sub>2</sub>. The medium was changed on 6 days per week by completely removing and replacing the medium with fresh mTeSR1 or iPSBrew (2 mL) iPSC medium. On the sixth day of feeding, 4 mL of the respective medium were added, to substitute for the feeding-free seventh day. Passaging was performed with 0.5 mM EDTA (#15575020, ThermoFisher Scientific, USA).

The neural induction of hiPSC cultures was initiated by incubating the cells with ROCK inhibitor (10 µM; ROCK INHIBITOR, #HB2297, Hello Bio, Great Britain) in mTeSR1 or iPSBrew medium for 1 h at 37 °C and 5% CO<sub>2</sub>. Subsequently, the cells were washed with PBS including 1% (v/v) Penicillin/Streptomycin (P06-07100, PAN-Biotech, Aidenbach, Germany) and neural induction medium (NIM; 1 ml), containing DMEM/F12 (31330038, Invitrogen, Waltham, USA), 1:50 B27 supplement (17504-044, Invitrogen, Waltham, USA), 1:100 (v/v) Penicillin/Streptomycin (P06-07100, PAN-Biotech, Aidenbach, Germany), 20 ng/ml Epidermal growth factor (EGF; PHG0313, Invitrogen, Waltham, USA), 20% (v/v) Knockout Serum Replacement (10828028, Invitrogen, Waltham, USA), 1:100 N2 supplement (17502-048, Invitrogen, Waltham, USA), 10 µM SB-431542 (S4317, Sigma Aldrich) and 0.5 µM LDN-193189 (SML0559, Sigma Aldrich, Burlington, USA) was added. Colonies were then fragmented with a StemPro EZPassage Disposable Stem Cell Passaging Tool (Thermo Fisher Scientific, Waltham, USA) and transferred into Poly-HEMA-coated 6 cm dishes (#P3932, Merck, Darmstadt, Germany) filled with NIM (5 ml). 10 µM ROCK inhibitor were added for at least 24 h. The medium was changed every second day. On day 7, spheres were collected and transferred into new Poly-HEMA-coated 6 cm dishes with 5 ml NIM and hFGF (10 ng/mL; #233-FB, R&D Systems, Minneapolis, USA) and the spheres were cultured for another 14 days. On day 21 the generated hiNPCs were transferred into new Poly-HEMA-coated 10 cm dishes filled with 20 ml NPC proliferation medium, containing DMEM/F12 (31330038, Invitrogen, Waltham, USA), 1:50 B27 supplement (17504-044, Invitrogen, Waltham, USA), 1:100 (v/v) Penicillin/Streptomycin (P06-07100, PAN-Biotech, Aidenbach, Germany), 20 ng/ml Epidermal growth factor (EGF; PHG0313, Invitrogen, Waltham, USA) and hFGF (20 ng/ml, #233-FB, R&D Systems, Minneapolis, USA). Cells were fed every second day with NPC proliferation medium and mechanically passaged to 0.2 mm diameter when exceeding a size of ≈0.5 mm, or when clumping occurs (McIlwain Tissue Chopper, Ted Pella, Redding, USA). Spheres were maintained in proliferation medium for subsequent cultivation.

2D neural inductions were performed with cell lines IMR90<sup>WT</sup> and IMR90<sup>KO</sup>, specifically for the generation of electrically active neural networks, which could not be achieved with the 3D induction protocol. The 2D inductions were performed according to Hartmann et al.<sup>35</sup>. HiPSC-colonies were dissociated using the Gentle Cell Dissociation Reagent (#100-0485, Stemcell Technologies, Vancouver, Canada) and subsequently seeded with a cell density of  $2 \times 10^6$  cells per well of a 6-well plate coated with polyethyleneimine (PEI, 0.1 %; #181978, Sigma-Aldrich, Burlington, USA) and laminin (15 µg/ml; #LN521, Biolamina, Sweden), and cultivated in NIM medium supplemented with 10 µM ROCK inhibitor (only for the first 24 h after passaging; #HB2297, Hello Bio, Great Britain) under humidified

conditions at 37 °C and 5 % CO<sub>2</sub>. Cells were cultivated for 12 days, before medium was changed to neural progenitor medium (NPM), containing proliferation medium without hFGF, 20% (v/v) Knockout Serum Replacement (10828028, Invitrogen, Waltham, USA), 1:100 N2 supplement (17502-048, Invitrogen, Waltham, USA) and 20 ng/ml hFGF (#233-FB, R&D Systems, Minneapolis, USA). Medium was completely changed every second day. Cells were passaged on days 12 and 17 through enzymatic dissociation with Accutase (#07920, Stemcell Technologies, Canada) and transferred to a new PEI-laminin-coated 6-well plate. On day 21, hiNPCs were singularized with Accutase and frozen in neural progenitor medium containing 10 % dimethyl sulfoxide (DMSO, #A994.1, Carl-Roth, Germany) and 10 μM ROCK inhibitor. Each thawed hiNPCs vial was diluted in 10 ml of the respective neural progenitor medium with 10 μM ROCK inhibitor (#HB2297, Hello Bio, Great Britain) and centrifuged at 300 g for 5 min. The cell pellet was resuspended in 4 ml NPM medium with 10 μM ROCK inhibitor (#HB2297, Hello Bio, Great Britain) and transferred to one well of a 6-well plate (#83.3920, Sarstedt, Germany) coated with anti-adherence rinsing solution (#07010, Stemcell Technologies, Vancouver, Canada). Cells were cultivated in an orbital shaking incubator (#LT-X, Kuhner Shaker GmbH, Swiss) at 140 rpm, 12.5 mm diameter, 37 °C, 5 % CO<sub>2</sub>, and 85 % humidity for 7 days without feeding, to allow sphere formation. Medium was changed to NPC proliferation medium on day 7 for culture maintenance. Cells were fed every second day with NPC proliferation medium and mechanically passaged to 0.2 mm diameter when exceeding a size of ≈0.5 mm (Mellwain Tissue Chopper, Ted Pella). Spheres were maintained in proliferation medium for culture maintenance.

BrainSpheres differentiation was conducted according to the needs of the respective readout. Protocols are described in each section.

### ***Oligodendrocyte Differentiation***

Differentiation of hiNPCs from 3D neural inductions to oligodendrocyte-containing BrainSpheres was conducted based on the protocol published by Pamies et al.<sup>59</sup>. Proliferating hiNPC spheres were mechanically passaged to 0.1 mm diameter 1-2 days before the start of the differentiation. Spheres were transferred into 4 ml oligodendrocyte differentiation medium (ODM), containing Neurobasal Electro Medium (A1413701, Thermo Fisher, Waltham, USA), 1:50 B-27 Electrophysiology supplement (A1413701, Thermo Fisher, Waltham, USA), 1:100 Glutamax (A1286001, Thermo Fisher, Waltham, USA), 20 ng/ml human recombinant GDNF (212-GMP-010, RnD Systems, Minneapolis, USA), 20 ng/ml human recombinant BDNF (450-02, Peprotech, Rock Hill USA), 1% (v/v) Penicillin/Streptomycin (P06-07100, PAN-Biotech, Aidenbach, Germany), 1:100 db-cAMP (D0260, Sigma Aldrich, Burlington, USA), 60 ng/ml Triiodothyronine (T3; T2877, Merck, Darmstadt, Germany) and 20 μg/ml Ascorbic acid (A5960, Sigma Aldrich, Burlington, USA), per well of 6-well plates (#83.3920, Sarstedt, Germany) coated with anti-adherence rinsing solution (#07010, Stemcell Technologies, Vancouver, Canada). Spheres were cultivated free-floating, in an orbital shaking incubator (#LT-X, Kuhner Shaker GmbH, Swiss) at 140 rpm, 12.5 mm diameter, 37 °C, 5 % CO<sub>2</sub>, and 85 % humidity for up to 8 weeks. Half of the medium was changed for new ODM every second to third day. For rescue treatments between week 6 and week 8, medium was completely changed for ODM including 250 nM tubastatin A (#SML004, Sigma Aldrich, Missouri, USA) or 50 nM SAHA (#Cay10009929, Biomol, Hamburg, Germany). Exposed spheres were fed with ODM including the substance every second to third day until week 8.

### ***Migration***

Cell migration was assessed as described previously<sup>76</sup>. Briefly, one sphere of 0.3 mm diameter was plated per well of a 96-well plate coated with poly-d-lysine (PDL, 0.1 mg/mL, Merck, #P0899) and laminin (0.0125 mg/mL, Merck, #L2020). Spheres were cultivated under differentiation conditions in 100 μl CINDA medium, containing DMEM/F12 (31330038, Invitrogen, Waltham, USA), 1:50 B27 supplement (17504-044, Invitrogen, Waltham, USA), 1:100 N2 supplement (17502-048, Invitrogen, Waltham, USA), 644 mg/ml creatin monohydrate (C3630, Sigma Aldrich, Burlington, USA), 100 U/ml Interferon-γ (300-02, Peprotech, Rock Hill USA), 20 ng/ml Neurotrophin-3 (450-03, Peprotech, Rock

Hill USA), 20 $\mu$ M Ascorbic acid (A5960, Sigma Aldrich, Burlington, USA), 1:100 (v/v) Penicillin/Streptomycin (P06-07100, PAN-Biotech, Aidenbach, Germany) and 300 $\mu$ M d-cAMP (D0260, Sigma Aldrich, Burlington, USA) for 3 days before the cells were imaged in brightfield mode (Cellomics ArrayScan, Thermo Fisher Scientific, Waltham, USA). Migration distance was measured from the sphere core to the furthest migrated cells using Fiji Image J software (v1.53f51, <https://imagej.net/software/fiji/>). Additionally, cells were fixed with 4% paraformaldehyde (#P6148, Sigma Aldrich, Missouri, USA) for 30 min at 37°C, followed by three PBS washing steps. The nuclei were stained with 1% Hoechst (H21486, Thermo Scientific, Waltham, USA) and the cells were imaged (Cellomics ArrayScan). The Cellomics Spot Detection Tool was used to automatically count all cells outside of the sphere core, to assess the number of migrated nuclei. For treatment experiments, cells were cultivated in CINDA differentiation medium supplemented with SAHA (#Cay10009929, Biomol, Hamburg, Germany), Tubastatin A (#SML004, Sigma Aldrich, Missouri, USA), Chloroquine (Sigma, #C6628) or the respective solvent control. Endpoint assessment was performed as described above. Additionally, cell viability was measured with an Alamar Blue assay (Cell Titer-Blue® (CTB) Viability Assay; #G8080, Promega, Germany) according to manufacturer's instructions. Cytotoxicity was assessed by measuring lactate dehydrogenase (LDH) exclusion (#G7890, CytoTox-One, Promega) following the manufacturer's guidelines. Only non-cytotoxic concentrations were evaluated for statistical analyses, using a cut-off of 20% cytotoxicity. Three biological replicates with three to ten technical replicates per cell line and condition were performed in each experiment.

### ***Proliferation***

Human hiNPC spheres of 0.3 mm diameter were placed into separate wells of a Poly-HEMA-coated (#P3932, Merck, Darmstadt, Germany) U-bottom 96-well plate (Greiner, Austria) and cultured in proliferation medium for 3 days. The proliferation was assessed by measuring the increase in sphere size and by assessing the incorporation of BrdU into newly synthesized DNA. Spheres were imaged in brightfield mode (Thermo Fisher Scientific, Waltham, USA) from d0- to d3. The sphere size was automatically measured using the Cellomics ArrayScan Software and the slope of the size increase was calculated for each sphere. The cell proliferation BrdU assay was performed on day 3 (#11669915001, Sigma Aldrich, Missouri, USA) according to the manufacturer's instructions. Three biological replicates with a minimum of 3-5 technical replicates per cell line were performed.

### ***Immunocytochemistry (ICC)***

Samples were fixed with a final concentration of 4% paraformaldehyde (#P6148, Sigma Aldrich, Missouri, USA) for 30 min at 37°C, followed by three PBS washing steps. The desired primary antibodies were diluted in 2% goat serum (G9023, Sigma Aldrich, Missouri, USA) and PBS-T (PBS in 0.1% (v/v) Triton X-100 (#T8787, Sigma Aldrich, Missouri, USA)). Subsequently, the antibody solution was added to the samples and incubated at 4 °C overnight. Samples were washed three times with PBS. Next, the secondary antibodies, or conjugated antibodies, were added to 1% Hoechst (33258, Sigma Aldrich, Missouri, USA) and 2% goat serum in PBS. The samples were incubated with the secondary antibody solution at 37°C for 1 h. Finally, the samples were washed three times with PBS and imaged with the confocal laser scanning microscope TCS SP8 (Inverse DMi8CS, Leica Microsystems) or the Cellomics ArrayScan (Thermo Fisher Scientific, Waltham, USA). Floating spheres were positioned onto microscopy glass slides and covered with Aqua-Poly/Mount (#18606-20, Polysciences Inc., USA) and a cover glass before imaging. All antibodies are listed in the key resource table.

ICC image detection and quantification by high-content imaging analysis (HCA) was done using the Cellomics ArrayScan. Respective channels were automatically acquired with a 40x objective magnification and a resolution of 552  $\times$  552 pixel. 30 randomly assigned fields of each 96-well were scanned. Automated image analysis was performed with the Thermo Scientific HCS Studio software, using the Colocalization analysis tool. Specifically, all O4 positive cells were detected and normalized to the total number of detected nuclei. Four biological replicates with three to five technical replicates per cell line were analyzed.

## ***RNA Sequencing***

IMR90<sup>WT</sup> and IMR90<sup>KO</sup> lines were used for transcriptome analyses. Here, 500 hiNPC spheres with a 0.1 mm diameter were plated onto poly-d-lysine (PDL, 0.1 mg/mL, Merck, #P0899) and laminin (0.0125 mg/mL, Merck, #L2020)-coated 6-well plates and differentiated in CINDA medium for 3, 14 or 21 days. Total RNA was isolated using the RNeasy Mini Kit (#74104, Qiagen, Hilden, Germany) according to the manufacturer's instructions. RNA was sent to BGI Genomics Co., Ltd. (China) for RNA sequencing using the DNBseq platform and the reads were mapped to human reference genome hg38. Three biological replicates were performed for each cell line.

Library preparation: Total RNA sample quality control (QC) was done using the Agilent 2100 Bio analyzer (Agilent RNA 6000 Nano Kit). Subsequently, mRNA was purified using oligo(dT)-attached magnetic beads, and fragmented. After, synthesis of the first and second cDNA strands, end repair and "A" base was added to the 3' end. Adaptor ligands were added, and PCR was performed. PCR product purification was done with XP beads. QC was again done using the Agilent 2100 Bio analyzer. Double stranded PCR products were denatured and circularized by splint oligo sequencing. Resulting single strand circle DNA was formatted as the final library. The library was amplified with phi29 to make DNA nanoball (DNB). The DNBs were loaded into the patterned nanoarray and single end 50 (pair end 100/150) bases reads were generated in the way of combinatorial Probe Anchor Synthesis (cPAS).

Sequence data analysis: First, reads mapping to rRNAs were removed. Next, low quality reads (>40% of bases qualities <20), reads with adaptors and reads with unknown bases (N bases >0.1%) were removed, to get the clean reads (20M clean reads per sample, BGI software SOAPnuke v1.5.2). These clean reads were stored as FASTQ files. Reads were subsequently mapped to the reference genome (GCF\_000001405.39\_GRCh38.p13) using the Hierarchical Indexing for Spliced Alignment of Transcripts software (HISAT2, v2.0.4). Additionally, novel transcript prediction (StringTie v1.0.4; Cuffcompare v2.2.1; CPC v0.9-r2), SNP & INDEL calling (GATK) and gene-splicing detection were done (rMATS v4.0.2). Gene expression analysis was performed, by mapping the clean reads to the reference genome (Bowtie2 v2.2.5) and calculating the expression levels with RSEM (v1.2.12). Differentially expressed genes (DEGs) between IMR90<sup>WT</sup> and IMR90<sup>KO</sup> lines were identified with DEseq2<sup>77</sup>.

## ***Quantitative polymerase chain reaction (qPCR)***

For KCC2 and NKCC1 expression, 60 hiNPC spheres of 0.1 mm diameter were plated onto poly-d-lysine (PDL, 0.1 mg/mL, Merck, #P0899) and laminin (0.0125 mg/mL, Merck, #L2020)-coated 48-well plates and differentiated in CINDA for 3, 14 or 21 days. For oligodendrocyte marker expression analyses, spheres were differentiated as described in the oligodendrocyte differentiation protocol, before harvesting. Total RNA was isolated using the RNeasy Mini Kit (#74104, Qiagen, Hilden, Germany) according to manufacturer's instructions. RNA was then reverse transcribed to cDNA (#205314, QuantiTec Reverse Transcription Kit, Qiagen, Hilden, Germany) according to the manufacturer's instructions and qPCR was performed (#204057, Quanti Fast SYBR Green Kit, Qiagen, Hilden, Germany) using the PCR-Cycler Rotor-Gene Q (Qiagen, Hilden, Germany). Primer sequences are listed in the SI Table S2. Three biological replicates were performed for each cell line.

## ***Western Blot (WB)***

For CSB protein analyses, proliferating hiNPC spheres were analyzed. For all other markers, 750 hiNPC spheres with a diameter 0.1 mm diameter were plated into one well of a 6-well plate coated with poly-d-lysine (PDL, 0.1 mg/mL, Merck, #P0899) and laminin (0.0125 mg/mL, Merck, #L2020). Spheres were cultivated under differentiation conditions in CINDA medium for 3 days. Cell pellets of each well were lysed in RIPA buffer (Cell Signaling Technology, Massachusetts, USA) and 1 mM protease inhibitor PMSF (Cell Signaling Technology) on ice for 30 min and centrifuged for 15 min at 4°C at maximum speed. Supernatant of protein samples were separated by 10% SDS-polyacrylamide gel

electrophoresis and blotted onto PVDF membrane (BioRAD, Hercules, USA). Blots were blocked in 5% BSA diluted in 0.1% TBS-Tween-20 (TBS-T) for 1h at RT and subsequently incubated with antibodies of interest overnight at 4°C according to the manufacturer's instructions. Blots were washed in TBS-T for 30 min and incubated with a 1:1000 dilution of HRP-conjugated secondary antibody (LI-COR Biosciences, Nebraska, USA) in 5% BSA in TBS-T at RT for 1 h. After final washing step of 30 min bands were visualized using ECL Prime (GE Healthcare, Freiburg, Germany) chemiluminescence substrate and the Odyssey imaging system (LI-COR Biosciences). Densitometry was carried out using Image Studio Lite software (LI-COR Biosciences). Three biological replicates were performed for each cell line. All antibodies are listed in the key resource table.

### ***Multielectrode Arrays (MEA)***

96-well cyto-view MEA plates (#M768-tMEA-96B, Axion Biosystems, Atlanta, USA) were coated with poly-L ornithine (PLO, 0.1 mg/ml, #P3655, Sigma Aldrich, Missouri, USA) and laminin (#LN521-05, 50 µg/ml, Biolamina, Sundbyberg, Sweden). 3D induced hiNPCs of CS789<sup>Res</sup> and CS789 cell lines were mechanically passaged to 0.1 mm diameter and transferred into CINDA+ differentiation medium, containing DMEM/F12 (31330038, Invitrogen, Waltham, USA), 1:50 B27 Plus supplement (A35828-01, Gibco, Billings, USA), 1:100 N2 supplement (17502-048, Invitrogen, Waltham, USA), 644 mg/ml creatin monohydrate (C3630, Sigma Aldrich, Burlington, USA), 100 U/ml Interferon-γ (300-02, Peprotech, Rock Hill USA), 20 ng/ml Neurotrophin-3 (450-03, Peprotech, Rock Hill USA), 20µM Ascorbic acid (A5960, Sigma Aldrich, Burlington, USA), 1:100 (v/v) Penicillin/Streptomycin (P06-07100, PAN-Biotech, Aidenbach, Germany) and 300µM d-cAMP (D0260, Sigma Aldrich, Burlington, USA). 20 hiNPC spheres in 200µl CINDA+ were plated per well and 12 wells were prepared per cell line. For the IMR90<sup>WT</sup> and IMR90<sup>KO</sup> lines, 3D induced BrainSpheres did not yield sufficient electrical activity. Therefore, an adapted 2D induction protocol was used. Here, one proliferating sphere of approx. 0.2-0.3 mm size was plated in 200µl CINDA+ per well and 12 wells were prepared per cell line. All lines were subsequently cultivated at 37°C in a humidified atmosphere of 5% CO<sub>2</sub> for up to 7 weeks. Cells were fed every two to three days, by removing 100µl and adding 100µl CINDA+ medium. The electrical activity was measured for 15 min every week after an equilibration time of 15 min on the Maestro Pro MEA system (Axion Biosystems, Atlanta USA). During the time of the measurement, temperature and CO<sub>2</sub> were kept stable and equivalent to the cultivation conditions. Data recording was operated by the Axion Integrated Studios (AxIS) navigator software (version 3.1.2, Axion Biosystems, Atlanta, USA) with a sampling frequency of 12.5 kHz and a digital band-pass filter of 200-3000 Hz. Subsequent spike detection was performed using the method “adaptive threshold crossing” with a threshold of 6 root mean square (rms) noise on each electrode and a pre- and post-spike duration of 0.84 ms and 2.16 ms, respectively. An electrode was termed “active” with at least 5 spikes per min. Quantification of general electrical activity and neuronal network activity was performed with the Neural Metric Tool software (version 3.1.7, Axion Biosystems, Atlanta, USA). For burst detection, the method “Inter-spike interval (ISI) threshold” was used with a minimum of 5 contributing spikes and a maximum ISI of 100 ms. Network bursts were identified using the algorithm “envelope” with a threshold factor of 1.5, a minimal inter-burst interval (IBI) of 100 ms, at least 35% participating electrodes, and 75 % burst inclusion. Parameters for neuronal activity (percentage of active electrodes and number of spikes) as well as for network maturation and synchronicity (number of network bursts, number of spikes per network bursts and area under normalized cross correlation) were analyzed.

### ***GC-Mass Spectrometry***

For GC-MS analyses, 500 hiNPC spheres with a diameter of 0.1 mm were plated into one well of a 6-well plate coated with poly-d-lysine (PDL, 0.1 mg/ml, Merck, #P0899) and laminin (0.0125 mg/ml, Merck, #L2020). Spheres were cultivated under differentiation conditions in CINDA medium for 14 days. As a wash control, 1mM Tricarballic acid (T53503, Sigma Aldrich, Missouri, USA) was added to each well of the cell culture medium, immediately before harvesting on day 14. Cells in each well were washed four times with ice cold 0.9% (w/v) saline in MilliQ water, before being collected in 2 ml

of 0.9% (w/v) saline (3957.1, Roth, Karlsruhe, Germany) in MilliQ water. 2 ml methanol (N41.1, Roth, Karlsruhe, Germany) were supplemented with 250µl internal standard (ISTD; 10µM final; ribitol; A5502-5G, Sigma Aldrich, Missouri, USA). 2 ml methanol-ISTD solution was added to 2 ml of cell suspension and samples were shock frozen in liquid nitrogen. Upon thawing on ice, 1 ml chloroform (3313.1 Roth, Karlsruhe, Germany) was added to 4 ml sample solution and the mixture was incubated on ice and frequently vortexed for 10 min, before resting for 5 min on ice. The samples were centrifuged for 10 min at 4°C and 4000g. Subsequently, the aqueous phase (top layer) was collected in a separate tube and the remaining organic phase was washed with 2 ml ice-cold MilliQ water. After another centrifugation cycle at 4°C and 4000g for 10 min, the aqueous phase was collected and pooled with the first collection tube. The sample was filled with 11.5 ml MilliQ water, to reduce the amount of the organic solvent <15%. Samples were frozen for at -80°C, before lyophilization was carried out. Dried samples were resuspended in 500µl MilliQ water, of which 20 µl were mixed with 50 µl methanol and dried via vacuum centrifugation for derivatization and GC-MS measurement.

The polar metabolites were derivatized for GC-MS analysis according to the method described by Gu et al.<sup>78</sup>. The derivatization process was executed using an MPS-Dual-head autosampler (Gerstel, Mülheim an der Ruhr, Germany). First, 10 µl of methoxyamine hydrochloride (10440364, Thermo Fisher Scientific, Fisher Scientific Chemicals, Waltham, Massachusetts, USA; freshly prepared at 20 mg ml<sup>-1</sup> in pure pyridine from) were added, and the samples were shaken at 37 °C for 90 minutes. Next, 90 µl of N-Methyl-N-(trimethylsilyl)trifluoroacetamide (MSTFA; Macherey-Nagel, Düren, Germany) were added and shaken at 37 °C for 30 minutes, followed by a 2-hour incubation at room temperature. Metabolite analysis was conducted using a 7890B gas chromatography system connected to a 7200 QTOF mass spectrometer from Agilent Technologies, as previously described by Shim et al.<sup>79</sup>. Compound identification was performed using MassHunter Qualitative software (v b08, Agilent Technologies, Santa Clara, USA) by comparing the mass spectra to an in-house library of authentic standards and the NIST14 Mass Spectral Library (available at <https://www.nist.gov/srd/nist-standard-reference-database-1a-v14>). Peak areas were integrated using MassHunter Quantitative software (v b08, Agilent Technologies, Santa Clara, USA) and normalized to the internal standard ribitol (Sigma Aldrich, Missouri, USA).

## **Quantification and statistical analysis**

### ***Migration, Proliferation, Western Blot and Mass Spectrometry analyses***

GraphPad Prism was used to create visual graphs and analyses. Statistical significance was determined by unpaired two-tailed t-tests. Migration rescue experiments were analyzed using ANOVA with the Dunnett test for multiple comparisons. A p value below 0.05 was termed significant.

### ***qPCR***

Fold change values were determined by 2<sup>-ddCt</sup>. Statistical significance was determined by unpaired two-tailed t-tests in GraphPad Prism. A p value below 0.05 was termed significant.

### ***RNA Seq***

DEG criteria was set to  $|\log_2| \geq 1$  and Qvalue of  $\leq 0.05$  were used for subsequent analyses and KEGG pathway mapping. Individually analyzed genes had a minimum FPKM of 1. Analyses and visualization of gene expression parameters were done using the Dr. Tom software (BGI Genomics Co., Ltd.).

### ***MEAs***

Statistical analyses of MEA results were performed in GraphPad using Mixed-effects analysis with the Sidak test for multiple comparisons (N=8-12 wells with n=64-96 electrodes). A p value below 0.05 was termed significant.

## References

1. Laugel, V., Dalloz, C., Tobias, E.S., Tolmie, J.L., Martin-Coignard, D., Drouin-Garraud, V., Valayannopoulos, V., Sarasin, A., and Dollfus, H. (2008). Cerebro-oculo-facio-skeletal syndrome: Three additional cases with CSB mutations, new diagnostic criteria and an approach to investigation. *J. Med. Genet.* *45*, 564–571. 10.1136/jmg.2007.057141.
2. R. D. Schmickel, E. H. Y. Chu, J.E.T. and C.C.C. (1977). Cockayne Syndrome: A Cellular Sensitivity to Ultraviolet Light. *Pediatrics* *60*, 135–139.
3. P. M. Paddison, J. Moossy, V. J. Derbres, W.K. (1963). COCKAYNE'S SYNDROME. A REPORT OF FIVE NEW CASES WITH BIOCHEMICAL, CHROMOSOMAL, DERMATOLOGIC, GENETIC AND NEUROPATHOLOGIC OBSERVATIONS. *Dermatol Trop Ecol Geogr.* *15*, 195–203.
4. Moossy, J. (1967). The neuropathology of cockayne's syndrome. *J. Neuropathol. Exp. Neurol.* *26*, 654–660. 10.1097/00005072-196710000-00010.
5. Sugarman, G.I., Landing, B.H., and Reed, W.B. (1977). Cockayne syndrome: clinical study of two patients and neuropathologic findings in one. *Clin. Pediatr. (Phila).* *16*, 225–232. 10.1177/000992287701600304.
6. Laugel, V., Dalloz, C., Durand, M., Sauvanaud, F., Kristensen, U., Vincent, M.C., Pasquier, L., Odent, S., Cormier-Daire, V., Gener, B., et al. (2010). Mutation update for the CSB/ERCC6 and CSA/ERCC8 genes involved in Cockayne syndrome. *Hum. Mutat.* *31*, 113–126. 10.1002/humu.21154.
7. Kraemer, K.H., Patronas, N.J., Schiffmann, R., Brooks, B.P., Tamura, D., and Digiovanna, J.J. (2008). Cockayne Syndrome : a Complex Genotype-Phenotype. *Neuroscience* *145*, 1388–1396.
8. De Waard, H., De Wit, J., Gorgels, T.G.M.F., Van den Aardweg, G., Andressoo, J.O., Vermeij, M., Van Steeg, H., Hoeijmakers, J.H.J., and Van der Horst, G.T.J. (2003). Cell type-specific hypersensitivity to oxidative damage in CSB and XPA mice. *DNA Repair (Amst).* *2*, 13–25. 10.1016/S1568-7864(02)00188-X.
9. Gorgels, T.G.M.F., van der Pluijm, I., Brandt, R.M.C., Garinis, G.A., van Steeg, H., van den Aardweg, G., Jansen, G.H., Ruijter, J.M., Bergen, A.A.B., van Norren, D., et al. (2007). Retinal Degeneration and Ionizing Radiation Hypersensitivity in a Mouse Model for Cockayne Syndrome. *Mol. Cell. Biol.* *27*, 1433–1441. 10.1128/mcb.01037-06.
10. Jaarsma, D., van der Pluijm, I., van der Horst, G.T.J., and Hoeijmakers, J.H.J. (2013). Cockayne syndrome pathogenesis: Lessons from mouse models. *Mech. Ageing Dev.* *134*, 180–195. 10.1016/j.mad.2013.04.003.
11. Vessoni, A.T., Guerra, C.C.C., Kajitani, G.S., Nascimento, L.L.S., and Garcia, C.C.M. (2020). Cockayne syndrome: The many challenges and approaches to understand a multifaceted disease. *Genet. Mol. Biol.* *43*. 10.1590/1678-4685-GMB-2019-0085.
12. Xu, Y., Wu, Z., Liu, L., Liu, J., and Wang, Y. (2019). Rat Model of Cockayne Syndrome Neurological Disease. *Cell Rep.* *29*, 800-809.e5. 10.1016/j.celrep.2019.09.028.
13. Van der Horst, G.T.J., Van Steeg, H., Berg, R.J.W., Van Gool, A.J., De Wit, J., Weeda, G., Morreau, H., Beems, R.B., Van Kreijl, C.F., De Gruijl, F.R., et al. (1997). Defective transcription-coupled repair in Cockayne syndrome B mice is associated with skin cancer predisposition. *Cell* *89*, 425–435. 10.1016/S0092-8674(00)80223-8.
14. Frouin, E., Laugel, V., Durand, M., Dollfus, H., and Lipsker, D. (2013). Dermatologic findings in 16 patients with cockayne syndrome and cerebro-oculo-facial-skeletal syndrome. *JAMA Dermatology* *149*, 1414–1418. 10.1001/jamadermatol.2013.6683.
15. Majora, M., Sondenheimer, K., Knechten, M., Uthe, I., Esser, C., Schiavi, A., Ventura, N., and

- Krutmann, J. (2018). HDAC inhibition improves autophagic and lysosomal function to prevent loss of subcutaneous fat in a mouse model of Cockayne syndrome. *Sci. Transl. Med.* *10*. 10.1126/scitranslmed.aam7510.
16. Fritsche, E., Tigges, J., Hartmann, J., Kapr, J., Serafini, M.M., and Viviani, B. (2020). Neural In Vitro Models for Studying Substances Acting on the Central Nervous System. *Handb Exp Pharmacol.* 10.1007/164\_2020\_367.
  17. Fritsche, E., Haarmann-Stemmann, T., Kapr, J., Galanjuk, S., Hartmann, J., Mertens, P.R., Kämpfer, A.A.M., Schins, R.P.F., Tigges, J., and Koch, K. (2020). Stem Cells for Next Level Toxicity Testing in the 21st Century. *Small* *2006252*, 1–31. 10.1002/sml.202006252.
  18. Azar, J., Bahmad, H.F., Daher, D., Moubarak, M.M., Hadadeh, O., Monzer, A., Bitar, S. Al, Jamal, M., Al-Sayegh, M., and Abou-Kheir, W. (2021). The use of stem cell-derived organoids in disease modeling: An update. *Int. J. Mol. Sci.* *22*. 10.3390/ijms22147667.
  19. Pamies, D., Wiersma, D., Katt, M.E., Zhao, L., Burtscher, J., Harris, G., Smirnova, L., Searson, P.C., Hartung, T., and Hogberg, H.T. (2022). Human organotypic brain model as a tool to study chemical-induced dopaminergic neuronal toxicity. *Neurobiol. Dis.* *169*, 105719. 10.1016/j.nbd.2022.105719.
  20. Park, J., Wetzel, I., Marriott, I., Dréau, D., D’Avanzo, C., Kim, D.Y., Tanzi, R.E., and Cho, H. (2018). A 3D human triculture system modeling neurodegeneration and neuroinflammation in Alzheimer’s disease. *Nat. Neurosci.* *21*, 941–951. 10.1038/s41593-018-0175-4.
  21. Martins, S., Hacheney, I., Teichweyde, N., Hildebrandt, B., Krutmann, J., and Rossi, A. (2021). Generation of an induced pluripotent stem cell line (iUFI001) from a Cockayne syndrome patient carrying a mutation in the ERCC6 gene. *Stem Cell Res.* *55*. 10.1016/j.scr.2021.102456.
  22. Pasca, A.M., Sloan, S.A., Clarke, L.E., Tian, Y., Makinson, C.D., Huber, N., Kim, C.H., Park, J.Y., O’Rourke, N.A., Nguyen, K.D., et al. (2015). Functional cortical neurons and astrocytes from human pluripotent stem cells in 3D culture. *Nat. Methods* *12*, 671–678. 10.1038/nmeth.3415.
  23. Mayne, L., and Lehmann, A.R. (1982). Failure of RNA synthesis to recover after UV irradiation: An early defect in cells from individuals with Cockayne syndrome and xeroderma pigmentosum. *Mutat. Res.* *96*, 140. 10.1016/0027-5107(82)90047-1.
  24. Troelstra, C., van Gool, A., de Wit, J., Vermeulen, W., Bootsma, D., and Hoeijmakers, J.H.J. (1992). ERCC6, a member of a subfamily of putative helicases, is involved in Cockayne’s syndrome and preferential repair of active genes. *Cell* *71*, 939–953. 10.1016/0092-8674(92)90390-X.
  25. Rapin, I., Lindenbaum, Y., Dickson, D.W., Kraemer, K.H., and Robbins, J.H. (2000). Cockayne syndrome and xeroderma pigmentosum: DNA repair disorders with overlaps and paradoxes. *Neurology* *55*, 1442–1449. 10.1212/WNL.55.10.1442.
  26. Lindenbaum, Y., Dickson, D., Rosenbaum, P., Kraemer, K., Robbins, J., and Rapin, I. (2001). Xeroderma pigmentosum/Cockayne syndrome complex: First neuropathological study and review of eight other cases. *Eur. J. Paediatr. Neurol.* *5*, 225–242. 10.1053/ejpn.2001.0523.
  27. Ciuffardini, F., Nicolai, S., Caputo, M., Canu, G., Paccosi, E., Costantino, M., Frontini, M., Balajee, A.S., and Proietti-De-Santis, L. (2014). The cockayne syndrome B protein is essential for neuronal differentiation and neuritogenesis. *Cell Death Dis.* *5*, e1268-11. 10.1038/cddis.2014.228.
  28. Wang, Y., Jones-Tabah, J., Chakravarty, P., Stewart, A., Muotri, A., Laposa, R.R., and Svejstrup, J.Q. (2016). Pharmacological Bypass of Cockayne Syndrome B Function in Neuronal Differentiation. *Cell Rep.* *14*, 2554–2561. 10.1016/j.celrep.2016.02.051.
  29. Vessoni, A.T., Herai, R.H., Karpiak, J. V., Leal, A.M.S., Trujillo, C.A., Quinet, A., Agnez

- Lima, L.F., Menck, C.F.M., and Muotri, A.R. (2016). Cockayne syndrome-derived neurons display reduced synapse density and altered neural network synchrony. *Hum. Mol. Genet.* 25, 1271–1280. 10.1093/hmg/ddw008.
30. Liang, F., Li, B., Xu, Y., Gong, J., Zheng, S., Zhang, Y., and Wang, Y. (2023). Identification and characterization of Necdin as a target for the Cockayne syndrome B protein in promoting neuronal differentiation and maintenance. *Pharmacol. Res.* 187, 106637. 10.1016/j.phrs.2022.106637.
  31. Brunner, J.W., Lammertse, H.C.A., van Berkel, A.A., Koopmans, F., Li, K.W., Smit, A.B., Toonen, R.F., Verhage, M., and van der Sluis, S. (2023). Power and optimal study design in iPSC-based brain disease modelling. *Mol. Psychiatry* 28, 1545–1556. 10.1038/s41380-022-01866-3.
  32. Hofrichter, M., Nimtz, L., Tigges, J., Kabiri, Y., Schröter, F., Royer-Pokora, B., Hildebrandt, B., Schmuck, M., Epanchintsev, A., Theiss, S., et al. (2017). Comparative performance analysis of human iPSC-derived and primary neural progenitor cells (NPC) grown as neurospheres in vitro. *Stem Cell Res.* 25, 72–82. 10.1016/j.scr.2017.10.013.
  33. Nimtz, L., Hartmann, J., Tigges, J., Masjosthusmann, S., Schmuck, M., Keßel, E., Theiss, S., Köhrer, K., Petzsch, P., Adjaye, J., et al. (2020). Characterization and application of electrically active neuronal networks established from human induced pluripotent stem cell-derived neural progenitor cells for neurotoxicity evaluation. *Stem Cell Res.* 45, 101761. 10.1016/j.scr.2020.101761.
  34. Pamies, D., Chesnut, M., Smirnova, L., Mutallimov, A., Maillard, V., Repond, C., Hartung, T., Zurich, M.-G., and Hogberg, H. (2021). Human 3D iPSC-derived brain model to study chemical-induced myelin disruption. *Glia* 69, E392–E394.
  35. Hartmann, J., Henschel, N., Bartmann, K., Dönmez, A., Brockerhoff, G., Koch, K., and Fritsche, E. (2023). Molecular and Functional Characterization of Different BrainSphere Models for Use in Neurotoxicity Testing on Microelectrode Arrays. *cells* 12. 10.3390/cells12091270.
  36. Tigges, J., Bielec, K., Brockerhoff, G., Hildebrandt, B., Hübenthal, U., Kapr, J., Koch, K., Teichweyde, N., Wieczorek, D., Rossi, A., et al. (2021). Academic application of Good Cell Culture Practice for induced pluripotent stem cells. *ALTEX*. <https://doi.org/10.14573/altex.2101221>.
  37. Karikkineth, A.C., Scheibye-Knudsen, M., Fivenson, E., Croteau, D.L., and Bohr, V.A. (2017). Cockayne syndrome: Clinical features, model systems and pathways. *Ageing Res. Rev.* 33, 3–17. 10.1016/j.arr.2016.08.002.
  38. Poirier, K., Lebrun, N., Broix, L., Tian, G., Saillour, Y., Boscheron, C., Parrini, E., Valence, S., Pierre, B., Saint, Oger, M., et al. (2013). Mutations in TUBG1, DYNC1H1, KIF5C and KIF2A cause malformations of cortical development and microcephaly. *Nat. Genet.* 45, 639–647. 10.1038/ng.2613.
  39. Becerra-Solano, L.E., Mateos-Sánchez, L., and López-Muñoz, E. (2021). Microcephaly, an etiopathogenic vision. *Pediatr. Neonatol.* 62, 354–360. 10.1016/j.pedneo.2021.05.008.
  40. Laugel, V., Dalloz, C., Stary, A., Cormier-Daire, V., Desguerre, I., Renouil, M., Fourmaintraux, A., Velez-Cruz, R., Egly, J.-M., Sarasin, A., et al. (2008). Deletion of 5' sequences of the CSB gene provides insight into the pathophysiology of Cockayne syndrome. *Eur. J. Hum. Genet.* 16, 320–327. 10.1038/sj.ejhg.5201991.
  41. Bartmann, K., Bendt, F., Dönmez, A., Haag, D., Keßel, E., Masjosthusmann, S., Noel, C., Wu, J., Zhou, P., and Fritsche, E. (2023). A human iPSC-based in vitro neural network formation assay to investigate neurodevelopmental toxicity of pesticides. *biorxiv* 12. 10.1101/2023.01.12.523741.

42. Ben-Ari, Y. (2002). Excitatory actions of GABA during development: The nature of the nurture. *Nat. Rev. Neurosci.* *3*, 728–739. 10.1038/nrn920.
43. Kenific, C.M., Wittmann, T., and Debnath, J. (2016). Autophagy in adhesion and migration. *J. Cell Sci.* *129*, 3685–3693. 10.1242/jcs.188490.
44. Kenific, C.M., Stehbens, S.J., Goldsmith, J., Leidal, A.M., Faure, N., Ye, J., Wittmann, T., and Debnath, J. (2016). NBR 1 enables autophagy-dependent focal adhesion turnover. *J. Cell Biol.* *212*, 577–590. 10.1083/jcb.201503075.
45. Hernandez, S.J., Fote, G., Reyes-Ortiz, A.M., Steffan, J.S., and Thompson, L.M. (2021). Cooperation of cell adhesion and autophagy in the brain: Functional roles in development and neurodegenerative disease. *Matrix Biol. Plus* *12*, 100089. 10.1016/j.mbplus.2021.100089.
46. Clawson, G.A. (2016). Histone deacetylase inhibitors as cancer therapeutics. *Ann. Transl. Med.* *4*. 10.21037/atm.2016.07.22.
47. Hartlaub, A.M., McElroy, C.A., Maitre, N.L., and Hester, M.E. (2019). Modeling human brain circuitry using pluripotent stem cell platforms. *Front. Pediatr.* *7*, 1–8. 10.3389/fped.2019.00057.
48. Pelkonen, A., Pistono, C., Klecki, P., Gómez-Budia, M., Dougalis, A., Konttinen, H., Stanová, I., Fagerlund, I., Leinonen, V., Korhonen, P., et al. (2022). Functional characterization of human pluripotent stem cell-derived models of the brain with microelectrode arrays. *Cells* *11*. 10.3390/cells11010106.
49. Silbereis, J.C., Pochareddy, S., Zhu, Y., Li, M., and Sestan, N. (2016). The Cellular and Molecular Landscapes of the Developing Human Central Nervous System. *Neuron* *89*, 248. 10.1016/j.neuron.2015.12.008.
50. Budday, S., Steinmann, P., and Kuhl, E. (2015). Physical biology of human brain development. *Front. Cell. Neurosci.* *9*, 1–17. 10.3389/fncel.2015.00257.
51. Vasudevan, P., and Suri, M. (2017). A clinical approach to developmental delay and intellectual disability. *Clin. Med. J. R. Coll. Physicians London* *17*, 558–561. 10.7861/clinmedicine.17-6-558.
52. Peerboom, C., and Wierenga, C.J. (2021). The postnatal GABA shift: A developmental perspective. *Neurosci. Biobehav. Rev.* *124*, 179–192. 10.1016/j.neubiorev.2021.01.024.
53. Pozzi, D., Rasile, M., Corradini, I., and Matteoli, M. (2020). Environmental regulation of the chloride transporter KCC2: switching inflammation off to switch the GABA on? *Transl. Psychiatry* *10*. 10.1038/s41398-020-01027-6.
54. Gitiaux, C., Blin-Rochemaure, N., Hully, M., Echaniz-Laguna, A., Calmels, N., Bahi-Buisson, N., Desguerre, I., Dabaj, I., Wehbi, S., Quijano-Roy, S., et al. (2015). Progressive demyelinating neuropathy correlates with clinical severity in Cockayne syndrome. *Clin. Neurophysiol.* *126*, 1435–1439. 10.1016/j.clinph.2014.10.014.
55. Ying, Y. qin, Yan, X. qin, Jin, S. juan, Liang, Y., Hou, L., Niu, W. ting, and Luo, X. ping (2018). Inhibitory Effect of LPS on the Proliferation of Oligodendrocyte Precursor Cells through the Notch Signaling Pathway in Intrauterine Infection-induced Rats. *Curr. Med. Sci.* *38*, 840–846. 10.1007/s11596-018-1951-9.
56. Volpe, J.J., Kinney, H.C., Jensen, F.E., and Rosenberg, P.A. (2011). The developing oligodendrocyte: Key cellular target in brain injury in the premature infant. *Int. J. Dev. Neurosci.* *29*, 423–440. 10.1016/j.ijdevneu.2011.02.012.
57. Dach, K., Bendt, F., Huebenthal, U., Giersiefer, S., Lein, P.J., Heuer, H., and Fritsche, E. (2017). BDE-99 impairs differentiation of human and mouse NPCs into the oligodendroglial lineage by species-specific modes of action. *Sci. Rep.* *7*. 10.1038/srep44861.

58. Ehrlich, M., Mozafari, S., Glatza, M., Starost, L., Velychko, S., Hallmann, A.L., Cui, Q.L., Schambach, A., Kim, K.P., Bachelin, C., et al. (2017). Rapid and efficient generation of oligodendrocytes from human induced pluripotent stem cells using transcription factors. *Proc. Natl. Acad. Sci. U. S. A.* *114*, E2243–E2252. 10.1073/pnas.1614412114.
59. Pamies, D., Barreras, P., Block, K., Makri, G., Kumar, A., Wiersma, D., Smirnova, L., Zhang, C., Bressler, J., Christian, K.M., et al. (2017). A human brain microphysiological system derived from induced pluripotent stem cells to study neurological diseases and toxicity. *ALTEX* *34*, 362–376. 10.14573/altex.1609122.
60. Chesnut, M., Hartung, T., Hogberg, H., and Pamies, D. (2021). Human Oligodendrocytes and Myelin In Vitro to Evaluate Developmental Neurotoxicity. *Int. J. Mol. Sci.* *22*, 7929. 10.3390/ijms22157929.
61. Douvaras, P., and Fossati, V. (2015). Generation and isolation of oligodendrocyte progenitor cells from human pluripotent stem cells. *Nat. Protoc.* *10*, 1143–1154. 10.1038/nprot.2015.075.
62. Noack, M., Leyk, J., and Richter-Landsberg, C. (2014). HDAC6 inhibition results in tau acetylation and modulates tau phosphorylation and degradation in oligodendrocytes. *Glia* *62*, 535–547. 10.1002/glia.22624.
63. Liu, B., Chen, X., Wang, Z.Q., and Tong, W.M. (2014). Nbn gene inactivation in the CNS of mouse inhibits the myelinating ability of the mature cortical oligodendrocytes. *Glia* *62*, 133–144. 10.1002/glia.22593.
64. Tauheed, A.M., Ayo, J.O., and Kawu, M.U. (2016). Regulation of oligodendrocyte differentiation: Insights and approaches for the management of neurodegenerative disease. *Pathophysiology* *23*, 203–210. 10.1016/j.pathophys.2016.05.007.
65. Yadav, R., Mishra, P., and Yadav, D. (2019). Histone deacetylase inhibitors: A prospect in drug discovery. *Turkish J. Pharm. Sci.* *16*, 101–114. 10.4274/tjps.75047.
66. Smalley, J.P., Cowley, S.M., and Hodgkinson, J.T. (2020). Bifunctional HDAC therapeutics: One drug to rule them all? *Molecules* *25*. 10.3390/molecules25194394.
67. Bondarev, A.D., Attwood, M.M., Jonsson, J., Chubarev, V.N., Tarasov, V. V., and Schiöth, H.B. (2021). Recent developments of HDAC inhibitors: Emerging indications and novel molecules. *Br. J. Clin. Pharmacol.* *87*, 4577–4597. 10.1111/bcp.14889.
68. Tang, X., Kim, J., Zhou, L., Wengert, E., Zhang, L., Wu, Z., Carromeu, C., Muotri, A.R., Marchetto, M.C.N., Gage, F.H., et al. (2016). KCC2 rescues functional deficits in human neurons derived from patients with Rett syndrome. *Proc. Natl. Acad. Sci. U. S. A.* *113*, 751–756. 10.1073/pnas.1524013113.
69. Toritsuka, M., Yoshino, H., Makinodan, M., Ikawa, D., Kimoto, S., Yamamuro, K., Okamura, K., Akamatsu, W., Okada, Y., Matsumoto, T., et al. (2021). Developmental dysregulation of excitatory-to-inhibitory GABA-polarity switch may underlie schizophrenia pathology: A monozygotic-twin discordant case analysis in human iPS cell-derived neurons. *Neurochem. Int.* *150*. 10.1016/j.neuint.2021.105179.
70. Menassa, D.A., and Gomez-Nicola, D. (2018). Microglial dynamics during human brain development. *Front. Immunol.* *9*. 10.3389/fimmu.2018.01014.
71. Allen, N.J., and Lyons, D.A. (2018). Glia as architects of central nervous system formation and function. *Science* (80-. ). *185*, 181–185.
72. Bar, E., and Barak, B. (2019). Microglia roles in synaptic plasticity and myelination in homeostatic conditions and neurodevelopmental disorders. *Glia* *67*, 2125–2141. 10.1002/glia.23637.
73. Tau, G.Z., and Peterson, B.S. (2010). Normal development of brain circuits.

- Neuropsychopharmacology 35, 147–168. 10.1038/npp.2009.115.
74. Ramachandran, H., Martins, S., Kontarakis, Z., Krutmann, J., and Rossi, A. (2021). Fast but not furious: A streamlined selection method for genome-edited cells. *Life Sci. Alliance* 4. 10.26508/lsa.202101051.
  75. Nguyen, T., Ramachandran, H., Martins, S., Krutmann, J., and Rossi, A. (2022). Identification of genome edited cells using CRISPRnano. *Nucleic Acids Res.* 50, W199–W203. 10.1093/nar/gkac440.
  76. Baumann, J., Gassmann, K., Masjosthusmann, S., DeBoer, D., Bendt, F., Giersiefer, S., and Fritsche, E. (2016). Comparative human and rat neurospheres reveal species differences in chemical effects on neurodevelopmental key events. *Arch. Toxicol.* 90, 1415–1427. 10.1007/s00204-015-1568-8.
  77. Kong, L., Zhang, Y., Ye, Z.Q., Liu, X.Q., Zhao, S.Q., Wei, L., and Gao, G. (2007). CPC: Assess the protein-coding potential of transcripts using sequence features and support vector machine. *Nucleic Acids Res.* 35. 10.1093/nar/gkm391.
  78. Gu, J., Weber, K., Klemp, E., Winters, G., Franssen, S.U., Wienpahl, I., Huylmans, A.K., Zecher, K., Reusch, T.B.H., Bornberg-Bauer, E., et al. (2012). Identifying core features of adaptive metabolic mechanisms for chronic heat stress attenuation contributing to systems robustness. *Integr. Biol.* 4, 480–493. 10.1039/c2ib00109h.
  79. Shim, S.H., Lee, S.K., Lee, D.W., Brilhaus, D., Wu, G., Ko, S., Lee, C.H., Weber, A.P.M., and Jeon, J.S. (2020). Loss of Function of Rice Plastidic Glycolate/Glycerate Translocator 1 Impairs Photorespiration and Plant Growth. *Front. Plant Sci.* 10. 10.3389/fpls.2019.01726.

## STAR Methods

### Key Resources Table

REAGENT or RESOURCE	SOURCE	IDENTIFIER
<b>Antibodies</b>		
Anti-beta III tubulin conjugated to Alexa Fluor 647	Abcam	ab190575
Anti-MAP2	Thermo Fisher	13-1500; RRID:AB_2533001
Anti-AQP4	Merck	HPA014784; RRID:AB_1844967
Anti-LAMP2	Santa Cruz	sc-18822; RRID:AB_626858
Anti-O4	R&D Systems	MAB1326; RRID:AB_357617
Anti-CSB	GeneTex	GTX104589
Anti-LC3A	Abcam	ab52768; RRID:AB_881226
Anti-mTOR	Cell Signaling	mAb2983
Anti-acetyl-alpha-tubulin	Cell Signaling	mAb5335
Anti-HADC6	Cell Signaling	mAb7558
Anti-HSP90	Cell Signaling	mAb4877
Hoechst 34580	Thermo Fisher	H21486
Alexa Fluor 488 Phalloidin	Invitrogen	A12379
Anti-mouse Alexa Fluor 488	Invitrogen	A11001; RRID:AB_2534069
Anti-mouse Alexa Fluor 546	Invitrogen	A11030; RRID:AB_2534089
Anti-rabbit Alexa Fluor 546	Invitrogen	A11010; RRID:AB_2534077
Anti-mouse Alexa Fluor 488	Invitrogen	A-21042; RRID:AB_2535711
Anti-mouse	LI-COR Bioscience	926-80010
Anti-rabbit	LI-COR Biosciences	926-80011
<b>Chemicals, peptides, and recombinant proteins</b>		
Laminin521	Biolamina	LN521-05
Laminin111	Merck	L2020
EDTA	Thermo Fisher	15575020
ROCK inhibitor	Hello Bio	HB2297
Penicillin/Streptomycin	PAN-Biotech	P06-07100
Human recombinant fibroblast growth factor (hFGF)	R&D Systems	233-FB
mTeSR1	StemCell Technologies	5850
mTeSR1 supplement	StemCell Technologies	5850
Penicillin/Streptomycin	PAN-Biotech	P06-07100
iPS-brew XF, human	StemMACS	130-104-368
iPS Brew XF supplement	StemMACS	130-104-368
Penicillin/Streptomycin	PAN-Biotech	P06-07100
Knockout Serum Replacement	Invitrogen	10828028
N2 supplement	Invitrogen	17502-048
SB-431542	Sigma Aldrich	S4317
LDN-193189	Sigma Aldrich	SML0559
DMEM/F12	Invitrogen	31330038

B27 supplement	Invitrogen	17504-044
B27 Plus supplement	Gibco	A35828-01
Creatin monohydrate	Sigma Aldrich	C3630
Interferon- $\gamma$	Peprtech	300-02
Neurotrophin-3	Peprtech	450-03
Ascorbic acid	Sigma Aldrich	A5960
db-cAMP	Sigma Aldrich	D0260
Neurobasal Electro Medium	Thermo Fisher	A1413701
B-27 Electrophysiology supplement	Thermo Fisher	A1413701
Glutamax	Thermo Fisher	A1286001
human recombinant GDNF	RnD Systems	212-GMP-010
human recombinant BDNF	Peprtech	450-02
Triiodothyronine (T3)	Merck	T2877
Gentle Cell Dissociation Reagent	Stemcell Technologies	100-0485
Polyethyleneimine (PEI)	Sigma-Aldrich	181978
Accutase	Stemcell Technologies	07920
Dimethyl sulfoxide (DMSO)	Carl-Roth	A994.1
Anti-adherence rinsing solution	Stemcell Technologies	07010
Matrigel	Corning	354277
Tubastatin A	Sigma Aldrich	SML004
Suberoylanilide hydroxamic acid (SAHA)	Biomol	Cay10009929
Poly-d-lysine (PDL)	Merck	P0899
Chloroquine	Sigma	C6628
Poly-HEMA	Merck	P3932
Paraformaldehyde	Sigma Aldrich	P6148
Goat serum	Sigma Aldrich	G9023
Triton X-100	Sigma Aldrich	T8787
Poly-L ornithine	Sigma Aldrich	P3655
Tricarballic acid	Sigma Aldrich	T53503
Methanol	Roth	N41.1
Chloroform	Roth	3313.1
Natriumchloride	Roth	3957.1
Methoxyamine hydrochloride	Thermo Fisher	10440364
Ribitol	Sigma Aldrich	A5502-5G
Aqua-Poly/Mount	Polysciences Inc.	18606-20
Critical commercial assays		
Cell Titer-Blue® Viability Assay (CTB)	Promega	G8080
Lactate dehydrogenase Assay (LDH)	Promega	G7890
Cell Proliferation BrdU Assay	Sigma Aldrich	11669915001
RNeasy Mini Kit	Qiagen	74104
QuantiTec Reverse Transcription Kit	Qiagen	205314
Quanti Fast SYBR Green Kit	Qiagen	204057
Deposited data		
RNA Sequencing		GEO: GSE240972
Experimental models: Cell lines		
hiPSC-IMR90 clone 4 (IMR90 <sup>WT</sup> )	WiCell	RRID:CVCL_C437
CS789	Prof. Dr. Egly, IGBMC Strasbourg	N/A
CS789 <sup>Res</sup>	GEMD, Leibniz IUF Düsseldorf	N/A
IMR90 <sup>KO</sup>	GEMD, Leibniz IUF Düsseldorf	N/A
Oligonucleotides		

Primers listed in supplemental information table S2.	Eurofins	N/A
Recombinant DNA		
PX458	Addgene	48138
Software and algorithms		
CRISPR design tool CHOPCHOP	<a href="https://chopchop.cbu.uib.no/">https://chopchop.cbu.uib.no/</a>	N/A
CRISPRnano	Nguyen et al. (2022). <a href="https://doi.org/10.1093/nar/gkac440">10.1093/nar/gkac440</a> <sup>73</sup>	N/A
Fiji Image J (v1.53f51)	<a href="https://imagej.net/software/fiji/">https://imagej.net/software/fiji/</a>	N/A
Image Studio Lite (v5.2)	LI-COR Biosciences	N/A
Axion Integrated Studios (AxIS) navigator software (version 3.1.2)	Axion Biosystems	N/A
Neural Metric Tool software (version 3.1.7)	Axion Biosystems	N/A
MassHunter Qualitative software (vb08)	Agilent Technologies	N/A
NIST14 Mass Spectral Library	<a href="https://www.nist.gov/srd/nist-standard-reference-database-1a-v14">https://www.nist.gov/srd/nist-standard-reference-database-1a-v14</a>	N/A
GraphPad Prism (v9.5.1)	<a href="https://www.graphpad.com">https://www.graphpad.com</a>	N/A

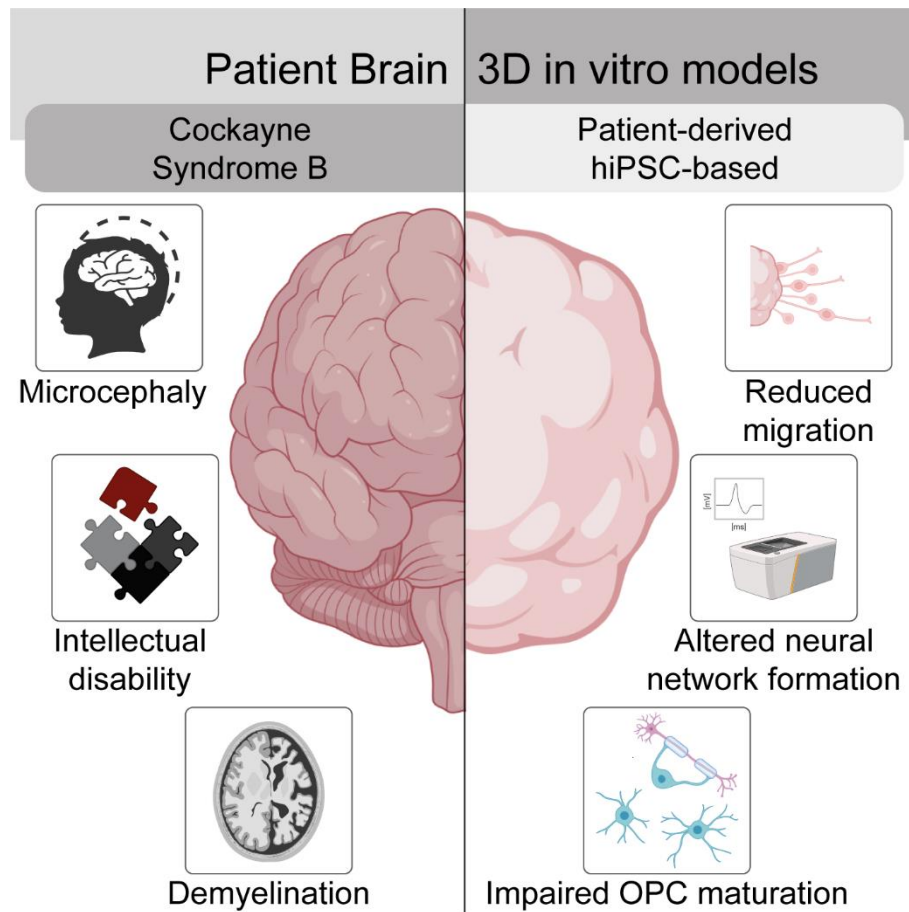


Figure 1

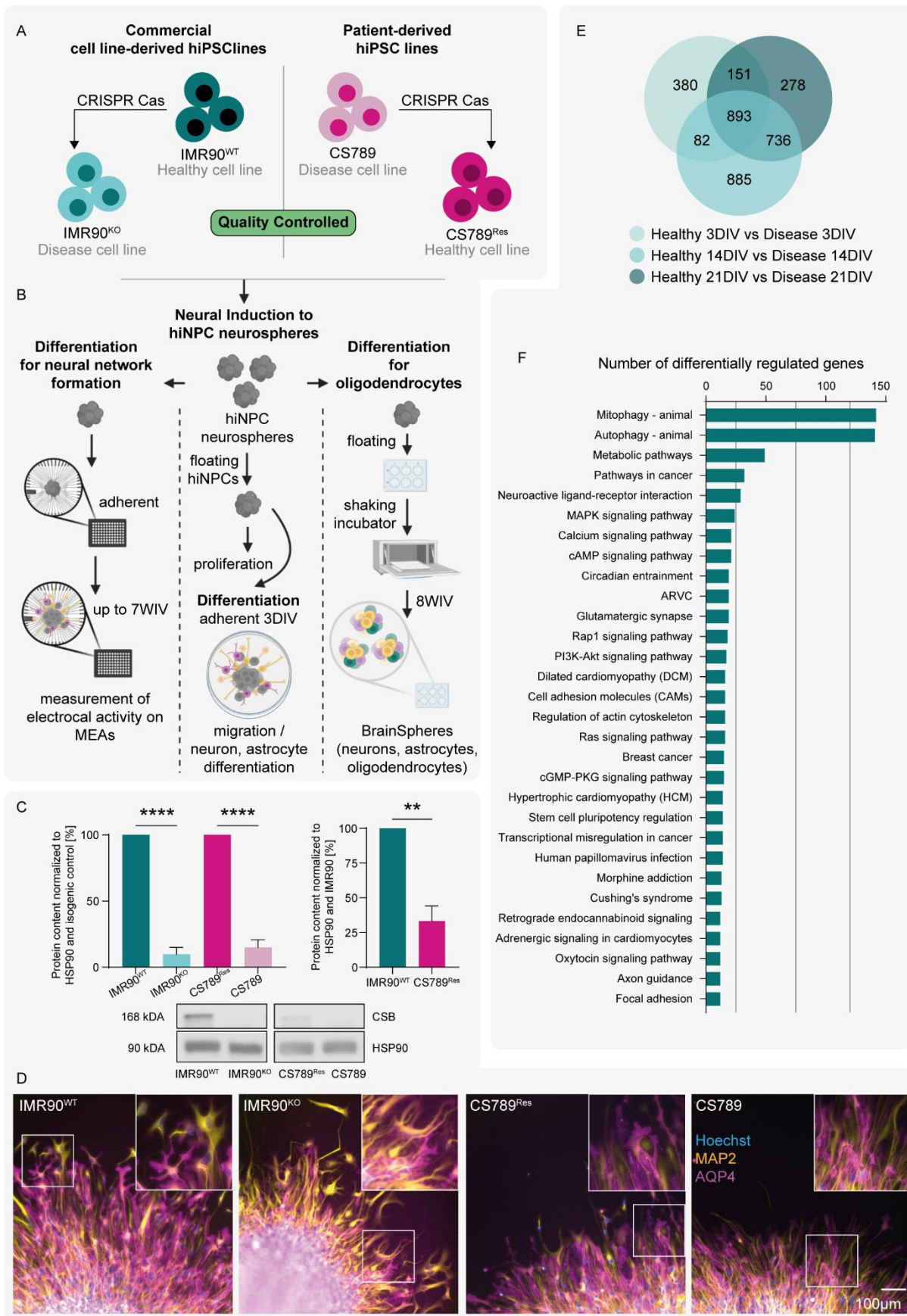


Figure 2

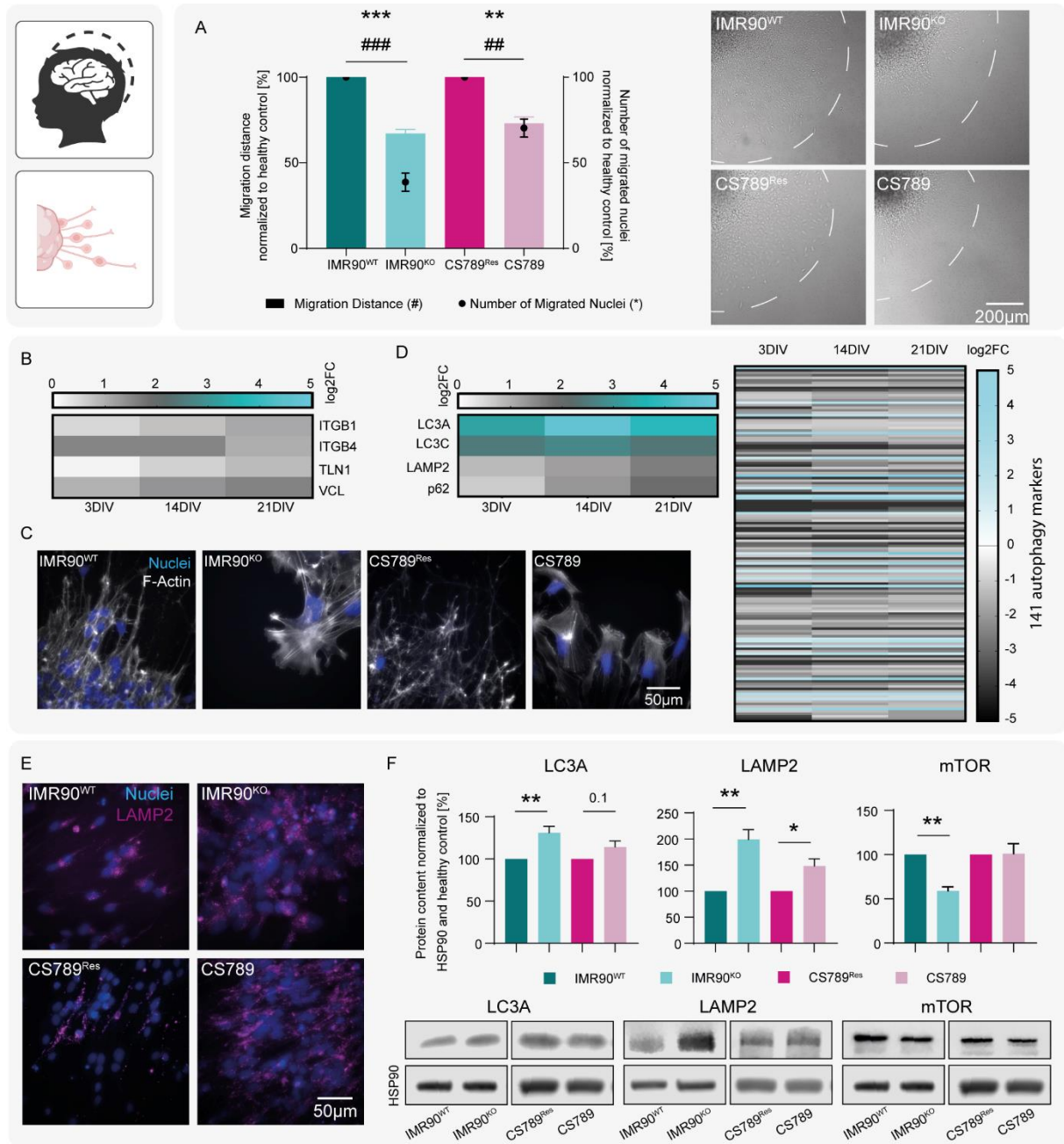


Figure 3

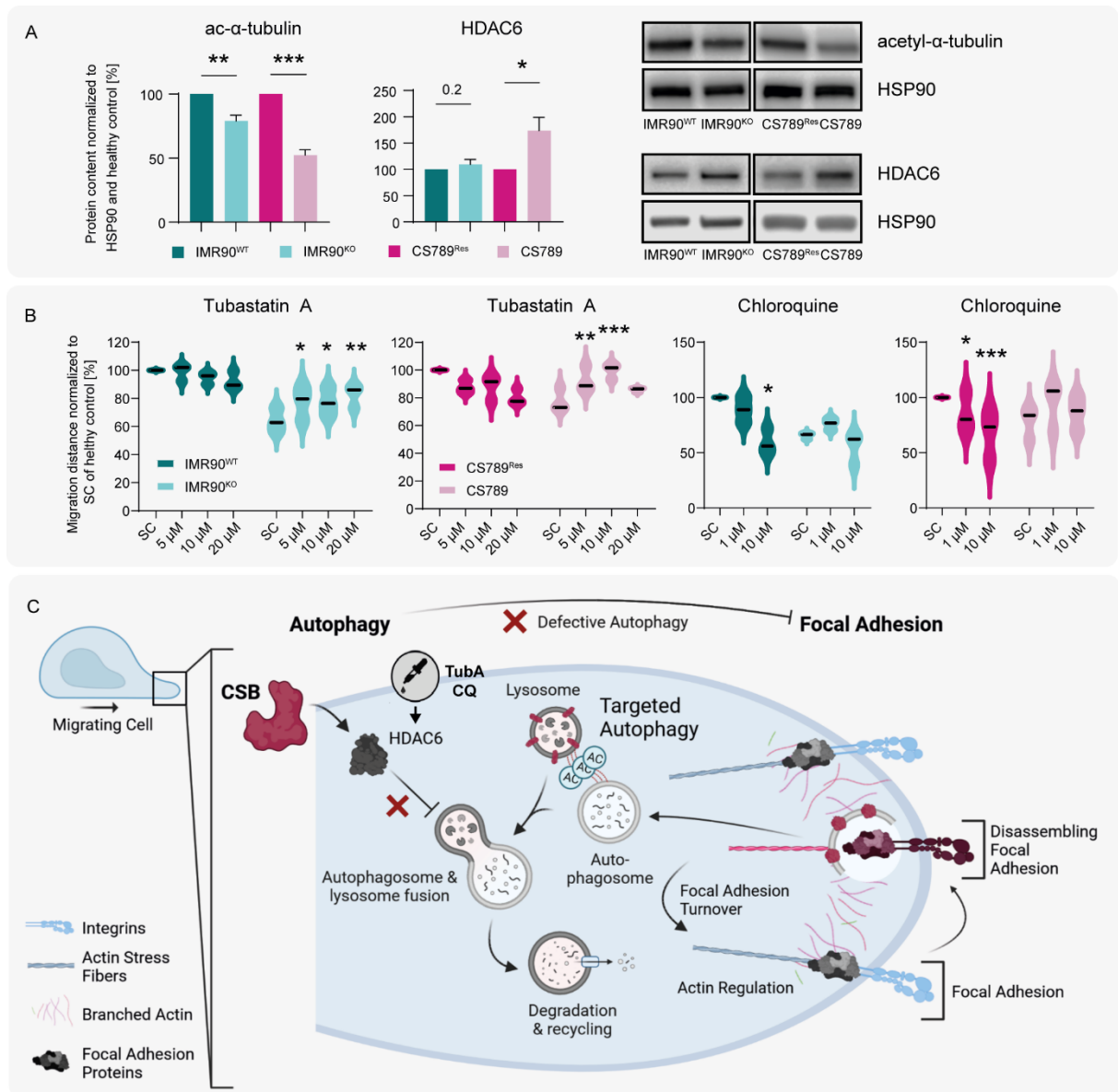




Figure 5

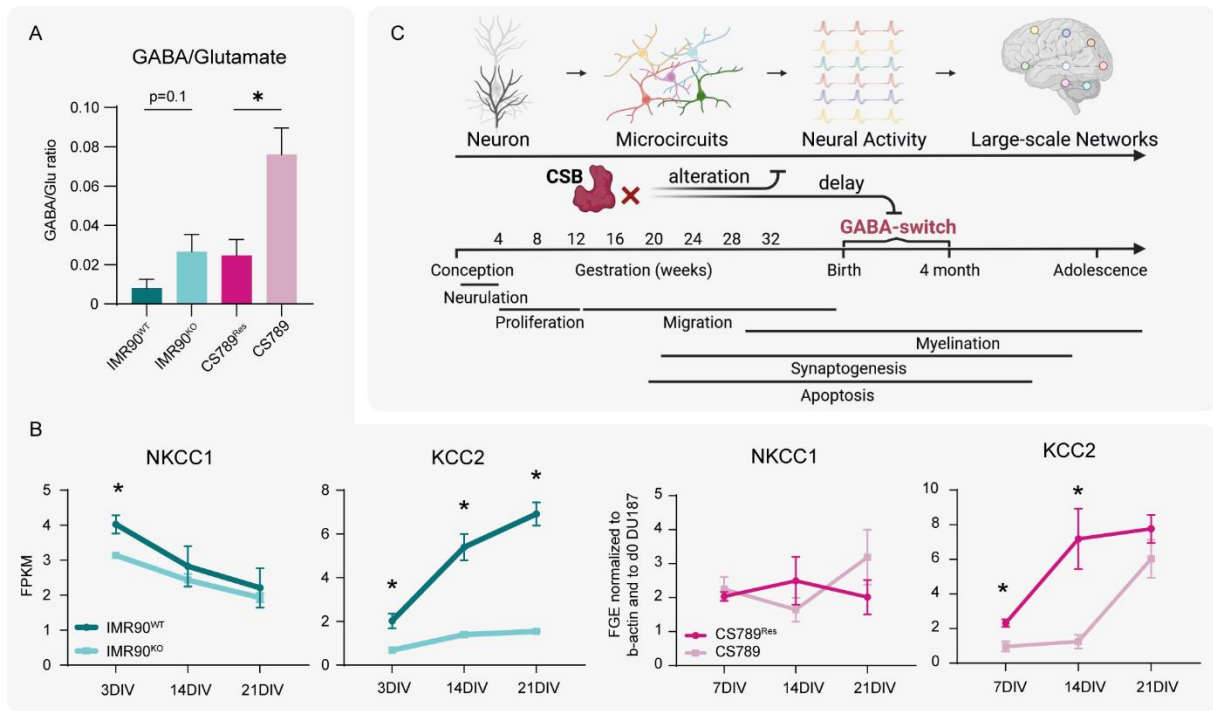
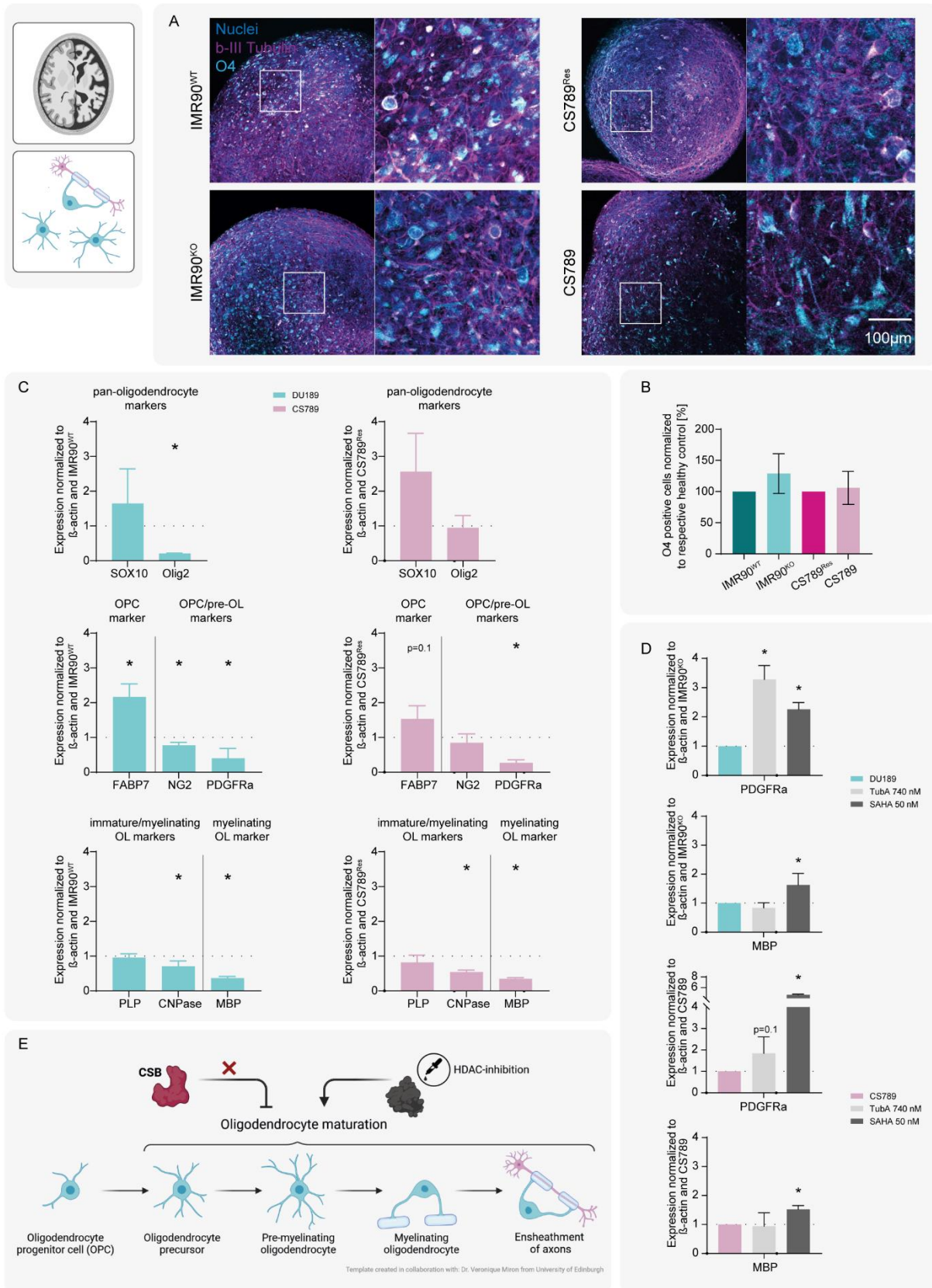
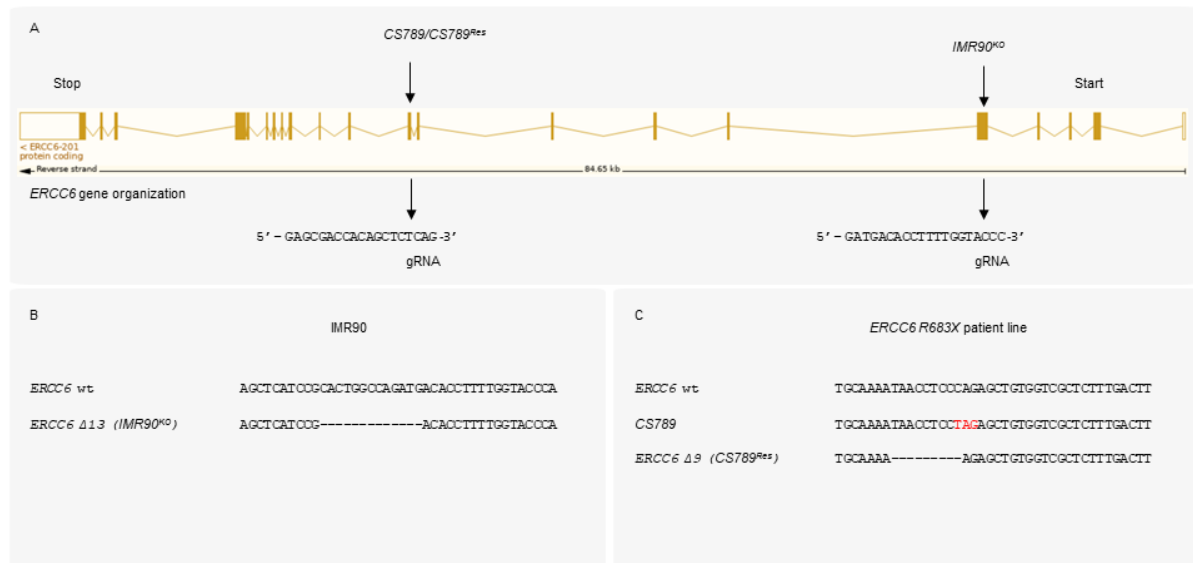


Figure 6

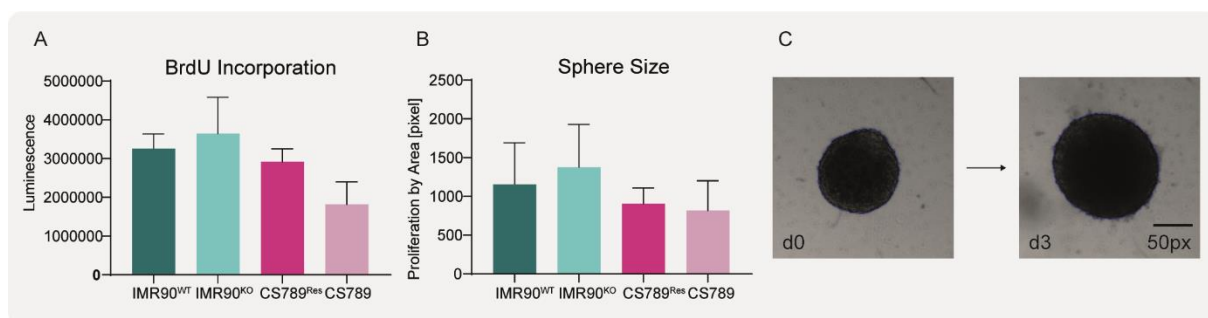


## Supplemental Information

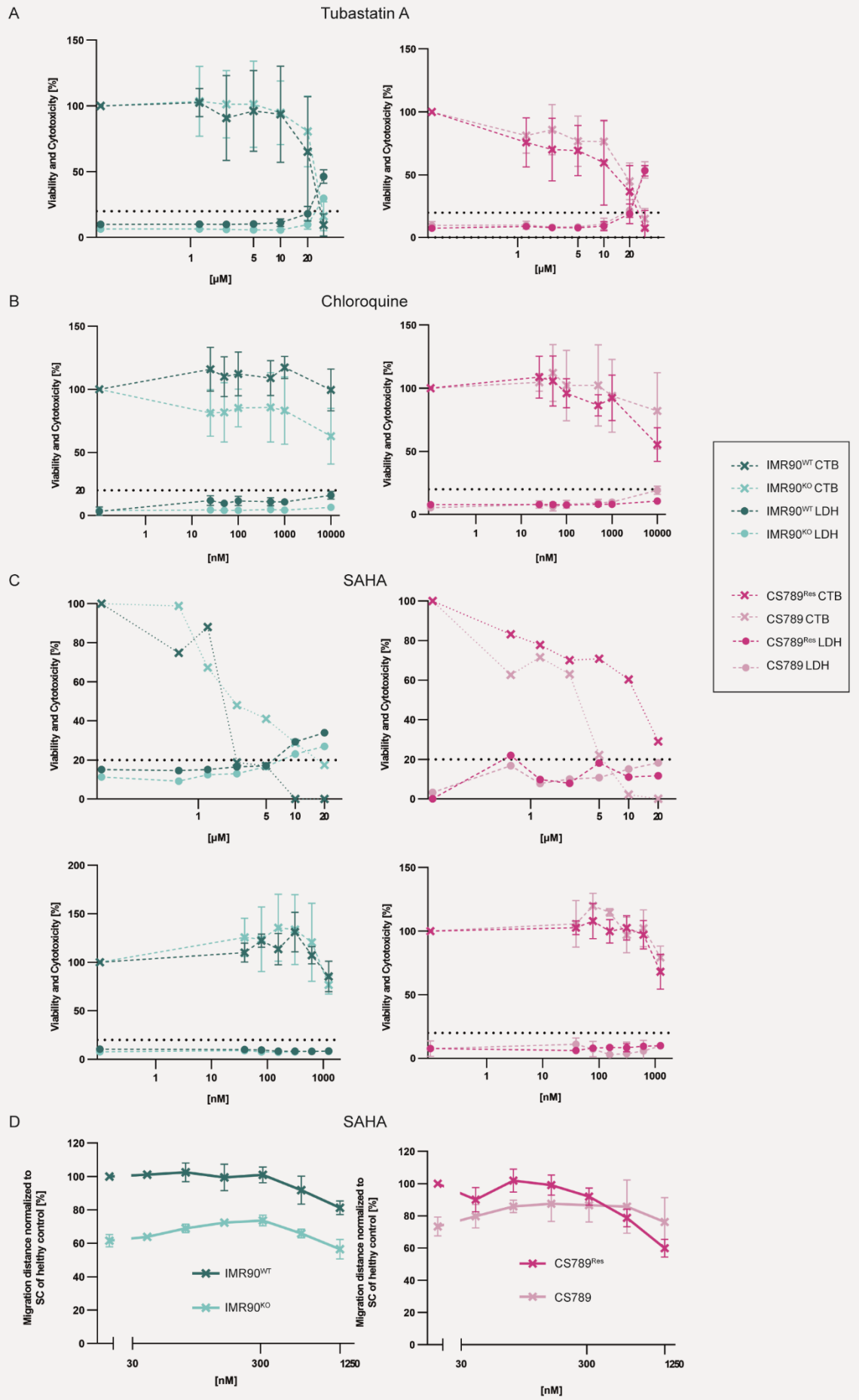
## Figures



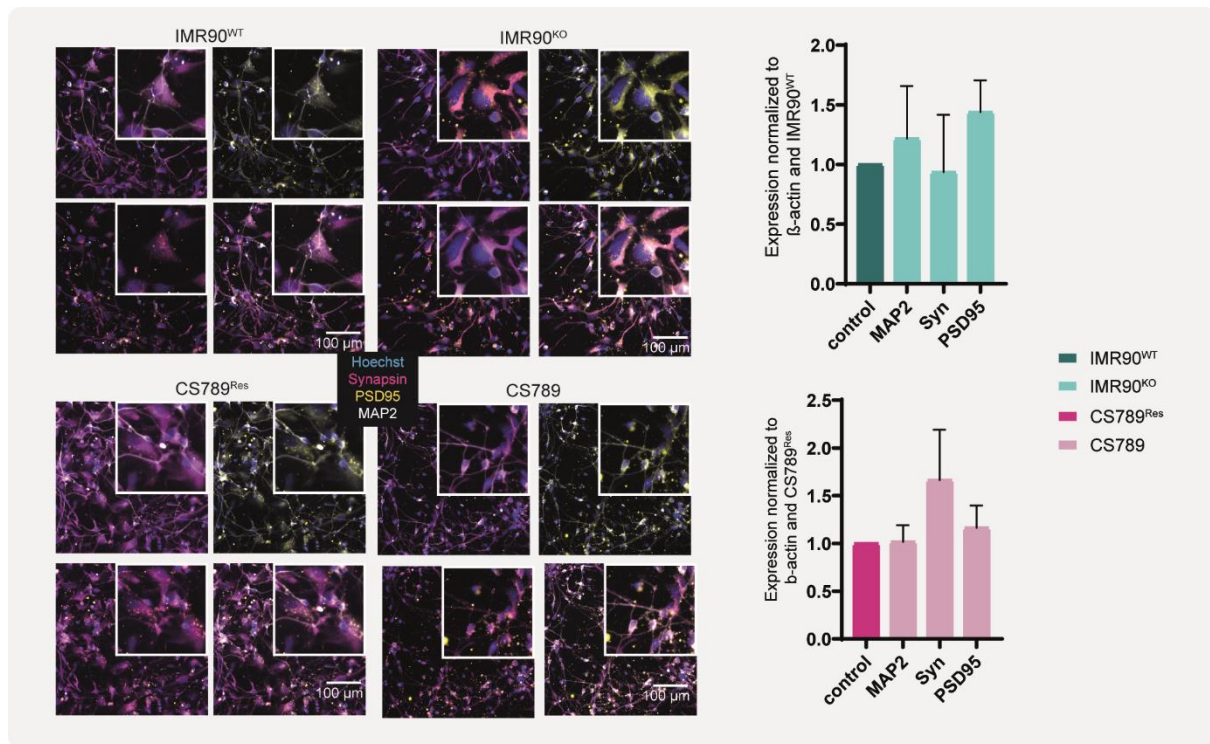
**SI Figure S1. Cell Line Information – related to ‘Two hiPSC models for neurodevelopmental key event analyses in the Cockayne Syndrome B’.** (A) Schematic view of ERCC6 gene structure modified from Ensembl (ENT00000355832). Top, ERCC6 iPSC mutants (CS789<sup>Res</sup>, CS789 and IMR90<sup>KO</sup>) carry mutations in exons pointed to by the arrows. IMR90<sup>KO</sup> ERCC6 mutant was generated using commercially available iPSCs (IMR90<sup>WT</sup>). CS789<sup>Res</sup> mutant was generated using the CS789 patient-derived iPSC line. Bottom, arrows point to the gRNA sequences used to generate ERCC6 mutants (CS789 and IMR90<sup>KO</sup>). (B) Next generation sequencing alignment of IMR90<sup>WT</sup> and IMR90<sup>KO</sup> mutant. Depicted is a deletion of 13 bp in the IMR90<sup>KO</sup> mutant. (C) Next generation sequencing alignment of IMR90<sup>WT</sup>, CS789 (the stop codon is depicted in red), and CS789<sup>Res</sup> mutant that carries 9 bp in-frame deletion that removes the premature stop codon present in the CS789 patient line.



**SI Figure S2. CSB-deficient cell lines do not show altered proliferation – related to ‘CSB-deficiency is associated with inhibited neural progenitor cell migration and alterations in focal adhesion and autophagy’.** Proliferation of all cell lines was assessed in hiNPCs using the BrdU assay and area measurement. Spheres were cultivated in proliferation medium for 3 days. (A) The BrdU incorporation on day 3. The graph depicts the luminescence of each cell line. (B) The area was measured every day, and the increase in Area is depicted for each cell line. (C) Exemplary images of sphere growth from d0 to d3. N=3 biological replicates with n=3-5 spheres. All graphs depict the mean ± SEM. Abbreviations: hiNPC, human induced neural progenitor cell; BrdU, bromodeoxyuridine / 5-bromo-2'-deoxyuridine.



**SI Figure S3. Migration treatment supplemental information – related to ‘The HDAC6-inhibitor Tubastatin A partially rescues the migration phenotype of disease hiNPC neurospheres’.** Cytotoxicity (LDH) and viability (CTB) were measured for all Tubastatin A (A), Chloroquine (B) and SAHA (C) treatments. (C) The top two graphs depict an N=1 biological replicate with n=3-5 spheres. All other Graphs depict N=3 biological replicates with n=3-5 spheres. (D) Migration in differentiation BrainSpheres treated with different SAHA concentrations. N=3 biological replicates with n=3-5 spheres. All graphs depict the mean  $\pm$  SEM.



**SI Figure S4. Neuronal and synaptic markers – related to ‘Microelectrode Array measurements reveal altered neural network activity in CSB-deficient networks’.** Left: ICC stainings of plated hiNPC spheres after 3 DIV. Representative images of each cell line are depicted. Right: qPCR analyses of MAP2 (neuronal marker), SYN (pre-synaptic marker) and PSD95 (post-synaptic marker) after 3 DIV, normalized to the housekeeper  $\beta$ -actin and the respective control cell line. Graps depict mean  $\pm$  SEM. Abbreviations: ICC, immunocytochemistry; hiNPC, human induced neural progenitor cell; DIV, days in vitro.

## Tables

**SI Table S1. CS789 – Patient information<sup>1</sup> – related to ‘Two hiPSC models for neurodevelopmental key event analyses in the Cockayne Syndrome B’.**

Patient ID	CS789VI
Origin	UK
Mutation	Point mutation (2047C>T; p.Arg683x)
Donor Cell Type	Dermal fibroblasts, male
Clinical Classification	Cerebro-oculofacio-skeletal syndrome (COFS)
Growth failure	+
Low birth weight	+
Cachexia	-
Intellectual Disability	Severe
Microcephaly	Congenital
Seizures	+
Cataracts	Congenital
Microphthalmia	+
Retinal degradation	-
Deafness	+
Clinical photosensitivity	+
Dental anomalies	-
Arthrogryposis	+
Age at Death	10 months

**SI Table S2. qPCR Primers – related to ‘Key Resource Table’.** All primers supplied by Eurofins.

β-actin	FW	CAG GAA GTC CCT TGC CAT CC
	RV	ACC AAA AGC CTT CAT ACA TCT CA
NKCC1	FW	ACA AAG TTG AGG AAG AGG ATG GC
	RV	CCT GAT CTG CCG GTA TGT CTT GG
KCC2	FW	CTA CAG CGA ACG AGA GAG CG
	RV	CCA TCT CCT CCT CAA ACA AGG C
FABP7	FW	TCA TCA GGA CTC TCA GCA CA
	RV	GAA CAG CAA CCA CAT CAC CA
NG2	FW	CGG ACA CTT CTT CCG AGT GA
	RV	TAT TCC CAG CGT AGA CCT CTG
PLP	FW	TTG GCG ACT ACA AGA CCA CC
	RV	GGG AAG GCA ATA GAC TGG CA
PDGFRa	FW	ATT AAG CCG GTC CCA ACC TG
	RV	AGC TCC GTG TGC TTT CAT CA
CNPase	FW	ACT CAG GCA TCA TTC CAC CA
	RV	TGT CAA GCG TGG TGT TCA AG
Olig2	FW	CCG ATG ACC TTT TTC TGC CG
	RV	CCA CTG CCT CCT AGC TTG TC
MBP	FW	CAG AGC GTC CGA CTA TAA ATC G
	RV	GGT GGG TTT TCA GCG TCT A

## References

1. Laugel, V., Dalloz, C., Durand, M., Sauvanaud, F., Kristensen, U., Vincent, M.C., Pasquier, L., Odent, S., Cormier-Daire, V., Gener, B., et al. (2010). Mutation update for the CSB/ERCC6 and CSA/ERCC8 genes involved in Cockayne syndrome. *Hum. Mutat.* 31, 113–126. 10.1002/humu.21154.

## 3 Discussion

A distinct shift from animal models to in vitro alternatives is evident across academia, industry and regulatory bodies. This movement leads to new guidelines and an improved acceptance of new approach methodologies (NAMs), like those addressing skin sensitization (OECD guideline no.497 2023), in the context of the 3R principles (replacement, reduction, and refinement of animal testing). The 3R initiative is a movement initiated by Russell and Burch already in 1959, that supports and guides the development of alternatives to animal experiments with the perspective of regulatory acceptance. In this context, the establishment of complex and robust models and reliable cultivation systems that reflect human physiology becomes essential (Krewski et al. 2010). At the forefront of NAM development are stem cell-, especially hiPSC-based models, due to their pluripotency, human relevance and virtually unlimited availability (manuscript 2.1). This thesis ties in with the aforementioned goals, by characterizing and optimizing hiPSC-derived 3D in vitro models to gain valuable insights into neurodevelopmental pathomechanisms and their application as NAMs. The thesis further supports the versatility of such models beyond disease modeling, extending the relevance of hiPSC-derived in vitro systems to other biomedical fields like toxicology.

### 3.1 Human iPSCs as basis for neural in vitro models

Although many efforts in the field of neural in vitro modeling rely on primary or rodent cell cultures (Meyer, Lotze, and Riess 2022; Baumann et al. 2016; Koch et al. 2022), hiPSCs are up and coming (Tukker et al. 2020; Rowe and Daley 2019; Ebert, Liang, and Wu 2012), aiding the development of physiologically relevant NAMs. Human iPSC-based NAMs have proven to be valuable tools for the investigation of human brain development in vitro, as reviewed in manuscript 2.2. However, limitations and drawbacks need to be considered, in order to correctly implement and analyze these models.

Beyond the regularly argued ethical acceptance, a significant advantage of hiPSCs is their human, often patient-specific origin. This intrinsic quality aids the recapitulation

of specific genetic phenotypes, granting them substantial relevance and predictive capacity. For instance, Li et al. (2018) used a patient-specific hiPSC-based model with mutations in the GFAP gene, to identify impaired OPC proliferation and myelination as underlying mechanisms in the Alexander disease. The genetic heterogeneity inherent in different hiPSC lines, arising from their donor-specificity, further strengthens their predictivity by reflecting the broad patient heterogeneity. This enables the investigation of how patient-derived hiPSCs of donors with heterogenous psychiatric conditions, such as schizophrenia, react to drug administration (Collo et al. 2020). In addition, larger-scale applications such as drug screenings and toxicological hazard assessments could profit from this genetic diversity. Nevertheless, one should err on the side of caution, when comparing single healthy and disease cell lines from different donors with respect to their individual behavior and response to substances (Volpato and Webber 2020).

An effective strategy to navigate challenges posed by, and even leverage, donor variability involves creating isogenic control cell lines for disease-specific and patient-derived hiPSC models. Isogenic controls enable a direct comparison between a mutated cell line and its rescued control, possessing otherwise identical genetic backgrounds. This allows the distinction between effects attributed to the mutation itself and those arising from the genetic background. Despite a growing number of studies employing isogenic controls, the potential advantages they offer remain underutilized. In an extensive study, Brunner et al. (2023) analyzed and compared multiple endpoints (immunocytochemistry, electrophysiological measurement, proteomic data) for neurons derived from different hiPSC lines, revealing low statistic power in current neural disease modeling setups. However, they state a strong increase of statistical power in studies using multiple isogenic control designs. Two pairs of isogenic control lines were utilized in manuscript 2.7, as discussed in section 3.4.1 of this thesis.

A high cellular and structural complexity can be achieved using hiPSCs. Neurons and astrocytes are readily differentiated from hiPSCs (Chambers et al. 2009; Hofrichter et al. 2017; Hartmann et al. 2023), whereas the generation of oligodendrocytes and microglia was impossible for a long time. Although still challenging, both cell types can now be obtained from differentiating hiPSCs in vitro (Abreu et al. 2018; David Pamies et al. 2017;

Douvaras and Fossati 2015; McPhie et al. 2018). The added model complexity in multicellular and 3D cultures, compared to monocultures, enables the investigation of inter-cellular interactions, such as during neuronal migration, and cell-type specific effects, such as oligodendrocyte sensitivity to oxidative stress (Alépée et al. 2014).

Human iPSCs can be massively expanded in culture, thereby generating a virtually inexhaustible cell source. This is a big advantage for long-term or screening studies. However, researchers should always be aware of risk factors, such as genomic instability (Yoshihara, Oguchi, and Murakawa 2019) and mycoplasma contaminations (Drexler and Uphoff 2002; Nikfarjam and Farzaneh 2012), which can lead to severe reliability and reproducibility issues. To date, no gold standard is set for quality-controlled cell culture material in academia, which leads to high variances in quality control standards (Pamies, Leist, et al. 2022). In manuscript 2.6, the generation of a quality-controlled banking process for hiPSCs is suggested, including assays to assess cell morphology, mycoplasma contamination, short tandem repeats (STR) and karyotype analysis, as well as pluripotency and viability tests. Such a quality control may seem extensive, but only comes with an average cost of 2,340 Euros per master cell bank (50 vials) – a reasonable price for improved data reliability within the academic research community. All hiPSC lines used in this thesis were quality controlled and banked according to manuscript 2.6, to ensure high and reliable culture quality. This thesis therefore provides a proof of principle for the applicability of good cell culture practice for in vitro models.

## 3.2 Human iPSC-based neural models in 2D and 3D

### 3.2.1 *From 2D to 3D cultures*

From 2D mono-cultures (Washer et al. 2022; Quist, Ahlenius, and Canals 2021) over multicellular spheroid cultures (Y. K. Lee et al. 2020; Raja et al. 2022; Hofrichter et al. 2017; Pamies et al. 2017) to complex bioengineered 3D models (manuscript 2.3 and manuscript 2.4; Antill-O'Brien, Bourke, and O'Connell 2019), the application of hiPSCs is manifold. The conventional approach to neural in vitro modeling involved utilizing 2D models cultivated on coated plastic or glass surfaces. These models are advantageous

due to their simplicity and efficiency in generating homogeneous and reproducible cultures, facilitating well-established readouts (Table 3.1; Centeno, Cimarosti, and Bithell 2018). HiPSC-derived neural 2D cultures have been employed in the investigation of diseases such as Alzheimer's disease (Kondo et al. 2013; Hossini et al. 2015), Huntington's disease (Mattis et al. 2012), and Parkinson's disease (Cooper et al. 2010; Soldner et al. 2009). However, the human brain is one of the most complex tissues in the body. Stem cells underlay a defined spatial and temporal exposure to signaling molecules, cell-cell and cell-matrix interactions (Farrukh, Zhao, and del Campo 2018) thus determines their fate and organization (Discher, Mooney, and Zandstra 2009). These interactions are largely absent in 2D models, causing them to fall short in capturing the complexity of human in vivo physiology (Table 3.1; Hopkins et al. 2015; Morrison, Cullen, and LaPlaca 2011). Consequently, this can lead to alterations in cell morphology, proliferation and differentiation (T. Xu et al. 2009; Brännvall et al. 2007; Zhang et al. 2014).

3D models augment the complexity of conventional cell cultures, rendering them more predictive and physiologically relevant (Bahram, Mohseni, and Moghtader 2016; Q. Gu et al. 2018; Pacitti, Privolizzi, and Bax 2019; Fritsche, Gassmann, and Schreiber 2011; Zhuang, Sun, et al. 2018; Centeno, Cimarosti, and Bithell 2018; D'Aiuto et al. 2018). These models provide crucial cell-cell and cell-matrix interactions, establishing a certain degree of spatial organization and the potential for a customized physiological microenvironment. These qualities make these models adaptable to individual research needs (Table 3.1; manuscripts 2.3 and 2.4; Madl and Heilshorn 2018; Zhuang, An, et al. 2018; Fabbri et al. 2023). However, this increased complexity may entail elevated cell culture costs, particularly if additional equipment or materials are necessary. This is accompanied by greater challenges in method development, including tasks like image analysis and quantification (Table 3.1).

Two distinct strategies for 3D model development have arisen: scaffold-free and scaffold-based approaches. Both strategies will be elaborated upon in the next section.

**Table 3.1 Comparison of 2D and 3D neural models.** Adapted from Centeno, Cimarosti, and Bithell (2018).

	<b>Two-dimensional (2D)</b>	<b>Three-dimensional (3D)</b>
	Mono- or multi-cell type models cultivated on coated surfaces (often glass or plastic).	Scaffold-free or scaffold-based models, adherent or non-adherent.
Advantages	Simple to use Inexpensive Homogenous culture Reproducible Well-established techniques Easy downstream processing	Complex cell-cell interactions Cell-matrix interactions Spatial organization Higher degree of complexity Design of microenvironment Higher physiological relevance
Limitations	Non-physiological Cell-cell interactions limited Altered Cell-matrix interaction Low predictability Altered cell morphology and behavior	Potentially more expensive Can be challenging for methods and readouts Potential variability in reproduction Downstream processing can be difficult

### 3.2.2 Scaffold-free and scaffold-based 3D models

In this study, different scaffold-free and scaffold-based approaches were established and employed to generate hiPSC-derived fit-for-purpose models (Figure 3.1).

Initially, hiPSCs were neurally induced to hiNPCs neurospheres, a process attainable by dual-SMAD inhibition in 2D or 3D (Hofrichter et al. 2017; Hartmann et al. 2023). The hiNPC neurospheres were further differentiated into neurons and astrocytes, oligodendrocyte-containing BrainSpheres (both scaffold-free) or bioengineered hydrogel cultures (scaffold-based, Figure 3.1, manuscripts 2.3, 2.4 and 2.7). Neurospheres consist of proliferative hiNPCs and serve as a platform to investigate proliferation and migration, as well as terminal differentiation into neurons and astrocytes. Their quick and reproducible generation makes them ideal for the screening of adverse effects induced by genetic or external factors (manuscript 2.7; Hofrichter et al. 2017; Boutin et al. 2022). Test methods based on primary fetal neurospheres have been previously established for DNT hazard identification (Harrill et al. 2018; Masjosthusmann et al. 2019; Fritsche et al.

2018b; Koch et al. 2022), which gives reason to expect further application of hiPSC-based neurospheres in drug screening and toxicological hazard assessment. BrainSpheres are generally cultured under differentiating conditions for up to 8 weeks and comprise various cell types, including neurons, astrocytes and oligodendrocytes. This composition enables the modeling of oligodendrogenesis and its disruption in 3D (manuscript 2.7; Abreu et al. 2018; David Pamies et al. 2017; D Pamies et al. 2021). Both neurospheres and BrainSpheres were utilized in manuscript 2.7, as closely discussed in section 3.4 of this thesis.

Human iPSC-derived and differentiated neurospheres and BrainSpheres develop electrically active neural networks, despite their early maturation stage. This enables the analysis of further neurodevelopmental KEs, such as neural network formation and synaptogenesis (manuscript 2.5, manuscript 2.7; Nimtz et al. 2020; Hartmann et al. 2023). Neural network formation (NNF) can be measured during the differentiation on MEAs over time, or in acute measurements at a designated timepoint (Pelkonen et al. 2022). This is useful for analyzing NNF in neurodevelopmental and neurodegenerative disorders, such as Kleefstra syndrome (Frega et al. 2019), amyotrophic lateral sclerosis (ALS; Wainger et al. 2014; Szebényi et al. 2021), Schizophrenia (Kathuria, Lopez-Lengowski, Jagtap, et al. 2020), Bipolar disorder (Kathuria, Lopez-Lengowski, et al. 2020), Parkinson's disease (Ronchi et al. 2021), Alzheimer's disease (Ghatak et al. 2021) and other encephalomyopathic disorders (Ekert et al. 2020; Simkin et al. 2021; Ichise et al. 2021). As an example, Linda et al. (2022) investigated the Koolen-de Vries (KdV) syndrome, a neurological disease with developmental delays, epilepsy and congenital malformations, by analyzing the neural network function of patient-based hiPSC models on MEAs. They identified impaired NNF and reduced synaptic density as an in vitro phenotype of KdV. Human iPSC-derived neural models on MEAs can also be used for measuring acute or long-term responses to substance exposure (Odawara et al. 2018; Que et al. 2021; Hartmann et al. 2023). Bartmann et al. (2023) used hiPSC-derived neural networks to assess neurodevelopmental pesticide toxicity on MEAs. They challenged the neural networks with 28 compounds to identify and quantify their DNT potential. The

option to closely monitor potential delays or shifts in network formation of hiPSC-based models can thus provide valuable insights into various aspects of brain development.

Scaffold-based approaches to 3D in vitro modeling provide their own distinct advantages and limitations. Since the brain is one of the softest tissues in the human body, with a Young's elastic modulus of 0.5-50 kPa (Leipzig and Shoichet 2009; S. Budday et al. 2017), mimicking the brain's ECM in vitro is highly challenging (Axpe et al. 2020). Hydrogels feature advantageous properties for the 3D cultivation of neural models, such as the high water content (>90%), potential for functionalization, as well as chemical and physical tunability (David Pamies et al. 2018). However, high variability and low throughput ask for better hydrogel compositions and characterization. In this thesis we developed different well-characterized hydrogels with distinct properties for the cultivation and differentiation of hiPSC-derived neural fit-for-purpose models (manuscript 2.3, manuscript 2.4).

In manuscript 2.3 we show the cytocompatibility of oxidized alginate-gelatin-laminin (ADA-GEL-LAM, 2.5%/2.5%/0.01%) hydrogels for neurospheres, as well as their subsequent differentiation and neuronal outgrowth. ADA provides an ECM surrogate which can easily be crosslinked by  $\text{Ca}^{2+}$  ions, while GEL contributes cell adhesion motifs to the hydrogel (Sarker et al. 2014; Hofrichter et al. 2017; Thomas Distler et al. 2020). Both components degrade over time, thus enabling neural outgrowth and migration (Sarker et al. 2014). The ADA-GEL was additionally functionalized with the integrin binding motif LAM, which plays a major role in cell adhesion, migration and differentiation in the developing brain (Flanagan et al. 2006; Tzu and Marinkovich 2008; Paulsson 1992; Georges-Labouesse et al. 1998; Campos et al. 2004). Integrins have already proven beneficial in vitro, e.g. by improving human neural stem cells differentiation (P. Wu et al. 2002; G. A. Silva et al. 2004; Caldwell et al. 2001). LAM-functionalization in the ADA-GEL hydrogels increased neuronal outgrowth over 14 days, thus showing the necessity of appropriate binding-motifs in 3D hydrogels. The initial stiffness of approx. 5 kPa in the ADA-GEL-LAM hydrogel roughly reflects the stiffness of the brain tissue (S. Budday et al. 2017). However, beneficial hydrogel degradation over time may decrease the stiffness, therefore further aiding progenitor stemness (Madl et

al. 2017) and subsequent neuronal outgrowth and migration. In addition, this hydrogel model allows downstream analysis of cell viability through live/dead staining and the quantification of neuronal outgrowth via ICC images. These options, together with the cost-efficiency and tissue-like properties of the hydrogels, are beneficial for future application of this hiPSC-based model in disease modeling or substance testing. Adaptation of the hydrogel may be necessary to study functional readouts or for bioprinting applications.

With manuscript 2.4, we characterized additional hydrogel variations with different characteristics. We present two cytocompatible alginate-gellan gum-laminin (ALG-GG-LAM) hydrogel blends for the generation of hiPSC-based 3D neural models with spontaneous intracellular calcium signals and the compatibility with bioprinting. ALG-based hydrogels were previously shown to support neurite outgrowth and increase the resistance to oxidative stress in neurons, while GG-based hydrogels support migration and maturation of neuronal cultures (Koivisto et al. 2017; Matyash et al. 2012). Both gels are inexpensive and enable easy and fast processing. However, they don't have specific cell binding sites (Sun and Tan 2013; Ferris et al. 2013), which is why LAM was used to functionalize the ALG-GG blend. LAM supports cell-matrix interaction (Lozano et al. 2015; Sakaguchi et al. 2019), as discussed above for manuscript 2.3. We designed two hydrogel blends (i) 0.3% ALG / 0.8% GG / 0.01% LAM and (ii) 1.5% ALG / 0.5% GG / 0.01% LAM, within the appropriate stiffness range (approx. 20-35 kPa). Interestingly, a reduced ALG content increased the stress relaxation time of the 0.3% ALG / 0.8% GG / 0.01% LAM hydrogel significantly, suggesting ALG or GG to act similar to spacer molecules. Spacer molecules were previously shown to control and accelerate stress relaxation of other materials and hydrogels (Zhu et al. 2010). Since the brains ECM components are viscoelastic, with time-dependent mechanical responses to stress, quick stress relaxation times seem to be a crucial property to mimic in vitro (Madl and Heilshorn 2018; Axpe et al. 2020). We also confirm slow degradation of the ALG-GG-LAM gel blends over time, which benefits cellular outgrowth and migration (Yildirim and Seifalian 2014). Further investigations and multimodal mechanical testing are necessary to

properly investigate the brain tissue and brain-mimicking materials (Leipzig and Shoichet 2009; T. Distler et al. 2020).

Spontaneous calcium signals are important for cellular regulation of e.g. gene expression, neuronal outgrowth and differentiation (Dolmetsch, Xu, and Lewis 1998; West et al. 2001; Lankford and Letourneau 1989). Calcium imaging has been previously applied to study tissue slices, human neural aggregates, primary human neurospheres and brain organoids (Sutherland, Pujic, and Goodhill 2014; Rosenberg and Spitzer 2011; Lancaster et al. 2013; Gualda et al. 2014). In this manuscript we are, to the best of our knowledge, the first to establish calcium imaging in slices of in vitro 3D-cultivated neural samples. We generated two fit-for-purpose models to suit different modeling needs. The first model consists of hiNPC neurospheres in 0.3% ALG / 0.8% GG / 0.01% LAM hydrogels. This softer gel model supports cellular outgrowth, migration and differentiation to form complex microtissues containing astrocytes and neurons. Spontaneous calcium signals can be measured after 3 WIV. We suggest this model to be valuable for applications requiring a high degree of complexity, but less throughput, such as disease modeling and long-term exposure studies. We also successfully generated a hydrogel model based on a disease hiPSC line, derived from a donor afflicted with the Cockayne Syndrome B. This disease is associated with severe neurological defects. A closer discussion on the disease is given in section 3.4 of this thesis. The second model features 2 weeks pre-differentiated hiNPC spheres embedded into 1.5% ALG / 0.5% GG / 0.01% LAM. These models are especially easy to handle for calcium imaging due to their slightly higher stiffness. They quickly produced dense intra-spherical networks containing neurons and astrocytes, and showed spontaneous calcium signals after one week within the hydrogel. This model could be suitable for higher throughput applications, such as acute exposures to chemicals or substance screenings, due to their fast and easy production and improved handling during  $Ca^{2+}$  imaging, compared to suspension spheres.

Advanced biofabrication techniques like 3D bioprinting are up and rising in fields like tissue engineering and substance testing (Parrish et al. 2019; Ong et al. 2018; Cui et al. 2017; Z. Gu et al. 2020; Zhuang, An, et al. 2018). Bioprinting can be utilized to design and

build complex and reproducible scaffolds with cell-laden materials (bioinks) like hydrogels (Fantini et al. 2019; R. Sharma et al. 2020). In manuscript 2.4 we utilized the developed hydrogel blends to print single hiNPCs in squared structures for the precise deposition on 96-well MEA electrodes. This approach aimed at increasing the reliable deposition of cell material onto the electrodes for higher throughput applications (Ylä-Outinen et al. 2019; Parrish et al. 2019). We successfully printed the cell-laden hydrogels in millimeter-sized squares, however higher than expected MEA plate variability concerning the position of the electrodes due to the manufacturer's quality criteria, prevented the successful production of ready-to-use 3D bioprinted neural models. Notably, un-crosslinked 1% ALG was not printable and GG alone was not adherent to coated cell culture surfaces, making the here discovered hydrogel blends valuable for 3D bioprinting applications.

Further characterization and adaptations are necessary to bring the scaffold-based 3D models into application for disease modeling or substance screenings. For long-term cultivations, these models could be improved, by adding other native ECM molecules like collagen, fibronectin or hyaluronic acid (Gassmann et al. 2012; N. A. Silva et al. 2012; Antman-Passig et al. 2017; Licht et al. 2019; Seidlits et al. 2010). Downstream readouts like cellular migration, viability and neural network activity need to be further established and characterized in healthy hiPSC-based models, to increase their relevance in disease modeling. Nevertheless, with manuscripts 2.3 and 2.4 we contribute to the evolution of 3D scaffold-based neural in vitro models.

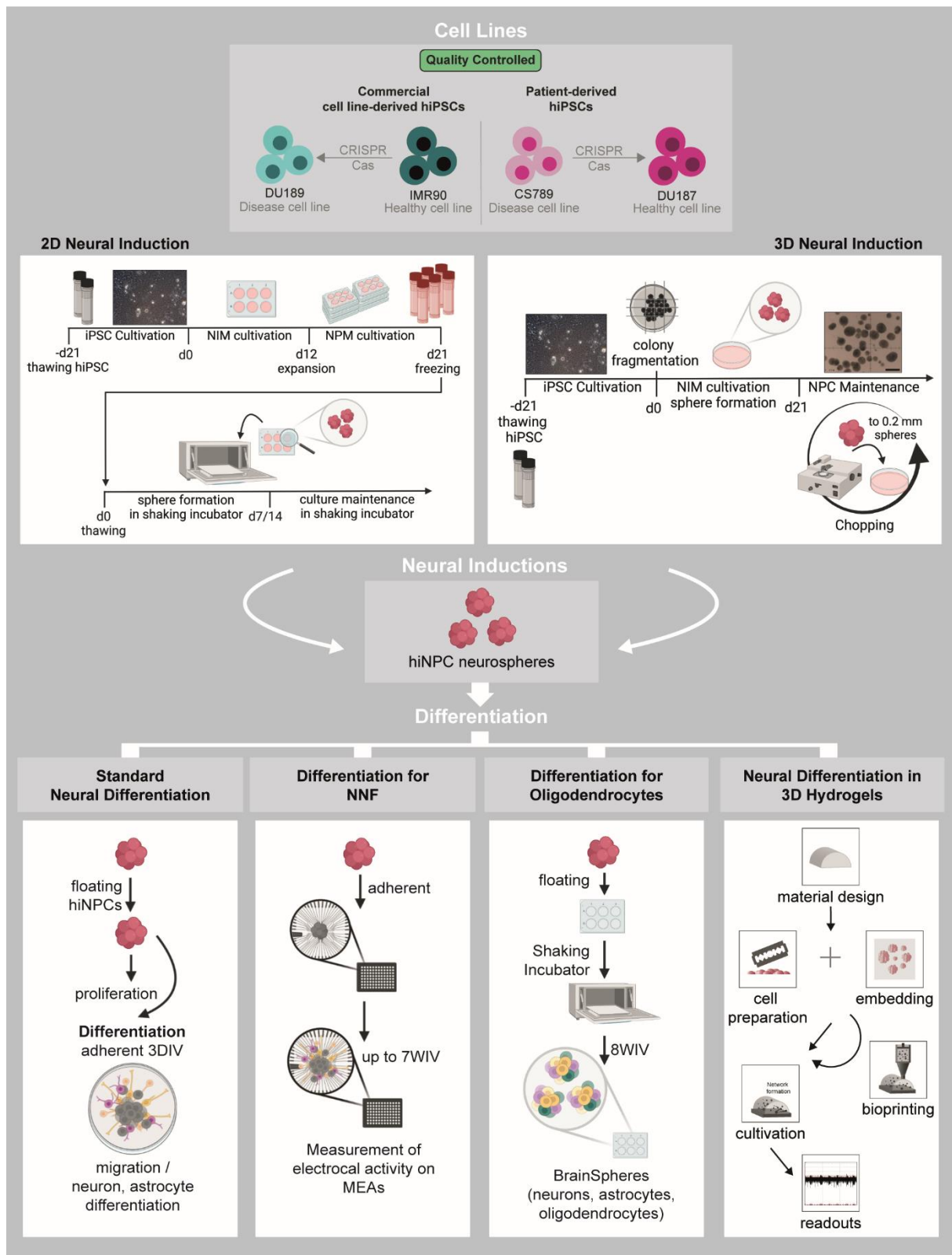


**Figure 3.1. Human iPSC-derived fit-for-purpose neural models used in this thesis.** Human induced pluripotent stem cells (hiPSCs) from different donors, genetically modified if necessary, can be neurally induced in 2D or 3D to form 3D neurospheres, consisting of human induced neural progenitor cells (hiNPCs). In a fit-for-purpose approach, these hiNPC neurospheres can then be differentiated depending on the desired readout. Proliferation can be assessed in proliferating hiNPC neurospheres,

while migration and differentiation into neurons and astrocytes can be analyzed in differentiating neurospheres plated onto coated surfaces after 3 DIV (standard neural differentiation). In an adapted protocol, hiNPC neurospheres are plated onto coated microelectrode array (MEA) plates for subsequent neural network formation and measurement of electrical activity for up to 7 WIV (differentiation for NNF). The differentiation protocol for oligodendrocytes requires long-term differentiation of hiNPC neurospheres in a shaking incubator, to obtain BrainSpheres consisting of neurons, astrocytes and oligodendrocytes (differentiation for oligodendrocytes). HiNPC neurospheres or single cell hiNPCs can be embedded into specifically designed hydrogels for subsequent differentiation and analyses in 3D. Hydrogel-embedded cells can also be bioprinted to obtain desired 3D structures in vitro. Abbreviations: hiPSC, human induced pluripotent stem cell; hiNPC, human induced pluripotent stem cell; NIM, neural induction; NPM, neural progenitor medium; NNF, neural network formation; DIV, days in vitro; WIV, weeks in vitro; MEA, microelectrode array. Figure made using biorender.com.

### 3.3 In vitro modeling of human brain pathology

Each neurological disease has its individual features evoked by a specific neuropathology. Modeling such diseases in vitro hence calls for distinct solutions as outlined in Figure 3.2. When investigating human disease in vitro, it is crucial to first pinpoint the existing data gaps in order to formulate the research questions. The chosen model systems should in principle be suitable to investigate these research questions through relevant methods and readouts, while also recognizing any inherent limitations. Considerations for choosing fit-for-purpose models are discussed below.

From the pathophysiological point of view, neurodevelopmental and adult neurological diseases are to be distinguished. Within the perinatal period, developmental timing governs distinct windows wherein specific developmental key processes take place. Hence, the selected model system should recapitulate the age of disease onset and/or progression. Studying neurodevelopmental disorders requires models that recapitulate early KEs of human brain development. Such KEs include proliferation, migration, differentiation, as well as neural network formation and function (Bal-Price et al. 2018). Their genetically or environmentally-induced disruption leads to severe structural, functional and metabolic changes in the developing brain (manuscript 2.1, manuscript 2.2). Human iPSC-based 3D models like neurospheres and BrainSpheres emerge as ideal

systems to investigate brain development in vitro (manuscript 2.7; Abreu et al. 2018; David Pamies et al. 2017; Nimtz et al. 2020; D Pamies et al. 2021). The effect of patient-specific genetic mutations on brain development can be addressed using in vitro models thanks to the development of genome editing technologies. The discovery and adaptation of the CRISPR (clustered regularly interspaced short palindromic repeats)/Cas (CRISPR-associated) system now enables highly specific editing of the human genome in vitro. The CRISPR/Cas system was originally discovered in bacteria and archaea as an RNA-mediated defense mechanism against viruses and foreign plasmids (Garneau et al. 2010; Marraffini and Sontheimer 2010; Wiedenheft, Sternberg, and Doudna 2012). A guide RNA (gRNA) that matches the foreign DNA leads the endonuclease Cas9 to the virus, where it induces a double-strand break (DSB) to inactivating the virus. This system has been engineered for improved site specificity and functionality in human cells such as hiPSCs, compared to the initial machinery. This makes it possible to introduced Cas9-mediated DSBs at a precisely chosen location, by designing the gDNA to match the target sequence (Jinek et al. 2012; S. W. Cho et al. 2013; Cong et al. 2013). Subsequently, gene disruption through deletions or insertions, or gene corrections through homologous recombination can be achieved (Yang et al. 2014; Doetschman and Georgieva 2017). Two examples demonstrate the usefulness of the CRISPR/Cas system for understanding pathomechanisms of rare hereditary diseases. Tan et al. (2020) generated CSB and RAD52 knockout cell lines of different origins to investigate reactive oxygen species (ROS)-induced DNA damage and Yoon et al. (2022) inserted a Ndufs4 deletion in hiPSCs to study the Leigh Syndrome in hiPSC-derived cardiomyocytes.

Aging-related neurodegenerative disorders such as Alzheimer's disease and Parkinson's disease require highly mature models (N. S. Sharma et al. 2021; Barak et al. 2022; Kwak et al. 2020), which is to date a considerable challenge. Organoids are generated over several months and are often used to model neurodegenerative disorders as reviewed by Wray (2021). Yet, hiPSC-derived organoids show a transcriptome roughly comparable to the prenatal brain (Camp et al. 2015). This intrinsic immaturity of hiPSC-based in vitro models still hinders the translation of findings from bench to bedside. However,

advancing methods enable long-term cultivations and improved maturation of crucial cell populations like oligodendrocytes and microglia within intricate 3D models (A. Sharma et al. 2020). For instance, Kwak et al. (2020) were able to advance the maturation of hiPSC-derived midbrain-like organoids towards an in-vivo-like cellular composition with neurons, astrocytes and oligodendrocytes, by optimizing culture conditions, thereby providing an improved platform to study Parkinson's disease. Nevertheless, a lack of vascularization and relevant barriers limits even the most complex organoid models. Organ-on-a-chip (OOAC) approaches currently provide a promising option to recapitulate complex barriers like the blood-brain-barrier (BBB). Maoz et al. (2018) have developed microfluidic organ chips to analyze the role of different cell types in the BBB. They coupled three chips to model (i) the influx across the BBB, (ii) the brain parenchyma including astrocytes and neurons and (iii) the efflux across the BBB. With this system they modeled methamphetamine administration and identified specific metabolic coupling of the compartments.

In summary, it may be necessary to develop multiple fit-for-purpose models to investigate the disease of interest, similar to the approach taken in manuscript 2.7, or consider additional animal models to study distinct phenotypes (Figure 3.2).

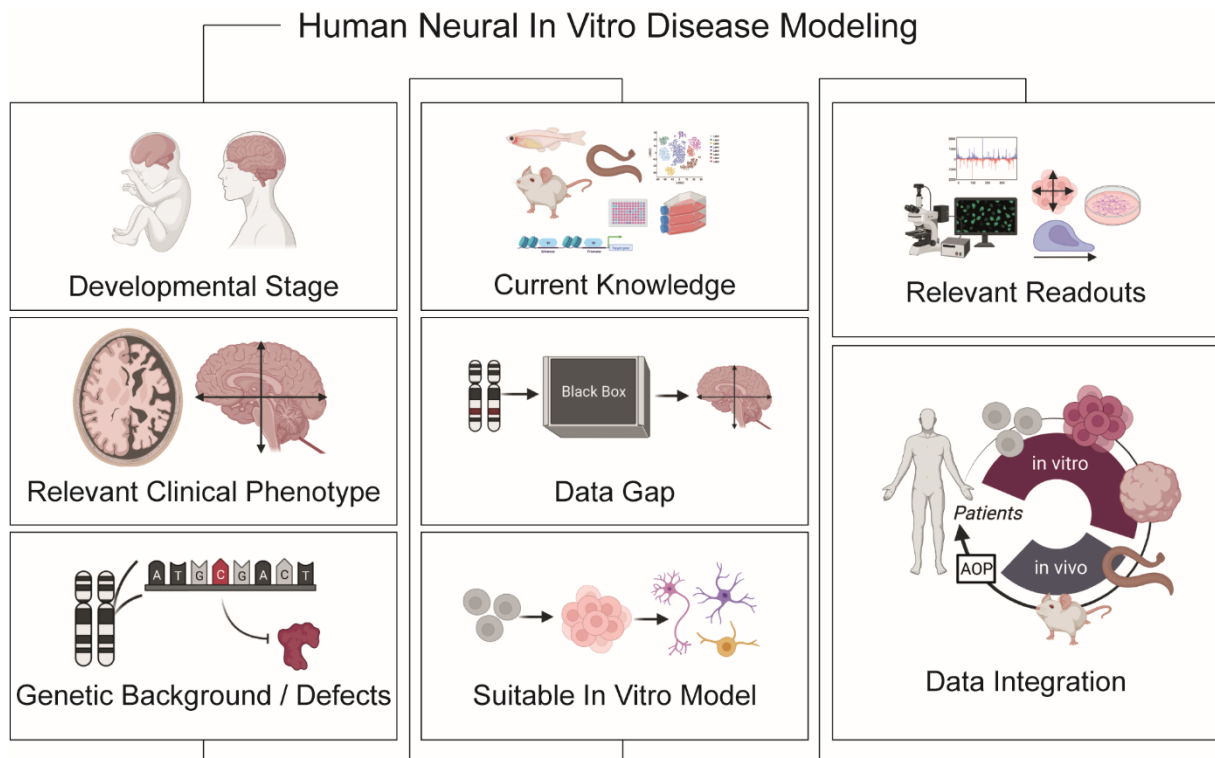


**Figure 3.2. Identification of relevant in vitro model systems for disease-specific applications.** The developmental stage in which the disease develops or surfaces needs to be identified, together with the relevant clinical phenotypes that need to be modeled. It may be necessary to develop more than one model to investigate all identified clinical phenotypes. Genetic predispositions or mutations need to be identified and incorporated within the model, if applicable. Upon reviewing the current knowledge, data gaps need to be identified. The subsequently chosen in vitro model and associated readouts should be able to recapitulate the aforementioned aspects of the disease. Data integration of different studies and model systems can be achieved e.g. through the generation of adverse outcome pathways (AOPs). Figure made using biorender.com.

### 3.4 The Cockayne Syndrome B (CSB)

The Cockayne Syndrome B (CSB) is a rare hereditary recessive disease with severe dermatological and neurological symptoms (Laugel 2013; Vessoni et al. 2020). CSB is caused by mutations in the ERCC6 gene, which encodes for the CSB protein (Troelstra et al. 1992). The lack of CSB protein results in defective brain development already in the prenatal phase (Laugel 2013; Alexandre Teixeira Vessoni et al. 2020). CSB is known to be involved in the TC-NER (Lindenbaum et al. 2001; Rapin et al. 2000), which has been linked to the dermatological phenotype of CSB, which is caused by ultraviolet (UV) light-induced DNA damage. However, the mechanism of DNA damage alone cannot be

responsible for the severe neurodevelopmental symptoms observed in children with the disease, which is why alternative functions of the CSB protein need to be unraveled. Due to very limited understanding of the CSB pathomechanisms, resulting from a lack of human-relevant models, there is no treatment for the children with CSB to date. This thesis aimed to help close the current knowledge gap by developing 3D hiPSC-based CSB disease models to investigate the cardinal brain phenotypes of CSB: 1) microcephaly, 2) intellectual disability and 3) demyelination (Laugel et al. 2010; Alexandre Teixeira Vessoni et al. 2020; Laugel et al. 2008; Karikkineth et al. 2017).

### *3.4.1 Fit-for-purpose models to study CSB in vitro*

Human iPSC-based models like neurospheres and BrainSpheres recapitulate early neurodevelopmental processes and are thus the ideal tools to gain a mechanistic understanding of the CSB neuropathology. A previous study has used iPSC-based neuron/astrocyte mixed cultures to investigate the neuropathology of CSB (Vessoni et al. 2016) and another study by Wang et al. (2020) utilized hiPSCs of CSB patients and a respective isogenic control line to study DNA repair defects in mesenchymal and neural stem cells. Other previous studies on CSB have employed non-hiPSC systems, such as immortalized hNPCs (Ciaffardini et al. 2014; Wang et al. 2016) and neuroblastoma cells (Liang et al. 2023). However, immortalized and tumor cell lines are limited in recapitulating a patient's in vivo situation and may therefore cause misleading results.

Hence, this thesis focused on utilizing hiPSCs for in vitro disease modeling. For increased predictivity (Brunner et al. 2023), we generated two distinct hiPSC-based models, each including a disease and isogenic control cell line. The first model consists of the commercially available hiPSC line IMR90<sup>WT</sup>, and an IMR90<sup>KO</sup> line generated via CRISPR/Cas9, by introducing a 13bp deletion into exon 5 of the ERCC6 gene. The second model consists of the patient-derived hiPSC line CS789 and the isogenic control line CS789<sup>Res</sup>. The patient cell line holds a point mutation (2047C>T) in exon 10 of the ERCC6 gene, which leads to a premature stop codon. The genetic rescue of the CS789 disease cell line via CRISPR/Cas9 through a 9bp in-frame deletion, which removes the stop

codon, results in the isogenic control line CS789<sup>Res</sup>. The two CSB models allow for the distinction between sole CSB-specific effects (IMR90<sup>WT</sup>/IMR90<sup>KO</sup> model) and additional influences of the patient's genetic background (CS789/ CS789<sup>Res</sup>). In addition, the isogenic nature of each model enables the direct comparison of disease and control condition, thereby adding different levels of analysis to the study design. Although the type of CSB mutation differs between the two models, both lead to a loss of CSB protein (manuscript 2.7). The CSB-proficient IMR90<sup>WT</sup> and CS789<sup>Res</sup> lines express significantly different protein levels, which can be expected due to the non-isogenic nature of the two lines. In general, the direct comparison of protein levels of different individual donors can be challenging due to potential genetic variations, such as single nucleotide polymorphisms (SNPs), and other genomic variances that can influence gene expression and protein production (Beekhuis-Hoekstra et al. 2021; Geiger et al. 2012). Therefore, the usage of isogenic controls is highly advantageous when studying human diseases in vitro.

Taken to together, CSB manifests in multiple neurological phenotypes each having different modeling needs, thus benefiting from the here provided fit-for-purpose models.

### *3.4.2 Mechanisms underlying the neuropathology of CSB*

CSB is a heterogeneous disease with a spectrum of symptoms, yet common pathophysiological features include microcephaly, intellectual disability and demyelination (Laugel et al. 2008; 2010; Vessoni et al. 2020; Karikkineth et al. 2017). In this thesis, in vitro disease modeling was applied to reveal CSB endophenotypes of altered migration, neural network activity and oligodendrocyte maturation. These findings link cellular pathomechanisms to the cardinal clinical symptoms seen in CSB.

Altered migration has previously been linked to microcephaly (reviewed by Becerra-Solano, Mateos-Sánchez, and López-Muñoz 2021 and Poirier et al. 2013), such as in the Meckel syndrome or different tubulinopathies (Pirozzi, Nelson, and Mirzaa 2018). Not only hampered migration, but also impaired NPC proliferation, neuronal differentiation

or apoptosis can be the underlying causes for microcephaly (Becerra-Solano, Mateos-Sánchez, and López-Muñoz 2021). For instance, others found disrupted neuronal differentiation and neurite outgrowth in 2D CSB-deficient immortalized NPC and hiPSC-derived neurons, respectively (Ciuffardini et al. 2014; Y. Wang et al. 2016). For instance, Ciuffardini et al. (2014) utilized ReNcell VM cells, an immortalized hNPC line, and a short hairpin RNAs (shRNA)-silenced CSB knockout line to investigate the role of CSB in neuritogenesis. The group subsequently differentiated the cell lines in 2D, identifying inhibited neurite outgrowth and impaired MAP2 expression in CSB-suppressed neuronal-astrocyte co-cultures. Both cell systems used in this thesis do not display impaired NPC proliferation or neuronal differentiation, including no alteration of MAP2 expression, and no increase in cell death was observed. The differences to the in vitro readouts observed by others could be explained with the large heterogeneity between CSB mutations, the usage of different non-hiPSC models or the lack of isogenic controls.

The disrupted migration of hiNPCs is accompanied by altered autophagy in our CSB-deficient models. Genes associated with autophagy are highly differentially expressed between the healthy and the disease cells, as identified via RNA sequencing. HDAC-dependent dysregulation of autophagy has recently been identified to play a major role in the dermatological defects of CSB patients (Majora et al. 2018). Here we show that the HDAC6-specific inhibitor Tubastatin A rescues the inhibited migration in the CSB models leading us to hypothesize that defective autophagy is the mechanistic link between the lack of CSB protein and the impaired migration. This hypothesis is supported by the well-established knowledge that targeted autophagy plays a major role in focal adhesion turnover, which in turn facilitates cell migration (Hernandez et al. 2021; Kenific, Wittmann, and Debnath 2016; Kenific et al. 2016).

Brain circuit formation is precisely orchestrated and a disruption leads to numerous pathological defects, many of which culminate in intellectual disabilities (Silbereis et al. 2016; Silvia Budday, Steinmann, and Kuhl 2015; Vasudevan and Suri 2017). CSB patients are generally afflicted with impaired cognitive function (Laugel et al. 2008; 2010; Karikkineth et al. 2017), with the donor of the patient cell line used in this thesis additionally being afflicted with seizures. The in vitro counterpart of circuit formation is

the ability of neural cells to form functional and synchronized networks e.g. on microelectrode arrays (MEAs). Therefore, we studied the ability of the healthy and corresponding disease hiPSC-derived neural models to form functional and synchronized neural networks. MEAs provide an excellent tool to investigate disease-associated alterations in NNF in vitro (Hartlaub et al. 2019; Pelkonen et al. 2022). Our CSB-deficient neural networks show significantly increased network activity over the course of 7 WIV. We underline similar, however reverse, findings of a study conducted by Vessoni et al. (2016). The group utilized two patient-based and three control hiPSC lines, none of which were isogenic pairs. The first patient line holds heterozygous point mutations (A>T and C>T; unknown clinical classification), while the second patient line is homozygous for a single point mutation (C>T; CSI clinical classification). The group found CSB-related alterations in synapse density and reduced electrical activity in 2D cultures of the hiPSC-derived neuron-astrocyte co-cultures after 5 WIV. The difference to our data could be explained by differences in patient and control cells' genetic backgrounds, endpoint measures only at one time point, general low network activity (approx. 30-160 spikes/min vs approx. 600-2000 spikes/min in our models after 5 WIV) or other aspects of the MEA protocol. The altered neural network activity in our CSB-deficient cells could not be antagonized via HDAC-inhibition, which suggests another HDAC-independent role of CSB. The increased neural network activity is, however, accompanied by elevated GABA levels and decreased KCC2 expression, which could be a possible underlying reason for the increased electrophysiological activities on MEAs. GABA is a fundamentally important neurotransmitter, with a crucial shift from excitatory to inhibitory actions during postnatal brain development. Upregulation of the K/Cl co-transporter KCC2 initiates the GABA switch. A disruption of this pivotal shift causes developmental delays and disorders, such as autism, ADHD and various psychiatric conditions (Peerboom and Wierenga 2021; Pozzi et al. 2020). KCC2 is not a novel therapeutic target, but has been addressed in epilepsy, neuropathic pain, spinal cord injury and the Rett syndrome (Tang 2020; Duy et al. 2020). A promising KCC2-upregulator for testing in CSB models could be the FDA-approved drug prochlorperazine (Liabeuf et al. 2017), which is usually administered as a conventional antipsychotic, but also gained interest in e.g. treating epileptic conditions.

A third neuropathological phenotype found in CSB patients is hypomyelination (Laugel et al. 2010; Vessoni et al. 2020; Karikkineth et al. 2017; Gitiaux et al. 2015). Exemplary causes of altered myelination are disturbed OPC proliferation (e.g. through Notch pathway inhibition), OPC death (e.g. by increased oxidative stress or excitotoxicity) or inhibited oligodendrocyte maturation (e.g. by thyroid hormone deficiency), clinically leading to e.g. cerebral motor deficits, microcephaly, lower IQ, attention deficits and hyperactivity (Ying et al. 2018; Volpe et al. 2011; Dach et al. 2017). The study of demyelination in hiPSC-based vitro models was a great challenge, because most neural differentiation protocols do not support oligodendrocyte differentiation. However, there are specialized protocols that allow the generation of oligodendrocytes in hiPSC-based models (David Pamies et al. 2017; Marton et al. 2019; Chesnut et al. 2021; Douvaras and Fossati 2015). In this thesis, hiPSC-based 3D BrainSpheres, which consist of neurons, astrocytes and oligodendrocytes were employed to investigate the hypomyelination phenotype caused by CSB-deficiency in vitro. We used hiNPC neurospheres that were neurally induced in 3D for subsequent BrainSphere differentiation as described by Pamies et al. (2017). CSB-deficient BrainSpheres revealed no difference in the number of O4+ oligodendrocytes compared to CSB-proficient BrainSpheres. However, gene expression analyses indicated inhibited oligodendrocyte maturation in CSB-deficient BrainSpheres due to overexpression of early versus later oligodendrocyte maturation markers. The early oligodendrocyte progenitor cell (OPC) marker FABP7 was overexpressed, while later the stage markers PDGFR $\alpha$ , CNPase and MBP were underexpressed in both CSB-deficient BrainSpheres, compared to their respective isogenic controls. This inhibited oligodendrocyte maturation can be partially rescued through HDAC-inhibition via the HDAC6-specific inhibitor Tubastatin A and the pan HDAC-inhibitor SAHA. A number of studies have suggested a role of HDACs in the regulation of rodent oligodendrocyte differentiation and maturation, which renders them promising targets in different neurological pathologies (Noack, Leyk, and Richter-Landsberg 2014; Liu et al. 2014; Tauheed, Ayo, and Kawu 2016). Here we show for the first time that altered human oligodendrocyte maturation can be rescued by pharmacological intervention using HDAC inhibitors in an organotypic CSB disease model. This leads us to suggest HDACs as possible drug targets for CSB. Clinically approved HDAC-inhibitors

like SAHA (aka Vorinostat), are currently employed as anti-cancer agents (Yadav, Mishra, and Yadav 2019; Smalley, Cowley, and Hodgkinson 2020). However, novel applications, e.g. for treating HIV infections, muscular dystrophies, inflammatory diseases, as well as neurodegenerative diseases, such as Alzheimer's Disease, frontotemporal dementia and Friedreich's ataxia (as reviewed by Bondarev et al. 2021) are being investigated.

Our combined endophenotypic data of disturbed migration, neural network formation, GABA switch and oligodendrocyte maturation suggest the involvement of HDAC-dependent and -independent mechanisms in CSB, therefore leading us to believe that a combination of drugs might be necessary to target the different cellular adversities observed in the CSB-deficient neural models. However, further investigation is necessary to fully uncover the pathomechanisms underlying CSB on the molecular level. Especially the delayed GABA switch in CSB-deficient hiPSC-based neural in vitro models should be investigated in more detail. Furthermore, the applied CSB models lack microglia, which influence brain development, e.g. by refining synapse formation, circuit sculpting, myelination, plasticity, and cognition. Alterations in microglia function have been linked to neurodevelopmental diseases like autism spectrum disorder, Williams syndrome, Schizophrenia or Rett Syndrome (Allen and Lyons 2018; Bar and Barak 2019). It is however not known, how and if microglia are affected in CSB patients. The integration of microglia into the BrainSpheres would nevertheless increase their physiological relevance.

### 3.5 Implications for the future of disease modeling

With the fit-for-purpose models (manuscript 2.7), the thesis provides human-relevant multicellular systems that are advantageous over tumor or monocellular cultures. However, the models lack the organism complexity, therefore limiting the disease model in relation to inter-organ-crosstalk. An interesting perspective is the development of linked organ-on-chip devices, where interaction between multiple organ models can be studied (manuscript 2.1; Maoz et al. 2018; Alépée et al. 2014; Watson, Hunziker, and Wikswo 2017; Wnorowski, Yang, and Wu 2019). Nevertheless, this thesis shows that

NAMs can provide what animal models often cannot: revealing fundamental disease mechanisms and therapeutic targets (manuscript 2.7).

The application of NAMs cannot stand alone, but rather needs to be integrated into overarching frameworks including *in vitro*, *in vivo* and *in silico* approaches (Shcheglovitov and Peterson 2021; Engdahl et al. 2021; Restuadi et al. 2022). Such integration supports data interpretation, ultimately leading to better predictivity and reliability. This thesis is part of a consortium investigating the CSB using different *in vitro* and *in vivo* approaches. Data obtained in this thesis will be further validated within this consortium. Linking data from different studies and model systems can be challenging, which is why the development of adverse outcome pathways (AOPs) gained more and more attention during the past years. This organizational tool helps to integrate data from different sources to identify the relation between molecular initiating events (MIE), key events (KE), and adverse outcomes (AO; Villeneuve et al. 2014a; 2014b). AOPs have especially been used in the field of toxicity. However, they could also help to understand and link data for disease modeling (Carusi et al. 2018). Future efforts could therefore focus on establishing an AOP network describing CSB, thereby integrating data of different model systems (Figure 3.3 includes data from this study only).

The findings from this thesis intend to spark further investigation into the pathophysiological mechanisms of CSB specifically, and the use of hiPSC-based 3D cultures for disease modeling and personalized medicine in general.

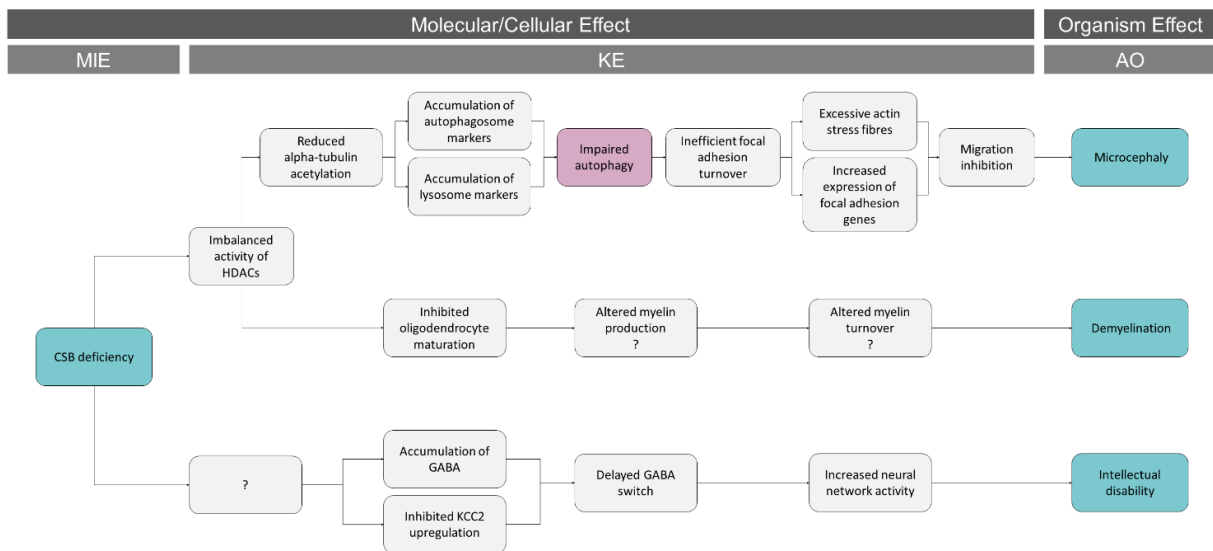


**Figure 3.3. Suggested adverse outcome pathway (AOP) network for the Cockayne Syndrome B (CSB) neuropathology.** AOP1: CSB-deficiency as MIE causes imbalanced activity of HDACs. This imbalanced activity leads to reduced alpha-tubulin acetylation, as well as the accumulation of autophagosome and lysosome markers, thereby impairing cellular autophagy. Impaired autophagy causes inefficient focal adhesion turnover, leading to excessive actin stress fibers and increased expression of focal adhesion genes. The resulting inhibition of cell migration may contribute to the microcephaly phenotype seen in CSB patients. AOP2: CSB-deficiency as MIE causes imbalanced activity of HDACs. This imbalance leads, through unknown molecular effects, to inhibited oligodendrocyte maturation. We presume altered myelin production and myelin turnover as a result, contributing to the demyelination phenotype seen in patients. AOP3: CSB-deficiency as MIE has an HDAC-independent, but unknown molecular effect during neural network formation. Subsequently GABA accumulates and KCC2 upregulation is inhibited. This leads to a delayed GABA switch and increased neural network activity, which may play a role in the intellectual disability seen in CSB patients. The AOP network with all KEs is a suggestion of the data obtain during this thesis. Abbreviations: MIE, molecular initiating event; KE, key event; AO, adverse outcome.



## Abbreviations

2D	Two-dimensional
3D	Three-dimensional
3Rs	Reduce, replace, refine
ACC	Corpus callosum
ACTB	Beta actin
ADA	Oxidized alginate
ADHD	Attention deficite hyperactivity disorder
ALG	Alginate
AO	Adverse outcome
AOP	Adverse outcome pathway
BBB	Blood Brain Barrier
CNS	Central nervous system
COFS	Cerebro-Oculo-Facio-Skeletal
CRISPR	Clustered regularly interspaced short palindromic repeats
CSB	Cockayne syndrome B
DIV	Days in vitro
DNA	Deoxyribonucleic acid
DNT	Developmental neurotoxicity
DSB	Double-strand break
EB	Embryoid Body
ECM	Extracellular matrix
ERCC6	Excision-repair cross complementing group 6
GW	Gastational week
GFAP	Glial fibrillary acidic protein
GG	Gellan Gum
gRNA	Guide RNA
hESC	Human embryonic stem cells

hiPSC	Human induced pluripotent stem cell
hiNPC	Human induced neural progenitor cell
hNPC	Human neural progenitor cell
HTS	High-throughput screening
KCC2	K-Cl cotransporter isoform 2
KdV	Koolen-de Vries
KE	Key event
LAM	Laminin
MAP2	Microtubule-associated protein 2
MEA	Multielectrode array
MIE	Molecular initiating event
MoA	Mode-of-action
MPPH	Megalencephaly-polymicrogyria-polydactyly-hydrocephalus
mRNA	Messenger ribonucleic acid
NAMs	New approach methodologies
NDN	Necdin
NTC	Neural tube closure
NKCC1	Na-K-2Cl cotransporter isoform 1
NNF	Neural network formation
NPC	Neural progenitor cell
NTC	Neural tube closure
O4	Oligodendrocyte marker O4
OPC	Oligodendrocyte precursors
PVL	Perivascular leukomalacia
RG	Radial glia
RNA	Ribonucleic acid
ROS	Reactive oxygen species
shRNA	Short hairpin RNAs
SNPs	Single nucleotide polymorphisms
TC-NER	Transcription-coupled nucleotide excision repair

UVSS	UV-sensitivity syndrome
WIV	Weeks in vitro
XP	Xeroderma pigmentosum



## References

- Abreu, Celina Monteiro, Lucio Gama, Susanne Krasemann, Megan Chesnut, Shelly Odwin-Dacosta, Helena T. Hogberg, Thomas Hartung, and David Pamies. 2018. "Microglia Increase Inflammatory Responses in iPSC-Derived Human BrainSpheres." *Frontiers in Microbiology* 9. <https://doi.org/10.3389/fmicb.2018.02766>.
- Alépée, Natalie, Anthony Bahinski, Mardas Daneshian, Bart De Wever, Ellen Fritsche, Alan Goldberg, Jan Hansmann, et al. 2014. "State-of-the-Art of 3D Cultures (Organs-on-a-Chip) in Safety Testing and Pathophysiology." *Altex* 31 (4): 441–77. <https://doi.org/10.14573/altex1406111>.
- Allen, Nicola J, and David A Lyons. 2018. "Glia as Architects of Central Nervous System Formation and Function." *Science* 185 (October): 181–85.
- Antill-O'Brien, Natasha, Justin Bourke, and Cathal D. O'Connell. 2019. "Layer-by-Layer: The Case for 3D Bioprinting Neurons to Create Patient-Specific Epilepsy Models." *Materials* 12 (19). <https://doi.org/10.3390/ma12193218>.
- Antman-Passig, Merav, Shahar Levy, Chaim Gartenberg, Hadas Schori, and Orit Shefi. 2017. *Mechanically Oriented 3D Collagen Hydrogel for Directing Neurite Growth. Tissue Engineering - Part A*. Vol. 23. <https://doi.org/10.1089/ten.tea.2016.0185>.
- Arber, Charles, Christopher Lovejoy, and Selina Wray. 2017. "Stem Cell Models of Alzheimer's Disease: Progress and Challenges." *Alzheimer's Research and Therapy* 9 (1). <https://doi.org/10.1186/s13195-017-0268-4>.
- Arrowsmith, John, and Philip Miller. 2013. "Trial Watch: Phase II and Phase III Attrition Rates 2011-2012." *Nature Reviews Drug Discovery* 12 (8): 569. <https://doi.org/10.1038/nrd4090>.
- Axpe, Eneko, Gorka Orive, Kristian Franze, and Eric A. Appel. 2020. "Towards Brain-Tissue-like Biomaterials." *Nature Communications* 11 (1): 10–13. <https://doi.org/10.1038/s41467-020-17245-x>.
- Azar, Joseph, Hisham F. Bahmad, Darine Daher, Maya M. Moubarak, Ola Hadadeh, Alissar Monzer, Samar Al Bitar, Mohamed Jamal, Mohamed Al-Sayegh, and Wassim Abou-Kheir. 2021. "The Use of Stem Cell-Derived Organoids in Disease Modeling: An Update." *International Journal of Molecular Sciences* 22 (14). <https://doi.org/10.3390/ijms22147667>.
- Back, Stephen A., Ning Ling Luo, Natalya S. Borenstein, Joel M. Levine, Joseph J. Volpe, and Hannah C. Kinney. 2001. "Late Oligodendrocyte Progenitors Coincide with the Developmental Window of Vulnerability for Human Perinatal White Matter Injury." *Journal of Neuroscience* 21 (4): 1302–12. <https://doi.org/10.1523/jneurosci.21-04-01302.2001>.
- Bagley, Joshua A., Daniel Reumann, Shan Bian, Julie Lévi-Strauss, and Juergen A. Knoblich. 2017. "Fused Cerebral Organoids Model Interactions between Brain

- Regions." *Nature Methods* 14 (7): 743–51. <https://doi.org/10.1038/nmeth.4304>.
- Bahram, Morteza, Naimeh Mohseni, and Mehdi Moghtader. 2016. "An Introduction to Hydrogels and Some Recent Applications." *Emerging Concepts in Analysis and Applications of Hydrogels*. <https://doi.org/10.5772/64301>.
- Bal-Price, Anna, Helena T. Hogberg, Kevin M. Crofton, Mardas Daneshian, Rex E. FitzGerald, Ellen Fritsche, Tuula Heinonen, et al. 2018. "Recommendation on Test Readiness Criteria for New Approach Methods in Toxicology: Exemplified for Developmental Neurotoxicity." *Altex* 35 (3): 306–52. <https://doi.org/10.14573/altex.1712081>.
- Bar, Ela, and Boaz Barak. 2019. "Microglia Roles in Synaptic Plasticity and Myelination in Homeostatic Conditions and Neurodevelopmental Disorders." *Glia* 67 (11): 2125–41. <https://doi.org/10.1002/glia.23637>.
- Barak, Martin, Veronika Fedorova, Veronika Pospisilova, Jan Raska, Simona Vochyanova, Jiri Sedmik, Hana Hribkova, Hana Klimova, Tereza Vanova, and Dasa Bohaciakova. 2022. "Human iPSC-Derived Neural Models for Studying Alzheimer's Disease: From Neural Stem Cells to Cerebral Organoids." *Stem Cell Reviews and Reports* 18 (2): 792–820. <https://doi.org/10.1007/s12015-021-10254-3>.
- Barnea-Goraly, Naama, Vinod Menon, Mark Eckert, Leanne Tamm, Roland Bammer, Asya Karchemskiy, Christopher C. Dant, and Allan L. Reiss. 2005. "White Matter Development during Childhood and Adolescence: A Cross-Sectional Diffusion Tensor Imaging Study." *Cerebral Cortex* 15 (12): 1848–54. <https://doi.org/10.1093/cercor/bhi062>.
- Bartmann, Kristina, Farina Bendt, Arif Dönmez, Daniel Haag, Eike Keßel, Stefan Masjosthusmann, Christopher Noel, Ji Wu, Peng Zhou, and Ellen Fritsche. 2023. "A Human iPSC-Based in Vitro Neural Network Formation Assay to Investigate Neurodevelopmental Toxicity of Pesticides." *Biorxiv* 12. <https://doi.org/10.1101/2023.01.12.523741>.
- Baumann, Jenny, Kathrin Gassmann, Stefan Masjosthusmann, Denise DeBoer, Farina Bendt, Susanne Giersiefer, and Ellen Fritsche. 2016. "Comparative Human and Rat Neurospheres Reveal Species Differences in Chemical Effects on Neurodevelopmental Key Events." *Archives of Toxicology* 90 (6): 1415–27. <https://doi.org/10.1007/s00204-015-1568-8>.
- Becerra-Solano, Luis Eduardo, Leovigildo Mateos-Sánchez, and Eunice López-Muñoz. 2021. "Microcephaly, an Etiopathogenic Vision." *Pediatrics and Neonatology* 62 (4): 354–60. <https://doi.org/10.1016/j.pedneo.2021.05.008>.
- Beekhuis-Hoekstra, Stephanie D., Kyoko Watanabe, Josefin Werme, Christiaan A. de Leeuw, Iryna Paliukhovich, Ka Wan Li, Frank Koopmans, August B. Smit, Danielle Posthuma, and Vivi M. Heine. 2021. "Systematic Assessment of Variability in the Proteome of iPSC Derivatives." *Stem Cell Research* 56. <https://doi.org/10.1016/j.scr.2021.102512>.

- Ben-Ari, Yehezkel. 2002. "Excitatory Actions of GABA during Development: The Nature of the Nurture." *Nature Reviews Neuroscience* 3 (9): 728–39. <https://doi.org/10.1038/nrn920>.
- Blum, Jonathan, Stefan Masjosthusmann, Kristina Bartmann, Farina Bendt, Xenia Dolde, Arif Dönmez, Nils Förster, et al. 2023. "Establishment of a Human Cell-Based in Vitro Battery to Assess Developmental Neurotoxicity Hazard of Chemicals." *Chemosphere* 311. <https://doi.org/10.1016/j.chemosphere.2022.137035>.
- Boer, Jan De, and Jan H.J. Hoeijmakers. 2000. "Nucleotide Excision Repair and Human Syndromes." *Carcinogenesis* 21 (3): 453–60. <https://doi.org/10.1093/carcin/21.3.453>.
- Bondarev, Andrey D., Misty M. Attwood, Jörgen Jonsson, Vladimir N. Chubarev, Vadim V. Tarasov, and Helgi B. Schiöth. 2021. "Recent Developments of HDAC Inhibitors: Emerging Indications and Novel Molecules." *British Journal of Clinical Pharmacology* 87 (12): 4577–97. <https://doi.org/10.1111/bcp.14889>.
- Boutin, Molly E., Caroline E. Strong, Brittney Van Hese, Xin Hu, Zina Itkin, Yu Chi Chen, Andrew LaCroix, et al. 2022. "A Multiparametric Calcium Signal Screening Platform Using iPSC-Derived Cortical Neural Spheroids." *SLAS Discovery* 27 (January): 209–18. <https://doi.org/10.1016/j.slasd.2022.01.003>.
- Brännvall, K., K. Bergman, U. Wallenquist, S. Svahn, T. Bowden, J. Hilborn, and Karin Forsberg-Nilsson. 2007. "Enhanced Neuronal Differentiation in a Three-Dimensional Collagen-Hyaluronan Matrix." *Journal of Neuroscience Research* 85 (10): 2138–46. <https://doi.org/10.1002/jnr.21358>.
- Brunner, Jessie W., Hanna C.A. Lammertse, Annemiek A. van Berkel, Frank Koopmans, Ka Wan Li, August B. Smit, Ruud F. Toonen, Matthijs Verhage, and Sophie van der Sluis. 2023. "Power and Optimal Study Design in iPSC-Based Brain Disease Modelling." *Molecular Psychiatry* 28 (4): 1545–56. <https://doi.org/10.1038/s41380-022-01866-3>.
- Buchsbaum, Isabel Yasmin, and Silvia Cappello. 2019. "Neuronal Migration in the CNS during Development and Disease: Insights from in Vivo and in Vitro Models." *Development (Cambridge)* 146 (1). <https://doi.org/10.1242/dev.163766>.
- Budday, S., G. Sommer, J. Haybaeck, P. Steinmann, G. A. Holzapfel, and E. Kuhl. 2017. "Rheological Characterization of Human Brain Tissue." *Acta Biomaterialia* 60: 315–29. <https://doi.org/10.1016/j.actbio.2017.06.024>.
- Budday, Silvia, Paul Steinmann, and Ellen Kuhl. 2015. "Physical Biology of Human Brain Development." *Frontiers in Cellular Neuroscience* 9 (JULY): 1–17. <https://doi.org/10.3389/fncel.2015.00257>.
- Caldwell, Maeve A., Xiaoling He, Neil Wilkie, Scott Pollack, George Marshall, Keith A. Wafford, and Clive N. Svendsen. 2001. "Growth Factors Regulate the Survival and Fate of Cells Derived from Human Neurospheres." *Nature Biotechnology* 19 (5): 475–79. <https://doi.org/10.1038/88158>.

- Camp, J. Gray, Farhath Badsha, Marta Florio, Sabina Kanton, Tobias Gerber, Michaela Wilsch-Bräuninger, Eric Lewitus, et al. 2015. "Human Cerebral Organoids Recapitulate Gene Expression Programs of Fetal Neocortex Development." *Proceedings of the National Academy of Sciences of the United States of America* 112 (51): 15672–77. <https://doi.org/10.1073/pnas.1520760112>.
- Campos, Lia S., Dino P. Leone, Joao B. Relvas, Cord Brakebusch, Reinhard Fässler, Ueli Suter, and Charles Ffrench-Constant. 2004. "β1 Integrins Activate a MAPK Signalling Pathway in Neural Stem Cells That Contributes to Their Maintenance." *Development* 131 (14): 3433–44. <https://doi.org/10.1242/dev.01199>.
- Carusi, Annamaria, Mark R. Davies, Giovanni De Grandis, Beate I. Escher, Geoff Hodges, Kenneth M.Y. Leung, Maurice Whelan, Catherine Willett, and Gerald T. Ankley. 2018. "Harvesting the Promise of AOPs: An Assessment and Recommendations." *Science of the Total Environment* 628–629: 1542–56. <https://doi.org/10.1016/j.scitotenv.2018.02.015>.
- Centeno, Eduarda G.Z., Helena Cimarosti, and Angela Bithell. 2018. "2D versus 3D Human Induced Pluripotent Stem Cell-Derived Cultures for Neurodegenerative Disease Modelling." *Molecular Neurodegeneration* 13 (1): 1–15. <https://doi.org/10.1186/s13024-018-0258-4>.
- Chai, Qinyuan, Yang Jiao, and Xinjun Yu. 2017. "Hydrogels for Biomedical Applications: Their Characteristics and the Mechanisms behind Them." *Gels* 3 (1): 6. <https://doi.org/10.3390/gels3010006>.
- Chambers, Stuart M., Christopher A. Fasano, Eirini P. Papapetrou, Mark Tomishima, Michel Sadelain, and Lorenz Studer. 2009. "Highly Efficient Neural Conversion of Human ES and IPS Cells by Dual Inhibition of SMAD Signaling." *Nature Biotechnology* 27 (3): 275–80. <https://doi.org/10.1038/nbt.1529>.
- Chao, Daniel L., Le Ma, and Kang Shen. 2009. "Transient Cell-Cell Interactions in Neural Circuit Formation." *Nature Reviews Neuroscience* 10 (4): 262–71. <https://doi.org/10.1038/nrn2594>.
- Chesnut, Megan, Thomas Hartung, Helena Hogberg, and David Pamies. 2021. "Human Oligodendrocytes and Myelin In Vitro to Evaluate Developmental Neurotoxicity." *International Journal of Molecular Sciences* 22 (15): 7929. <https://doi.org/10.3390/ijms22157929>.
- Cho, Iltaeg, Pei Fang Tsai, Robert J. Lake, Asjad Basheer, and Hua Ying Fan. 2013. "ATP-Dependent Chromatin Remodeling by Cockayne Syndrome Protein B and NAP1-Like Histone Chaperones Is Required for Efficient Transcription-Coupled DNA Repair." *PLoS Genetics* 9 (4). <https://doi.org/10.1371/journal.pgen.1003407>.
- Cho, Seung Woo, Sojung Kim, Jong Min Kim, and Jin Soo Kim. 2013. "Targeted Genome Engineering in Human Cells with the Cas9 RNA-Guided Endonuclease." *Nature Biotechnology* 31 (3): 230–32. <https://doi.org/10.1038/nbt.2507>.
- Ciaffardini, F., S. Nicolai, M. Caputo, G. Canu, E. Paccosi, M. Costantino, M. Frontini, A. S.

- Balajee, and L. Proietti-De-Santis. 2014. "The Cockayne Syndrome B Protein Is Essential for Neuronal Differentiation and Neuritogenesis." *Cell Death and Disease* 5 (5): e1268-11. <https://doi.org/10.1038/cddis.2014.228>.
- Citterio, Elisabetta, Vincent Van Den Boom, Gavin Schnitzler, Roland Kanaar, Edgar Bonte, Robert E. Kingston, Jan H. J. Hoeijmakers, and Wim Vermeulen. 2000. "ATP-Dependent Chromatin Remodeling by the Cockayne Syndrome B DNA Repair-Transcription-Coupling Factor." *Molecular and Cellular Biology* 20 (20): 7643–53. <https://doi.org/10.1128/mcb.20.20.7643-7653.2000>.
- Collo, Ginetta, Armida Mucci, Giulia M. Giordano, Emilio Merlo Pich, and Silvana Galderisi. 2020. "Negative Symptoms of Schizophrenia and Dopaminergic Transmission: Translational Models and Perspectives Opened by iPSC Techniques." *Frontiers in Neuroscience* 14. <https://doi.org/10.3389/fnins.2020.00632>.
- Cong, Le, F. Ann Ran, David Cox, Shuailiang Lin, Robert Barretto, Naomi Habib, Patrick D. Hsu, et al. 2013. "Multiplex Genome Engineering Using CRISPR/Cas Systems." *Science* 339 (6121): 819–23. <https://doi.org/10.1126/science.1231143>.
- Cooper, Oliver, Gunnar Hargus, Michela Deleidi, Alexandra Blak, Teresia Osborn, Elizabeth Marlow, Kristen Lee, et al. 2010. "Differentiation of Human ES and Parkinson's Disease IPS Cells into Ventral Midbrain Dopaminergic Neurons Requires a High Activity Form of SHH, FGF8a and Specific Regionalization by Retinoic Acid." *Molecular and Cellular Neuroscience* 45 (3): 258–66. <https://doi.org/10.1016/j.mcn.2010.06.017>.
- Cui, Haitao, Margaret Nowicki, John P. Fisher, and Lijie Grace Zhang. 2017. "3D Bioprinting for Organ Regeneration." *Advanced Healthcare Materials* 6 (1). <https://doi.org/10.1002/adhm.201601118>.
- Cummings, Jeffrey L., Travis Morstorf, and Kate Zhong. 2014. "Alzheimer's Disease Drug-Development Pipeline: Few Candidates, Frequent Failures." *Alzheimer's Research and Therapy* 6 (4). <https://doi.org/10.1186/alzrt269>.
- D'Aiuto, Leonardo, Jennifer Naciri, Nicholas Radio, Sessa Tekur, Dennis Clayton, Gerard Apodaca, Roberto Di Maio, et al. 2018. "Generation of Three-Dimensional Human Neuronal Cultures: Application to Modeling CNS Viral Infections." *Stem Cell Research and Therapy* 9 (1). <https://doi.org/10.1186/s13287-018-0881-6>.
- D'Antoni, Chiara, Lorenza Mautone, Caterina Sanchini, Lucrezia Tondo, Greta Grassmann, Gianluca Cidonio, Paola Bezzi, Federica Cordella, and Silvia Di Angelantonio. 2023. "Unlocking Neural Function with 3D In Vitro Models: A Technical Review of Self-Assembled, Guided, and Bioprinted Brain Organoids and Their Applications in the Study of Neurodevelopmental and Neurodegenerative Disorders." *International Journal of Molecular Sciences* 24 (13): 10762. <https://doi.org/10.3390/ijms241310762>.
- Dach, Katharina, Farina Bendt, Ulrike Huebenthal, Susanne Giersiefer, Pamela J. Lein, Heike Heuer, and Ellen Fritsche. 2017. "BDE-99 Impairs Differentiation of Human and Mouse NPCs into the Oligodendroglial Lineage by Species-Specific Modes of

- Action." *Scientific Reports* 7. <https://doi.org/10.1038/srep44861>.
- Dekaban, Anatole S., and Doris Sadowsky. 1978. "Changes in Brain Weights during the Span of Human Life: Relation of Brain Weights to Body Heights and Body Weights." *Annals of Neurology* 4 (4): 345–56. <https://doi.org/10.1002/ana.410040410>.
- Discher, Dennis E., David J. Mooney, and Peter W. Zandstra. 2009. "Growth Factors, Matrices, and Forces Combine and Control Stem Cells." *Science* 324 (5935): 1673–77. <https://doi.org/10.1126/science.1171643>.
- Distler, T., E. Schaller, P. Steinmann, A. R. Boccaccini, and S. Budday. 2020. "Alginate-Based Hydrogels Show the Same Complex Mechanical Behavior as Brain Tissue." *Journal of the Mechanical Behavior of Biomedical Materials* 111. <https://doi.org/10.1016/j.jmbbm.2020.103979>.
- Distler, Thomas, Aditya A. Solisito, Dominik Schneidereit, Oliver Friedrich, Rainer Detsch, and Aldo R. Boccaccini. 2020. "3D Printed Oxidized Alginate-Gelatin Bioink Provides Guidance for C2C12 Muscle Precursor Cell Orientation and Differentiation via Shear Stress during Bioprinting." *Biofabrication* 12 (4). <https://doi.org/10.1088/1758-5090/ab98e4>.
- Doetschman, Thomas, and Teodora Georgieva. 2017. "Gene Editing with CRISPR/Cas9 RNA-Directed Nuclease." *Circulation Research* 120 (5): 876–94. <https://doi.org/10.1161/CIRCRESAHA.116.309727>.
- Dolmetsch, Ricardo E., Keli Xu, and Richard S. Lewis. 1998. "Calcium Oscillations Increase the Efficiency and Specificity of Gene Expression." *Nature* 392 (6679): 933–36. <https://doi.org/10.1038/31960>.
- Donato, Nataliya Di, Sara Chiari, Ghayda M. Mirzaa, Kimberly Aldinger, Elena Parrini, Carissa Olds, A. James Barkovich, Renzo Guerrini, and William B. Dobyns. 2017. "Lissencephaly: Expanded Imaging and Clinical Classification." *American Journal of Medical Genetics, Part A* 173 (6): 1473–88. <https://doi.org/10.1002/ajmg.a.38245>.
- Douvaras, Panagiotis, and Valentina Fossati. 2015. "Generation and Isolation of Oligodendrocyte Progenitor Cells from Human Pluripotent Stem Cells." *Nature Protocols* 10 (8): 1143–54. <https://doi.org/10.1038/nprot.2015.075>.
- Drexler, Hans G., and Cord C. Uphoff. 2002. "Mycoplasma Contamination of Cell Cultures: Incidence, Sources, Effects, Detection, Elimination, Prevention." *Cytotechnology* 39 (2): 75–90. <https://doi.org/10.1023/A:1022913015916>.
- Duan, Mingrui, Rachel M. Speer, Jenna Ulibarri, Ke Jian Liu, and Peng Mao. 2021. "Transcription-Coupled Nucleotide Excision Repair: New Insights Revealed by Genomic Approaches." *DNA Repair* 103. <https://doi.org/10.1016/j.dnarep.2021.103126>.
- Duy, Phan Q., Miao He, Zhigang He, and Kristopher T. Kahle. 2020. "Preclinical Insights into Therapeutic Targeting of KCC2 for Disorders of Neuronal Hyperexcitability." *Expert Opinion on Therapeutic Targets* 24 (7): 629–37.

<https://doi.org/10.1080/14728222.2020.1762174>.

Ebert, Antje D., Ping Liang, and Joseph C. Wu. 2012. "Induced Pluripotent Stem Cells as a Disease Modeling and Drug Screening Platform." *Journal of Cardiovascular Pharmacology* 60 (4): 408–16. <https://doi.org/10.1097/FJC.0b013e318247f642>.

Ekert, Jason E., Julianna Deakyne, Philippa Pribul-Allen, Rebecca Terry, Christopher Schofield, Claire G. Jeong, Joanne Storey, et al. 2020. "Recommended Guidelines for Developing, Qualifying, and Implementing Complex In Vitro Models (CIVMs) for Drug Discovery." *SLAS Discovery* 25 (10): 1174–90. <https://doi.org/10.1177/2472555220923332>.

Engdahl, Elin, Maarten D.M. van Schijndel, Dimitrios Voulgaris, Michela Di Criscio, Kerry A. Ramsbottom, Daniel J. Rigden, Anna Herland, and Joëlle Rüegg. 2021. "Bisphenol a Inhibits the Transporter Function of the Blood-Brain Barrier by Directly Interacting with the Abc Transporter Breast Cancer Resistance Protein (Bcrp)." *International Journal of Molecular Sciences* 22 (11). <https://doi.org/10.3390/ijms22115534>.

Fabbri, Rachele, Ludovica Cacopardo, Arti Ahluwalia, and Chiara Magliaro. 2023. "Advanced 3D Models of Human Brain Tissue Using Neural Cell Lines: State-of-the-Art and Future Prospects." *Cells* 12 (8): 1–17. <https://doi.org/10.3390/cells12081181>.

Fantini, Valentina, Matteo Bordoni, Franca Scocozza, Michele Conti, Eveljn Scarian, Stephana Carelli, Anna Maria Di Giulio, et al. 2019. "Bioink Composition and Printing Parameters for 3D Modeling Neural Tissue." *Cells* 8 (8): 830. <https://doi.org/10.3390/cells8080830>.

Farrukh, Aleeza, Shifang Zhao, and Aránzazu del Campo. 2018. "Microenvironments Designed to Support Growth and Function of Neuronal Cells." *Frontiers in Materials* 5. <https://doi.org/10.3389/fmats.2018.00062>.

Fedorova, Veronika, Tereza Vanova, Lina Elrefae, Jakub Pospisil, Martina Petrasova, Veronika Kolajova, Zuzana Hudacova, et al. 2019. "Differentiation of Neural Rosettes from Human Pluripotent Stem Cells in Vitro Is Sequentially Regulated on a Molecular Level and Accomplished by the Mechanism Reminiscent of Secondary Neurulation." *Stem Cell Research* 40. <https://doi.org/10.1016/j.scr.2019.101563>.

Ferris, Cameron J., Kerry J. Gilmore, Gordon G. Wallace, and Marc In Het Panhuis. 2013. "Modified Gellan Gum Hydrogels for Tissue Engineering Applications." *Soft Matter* 9 (14): 3705–11. <https://doi.org/10.1039/c3sm27389j>.

Flanagan, Lisa A., Liza M. Rebaza, Stanislava Derzic, Philip H. Schwartz, and Edwin S. Monuki. 2006. "Regulation of Human Neural Precursor Cells by Laminin and Integrins." *Journal of Neuroscience Research* 83 (5): 845–56. <https://doi.org/10.1002/jnr.20778>.

Fox, Jeremy W., and Christopher A. Walsh. 1999. "Periventricular Heterotopia and the Genetics of Neuronal Migration in the Cerebral Cortex." *American Journal of*

- Human Genetics* 65 (1): 19–24. <https://doi.org/10.1086/302474>.
- Frega, Monica, Katrin Linda, Jason M. Keller, Güvem Gümüþ-Akay, Britt Mossink, Jon Ruben van Rhijn, Moritz Negwer, et al. 2019. “Neuronal Network Dysfunction in a Model for Kleefstra Syndrome Mediated by Enhanced NMDAR Signaling.” *Nature Communications* 10 (1). <https://doi.org/10.1038/s41467-019-12947-3>.
- Fritsche, Ellen, Marta Barenys, Jödis Klose, Stefan Masjosthusmann, Laura Nimtz, Martin Schmuck, Saskia Wuttke, and Julia Tigges. 2018a. “Current Availability of Stem Cell-Based in Vitro Methods for Developmental Neurotoxicity (DNT) Testing.” *Toxicological Sciences* 165 (1): 21–30. <https://doi.org/10.1093/toxsci/kfy178>.
- . 2018b. “Development of the Concept for Stem Cell-Based Developmental Neurotoxicity Evaluation.” *Toxicological Sciences* 165 (1): 14–20. <https://doi.org/10.1093/toxsci/kfy175>.
- Fritsche, Ellen, Kathrin Gassmann, and Timm Schreiber. 2011. “Neurospheres as a Model for Developmental Neurotoxicity Testing.” *Methods in Molecular Biology* 758: 99–114. [https://doi.org/10.1007/978-1-61779-170-3\\_7](https://doi.org/10.1007/978-1-61779-170-3_7).
- Galiakberova, Adelya A., and Erdem B. Dashinimaev. 2020. “Neural Stem Cells and Methods for Their Generation From Induced Pluripotent Stem Cells in Vitro.” *Frontiers in Cell and Developmental Biology* 8 (October). <https://doi.org/10.3389/fcell.2020.00815>.
- Garel, C., E. Chantrel, H. Brisse, M. Elmaleh, D. Luton, J. F. Oury, G. Sebag, and M. Hassan. 2001. “Fetal Cerebral Cortex: Normal Gestational Landmarks Identified Using Prenatal MR Imaging.” *American Journal of Neuroradiology* 22 (1): 184–89.
- Garneau, Josiane E., Marie Ève Dupuis, Manuela Villion, Dennis A. Romero, Rodolphe Barrangou, Patrick Boyaval, Christophe Fremaux, Philippe Horvath, Alfonso H. Magadán, and Sylvain Moineau. 2010. “The CRISPR/Cas Bacterial Immune System Cleaves Bacteriophage and Plasmid DNA.” *Nature* 468 (7320): 67–71. <https://doi.org/10.1038/nature09523>.
- Gassmann, K., J. Baumann, S. Giersiefer, J. Schuwald, T. Schreiber, H. F. Merk, and E. Fritsche. 2012. “Automated Neurosphere Sorting and Plating by the COPAS Large Particle Sorter Is a Suitable Method for High-Throughput 3D in Vitro Applications.” *Toxicology in Vitro* 26 (6): 993–1000. <https://doi.org/10.1016/j.tiv.2012.04.025>.
- Geiger, Tamar, Anja Wehner, Christoph Schaab, Juergen Cox, and Matthias Mann. 2012. “Comparative Proteomic Analysis of Eleven Common Cell Lines Reveals Ubiquitous but Varying Expression of Most Proteins.” *Molecular and Cellular Proteomics* 11 (3). <https://doi.org/10.1074/mcp.M111.014050>.
- Georges-Labouesse, Elisabeth, Manuel Mark, Nadia Messaddeq, and Anne Gansmüller. 1998. “Essential Role of A6 Integrins in Cortical and Retinal Lamination.” *Current Biology* 8 (17): 983–86. [https://doi.org/10.1016/s0960-9822\(98\)70402-6](https://doi.org/10.1016/s0960-9822(98)70402-6).
- Ghatak, Swagata, Nima Dolatabadi, Richard Gao, Yin Wu, Henry Scott, Dorit Trudler, Abdullah Sultan, et al. 2021. “NitroSynapsin Ameliorates Hypersynchronous Neural

- Network Activity in Alzheimer HiPSC Models.” *Molecular Psychiatry* 26 (10): 5751–65. <https://doi.org/10.1038/s41380-020-0776-7>.
- Gitiaux, Cyril, Nathalie Blin-Rochemaure, Marie Hully, Andoni Echaniz-Laguna, Nadège Calmels, Nadia Bahi-Buisson, Isabelle Desguerre, et al. 2015. “Progressive Demyelinating Neuropathy Correlates with Clinical Severity in Cockayne Syndrome.” *Clinical Neurophysiology* 126 (7): 1435–39. <https://doi.org/10.1016/j.clinph.2014.10.014>.
- Graaf-Peters, Victorine B. de, and Mijna Hadders-Algra. 2006. “Ontogeny of the Human Central Nervous System: What Is Happening When?” *Early Human Development* 82 (4): 257–66. <https://doi.org/10.1016/j.earlhumdev.2005.10.013>.
- Gressens, Pierre. 2000. “Mechanisms and Disturbances of Neuronal Migration.” *Pediatric Research* 48 (6): 725–30. <https://doi.org/10.1203/00006450-200012000-00004>.
- Gu, Qi, Eva Tomaskovic-Crook, Gordon G. Wallace, and Jeremy M. Crook. 2018. “Engineering Human Neural Tissue by 3D Bioprinting.” *Methods in Molecular Biology* 1758: 129–38. [https://doi.org/10.1007/978-1-4939-7741-3\\_10](https://doi.org/10.1007/978-1-4939-7741-3_10).
- Gu, Zeming, Jianzhong Fu, Hui Lin, and Yong He. 2020. “Development of 3D Bioprinting: From Printing Methods to Biomedical Applications.” *Asian Journal of Pharmaceutical Sciences*. <https://doi.org/10.1016/j.ajps.2019.11.003>.
- Gualda, Emilio J., Daniel Simão, Catarina Pinto, Paula M. Alves, and Catarina Brito. 2014. “Imaging of Human Differentiated 3D Neural Aggregates Using Light Sheet Fluorescence Microscopy.” *Frontiers in Cellular Neuroscience* 8 (AUG): 1–10. <https://doi.org/10.3389/fncel.2014.00221>.
- Hanawalt, Philip C., and Graciela Spivak. 2008. “Transcription-Coupled DNA Repair: Two Decades of Progress and Surprises.” *Nature Reviews Molecular Cell Biology* 9 (12): 958–70. <https://doi.org/10.1038/nrm2549>.
- Haring, Alexander P., Harald Sontheimer, and Blake N. Johnson. 2017. “Microphysiological Human Brain and Neural Systems-on-a-Chip: Potential Alternatives to Small Animal Models and Emerging Platforms for Drug Discovery and Personalized Medicine.” *Stem Cell Reviews and Reports* 13 (3): 381–406. <https://doi.org/10.1007/s12015-017-9738-0>.
- Harrill, Joshua A., Theresa Freudenrich, Kathleen Wallace, Kenneth Ball, Timothy J. Shafer, and William R. Mundy. 2018. “Testing for Developmental Neurotoxicity Using a Battery of in Vitro Assays for Key Cellular Events in Neurodevelopment.” *Toxicology and Applied Pharmacology* 354: 24–39. <https://doi.org/10.1016/j.taap.2018.04.001>.
- Hartfield, Elizabeth M., Michiko Yamasaki-Mann, Hugo J. Ribeiro Fernandes, Jane Vowles, William S. James, Sally A. Cowley, and Richard Wade-Martins. 2014. “Physiological Characterisation of Human IPS-Derived Dopaminergic Neurons.” *PLoS ONE* 9 (2). <https://doi.org/10.1371/journal.pone.0087388>.

- Hartlaub, Annalisa M., Craig A. McElroy, Nathalie L. Maitre, and Mark E. Hester. 2019. "Modeling Human Brain Circuitry Using Pluripotent Stem Cell Platforms." *Frontiers in Pediatrics* 7 (MAR): 1–8. <https://doi.org/10.3389/fped.2019.00057>.
- Hartmann, Julia, Noah Henschel, Kristina Bartmann, Arif Dönmez, Gabriele Brockerhoff, Katharina Koch, and Ellen Fritsche. 2023. "Molecular and Functional Characterization of Different BrainSphere Models for Use in Neurotoxicity Testing on Microelectrode Arrays." *Cells* 12. <https://doi.org/10.3390/cells12091270>.
- Hatten, Mary E. 1999. "Central Nervous System Neuronal Migration." *Annual Review of Neuroscience* 22: 511–39. <https://doi.org/10.1146/annurev.neuro.22.1.511>.
- Hernandez, Sarah J., Gianna Fote, Andrea M. Reyes-Ortiz, Joan S. Steffan, and Leslie M. Thompson. 2021. "Cooperation of Cell Adhesion and Autophagy in the Brain: Functional Roles in Development and Neurodegenerative Disease." *Matrix Biology Plus* 12: 100089. <https://doi.org/10.1016/j.mbplus.2021.100089>.
- Hoar, D. I., and C. Waghorne. 1978. "DNA Repair in Cockayne Syndrome." *American Journal of Human Genetics* 30 (6): 590–601.
- Hofrichter, Maxi, Laura Nimtz, Julia Tigges, Yaschar Kabiri, Friederike Schröter, Brigitte Royer-Pokora, Barbara Hildebrandt, et al. 2017. "Comparative Performance Analysis of Human iPSC-Derived and Primary Neural Progenitor Cells (NPC) Grown as Neurospheres in Vitro." *Stem Cell Research* 25: 72–82. <https://doi.org/10.1016/j.scr.2017.10.013>.
- Hopkins, Amy M., Elise DeSimone, Karolina Chwalek, and David L. Kaplan. 2015. "3D in Vitro Modeling of the Central Nervous System." *Progress in Neurobiology* 125: 1–25. <https://doi.org/10.1016/j.pneurobio.2014.11.003>.
- Horst, Gijsbertus T.J. Van der, Harry Van Steeg, Rob J.W. Berg, Alain J. Van Gool, Jan De Wit, Geert Weeda, Hans Morreau, et al. 1997. "Defective Transcription-Coupled Repair in Cockayne Syndrome B Mice Is Associated with Skin Cancer Predisposition." *Cell* 89 (3): 425–35. [https://doi.org/10.1016/S0092-8674\(00\)80223-8](https://doi.org/10.1016/S0092-8674(00)80223-8).
- Hossini, Amir M., Matthias Megges, Alessandro Prigione, Bjoern Lichtner, Mohammad R. Toliat, Wasco Wruck, Friederike Schröter, et al. 2015. "Induced Pluripotent Stem Cell-Derived Neuronal Cells from a Sporadic Alzheimer's Disease Donor as a Model for Investigating AD-Associated Gene Regulatory Networks." *BMC Genomics* 16 (1). <https://doi.org/10.1186/s12864-015-1262-5>.
- Howard, Brian M., Zhicheng Mo, Radmila Filipovic, Anna R. Moore, Srdjan D. Antic, and Nada Zecevic. 2008. "Radial Glia Cells in the Developing Human Brain." *Neuroscientist* 14 (5): 459–73. <https://doi.org/10.1177/1073858407313512>.
- Hu, Jia, Ge Li, Liuqing Qu, Ning Li, Wei Liu, Dan Xia, Beiqi Hongdu, et al. 2016. "TMEM166/EVA1A Interacts with ATG16L1 and Induces Autophagosome Formation and Cell Death." *Cell Death and Disease* 7 (8): 1–13. <https://doi.org/10.1038/cddis.2016.230>.

- Huttenlocher, P. R., C. De Courten, L. J. Garey, and H. Van der Loos. 1982. "Synaptic Development in Human Cerebral Cortex." *International Journal of Neurology* 16–17: 144–54.
- Ichise, Eisuke, Tomohiro Chiyonobu, Mitsuru Ishikawa, Yasuyoshi Tanaka, Mami Shibata, Takenori Tozawa, Yoshihiro Taura, et al. 2021. "Impaired Neuronal Activity and Differential Gene Expression in STXBP1 Encephalopathy Patient iPSC-Derived GABAergic Neurons." *Human Molecular Genetics* 30 (14): 1337–48. <https://doi.org/10.1093/hmg/ddab113>.
- Insel, Thomas R. 2010. "Rethinking Schizophrenia." *Nature* 468 (7321): 187–93. <https://doi.org/10.1038/nature09552>.
- Jessell, Thomas M., and Joshua R. Sanes. 2000. "Development: The Decade of the Developing Brain." *Current Opinion in Neurobiology* 10 (5): 599–611. [https://doi.org/10.1016/S0959-4388\(00\)00136-7](https://doi.org/10.1016/S0959-4388(00)00136-7).
- Jinek, Martin, Krzysztof Chylinski, Ines Fonfara, Michael Hauer, Jennifer A. Doudna, and Emmanuelle Charpentier. 2012. "A Programmable Dual-RNA-Guided DNA Endonuclease in Adaptive Bacterial Immunity." *Science* 337 (6096): 816–21. <https://doi.org/10.1126/science.1225829>.
- Joseph, Leena, Pushpalatha, and Sarah Kuruvilla. 2008. "Cytomegalovirus Infection with Lissencephaly." *Indian Journal of Pathology and Microbiology* 51 (3): 402–4. <https://doi.org/10.4103/0377-4929.42534>.
- Karikkineth, Ajay C., Morten Scheibye-Knudsen, Elayne Fivenson, Deborah L. Croteau, and Vilhelm A. Bohr. 2017. "Cockayne Syndrome: Clinical Features, Model Systems and Pathways." *Ageing Research Reviews* 33 (1): 3–17. <https://doi.org/10.1016/j.arr.2016.08.002>.
- Kathuria, Annie, Kara Lopez-Lengowski, Smita S. Jagtap, Donna McPhie, Roy H. Perlis, Bruce M. Cohen, and Rakesh Karmacharya. 2020. "Transcriptomic Landscape and Functional Characterization of Induced Pluripotent Stem Cell-Derived Cerebral Organoids in Schizophrenia." *JAMA Psychiatry* 77 (7): 745–54. <https://doi.org/10.1001/jamapsychiatry.2020.0196>.
- Kathuria, Annie, Kara Lopez-Lengowski, Magdalena Vater, Donna McPhie, Bruce M. Cohen, and Rakesh Karmacharya. 2020. "Transcriptome Analysis and Functional Characterization of Cerebral Organoids in Bipolar Disorder." *Genome Medicine* 12 (1). <https://doi.org/10.1186/s13073-020-00733-6>.
- Kenific, Candia M., Samantha J. Stehbens, Juliet Goldsmith, Andrew M. Leidal, Nathalie Faure, Jordan Ye, Torsten Wittmann, and Jayanta Debnath. 2016. "NBR 1 Enables Autophagy-Dependent Focal Adhesion Turnover." *Journal of Cell Biology* 212 (5): 577–90. <https://doi.org/10.1083/jcb.201503075>.
- Kenific, Candia M., Torsten Wittmann, and Jayanta Debnath. 2016. "Autophagy in Adhesion and Migration." *Journal of Cell Science* 129 (20): 3685–93. <https://doi.org/10.1242/jcs.188490>.

- Kim, Ji Eun, Matthew L. O'Sullivan, Christopher A. Sanchez, Minju Hwang, Mason A. Israel, Kristen Brennand, Thomas J. Deerinck, et al. 2011. "Investigating Synapse Formation and Function Using Human Pluripotent Stem Cell-Derived Neurons." *Proceedings of the National Academy of Sciences of the United States of America* 108 (7): 3005–10. <https://doi.org/10.1073/pnas.1007753108>.
- Kinney, H. C., and S. A. Back. 1998. "Human Oligodendroglial Development: Relationship to Periventricular Leukomalacia." *Seminars in Pediatric Neurology* 5 (3): 180–89. [https://doi.org/10.1016/S1071-9091\(98\)80033-8](https://doi.org/10.1016/S1071-9091(98)80033-8).
- Koch, Katharina, Kristina Bartmann, Julia Hartmann, Julia Kapr, Jördis Klose, Eliška Kuchovská, Melanie Pahl, Kevin Schlüppmann, Etta Zühr, and Ellen Fritsche. 2022. "Scientific Validation of Human Neurosphere Assays for Developmental Neurotoxicity Evaluation." *Frontiers in Toxicology* 4 (March): 7. <https://doi.org/10.3389/ftox.2022.816370>.
- Koivisto, Janne T., Tiina Joki, Jenny E. Parraga, Rami Paakkönen, Laura Ylä-Outinen, Laura Salonen, Ilari Jönkkari, et al. 2017. "Bioamine-Crosslinked Gellan Gum Hydrogel for Neural Tissue Engineering." *Biomedical Materials (Bristol)* 12 (2): 0–25. <https://doi.org/10.1088/1748-605X/aa62b0>.
- Kondo, Takayuki, Masashi Asai, Kayoko Tsukita, Yumiko Kutoku, Yutaka Ohsawa, Yoshihide Sunada, Keiko Imamura, et al. 2013. "Modeling Alzheimer's Disease with iPSCs Reveals Stress Phenotypes Associated with Intracellular A $\beta$  and Differential Drug Responsiveness." *Cell Stem Cell* 12 (4): 487–96. <https://doi.org/10.1016/j.stem.2013.01.009>.
- Kraemer, Kenneth H, Nicholas J Patronas, Raphael Schiffmann, Brian P Brooks, Deborah Tamura, and John J Digiovanna. 2008. "Cockayne Syndrome : A Complex Genotype-Phenotype." *Neuroscience* 145 (4): 1388–96.
- Krewski, Daniel, Daniel Acosta, Melvin Andersen, Henry Anderson, John C. Bailar, Kim Boekelheide, Robert Brent, et al. 2010. "Toxicity Testing in the 21st Century: A Vision and a Strategy." *Journal of Toxicology and Environmental Health - Part B: Critical Reviews* 13 (2–4): 51–138. <https://doi.org/10.1080/10937404.2010.483176>.
- Kuhn, Sarah, Laura Gritti, Daniel Crooks, and Yvonne Dombrowski. 2019. "Oligodendrocytes in Development, Myelin Generation and Beyond." *Cells* 8 (11): ix. <https://doi.org/10.3390/cells8111424>.
- Kwak, Tae Hwan, Ji Hyun Kang, Sai Hali, Jonghun Kim, Kee Pyo Kim, Chanhyeok Park, Ju Hyun Lee, et al. 2020. "Generation of Homogeneous Midbrain Organoids with in Vivo-like Cellular Composition Facilitates Neurotoxin-Based Parkinson's Disease Modeling." *Stem Cells* 38 (6): 727–40. <https://doi.org/10.1002/stem.3163>.
- Lancaster, Madeline A., Nina S. Corsini, Simone Wolfinger, E. Hilary Gustafson, Alex W. Phillips, Thomas R. Burkard, Tomoki Otani, Frederick J. Livesey, and Juergen A. Knoblich. 2017. "Guided Self-Organization and Cortical Plate Formation in Human Brain Organoids." *Nature Biotechnology* 35 (7): 659–66. <https://doi.org/10.1038/nbt.3906>.

- Lancaster, Madeline A., and Juergen A. Knoblich. 2014. "Organogenesis in a Dish: Modeling Development and Disease Using Organoid Technologies." *Science* 345 (6194). <https://doi.org/10.1126/science.1247125>.
- Lancaster, Madeline A., Magdalena Renner, Carol Anne Martin, Daniel Wenzel, Louise S. Bicknell, Matthew E. Hurles, Tessa Homfray, Josef M. Penninger, Andrew P. Jackson, and Juergen A. Knoblich. 2013. "Cerebral Organoids Model Human Brain Development and Microcephaly." *Nature* 501 (7467): 373–79. <https://doi.org/10.1038/nature12517>.
- Lankford, K. L., and P. C. Letourneau. 1989. "Evidence That Calcium May Control Neurite Outgrowth by Regulating the Stability of Actin Filaments." *Journal of Cell Biology* 109 (3): 1229–43. <https://doi.org/10.1083/jcb.109.3.1229>.
- Laugel, Vincent. 2013. "Cockayne Syndrome: The Expanding Clinical and Mutational Spectrum." *Mechanisms of Ageing and Development* 134 (5–6): 161–70. <https://doi.org/10.1016/j.mad.2013.02.006>.
- Laugel, Vincent, C. Dalloz, M. Durand, F. Sauvanaud, U. Kristensen, M. C. Vincent, L. Pasquier, et al. 2010. "Mutation Update for the CSB/ERCC6 and CSA/ERCC8 Genes Involved in Cockayne Syndrome." *Human Mutation* 31 (2): 113–26. <https://doi.org/10.1002/humu.21154>.
- Laugel, Vincent, C. Dalloz, E. S. Tobias, J. L. Tolmie, D. Martin-Coignard, V. Drouin-Garraud, V. Valayannopoulos, A. Sarasin, and H. Dollfus. 2008. "Cerebro-Oculo-Facio-Skeletal Syndrome: Three Additional Cases with CSB Mutations, New Diagnostic Criteria and an Approach to Investigation." *Journal of Medical Genetics* 45 (9): 564–71. <https://doi.org/10.1136/jmg.2007.057141>.
- Lebedeva, O. S., and M. A. Lagarkova. 2018. "Pluripotent Stem Cells for Modelling and Cell Therapy of Parkinson's Disease." *Biochemistry (Moscow)* 83 (9): 1046–56. <https://doi.org/10.1134/S0006297918090067>.
- Lee, Francis S., Hakon Heimer, Jay N. Giedd, Edward S. Lein, Nenad Šestan, Daniel R. Weinberger, and B. J. Casey. 2014. "Adolescent Mental Health-Opportunity and Obligation: Emerging Neuroscience Offers Hope for Treatments." *Science* 346 (6209): 547–49. <https://doi.org/10.1126/science.1260497>.
- Lee, You Kyung, Su Kyeong Hwang, Soo Kyung Lee, Jung Eun Yang, Ji Hye Kwak, Hyunhyo Seo, Hyunjun Ahn, et al. 2020. "Cohen Syndrome Patient Ipsc-Derived Neurospheres and Forebrain-like Glutamatergic Neurons Reveal Reduced Proliferation of Neural Progenitor Cells and Altered Expression of Synapse Genes." *Journal of Clinical Medicine* 9 (6): 1–20. <https://doi.org/10.3390/jcm9061886>.
- Lehmann, Alan R., David McGibbon, and Miria Stefanini. 2011. "Xeroderma Pigmentosum." *Orphanet Journal of Rare Diseases* 6 (1). <https://doi.org/10.1186/1750-1172-6-70>.
- Leipzig, Nic D., and Molly S. Shoichet. 2009. "The Effect of Substrate Stiffness on Adult Neural Stem Cell Behavior." *Biomaterials* 30 (36): 6867–78.

<https://doi.org/10.1016/j.biomaterials.2009.09.002>.

- Leung, Alexander K.C., Benjamin Barankin, Joseph M. Lam, Kin Fon Leong, and Kam Lun Hon. 2022. "Xeroderma Pigmentosum: An Updated Review." *Drugs in Context* 11. <https://doi.org/10.7573/dic.2022-2-5>.
- Li, Li, E. Tian, Xianwei Chen, Jianfei Chao, Jeremy Klein, Qiu hao Qu, Guihua Sun, et al. 2018. "GFAP Mutations in Astrocytes Impair Oligodendrocyte Progenitor Proliferation and Myelination in an iPSC Model of Alexander Disease." *Cell Stem Cell* 23 (2): 239–251.e6. <https://doi.org/10.1016/j.stem.2018.07.009>.
- Liabeuf, Sylvie, Laetitia Stuhl-Gourmand, Florian Gackière, Renzo Mancuso, Irene Sanchez Brualla, Philippe Marino, Frédéric Brocard, and Laurent Vinay. 2017. "Prochlorperazine Increases KCC2 Function and Reduces Spasticity after Spinal Cord Injury." *Journal of Neurotrauma* 34 (24): 3397–3406. <https://doi.org/10.1089/neu.2017.5152>.
- Liang, Fangkeng, Bijuan Li, Yingying Xu, Junwei Gong, Shaohui Zheng, Yunlong Zhang, and Yuming Wang. 2023. "Identification and Characterization of Necdin as a Target for the Cockayne Syndrome B Protein in Promoting Neuronal Differentiation and Maintenance." *Pharmacological Research* 187 (December 2022): 106637. <https://doi.org/10.1016/j.phrs.2022.106637>.
- Licht, Christopher, Jonas C. Rose, Abdolrahman Omidinia Anarkoli, Delphine Blondel, Marta Roccio, Tamás Haraszti, David B. Gehlen, Jeffrey A. Hubbell, Matthias P. Lutolf, and Laura De Laporte. 2019. "Synthetic 3D PEG-Anisogel Tailored with Fibronectin Fragments Induce Aligned Nerve Extension." *Biomacromolecules* 20 (11): 4075–87. <https://doi.org/10.1021/acs.biomac.9b00891>.
- Linda, Katrin, Elly I. Lewerissa, Anouk H.A. Verboven, Michele Gabriele, Monica Frega, Teun M. Klein Gunnewiek, Lynn Devilee, et al. 2022. "Imbalanced Autophagy Causes Synaptic Deficits in a Human Model for Neurodevelopmental Disorders." *Autophagy* 18 (2): 423–42. <https://doi.org/10.1080/15548627.2021.1936777>.
- Lindenbaum, Y., D. Dickson, Ps Rosenbaum, Kh Kraemer, Jh Robbins, and I. Rapin. 2001. "Xeroderma Pigmentosum/Cockayne Syndrome Complex: First Neuropathological Study and Review of Eight Other Cases." *European Journal of Paediatric Neurology* 5 (6): 225–42. <https://doi.org/10.1053/ejpn.2001.0523>.
- Liu, Bo, Xin Chen, Zhao Qi Wang, and Wei Min Tong. 2014. "Nbn Gene Inactivation in the CNS of Mouse Inhibits the Myelinating Ability of the Mature Cortical Oligodendrocytes." *Glia* 62 (1): 133–44. <https://doi.org/10.1002/glia.22593>.
- López-Tobón, Alejandro, Carlo Emanuele Villa, Cristina Cheroni, Sebastiano Trattaro, Nicolò Caporale, Paola Conforti, Raffaele Iennaco, et al. 2019. "Human Cortical Organoids Expose a Differential Function of GSK3 on Cortical Neurogenesis." *Stem Cell Reports* 13 (5): 847–61. <https://doi.org/10.1016/j.stemcr.2019.09.005>.
- Lovinger, David M. 2008. "Communication Networks in the Brain: Neurons, Receptors, Neurotransmitters, and Alcohol." *Alcohol Res Health*. 31 (3): 196–214.

- Lozano, Rodrigo, Leo Stevens, Brianna C. Thompson, Kerry J. Gilmore, Robert Gorkin, Elise M. Stewart, Marc in het Panhuis, Mario Romero-Ortega, and Gordon G. Wallace. 2015. "3D Printing of Layered Brain-like Structures Using Peptide Modified Gellan Gum Substrates." *Biomaterials* 67: 264–73. <https://doi.org/10.1016/j.biomaterials.2015.07.022>.
- Lullo, Elizabeth Di, and Arnold R. Kriegstein. 2017. "The Use of Brain Organoids to Investigate Neural Development and Disease." *Nature Reviews Neuroscience* 18 (10): 573–84. <https://doi.org/10.1038/nrn.2017.107>.
- Madl, Christopher M., and Sarah C. Heilshorn. 2018. "Engineering Hydrogel Microenvironments to Recapitulate the Stem Cell Niche." *Annual Review of Biomedical Engineering* 20 (5): 21–47. <https://doi.org/10.1146/annurev-bioeng-062117-120954>.
- Madl, Christopher M., Bauer L. Lesavage, Ruby E. Dewi, Cong B. Dinh, Ryan S. Stowers, Margarita Khariton, Kyle J. Lampe, et al. 2017. "Maintenance of Neural Progenitor Cell Stemness in 3D Hydrogels Requires Matrix Remodelling." *Nature Materials* 16 (12): 1233–42. <https://doi.org/10.1038/nmat5020>.
- Majora, Marc, Kevin Sondenheimer, Maren Knechten, Ingo Uthe, Charlotte Esser, Alfonso Schiavi, Natascia Ventura, and Jean Krutmann. 2018. "HDAC Inhibition Improves Autophagic and Lysosomal Function to Prevent Loss of Subcutaneous Fat in a Mouse Model of Cockayne Syndrome." *Science Translational Medicine* 10 (456). <https://doi.org/10.1126/scitranslmed.aam7510>.
- Malatesta, Paolo, Michael A. Hack, Eva Hartfuss, Helmut Kettenmann, Wolfgang Klinkert, Frank Kirchhoff, and Magdalena Götz. 2003. "Neuronal or Glial Progeny: Regional Differences in Radial Glia Fate." *Neuron* 37 (5): 751–64. [https://doi.org/10.1016/S0896-6273\(03\)00116-8](https://doi.org/10.1016/S0896-6273(03)00116-8).
- Mallery, Donna L., Bianca Tanganelli, Stefano Colella, Herdis Steingrimsdottir, Alain J. Van Gool, Christine Troelstra, Miria Stefanini, and Alan R. Lehmann. 1998. "Molecular Analysis of Mutations in the CSB (ERCC6) Gene in Patients with Cockayne Syndrome." *American Journal of Human Genetics* 62 (1): 77–85. <https://doi.org/10.1086/301686>.
- Maoz, Ben M., Anna Herland, Edward A. Fitzgerald, Thomas Grevesse, Charles Vidoudez, Alan R. Pacheco, Sean P. Sheehy, et al. 2018. "A Linked Organ-on-Chip Model of the Human Neurovascular Unit Reveals the Metabolic Coupling of Endothelial and Neuronal Cells." *Nature Biotechnology* 36 (9): 865–77. <https://doi.org/10.1038/nbt.4226>.
- Margolis, Seth S., Gabrielle L. Sell, Mark A. Zbinden, and Lynne M. Bird. 2015. "Angelman Syndrome." *Neurotherapeutics* 12 (3): 641–50. <https://doi.org/10.1007/s13311-015-0361-y>.
- Marraffini, Luciano A., and Erik J. Sonthheimer. 2010. "CRISPR Interference: RNA-Directed Adaptive Immunity in Bacteria and Archaea." *Nature Reviews Genetics* 11 (3): 181–90. <https://doi.org/10.1038/nrg2749>.

- Martins, Soraia, Inken Hachene, Nadine Teichweyde, Barbara Hildebrandt, Jean Krutmann, and Andrea Rossi. 2021. "Generation of an Induced Pluripotent Stem Cell Line (IUFi001) from a Cockayne Syndrome Patient Carrying a Mutation in the ERCC6 Gene." *Stem Cell Research* 55. <https://doi.org/10.1016/j.scr.2021.102456>.
- Marton, Rebecca M., Yuki Miura, Steven A. Sloan, Qingyun Li, Omer Revah, Rebecca J. Levy, John R. Huguenard, and Sergiu P. Paşca. 2019. "Differentiation and Maturation of Oligodendrocytes in Human Three-Dimensional Neural Cultures." *Nature Neuroscience* 22 (3): 484–91. <https://doi.org/10.1038/s41593-018-0316-9>.
- Masjosthusmann, Stefan, Clara Siebert, Ulrike Hübenthal, Farina Bendt, Jenny Baumann, and Ellen Fritsche. 2019. "Arsenite Interrupts Neurodevelopmental Processes of Human and Rat Neural Progenitor Cells: The Role of Reactive Oxygen Species and Species-Specific Antioxidative Defense." *Chemosphere* 235: 447–56. <https://doi.org/10.1016/j.chemosphere.2019.06.123>.
- Matsui, Takeshi K., Masaya Matsubayashi, Yoshihiko M. Sakaguchi, Ryusei K. Hayashi, Canbin Zheng, Kazuma Sugie, Masatoshi Hasegawa, Takahiko Nakagawa, and Eiichiro Mori. 2018. "Six-Month Cultured Cerebral Organoids from Human ES Cells Contain Matured Neural Cells." *Neuroscience Letters* 670: 75–82. <https://doi.org/10.1016/j.neulet.2018.01.040>.
- Mattis, Virginia B., Soshana P. Svendsen, Allison Ebert, Clive N. Svendsen, Alvin R. King, Malcolm Casale, Sara T. Winokur, et al. 2012. "Induced Pluripotent Stem Cells from Patients with Huntington's Disease Show CAG Repeat Expansion Associated Phenotypes." *Cell Stem Cell* 11 (2): 264–78. <https://doi.org/10.1016/j.stem.2012.04.027>.
- Matyash, Marina, Florian Despang, Rakesh Mandal, Diccon Fiore, Michael Gelinsky, and Chrysanthy Ikonomidou. 2012. "Novel Soft Alginate Hydrogel Strongly Supports Neurite Growth and Protects Neurons against Oxidative Stress." *Tissue Engineering - Part A* 18 (1–2): 55–66. <https://doi.org/10.1089/ten.tea.2011.0097>.
- McPhie, Donna L., Ralda Nehme, Caitlin Ravichandran, Suzann M. Babb, Sulagna Dia Ghosh, Alexandra Staskus, Amy Kalinowski, et al. 2018. "Oligodendrocyte Differentiation of Induced Pluripotent Stem Cells Derived from Subjects with Schizophrenias Implicate Abnormalities in Development." *Translational Psychiatry* 8 (1). <https://doi.org/10.1038/s41398-018-0284-6>.
- Melis, Joost P.M., Harry Van Steeg, and Mirjam Luijten. 2013. "Oxidative DNA Damage and Nucleotide Excision Repair." *Antioxidants and Redox Signaling* 18 (18): 2409–19. <https://doi.org/10.1089/ars.2012.5036>.
- Meyer, Luise J., Felicia P. Lotze, and Matthias L. Riess. 2022. "Simulated Traumatic Brain Injury in In-Vitro Mouse Neuronal and Brain Endothelial Cell Culture Models." *Journal of Pharmacological and Toxicological Methods* 114. <https://doi.org/10.1016/j.vascn.2022.107159>.
- Mittal, Nishka, Jaydev Dave, Magdalena Harakalova, J. Peter van Tintelen, Folkert W. Asselbergs, Pieter A. Doevendans, Kevin D. Costa, Irene C. Turnbull, and Francesca

- Stillitano. 2022. "Generation of Human Induced 4x44 Stem Cell (iPSC) Lines Derived from Five Patients Carrying the Pathogenic Phospholamban-R14del (PLN-R14del) Variant and Three Non-Carrier Family Members." *Stem Cell Research* 60. <https://doi.org/10.1016/j.scr.2022.102737>.
- Miyahara, Hiroaki, Tomoyo Itonaga, Tomoki Maeda, Tatsuro Izumi, and Kenji Ihara. 2015. "Overexpression of P53 but Not Rb in the Cytoplasm of Neurons and Small Vessels in an Autopsy of a Patient with Cockayne Syndrome." *Neuropathology* 35 (3): 266–72. <https://doi.org/10.1111/neup.12183>.
- Monk, C. S., S. J. Webb, and C. A. Nelson. 2001. "Prenatal Neurobiological Development: Molecular Mechanisms and Anatomical Change." *Developmental Neuropsychology* 19 (2): 211–36. [https://doi.org/10.1207/S15326942DN1902\\_5](https://doi.org/10.1207/S15326942DN1902_5).
- Moossy, John. 1967. "The Neuropathology of Cockayne's Syndrome." *Journal of Neuropathology and Experimental Neurology* 26 (4): 654–60. <https://doi.org/10.1097/00005072-196710000-00010>.
- Morizane, Asuka, Daisuke Doi, Tetsuhiro Kikuchi, Kaneyasu Nishimura, and Jun Takahashi. 2011. "Small-Molecule Inhibitors of Bone Morphogenetic Protein and Activin/Nodal Signals Promote Highly Efficient Neural Induction from Human Pluripotent Stem Cells." *Journal of Neuroscience Research* 89 (2): 117–26. <https://doi.org/10.1002/jnr.22547>.
- Morrison, Barclay, D. Kacy Cullen, and Michelle LaPlaca. 2011. "In Vitro Models for Biomechanical Studies of Neural Tissues." *Studies in Mechanobiology, Tissue Engineering and Biomaterials* 3: 247–85. [https://doi.org/10.1007/8415\\_2011\\_79](https://doi.org/10.1007/8415_2011_79).
- Motavaf, Mahsa, and Xianhua Piao. 2021. "Oligodendrocyte Development and Implication in Perinatal White Matter Injury." *Frontiers in Cellular Neuroscience* 15. <https://doi.org/10.3389/fncel.2021.764486>.
- Murai, Machiko, Yasushi Enokido, Naoko Inamura, Masafumi Yoshino, Yoshimichi Nakatsu, Gijsbertus T.J. Van Der Horst, Jan H.J. Hoeijmakers, Kiyoji Tanaka, and Hiroshi Hatanaka. 2001. "Early Postnatal Ataxia and Abnormal Cerebellar Development in Mice Lacking Xeroderma Pigmentosum Group A and Cockayne Syndrome Group B DNA Repair Genes." *Proceedings of the National Academy of Sciences of the United States of America* 98 (23): 13379–84. <https://doi.org/10.1073/pnas.231329598>.
- Nakagawa, Masato, Michiyo Koyanagi, Koji Tanabe, Kazutoshi Takahashi, Tomoko Ichisaka, Takashi Aoi, Keisuke Okita, Yuji Mochizuki, Nanako Takizawa, and Shinya Yamanaka. 2008. "Generation of Induced Pluripotent Stem Cells without Myc from Mouse and Human Fibroblasts." *Nature Biotechnology* 26 (1): 101–6. <https://doi.org/10.1038/nbt1374>.
- Nakazawa, Yuka, Kensaku Sasaki, Norisato Mitsutake, Michiko Matsuse, Mayuko Shimada, Tiziana Nardo, Yoshito Takahashi, et al. 2012. "Mutations in UVSSA Cause UV-Sensitive Syndrome and Impair RNA Polymerase IIo Processing in Transcription-Coupled Nucleotide-Excision Repair." *Nature Genetics* 44 (5): 586–

92. <https://doi.org/10.1038/ng.2229>.

- Ness, Jennifer K., Michael J. Romanko, Raymond P. Rothstein, Teresa L. Wood, and Steven W. Levison. 2001. "Perinatal Hypoxia-Ischemia Induces Apoptotic and Excitotoxic Death of Periventricular White Matter Oligodendrocyte Progenitors." *Developmental Neuroscience* 23 (3): 203–8. <https://doi.org/10.1159/000046144>.
- Newman, John C., Arnold D. Bailey, and Alan M. Weiner. 2006. "Cockayne Syndrome Group B Protein (CSB) Plays a General Role in Chromatin Maintenance and Remodeling." *Proceedings of the National Academy of Sciences of the United States of America* 103 (25): 9613–18. <https://doi.org/10.1073/pnas.0510909103>.
- Nikfarjam, Laleh, and Parvaneh Farzaneh. 2012. "Prevention and Detection of Mycoplasma Contamination in Cell Culture." *Cell Journal* 13 (4): 203–12.
- Nikolopoulou, Evanthia, Gabriel L. Galea, Ana Rolo, Nicholas D.E. Greene, and Andrew J. Copp. 2017. "Neural Tube Closure: Cellular, Molecular and Biomechanical Mechanisms." *Development (Cambridge)* 144 (4): 552–66. <https://doi.org/10.1242/dev.145904>.
- Nimtz, Laura, Julia Hartmann, Julia Tigges, Stefan Masjosthusmann, Martin Schmuck, Eike Keßel, Stephan Theiss, et al. 2020. "Characterization and Application of Electrically Active Neuronal Networks Established from Human Induced Pluripotent Stem Cell-Derived Neural Progenitor Cells for Neurotoxicity Evaluation." *Stem Cell Research* 45: 101761. <https://doi.org/10.1016/j.scr.2020.101761>.
- Noack, Monika, Janina Leyk, and Christiane Richter-Landsberg. 2014. "HDAC6 Inhibition Results in Tau Acetylation and Modulates Tau Phosphorylation and Degradation in Oligodendrocytes." *Glia* 62 (4): 535–47. <https://doi.org/10.1002/glia.22624>.
- O’Rahilly, Ronan, and Fabiola Müller. 2005. *The Embryonic Human Brain: An Atlas of Developmental Stages, Third Edition*. *The Embryonic Human Brain: An Atlas of Developmental Stages, Third Edition*. <https://doi.org/10.1002/0471973084>.
- Odawara, A., N. Matsuda, Y. Ishibashi, R. Yokoi, and I. Suzuki. 2018. "Toxicological Evaluation of Convulsant and Anticonvulsant Drugs in Human Induced Pluripotent Stem Cell-Derived Cortical Neuronal Networks Using an MEA System." *Scientific Reports* 8 (1). <https://doi.org/10.1038/s41598-018-28835-7>.
- Okita, Keisuke, Yasuko Matsumura, Yoshiko Sato, Aki Okada, Asuka Morizane, Satoshi Okamoto, Hyenjong Hong, et al. 2011. "A More Efficient Method to Generate Integration-Free Human IPS Cells." *Nature Methods* 8 (5): 409–12. <https://doi.org/10.1038/nmeth.1591>.
- Ong, Chin Siang, Pooja Yesantharao, Chen Yu Huang, Gunnar Mattson, Joseph Bektor, Takuma Fukunishi, Huaitao Zhang, and Narutoshi Hibino. 2018. "3D Bioprinting Using Stem Cells." *Pediatric Research* 83 (1–2): 223–31. <https://doi.org/10.1038/pr.2017.252>.
- P. M. Paddison, J. Moossy, V. J. Derbres, W. Kloepfer. 1963. "COCKAYNE’S SYNDROME. A

REPORT OF FIVE NEW CASES WITH BIOCHEMICAL, CHROMOSOMAL, DERMATOLOGIC, GENETIC AND NEUROPATHOLOGIC OBSERVATIONS.” *Dermatol Trop Ecol Geogr.* 15: 195–203.

- Pacitti, Dario, Riccardo Privolizzi, and Bridget E. Bax. 2019. “Organs to Cells and Cells to Organoids: The Evolution of In Vitro Central Nervous System Modelling.” *Frontiers in Cellular Neuroscience* 13. <https://doi.org/10.3389/fncel.2019.00129>.
- Pamies, D, M Chesnut, L Smirnova, A Mutallimov, V Maillard, C Repond, T Hartung, M.-G. Zurich, and H Hogberg. 2021. “Human 3D iPSC-Derived Brain Model to Study Chemical-Induced Myelin Disruption.” *Glia* 69 (SUPPL 1): E392–94. <https://www.embase.com/search/results?subaction=viewrecord&id=L635487710&from=export%0Ahttp://dx.doi.org/10.1002/glia.24036>.
- Pamies, David, Paula Barreras, Katharina Block, Georgia Makri, Anupama Kumar, Daphne Wiersma, Lena Smirnova, et al. 2017. “A Human Brain Microphysiological System Derived from Induced Pluripotent Stem Cells to Study Neurological Diseases and Toxicity.” *Altex* 34 (3): 362–76. <https://doi.org/10.14573/altex.1609122>.
- Pamies, David, Katharina Block, Pierre Lau, Laura Gribaldo, Carlos A. Pardo, Paula Barreras, Lena Smirnova, et al. 2018. “Rotenone Exerts Developmental Neurotoxicity in a Human Brain Spheroid Model.” *Toxicology and Applied Pharmacology* 354: 101–14. <https://doi.org/10.1016/j.taap.2018.02.003>.
- Pamies, David, Marcel Leist, Sandra Coecke, Gerard Bowe, David G. Allen, Gerhard Gstraunthaler, Anna Bal-Price, et al. 2022. “Guidance Document on Good Cell and Tissue Culture Practice 2.0 (GCCP 2.0).” *Altex* 39 (1): 30–70. <https://doi.org/10.14573/altex.2111011>.
- Pamies, David, Daphne Wiersma, Moriah E. Katt, Liang Zhao, Johannes Burtscher, Georgina Harris, Lena Smirnova, Peter C. Searson, Thomas Hartung, and Helena T. Hogberg. 2022. “Human Organotypic Brain Model as a Tool to Study Chemical-Induced Dopaminergic Neuronal Toxicity.” *Neurobiology of Disease* 169 (February): 105719. <https://doi.org/10.1016/j.nbd.2022.105719>.
- Park, In Hyun, Paul H. Lerou, Rui Zhao, Hongguang Huo, and George Q. Daley. 2008. “Generation of Human-Induced Pluripotent Stem Cells.” *Nature Protocols* 3 (7): 1180–86. <https://doi.org/10.1038/nprot.2008.92>.
- Park, In Hyun, Rui Zhao, Jason A. West, Akiko Yabuuchi, Hongguang Huo, Tan A. Ince, Paul H. Lerou, M. William Lensch, and George Q. Daley. 2008. “Reprogramming of Human Somatic Cells to Pluripotency with Defined Factors.” *Nature* 451 (7175): 141–46. <https://doi.org/10.1038/nature06534>.
- Park, Joseph, Isaac Wetzel, Ian Marriott, Didier Dréau, Carla D’Avanzo, Doo Yeon Kim, Rudolph E. Tanzi, and Hansang Cho. 2018. “A 3D Human Triculture System Modeling Neurodegeneration and Neuroinflammation in Alzheimer’s Disease.” *Nature Neuroscience* 21 (7): 941–51. <https://doi.org/10.1038/s41593-018-0175-4>.

- Parrish, Jonathon, Khoon Lim, Boyang Zhang, Milica Radisic, and Tim B.F. Woodfield. 2019. "New Frontiers for Biofabrication and Bioreactor Design in Microphysiological System Development." *Trends in Biotechnology* 37 (12): 1327–43. <https://doi.org/10.1016/j.tibtech.2019.04.009>.
- Pasca, Anca M., Steven A. Sloan, Laura E. Clarke, Yuan Tian, Christopher D. Makinson, Nina Huber, Chul Hoon Kim, et al. 2015. "Functional Cortical Neurons and Astrocytes from Human Pluripotent Stem Cells in 3D Culture." *Nature Methods* 12 (7): 671–78. <https://doi.org/10.1038/nmeth.3415>.
- Pasca, Sergiu P. 2018. "The Rise of Three-Dimensional Human Brain Cultures." *Nature* 553 (7689): 437–45. <https://doi.org/10.1038/nature25032>.
- Paşca, Sergiu P., Paola Arlotta, Helen S. Bateup, J. Gray Camp, Silvia Cappello, Fred H. Gage, Jürgen A. Knoblich, et al. 2022. "A Nomenclature Consensus for Nervous System Organoids and Assembloids." *Nature* 609 (7929): 907–10. <https://doi.org/10.1038/s41586-022-05219-6>.
- Paulsson, Mats. 1992. "The Role of Laminin in Attachment, Growth, and Differentiation of Cultured Cells: A Brief Review." *Cytotechnology* 9 (1–3): 99–106. <https://doi.org/10.1007/BF02521736>.
- Paus, Tomáš, Matcheri Keshavan, and Jay N. Giedd. 2008. "Why Do Many Psychiatric Disorders Emerge during Adolescence?" *Nature Reviews Neuroscience* 9 (12): 947–57. <https://doi.org/10.1038/nrn2513>.
- Peerboom, Carlijn, and Corette J. Wierenga. 2021. "The Postnatal GABA Shift: A Developmental Perspective." *Neuroscience and Biobehavioral Reviews* 124 (January): 179–92. <https://doi.org/10.1016/j.neubiorev.2021.01.024>.
- Pei, Ying, Jun Peng, Mamta Behl, Nisha S. Sipes, Keith R. Shockley, Mahendra S. Rao, Raymond R. Tice, and Xianmin Zeng. 2016. "Comparative Neurotoxicity Screening in Human iPSC-Derived Neural Stem Cells, Neurons and Astrocytes." *Brain Research* 1638: 57–73. <https://doi.org/10.1016/j.brainres.2015.07.048>.
- Pelkonen, Anssi, Cristiana Pistono, Pamela Klecki, Mireia Gómez-Budia, Antonios Dougalis, Henna Konttinen, Iveta Stanová, et al. 2022. "Functional Characterization of Human Pluripotent Stem Cell-Derived Models of the Brain with Microelectrode Arrays." *Cells* 11 (1). <https://doi.org/10.3390/cells11010106>.
- Pencea, Viorica, Kimberly D. Bingaman, Lorin J. Freedman, and Marla B. Luskin. 2001. "Neurogenesis in the Subventricular Zone and Rostral Migratory Stream of the Neonatal and Adult Primate Forebrain." *Experimental Neurology* 172 (1): 1–16. <https://doi.org/10.1006/exnr.2001.7768>.
- Penney, Jay, William T. Ralvenius, and Li Huei Tsai. 2020. "Modeling Alzheimer's Disease with iPSC-Derived Brain Cells." *Molecular Psychiatry* 25 (1): 148–67. <https://doi.org/10.1038/s41380-019-0468-3>.
- Petanjek, Zdravko, Miloš Judaš, Ivica Kostović, and Harry B.M. Uylings. 2008. "Lifespan Alterations of Basal Dendritic Trees of Pyramidal Neurons in the Human Prefrontal

- Cortex: A Layer-Specific Pattern." *Cerebral Cortex* 18 (4): 915–29. <https://doi.org/10.1093/cercor/bhm124>.
- Petanjek, Zdravko, Miloš Judaš, Goran Šimić, Mladen Roko Rašin, Harry B.M. Uylings, Pasko Rakic, and Ivica Kostović. 2011. "Extraordinary Neoteny of Synaptic Spines in the Human Prefrontal Cortex." *Proceedings of the National Academy of Sciences of the United States of America* 108 (32): 13281–86. <https://doi.org/10.1073/pnas.1105108108>.
- Peuchen, Stefan, Juan P. Bolaños, Simon J.R. Heales, Angeles Almeida, Michael R. Duchon, and John B. Clark. 1997. "Interrelationships between Astrocyte Function, Oxidative Stress and Antioxidant Status within the Central Nervous System." *Progress in Neurobiology* 52 (4): 261–81. [https://doi.org/10.1016/S0301-0082\(97\)00010-5](https://doi.org/10.1016/S0301-0082(97)00010-5).
- Pirozzi, Filomena, Branden Nelson, and Ghayda Mirzaa. 2018. "From Microcephaly to Megalencephaly: Determinants of Brain Size." *Dialogues in Clinical Neuroscience* 20 (4): 267–82. <https://doi.org/10.31887/dcns.2018.20.4/gmirzaa>.
- Pizzarelli, Rocco, and Enrico Cherubini. 2011. "Alterations of GABAergic Signaling in Autism Spectrum Disorders." *Neural Plasticity* 2011. <https://doi.org/10.1155/2011/297153>.
- Poirier, Karine, Nicolas Lebrun, Loic Broix, Guoling Tian, Yoann Saillour, Cécile Boscheron, Elena Parrini, et al. 2013. "Mutations in TUBG1, DYNC1H1, KIF5C and KIF2A Cause Malformations of Cortical Development and Microcephaly." *Nature Genetics* 45 (6): 639–47. <https://doi.org/10.1038/ng.2613>.
- Pozzi, Davide, Marco Rasile, Irene Corradini, and Michela Matteoli. 2020. "Environmental Regulation of the Chloride Transporter KCC2: Switching Inflammation off to Switch the GABA On?" *Translational Psychiatry* 10 (1). <https://doi.org/10.1038/s41398-020-01027-6>.
- Qian, Xuyu, Ha Nam Nguyen, Mingxi M. Song, Christopher Hadiono, Sarah C. Ogden, Christy Hammack, Bing Yao, et al. 2016. "Brain-Region-Specific Organoids Using Mini-Bioreactors for Modeling ZIKV Exposure." *Cell* 165 (5): 1238–54. <https://doi.org/10.1016/j.cell.2016.04.032>.
- Quadrato, Giorgia, Tuan Nguyen, Evan Z. Macosko, John L. Sherwood, Sung Min Yang, Daniel R. Berger, Natalie Maria, et al. 2017. "Cell Diversity and Network Dynamics in Photosensitive Human Brain Organoids." *Nature* 545 (7652): 48–53. <https://doi.org/10.1038/nature22047>.
- Que, Zhefu, Maria I. Olivero-Acosta, Jingliang Zhang, Muriel Eaton, Anke M. Tukker, Xiaoling Chen, Jiayang Wu, et al. 2021. "Hyperexcitability and Pharmacological Responsiveness of Cortical Neurons Derived from Human iPSCs Carrying Epilepsy-Associated Sodium Channel Nav1.2-L1342P Genetic Variant." *Journal of Neuroscience* 41 (49): 10194–208. <https://doi.org/10.1523/JNEUROSCI.0564-21.2021>.

- Quist, Ella, Henrik Ahlenius, and Isaac Canals. 2021. "Transcription Factor Programming of Human Pluripotent Stem Cells to Functionally Mature Astrocytes for Monocultures and Cocultures with Neurons." *Methods in Molecular Biology* 2352: 133–48. [https://doi.org/10.1007/978-1-0716-1601-7\\_10](https://doi.org/10.1007/978-1-0716-1601-7_10).
- R. D. Schmickel, E. H. Y. Chu, J. E. Trosko and C. C. Chang. 1977. "Cockayne Syndrome: A Cellular Sensitivity to Ultraviolet Light." *Pediatrics* 60 (2): 135–39.
- Raja, Waseem K., Esther Neves, Christopher Burke, Xin Jiang, Ping Xu, Kenneth J. Rhodes, Vikram Khurana, Robert H. Scannevin, and Chee Yeun Chung. 2022. "Patient-Derived Three-Dimensional Cortical Neurospheres to Model Parkinson's Disease." *PLoS ONE* 17 (12 December). <https://doi.org/10.1371/journal.pone.0277532>.
- Rakic, P. 1982. "Early Developmental Events: Cell Lineages, Acquisition of Neuronal Positions, and Areal and Laminar Development." *Neurosciences Research Program Bulletin* 20 (4): 439–51.
- Rapin, Isabelle, Y. Lindenbaum, D. W. Dickson, K. H. Kraemer, and J. H. Robbins. 2000. "Cockayne Syndrome and Xeroderma Pigmentosum: DNA Repair Disorders with Overlaps and Paradoxes." *Neurology* 55 (10): 1442–49. <https://doi.org/10.1212/WNL.55.10.1442>.
- Rash, Brian G., and Elizabeth A. Grove. 2006. "Area and Layer Patterning in the Developing Cerebral Cortex." *Current Opinion in Neurobiology* 16 (1): 25–34. <https://doi.org/10.1016/j.conb.2006.01.004>.
- Rebel, Heggert, Nicolien Kram, Anja Westerman, Sander Banus, Henk J. van Kranen, and Frank R. de Gruijl. 2005. "Relationship between UV-Induced Mutant P53 Patches and Skin Tumours, Analysed by Mutation Spectra and by Induction Kinetics in Various DNA-Repair-Deficient Mice." *Carcinogenesis* 26 (12): 2123–30. <https://doi.org/10.1093/carcin/bgi198>.
- Restuadi, Restuadi, Frederik J. Steyn, Edor Kabashi, Shyuan T. Ngo, Fei Fei Cheng, Marta F. Nabais, Mike J. Thompson, et al. 2022. "Functional Characterisation of the Amyotrophic Lateral Sclerosis Risk Locus GPX3/TNIP1." *Genome Medicine* 14 (1). <https://doi.org/10.1186/s13073-021-01006-6>.
- Revet, Ingrid, Luzviminda Feeney, Amy A. Tang, Eric J. Huang, and James E. Cleaver. 2012. "Dysmyelination Not Demyelination Causes Neurological Symptoms in Preweaned Mice in a Murine Model of Cockayne Syndrome." *Proceedings of the National Academy of Sciences of the United States of America* 109 (12): 4627–32. <https://doi.org/10.1073/pnas.1202621109>.
- Rhinn, Muriel, Alexander Picker, and Michael Brand. 2006. "Global and Local Mechanisms of Forebrain and Midbrain Patterning." *Current Opinion in Neurobiology* 16 (1): 5–12. <https://doi.org/10.1016/j.conb.2006.01.005>.
- Ronchi, Silvia, Alessio Paolo Buccino, Gustavo Prack, Sreedhar Saseendran Kumar, Manuel Schröter, Michele Fiscella, and Andreas Hierlemann. 2021.

- “Electrophysiological Phenotype Characterization of Human iPSC-Derived Neuronal Cell Lines by Means of High-Density Microelectrode Arrays.” *Advanced Biology* 5 (3). <https://doi.org/10.1002/adbi.202000223>.
- Rosati, Jessica, Daniela Ferrari, Filomena Altieri, Silvia Tardivo, Claudia Ricciolini, Caterina Fusilli, Cristina Zalfa, et al. 2018. “Establishment of Stable IPS-Derived Human Neural Stem Cell Lines Suitable for Cell Therapies.” *Cell Death and Disease* 9 (10). <https://doi.org/10.1038/s41419-018-0990-2>.
- Rosenberg, Sheila S., and Nicholas C. Spitzer. 2011. “Calcium Signaling in Neuronal Development.” *Cold Spring Harbor Perspectives in Biology* 3 (10): 1–13. <https://doi.org/10.1101/cshperspect.a004259>.
- Rotmensch, Siegfried, and Ana Monteagudo. 2020. “Agenesis of the Corpus Callosum.” *American Journal of Obstetrics and Gynecology* 223 (6): B17–22. <https://doi.org/10.1016/j.ajog.2020.08.179>.
- Rowe, R. Grant, and George Q. Daley. 2019. “Induced Pluripotent Stem Cells in Disease Modelling and Drug Discovery.” *Nature Reviews Genetics* 20 (7): 377–88. <https://doi.org/10.1038/s41576-019-0100-z>.
- Russell, W.M.S., and R.L. Burch. 1959. “The Principles of Humane Experimental Technique.” In , xiv + 238pp. London: UK: Methuen & Co LTD.
- Saili, Katerine S., Todd J. Zurlinden, Andrew J. Schwab, Aymeric Silvin, Nancy C. Baker, E. Sidney Hunter, Florent Ginhoux, and Thomas B. Knudsen. 2017. “Blood-Brain Barrier Development: Systems Modeling and Predictive Toxicology.” *Birth Defects Research* 109 (20): 1680–1710. <https://doi.org/10.1002/bdr2.1180>.
- Sakaguchi, Hideya, Yuki Ozaki, Tomoka Ashida, Takayoshi Matsubara, Naotaka Oishi, Shunsuke Kihara, and Jun Takahashi. 2019. “Self-Organized Synchronous Calcium Transients in a Cultured Human Neural Network Derived from Cerebral Organoids.” *Stem Cell Reports* 13 (3): 458–73. <https://doi.org/10.1016/j.stemcr.2019.05.029>.
- Santello, Mirko, Nicolas Toni, and Andrea Volterra. 2019. “Astrocyte Function from Information Processing to Cognition and Cognitive Impairment.” *Nature Neuroscience* 22 (2): 154–66. <https://doi.org/10.1038/s41593-018-0325-8>.
- Sarker, Bapi, Dimitrios G. Papageorgiou, Raquel Silva, Tobias Zehnder, Farhana Gul-E-Noor, Marko Bertmer, Joachim Kaschta, Konstantinos Chrissafis, Rainer Detsch, and Aldo R. Boccaccini. 2014. “Fabrication of Alginate-Gelatin Crosslinked Hydrogel Microcapsules and Evaluation of the Microstructure and Physico-Chemical Properties.” *Journal of Materials Chemistry B* 2 (11): 1470–82. <https://doi.org/10.1039/c3tb21509a>.
- Scheibye-Knudsen, Morten, Mahesh Ramamoorthy, Peter Sykora, Scott Maynard, Ping Chang Lin, Robin K. Minor, David M. Wilson, et al. 2012. “Cockayne Syndrome Group B Protein Prevents the Accumulation of Damaged Mitochondria by Promoting Mitochondrial Autophagy.” *Journal of Experimental Medicine* 209 (4): 855–69. <https://doi.org/10.1084/jem.20111721>.

- Schmidt, Martin J., and Karoly Mirnics. 2015. "Neurodevelopment, GABA System Dysfunction, and Schizophrenia." *Neuropsychopharmacology* 40 (1): 190–206. <https://doi.org/10.1038/npp.2014.95>.
- Seidlits, Stephanie K., Zin Z. Khaing, Rebecca R. Petersen, Jonathan D. Nickels, Jennifer E. Vanscoy, Jason B. Shear, and Christine E. Schmidt. 2010. "The Effects of Hyaluronic Acid Hydrogels with Tunable Mechanical Properties on Neural Progenitor Cell Differentiation." *Biomaterials* 31 (14): 3930–40. <https://doi.org/10.1016/j.biomaterials.2010.01.125>.
- Shaker, Mohammed R., Giovanni Pietrogrande, Sally Martin, Ju Hyun Lee, Woong Sun, and Ernst J. Wolvetang. 2021. "Rapid and Efficient Generation of Myelinating Human Oligodendrocytes in Organoids." *Frontiers in Cellular Neuroscience* 15 (March): 1–11. <https://doi.org/10.3389/fncel.2021.631548>.
- Sharma, Arun, Samuel Sances, Michael J. Workman, and Clive N. Svendsen. 2020. "Multi-Lineage Human iPSC-Derived Platforms for Disease Modeling and Drug Discovery." *Cell Stem Cell* 26 (3): 309–29. <https://doi.org/10.1016/j.stem.2020.02.011>.
- Sharma, Navatha Shree, Anik Karan, Donghee Lee, Zheng Yan, and Jingwei Xie. 2021. "Advances in Modeling Alzheimer's Disease In Vitro." *Advanced NanoBiomed Research* 1 (12). <https://doi.org/10.1002/anbr.202100097>.
- Sharma, Ruchi, Imke P.M. Smits, Laura De La Vega, Christopher Lee, and Stephanie M. Willerth. 2020. "3D Bioprinting Pluripotent Stem Cell Derived Neural Tissues Using a Novel Fibrin Bioink Containing Drug Releasing Microspheres." *Frontiers in Bioengineering and Biotechnology* 8. <https://doi.org/10.3389/fbioe.2020.00057>.
- Shcheglovitov, Aleksandr, and Randall T. Peterson. 2021. "Screening Platforms for Genetic Epilepsies—Zebrafish, iPSC-Derived Neurons, and Organoids." *Neurotherapeutics* 18 (3): 1478–89. <https://doi.org/10.1007/s13311-021-01115-5>.
- Si-Tayeb, Karim, Fallon K. Noto, Ana Sepac, Filip Sedlic, Zeljko J. Bosnjak, John W. Lough, and Stephen A. Duncan. 2010. "Generation of Human Induced Pluripotent Stem Cells by Simple Transient Transfection of Plasmid DNA Encoding Reprogramming Factors." *BMC Developmental Biology* 10. <https://doi.org/10.1186/1471-213X-10-81>.
- Silbereis, John C., Sirisha Pochareddy, Ying Zhu, Mingfeng Li, and Nenad Sestan. 2016. "The Cellular and Molecular Landscapes of the Developing Human Central Nervous System." *Neuron* 89 (2): 248. <https://doi.org/10.1016/j.neuron.2015.12.008>.
- Silva, Gabriel A., Catherine Czeisler, Krista L. Niece, Elia Beniash, Daniel A. Harrington, John A. Kessler, and Samuel I. Stupp. 2004. "Selective Differentiation of Neural Progenitor Cells by High-Epitope Density Nanofibers." *Science* 303 (5662): 1352–55. <https://doi.org/10.1126/science.1093783>.
- Silva, Nuno A., Michael J. Cooke, Roger Y. Tam, Nuno Sousa, António J. Salgado, Rui L. Reis, and Molly S. Shoichet. 2012. "The Effects of Peptide Modified Gellan Gum and

- Olfactory Ensheathing Glia Cells on Neural Stem/Progenitor Cell Fate.” *Biomaterials* 33 (27): 6345–54. <https://doi.org/10.1016/j.biomaterials.2012.05.050>.
- Simkin, Dina, Kelly A. Marshall, Carlos G. Vanoye, Reshma R. Desai, Bernabe I. Bustos, Brandon N. Piyevesky, Juan A. Ortega, et al. 2021. “Dyshomeostatic Modulation of Ca<sup>2+</sup>-Activated K<sup>+</sup> Channels in a Human Neuronal Model of Kcnq2 Encephalopathy.” *ELife* 10: 1–32. <https://doi.org/10.7554/eLife.64434>.
- Smalley, Joshua P., Shaun M. Cowley, and James T. Hodgkinson. 2020. “Bifunctional HDAC Therapeutics: One Drug to Rule Them All?” *Molecules* 25 (19). <https://doi.org/10.3390/molecules25194394>.
- Snaidero, Nicolas, and Mikael Simons. 2014. “Myelination at a Glance.” *Journal of Cell Science* 127 (14): 2999–3004. <https://doi.org/10.1242/jcs.151043>.
- Soldner, Frank, Dirk Hockemeyer, Caroline Beard, Qing Gao, George W. Bell, Elizabeth G. Cook, Gunnar Hargus, et al. 2009. “Parkinson’s Disease Patient-Derived Induced Pluripotent Stem Cells Free of Viral Reprogramming Factors.” *Cell* 136 (5): 964–77. <https://doi.org/10.1016/j.cell.2009.02.013>.
- Spaas, Jan, Lieve van Veggel, Melissa Schepers, Assia Tiane, Jack van Horssen, David M. Wilson, Pablo R. Moya, et al. 2021. “Oxidative Stress and Impaired Oligodendrocyte Precursor Cell Differentiation in Neurological Disorders.” *Cellular and Molecular Life Sciences* 78 (10): 4615–37. <https://doi.org/10.1007/s00018-021-03802-0>.
- Stadelmann, Christine, Sebastian Timmler, Alonso Barrantes-Freer, and Mikael Simons. 2019. “Myelin in the Central Nervous System: Structure, Function, and Pathology.” *Physiological Reviews* 99 (3): 1381–1431. <https://doi.org/10.1152/physrev.00031.2018>.
- Stern, Claudio D. 2001. “Initial Patterning of the Central Nervous System: How Many Organizers?” *Nature Reviews Neuroscience* 2 (2): 92–98. <https://doi.org/10.1038/35053563>.
- Stevnsner, Tinna, Simon Nyaga, Nadja C. De Souza-Pinto, Gijsbertus T.J. Van der Horst, Theo G.M.F. Gorgels, Barbara A. Hogue, Tina Thorslund, and Vilhelm A. Bohr. 2002. “Mitochondrial Repair of 8-Oxoguanine Is Deficient in Cockayne Syndrome Group B.” *Oncogene* 21 (57): 8675–82. <https://doi.org/10.1038/sj.onc.1205994>.
- Stiles, Joan, and Terry L. Jernigan. 2010. “The Basics of Brain Development.” *Neuropsychology Review* 20 (4): 327–48. <https://doi.org/10.1007/s11065-010-9148-4>.
- Sugarman, G. I., B. H. Landing, and W. B. Reed. 1977. “Cockayne Syndrome: Clinical Study of Two Patients and Neuropathologic Findings in One.” *Clinical Pediatrics* 16 (3): 225–32. <https://doi.org/10.1177/000992287701600304>.
- Sugita, Katsuo, Xiao Jun Chi, Takaki Hiwasa, and Nobuo Nobuo. 2001. “Studies on P53 and Bax Protein Expression in Cockayne Syndrome Cells after UV Irradiation and Interferon- $\beta$  Treatment.” *Cell Biochemistry and Function* 19 (3): 221–25.

- <https://doi.org/10.1002/cbf.917>.
- Sun, Jinchun, and Huaping Tan. 2013. "Alginate-Based Biomaterials for Regenerative Medicine Applications." *Materials* 6 (4): 1285–1309. <https://doi.org/10.3390/ma6041285>.
- Sutherland, Daniel J., Zac Pujic, and Geoffrey J. Goodhill. 2014. "Calcium Signaling in Axon Guidance." *Trends in Neurosciences* 37 (8): 424–32. <https://doi.org/10.1016/j.tins.2014.05.008>.
- Sweeney, Melanie D., Zhen Zhao, Axel Montagne, Amy R. Nelson, and Berislav V. Zlokovic. 2019. "Blood-Brain Barrier: From Physiology to Disease and Back." *Physiological Reviews* 99 (1): 21–78. <https://doi.org/10.1152/physrev.00050.2017>.
- Szebényi, Kornélia, Léa M.D. Wenger, Yu Sun, Alexander W.E. Dunn, Colleen A. Limegrover, George M. Gibbons, Elena Conci, et al. 2021. "Human ALS/FTD Brain Organoid Slice Cultures Display Distinct Early Astrocyte and Targetable Neuronal Pathology." *Nature Neuroscience* 24 (11): 1542–54. <https://doi.org/10.1038/s41593-021-00923-4>.
- Takahashi, Kazutoshi, Koji Tanabe, Mari Ohnuki, Megumi Narita, Tomoko Ichisaka, Kiichiro Tomoda, and Shinya Yamanaka. 2007. "Induction of Pluripotent Stem Cells from Adult Human Fibroblasts by Defined Factors." *Cell* 131 (5): 861–72. <https://doi.org/10.1016/j.cell.2007.11.019>.
- Tan, Jun, Meihan Duan, Tribhuvan Yadav, Laiyee Phoon, Xiangyu Wang, Jia Min Zhang, Lee Zou, and Li Lan. 2020. "An R-Loop-Initiated CSB-RAD52-POLD3 Pathway Suppresses ROS-Induced Telomeric DNA Breaks." *Nucleic Acids Research* 48 (3): 1285–1300. <https://doi.org/10.1093/nar/gkz1114>.
- Tanaka, Kiyoji, Kazuhiko Kawai, Yuichi Kumahara, Mituo Ikenaga, and Yoshio Okada. 1981. "Genetic Complementation Groups in Cockayne Syndrome." *Somatic Cell Genetics* 7 (4): 445–55. <https://doi.org/10.1007/BF01542989>.
- Tang, Bor Luen. 2020. "The Expanding Therapeutic Potential of Neuronal KCC2." *Cells* 9 (1): 1–15. <https://doi.org/10.3390/cells9010240>.
- Tau, Gregory Z., and Bradley S. Peterson. 2010. "Normal Development of Brain Circuits." *Neuropsychopharmacology* 35 (1): 147–68. <https://doi.org/10.1038/npp.2009.115>.
- Tauheed, Abdullah Mohammad, Joseph Olusegun Ayo, and Mohammed Umaru Kawu. 2016. "Regulation of Oligodendrocyte Differentiation: Insights and Approaches for the Management of Neurodegenerative Disease." *Pathophysiology* 23 (3): 203–10. <https://doi.org/10.1016/j.pathophys.2016.05.007>.
- Treiman, David M. 2001. "GABAergic Mechanisms in Epilepsy." *Epilepsia* 42 (SUPPL. 3): 8–12. <https://doi.org/10.1046/j.1528-1157.2001.042Suppl.3008.x>.
- Troelstra, C., R. M. Landsvater, J. Wiegant, M. van der Ploeg, G. Viel, C. H.C.M. Buys, and J. H.J. Hoeijmakers. 1992. "Localization of the Nucleotide Excision Repair Gene ERCC6 to Human Chromosome 10q11-Q21." *Genomics* 12 (4): 745–49.

[https://doi.org/10.1016/0888-7543\(92\)90304-B](https://doi.org/10.1016/0888-7543(92)90304-B).

- Troelstra, Christine, Alain van Gool, Jan de Wit, Wim Vermeulen, Dirk Bootsma, and Jan H.J. Hoeijmakers. 1992. "ERCC6, a Member of a Subfamily of Putative Helicases, Is Involved in Cockayne's Syndrome and Preferential Repair of Active Genes." *Cell* 71 (6): 939–53. [https://doi.org/10.1016/0092-8674\(92\)90390-X](https://doi.org/10.1016/0092-8674(92)90390-X).
- Tsubooka, Noriko, Tomoko Ichisaka, Keisuke Okita, Kazutoshi Takahashi, Masato Nakagawa, and Shinya Yamanaka. 2009. "Roles of Sall4 in the Generation of Pluripotent Stem Cells from Blastocysts and Fibroblasts." *Genes to Cells* 14 (6): 683–94. <https://doi.org/10.1111/j.1365-2443.2009.01301.x>.
- Tukker, Anke M., Regina G.D.M. Van Kleef, Fiona M.J. Wijnolts, Aart De Groot, and Remco H.S. Westerink. 2020. "Towards Animal-Free Neurotoxicity Screening: Applicability of HiPSC-Derived Neuronal Models for in Vitro Seizure Liability Assessment." *Altex* 37 (1): 121–35. <https://doi.org/10.14573/altex.1907121>.
- Tukker, Anke M., Fiona M.J. Wijnolts, Aart de Groot, and Remco H.S. Westerink. 2018. "Human iPSC-Derived Neuronal Models for in Vitro Neurotoxicity Assessment." *NeuroToxicology* 67: 215–25. <https://doi.org/10.1016/j.neuro.2018.06.007>.
- Tuo, Jingsheng, Catheryne Chen, Xianmin Zeng, Mette Christiansen, and Vilhelm A. Bohr. 2002. "Functional Crosstalk between HOG1 and the Helicase Domain of Cockayne Syndrome Group B Protein." *DNA Repair* 1 (11): 913–27. [https://doi.org/10.1016/S1568-7864\(02\)00116-7](https://doi.org/10.1016/S1568-7864(02)00116-7).
- Tzu, Julia, and M. Peter Marinkovich. 2008. "Bridging Structure with Function: Structural, Regulatory, and Developmental Role of Laminins." *International Journal of Biochemistry and Cell Biology* 40 (2): 199–214. <https://doi.org/10.1016/j.biocel.2007.07.015>.
- Vasudevan, Pradeep, and Mohnish Suri. 2017. "A Clinical Approach to Developmental Delay and Intellectual Disability." *Clinical Medicine, Journal of the Royal College of Physicians of London* 17 (6): 558–61. <https://doi.org/10.7861/clinmedicine.17-6-558>.
- Vessoni, Alexandre T., Roberto H. Herai, Jerome V. Karpiak, Angelica M.S. Leal, Cleber A. Trujillo, Annabel Quinet, Lucymara F. Agnez Lima, Carlos F.M. Menck, and Alysso R. Muotri. 2016. "Cockayne Syndrome-Derived Neurons Display Reduced Synapse Density and Altered Neural Network Synchrony." *Human Molecular Genetics* 25 (7): 1271–80. <https://doi.org/10.1093/hmg/ddw008>.
- Vessoni, Alexandre Teixeira, Camila Chaves Coelho Guerra, Gustavo Satoru Kajitani, Livia Luz Souza Nascimento, and Camila Carrião Machado Garcia. 2020. "Cockayne Syndrome: The Many Challenges and Approaches to Understand a Multifaceted Disease." *Genetics and Molecular Biology* 43 (1). <https://doi.org/10.1590/1678-4685-GMB-2019-0085>.
- Villeneuve, Daniel L., Doug Crump, Natàlia Garcia-Reyero, Markus Hecker, Thomas H. Hutchinson, Carlie A. LaLone, Brigitte Landesmann, et al. 2014a. "Adverse Outcome

- Pathway (AOP) Development I: Strategies and Principles.” *Toxicological Sciences* 142 (2): 312–20. <https://doi.org/10.1093/toxsci/kfu199>.
- . 2014b. “Adverse Outcome Pathway Development II: Best Practices.” *Toxicological Sciences* 142 (2): 321–30. <https://doi.org/10.1093/toxsci/kfu200>.
- Volpato, Viola, and Caleb Webber. 2020. “Addressing Variability in iPSC-Derived Models of Human Disease: Guidelines to Promote Reproducibility.” *DMM Disease Models and Mechanisms* 13 (1). <https://doi.org/10.1242/dmm.042317>.
- Volpe, Joseph J., Hannah C. Kinney, Frances E. Jensen, and Paul A. Rosenberg. 2011. “The Developing Oligodendrocyte: Key Cellular Target in Brain Injury in the Premature Infant.” *International Journal of Developmental Neuroscience* 29 (4): 423–40. <https://doi.org/10.1016/j.ijdevneu.2011.02.012>.
- Wainger, Brian J., Evangelos Kiskinis, Cassidy Mellin, Ole Wiskow, Steve S.W. Han, Jackson Sandoe, Numa P. Perez, et al. 2014. “Intrinsic Membrane Hyperexcitability of Amyotrophic Lateral Sclerosis Patient-Derived Motor Neurons.” *Cell Reports* 7 (1): 1–11. <https://doi.org/10.1016/j.celrep.2014.03.019>.
- Wang, Si, Zheyang Min, Qianzhao Ji, Lingling Geng, Yao Su, Zunpeng Liu, Huifang Hu, et al. 2020. “Rescue of Premature Aging Defects in Cockayne Syndrome Stem Cells by CRISPR/Cas9-Mediated Gene Correction.” *Protein and Cell* 11 (1). <https://doi.org/10.1007/s13238-019-0623-2>.
- Wang, Yuming, Jace Jones-Tabah, Probir Chakravarty, Aengus Stewart, Alysso Muotri, Rebecca R. Laposa, and Jesper Q. Svejstrup. 2016. “Pharmacological Bypass of Cockayne Syndrome B Function in Neuronal Differentiation.” *Cell Reports* 14 (11): 2554–61. <https://doi.org/10.1016/j.celrep.2016.02.051>.
- Warren, Luigi, Philip D. Manos, Tim Ahfeldt, Yuin Han Loh, Hu Li, Frank Lau, Wataru Ebina, et al. 2010. “Highly Efficient Reprogramming to Pluripotency and Directed Differentiation of Human Cells with Synthetic Modified mRNA.” *Cell Stem Cell* 7 (5): 618–30. <https://doi.org/10.1016/j.stem.2010.08.012>.
- Washer, Sam J., Marta Perez-Alcantara, Yixi Chen, Juliette Steer, William S. James, Gosia Trynka, Andrew R. Bassett, and Sally A. Cowley. 2022. “Single-Cell Transcriptomics Defines an Improved, Validated Monoculture Protocol for Differentiation of Human iPSC to Microglia.” *Scientific Reports* 12 (1). <https://doi.org/10.1038/s41598-022-23477-2>.
- Watson, David E., Rosemarie Hunziker, and John P. Wikswo. 2017. “Fitting Tissue Chips and Microphysiological Systems into the Grand Scheme of Medicine, Biology, Pharmacology, and Toxicology.” *Experimental Biology and Medicine* 242 (16): 1559–72. <https://doi.org/10.1177/1535370217732765>.
- West, A. E., W. G. Chen, M. B. Dalva, R. E. Dolmetsch, J. M. Kornhauser, A. J. Shaywitz, M. A. Takasu, X. Tao, and M. E. Greenberg. 2001. “Calcium Regulation of Neuronal Gene Expression.” *Proceedings of the National Academy of Sciences of the United States of America* 98 (20): 11024–31. <https://doi.org/10.1073/pnas.191352298>.

- Wichterle, O., and D. Lím. 1960. "Hydrophilic Gels for Biological Use." *Nature* 185 (4706): 117–18. <https://doi.org/10.1038/185117a0>.
- Wiedenheft, Blake, Samuel H. Sternberg, and Jennifer A. Doudna. 2012. "RNA-Guided Genetic Silencing Systems in Bacteria and Archaea." *Nature* 482 (7385): 331–38. <https://doi.org/10.1038/nature10886>.
- Wnorowski, A., Huaxiao Yang, and Joseph C. Wu. 2019. "Progress, Obstacles, and Limitations in the Use of Stem Cells in Organ-on-a-Chip Models." *Advanced Drug Delivery Reviews* 140 (1): 3–11. <https://doi.org/10.1016/j.addr.2018.06.001>.
- Wray, Selina. 2021. "Modelling Neurodegenerative Disease Using Brain Organoids." *Seminars in Cell and Developmental Biology* 111: 60–66. <https://doi.org/10.1016/j.semcdb.2020.05.012>.
- Wu, Ping, Yevgeniya I. Tarasenko, Yanping Gu, Li Yen M. Huang, Richard E. Coggeshall, and Yongjia Yu. 2002. "Region-Specific Generation of Cholinergic Neurons from Fetal Human Neural Stem Cells Grafted in Adult Rat." *Nature Neuroscience* 5 (12): 1271–78. <https://doi.org/10.1038/nn974>.
- Wu, Zhenzhen, Xun Zhu, Qian Yu, Yingying Xu, and Yuming Wang. 2019. "Multisystem Analyses of Two Cockayne Syndrome Associated Proteins CSA and CSB Reveal Shared and Unique Functions." *DNA Repair* 83 (May): 102696. <https://doi.org/10.1016/j.dnarep.2019.102696>.
- Xu, Ranjie, Andrew T. Brawner, Shenglan Li, Jing Jing Liu, Hyosung Kim, Haipeng Xue, Zhiping P. Pang, et al. 2019. "OLIG2 Drives Abnormal Neurodevelopmental Phenotypes in Human iPSC-Based Organoid and Chimeric Mouse Models of Down Syndrome." *Cell Stem Cell* 24 (6): 908–926.e8. <https://doi.org/10.1016/j.stem.2019.04.014>.
- Xu, Tao, Peter Molnar, Cassie Gregory, Mainak Das, Thomas Boland, and James J. Hickman. 2009. "Electrophysiological Characterization of Embryonic Hippocampal Neurons Cultured in a 3D Collagen Hydrogel." *Biomaterials* 30 (26): 4377–83. <https://doi.org/10.1016/j.biomaterials.2009.04.047>.
- Xu, Yingying, Zhenzhen Wu, Lingyun Liu, Jiena Liu, and Yuming Wang. 2019. "Rat Model of Cockayne Syndrome Neurological Disease." *Cell Reports* 29 (4): 800–809.e5. <https://doi.org/10.1016/j.celrep.2019.09.028>.
- Yadav, Rakesh, Pooja Mishra, and Divya Yadav. 2019. "Histone Deacetylase Inhibitors: A Prospect in Drug Discovery." *Turkish Journal of Pharmaceutical Sciences* 16 (1): 101–14. <https://doi.org/10.4274/tjps.75047>.
- Yang, Luhan, Joyce L. Yang, Susan Byrne, Joshua Pan, and George M. Church. 2014. "CRISPR/Cas9-Directed Genome Editing of Cultured Cells." *Current Protocols in Molecular Biology* 2014 (July): 31.1.1–31.1.17. <https://doi.org/10.1002/0471142727.mb3101s107>.
- Yildirimer, Lara, and Alexander M. Seifalian. 2014. "Three-Dimensional Biomaterial Degradation - Material Choice, Design and Extrinsic Factor Considerations."

- Biotechnology Advances* 32 (5): 984–99.  
<https://doi.org/10.1016/j.biotechadv.2014.04.014>.
- Ying, Yan qin, Xue qin Yan, Sheng juan Jin, Yan Liang, Ling Hou, Wan ting Niu, and Xiao ping Luo. 2018. “Inhibitory Effect of LPS on the Proliferation of Oligodendrocyte Precursor Cells through the Notch Signaling Pathway in Intrauterine Infection-Induced Rats.” *Current Medical Science* 38 (5): 840–46.  
<https://doi.org/10.1007/s11596-018-1951-9>.
- Ylä-Outinen, Laura, Jarno M.A. Tanskanen, Fikret E. Kapucu, Anu Hyysalo, Jari A.K. Hyttinen, and Susanna Narkilahti. 2019. *Advances in Human Stem Cell-Derived Neuronal Cell Culturing and Analysis. Advances in Neurobiology*. Vol. 22.  
[https://doi.org/10.1007/978-3-030-11135-9\\_13](https://doi.org/10.1007/978-3-030-11135-9_13).
- Yoon, Jin-young, Nastaran Daneshgar, Biyi Chen, Marco Hefti, Ajit Vikram, Kaikobad Irani, Charles Brenner, et al. 2022. “Metabolic Rescue Ameliorates Mitochondrial Encephalo-Cardiomyopathy in Murine and Human iPSC Models of Leigh Syndrome,” no. January. <https://doi.org/10.1002/ctm2.954>.
- Yoon, Joy, and Yingwei Mao. 2021. “Dissecting Molecular Genetic Mechanisms of 1q21.1 Cnv in Neuropsychiatric Disorders.” *International Journal of Molecular Sciences* 22 (11). <https://doi.org/10.3390/ijms22115811>.
- Yoshihara, Masahito, Akiko Oguchi, and Yasuhiro Murakawa. 2019. “Genomic Instability of iPSCs and Challenges in Their Clinical Applications.” *Advances in Experimental Medicine and Biology* 1201: 23–47. [https://doi.org/10.1007/978-3-030-31206-0\\_2](https://doi.org/10.1007/978-3-030-31206-0_2).
- Yu, Adong, Hua Ying Fan, Daiqing Liao, Arnold D. Bailey, and Alan M. Weiner. 2000. “Activation of P53 or Loss of the Cockayne Syndrome Group B Repair Protein Causes Metaphase Fragility of Human U1, U2, and 5S Genes.” *Molecular Cell* 5 (5): 801–10. [https://doi.org/10.1016/S1097-2765\(00\)80320-2](https://doi.org/10.1016/S1097-2765(00)80320-2).
- Yu, Junying, Maxim A. Vodyanik, Kim Smuga-Otto, Jessica Antosiewicz-Bourget, Jennifer L. Frane, Shulan Tian, Jeff Nie, et al. 2007. “Induced Pluripotent Stem Cell Lines Derived from Human Somatic Cells.” *Science* 318 (5858): 1917–20.  
<https://doi.org/10.1126/science.1151526>.
- Zhang, Dawei, Mari Pekkanen-Mattila, Mansoureh Shahsavani, Anna Falk, Ana I. Teixeira, and Anna Herland. 2014. “A 3D Alzheimer’s Disease Culture Model and the Induction of P21-Activated Kinase Mediated Sensing in iPSC Derived Neurons.” *Biomaterials* 35 (5): 1420–28. <https://doi.org/10.1016/j.biomaterials.2013.11.028>.
- Zhao, Yang, Xiaolei Yin, Han Qin, Fangfang Zhu, Haisong Liu, Weifeng Yang, Qiang Zhang, et al. 2008. “Two Supporting Factors Greatly Improve the Efficiency of Human iPSC Generation.” *Cell Stem Cell* 3 (5): 475–79.  
<https://doi.org/10.1016/j.stem.2008.10.002>.
- Zhou, Ting, Lei Tan, Gustav Y. Cederquist, Yujie Fan, Brigham J. Hartley, Suranjit Mukherjee, Mark Tomishima, et al. 2017. “High-Content Screening in hPSC-Neural Progenitors Identifies Drug Candidates That Inhibit Zika Virus Infection in Fetal-

- like Organoids and Adult Brain.” *Cell Stem Cell* 21 (2): 274-283.e5.  
<https://doi.org/10.1016/j.stem.2017.06.017>.
- Zhou, Yi ye, and Fanyi Zeng. 2013. “Integration-Free Methods for Generating Induced Pluripotent Stem Cells.” *Genomics, Proteomics and Bioinformatics* 11 (5): 284–87.  
<https://doi.org/10.1016/j.gpb.2013.09.008>.
- Zhu, N., M. G. Li, Y. J. Guan, D. J. Schreyer, and X. B. Chen. 2010. “Effects of Laminin Blended with Chitosan on Axon Guidance on Patterned Substrates.” *Biofabrication* 2 (4). <https://doi.org/10.1088/1758-5082/2/4/045002>.
- Zhuang, Pei, Jia An, Lay Poh Tan, and Chee Kai Chua. 2018. “The Current Status of 3D Bioprinting for Neural Tissue Models.” *Proceedings of the International Conference on Progress in Additive Manufacturing 2018-May*: 183–88.  
<https://doi.org/10.25341/D4688F>.
- Zhuang, Pei, Alfred Xuyang Sun, Jia An, Chee Kai Chua, and Sing Yian Chew. 2018. “3D Neural Tissue Models: From Spheroids to Bioprinting.” *Biomaterials* 154: 113–33.  
<https://doi.org/10.1016/j.biomaterials.2017.10.002>.





## Danksagung

Ich möchte mich bei allen Personen bedanken, die mich in meinem Weg zur Promotion unterstützt und motiviert haben.

Ein besonderer Dank gilt Frau Prof. Dr. Ellen Fritsche, für die Aufnahme in ihre Arbeitsgruppe, zunächst für meine Masterarbeit und später für meine Promotion. Vielen Dank für die großzügige Förderung und das Vertrauen in mich und meine Fähigkeiten.

Auch danken möchte ich Herrn Prof. Dr. Jean Krutmann, welcher mir die Arbeit an diesem Leibniz Projekt ermöglichte. Innerhalb des von ihm geführten Konsortiums habe ich wertvolle Unterstützung für meine Forschung erhalten.

Bei Frau Prof. Dr. Vlada Urlacher bedanke ich mich besonders für die fakultätsübergreifende Betreuung und die Mentorenschaft, durch welche meine Promotion erst möglich wurde.

Ein großer Dank gilt meiner Betreuerin Katharina Koch, die mir immer mit Rat und Tat zur Seite gestanden hat. Vielen Dank für die fachliche und persönliche Unterstützung und dein offenes Ohr.

Auch bedanken möchte ich mich bei Ilka Egger, für ihre tolle Unterstützung im Labor und ihren unermüdlichen Eifer im Projekt.

Vielen Dank an alle meine Arbeitskollegen für die tolle Unterstützung und einen nie langweilig werdenden Arbeitsalltag. Besonderer Dank geht an die gesamte AG Fritsche für die tollen Erlebnisse innerhalb und außerhalb von Düsseldorf. Die Konferenzen, Urlaube und Feiern werden mir immer im Gedächtnis bleiben.

Außerdem danke ich allen meinen Freunden für ihre positive Energie und damit Motivation und Unterstützung in allen Phasen meiner Promotion.

Ein ganz besonderer Dank gebührt meiner Familie, die mir den nötigen Rückhalt gegeben hat, um kleine und große Aufgaben zu bewältigen. Danke für eure bedingungslose Unterstützung in allen Situationen und an allen Orten.

Vielen Dank für alles!



## Eidesstattliche Erklärung/Declaration

Hiermit versichere ich an Eides statt, dass die vorliegende Dissertation „Neurale 3D in vitro Modelle basierend auf humanen induzierten pluripotenten Stammzellen: Entwicklung, Qualitätskontrolle und Krankheitsmodellierung“ von mir selbständig und ohne unzulässige fremde Hilfe unter Beachtung der „Grundsätze zur Sicherung guter wissenschaftlicher Praxis and der Heinrich-Heine-Universität Düsseldorf“ erstellt worden ist. Die Dissertation wurde in der vorgelegten oder einer ähnlichen Form noch bei keiner anderen Institution eingereicht. Ich habe bisher keine erfolglosen Promotionsversuche unternommen.

I declare that I have developed and written the enclosed thesis ‘Human induced pluripotent stem cell-based 3D neural in vitro models: development, quality control and disease modeling’ completely by myself, and have not used sources or means without declaration in the text. Any thoughts from others or literal quotations are clearly marked. The thesis was prepared in compliance with the principles of ‘Good Scientific Practice at the Heinrich-Heine-University Dusseldorf’. The thesis was not used in the same or in a similar version to achieve an academic grading elsewhere.

Düsseldorf, den \_\_\_\_\_

-----

Julia Kapr